Université Libre de Bruxelles – Département des Sciences de la Terre et de l'Environnement

Musée Royal de l'Afrique Centrale – Département des Sciences de la Terre

Isotopic approaches of the silicon cycle:

The Southern Ocean case study

François Fripiat

Thèse présentée en vue de l'obtention du grade de Docteur en sciences de la terre et de l'environnement

Année académique 2009 – 2010

Composition du jury :

Pr. Christiane Lancelot (Université Libre de Bruxelles, Belgique) – Présidente

Pr. Nadine Mattielli (Université Libre de Bruxelles, Belgique) - Secrétaire

Pr. Luc André (Université Libre de Bruxelles – Musée Royal de l'Afrique Centrale, Belgique) – Promoteur

Dr. Damien Cardinal (Musée Royal de l'Afrique Centrale, Belgique) – Co-promoteur

Pr. Frank Dehairs (Vrije Universiteit Brussel, Belgique)

Pr. Christina De La Rocha (Institut Universitaire Européen de la Mer –Université de Bretagne Occidentale, France)

Dr. Karine Leblanc (Laboratoire d'Océanographie Physique et Biogéochimique – Centre Océanologie de Marseille, France)

Histoire élémentaire commune…

D'une étoile et de son explosion, nous apparaît une soupe isotopique constituant une jolie fresque élémentaire. Ces éléments, aujourd'hui, sont là tout autour de nous, sous diverses formes.

Nous-mêmes sommes formés d'une architecture de ces éléments créés et judicieusement sélectionnés. Prenons l'exemple de nos atomes de carbone. Ces derniers ont nécessairement pris diverses formes depuis leur création dans les étoiles.

Nos atomes de carbone «12», avec leurs potes phosphores «tous seuls», ont sûrement subi plusieurs cycles endogènes et exogènes passant d'une cheminée hydrothermale au primaire, à un baobab au secondaire et peut-être même une simple et jolie petite diatomée au tertiaire. En un sens, la géochimie m'a donné un ensemble et un petit bout d'éternité.

Bruxelles, 2009

Tout comme la fin de mes études, qui marque une page tournée de mon enfance, je dédicace cette thèse à «Dom», qui, depuis sa disparition, aura laissé lui aussi une part de mon enfance et de mon insouciance derrière moi…

Je tiens particulièrement à exprimer toute ma reconnaissance à

Luc André, mon promoteur de thèse;

Damien Cardinal, mon co-promoteur de thèse;

Frank Dehairs, le coordinateur du projet BELCANTOIII;

Et aux autres membres du jury;

Sans qui cette thèse n'aurait certainement pas abouti, sans oublier les nombreuses collaborations et amitiés données-reçues…

Table of Contents

Abstract

We investigate the silicon (Si) cycle in the Southern Ocean through two isotopic approaches: (1) ^{30}Si-incubation experiments and (2) natural silicon isotopic composition (δ^{30}Si). ^{30}Si-spiked incubation allows to discriminate the short-term (~ 1 day) net Si-uptake flux in $bSiO_2$ production and dissolution. δ^{30}Si of both biogenic silica and dissolved silicon integrates at seasonal/annual scale $bSiO_2$ production or dissolution and mixing.

(1) A new mass spectrometer method (HR-SF-ICPMS) has been developed for ^{30}Si-isotopic abundance measurements. This methodology is faster and easier than the previous available methodologies and has the same precision. A complete set of incubation was coupled with parallel ^{32}Si-incubations and the two methodologies give not significantly different $bSiO_2$ production rates. In the Southern Ocean, especially in the southern Antarctic Circumpolar Current, the large silicic acid concentration degrades the sensitivity of the method with Si dissolution fluxes staying generally below the detection limit. In contrast, the ^{28}Si-isotopic dilution was sensitive enough to assess low biogenic silica dissolution rates in silicic acid poor waters of the northern ACC. We show that large accumulation of detrital dissolving biogenic silica after productive period implies really efficient silicon loop with integrated (euphotic layer) dissolution:production ratio equal or larger than 1.

(2) We largely expand the silicic acid isotopic data in the open ocean. Relatively simple mass and isotopic balances have been performed in the Antarctic Zone and have allowed to apply for the first time δ^{30}Si in a quantitative way to estimate regional net silica production and quantify source waters fueling $bSiO_2$ productivity. We observe that at the end of the productive period as suggested with ^{30}Si-incubation, large accumulation of detrital biogenic silica in the surface waters increase the D:P ratio and subsequently dampens the $bSiO_2$ production mediated isotopic fractionation with residual biogenic silica carrying heavier δ^{30}Si than expected. Seasonal isotopic evolution is simulated and seems in agreement with our observations. These simulations strongly suggest working with non-zero order equations to fully assess the seasonal expression of the different processes involved: mixing, uptake, dissolution. Si-isotopes are also tracking the origin and fates of the different ACC pools across the Southern Ocean meridional circulation. Moreover during the circumpolar eastward pathway, the $bSiO_2$ dissolution in deep water decreases the corresponding δ^{30}Si values and this imprint is further transmitted via the upper limb of the meridional circulation in the intermediate water masses.

Thesis outline

Since decades, efforts are made by geoscientists to understand the processes driving the global biogeochemical cycles, and their interactions with the biosphere and the global environment. A thorough understanding of these interactions can help to decipher how climate evolved throughout earth's history and to predict how it might evolve in the future. Moreover, human activities significantly affect the earth elemental cycling pattern. For these purposes it is absolutely crucial to understand how global element cycles, such as the Si cycle, work and how they might change through time. This cycle is closely linked to other element cycles (N, P, Fe, Mg, Ca …), especially the C cycle which is presently the focus of investigations in the context of climate change. Indeed silicon cycle affects the carbon cycle mainly through two processes. (1) The "biological pump" (*Volk and Hoffert*, 1985) which is a complex ecosystem process that efficiently and consistently transports large amounts of carbon molecules in the form of particulate organic carbon along with biogenic silica from epipelagic (surface) to the deep interior of the world ocean and further to the abyssal floor. Some studies provided evidences for the important relationship between pelagic food-web structure (in particular the proportion of diatoms among primary producers) and the export flux from the surface ocean (*Boyd and Newton*, 1995, 1999a; *Buesseler*, 1998; *Jin et al*., 2006; *Boyd and Trull*, 2007; *Honjo et al*., 2008). (2) The weathering of Ca- and Mg- bearing silicate minerals/rocks liberates these species into the rivers and oceans where they react with HCO_3^- to form Ca- and Mg-bearing carbonates. This combination of silicate weathering and carbonate precipitation consumes atmospheric CO_2 which impacts the atmospheric CO_2 budget.

Over the past ca. 150 years, human activities have led to a large and rapid injection of CO_2 into Earth's atmosphere, largely through the combustion of fossil fuels as source of energy. In this process, organic carbon has been extracted from the slow carbon cycle of the lithosphere and placed into the rapid carbon cycle that includes the atmosphere/ocean abiotic exchanges, and biologically mediated exchanges (*Falkowski et al*., 2003). In the modern ocean, the biological pump transfers around 5-15 GT C yr^{-1} to the deep sea (*Falkowski et al*., 1998), which is returned in the atmosphere as part of the much larger overturning circulation of dissolved inorganic carbon (*circa* 100 GT C yr^{-1}; *Sarmiento et al*., 1998). These transfers are large in comparison to the *circa* 6 GT C yr^{-1} of anthropogenic CO_2 emission to the atmosphere so they could potentially mitigate part of the global warming. Only alteration of the biological and circulation driven transfers can influence the uptake by the ocean (*Falkowski et al*., 2003; *Boyd and Trull*, 2007). The circulation driven transfer responds directly to the increasing atmospheric CO_2 partial pressure, and removes *circa* 1/3 to 1/2 of the annual atmospheric load (*Sabine et al*., 2004). Modeling experiment indicates that changes in the strength and efficiency of the biological pump are also important (e.g. Sarmiento et al., 1998), but they are much less understood (*Falkowski et al*., 2000; *Sigman and Boyle*, 2000) and they are superimposed to circulation pattern adding difficulties to discern both effects (*Watson and Orr*., 2003). Given the potential of climate change in impacting the functioning of the biological pump and vice-versa (*Bopp et al.*, 2001; *Feely et al*., 2004), our ability to model downward particulate biogenic fluxes will be central to determine the role of oceanic biogeochemical feedbacks in the future.

The main goal of this thesis is to use two silicon isotopic approaches, based on natural silicon isotopic composition and ^{30}Si-spiked experiments, to better constrain the impact of diatoms productivity on the Si-biogeochemical cycle in the Southern Ocean. The Figure A shows that diverse processes controlling the Si-biogeochemical cycle (Figure A-a). Briefly, the silicon cycle in the ocean is balanced by uptake and

dissolution of biogenic silica in surface waters, its dissolution during its settling toward the seafloor and during diagenetic processes. Food web structures strongly impact on the origin and fates of biogenic silica through the water column. Several tools have been developed in order to quantify the different Si-flux (Figure A-b). However, the integrated rates of $bSiO_2$ production, dissolution, and export estimated from direct measures are plagued by the spatial and temporal variability of the surface ocean as well as artifacts associated with making these measurements (e.g. bottle effects and sediments trap artifacts). Dissolved geochemical tracers are useful because they integrate over heterogeneities and do not involve manipulation of the organisms responsible for the biogeochemical fluxes. Over the last forty years, there has been great progress in characterizing the spatial distribution of bioactive species in the ocean. The distributions of dissolved tracers (e.g. $Si(OH)_4$) are relatively well defined, and the databases are being

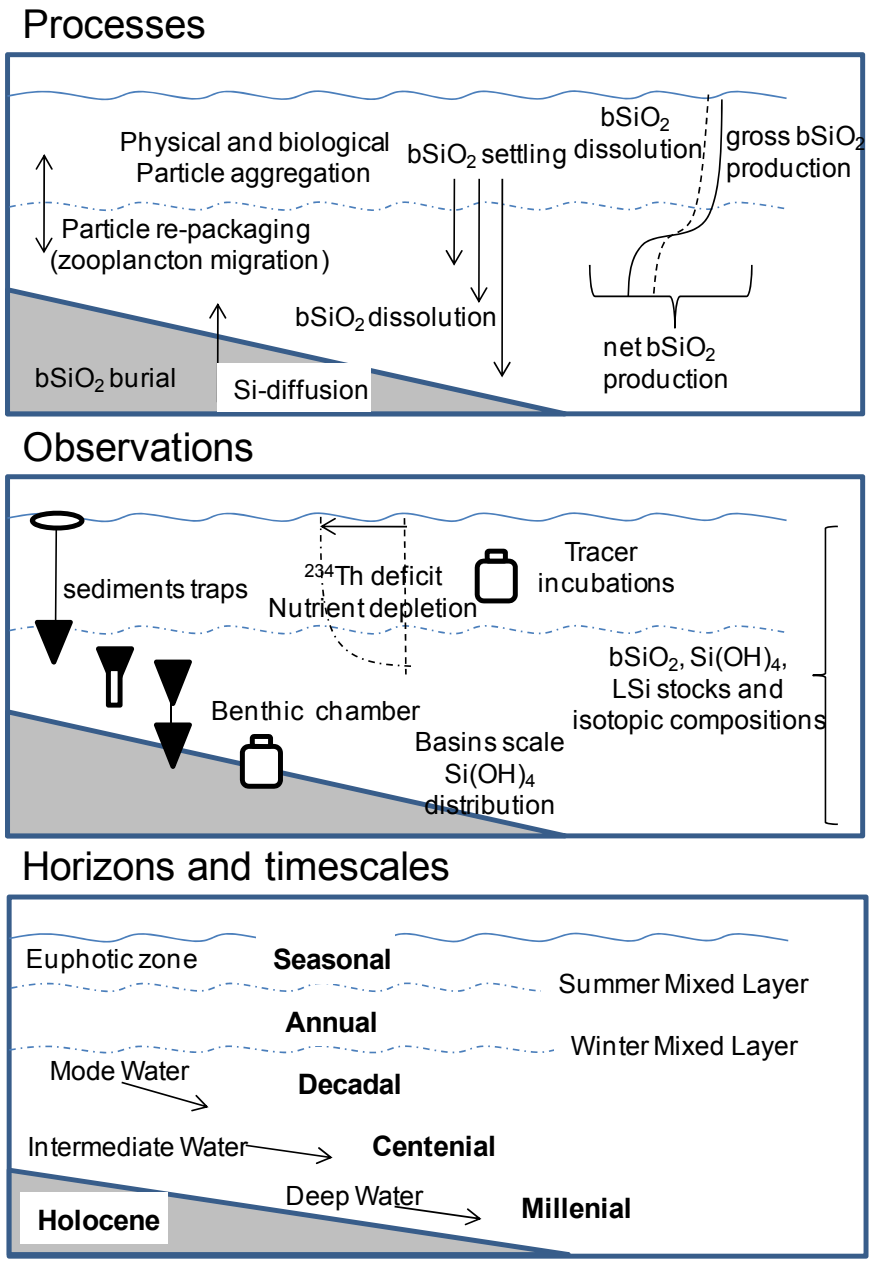

Figure A. Processes, observations, and depth horizons important in Si-biogeochemical cycle (adapted from Boyd and Trull, 2008, for Carbon export).

continuously improved (*Conkright et al*., 2002; *Key et al*., 2004). The use of these distributions to quantify physical and biological fluxes is an area of active research. If the ocean circulation is known, then the nutrient fields could be overlain on the circulation field to quantify the uptake of nutrients and carbon throughout the surface ocean, "nutrient restoring approach" (*Schlitzer*, 2002; *Jin and Gruber*, 2003; *Dunne et al*., 2005; *Jin et al*., 2006). However, uncertainties in the model-derived circulation compromise these estimates, especially for $Si(OH)_4$ (*Jin et al*., 2006). A similar conclusion could be reached for annual estimation of net $bSiO_2$ production from $Si(OH)_4$ seasonal depletion. Indeed, the nutrient depletion method is an underestimates of export production because it does not account for nutrient resupply to surface waters (*Wang et al*., 2001) and bias can emerge from estimation of initial conditions. Figure A-c illustrates the timescales involved at different depths which make difficult the interpretation of proxies integrating several timescales (e.g. days for incubations, season for nutrient depletion…).

The silicon isotopic composition, both in particulate and dissolved phase, integrates longer temporal- and larger spatial-scale than with direct measurement and allows tracking back the Si-sources. The mass and isotopic balances differ according to the processes involved: Si-uptake (*De La Rocha et al*., 1997), $bSiO_2$ dissolution (*Demarest et al*., 2009), and mixing. Incidentally this would permit to dissect the different flux acting in the same direction for the mass balance but not for isotopic balance, in a similar way than ^{30}Si incubation which allows discerning in the short time (~ 1 day) net $bSiO_2$ production, the $bSiO_2$ dissolution and the gross $bSiO_2$ production. Today, the sensibility of ^{30}Si-incubation with available methodologies could be only applied in the surface ocean. The difference between the two isotopic approaches for the surface oceans is the integration times. Indeed, silicon isotopic composition integrates seasonal timescale and ^{30}Si-incubations only ~ 1 day.

Part I. General overview

Chapter 1. Introduction

1.1 The superficial silicon cycle

The continental silicate crust is exposed to the atmosphere and hydrosphere and thus to the physical and chemical disintegrative processes of weathering. The weathering of silicate rocks contributes with solutes and particles to the load of rivers and finally to the world ocean. On it's way from the weathering site to the river and finally to the oceans (aquatic continuum) Si is involved in several biochemical and geochemical processes, such as the formation of weathering products (e.g. clays, opal phases) and biogenic silica (e.g. in phytoliths and diatoms). This thesis focuses on the marine Si-biogeochemical cycle, readers are referred to *Wollast and Mackenzie* (1983) and *Conley* (2002) for Si-continental cycle. Once reaching the ocean, some planktonic organisms (diatoms, silicoflagellates, and radiolarians) build up their biogenic silica skeletons by taking up silicic acid from seawater. Relatively little is known about the exact contribution of these different organisms to silica production but diatoms are by far the predominant

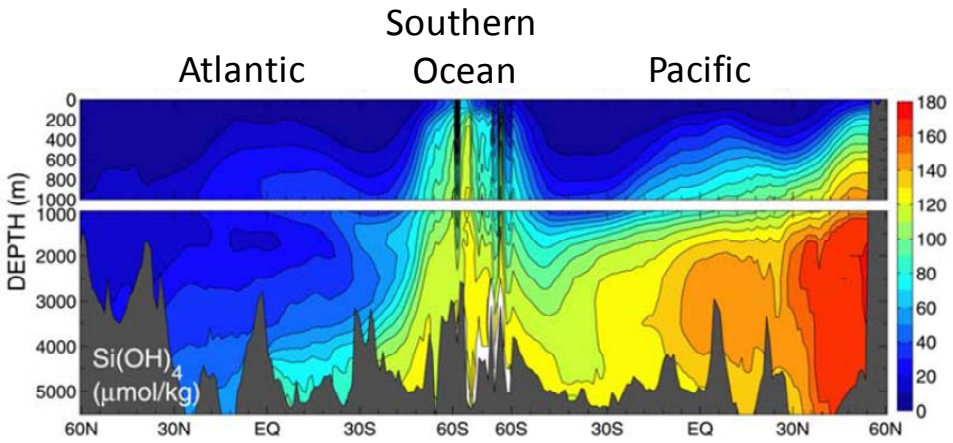

Figure 1.1. "Conveyor belt" section of silicic acid concentration using the World Ocean Atlas 2001 (Conkright et al., 2002). The Atlantic and Pacific basins are zonal means (From Sarmiento et al., 2007).

siliceous organisms in the modern marine environment and sediment (*Nelson et al*., 1995; *Tréguer et al*., 1995). Therefore in this manuscript, biogenic silica will refer mostly to diatoms.

The total content of silicic acid in the oceans is close to 10^{17} mol of Si. In the aqueous phase, there is more than one chemical form of dissolved silicon because of the hydrolysis of silicic acid, resulting in an equilibrium between the nonionized form $Si(OH)_4$ and anionic forms $SiO_x(OH)^{x-}_{4-x}$. The chemical speciation of the various interchangeable form of dissolved silicon can be calculated as a function of pH by using the appropriate dissociation constants (*Sjöberg et al*., 1981). At the natural pH of seawater (pH *circa* 8), undissociated silicic acid $Si(OH)_4$ is the dominant form (97% of total), with the remainder being largely $SiO(OH)_3^-$ (*Stumm and Morgan*, 1981). The concentration of silicic acid in the world ocean averages about 70 µmol Si l^{-1} with an oceanic residence time of *circa* 15000 yr (*Tréguer et al*., 1995). This long residence time would lead to a homogeneous distribution in the absence of biologic processes. Nevertheless, there

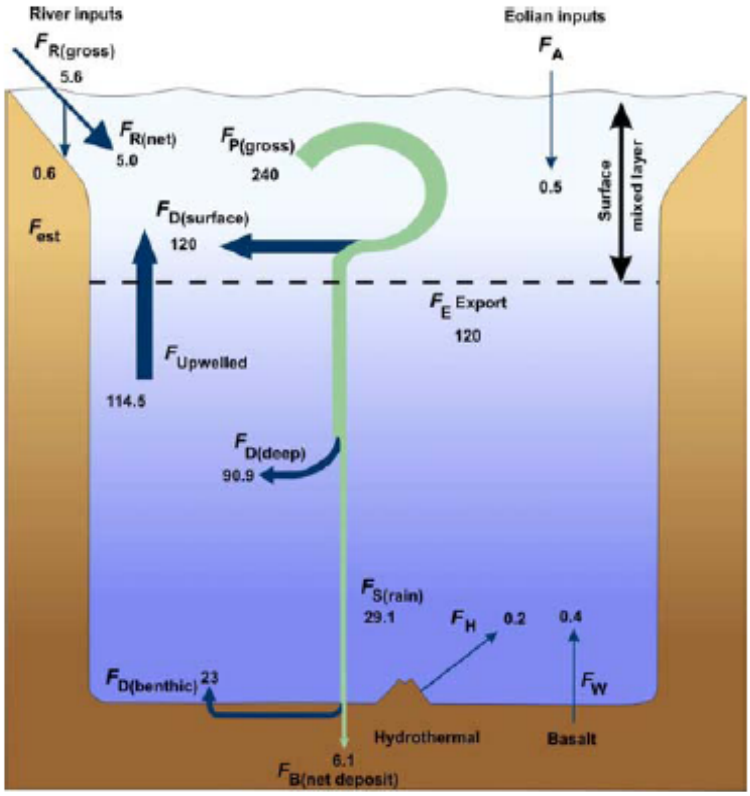

Figure 1.2: Biogeochemical cycle of Si in the world ocean at steady state (From Tréguer et al., 1995): a possible balance that is in reasonable agreement with individual range of each flux (F). Blue arrows, fluxes of silicic acid; green arrows, fluxes of particulate biogenic silica. All fluxes are in teramoles of Si per year. Abbreviations are as follows: River fluxes: gross input, $F_{R(gross)}$, and net inputs, $F_{R(Net)}$; eolian inputs, F_A; seafloor weathering inputs, F_W; hydrothermal inputs, F_H; net deposit of biogenic silica in estuaries, Fest: net deposit of biogenic silica in coastal and abyssal sediments, F_B; biogenic silica gross production, $F_{P(gross)}$; flux of silicic acid recycled in the surface reservoir, $F_{D(surface)}$; flux of biogenic silica exported toward the deep reservoir, F_E; flux of silicic acid recycled in the deep reservoir, $F_{D(deep)}$; and at the sediment interface, $F_{D(benthic)}$; flux of biogenic silica that reaches the sediment-water interface, $F_{S(rain)}$; and flux of silicic acid transferred from the deep reservoir to the surface mixed layer, $F_{upwelled}$.

are marked regional differences (Figure 1.1). In surface waters of oligotrophic areas the concentrations are usually less than 2 µmol Si l^{-1}, but south to the Antarctic Polar Front concentrations are as high as 80 to 100 µmol Si l^{-1}. Deep and bottom waters are usually silicic acid-rich, with concentrations varying from 10 to 40 µmol Si l^{-1} in the North Atlantic to 100 to 160 µmol Si l^{-1} in the Antarctic Circumpolar Current, and 140 to 180 µmol Si l^{-1} in the North Pacific (*Tréguer et al.,* 1995). This variability reflects the importance of Si for the ocean's biological pump, which strips nutrients and carbon from surface waters and export them to deep waters and are thereafter transported along the global meridional circulation, basically from North Atlantic to North Pacific (*Sarmiento et al.,* 2007). The silicic acid content is determined by the balance between geological and biological cycles of Si. A balanced Si-budget has been presented by *Tréguer et al.* (1995; Figure 1.2).

The surface reservoir receives silicic acid inputs from the lithosphere through river discharge, via chemical weathering of the continental crust, and eolian transport. Through high- and low-temperature alteration of the oceanic crust and its sedimentary cover, the ocean's deep reservoir also receives silicic acid inputs from the lithosphere (*Tréguer et al*., 1995). River input seems to dominate Si-supply to the ocean (85%, Figure 1.2).

In the ocean, the transfer of silicic acid from the hydrosphere to the biosphere initiates the biological cycle of Si; it is also a way to link the Si cycle to the one of carbon. Once the siliceous organisms die, the biogenic silica dissolves. The proportion of biogenic silica that escapes dissolution settles downward, ultimately reaching the sediments where diagenetic processes is a means for silica to re-enter the geological cycle. *Tréguer et al.* (1995) estimate that ~ 3% of the biogenic silica production is buried in the sediments with the burial equaling more or less the oceanic Si-supply. The Si delivered to the ocean passes through the biological uptake and dissolution cycle an average of about 39 times before being removed to the seabed. As seen on Figure 1.2, the marine Si-biogeochemical cycle is dominated by biogenic silica production-dissolution in the euphotic layer and by the overturning circulation component.

1.2 Diatoms Si-metabolism

Diatoms are eukaryotic unicellular microalgae with cell walls made of a composite of organic material and silica (Figure 1.3). Diatoms take up silicon from their surrounding environment in soluble form as silicic acid, transport it into the cell, and during the period of cell wall synthesis catalyze its polymerization into silica. This silica skeleton is called "frustule". The frustules are constituted of amorphous silica where the chaotic tetrahedrons are coordinated with water molecules (SiO_2. nH_2O, hereafter referred to as biogenic silica or $bSiO_2$). A striking feature is the diversity of structures that diatoms make on the nano- to

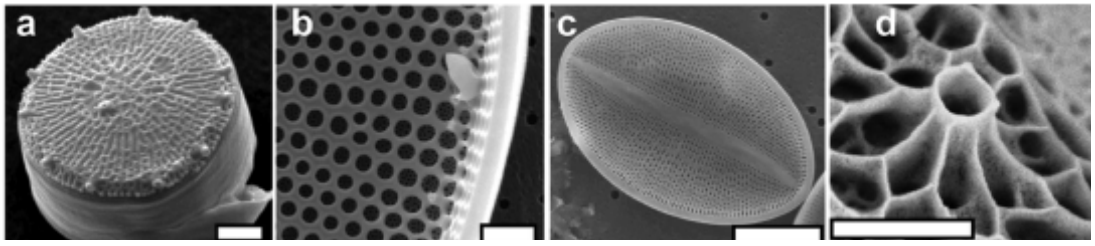

Figure 1.3: Diversity of diatom silica structures (from Hildebrand, 2008). Acid cleaned material from (a) *Thalassiosira pseudonana*, bar = 1µm, (b) close up of *Coscinodiscus*, bar = 5µm, (c) *Cocconeis sp*., bar = 10µm, and (d) close up of *Thalassiosira weissflogii*, bar = 500nm.

microscales, which is indicative of the molecular control of intracellular processes by which organics facilitate mineral formation (*Hildebrand*, 2008).

Silicon seems to be distributed throughout the cytoplasm and is not enriched in vesicle or other cellular locations (*Mehard et al*., 1974; *Rogerson et al*., 1987). The distribution data are consistent with the presence of ubiquitous silicic acid binding components in the cytoplasm (*Martin-Jézéquel et al*., 2000; *Thamatrakoln and Hildebrand*, 2008; *Hildebrand*, 2008). There is no clear evidence on the nature of this intracellular pool. It consists probably of mono or perhaps molecular weight poly-silicic acid complexes with organic material (*Martin-Jézéquel et al*., 2000). Thus the chemical form differs from free silicic acid found outside the cell. The solid phase of silica exists in the Silica Deposit Vesicle (SDV) where it is polymerized (*Martin-Jézéquel et al*., 2000). The different chemical forms of silicon are separated by membranes with significant potential implications in the cell Si-isotopic balance: the plasma membranes separates extracellular silicic acid from intracellular forms, and the silicalemma (SDV membrane) separates intracellular forms of silicon. The separations impose equilibrium effects on diatom silicon metabolism that relate to processes of transport and silica deposition (*Thamatrakoln and Hildebrand*, 2008).

The Si-biochemical pathways involved, and their regulation, are not well understood (review in *Martin-Jézéquel et al.,* 2000; and in *Hildebrand*, 2008). Most diatoms use the most common form in the ocean, $Si(OH)_4$ (*Del Amo and Brzezinksi*, 1999). The overall process of silicification involves transport of silicon across the plasmalemma and then through the cytoplasm to the site of polymerization into the silica deposition vesicle (SDV) (*Martin-Jézéquel et a*l., 2000). There are four important cellular fluxes of $Si(OH)_4$ (excluding the fluxes between intracellular compartments): (1) Influx is the transport rate across the plasmalemma from outside to inside the cell, (2) incorporation is the rate of frustule formation, (3) Efflux is the outward transport rate across the plasmalemma, and (4) dissolution is the rate of depolymerization of biogenic silica to silicic acid.

1.2.1 Si-transport and silica polymerization

A relatively large number of studies have examined the kinetic of Si-uptake by both natural diatoms assemblages and cultured clones. Both the specific Si uptake rate (V_{Si}; d^{-1}) and the specific Si-dependant cell-division rate (μ; d^{-1}), increase with increasing extracellular $[Si(OH)_4]$ in a manner that closely follows the Michaelis-Menten equation or Monod equation (1942) saturation function:

$$V_{Si} = \frac{V_{max}.[Si(OH)_4]}{K_{Si} + [Si(OH)_4]} \quad (1.1)$$

$$\mu = \frac{\mu_{max}.[Si(OH)_4]}{K_{\mu} + [Si(OH)_4]} \quad (1.2)$$

Where V_{max} and μ_{max} represent the maximum rates of uptake and division, respectively, at infinite substrate concentration; K_{Si} is the $Si(OH)_4$ concentration at 0.5 V_{max}; and K_{μ} is the $Si(OH)_4$ concentration that limits μ to 0.5 μ_{max} (*Martin-Jézéquel et al*., 2000; *Ragueneau et al.*, 2000). Notwithstanding, nonsaturable and biphasic kinetics have occasionally been observed (*Azam and Volcani*, 1974; *Nelson et*

al., 1976; *Del Amo and Brzezinski*, 1999; *Nelson et al.*, 2001; *Mosseri et al.*, 2008; *Thamatrakoln and Hildebrand*, 2008).

Examination of the kinetic response to short- and long-term Si starvation, and measurement of intracellular pools, indicates a major controlling factor regulating the transition from non-saturable to saturable uptake is the capacity of the intracellular pools to accommodate excess soluble Si (Figure 1.4; *Thamatrakoln and Hildebrand*, 2008). Saturable uptake is mediated by SITs (silicic acid transporters), specific membrane-associated proteins transporting silicic acid across the lipid bilayer membrane (*Hildebrand et al.*, 1997, 1998; *Sherbakova et al.*, 2005; *Thamatrakoln et al.*, 2006; *Thamatrakoln and Hildebrand*, 2007), and while nonsaturable Si-uptake is mediated by diffusion. In exponentially growing cultures, intracellular $Si(OH)_4$ levels are relatively low, but the capacity of pools is high (Figure 1.4a). *Thamatrakoln and Hildebrand* (2008) propose that during brief period (5-10 min) of Si starvation prior to the measurement of uptake, intracellular binding components continue to release their Si for incorporation, but because no extracellular Si is present, they are not recharged. Thus, when cells are subsequently in a Si-rich medium, the binding capacity of pools is high and a nonsaturable surge occurs

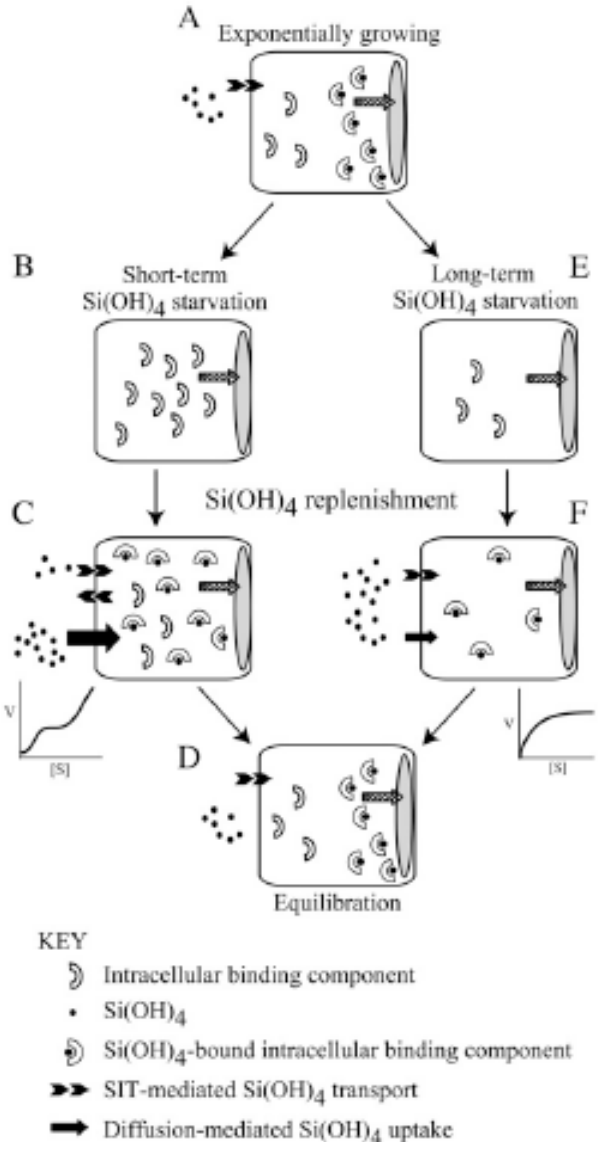

Figure 1.4. Proposed model of Si uptake in diatoms by Thamatrakoln and Hildebrand (2008). In each image, a diatom cell is represented as a rectangular box cell wall silica (i.e. the SDV) is represented as a gray elongated oval. Black dots represent intracellular Si-binding components that data suggest are present but have yet to be identified. Arrows denote direction of transport with magnitude indicated by their thickness. Black arrows represent SIT-mediated transport. Hatched arrows show movement of $Si(OH)_4$ into the SDV. Stylized graphs of uptake kinetic are shown for (c) and (e). (a), in exponentially growing cells, equilibration is achieved between uptake rate, intracellular pools, and cell wall silica incorporation. Uptake is internally controlled. (b), after a brief (5-10min) incubation in Si-free medium, levels of intracellular binding component have delivered $Si(OH)_4$ to the SDV and are predominantly in the uncomplexed state. (c), upon $Si(OH)_4$ replenishment, cells are able to accommodate surge uptake mediated by diffusion at high $Si(OH)_4$, and a non-saturable uptake kinetics are observed. Biphasic curves are seen because, at low $Si(OH)_4$ concentration, SITs are still capable of mediating uptake. SIT-mediated efflux aids in equilibration. (d), aftertime, equilibration is re-established between the level of binding component and the rate of silica incorporation, and uptake becomes internally controlled. (e), during long-term (24h) Si starvation, the level of binding component becomes reduced. (f), upon $Si(OH)_4$ replenishment, intracellular capacity is low, and cells are not able to accommodate surge uptake; thus, Michaelis-Menten type saturation is observed.

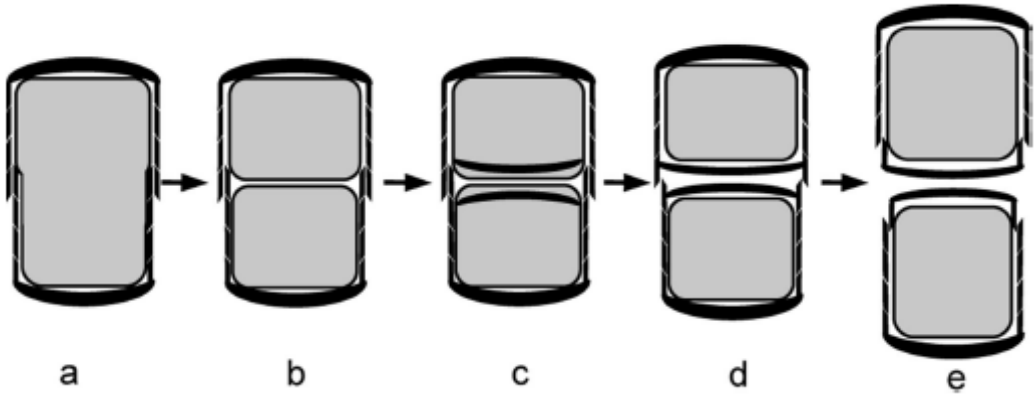

Figure 1.5: Schematic representation of diatom cell division (from Hildebrand, 2008): (a) vegetative mother cell, (b) after cytokinesis, showing the two daughter cell protoplasts within the mother cell thecae, (c) valve synthesis occurring within the daughter cell, (d) daughter cell valves after exocytosis, and (e) daughter cell separation.

(Figure 1.4c). Overtime, nonsaturable uptake transitions to saturable uptake because equilibrium is achieved between the capacity of binding components and their delivery rate of Si to the cell wall; thus, the rate of uptake becomes controlled by the rate of cell wall silica incorporation (i.e. internally controlled uptake). In extensively (24h) Si-starved cells the levels of soluble Si-binding component decrease (Figure 1.4e), and the diminished intracellular capacity results in saturable kinetics immediately upon addition of $Si(OH)_4$. Pools levels then gradually increase (*Hildebrand et al*., 2007) to maintain equilibrium with the increasing demand for silica incorporation, and presumably a concurrent increase in the amount of Si-binding component occurs. From this analysis, efflux seems a consequence of transient imbalances between uptake and deposition during surge uptake caused by a level of transport that exceeds the capacity of the intracellular silicon binding component (*Martin-Jézéquel et al*., 2000).

Silica polymerization occurs within a specialized intracellular compartment known as Silicon Deposition Vesicle (SDV), bound by a membrane called the silicalemma (review in *Martin-Jézéquel et al*., 2000). The

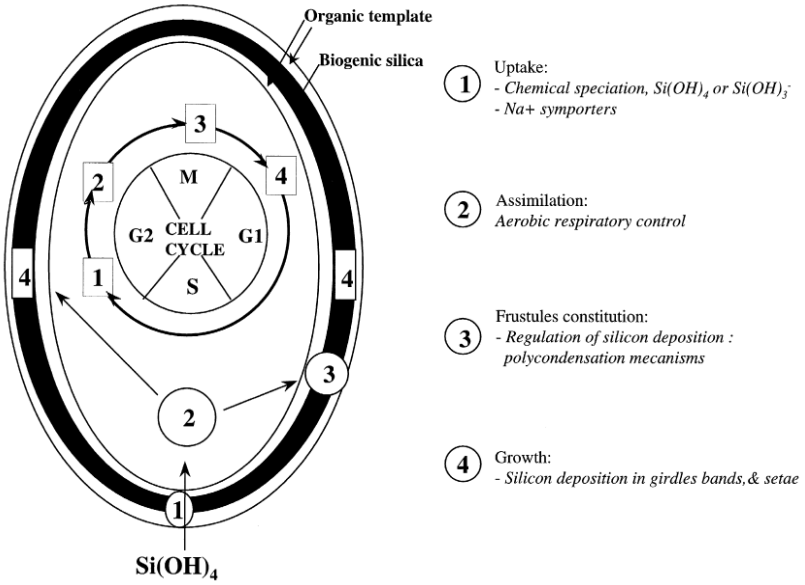

Figure 1.6: Schematic view of diatom cell, and events of the silicification processes in relation with the cell cycle (From Ragueneau et al., 2000). G1 and G2: gap phases; S: DNA replication; Mitosis:M.

internal pH of vesicle is acid (*Vrieling et al*., 1999) favoring polymerization of silicic acid. Once the silica structure in SDV is complete, the entire organelle is exocytosed to become part of the cell wall (*Pickett-Heaps et al*., 1990), without compromising cell integrity. As this membrane is formed of protein, the siliceous structure is subsequently protected by an organic coating (*Volcani*, 1981). The different key steps allowing the setting of SDV and subsequently the biogenic silica formation during cell division are shown in Figure 1.5.

As shown in Figure 1.6, silicon metabolism and photosynthesis (associated mainly with growth) are not directly coupled in diatoms, even though biogenic silica production profiles generally follow carbon primary production in the field (*Ragueneau et al*., 2000; *Martin-Jézéquel et al*., 2000). *Lobel et al*. (1996), using a biochemical simulation model, identify a possible low-energy reaction pathway for nucleation and biogenic silica growth during the mineralization process mainly coming from respiration. According to *Blank and Sullivan* (1979), the slight differential Si uptake sometimes occurring between light and dark should not reflect a light-dependent energy requirement for uptake itself, but rather synthesis or activation in the light of an unstable component of the transport system (*Hildebrand*, 2008).

$Si(OH)_4$ uptake and deposition appear to be mainly associated with the formation of new siliceous valves during the G2 and M phases just prior to cell division (*Round,* 1972). Many studies show that diatoms build thicker frustules when limited by temperature (*Durbin*, 1977), light (*Taylor*, 1985) or micronutrients, especially iron (*Takeda*, 1998; *Hutchins and Bruland*., 1998; *Franck et al*., 2003). *Martin-Jézéquel et al*. (2000) suggested that a decrease of growth rate entails an increase of silicate uptake. This has been later confirmed by *Claquin et al*. (2002) for light, N and P limitations (Figure 1.7) and by *Leynaert et al*. (2004) for Fe limitation. When growth rate is slowed down by various limitations, cells have longer in G2+M cell phases (Figure 1.6), which lead to an increase of the total amount of Si uptake and an increase of frustule thickness (i.e., $bSiO_2$ per cell surface). Variations in silicon content are thereby not so much linked to the type but rather to the intensity of limitation acting on the growth rate (Figure 1.7). Recently *Bucciarelli et*

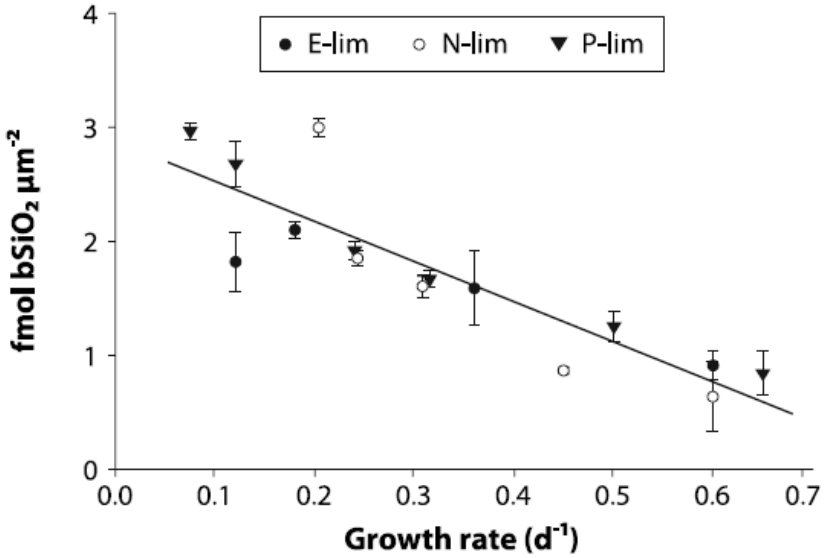

Figure 1.7. Silica cell content (bSiO2) per cell surface as a function of growth rate under light (E-lim), nitrogen (N-lim), and phosphorus (P-lim) limitation (From Claquin et al., 2002).

al. (2009) discuss on the intraspecific variability of this decoupling not still taking well into account.

1.2.2 Biogenic silica dissolution

Although $bSiO_2$ production and dissolution occur simultaneously in marine surface waters, for a given diatom cell these processes are uncoupled temporally, since it is not until after diatom death and degradation of its organic protective coating, which isolates silica from an undersaturated environment, that the $bSiO_2$ cell wall dissolves (*Lewin*, 1961; *Kamatan*i, 1982; *Bidle and Azam*, 1999, 2001; *Bidle et al*., 2003). Different external (physical, chemical, and biological) factors along with intrinsic properties control the dissolution efficiency of biogenic silica (review in *Ragueneau et al*., 2000).

The specific dissolution rate of opal in seawater (V_{dis} in d^{-1}) is given by (*Hurd and Birdwhistell*, 1983):

$$V_{diss} = k([Si(OH)_4]_{sat} - [Si(OH)_4]).A_{sp} \quad (1.3)$$

where k is the first-order rate constant (cm h^{-1}), $[Si(OH)_4]_{sat}$ the solubility of opal (mol cm^{-3}), $[Si(OH)_4]$ the ambient silicic acid concentration (mol cm^{-3}) and A_{sp} the specific surface area of the opal (cm^2 mol^{-1}). V_{dis} is expressed in h^{-1}. V_{dis} increases linearly with k, A_{sp}, and ($[Si(OH)_4]_{sat}$-$[Si(OH)_4]$). Both $[Si(OH)_4]_{sat}$ and k increase sharply with temperature (e.g. *Hurd*, 1972; *Kamatani*, 1982). The combined effect implies an almost 50-fold increase in V_{dis} between 0°C and 25°C (*Hurd and Birdwhistell*, 1983).

The incorporation of trace elements within the opaline matrix can decrease significantly opal solubility thus reduce the departure from equilibrium in the upper waters. *Lewin* (1961) showed that several metals (Al, Be, Fe, Ga, Gd, and Y) can combine with opaline matrix in ways that decrease its dissolution rate. The key role of Al has been reported by various authors (e.g. *Lewin*, 1961; *Van Bennekom et al*., 1989, 1991; *Van Beusekom et al*., 1997).

The specific dissolution rate varies from one species to another, spanning over an order of magnitude even at constant external conditions (*Kamatani*, 1982; *Tréguer et al*., 1989). Species-specific differences in dissolution rates reflect variability in specific surface areas (*Lewin*, 1961; *Lawson et al*., 1978; *Kamatani and Riley*, 1979) or morphology and structure of the frustules (*Kamatani et al*., 1980), as well as in the growth of organic and inorganic surface coating (*Lewin*, 1961; *Luce et al*., 1972; *Lawson et al*., 1978; *Kamatani et al*., 1988). Thus, any process that removes organic matter from the opal surfaces, and hence exposes silica directly to seawater, should increase V_{diss}. Both microbial degradation and grazing could potentially clean the silica surfaces in this way. *Bidle and Azam* (1999) and *Bidle et al*. (2001) observed that bacteria colonizing and degrading the protective organic matrix, subsequenlty increasing the V_{diss} of naked frustules. However, different bacterial assemblages and isolates involving different species composition, colonization dynamics, and metabolic state induce a relation between bacteria activity and specific dissolution rate which is not straightforward. Grazing could also impact V_{dis} but the effect can be different depending of grazers. Grazers such as heterotrophic dinoflagellates (*Jacobson and Anderson*, 1986) extract virtually all organic matter from diatoms, leaving exposed frustules free to dissolve. Nevertheless, grazing by microcrustaceans such as copepods could break diatoms frustules enhancing A_{sp} and subsequently V_{dis} (*Sullivan et al*., 1975; *Miller et al*., 1990), but opposite effect can occur since biogenic silica enclosed in faecal pellets with high settling rates can increase biogenic silica preservation.

1.3 Modern surface Si-cycle

1.3.1 Biogenic silica production in surface waters

1.3.1.1 Range of biogenic silica production rates in the ocean

Rates of biogenic silica production have been measured in numerous marine systems by means of isotopic tracers (^{30}Si by *Nelson and Goering*, 1977a; ^{32}Si by *Tréguer et al*., 1991). These rates are closely linked to the rates of Si-uptake in any incubation experiment longer than the relatively short residence time of Si in stored intracellular pools. Thus, the terms “Si uptake” and “biogenic silica production” are nearly synonymous when discussing field data. There are 531 published integrated profiles of direct

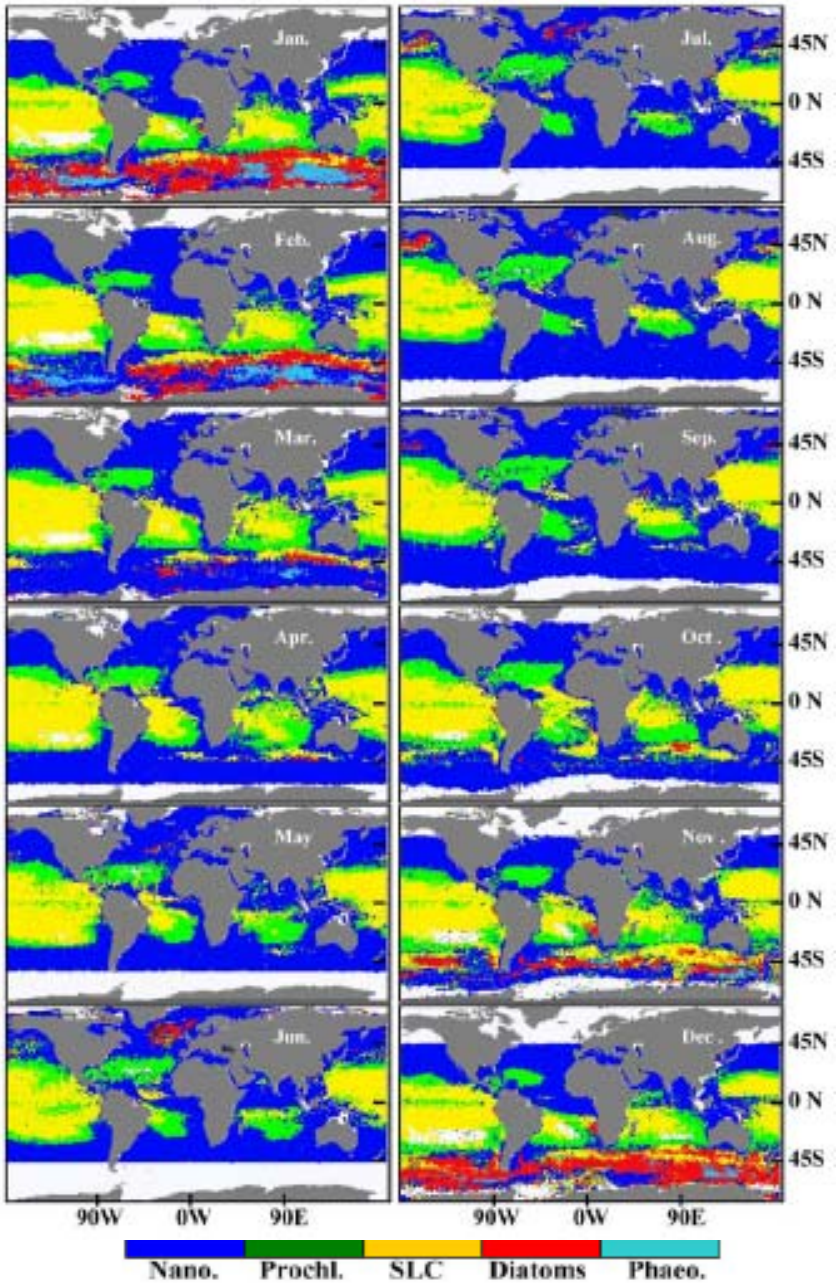

Figure 1.8: Monthly climatology (1998-2006) of the dominant phytoplankton group (from Alvain et al., 2008): respectively nanoeucaryotes, Prochlorococcus, Synechococcus, diatoms, and Phaeocystis.

measures of silica production rates in the ocean (Appendix A; *Ragueneau et al*., 2000; *Quéguiner*, 2001; *Brzezinski et al*., 2001; *Quéguiner and Brzezinski*, 2002; *Leblanc et al*., 2002, 2003, 2004; 2005a; *Beucher et al*., 2004a, 2004b; *Krause et al*., 2009; this thesis). There is an enormous spatial and temporal variability in euphotic integrated biogenic silica production with a range from 0.1 mmol Si m^{-2} d^{-1} in oligotrophic system to 1140 mmol Si m^{-2} d^{-1} in coastal upwelling system.

In agreement with $bSiO_2$ production rates, Diatoms abundances reveal that they tend to dominate whenever conditions become optimal for phytoplankton growth such as spring blooms, coastal upwelling's, equatorial divergences, river plumes, macrotidal coastal ecosystems, ice-edge bloom and transient open-ocean blooms triggered by pulse nutrient supply, decay of ocean eddies, and atmospheric dust inputs (review *Ragueneau et al*., 2000). Chl-a contribution of different phytoplankton groups are in agreement with this distribution where especially high diatoms bloom are observed in the Southern Ocean (Figure 1.8, from *Alvain et al*., 2008).

Most of these situations present hydrodynamical peculiarities (*Ragueneau et al*., 2002), which tend to favor large cells, as suggested by *Margalef* (1978) and *Legendre and Le Fèvre* (1989). Large phytoplankton cells (e.g. diatoms and dinoflagellates) have generally a low surface to volume ratio, which imply a need for a nutrient-rich habitat, in contrast to smaller phytoplankton whose higher surface to volume ratio leads to more efficient exploitation of low nutrient concentrations (*Chisholm,* 1992; *Timmermans et al.*, 2005).

Thus to explain why diatoms are currently highly ecologically successful, different mechanisms are proposed: (1) Si-uptake and deposition are mechanisms requiring less energy than for the elaboration of an organic cell wall (*Raven*, 1983), subsequently diatoms have a competitive advantage over other

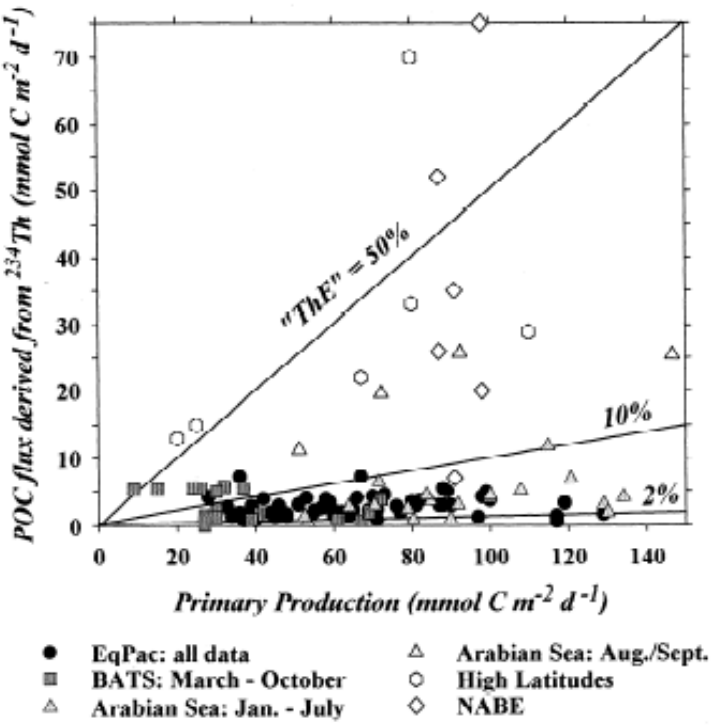

Figure 1.9: Summary plot of primary production versus POC flux derived from the ^{234}Th approach (from Buesseler, 1998)

organisms, (2) Silica frustules should facilitate the rapid absorption of nutrient offering a structure that maintains storage vacuoles, (3) Silica frustules should decrease mortality rates since grazing should be more difficult (*Smetacek*, 1999; *Smetacek et al*., 2004; *Pondaven et al*., 2007). A major strategy of diatoms is to acquire nutrients rapidly under highly physically dynamic conditions, and to store the nutrients in vacuoles for later cell growth (*Falkowski et al*., 2003). This strategy simultaneous deprives competing groups of phytoplankton of essential nutrients while allowing diatoms to grow rapidly forming blooms.

Diatoms are located in areas of relatively high carbon export efficiency (Figure 1.9), such as high latitudes bloom, seasonal or episodic export flux at low latitudes (*Buesseler*, 1998). Carbon export efficiency ("ThE ratio") is the ratio between C-export flux below surface layer and primary production (e.g. *Buesseler*, 1998). *Buesseler* (1998) observe a strong decoupling between production and particulate export in the ocean. Food web structure has prominent role in determining the extent to which organic C and associated nutrients are recycled within or exported from the surface ocean (*Buesseler*, 1998; *Boyd and Trull*, 2007). High export events appear to be related to the occurrence of diatom blooms and large cells that are quickly removed from the surface ocean via aggregation, settling or grazing.

1.3.1.2 Coupling with organic carbon

The increase of diatom productivity and silica production with increasing total primary productivity is non-linear. There exists important spatial variation in the Si:C production ratio.

-First, variations in the contribution of diatoms to primary production show large spatial and temporal variations, subsequently strongly impacting the values observed in the Si:C production and biomass ratios (*Ragueneau et al*., 2000).

- Several factors have been shown to influence the Si:C ratio with interspecific variability (*Bucciarelli et al*., 2009): temperature (*Durbin*, 1977), light intensity (*Claquin et al*., 2002), photoperiods (*Eppley et al.,* 1967), macronutrient limitation (*Claquin et al*., 2002), iron limitation (*Takeda*, 1998; *Hutchins and Bruland*, 1998; *Franck et al*., 2003). *Martin-Jézéquel et al*. (2000) and *Claquin et al*. (2002) link silicification to diatom growth rate, which is influenced by all these factors (see section 1.2.1).

- Typically, the half saturation constant for growth is less than for uptake (Eqs. 1.1 and 1.2), and diatoms can maintain division rates very close to μ_{max} at extracellular $Si(OH)_4$ concentration that limit Si-uptake (*Sarthou et al*., 2005). Since growth rate seems less Si-limited than Si-uptake, *Martin-Jézéquel et al.* (2000) suggest that under severe $Si(OH)_4$ limitation growth should be less affected than Si-uptake inducing lower silicification.

- Recently, *Pondaven et al*. (2007) observe that grazing induces change in cell wall silicification in marine diatoms in agreement with the view that grazing contributes to drive ecosystem structure and biogeochemical cycles in the ocean (*Smetacek et al*., 2004).

- Along with "silicate pump processes" (*Dugdale et al*., 1995), metabolic processes and kinetics of regeneration induce a preferential remineralization of the more labile organic matter compared to biogenic silica. Si:C ratio of biomass increase with maturation of biogenic particulate matter, both in surface and subsurface (*Quéguiner et al*., 1997; *Ragueneau et al*., 2002; *Brzezinski et al*., 2003a).

All this processes decouple C and Si biogeochemical cycles and have significant impact on biogeochemistry at global scale, especially in the Southern Ocean (*Sarmiento et al*., 2004, 2007), which is the focus of this thesis.

1.3.2 Biogenic silica dissolution in surface waters

There is a very limited data set available on direct measures of upper ocean biogenic silica dissolution. Only 57 individual profiles have been reported so far (*Nelson et al*., 1995; *Brzezinski et al*., 2003b; *Beucher et al*., 2004a, 2004b) exhibiting large spatial and temporal variations in surface waters (Appendix A; *Nelson et al*., 1995; *Brzezinski et al*., 2003b). Up to now biogenic silica dissolution rate can only be assessed using ^{30}Si-isotopic dilution, a technique initially developed by *Nelson et al*. (1977b). Dissolution-rate measurements are still relatively difficult to perform mainly due to the analytical difficulties and low sensitivity. Nevertheless, the present thesis we provide an additional set of 9 profiles, all from the Southern Ocean (chapter 8), acquired using a more efficient method we have developed (chapter 5).

The balance between integrated silica production and integrated silica dissolution in the euphotic zone, which we define as the integrated dissolution to production rate ratio (∫D:∫P), is a key determinant of the strength of the silicate pump. The quantity 1-(∫D:∫P) is the fraction of silica production supported by new silicic acid, in analogy to the f ratio (i.e., the fraction of N which is supported by new N, mainly NO_3 and N_2) (*Brzezinski et al*., 2003b). The range of variability of ∫D:∫P is very high for Si, with values as low as 0.1 and others exceeding 1.0 (*Nelson et al*., 1995; *Brzezinski et al*., 2003b; *Beucher et al*., 2004a, 2004b; chapter 6). This suggests there is a high degree of variability in the extent of silica recycling in the surface ocean and consequently in the efficiency of the silicate pump (*Brzezinski et al*., 2003b). The magnitude and variability of ∫D:∫P in different regions of the surface ocean is one of the greatest uncertainties in the global marine silica budget (Figure 1.2). *Nelson et al*. (1995) and *Brzezinski et al*. (2003b) estimate a global average for ∫D:∫P at 0.50. Despite the importance of silica dissolution in regenerating $Si(OH)_4$ in the surface ocean, great uncertainty remains regarding the factors controlling the temporal and spatial variability in the ∫D:∫P ratio in different regions of the global ocean and on the influence of this variation has on phytoplankton dynamics, the silica cycle, and the links between silica cycle and organic matter production and export (*Brzezinski et al*., 2003b). These authors realized the first attempt to examine whether ∫D:∫P varies in a systematic way relative to silica production. When the fraction of silica production supported by new silicic acid, 1-(∫D:∫P), is plotted as a function of the level of silica production (Figure 1.10), the data points fall along a hyperbolic curve. *Brzezinski et al*. (2003b) suggested that there is a shift the mode of functioning of the silica cycle, from silica dissolution supporting a small fraction of gross silica production during diatoms bloom, irrespective of the level of silica production within a given bloom, to silica dissolution supporting the majority of gross silica production during nonbloom periods when silica production is low. This analysis supports the hypothesis that there is a seasonal shift in the character of the silica cycle, from silica behaving mainly like a new nutrient during blooms to one behaving more like a regenerated nutrient afterward (*Brzezinski and Nelson*, 1989; *Brzezinski et al*., 2001).

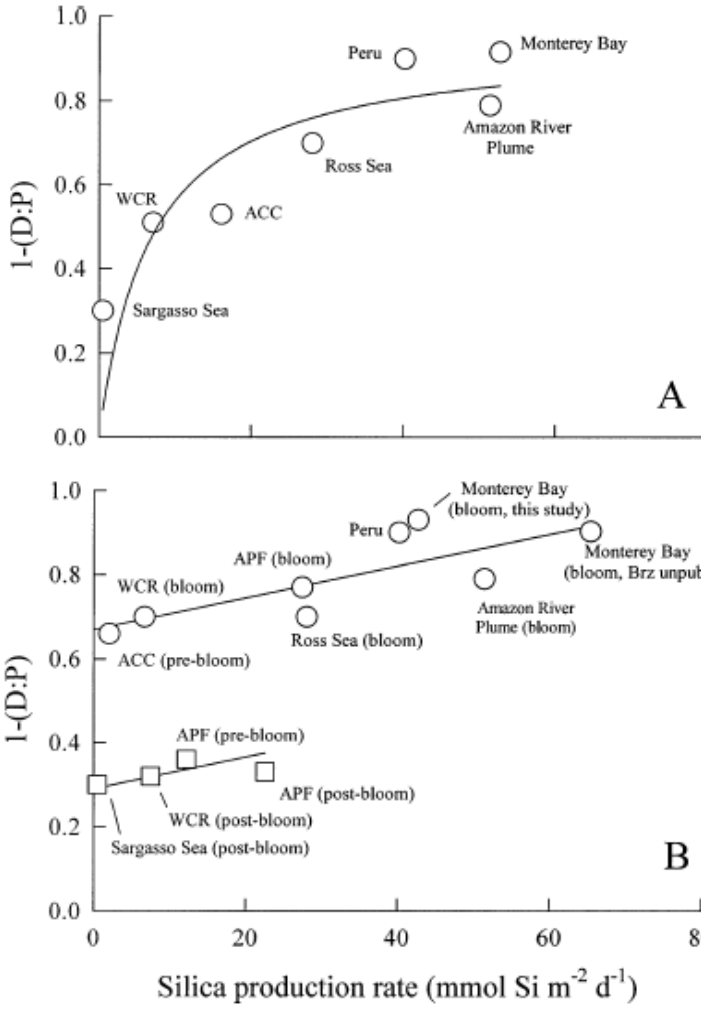

Figure 110. (from Brzezinski et al. (2003b): (a) The fraction of water column silica production supported by new silicic acid (1-ʃD:ʃP) as a function of mean silica production rate in the different regions of the global ocean. Data from all cruises within a given region were used to calculate each mean silica production rate and mean value of 1-ʃD:ʃP. The labels correspond to the following studies: Monteray Bay (Brzezinski et al., 2003b); Amazon River Plume (DeMaster et al., 1991), excluding data from stations inside of the turbid river plume: Peru coastal upwelling zone (Nelson et al., 1981; Antarctic Circumpolar Current (Nelson and Gordon, 1982; Brzezinski et al., 2001): WCR, Gulf Stream warm-core ring (Brzezinski and Nelson, 1989); Sargasso Sea (BATS) (Brzezinski and Nelson, 1995; Nelson and Brzezinski, 1997); Ross Sea, only data in the euphotic zone considered (Nelson et al., 1991). (b) Data from panel (a) plotted with each cruise represented as a separate data point. Where possible, each cruise is designated as having sampled bloom, prebloom, postbloom, or nonbloom conditions on the basis of the description provided in the original manuscripts for each study.

Since there is a decoupling between Si-uptake and dissolution, only naked (i.e., without their organic coating) dead diatoms are dissolving (see section 1.2.2). As discussed in *Brzezinski et al*. (2003b), one might predict a priori that ʃD:ʃP would increase following blooms because of an increase in the relative proportion of detrital biogenic silica in the water column (*Brzezinski and Nelson*, 1989; *Beucher et al*., 2004b; chapter 6) due to an increase of death cells, grazing pressure, and organic substrate favoring efficient bacterial activity. Nevertheless *Brzezinski et al*. (2001) show that the increase in ʃD:ʃP following the bloom was caused by a sharp decline in silica production with silica dissolution rates remaining relatively constant. This analysis suggests that different export mode and food web structure could strongly impact the mechanisms responsible for the increase ʃD:ʃP.

1.4 Southern Ocean case study

1.4.1 Southern Ocean dynamic and zonation

The region of the world ocean around the Antarctica continent is unique in many respects. First, it is the only region where the flow of water can circulate unhindered all around 360° of longitude. Second, the permanent thermocline usually present in the water column (interface between surface and deep water) reaches the surface in the SubTropical convergence, sometimes up to SubAntarctic Front, but does not extend into the polar regions; temperature differences between the sea surface and the ocean floor are

small: less than 1°C close to the continent and generally do not exceed 5°C, i.e. 20% only of the temperature difference found in the tropics (*Tomczak and Godfrey*, 2001). As a result, the water column is less stable than it is at lower latitudes. In Antarctic waters density variations with depth are small and the pressure gradient force is more evenly distributed over the water column. As a result, currents are not restricted to the upper few hundred meters of the ocean but extend to great depths. Antarctic Circumpolar Current (ACC) has the largest mass transport of all ocean currents: it moves eastward a slab of water more than 2000 meters thick with speeds comparable to other surface currents around Antarctica (*Tomczak and Godfrey*, 2001). The flow of the ACC has long been known to concentrate in a number of fronts characterized by enhanced meridional gradients of water properties (*Deacon*, 1937; *Nowlin and Clifford*, 1982; *Orsi et al*., 1995; *Belkin and Gordon*, 1996). Following *Orsi et al*. (1995), it is now traditional to identify three primary Southern Ocean fronts – the SubAntarctic Front (SAF), the Antarctic Polar Front (APF) and the southern ACC front (SACCF). A fourth feature, the southern boundary of the ACC (SB), marks the southern limit of the circumpolar flow. Each of the fronts is circumpolar in extent and extends from the sea surface to the seafloor. *Sokolov and Rintoul* (2002, 2009) demonstrate that each of the three primary ACC fronts consisted of multiple branches (jets and filaments). The intensity of the fronts varies along the fronts and the individual branches merge and diverge, often in response to interactions with bathymetry. The physical and chemical characteristics of Southern Ocean surface waters vary from north to south. These changes occur as a series of steps across each of the fronts. In between fronts, lie zones of weak flow and relatively uniform water properties with similar physical, chemical, biological properties and similar seasonal evolution (*Tréguer and Jacques*, 1992; *Rintoul and Trull*, 2001;

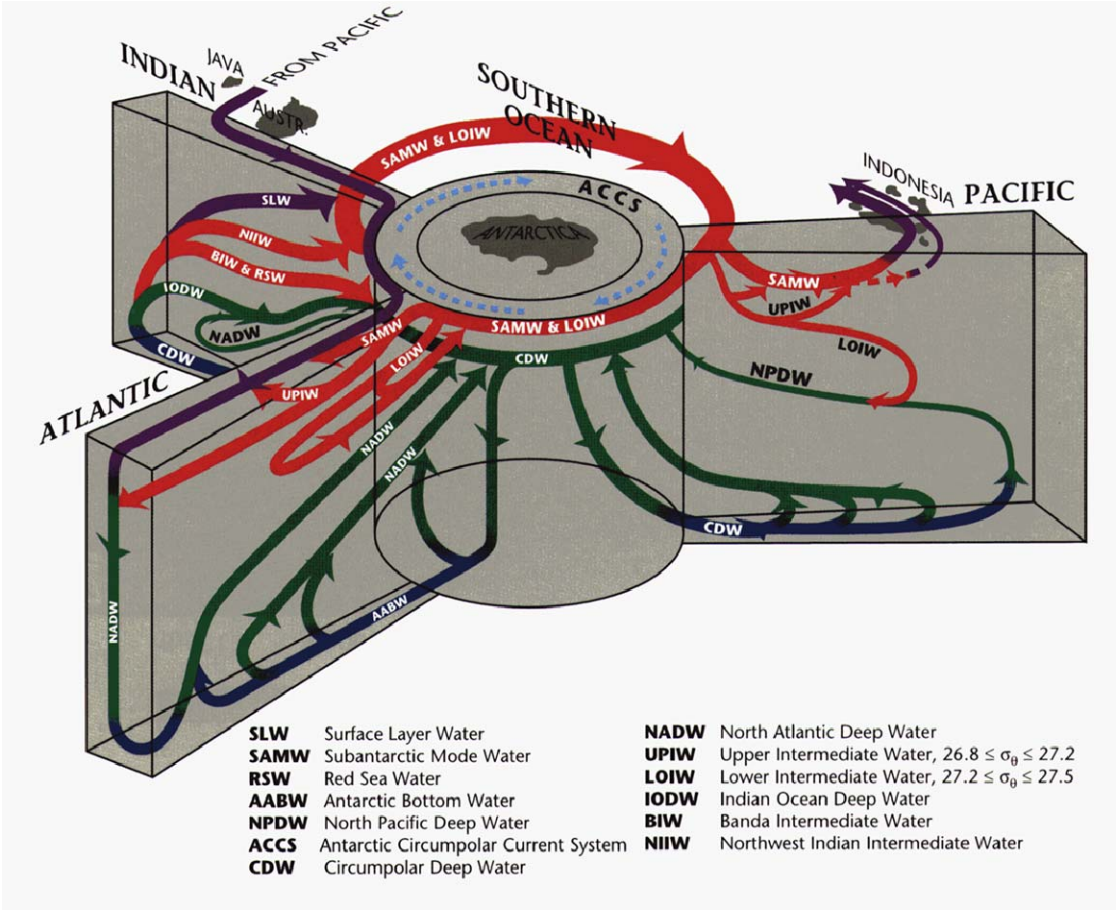

Figure 1.11. Water currents around Antarctica in a global circulation view (Rintoul et al., 2001).

Sokolov and Rintoul, 2007a). From North to South, these zones are the SubAntarctic Zone (SAZ), Polar Frontal Zone (PFZ), and the Antarctic Zone (AZ) (*Gordon et al*., 1977; *Whitworth*, 1980). Some authors divide AZ in Permanent Open Ocean Zone (POOZ) and Seasonal Ice Zone (SIZ) or Marginal Ice Zone (MIZ).

The Southern Ocean is not strictly speaking recognized by the International Hydrographic Bureau which generally delimits sea and ocean with geographical criteria with boundaries delimited by continent or referenced with regard to land positions. However, the Southern Ocean connects the three main ocean basins (Figure 1.11; Pacific, Atlantic, and Indian) and its unique features are repeated in each basin. Its most conventional definition is the region south of the Subtropical Front (STF). In practice, this is not a well defined line but a broad zone of transition between tropical/temperate and polar ocean dynamics. The surface area encompassed by the Southern Ocean represents roughly 77 .106 km^2, or 22% of the surface of the world ocean (*Tomczak and Godfrey*, 2001).

The overturning circulation driven by Antarctic divergence in the meridional plane is shown in Figure 1.12. Circumpolar Deep Water (upper, UCDW; and lower, LCDW) upwells mainly south to APF, where the Ekman transport is divergent. Part of the upwelled CDW loses buoyancy near Antarctica to form Antarctic Bottom Water (AABW). The remainder gains buoyancy due to warming and freshwater input as surface waters are driven north in the Ekman layer, ultimately sinking to form Antarctic Intermediate Water (AAIW) and SubAntarctic Mode Water (SAMW) (*Speer et al*., 2000; *Trull et al*., 2001). While the circumpolar average view in Figure 1.12 is broadly accurate for deep water masses, the sinking of surface water into the ocean (AAIW and SAMW) interior occurs in only few locations (*Tomczak and Godfrey*,

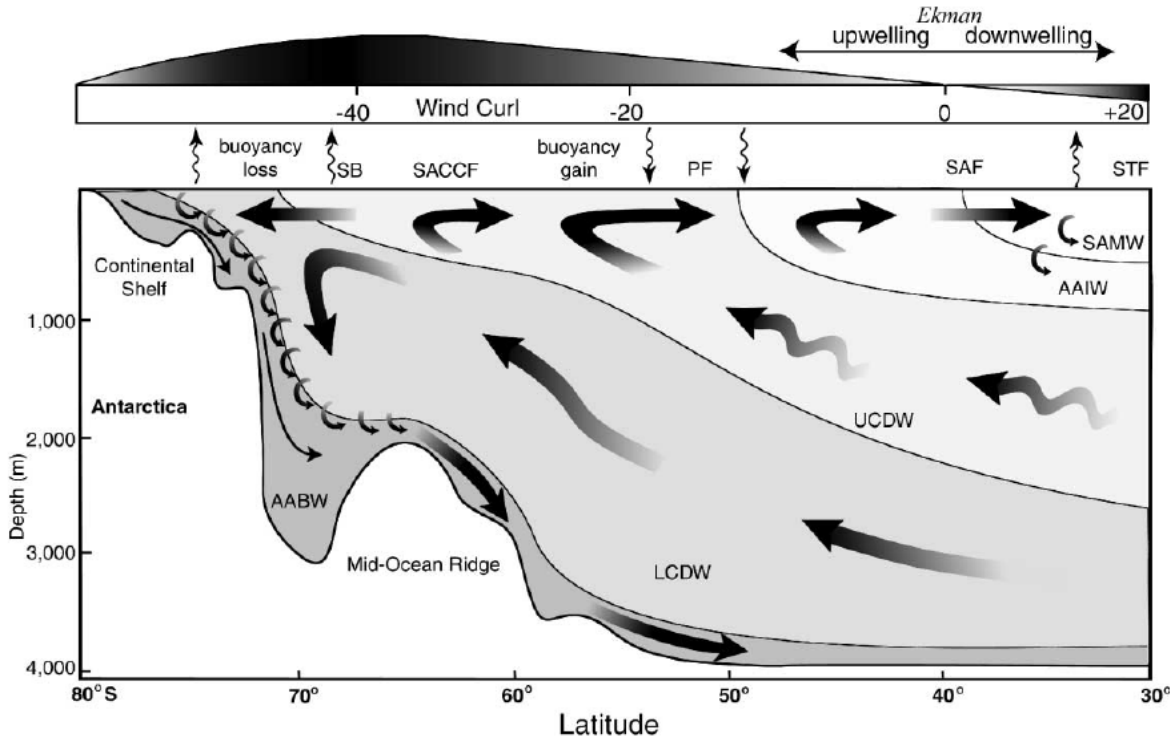

Figure 1.12: A schematic view of the meridional overturning circulation (from Trull et al., 2001), modified from (Speer et al., 2000) to show the annual mean wind-stress curl (10^9 dyn cm-2) from Trenberth et al (1989). Negative values of wind stress curl correspond to Ekman divergence and upwelling. The transition from upwelling and buoyancy in the south to downwelling and buoyancy loss in the north roughly coincides with the SubAntarctic Front. Antarctic Bottom Water (AABW) on the Antarctic Shelf occurs only in restricted locations.

2001).

1.4.2 Controls of primary production and biogeochemical processes involved in the Southern Ocean

Phytoplankton bloom dynamics in the Southern Ocean have long been a paradox for oceanographers. Despite high concentrations of available nitrate and phosphate due to the upwelling of deep nutrient-rich waters (Figure 1.12), chlorophyll concentrations in open ocean water is low (typically <0.5 mg m^{-3}; *Tréguer and Jacques*, 1992; *Comiso et al*., 1993; *Moore and Abbot*, 2000; *Sokolov and Rintoul*, 2007a). The Southern Ocean is the largest high-nutrient low chlorophyll (HNLC) region on Earth (*Martin*, 1990; *Minas and Minas*, 1992). The inefficient utilization of N and P is due to the low productivity for which three different but interacting factors are held responsible: growth limitation due to unfavorable light climate because of deep mixing (*Mitchell et al*., 1991; *Nelson and Smith*, 1991), trace elements (micro-nutrients) deficiency especially iron (review in *de Baar et al*., 2005) and, high mortality due to grazing pressure by proto- and metazooplankton in excess of growth rate of phytoplankton (*Smetacek et al*., 2004; *Safi et al*., 2007). The relative importance of these converging factors is still under debate (*Boyd*, 2002) but in recent years accumulated evidence has been reported indicating that iron availability is a key factor which limits phytoplankton growth rates along with light availability (*de Baar et al*., 2005).

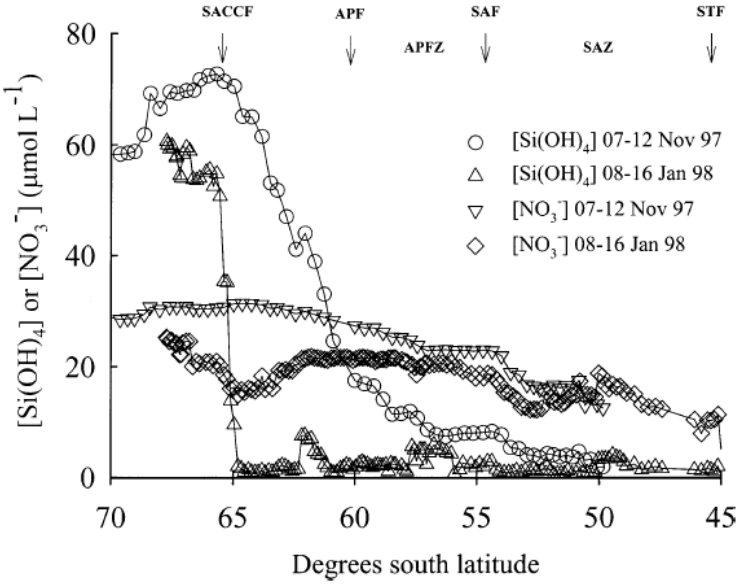

Figure 1.13: Surface silicic and nitrate concentrations (from Brzezinski et al., 2005) along 170°W longitude measured on 7-12 November 1997 and 8-16 January 1998 (adapted from Smith et al., 2000).

Unlike nitrate concentrations of macronutrients that remain high throughout the year across much of the ACC (Figure 1.13), the region of the ACC between the APF and the Seasonal Ice Zone is marked by an extremely strong latitudinal gradient in silicic acid concentration that increases southward (*Pondaven et al.*, 2000a; *Brzezinski et al*., 2001; *Quéguiner and Brzezinski*, 2002). Concentrations on the northern side of the gradient can decrease considerably down to less than 5 µmol Si l^{-1} and may rise up to more than 70 µmol Si l^{-1} to the south. This $Si(OH)_4$ gradient is centered on APF moving southward with the diatoms biomass tracking its center (*Brzezinski et al.,* 2001). The rate of Si uptake is almost always limited by $[Si(OH)_4]$ in the Si-depleted waters. Si-limiting conditions follow the bloom southward during spring and

summer (*Nelson et al*., 2001). Together with others factors influencing productivity, silicon can impose a secondary limitation on phytoplankton community structure by preventing the growth of diatoms, especially in the northern side of the ACC (*Hutchins et al*., 2001; *Sedwick et al*., 2002; *Boyd*, 2002; *Brzezinski et al*., 2005; *Leblanc et al*., 2005b).

*Sokolov and Rintou*l, 2007b have shown that the fronts define the limits of zones with similar concentrations and seasonality of surface chlorophyll. The overall pattern of surface chlorophyll is consistent with strongest vertical supply of nutrient-rich deep water south of the APF. The distribution of chlorophyll in the Southern Ocean is concentrated in a number of persistent blooms (Figure 1.14), observed downstream of islands and bathymetric features. Most regions of elevated chlorophyll in the open Southern Ocean can be explained by upwelling of nutrients (both macronutrients and micronutrients) where the ACC interacts with topography (Figure 1.14). The interaction of the flow with the topography therefore establishes both the large-scale dynamic balance of the ACC and determines the productivity of the open Southern Ocean (*Sokolov and Rintoul*, 2007a). Phytoplankton blooms where chlorophyll concentration exceeds 1.0 mg m^{-3} are also observed in coastal/shelf waters and areas associated with the seasonal sea ice retreat (*Comiso et al*., 1993; *Moore and Abbott*, 2000; *Arrigo et al*., 2008). These chlorophyll distribution patterns are consistent with an iron-limited system since all these areas are supposed to receive more iron (*Comiso et al*., 1993; *Moore and Abbot*, 2000; *Arrigo et al*., 2008). Most regions display a seasonal peak in chlorophyll concentration during December in phase with the seasonal solar radiation cycle (*Moore and Abbot*, 2000).

The highest primary production occurs also in December, with maximum values in the coastal/shelf waters off South America, Africa, Australia, and New Zealand and in the southern Weddell and Ross seas

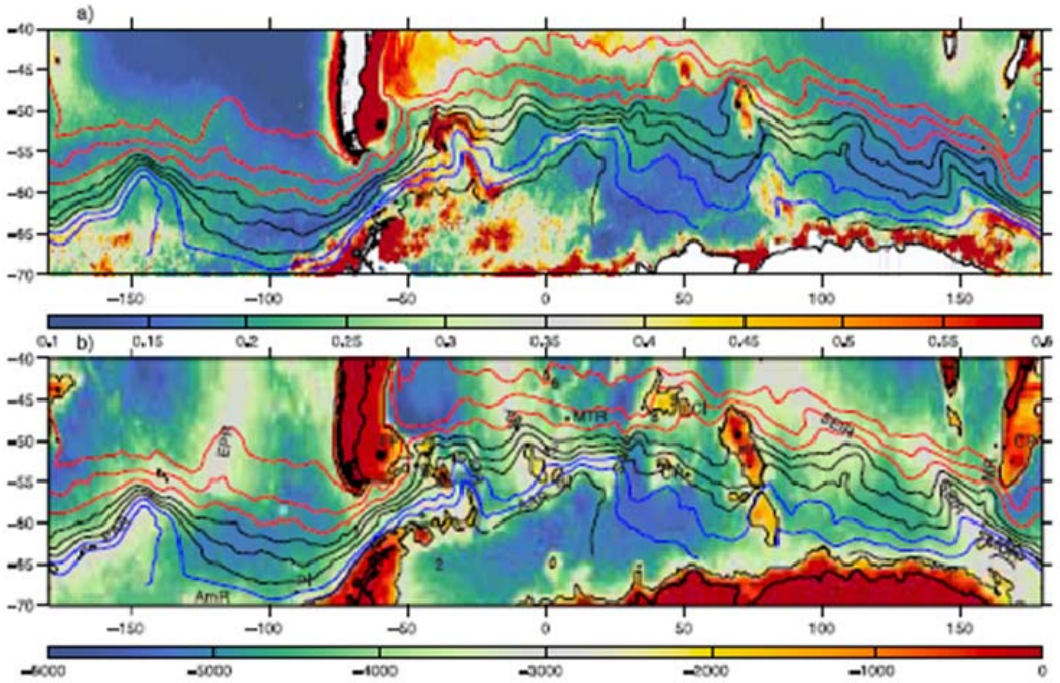

Figure 1.14. (a) mean chlorophyll distribution in the Southern Ocean averaged over the period from October 1997 to October 2002. (b) Bathymetry of the Southern Ocean. Positions of the ACC fronts are color-coded from north to south: SAF (blue), APF (red), SACCF (black), and SB (blue) (from Sokolov and Rintoul, 2007a).

(*Moore and Abbott*, 2000; *Arrigo et al*., 2008). In the open Southern Ocean there is a latitudinal general gradient of primary production with increasing production northwards (*Reuer et al*., 2007). *Moore and Abbot* (2000) estimate a total primary production (>30°S) at 14.2 Gt C yr^{-1} of which 80% are between 30 and 50°S corresponding roughly to SAZ and south STZ (also seen on Figure 1.16). This gradient could be linked to the shorter growth season, light limitation, and lower Sea Surface Temperature (SST) to the south together with lower atmospheric iron deposition (*Moore and Abbott*, 2000; *Cassar et al*., 2007). The ACC primary production is in the lower range of the primary production measurement (PP; Figure 1.15) (*El-Sayed and Turner*, 1975; *Behrenfield and Falkowski*, 1997; *Nelson et al*., 2002; *Falkowski et al*., 2003). Figure 1.16 highlights the decoupling between primary production and export production through a model analysis (*Behrenfield and Falkowski*, 1997; *Laws et al*., 2000) in agreement with observations (*Falkowski et al*., 2003). *Nelson et al*. (2002) suggest that 57-90% of gross photosynthetic production was remineralized with the euphotic zone across the ACC, with intensity of the recycling diminishing to the South (*Sambrotto and Mace*, 2000; *Buesseler et al*., 2001). The relatively higher export efficiency (export production:primary production) in the Southern ACC result in annual POC export that is similar than in more productive systems at lower latitudes, in spite of the lower primary production (*Buesseler*, 1998; *Nelson et al.*, 2002). *Laws et al.* (2000) suggest that both the level of primary production and temperature are needed to explain the temporal and spatial variability of the export efficiency. Qualitatively the temperature effect is easy to understand. At high temperatures the potential growth rates of microorganisms are high, and most organic matter is decomposed before it has a chance to leave the euphotic zone. A cold temperature, the potential growth rates of heterotrophic organisms are much lower, and at moderate to high rates of primary production, much of the organic matter produced in the euphotic zone is exported before it has a chance to decompose. In fact, the autotrophic community is nutrient limited, and the heterotrophic community is temperature limited.

In the ACC, there is a pronounced southward increase in both gross silica and net silica productions

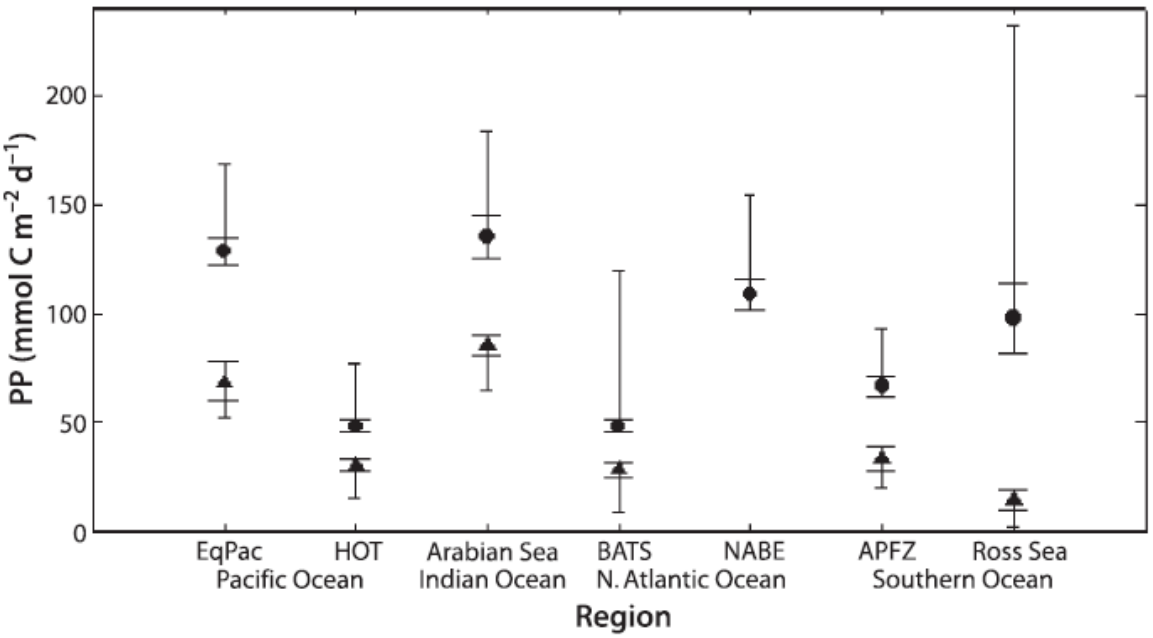

Figure 1.15. Summary of U.S. JGOFS primary productivity from five process studies and two times series studies (HOT and BATS). The circle and their errors bars show the mean and standard error of the maximum of productivity. Triangles and their error bars show the mean and standard error of the period of minimum productivity (from Falkowski et al., 2003).

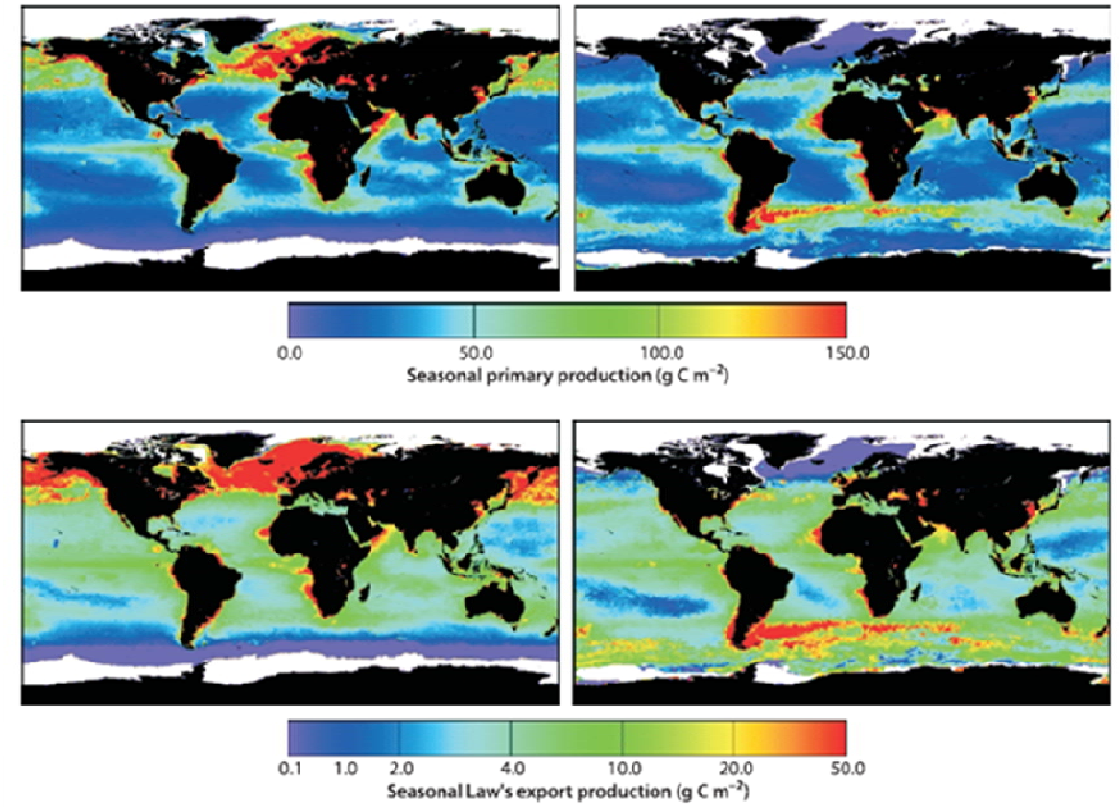

Figure 1.16. Boreal summer (left column) and winter (right column) distributions of primary production and export production (from Falkowski et al., 2003). Primary production was estimated using light dependent, depth resolved model for carbon fixation (Behrenfield and Falkowski, 1997). Export production was estimated using a pelagic food web model (Laws et al., 2000).

(*Pondaven et al*., 2000a; *Nelson et al*., 2002). *Nelson et al.* (2002) suggest that the main factor controlling this southward increase appears to be the standing stock of $Si(OH)_4$ in surface waters at the end of winter. It is in agreement with a progressive shoaling of the isopycnal to the surface with higher $Si(OH)_4$ content southward (*Pollard et al*., 2006). Taking together, the high rates of $bSiO_2$ production and export, low primary production and moderate POC export imply that the relationship between carbon and silicon cycles in Southern Ocean surface waters is very different from that in other oceans (*Ragueneau et al*., 2000). Primary production in the Southern Ocean is strongly limited by several factors (*Boyd*, 2002). Subsequently, growth rate is low and as suggested in section 1.2.1, the degree of silicification of diatoms cells is inversely correlated to growth rate (*Martin-Jézéquel et al*., 2000; *Claquin et al*., 2002). Such decoupling could explain the low Carbon productivity together with high opal production, at least for the Southern ACC where Si is not limiting for the diatoms community (*Nelson et al*., 2001). The association of diatoms with area of high export efficiency is in agreement with *Buesseler* (1998; section 1.3.1.1) and should work together with low temperature (*Laws et al*., 2000).

In low silicic acid regions of the Northern ACC with higher annual primary production (Figure 1.16) (*Reuer et al*., 2007), silicon impose a control on the community structure favoring the growth of nonsiliceous, ammonium-driven, iron efficient phytoplankton species (*Hutchins et al.*, 2001; *Smetacek et al.*, 2004). Such conditions are reported to have low export efficiency *(Buesseler*, 1998; *Buesseler et al*., 2001, 2005; *Savoye et al.*, 2004). Nevertheless, pulse or stratification events would impose some variability and sustain significant export production during the growth season (*McGillicuddy et al.*, 2007;

Benitez-Nelson et al., 2007) and probably diatoms contribution (*Krause et al.*, 2009). Unfortunately no extensive Si-biogeochemical studies has been performed in SAZ in spring when $Si(OH)_4$ concentration (*Griffiths et al.*, 1999) and productivity are expected to be higher (*Reuer et al.*, 2007) driven the seasonal Si-depletion.

1.4.3 Global impact of biogeochemical processes in the Southern Ocean

A new meridional overturning circulation paradigm has begun to emerge compared to the previous one (*Broecker*, 1991). The upwelling of deep water is now primarily confined to the Southern Ocean (Figure 1.11; *Sarmiento et al.*, 2004, 2007; *Gnadadesikan et al.*, 2004; *Hallberg and Gnanadesikan*, 2007), but also includes significant vertical mixing and/or upwelling in the North Pacific. *Sarmiento et al.* (2004) suggest that the low-latitude thermocline chemical properties are set by the preformed nutrient concentrations of waters feeding into the main thermocline from surface waters of the Southern Ocean. Hence, biogeochemical processes occurring in the surface Southern Ocean impose a strong control on biogeochemical properties of the low-latitude thermocline (*circa* 75%) feeding low latitude mixed layer in

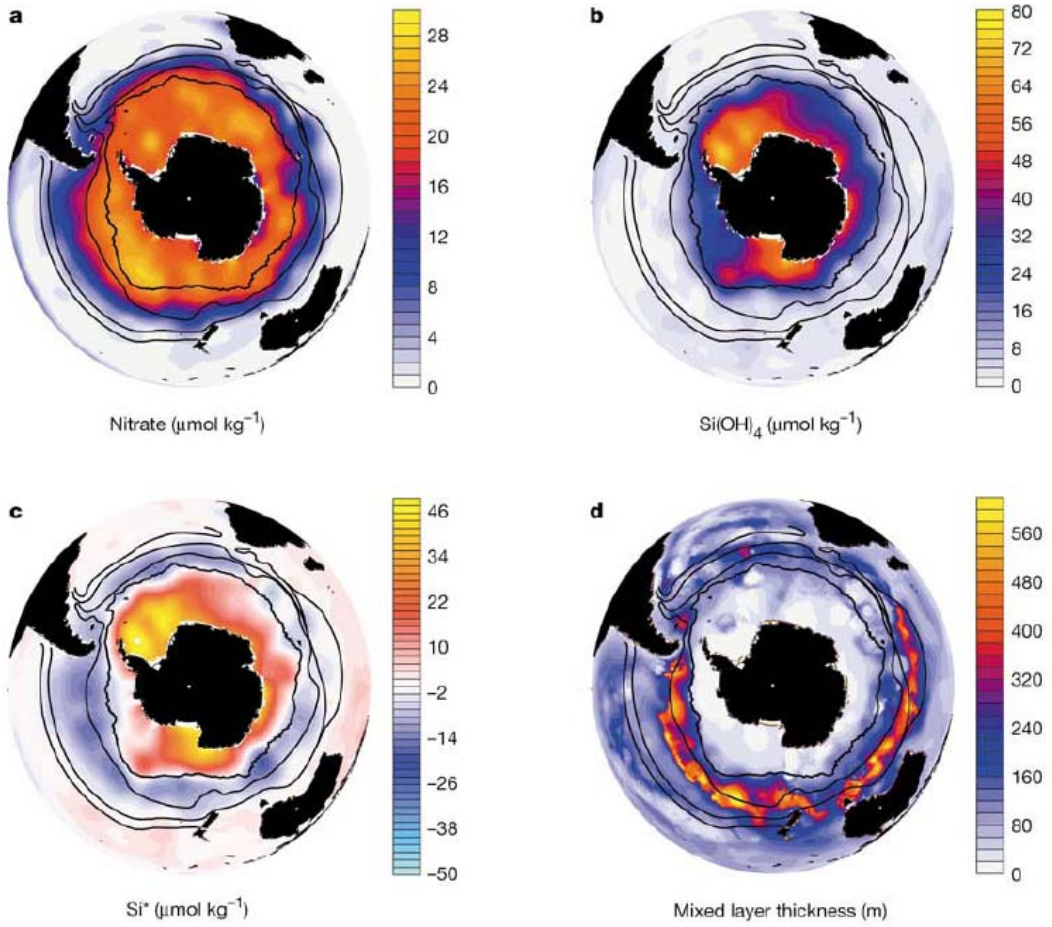

Figure 1.17: Polar stereographic maps of upper ocean nutrients and physics (from Sarmiento et al., 2004). (a) annual mean nitrate; (b) annual mean silicic acid; (c) annual mean Si*; (d) winter mixed layer thickness averaged over the July-September period. The southern line denotes the mean position of the Polar Front (from Moore et al., 1999). In sequence from south to north, the remaining lines denote the position of the SubAntarctic Front, the Southern SubTropical Front, and Northern SubTropical Front (from Belkin and Gordon, 1996). Nutrient data are from Levitus et al. (1998) and winter mixed layer depth from Kara et al. (2003).

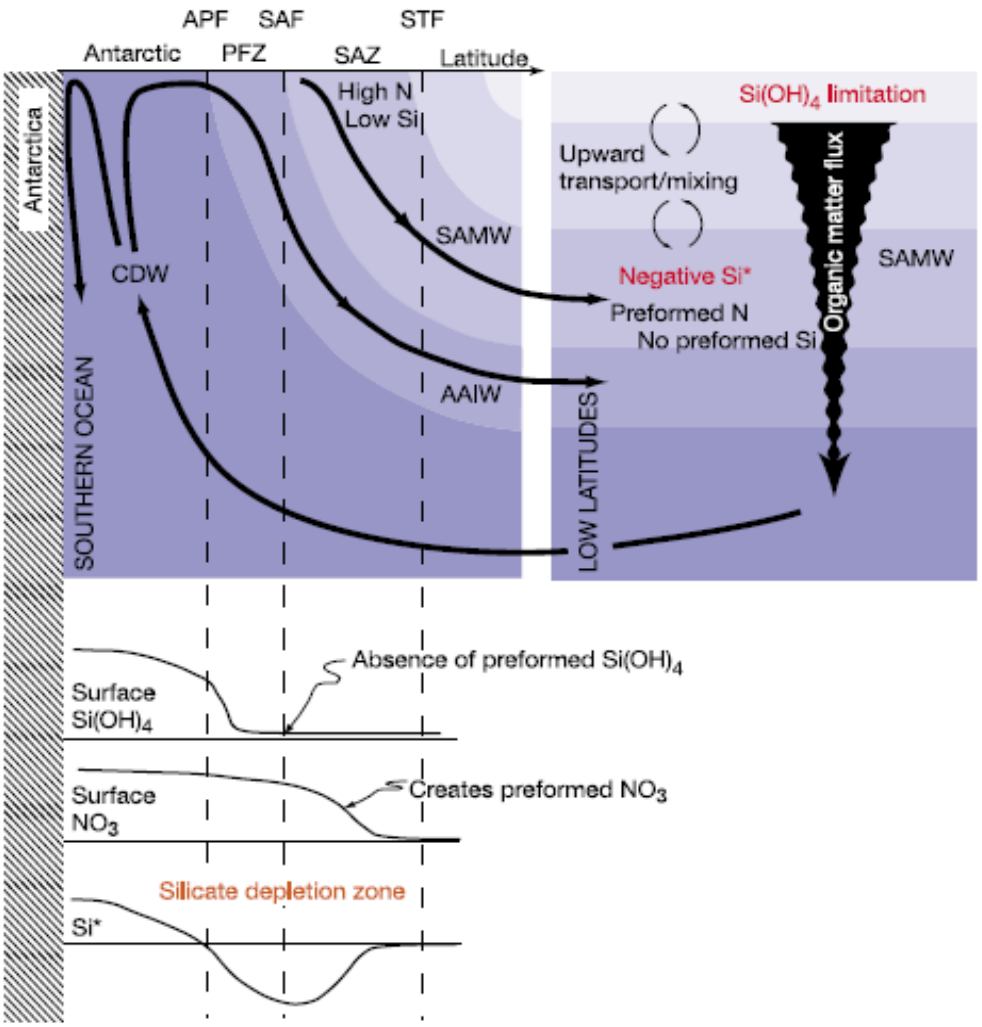

Figure 1.18. Southern Ocean control on thermocline nutrient concentrations (from Sarmiento et al., 2004). Conceptual diagram depicting the Southern Ocean physical and biological processes that form low-Si* waters and feed them in the global thermocline. Top, water pathways; bottom details of surface processes. Upper Circumpolar Deep Water (UCDW) upwells to the surface in the Southern Ocean, and is transported to the north across the Antarctic Polar Front (APF) into the Polar Frontal Zone (PFZ), where Antarctic Intermediate Waters (AAIW) forms and then across the SubAntarctic Front (SAF) into the SubAntarctic Zone (SAZ), which is bounded to the north by the SubTropical Front (STF). Silicic acid is stripped out preferentially over nitrate as the water moves to the north, thus generating negative Si* values. This negative-Si* water is SubAntarctic Mode Water (SAMW) and Antarctic Intermediate Water (AAIW), which sinks into the base of the main thermocline and feeds biological production in the low latitudes.

nutrients via the upper limb of Southern Ocean meridional circulation (Figure 1.12, *Sarmiento et al*., 2004). AAIW and SAMW are formed by deep winter convective mixing in some places with surface waters in PFZ and SAZ (Figures 1.12 and 1.17d). One unusual characteristic of these water masses is that they have high concentration of nitrate, but low concentration of silicic acid (Figure 1.17a, b). *Sarmiento et al*. (2004) defined a new tracer, Si* = [$Si(OH)_4 – NO_3$], with strong negative values in PFZ and SAZ (Figure 1.17c). They observed that Si* signatures of these water masses spread into the Southern Hemisphere subtropical gyres and into the North Atlantic, where it is part of the upper water return flow of the global thermohaline circulation.

Antarctic surface waters are carried northward by Ekman transport from the south of APF, where upwelling brings water with extremely high nutrient concentrations to the surface of the Southern Ocean

(Figures 1.12 and 1.18). During the northward movement in the Ekman layer, phytoplankton in the euphotic strip nutrients from surface to deep waters (biological pump) with preferentially $Si(OH)_4$ removal than NO_3. The preferential removal of silicic acid that would be required in order to generate such decrease in Si* is generally attributed to the influence of iron-light limitations and silicate pump processes especially exacerbated in the Southern Ocean (section 1.4.3).

Sarmiento et al. (2004) analysis shows important implications for the impact of climate change on the global nutricline, biological productivity and the carbon cycle. The Southern Ocean has long been recognized as playing a central role in the global carbon cycle and biological productivity, and in their response to climate change (*Sarmiento et al*., 1998; *Sigman and Boyle*., 2000; *Anderson et al*., 2002; *Matsumoto and Sarmiento*, 2008). Processes determining the properties of intermediate water masses, and the mechanisms leading to their formation have crucial implications in determining how Southern Ocean processes affect the supply of nutrients to the main thermocline and low-latitude productivity (Figure 1.18).

1.4.4 The Southern Ocean's biological pump on glacial-integlacial timescale

Shortly after *Delmas et al.* (1980) and *Neftel et al*. (1982) discovered that atmospheric CO_2 was lower at the peak of the last ice age, *Broecker* (1982) suggested that the CO_2 reduction was due to an increase in the ocean's biological activity: a larger flux of sinking organic particles through an enhancing of biological pump in a more productive glacial ocean would be in balance with a larger CO_2 gradient between the surface ocean and deep ocean. A larger CO_2 gradient would put more CO_2 into the deep ocean and leave less CO_2 for the atmosphere and surface ocean. Evidence to support a massive increase in biological productivity never materialized, however, and the search for a cause shifted to the Southern Ocean after the publication of the "Harvardton Bears" papers in 1984 (*Sarmiento and Toggweiler*, 1984; *Sigenthaler and Wenk*, 1984; *Knox and McElroy*, 1984). Synchronous changes in atmospheric CO_2 and Antarctic temperature are evident in high-resolution records covering major climate transitions, such as glacial terminations (*Broecker and Henderson*, 1998; *Petit et al*., 1999) and during abrupt warming of shorter duration (*Indermühle et al*., 2000; *Monnin et al*., 2001). These correlations provide strong circumstantial evidence for a Southern Ocean origin of climate-related changes in atmospheric CO_2 (*Anderson et al*., 2002).

Several proxies (review in *Anderson et al.*, 2002) allow indirect reconstruction of past changes in ocean circulation, biological pump and food web structure. However, none of these is a perfect proxy since they are influenced by multiple factors, and the sensitivity of each proxy to these factors will likely change in space and time (*Anderson et al*., 2002; *Anderson and Winckler*, 2005). A better calibration along with a better understanding of the influencing factors is required. Moreover these proxies required independent constraints on ocean circulation and related boundary conditions (e.g. winds, sea ice, …). This approach has not yet produced a general consensus, as proxies of export production are subject to different interpretations, and the reconstruction of ocean circulation and related boundary conditions during the LGM is controversial as well (*Anderson et al*., 2002; *Toggweiler et al*., 2006). The current debate about the role of the Southern Ocean is framed around two perspectives on the Harvardton Bears results. One builds on the biological pump idea (1). The other is built on circulation and gas exchange (2). Reality can lie between these two end-member processes (review in *Toggweiler et al*., 2006).

1.5 Silicon isotopic system

1.5.1 Si-isotope fractionation processes

Isotopes of one element are atoms with similar number of protons (Z) and electrons but differing by their number of neutrons (n). Therefore isotopes have different atomic mass (m) given by the total protons and neutrons (Z + n). The term "stable isotopes" is used in opposition to isotopes that have a limited life time (i.e. radioactive decay). Every isotope is characterized by its own vibration energy and capacity of movement depending on its mass: light isotopes react faster than heavy isotopes in a chemical reaction. This comes from the fact that light isotope bonds are slightly wider and have more potential energy (as mainly vibration energy) than heavy isotope bonds. The partitioning of isotope between two substances or two phases of the same substance with different isotope ratios is called "isotopic fractionation". Isotopic fractionation occurs in many of chemical and physical reactions.

Depending if the reaction is unidirectional or bidirectional, the isotopic fractionation is referred to as respectively kinetics or equilibrium. Kinetic fractionation is usually associated with fast and incomplete reactions. Equilibrium isotope reaction occurs when the isotopes are exchange between different chemical substances, between different phases, or between individual molecules. Those reactions are usually slow meaning that the products formed can react with the reactant. Heavy isotopes would be usually more abundant in the phase with the lower energy state (*Hoefs*, 2009).

Four isotopes of silicon exist in natural environment: ^{28}Si, ^{29}Si, ^{30}Si, and ^{32}Si. The first three isotopes are stable and the last one is a radioactive isotope of cosmogenic origin (half life of 140 ± 6 years). The atomic mass units (amu) for the three stable Si-isotopes are respectively 27.976927, 28.976495, and 29.973770 with respective abundance of 92.23%, 4.68%, and 3.09% (*Rosman and Taylor*, 1998). Natural silicon isotopic composition is expressed in δ values:

$$\delta^{30}\mathrm{Si}(‰) = \left(\frac{\left(\frac{^{30}\mathrm{Si}}{^{28}\mathrm{Si}}\right)_{\mathrm{sample}}}{\left(\frac{^{30}\mathrm{Si}}{^{28}\mathrm{Si}}\right)_{\mathrm{NBS28}}} - 1 \right) \cdot 1000 \quad (1.5)$$

$$\delta^{29}\mathrm{Si}(‰) = \left(\frac{\left(\frac{^{29}\mathrm{Si}}{^{28}\mathrm{Si}}\right)_{\mathrm{sample}}}{\left(\frac{^{29}\mathrm{Si}}{^{28}\mathrm{Si}}\right)_{\mathrm{NBS28}}} - 1 \right) \cdot 1000 \quad (1.6)$$

The δ values denote a difference measurement made relative to a standard, the NBS28 silica sand standard for silicon (National Institute of Standard and Technology RM #8546) (*Carignan et al*., 2004).

The isotope fractionation that occurs during a chemical reaction is indicated by the fractionation factor which is defined as:

$$\alpha = \frac{R_A}{R_B} \quad (1.7)$$

where R_A is the ratio of the heavy (^{30}Si or ^{29}Si) to the light isotope (^{28}Si) in molecule or phase A (e.g. biogenic silica) and R_B is the same in phase B (e.g. silicic acid). To make this fractionation difference easier to work with, ε values are derived from α values and are expressed in permil (‰):

$$\varepsilon = (\alpha - 1) \cdot 1000 \quad (1.8)$$

The first report of Si-isotopic fractionation factor ($^{30}\varepsilon$) induced by diatoms was in *De La Rocha et al*. (1997). This study highlights the preferential incorporation of ^{28}Si into diatoms. The isotopic fractionation factor seems constant even though there is a large standard deviation (*circa* -1.1 ± 0.4‰), and independent of the temperature (12-22°C), salinity (fresh and marine environments), growth rates, species, and cell-sizes (*De La Rocha et al*., 1997; *Milligan et al*., 2004; *Alleman et al*., 2005; *Cardinal et al*., 2007). The range of *in situ* and *in vitro* fractionation estimates covers -0.4 to -2.2‰ (*De la Rocha et al*., 1997, 2000; *Varela et al*., 2004; *Milligan et al*., 2004; *Cardinal et al*., 2005, 2007; *Reynolds et al*., 2006; *Beucher et al*., 2008; *Cavagna et al*., in revision; chapters 4 and 5). Due to the enzymatic character of Si-transport/silica polymerization process via protein transport and complexation through the plasma and SDV membranes, and cell plasma (*Hildebrand*, 2008), the Si-isotopic fractionation should probably be a kinetic fractionation as for C and N isotopic fractionations during phytoplankton assimilation processes (*François et al*., 1993; *Sigman et al.*, 2009). Indeed, it seems unrealistic to have an isotopic equilibrium between the SITs or silicon binding component and substrates (turnover time less than one day). Light Si-isotopes should bond faster with the SITs and intracellular binding components than heavy isotopes under incomplete reaction since the silicic acid pool is virtually too large at diatom scale. Moreover as for C isotopes (*Popp et al*., 1989; *François et al*., 1993; *Cassar*, 2003) this fractionation factor should be a balance between the different isotopic discrimination effects involved in the cellular-scale Si-metabolism balance (*Milligan et al*., 2004; *Demarest et al*., 2009), discussed in section 1.2.

During the physico-chemical dissolution of biogenic silica, the Si-isotopic fractionation seems to be in equilibrium (isotopic exchange reaction) through a process of bidirectional isotope exchange (*Demarest et al*., 2009).

1.5.2 Silicon isotopic variation on earth

The relative mass difference (Δm/m) is 7.8% between ^{30}Si and ^{28}Si compared to 3.5% between ^{29}Si and ^{28}Si. The larger the relative mass difference is, the stronger the degree of isotopic fractionation is expected. Isotopic fractionation is highly dependent on the chemical and physical properties of the corresponding element. Among these characters the most important factors are whether the element can form compounds of different valences and whether the element can form gas compounds. Silicon has only a valence 4^+, has no gas compounds in nature and only mainly form compounds with Si-O bond. This is why, there is no large silicon isotopic fractionation in terrestrial samples (*Douthitt*, 1982; *Ding et al*., 1996; *Basile-Doelsch*, 2006) in contrast to those found for other light elements, e.g. C, N, O. The range of Si-isotopic variations on Earth surface is 11.8‰ from $\delta^{30}Si$ of -5.7‰ in silcretes (*Basile-Doelsch*, 2006) to 6.1‰ in rice grains (*Ding et al*., 2005). Si-isotopic data have been compiled in review papers (*Douthit*, 1982; *Ding et al.*, 1996; *Basile-Doelsch*, 2006) but since new studies have largely increased the data available since 2005, we present in Figure 1.19 an update of the different reservoirs in continental and marine environments. Dissolved Si in fresh waters (rivers and lakes) and seawater is ^{30}Si-enriched. Seawater and brines in sea ice display signatures between 0.4 and 3.2‰. Biomineralization induces a

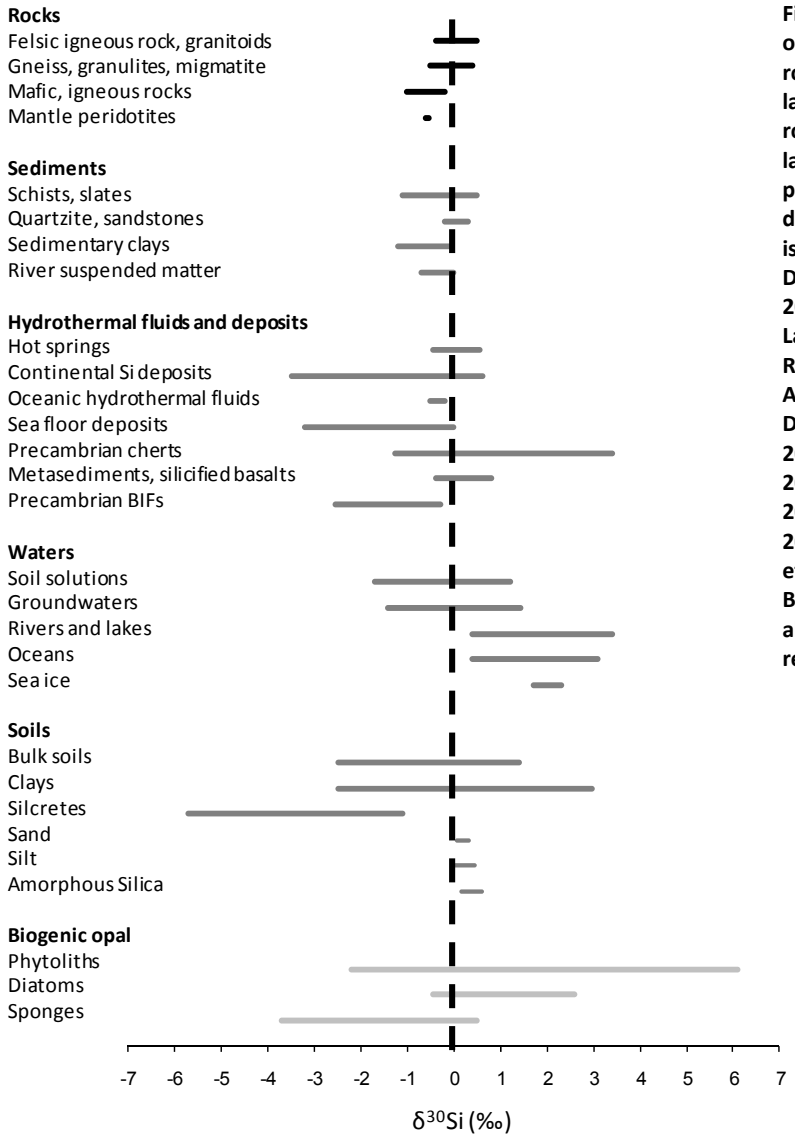

Figure 1.19. Si-isotopic variations on Earth: small fractionation by rock-forming processes (black), larger fractionation with water-rock interactions (dark grey), and large fractionation with biogenic processes (light grey). The vertical dotted line represents the crustal isotopic composition. From Douthit, 1982; Ding et al., 1996, 2004, 2005, 2007, 2008, 2009; De La Rocha et al., 2000b; De La Rocha, 2003; Ziegler et al., 2005; Alleman et al., 2005; Basile-Doelsch, 2006; Cardinal et al., 2005, 2007; Georg et al., 2006b, 2007a, 2009a, 2009b; André et al., 2006; Robert and Chaussidon, 2006; Reynolds et al., 2006 ; Fripiat et al., 2007; Abraham et al., 2008; Beucher et al., 2008 ; Opfergelt et al., 2008; 2009 ; Cavagna et al., in revision ; chapters 4 and 5.

range of isotopic variations of 9.8‰ corresponding to 83% of the whole terrestrial isotopic range which gives to this pool the largest impact on the Si-isotopic budget.

1.5.3 Si-isotopic distribution in the Ocean

Figure 1.20 shows the different Si-isotopic studies in the modern ocean. Whereas the data are still scarce for $\delta^{30}Si$ of silicic acid, this is even worse for biogenic silica isotopic compositions which are only available from four published studies, all in the Southern Ocean (*Varela et al*., 2004; *Cardinal et al*., 2007; *Fripiat et al*., 2007; *Cavagna et al*., in revision; chapter 4).

In the ocean, an inverse relationship exists between silicic acid concentration and $\delta^{30}Si$ because diatoms take preferentially light Si-isotopes composition to construct their opaline cell walls. This relationship is not straightforward due to the additional isotopic effects such as $bSiO_2$ dissolution and mixing which dampen this simple relation. Water column profiles of $Si(OH)_4$ concentration and isotopic composition display a heavier isotopic composition in surface relative to deep waters coinciding with Si-depletion (Figure 1.21 and *De La Rocha et al*., 2000b; *Cardinal et al*., 2005; *Reynolds et al*., 2006; *Beucher et al*.,

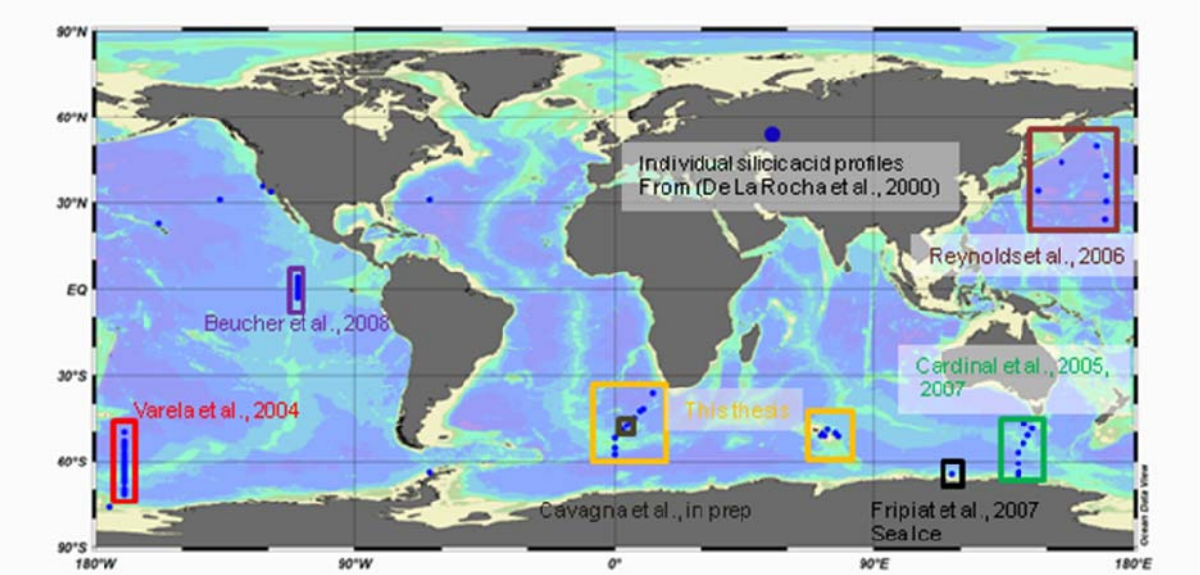

Figure 1.20. Geographic location of the whole modern $\delta^{30}Si$ oceanic data's. Cardinal et al. (2005), Reynolds et al. (2006), Beucher et al. (2008), Cavagna et al. (in revision), this thesis: $Si(OH)_4$ from complete water column profiles. De La Rocha et al. (2000b): One $Si(OH)_4$ profile by circle (no mixed layer $\delta^{30}Si$ except for coastal areas. Varela et al. (2004), Fripiat et al. (2007): $Si(OH)_4$ and $bSiO_2$ only for surface waters. Cardinal et al. (2007), Cavagna et al. (in revision); this thesis: $bSiO_2$ for surface waters

2008). Such vertical gradients are driven by diatom production combined with vertical mixing reuniting the previously fractionated Si-isotopes (*Cardinal et al.*, 2005; *Reynolds et al.*, 2006). In the Southern Ocean,

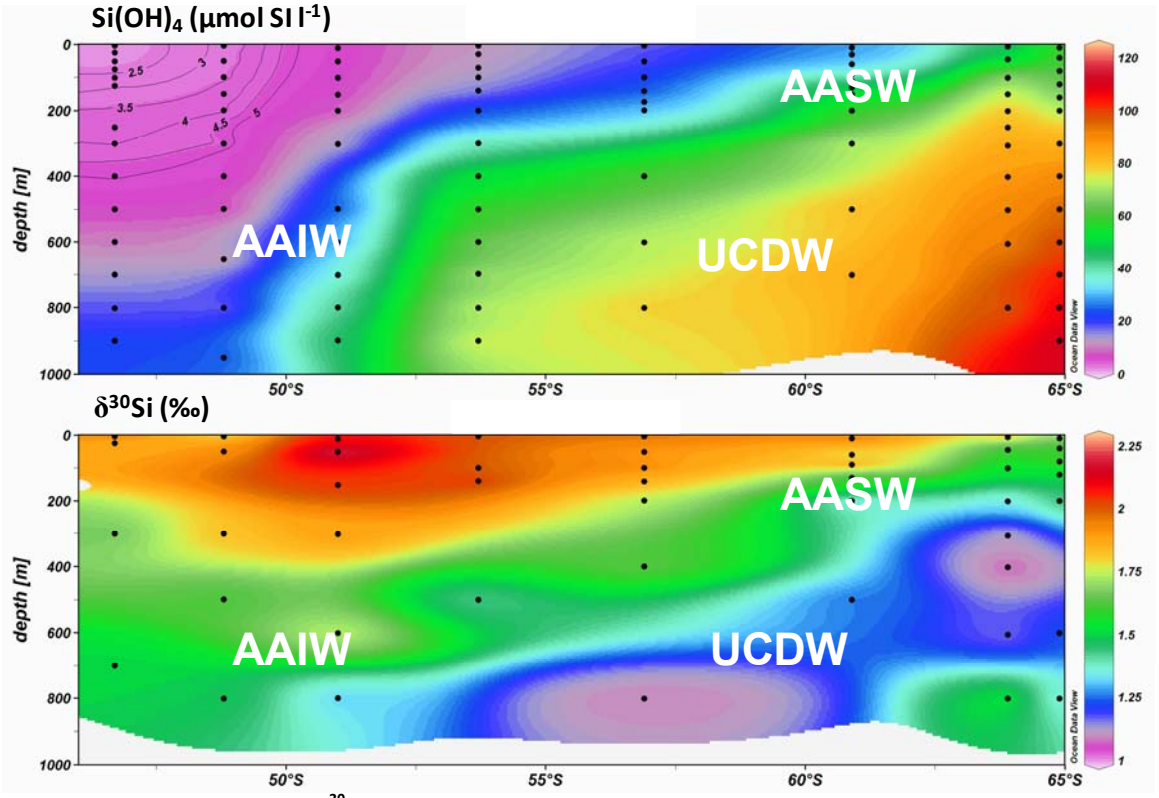

Figure 1.21. Interpolation of $\delta^{30}Si$, $Si(OH)_4$ concentration in the upper 1000m of the CLIVAR-SR3 latitudinal transect in the Southern Ocean south of Tasmania (adapted from Cardinal et al., 2005). Interpolation is from R. Schlitzer (Ocean Data View, 2003).

the main Si-isotopic variation is observed in the upper 1000m layer (Figure 1.21) reflecting (1) the shoaling of the isopycnal surface (CDW) southward towards the Antarctic divergence. (2) The Surface waters are advected northward in the Ekman layer where Si-uptake is occurring and subsequently (3) subducted (AAIW, SAMW) via the upper limb of the meridional circulation carrying heavier $\delta^{30}Si$ resulting from previous Si-consumption (Figures 1.12 and 1.18; *Cardinal et al.*, 2005).

Reactions convert substrate to product over time. The simplest way to produce isotopically distinct reservoirs between them is by their reaction equilibrium isotopic interchanges. This results in a maintained stable isotopic contrast between the substrates and products that is commonly referred as a closed system equilibrium (*Criss*, 1999; *Johnson et al*., 2004). When the product stops exchanging with the substrates, a Rayleigh fractionation (initially developed by Lord Rayleigh in 1902 for distillation processes) describes the change in δ values between the reaction-involved components (*Johnson et al*., 2004). In the case of Si-isotopic fractionation induced by diatoms, the formed biogenic silica is internally isolated ("fractionated") from the substrate. This is the reason why silicon isotopic fractionation in an overall closed mixed layer may follow a Rayleigh fractionation law. Therefore products can be removed internally within closed-systems along a classical Rayleigh fractionation law (*Rayleigh*, 1902; *Mariotti et al*., 1981; *Fry*, 2006). In the Ocean, there are two general systems for describing the isotopic effect induced by the Si-utilization by diatoms in surface ocean, assuming a kinetic fractionation (Figure 1.22). The closed system (also referred to as Rayleigh model in this thesis) is characterized by the lack of new inputs, and reactions progress in a sequential mode over time, consuming substrate (here silicic acid) that was present at the

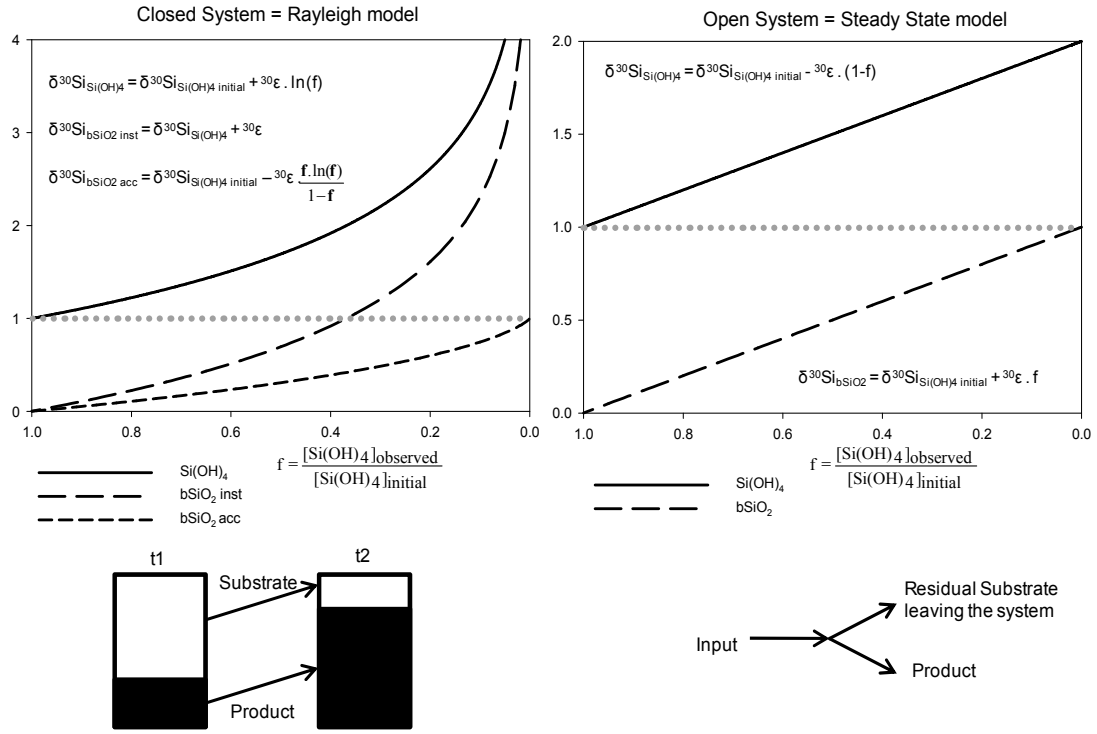

Figure 1.22. Si-isotopic dynamic in closed system (a) and open system (b) for a substrate and a product which are respectively silicic acid and biogenic silica. Isotope fractionation is 1‰ in the illustrate examples, and lead to lighter biogenic silica (lower δ) and by difference, heavier residual silicic acid (higher δ). In the closed system, there are two products, one that accumulates over time (accumulated biogenic silica) and one that is transient, forming instant by instant in time (instantaneous biogenic silica). Under open, flow-through system, where the reaction are split or branched, there is only one product (biogenic silica) (adapted from Fry, 2006).

beginning. The contrasting system is an open flow-through system (also referred to as steady state model in this thesis) when the inputs balance the outputs (e.g. *Fry*, 2006). In such a case, the counterbalanced flux imposes a stable isotopic fractionation than mimics a "closed system equilibrium". The equations governing the isotope dynamics in these ideal closed and open systems are well known (Figure 1.22). In the closed system, the step fractional reaction bears an indirect, unfixed, potentially discontinuous, time relationship. There are two products in the closed system, the long-term product that accumulates and the short-term instantaneous product. In the steady state system, there is a simpler overall isotope dynamics, with linear changes in isotope composition. Only one product forms from substrate at an instant in time, then both product and residual substrate are exported (*Fry*, 2006). This model just represents a final snapshot and does not reflect any temporal evolution. In many systems, the reactions can proceed in a mixed way. For Si, depending on the Si- supply:Si-uptake ratio and its seasonality, the true situation will likely lie between these two ideal situations (*Fry*, 2006). The Southern Ocean would be particularly behaving in a mixed way since large Si-utilization is occurring in a place with extremely deep mixed layer and regular mixing events are expected supplying the mixed layer in silicic acid (*Altabet and François*, 2001; *Varela et al*., 2004; *Cardinal et al*., 2005).

During this thesis, efforts will be made to use the different sensitivity of the Si-isotopic proxy in the modern ocean to different processes (uptake, dissolution, mixing) incidentally constraining the seasonal mass Si-balance (Figure 1.23).

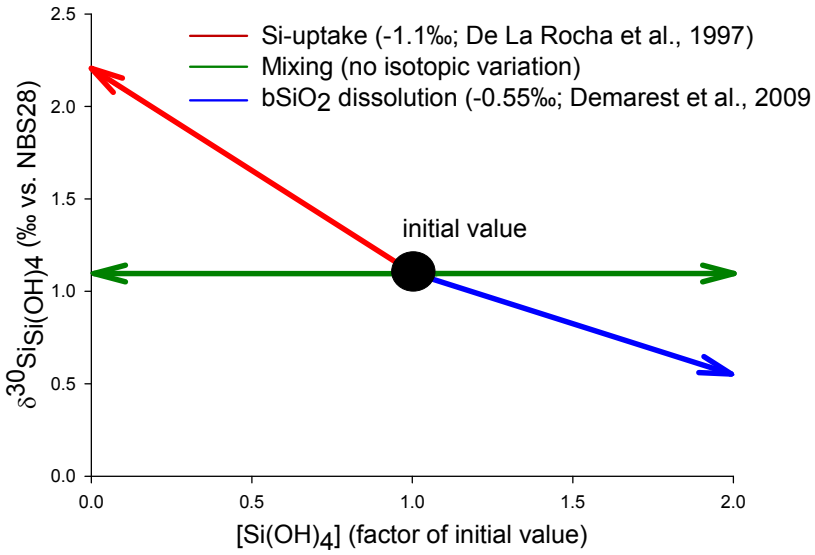

Figure 1.23. The instantaneous effect of different marine Si-cycle processes on silicic acid δ^{30}Si. The trajectories are for reasonable estimates of the fractionation factors and they depend on the initial silicic acid δ^{30}Si as well of the relative amplitude of the changes in silicic acid concentration.

1.5.4 δ^{30}Si palaeoceanographic implications

Few studies report Si-isotopic composition in the sediments: from the Southern Ocean during several interglacial-glacial cycles (*De La Rocha et al*., 1998*; Brzezinski et al*., 2002; *Beucher et al*., 2007), the North

Pacific Ocean in a transition state 2.8 million year ago (*Reynolds et al*., 2008), and in Equatorial Pacific Ocean from the last interglacial-glacial cycle (*Pichevin et al*., 2009). All these studies show significant variation in Si-isotopic composition with glacial-interglacial timescale (Figure 1.24; Antarctic Zone). Si-isotopic signature, whatever the oceanic basins, is lighter during glacial periods suggesting a lower Si-utilization by diatoms in the corresponding surface waters (*De La Rocha et al*., 1998). Nevertheless as all proxies, this relation needs to be constrained in the modern ocean with a comprehensive understanding of the processes which control it, both biological and physical, since $\delta^{30}Si$ is not only dependent on the relative Si utilization, but also on the $\delta^{30}Si$ signature, Si content of the source and fractionation factor (Figure 1.22).

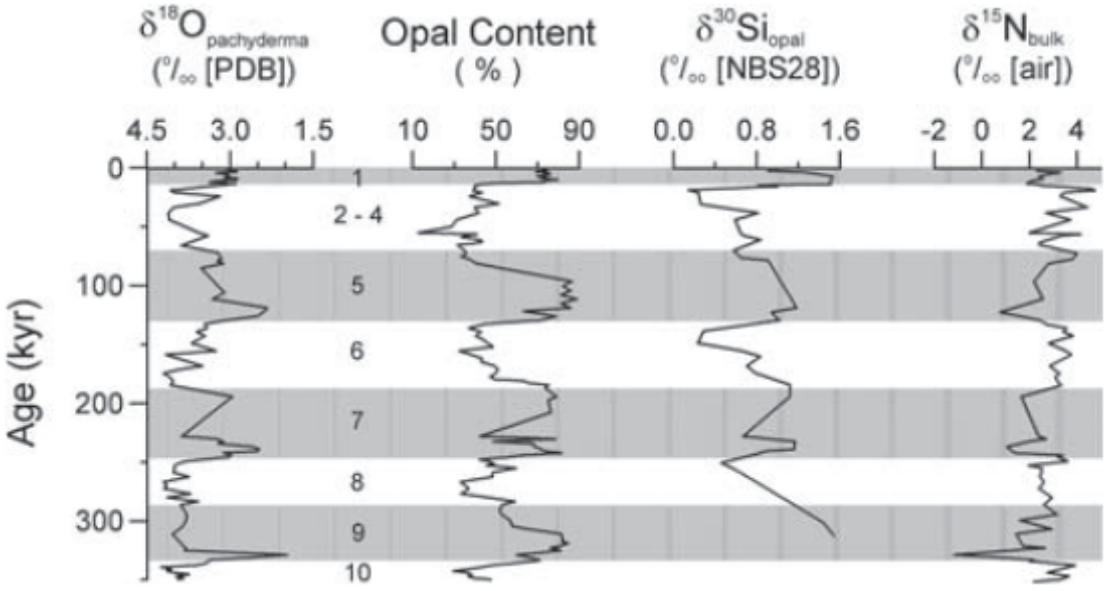

Figure 1.24. $\delta^{18}O$ (N. pachyderma) (Charles et al., 1991), opal content (charles et al., 1991), $\delta^{30}Si$ of diatom (Brzezinski et al., 2002) , and $\delta^{15}N$ of bulk sediment (Rau adn Froelich, 1993) from RC13-259 in the Antarctic Zone (53°53°S ; 4°56°W ; 2677m). Numbers indicate oxygen isotope states 1-10 (from Brzezinski et al., 2002).

Chapter 2. Thesis objectives

Marine Si-biogeochemical cycle is dominated by biogenic silica production and dissolution in the euphotic zone (*Tréguer et al.*, 1995). Southern Ocean plays a key role in the global Si-biogeochemical cycle since diatoms are major player of the biological pump in this area (*Buesseler et al*., 2001; *Jin et al.*, 2006; *Honjo et al*., 2008) driving the largest $Si(OH)_4$ gradient, both in surface and subsurface ocean (*Brzezinski et al*., 2001; *Sarmiento et al*., 2004, 2007) and accounting for 20-35% of the global marine biogenic silica production (*Pondaven et al*., 2000a). This circumpolar feature coincides with the most important sink for silica in the global ocean, accounting for 37% of the global opal accumulation (*DeMaster*, 2002). This north-south $Si(OH)_4$ gradient which is not observed for other major nutrients, has significant implications, both in modern and past ocean, on global biogeochemistry since the upper limb of the Southern Ocean circulation redistributes nutrient into the main global ocean thermocline driven 75% of the low-latitude productivity (*Sarmiento et al*., 2004). Notwithstanding, large uncertainties still persist due to the scarcity of data and the difficulty to discriminate different process (mixing, uptake, dissolution) from mass balance alone.

During this thesis, the Si-biogeochemical cycle of the Southern Ocean will be assessed mainly through two isotopic approaches:

(1) Natural silicon isotopic composition ($\delta^{30}Si$) of biogenic silica and silicic acid.

(2) Biogenic silica production and dissolution rates in the euphotic layer using ^{30}Si-isotopic dilution methods (Nelson and Goering, 1977a, 1977b).

(1) The estimation of the oceanic silicon mass balance from direct measurements is plagued by their strong temporal and spatial variability. The utilization of dissolved tracers distribution to quantify the silicic acid uptake in superimposing oceanic circulation encounters difficulties since the different mixing models give significantly different results, especially for Si (*Jin et al*., 2006). An alternative is to use natural silicon isotopic compositions, both in biogenic silica and silicic acid, since this proxy exhibits different sensitivities to uptake and mixing processes, and presents the advantage to integrate longer timescale. Thus uptake and mixing in the upper ocean should be distinguishable when element and isotope constraints are coupled. This thesis, attempts to use natural Si-isotopic compositions as a constraint to close Si-mass balance. This thesis widely expands the few available

Si-isotopic data (*De la Rocha et al*., 2000b; *Varela et al*., 2004; *Cardinal et al*., 2005; *Reynolds et al*., 2006; *Cardinal et al.*, 2007; *Beucher et al*., 2008), both for biogenic silica and silicic acid, in the different zones of the ACC during KEOPS and BONUS-goodhope cruises. Given the potential of this proxy to track back past Si-utilization (*De La Rocha et al*., 1998; *Brzezinski et al*., 2002; *Beucher et al*., 2007), it is necessary to determinate better origin and fate of the $\delta^{30}Si$ of $bSiO_2$ in the water column as well as the sediment-water interface. The fates of $bSiO_2$ are not the aim of this thesis but need clearly to be constrained (*Demarest et al*., 2009). This thesis aims to constrain the fractionation factor under Antarctic conditions (*in situ* estimation) with the different ACC Si-sources. Both parameters require quantification in the modern ocean, assessment of their variability, and the development of a mechanistic understanding of the parameters that control them.

(2) The balance between integrated silica production and dissolution in the euphotic zone is a key factor of the strength of the silicate pump. Up to now, only 30 profiles of biogenic production and dissolution rates in the euphotic layer of the Southern Ocean have been measured (*Nelson and Gordon*, 1982; *Nelson et al*., 1991; *Brzezinski et al*., 2001; *Beucher et al*., 2004b) showing already a large variability. This implies a high degree of change in the extent of silica recycling in the open ocean. The scarcity of existing data results from the difficulty of the preexisting mass spectrometer methods. So a new mass spectrometer method (HR-SF-ICPMS) has been developed easier and faster than previous methods. Moreover, biogenic silica production and dissolution rates have been assessed during two oceanographic cruises in summer (SAZ-Sense and BONUS-goodhope) and expand the available profiles to 48. It is necessary to expand the available datasets of $bSiO_2$ production and dissolution in the ocean since these processes drive the marine Si-biogeochemical cycle (Figure 1.2) and is one of the greatest uncertainties in the global marine budget.

The main results (chapter 5 to chapter 8) are presented as a succession of articles either published/submitted or prepared for submission to peer review journals. This presentation has the advantage that each chapter can be easily read and understood independently. Nevertheless, I would like to apologize for the discomfort that the redundancies among chapters may provide to people who would afford a complete and continuous reading.

The thesis is structured in five parts.

Part I give a general introduction (chapter 1) of the thesis context and scientific motivation. Marine Si-biogeochemical cycle is introduced along with a brief description of isotopic fractionation and Si-isotopes applications. A special emphasis is given on the Southern Ocean because it represents the main area of investigation in this thesis.

Part II focuses on used methodology. Chapter 3 is centered on basic concepts of ICP-MS. Chapter 4 is dedicated to the $\delta^{30}Si$ measurements through an instrumental upgrade of the previous methodology developed in *Cardinal et al*. (2003) allowing to resolve the ^{30}Si interferences and get directly $\delta^{30}Si$ instead of only $\delta^{29}Si$ (*Abraham et al*., 2008). Preliminary results from an intercomparison in the framework of GEOTRACES program are presented for $\delta^{30}Si$. Chapter 5 develops the new methodology for ^{30}Si-isotopic abundance measurement (^{30}Si atom%) using a HR-SFICPMS (Element2) for ^{30}Si-spiked incubations (*Fripiat et al*., 2009).

Part III is centered on natural Si-isotopic composition investigated during two oceanic cruises: KEOPS (Jan-Feb 2005; chapter 6) and BONUS-goodhope (Feb-March 2008; chapter 7). Natural isotopic composition is discussed in term of Si-source and fates for the different Si-pool observed in complete water column. When it is possible, simple annual mass balance are realized for surface waters (Annual Si-supply, Summer Si-supply, net $bSiO_2$ production).

Part IV focuses on $bSiO_2$ production and dissolution rates assessed during SAZ-Sense cruise (Jan-Feb 2007; chapter 8). During SAZ-Sense, the Si-cycle was fully investigated through ^{30}Si-incubations, ^{32}Si-incubation, PDMPO-incubation, taxonomy (collaboration with Karine Leblanc and Bernard Quéguiner, COM) and coupled with ^{15}N and ^{13}C incubations (*Cavagna et al.*, in revision). In this thesis, Si-budget is discussed with the Si:C ratios from uptake rates and particulate stocks.

Part V is a general discussion of the results presented in this thesis along with the conclusions and perspectives.

Part II. Analytical development

Chapter 3. Inductively coupled plasma mass spectrometry

Isotope ratio measurements are important in a number of different application fields (*Becker and Dietze*, 2000), for example for the determination of stable isotopes and long-lived radionuclides when studying biological processes and geochronology, the quality assurance of fuel material, radioactive waste control or in environmental monitoring. Furthermore isotope ratio measurements are of interest for tracer experiments with the addition of enriched stable or unstable isotopes ("spikes") in biological and medical research, studies of chemical reactions, metabolism studies and in the isotope dilution technique, the most precise method for the determination of element concentrations at the trace and ultratrace level. For many decades atomic mass spectrometry has occupied an outstanding position among the analytical techniques due to its universality, high sensitivity and wide fields of application in elemental and isotopic analysis (*Becker*, 2002). One of the main characteristics of mass spectrometry is the possibility of precise and accurate isotope ratio measurements (*Becker*, 2005). This thesis used two different silicon isotopic approaches to constrain the marine Si-biogeochemical cycle: the natural silicon isotopic composition in silicic acid and biogenic silica (*De La Rocha et al*., 1996, 1997), and the ^{28}Si-isotopic dilution method for the assessment of biogenic silica production and dissolution rates (*Nelson and Goering*, 1977a, 1977b). These two approaches require different samples processing and Mass Spectrometers (MS). The major difference results in the precision requirement. The ^{30}Si:^{28}Si isotopic ratio difference between the two extreme isotopic end-members measured so far on Earth is only 0.0118 corresponding to 11.8‰: the lightest endmember is silcretes from Southeast France (*Basile-Doelsch et al*. 2005) and the heaviest, rice grain from China (*Ding et al*. (2005). In contrast, ^{30}Si-spiked incubations largely exceed natural isotopic variation by one or two orders of magnitude with an isotopic difference between samples from 0.10 to 7.

We use the Inductively Coupled Plasma (ICP) as ionization source on two different mass spectrometers: a MultiCollector (MC)-ICP-MS (Nu Plasma, Nu Instruments, Wrexham, UK) for natural isotopic composition and a High Resolution (HR) Sector Field (SF)-ICP-MS (Element2, Thermo, Bremen, Germany) for spiked isotopic composition. We will start with a brief description of the fundamental principles used in ICP-MS – the use of a high temperature plasma discharge to generate positively charged ions. Among the inorganic mass spectrometric techniques, ICP-MS has been established as an extremely efficient and sensitive analytical mass spectrometric technique for the multi-element determination of elements in aqueous

solutions and digested solid samples at the trace and ultratrace concentration level and it has successfully been applied for precise and accurate isotopic analysis. This is demonstrated by a rapid growth of ICP mass spectrometer installations world-wide (*Becker and Dietze*, 2000). The sample, typically in liquid form, is pumped into the sample introduction system, which consists in a spray chamber and nebulizer. It exits the spray chamber as an aerosol and eventually finds its way into the plasma. As it travels through the different heating zones of the plasma torch it is successively and extremely quickly dried, vaporized, atomized, and ionized (Figure 3.1; *Thomas,* 2002). The plasma can be described as an excited argon gas that is partly ionized. The plasma is formed within an Ar stream at the end of the plasma torch, where the Ar meets a high frequency (27 MHz) electro-magnetic field. The electro-magnetic field is induced by a high frequency oscillating current within the RF coil controlled by the RF generator, which has an output power of *circa* 1350 W. A high-voltage initiation spark is applied to the Ar gas and causes electrons to be stripped off some Ar atoms. Where free electrons are available they get accelerated within the induced electro-magnetic field and initiate a chain reaction by colliding in turn with other Ar atoms and causing electrons to be stripped away. The energy required to ionize Ar atoms (~ 15.8 eV) is high enough to ionize most elements of the periodic table.

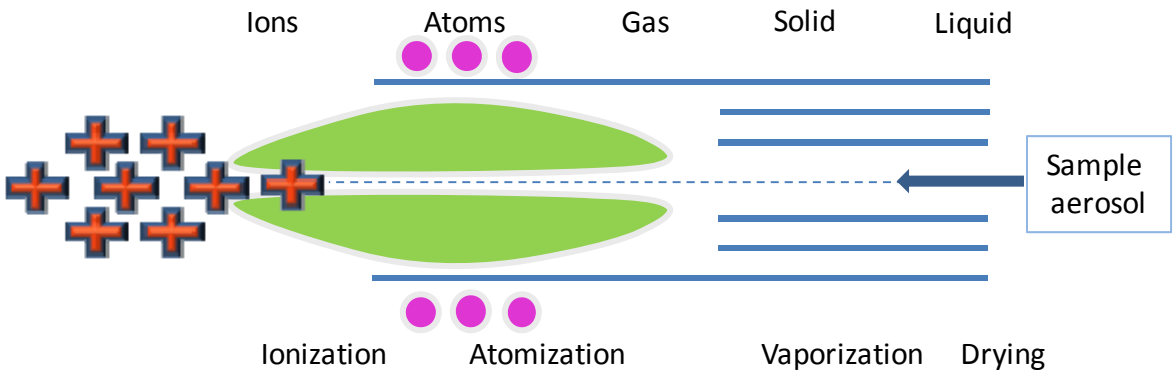

Figure 3.1. Generation of positively charged ions in the plasma (adapted from Thomas, 2002).

These ions are transferred through the sample and skimmer nickel cones defining the interface region where they get separated from the plasma and accelerated into the mass spectrometer through high voltage. The role of the interface is to transport the ions efficiently, consistently, and with electrical integrity from the plasma, which is at atmospheric pressure to the mass spectrometer analyzer part, which is at approximately ~ 3-4 10^{-9} bar. The ion beam is focused before it enters the mass analyzer. Sometimes known as ion optics, it comprises one or more ion lenses components (metallic plates, barrels, or cylinders that have a voltage placed on them), which electrostatically steer the analyte ions from the interface region into the mass separation device. Although the detection capability of ICP-MS is generally recognized as being superior to any of the other atomic spectroscopic techniques, it is probably most sensitive to the sample's matrix component. The inherent problem lies in the fact that ICP-MS yield at the interface is relatively inefficient: out of every million ions generated in the plasma (ICP), only one actually reaches the detector (MS). One of the main contributing factors to the low efficiency is the higher concentration of matrix elements compared to the analyte, which has the effect of defocusing the ions and altering the transmission characteristics of the ion beam. The role of the ion focusing system is

therefore to transport the maximum number of analyte ions from the interface region to the mass separation device (*Thomas*, 2002).

The mass separation device (also referred to as the mass analyzer) is the region of the ICP mass spectrometer that separates the ions according to their mass to charge ratio (m/z). The mass analyser is positioned between the ion optics and the detector and is maintained as a vacuum of approximately 10^{-9} mbar with a second turbomolecular pump. There are basically four kinds of commercially available mass analyzer: quadrupole mass filters, double focusing magnetic sector, time-of-flight, and collision-reaction cell technology. HR-SF-ICP-MS and MC-ICP-MS are both using a double focusing magnetic sector thus in the following only this characteristic mass analyzer would be described which has found its niche in solving challenging application problems that require excellent detection capability, exceptional resolving power, or very high precision (*Thomas*, 2002). Today's instrumentation is based on two different approaches, commonly referred to as standard or reverse Nier-Johnson geometry. Both these designs, which use the same basic principles, consist of two analyzers – a traditional electromagnet and an electrostatic analyzer (ESA). In the standard design, the ESA is positioned before the magnet, and in the reverse design it is positioned after the magnet. The HR-SF-ICP-MS and MC-ICP-MS use the reverse and standard configurations, respectively (Figures 3.2 and 3.3). Ions are sampled from the plasma in a conventional manner and then accelerated in the ion optic region to a few kilovolts before they enter the mass analyzer. The mass separation due to the m/z ratio requires that all ions have the same kinetic energy, which is a function of the velocity of the ions, for a given mass and charge. However, plasma ion sources produce ion beams with large energy spreads (depending on the type of instrument), meaning that ions with the same m/z ratio have different kinetic energies/velocities and thus use different trajectories within the mass spectrometer. This would cause two ions, with similar m/z ratios but with

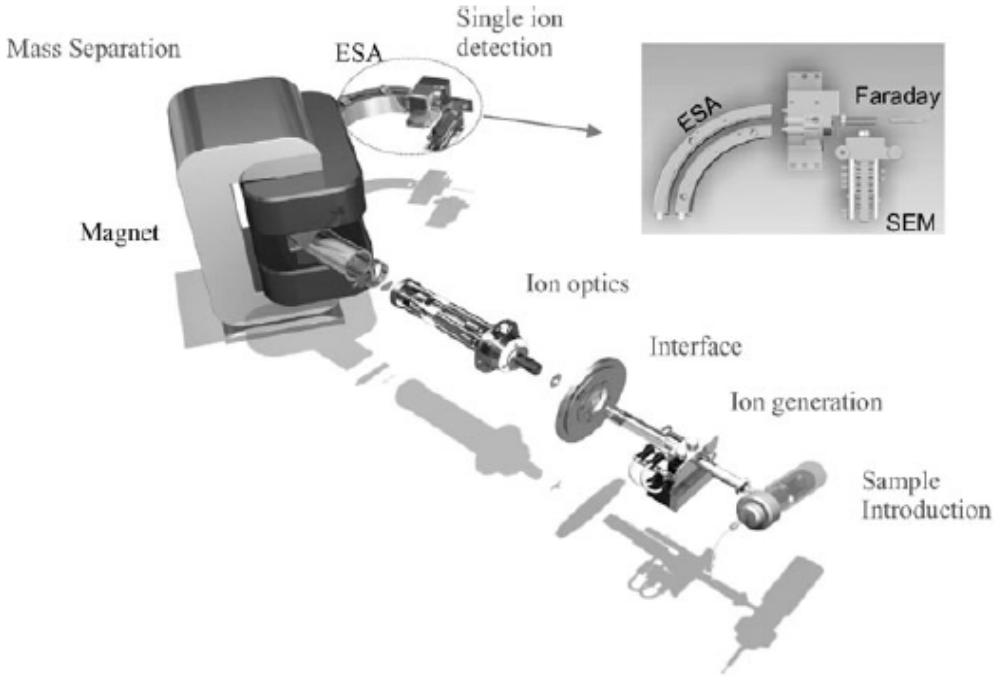

Figure 3.2. Double-focusing sector field ICP-MS (HRSF-ICP-MS, ELEMENT, Thermo, Bremen, Germany) (From Becker, 2005).

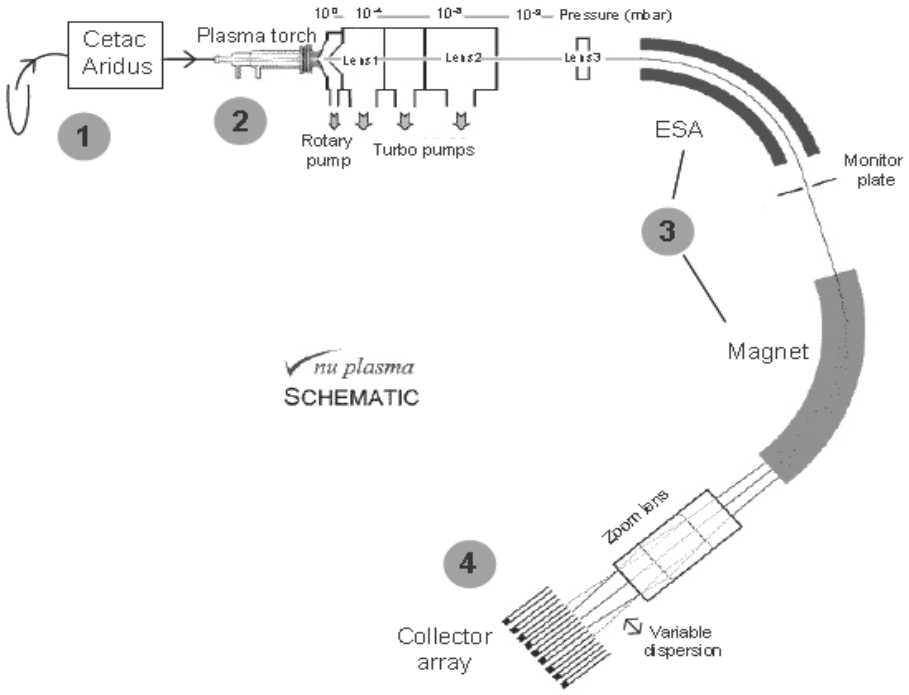

Figure 3.3. Schematic representation of a NuPlasma MC-ICP-MS, with (1) sample introduction system Cetac Aridus desolvating device, (2) Ar-plasma ion source, (3) mass analyzer consisting of ESA and magnet, and (4) detection unit with 12 fixed Faraday detectors (figure adapted from Nu Instruments).

different kinetic energies, to follow different trajectories before and after the mass separation. The mass spectrometer would measure two ions with different masses, although they have the same mass and charge. The double focusing magnetic sector allows to overcome such obstacle. In this device, the ion beam is focused in terms of energy and mass of the ions. The ESA deflects the ions as a function of their kinetic energy, such as slow ions with a lower kinetic energy are more deflected than faster ions. The magnet acts in the opposite sense but with the same magnitude, as it deflects faster ions more than slower ions. The combination of ESA and magnet ensures a good sample focusing on the same collector for similar m/z ratio entering the mass analyzer with different kinetic energy. The magnet needs to be calibrated for each range of masses of interest.

The resolving power (R: resolution) is calculated by the equation: $R = m/\Delta m$, where m is the nominal mass which the peak occurs and m is the mass difference between two resolved peaks. Because a double focusing magnetic sector instrument involves focusing ion angles and ion energies, mass resolution could be achieved by using two mechanical slits – one at the entrance to the mass spectrometer and another at the exit, before the detector. Varying resolution is achieved by scanning the magnetic field under different entrance- and exit-slit width conditions. Low resolution is achieved by using wide slits whereas high resolution is achieved with narrow slits. Varying the width of both the entrance and exit slits effectively changes the operating conditions. Besides high resolving power, another attractive feature of double focusing magnetic-sector instruments is their very high sensitivity combined with extremely low background levels. Another of the recognized benefits of the double focusing magnetic-sector approach is its ability to work with excellent precision. Measurement of the characteristically flat-topped spectral peaks translates directly into high-precision data (*Thomas*, 2002).

One of the main differences between HR-SF-ICP-MS and MC-ICP-MS resides in the detector configuration. HR-SF-ICP-MS has a single collector which perform rapid scan. The analytical performance of these instruments is thus restricted by the sequential measurement of the instable ions beams produced by plasma ionization incidentally implying lower precision (*Rehkämper et al*., 2004). The demand of ultrahigh-precision data, particularly in the field of geochemistry, has led to the development of instruments dedicated to isotope ratio analysis as Si-isotopes. MC-IPC-MS combine ICP source with the magnetic sector analyzer and multiple faraday cup array (multicollector) of Thermal Ionization MS (TIMS). The ICP source ensures excellent ionization efficiency, which is > 80% for most elements of the periodic table (*Rehkämper et al*., 2004). The magnetic sector analyzer (in conjunction with the slits of the ion-optical system) provided the flat-topped peak necessary for high precision isotope ratio measurements. The simultaneous measurements of mass-separated ion beam of several isotopes with multiple faraday cups (n = 12; equipped with $10^{11}\Omega$ resistors) cancels out the degradation of analytical precision due to temporally instable ions beams from the plasma in static mode. The MC-ICP-MS Nu Plasma has a variable dispersion zoom lens system behind the magnetic sector (*Belshaw et al*., 1998). Because the collector coincidences for static measurement of multiple ion beams are adjusted by changing the dispersion of the zoom lens system only, moveable Faraday cups are no longer required.

A significant feature of plasma source mass spectrometry is the large instrumental mass bias, which is related to the preferential extraction and transmission of the heavier ions. The large instrumental mass discrimination of plasma source mass spectrometry is ascribed by many to “space-charge effects” in the plasma and the focusing lens region (*Douglas and Tanner*, 1998; *Rehkämper et al*., 2004) but some debates on where the instrumental mass bias is occurring exist (*Maréchal et al*., 1999; *Rehkämper et al*., 2001). Regardless the origin, the large mass bias associated with plasma ionization clearly requires that mass discrimination is carefully controlled during isotope ratio measurements, if precise and accurate analytical results are to be obtained. Several techniques are available to correct instrumental mass bias. During this thesis, two of them are used: the “standard sample bracketing” and the “external normalization”. Standard sample bracketing technique is realized using alternating standards (with a known isotopic composition) and samples, such that each sample is referenced to the mean of the standards measured immediately before and afterwards. External normalization can be used for stable isotope analyses (*Belshaw et al*., 1998; *Rehkämper and Halliday*, 1998; *Maréchal et al*., 1999) by spiking with an external element close to the mass of the studied element with a constant isotopic composition, to precisely assess the mass. This procedure most commonly employs either a linear, power, or exponential law correction (review in *Rehkämper et al*., 2004). For the natural isotopic composition, both standard sample bracketing (NBS 28 certified standard) and external normalization with Mg using exponential mass bias are realized in dynamic mode (*Cardinal et al*., 2003). For the ^{30}Si-isotopic dilution isotopic measurement, only standard sample bracketing method is done with an unspiked standard (natural isotopic composition) sampled and processed in the same way than the sample (*Fripiat et al*., 2009).

Chapter 4. Measurement of the natural silicon isotopic composition

Before the development of the MC-ICP-MS, the natural silicon isotopic composition was measured with a fluorination line coupled to a gas source isotope ratio mass spectrometer (IRMS). This methodology has allowed reaching a good precision in the middle of nineties (Figure 4.1; *Ding et al*., 1996; *De La Rocha et al*., 1996). Only performed by three laboratories (Tiping Ding at the institute of mineral resources, CAGS in Beijing; Mark Brzezinski and Christina De La Rocha at the University of California, UCSB at Santa Barbara; Melanie Leng at Nottingham, UK), this methodology has a major inconvenient since the gaseous fluoride used is highly explosive which explains the scarcity of the data before 2000. Indeed, except the meteoritic studies presenting larger Si-isotopic fractionation requiring lower precision, only Tiping & collaborators in Beijing have measured earth Si-isotopic composition (mainly on geological reservoir but unfortunately mostly published in Chinese) in the 15 years following the seminal article of *Douthitt* (1982) who measured a large range of earth material samples (rocks, diatoms, phytoliths …). It is only after the work

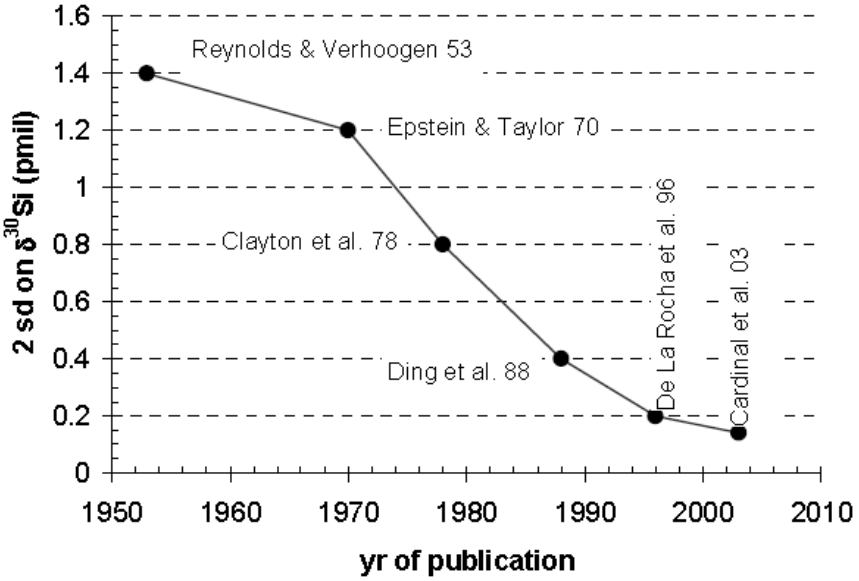

Figure 4.1. Evolution of the precision for Si isotope measurements through time (from Cardinal, 2008).

of *De La Rocha et al*. (1996) adapted from *De Freitas et al*. (1991) which facilitates the sample processing procedures and which allows the measurement of waters, that Si-isotopic application in biogeochemical studies is appeared. This purification involves the reaction of acid molybdate with silicic acid. The resulting silicomolybdic acid is then quantitatively precipitated by reaction with triethylamine hydrochloride. The silicon is recovered as silicon dioxide (SiO_2; mainly cristobalite) through stepwise combustion of the dried precipitate (up to 1000°C). This methodology was at the origin of the marine Si-isotopic studies (*De La Rocha et al*., 1997, 1998, 2000; *Brzezinski et al*., 2002) but the problem posed by fluorination still persists.

Recently, new areas of applications using MC-ICP-MS methodology have been opened with an increasing popularity in earth and environmental sciences for the rapid measurements of isotopic compositions, including silicon isotopes (*De La Rocha*, 2002; *Cardinal et al*., 2003; *Georg et al*., 2006a), at high precision (e.g. Hf, Pb, Ca, Cu, Zn, Mg, Mo, Nd …) (*Walder et al*., 1993; *Halliday et al*., 1998; *Halicz et al*., 1999; *Maréchal et al*., 1999 ; *Galy et al*., 2001 ; *Barling et al*., 2001 ; *Vance and Thirlwall*, 2002). Recent progress also in IRMS involved the conversion of silica to Cs_2SiF_6 by addition of HF and CsCl, followed by decomposition into SiF_4 by addition of sulfuric acid, thus avoiding the use of the direct fluorination method with dangerous BrF_5 reagent (*Brzezinski et al*., 2006). This method has a 0.1‰ precision, comparable to MC-ICP-MS method (*Reynolds et al*., 2007).

4.1 Sample processing for MC-ICP-MS

Before Si-isotopic analysis, samples have to be carefully purified in a clean air environment to avoid Si-contamination. Biogenic silica ($bSiO_2$) is dissolved using NaOH digestion (*Ragueneau et al*., 2005). It consists to extract biogenic silica by a single leaching step in order to minimize potential lithogenic contamination (40 min at 100°C with 0.2 M NaOH). Such alkaline leaching has been shown to extract quantitatively 10-15 µmol Si for every 4 ml NaOH 0.2 M. Dissolved Si from biogenic silica or seawater is then precipitated following the triethylamine molybdate co-precipitation method (*De La Rocha et al*., 1996) adapted from *de Freitas et al*. (1991). Complete Si recovery was monitored in the beginning of this thesis by checking periodically that no detectable amount of silicic acid remained in the water after filtering the molybdate precipitate. After combustion (1000°C) of the silicomolybdate precipitate in covered Pt crucibles, the pure cristobalite phase was transferred to pre-cleaned polypropylene vials and dissolved in a dilute HF/HCl mixture (*Cardinal et al*., 2003).

For silicic acid concentration less than 10 µmol Si l^{-1}, the precipitation protocol is inefficient, so we applied an additional pre-concentration step adapted by *Brzezinski et al*. (2003b) and *Reynolds et al*. (2006) from the MAGIC method (*Karl and Tien*, 1992). It consists of precipitating $Si(OH)_4$ along with brucite ($Mg(OH)_2$) by increasing the pH with ammonium hydroxide (*Brzezinski et al*., 2003b; *Cardinal et al*., 2005) or sodium hydroxide (*Reynolds et al*., 2006). *Cardinal et al*. (2005) and *Reynolds et al*. (2006) report that this method does not fractionate Si-isotopes but underlines the necessity to ensure 100% recovery. The precipitates were recovered either by centrifugation or filtration and redissolved with HCl. Both methods were compared and gave not significantly different results (Chapter 7). On BONUS-Goodhope samples, 22% of the preconcentration (total = 58) give unrealistic light $\delta^{30}Si$ results. This isotopic shift occurs only when initial seawater Si-content is below 1.6 µmol Si l^{-1}, but some replicated values at lower concentration give satisfactory results indicating that bias are not straightforward with the concentration. We first used NaOH (per analysis grade; 0.05% Si; *Reynolds et al*., 2006) but due to the potential Si-contamination at low

Si-concentration, we then used NH_4OH (suprapur; *Brzezinski et al*., 2003b; *Cardinal et al*., 2005) but the problem still persists. There is no difference in chemical composition (measured with ICP-AES) between non- and preconcentred analyte solutions precluding any matrix effect. An alternative cause is the incomplete recovery of $Si(OH)_4$ at low Si-concentration inducing a Si-isotopic fractionation with preferentially adsorption of light Si-isotopes on brucite (in a similar way than with iron oxides; *Delstanche et al*., 2009). It is difficult to measure Si-recovery for such silicon concentration (~0.04 ppm). Assuming a 95% recovery, the residual Si-concentration in the supernatant would be 0.002 ppm. Such very low level of Si-content is still hard to measure using conventional methods. Therefore, we recommend that samples needing pre-concentration to be systematically fully replicated in order to obtain consistent and reproducible $\delta^{30}Si$.

4.2 MC-ICP-MS Si-isotopic measurement

The MC-ICP-MS used has been installed in Brussels in 2001 (at Université Libre de Bruxelles, ULB). Our instrument (Figure 4.2) is a double-focusing MC-ICP-MS Nu Plasma (Nu Instruments, Wrexham, UK) already described in details elsewhere (*Belshaw et al*., 1998; *Young et al*., 2002).

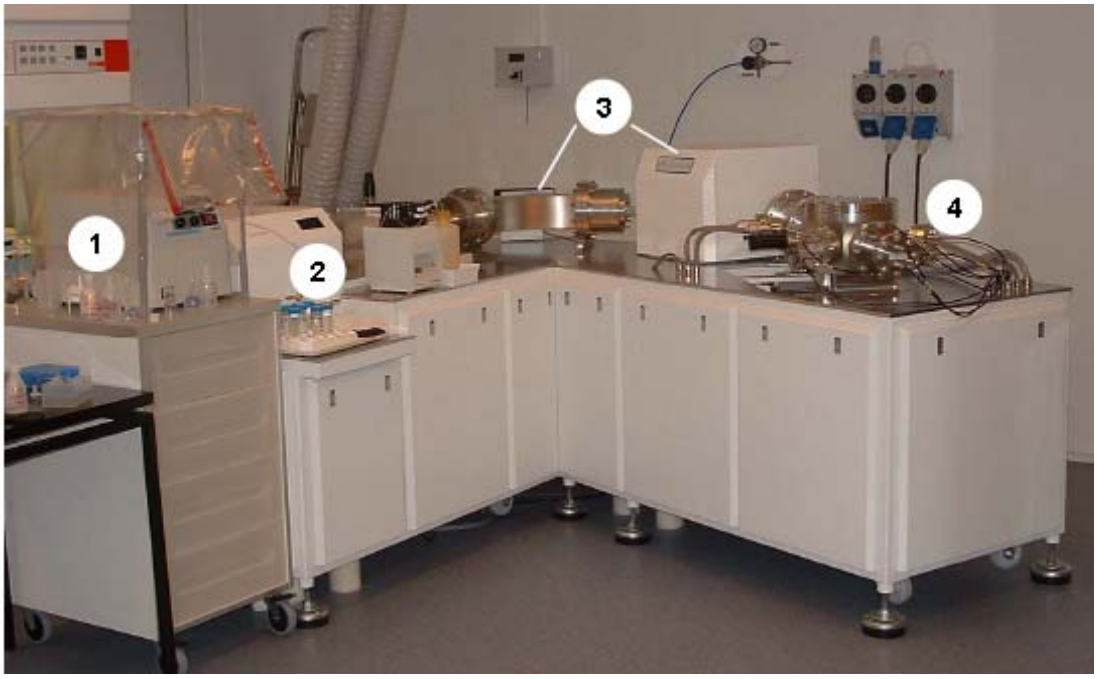

Figure 4.2. NuPlasma MC-ICP-MS in Brussels (ULB), with (1) sample introduction system Cetac Aridus desolvating device, (2) Ar-plasma ion source, (3) mass analyzer consisting of ESA and magnet, and (4) detection unit (From Opfergelt, 2008).

The first methodology dedicated to the measurements of Si-isotopic composition by MC-ICP-MS (*De La Rocha*, 2002) uses a wet plasma, requires solution with high Si content (10 ppm) and is time consuming (40 min by analysis). *Cardinal et al*. (2003) significantly improve the sensitivity and analysis time. In the latter, Si-isotopic measurements were realized in dry plasma mode using a Cetac Aridus desolvating nebulization system and an external normalization with Mg (SRM 980 Mg isotopic standard). Samples are injected into the argon plasma source through this desolvator device equipped with a PFA spray chamber (heated at 105°C) and a PFA microconcentric nebulizer from Elemental Scientific Inc. (Omaha, NE, USA) under free aspiration. The aerosol coming out of the spray chamber is dried through a semi-permeable

Teflon membrane heated at 160°C and conducted to the plasma by an argon flux. The removal of matrix components that could compete for ionization energy in the plasma greatly enhances the sensitivity as compared with wet plasma conditions. For a sample flow rate of 90 µl min^{-1}, the typical ^{28}Si and ^{24}Mg sensitivities are 6 V ppm^{-1} Si and 12 V ppm^{-1} Mg respectively. In comparison, *Cardinal et al*. (2003) find the sensitivity for a wet plasma run at 0.6 V ppm^{-1} Si using a cycling PFA spray chamber and a Polycon nebulizer (600µl min^{-1}) similar to the one obtained by *De La Rocha* (2002). For both studies, the same instrument is used.

Potential molecular interferences are $^{14}N_2$, $^{12}C^{16}O$, for ^{28}Si, $^{14}N_2{}^1H$, $^{12}C^1H^{16}O$, $^{15}N^{14}N$ for ^{29}Si and $^{14}N^{16}O$ for ^{30}Si. The Aridus desolvator drastically reduces the introduction of H_2O, CO_2, O_2 and N_2 into the plasma, thus decreasing the abundance of interfering molecular species. In figure 4.3, interferences measured in dilute HF-HCl solution are shown. The most prominent one is related to $^{14}N^{16}O$ at mass 29.99799, significantly overlying the ^{30}Si peak located nearby at mass 29.97377. This interference represents as much as 10 mV and cannot be eliminated by using the high resolution capacity of the initial Nu Plasma instruments (*De La Rocha*, 2002), or by measuring on the left side of the ^{30}Si flat peak. Therefore, *De La Rocha* (2002) and *Cardinal et al*. (2003) focused on the two lighter isotopes suffering much less from lower isobaric interferences, ^{28}Si found at mass 27.97693 with a small N_2 isobaric interference (usually 2 to 5 mV at mass 28.00615) and ^{29}Si without visible interference. The isotopic values are measured in $\delta^{29}Si$ and need to be converted in $\delta^{30}Si$ with the mass fractionation law (*Young et al*., 2002). This conversion factor slightly varies depending if we use the equilibrium (1.93) or kinetic (1.96) law. To date, the precision and the number of data are not sufficient enough to determine which factor is better. *Georg et al.* (2006b, 2007a) observe that the sample from the river environment, the isotopic fractionation is consistent with the equilibrium law and suggest to use the fractionation factor of 1.93. Nevertheless, the Si-isotopic oceanic distribution seems mainly controlled by Si-uptake, an enzymatic process (*De La Rocha et al*., 2000; *Milligan et al*., 2004). $bSiO_2$ production mediated isotopic fractionation should be a kinetic fractionation suggesting the utilization of the conversion factor of 1.96 for marine Si-isotopic studies.

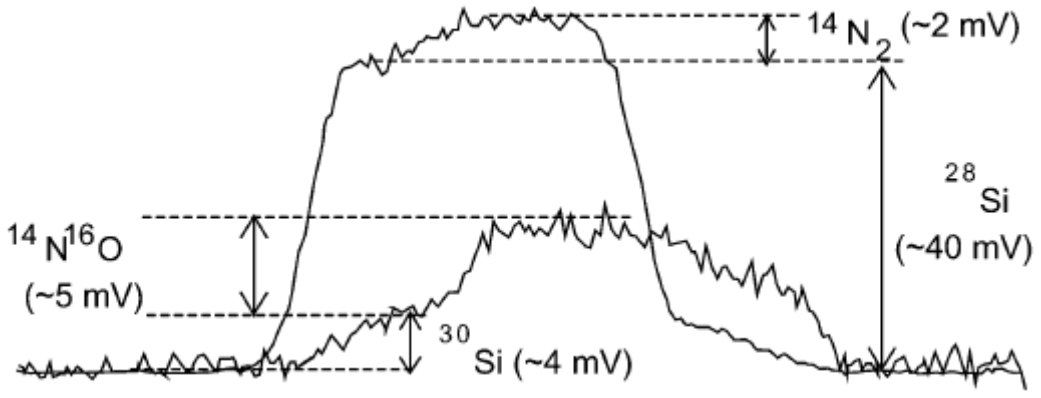

Figure 4.3. Diluted acid blank on the ^{28}Si and ^{30}Si isotopes where $^{14}N_2$ and $^{14}N^{16}O$ interferences are also seen on the left side of the peaks. No interference was observed on ^{29}Si (from Cardinal et al., 2003). Abscissa characterizes the magnet scan mass range on the axial collector.

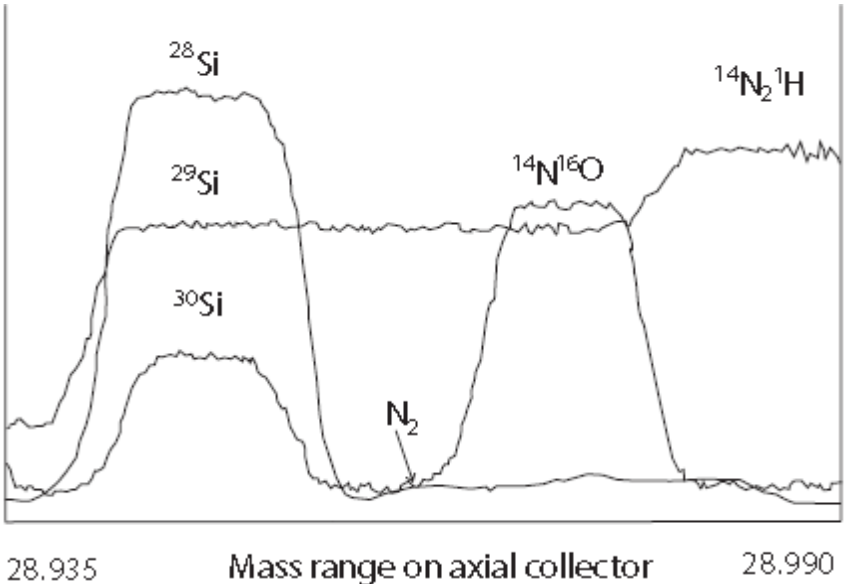

Figure 4.4. Magnet scan of an acid blank solution. Abscissa characterizes the magnet scan range on the axial collector. The ^{29}Si-peak was not separated from its $^{14}N_2{}^1$H interference due to the absence of a collector slit in front of the axial collector. Given that the analysis is centered on the ^{30}Si- and ^{28}Si-peaks, the measurement of ^{29}Si took place on the interference-free left side on the ^{29}Si-peak. Note that the $^{14}N_2{}^1$H interference was much higher, as in Cardinal et al. (2003), who report insignificant levels, probably related to the use of the new pump in combination with B-cones, causing a higher transmission of plasma-entrained atmospheric N into the mass spectrometer (from Abraham et al., 2008).

For ^{30}Si determinations, our Nu Plasma instrument was upgraded with the combination of two sets of adjustable slits (entrance and collector slits), high transmission B type cones and a new vacuum rotary pump (BOC Edwards E2M80), in order to accomplish a compromise between complete interference separation, flat-topped peak shape and sufficient signal intensity on all Si stable isotopes (*Abraham et al*., 2008). For Si isotope measurement, the entrance slit was set at medium resolution. Two collector slits were installed in front of the L4 and H5 faraday cups, where respectively ^{28}Si and ^{30}Si are measured. They were used to clip the interfering $^{14}N_2$ and $^{14}N^{16}O$ ion beams from the ^{28}Si and ^{30}Si beams to achieve full separation from the interference and to help peak-centering the instrument in dynamic mode (Figure 4.4). In the beginning of this thesis, the methodology used was the one from *Cardinal et al*. (2003) and at the end the one of *Abraham et al.* (2008). Chapter 6 on KEOPS cruise, the two methodologies have been used but for chapter 7 on BONUS-Goodhope cruise, only the last methodology has been employed. The operating conditions are presented in the Table 4.1. The isotopic variations were expressed as δ-values in per mil deviation from a reference material (NBS 28 or an in-house reference samples with δ-values not significantly different from 0: $pSiO_2$ or Quartz Merck). We applied mass bias correction using external Mg doping and measured Si and Mg in dynamic mode. In contrast to the low resolution mode (*Cardinal et al*., 2003), the analyte concentration were doubled (Table 4.1; *Abraham et al*., 2008) to compensate for the loss of sensitivity in medium resolution mode. Conversely, in order to minimize the use of HF, which induces a loss of Si in the desolvator (*Cardinal et al*, 2003; *Georg et al*., 2006a), the HF/HCl content was reduced by a factor of ~ 2 in *Abraham et al*. (2008). Silicon-rich sample solutions were diluted and spiked with Mg in order to reach approximately a 1:1 voltage intensity ratio (^{28}Si:^{24}Mg) at the mass spectrometer. HF, HCl, Mg, and Si contents of the running solutions were adjusted daily and kept constant throughout each analytical session.

Parameter	Running conditions
RF power	1350 W
Accelaration voltage	4 kV
Plasma mode	Dry plasma
Introduction system[1]	Cetac Aridus (I) desolvator
Introduction system[2]	Cetac Aridus (II) desolvator
Coolant gas flow rate	13 l min^{-1}
Auxiliary gas flow rate	0.7 l min^{-1}
Nebuliser gas flow rate	0.9 l min^{-1}
Nebuliser type	100 µl min^{-1} PFA microconcentric nebuliser (ESI)
Injector	Alumina injector (Glass expansion)
Cone type[1]	A
Cone type[2]	B
Plasma torch	semi-demountable glass torch
Aridus sweep gas flow rate	3.5 - 7 l min^{-1}
PFA Spray chamber temperature	105°C
Membrane temperature	160°C
Running concentration[1]	Si = 0.8 - 1.25 µg ml^{-1} - Mg = 0.4 - 0.6 µg ml^{-1}
Running concentration[2]	Si = 1.0 - 2.5 µg ml^{-1} - Mg = 0.5- 1.25 µg ml^{-1}
Intensity yields	^{28}Si - ^{24}Mg = 4 - 8 V
Background on HCl-HF [(~ 2 mmol l^{-1})[1] or (~ 1 mmol l^{-1})[2]] running solutions	^{28}Si ~ 50 mV - ^{24}Mg ~ 5 mV
Washout time	7 minutes
Stabilisation time before analysis	7 minutes
Analysis time	20 minutes
Cup configuration	L4 (^{28}Si), Ax (^{29}Si), H5 (^{30}Si), L5 (^{24}Mg), Ax(^{25}Mg), H6 (^{26}Mg)

[1]Cardinal et al. (2003)

[2]Abraham et al. (2008)

Table 4.1. Operating conditions for Si-isotopes determinations with a NuPlasma MC-ICP-MS (adapted from Cardinal et al., 2003 and Abraham et al., 2008).

The standard-sample bracketing technique can adequately correct for the instrumental mass bias present in ICP-MS instruments, long term drift, and is especially needed for light isotopes due to their high fractionation potential. It also has the advantage of cancelling out the Si blank and interferences since both affect the standard and sample almost equally as long as the intensity ratio of the sample and standard are close of the unity. The sample ratio is corrected as follows:

$$\delta^{30}Si = (\delta^{30}Si_1 + \delta^{30}Si_2)/2 \quad (4.1)$$

$$\delta^{30}Si_1 = \left[(^{30}Si/^{28}Si)_{sample}/(^{30}Si/^{28}Si)_{std1} - 1\right] \cdot 1000 \quad (4.2)$$

$$\delta^{30}Si_2 = \left[(^{30}Si/^{28}Si)_{sample}/(^{30}Si/^{28}Si)_{std2} - 1\right] \cdot 1000 \quad (4.3)$$

The instantaneous mass discrimination is corrected using external standardization. The solution is spiked with an external element, with a constant isotopic composition, close to the mass of the studied element, to precisely assess the mass fractionation (*Maréchal et al*., 1999). Mg with its three isotopes, 24, 25, and 26 is the most suitable external standard for silicon (*Cardinal et al*., 2003). Si isotope ratios are corrected with a fractionation factor (f_{Mg}) determined from the results of the ^{25}Mg:^{24}Mg ratio using the exponential mass bias law:

$$f_{Mg} = \ln\left(\frac{\left(\frac{^{25}Mg}{^{24}Mg}\right)_{true}}{\left(\frac{^{25}Mg}{^{24}Mg}\right)_{measured}}\right) \Big/ \ln\left(\frac{mass^{25}Mg}{mass^{24}Mg}\right) \quad (4.4)$$

By considering that the ratio between fractionation of Si and fractionation of Mg is constant during one analytical session (f_{Si}/f_{Mg} = constant), then f_{Mg} is applied to the measured $^{30}Si/^{28}Si$ ratio:

$$\left(\frac{^{30}Si}{^{28}Si}\right)_{true} = \left(\frac{^{30}Si}{^{28}Si}\right)_{measured} \cdot \left(\frac{mass^{30}Si}{mass^{28}Si}\right)^{f} \quad (4.5)$$

During one analytical session, the mass bias fractionation line between Mg isotopes displayed a constant slope around 0.51 (*Galy et al*., 2001; Figure 4.5a). Similarly, the mass bias fractionation line between Mg and Si isotopes has to be monitored for standards during one analytical session, and should display a constant slope during one day. Figure 4.5b displays the measured ratio of $\ln(^{30}Si/^{28}Si)$ vs $\ln(^{25}Mg/^{24}Mg)$ during three distinct analytical sessions (from December 2008 to March 2009). Using the atomic masses of Mg and Si, we can calculate the theoretical slope if $f_{Si} = f_{Mg}$, as assumed in Eq. 4.5:

$$slope = \frac{\ln\left(mass^{30}Si/mass^{28}Si\right)}{\ln\left(mass^{25}Mg/mass^{24}Mg\right)} = 1.690 \quad (4.6)$$

This theoretical slope is plotted in the Figure 4.5b It is obvious that the long-term measurements follow the Eq. 4.6 but shifts either in the slope and/or in the intercept appear between different analytical sessions. Although the linearity is respected (f_{Si}/f_{Mg} is constant during one session), the fractionation coefficients for Mg and Si are not equal and vary between the different analytical sessions as it has been frequently observed also for other external standardization procedures (e.g. *Maréchal et al*., 1999; *Cardinal et al*., 2003). Those variations might be corrected empirically by using the experimental slope on

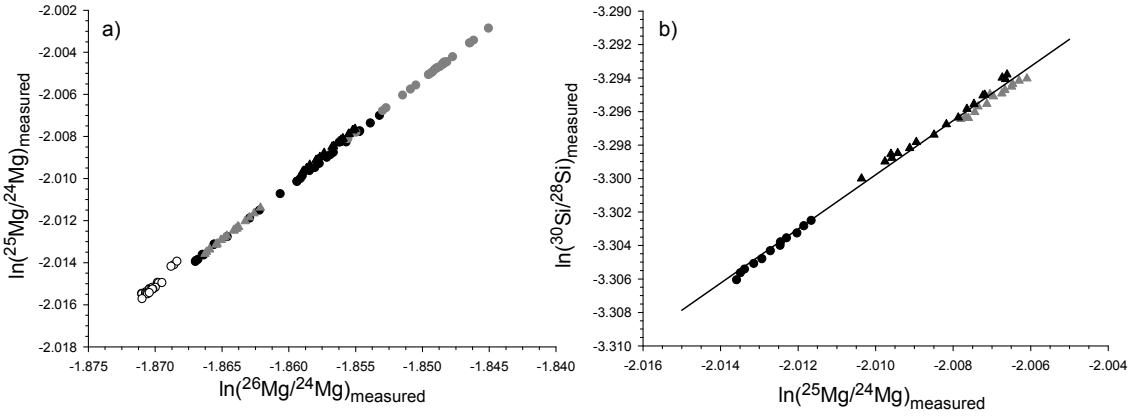

Figure 4.5. (a) Long term plot (December 2008 to March 2009; five analytical sessions) of measured Mg isotope ratio. (b) Long term plot (December 2008 to March 2009; three analytical sessions) of measured Si isotope ratios vs. measured Mg isotope ratios. Symbols represent an analytical session. The straight line represents the theoretical slope (see text).

a daily basis but it has also been demonstrated that such daily corrections can even induce a worse accuracy and reproducibility (*Cardinal et al*., 2003) or have a negligible impact when the standard-sample bracketing technique is used in combination with external normalization.

The average precision and reproducibility of the measurements are ± 0.15 ‰ (± 2 sd) for δ^{30}Si and ± 0.08 ‰ (± 2 sd) for δ^{29}Si. The accuracy of the measurements is checked on a daily basis on secondary reference materials (e.g. Diatomite, big batch) whose Si isotopic compositions are well known from an inter-comparison exercise (e.g. *Reynolds et al*., 2007). We are also involved in the inter-calibration for δ^{30}Si of silicic acid and biogenic silica launched in the framework of the international GEOTRACES project. Preliminary results for silicic acid are already available (*Brzezinski et al*., 2008) and give satisfactory results (Figure 4.6).

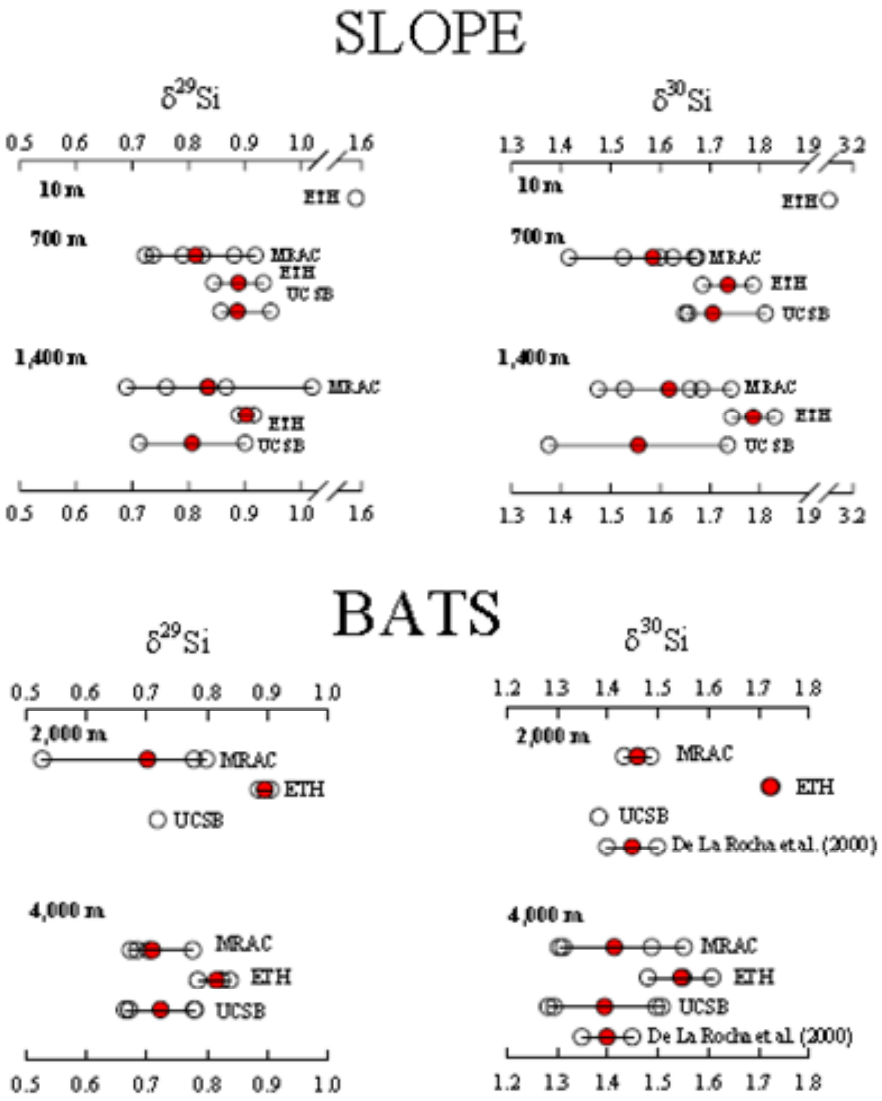

Figure 4.6. Intercomparison exercise during international GEOTRACE projects in Sargasso Sea close of Bermuda (from Brzezinski et al., 2008). MRAC = Musée Royal de l'Afrique Centrale (Belgium); ETH = Eidgenössische Technische Hochschule (Switzerland); UCSB = University of California Santa Barbara (U.S.A.); BATS = Bermuda Atlantic Time Series; Slope = Bermuda continental slope.

Chapter 5. Measurements of production-dissolution rates of marine biogenic silica by ^{30}Si-isotope dilution using a high resolution sector field ICP-MS[1]

Abstract

Regional and seasonal variability of the Si-dissolution rate : Si-production rate ratios in the surface ocean are poorly assessed. Here, we propose a new method for determination of these rates, using the ^{30}Si-isotopic dilution technique with a high resolution sector field inductively coupled plasma mass spectrometer (HR-SF-ICP-MS). Relative analytical precision of the isotopic measurement is better than 1%, similar to the one obtained by thermal ionization - quadrupole mass spectrometer (TIMS). Accuracy and reproducibility of the isotopic measurements have been checked on artificial and natural solutions by intercomparison between two HR-SF-ICP-MS instruments and one TIMS. Measurements of real Si production and dissolution rates are illustrated for two contrasted situations with an average relative precision of 10%, including one from waters with low Si content (2 µmol l^{-1}) which required an additional purification step by cation exchange chromatography. Si production rate from this later incubation was not significantly different from the one measured by radioactive ^{32}Si. The new method is faster and simpler than when using TIMS or isotope ratio mass spectrometer (IRMS). Its sensitivity is more than one order of magnitude better than TIMS and it can cover the whole range of Si concentrations encountered in the ocean.

[1] Adapted from Fripiat F., Corvaisier R., Navez J., Elskens M., Schoemann V., Leblanc K., André L., Cardinal D. (2009). Measuring production-dissolution rates of marine biogenic silica by ^{30}Si-isotope dilution using a high-resolution sector field inductively coupled plasma mass spectrometer. Limnology and Oceanography: methods 7: 470-478.

5.1 Introduction

The silicon (Si) biogeochemical cycle is linked to global CO_2 concentrations through chemical weathering of silicate minerals, which transfers carbon dioxide from the atmosphere to the lithosphere (e.g.*Wollast and Mackenzie*, 1983). Si also affects carbon cycling through production of marine siliceous phytoplankton such as diatoms, a group which has an absolute requirement for Si to build their cell wall (the frustule) and contributes from 25% to 75% of the ocean's total primary productivity (e.g. *Nelson et al.*, 1995; *Tréguer et al.*, 1995). As a result they are a key player in the carbon biological pump (*Buesseler et al.*, 1998; *Smetacek*, 2001) and contribute significantly to atmospheric CO_2 drawdown (*Tréguer and Pondaven*, 2000). They are the only ecologically dominant phytoplankton group requiring silicic acid ($Si(OH)_4$; DSi) for growth, whose availability in surface waters depends on both external inputs (mostly resupply of silicic acid from below the mixed layer or by advection) and internal recycling within the mixed layer. Indeed, very little is known about the exact contribution of this internal recycling to $Si(OH)_4$ availability in surface waters in different ecosystems on seasonal and annual time-scales (*Nelson et al.*, 1995; *Tréguer et al.*, 1995), mainly because accurate biogenic silica ($bSiO_2$) dissolution rates are still difficult to determine. In 2007 only 56 integrated profiles of the silicon budget ($\int D/\int P$) in the surface oceans were available (*Nelson and Goering*, 1977b; *Nelson and Gordon*, 1982; *Nelson et al*., 1981, 1995; *Nelson and Brzezinski*, 1997; *Brzezinski and Nelson*, 1989, 1995; *Brzezinski et al*., 2001, 2003b; *DeMaster et al.*, 1996; *Beucher et al.,* 2004a, 2004b). Therefore, the magnitude of the Si-dissolution rate : Si-production rate ratio (D:P) and its variability are not well defined. This constitutes a major remaining uncertainty in the global marine silica budget.

Since 1973, simultaneous measurements of the production and the dissolution rates of $bSiO_2$ have been performed using the ^{30}Si-isotopic dilution technique (*Goering et al.*, 1973; *Nelson and Goering*, 1977a, 1977b). Samples from the euphotic layer are spiked with $^{30}Si(OH)_4$ and incubated under controlled conditions (mainly temperature and light) for a specified time (usually 24h). The change in isotopic composition of the biogenic silica is used to estimate the production rate by measuring the enrichment in ^{30}Si of the particulate phase. To assess dissolution rates, the increase in ^{28}Si in the dissolved phase due to the dissolution of initial biogenic silica is measured.

Two different methods to measure the enriched isotopic Si compositions have been used so far. The first one developed by *Goering et al.* (1973), *Nelson and Goering* (1977a, b) uses a gas source mass spectrometer and measure abundance of SiF_3^+ ions. This requires the transformation of SiO_2 ($bSiO_2$) into $BaSiF_6$ by HF attack, then ($BaCl_2$) precipitation. For dissolved silicon, a prior extraction and purification of $Si(OH)_4$ into SiO_2 with Triethylamine-Molybdate is required (TEA-Moly, *De Freitas et al*., 1991; *De La Rocha et al*. 1996), or by using an ion-exchange resin (Sephadex) and subsequent transformation in $BaSiF_6$ by Na_2SiF_6 precipitation-HCl dissolution-($BaCl_2$) precipitation (*Brzezinski et al.,* 2003b). These procedures are time-consuming and use HF, which remains harmful. *Corvaisier et al.* (2005) proposed an alternative using thermal ionization - mass spectrometer (TIMS) with a quadrupole (THQ; Thermo, Bremen, Germany) and measure SiO_2^- ions from pure silica deposits. An alkaline digestion for biogenic silica is first applied. Purification and transformation of $Si(OH)_4$ into SiO_2 is performed subsequently following also the TEA-Moly coprecipitation completed by a mineralization at 1100°C. This method avoids the use of HF and allows accurate blank measurements although the procedure is still time-consuming.

Here we describe a new method for the simultaneous determination of the rates of production and dissolution of biogenic silica in the marine environment. We used the same sampling method and the calculation models described in *Corvaisier et al.* (2005) and *Elskens et al*. (2007) but we analyzed the isotopic composition by HR-SF-ICP-MS (Element 2) instead of TIMS or IRMS. Our procedure required a different sample processing protocol than the previous ones, but it is easier, 2-4 times faster, prevents the use of HF and uses HR-SF-ICP-MS instruments which are widespread and available in many laboratories.

5.2 Materials and procedures

5.2.1 Instrumentation

A standard High Resolution Sector Field Inductively Coupled Plasma Mass Spectrometer (HR-SF-ICP-MS, ELEMENT2, Thermo, Bremen, Germany) was used to measure the Si-isotopic abundances as described in equations 1 and 2 for ^{30}Si and ^{28}Si respectively.

$$\text{Atom \% } ^{30}Si = 100x\ [^{30}Si]/([^{28}Si]+[^{29}Si]+[^{30}Si])] \quad (5.1)$$

$$\text{Atom \% } ^{28}Si = 100x\ [^{28}Si]/([^{28}Si]+[^{29}Si]+[^{30}Si])] \quad (5.2)$$

Ionic currents were measured using a secondary electron multiplier in electric scanning mode (E-scan). For accurate determinations, all spectrometric interferences on silicon must be resolved. A mass resolution of 4000 (medium resolution mode of the Element 2) is adequate to avoid all possible interferences, mainly from $^{14}N^{16}O$, $^{12}N_2$ and ^{14}NH (*Klemens and Heumann*, 2001). The sample introduction system combined a glass concentric nebulizer (100 µl/min), a glass jacketed Tracey type cyclonic spray chamber (Glass Expansion, Hawthorn, Australia), a quartz injector and a quartz torch (Thermo, Bremen, Germany). This configuration provided the best blank : sample ratio (less than 10%) even when compared with a Teflon PFA sample introduction system. The HR-SF-ICP-MS operating conditions are summarized in Table 5.1.

Parameters	Running conditions
RF power	1210 W
Plasma gas	16 L min^{-1}
Auxiliary gas flow	1.0 - 1.3 L min^{-1}
Nebulizer gas flow	1.0 - 1.2 L min^{-1}
Sample uptake rate	100 µL min^{-1}
Mass resolution	4500
Acquisition mode	Electric scanning
Isotopes measured	^{28}Si, ^{29}Si, ^{30}Si
Detection mode	Pulse counting mode
Search window	80%
Integration window	40%
Integration type	Average
Time per scan	2.64 s
Number of samples per peak	50
Number of replicates	18 (3 runs, 6 passes)
Sensibility/100ppb Si	1-2 x 10^6 cps
Blank	0.4-2 x 10^5 cps

Table 5.1. Operating conditions of silicon isotope ratio measurement by HR-SF-ICP-MS.

A spectrophotometer (Genesys 10S UV, VWR) was used for quantification of biogenic silica and dissolved silicon concentrations, with a colorimetric method according to *Grasshoff et al.* (1983). The relative precision of the method for concentrations of biogenic silica and dissolved silicon were 10% and 2.5% respectively.

5.2.2 Reagents and standard solutions

All the solutions were prepared with 18 MΩ ultrapure deionised water. All sampling plastic ware (flasks, filtration units, decantation funnels, etc.) were pre-cleaned with 3% HCl (Merck, p.a.). The plastic ware used for the isotopic measurements were pre-cleaned with acid [2 times with distilled HNO_3 6.5% (Merck, p.a.), once with HF/HCl 4.5-3.2 % (Merck, suprapur) and then once with bidistilled HNO_3 6.5% (Merck, p.a.)].

Spike solutions of sodium silicate were prepared after the fusion of ^{30}Si enriched silica powder (99.62 %, Chemgas, Boulogne, France) with anhydrous sodium carbonate (Merck, Suprapur) (*Goering et al.*, 1973). Hot 0.2 M NaOH (Merck, p.a.) was used for alkaline digestion of biogenic silica and 1 M HCl for neutralization thereafter. Brucite co-precipitation adapted from MAGIC [MAGnesium Induced Coprecipitation (*Karl and Tien*, 1992)] in order to preconcentrate dissolved silicon was performed with sodium hydroxide 14 M. The brucite precipitate was re-dissolved in 3 M HCl. HNO_3 65 % and HCl 32% were used for the pre-cleaning of the cation-exchange resin. HNO_3 65 % was used to adjust the acidity of the HR-SF-ICP-MS solution matrix. All acids were bi-distilled or Suprapur grade (Merck).

5.2.3 Sample collection, spiking, and incubation

As described in *Corvaisier et al.* (2005) a variable volume of seawater, dictated by the initial Si content (usually 6 liters) was collected in the euphotic layer. The only difference between the sampling procedure described in *Corvaisier et al.* (2005) and ours resided in the fact that we sampled an additional ~2L of seawater to have a natural silicon isotopic standard (i.e., not spiked with ^{30}Si) to be processed along with the samples. This unspiked sample was immediately filtered (0.6µm, Nuclepore PC membrane) to separate $bSiO_2$ from DSi. The membrane was dried at room temperature under a laminar flow hood or at 50°C in an oven and the filtrate was directly pre-concentrated. These samples were used later on as analytical standards for natural biogenic and dissolved silicon isotopic composition to correct for the matrix effect inducing instrumental mass bias (see next section).

The 4-L sample aliquot was spiked with ^{30}Si in the form of Na_2SiO_3 solution, in a proportion usually lower than 10 % of the ambient DSi concentration. This minimized the perturbation on the natural DSi contents and provided sufficient sensitivity for the isotopic measurements.

After ^{30}Si spiking and gentle mixing, 2 liters were immediately filtered and processed in order to characterize the initial conditions.

The second half of the 4-L aliquot, was poured into a polycarbonate flask and incubated either at temperature and light conditions simulating those prevailing in situ (“on deck” incubation) or in laboratory controlled conditions (“*in vitro*” incubation), usually for 24h. At the end of the incubation period, the sample was filtered and treated as described above in order to characterize the final variables of the incubation.

5.2.4 Digestion of biogenic silica

The material collected on the polycarbonate membranes was digested in one step with 0.2M NaOH during 40 min at 100°C followed by a neutralization with HCl 1M (*Ragueneau et al.,* 2005).

A fraction of the digested sample was used to measure $bSiO_2$ concentration, while another one was diluted to ~100 ppb Si in a bidistilled 0.65% HNO_3 solution for the isotopic measurement.

5.2.5 Preconcentration of dissolved silicon

This preconcentration was achieved with a protocol adapted from the MAGIC method (*Karl and Tien,* 1992): a quantitative scavenging of $Si(OH)_4$ by the brucite [$Mg(OH)_2$] precipitate was obtained by adding 1 ml 14 M NaOH in 1 liter of seawater. *Brzezinski et al.* (2003b) report that this method does not fractionate at the precision level usually required for isotopic dilution experiments and *Cardinal et al.* (2005) have shown it is even suitable for measurements of natural Si isotopic compositions. The precipitate was recovered by filtration (0.8 µm, PC membrane Nuclepore) or by centrifugation and then redissolved in 4.3 ml of 3 M HCl. This step enhanced the Si:salinity ratio of the redissolved solution and reduced the Si-requirement of the whole method because the maximum salinity of the solution that can be introduced in the mass spectrometer is ~ 2 ‰ (see below). An aliquot of this solution was then diluted to ~100 ppb Si in 0.65% HNO_3 and run for the isotopic measurement.

5.2.6 Chromatographic purification of dissolved silicon

As the Si-requirement is both controlled by the maximum salinity (2‰) of the solution that can be introduced in the HR-SF-ICP-MS (mostly to avoid clogging of the cones) on the one hand and by the initial content of DSi in seawater on the other hand, the minimal DSi content in seawater should be ~2.8 µmol l^{-1} for measurement without purification. This estimation takes into account an average HR-SF-ICP-MS sensitivity of 1.10^6 cps/100ppb of Si in solution (Table 5.1) and a salinity of the MAGIC solution of 80 ± 8 ‰ by liter of coprecipitated seawater (average of 132 measurements). For $bSiO_2$, due to the low salinity (~ 10 ‰) of the alkaline digestion solution and the important Si concentration factor of this step (400 times for 2 L filtrated), the Si-requirement was not controlled by the salinity of the digested $bSiO_2$ solutions for the range of $bSiO_2$ concentration encountered in the ocean. In the case of DSi < 2.8 µmol l^{-1}, the salinity

Separatation stage	Solution matrix	Volume (ml)
Pre-cleaning	3 N HCl	3
Pre-cleaning	6 N HCl	3
Pre-cleaning	7 N HNO_3	3
Pre-cleaning	10 N HCl	3
Pre-cleaning	6 N HCl	3
Pre-cleaning	3 N HCl	3
Rinse	MQ-e*	8
		(pH should be neutral)
Sample load	diluted MAGIC solution	2-4 µg Si
Elution	MQ-e	2

* MQ-e is ultrapure deionized water.

Table 5.2. Separation scheme (Georg et al., 2006) of the cation-exchange chromatography applied to the MAGIC solution with low Si content (BioRad AG, 50W-X12, 1.8 mL resin bed).

constraint could be overcome by applying a purification step using the cation-exchange chromatography developed by *Georg et al.* (2006a) for the natural silicon isotopic composition measurements. The Si separation and purification were achieved with the BioRad cation exchange resin DOWEX 50W-X12 (200-400 mesh) in H^+ form, filled to a 1.8 ml resin bed in BioRad columns. The resin was pre-cleaned by several rinses with HCl, HNO_3 and ultrapure deionised water (18MΩ), as detailed in Table 5.2 and described in *Georg et al.* (2006a). Before loading the sample, the eluted water was checked for neutral pH to ensure complete removal of any acid. Since the prevailing Si species do not bind to the resin the elutant is water and silicic acid allowing complete Si recovery, the cation-exchange resin retaining effectively all the ambient cationic species (*Georg et al.*, 2006a).

Per column, 2 to 3.6 µg Si were loaded and purified by ion-exchange chromatography in about 12 h, including all pre-cleaning steps. The number of samples processed simultaneously is dependent on the number of available columns (usually 20-30).

One aliquot of the elutant was taken and diluted to ~100 ppb Si in a bidistilled 0.65% HNO_3 solution for the isotopic measurement.

5.2.7 Isotopic measurements

The solutions of ~100 ppb Si in bidistilled 0.65% HNO_3 were analyzed by HR-SF-ICP-MS to determine the silicon isotopic abundances. A single analysis took 4.5 minutes (2 minutes uptake time and 2.5 minutes analysis) and included 18 measurements (Table 5.1).

We applied the blank-standard-sample bracketing technique to correct for the instrumental mass bias (induced by matrix and temporal drift) and the blank using the linear law. Since the standard (which is the initial unspiked aliquot of the same sample) and the sample have exactly the same matrix, any matrix bias is avoided by the bracketing technique. The blank (ultrapure deionised water (18MΩ) with bidistilled 0.65% HNO_3) was subtracted to the sample. A complete analysis (2 blank, 2 standards, 1 sample) was achieved in less than 20 minutes and an autosampler can be used. No memory effect was observed since each spiked sample was bracketed with a standard bearing a natural isotopic composition and no significant difference was observed between two standards.

5.2.8 Determinations of production and dissolution rates

In order to calculate the flux rates (production and dissolution of biogenic silica, respectively ρ_P and ρ_D) from those measurements, it is necessary to postulate a model. Until now two different models exist, the linear one compartmental model described for production (*Nelson and Goering*, 1977a) and dissolution (*Neslon and Goering*, 1977b), and the nonlinear two compartmental model previously described in *Beucher et al.* (2004a), *de Brauwere et al.* (2005), and in *Elskens et al.* (2007).

The one compartmental model from *Neslon and Goering* (1977a, 1977b) is described respectively for production and dissolution rates by the equations 5.3 and 5.4.

$$\rho_p = [bSiO_2] \cdot \frac{Atom\,\%\ ^{30\text{-}28}Si - bSiO_{2(t)}}{t \cdot Atom\,\%\ ^{30\text{-}28}Si - DSi_{(0)}} \quad (5.3)$$

$$\rho_d = [DSi] \cdot \frac{Atom\,\%\ ^{30\text{-}28}Si\text{-}DSi_{(0)} - Atom\,\%\ ^{30\text{-}28}Si\text{-}DSi_{(t)}}{t \cdot Atom\,\%\ ^{30\text{-}28}Si\text{-}DSi_{(0)}} \quad (5.4)$$

[DSi] and [$bSiO_2$] are the dissolved and biosilica contents, respectively (in µmol l^{-1})

Atom % ^{30,28}Si-DSi and Atom % ^{30,28}Si-$bSiO_2$ are the abundances of ^{30,28}Si in DSi and $bSiO_2$ phases respectively (in Atom %), for the equations (5.3, 5.4, 5.7, 5.8) the abundances represent the abundance in excess (measured minus natural abundances).

Subscripts 0 and t refers to the initial and final samples

t is the incubation time

It is noted, however, that two different analytical solutions were gathered whether considering the sample concentration at the beginning or at the end of the incubation. To correct for these changes in concentration, *Neslon and Goering* (1977a, b) recommend using the geometric mean while calculating the rates.

The nonlinear two compartmental model from *Beucher et al.* (2004a) is described by the equations 5 to 8.

$$[DSi]_{(t)} = [DSi]_{(0)} + (\rho_d - \rho_p) \cdot t \quad (5.5)$$

$$[bSiO_2]_{(t)} = [bSiO_2]_{(0)} + (\rho_p - \rho_d) \cdot t \quad (5.6)$$

$$Atom\,\%\ ^{30\text{-}28}Si\text{-}DSi_{(t)} = Atom\,\%\ ^{30\text{-}28}Si\text{-}DSi_{(0)} \cdot \left(1 + \frac{\rho_d - \rho_p}{[DSi]_{(0)}} \cdot t\right)^{\frac{\rho_d}{\rho_p - \rho_d}} \quad (5.7)$$

$$Atom\,\%\ ^{30\text{-}28}Si\text{-}bSiO_{2(t)} = \frac{Atom\,\%\ ^{30\text{-}28}Si\text{-}DSi_{(0)} \cdot [DSi]_{(0)}}{[bSiO_2]_{(0)} + (\rho_p - \rho_D) \cdot t} \cdot \left(1 - \left(1 + \frac{\rho_D - \rho_P}{[DSi]_{(0)}} \cdot t\right)^{\frac{\rho_p}{\rho_p - \rho_D}}\right) \quad (5.8)$$

These parameters were constrained by the requirement to fit mass and isotopic balances of the dissolved and the particulate phases (i.e., 4 equations for 2 unknowns ρ_D and ρ_P); the best solution being found iteratively by minimizing the cost function for the four equations simultaneously. This model takes into account both isotope dilution and concentration changes occurring in the course of incubation which can induce biases in the estimations (*Elskens et al.,* 2007).

The comparison and the precision of the two models are out scope of this article which describes a new method for the Si-isotopic measurement. A detailed discussion on these issues is developed in *Elskens et al.* (2007).

The development of radioactive ^{32}Si isotope method (*Tréguer et al., 1991*; *Brzezinski and Phillips*, 1997) has significantly improved the measurements of biogenic silica production rates but is not able to measure dissolution rates. When production rates are calculated from ^{32}Si, dissolution rates can be calculated only if the ^{30}Si method is coupled to ^{32}Si method. In such case, equation 4 must be used [as in *Brzezinski et al.* (2001, 2003b)].

5.3 Assessment

5.3.1 Chromatographic purification step

Table 5.3 compares the $^{30\text{-}28}$Si-isotopic abundances for one solution after MAGIC preconcentration step with and without chromatographic purification. The results show that there was no significant difference, providing evidence that the purification step did not introduce any measurable isotopic bias as initially shown by *Georg et al.* (2006a).

	Atom % ^{30}Si (± sd)	rsd (%)	Atom % ^{28}Si (± sd)	rsd (%)	n
without Chromatographic purification[a]	6.37 ± 0.04	0.60	89.12 ± 0.05	0.05	10
with Chromatographic purification[b]	6.40 ± 0.04	0.26	89.09 ± 0.04	0.05	17

The resin was loaded with 500 µL solution diluted to 4 mL. RSD, relative standard deviation.

[a]Ten measurements performed during six analytical sessions over a 4-month period

[b]17 measurements performed during six analytical sessions over a 2-month period

Table 5.3. Average $^{30\text{-}28}$Si isotopic abundance, with absolute and relative standard deviations of the same solution (after MAGIC preconcentration step) without and with chromatographic purification.

5.3.2 Incubation experiments used to determine production and dissolution rates

Two contrasted incubations, including one which required a chromatographic purification step, have been conducted to test the precision and the accuracy of this analytical method. For the incubation 1, a 500 ml laboratory culture of diatoms *Chaetoceros brevis* was grown at 3°C in F/2 medium (*Veldhuis and Admiraal*, 1987; except for saline matrix which was natural seawater) and a 16:8 h light:dark cycle under light intensity of 120 µmol quanta m^{-2} s^{-1} in a incubation cabinet (RUMED). Three weeks after the inoculation, the incubation was spiked with ^{30}Si for 24h. For the incubation 2 (needing the purification step), a ^{30}Si-spiked 4l culture of natural seawater sample at 1% light level in the Antarctic Polar Frontal Zone south of Tasmania was left for 24h in on-deck incubator (SAZ-SENSE cruise onboard of the R/V *Aurora Australis*, summer 2007). The initial and final DSi and $bSiO_2$ concentrations of these incubations are given in the Table 5.4. The incubations were processed as described above.

		DSi ± SD, µmol L^{-1}	$bSiO_2$ ± SD, µmol L^{-1}
Incubation 1	initial	30.4 ± 0.8	9.5 ± 0.9
	final	24.9 ± 0.8	14.4 ± 1.4
Incubation 2	initial	1.98 ± 0.04	1.31 ± 0.13
	final	2.08 ± 0.04	0.89 ± 0.09

Table 5.4. Initial and final bSi_{O2} and DSi concentrations of incubations 1 and 2 to test the method.

In the case of the incubation 2, the spike addition represents ~ +20 % of the ambient DSi concentration, i.e. larger than the targeted spiking rate (< 10%) to avoid an artifact due to the possible disturbance of the ambient DSi availability. This over-spiking is due to the fact that during an oceanographic cruise, the DSi contents of the actual seawater sampled for incubations are usually not available at the time of spiking. Therefore previous data have to be used. During SAZ-SENSE we used the most recent nutrient value available, which was generally analyzed from Niskin samplings performed one day before ours. As implemented during a more recent cruise, it is indeed possible to have actual DSi analyses within 30' after Niskin sampling using an autoanalyser on-board. This permits ensuring that the amount of spike added is

systematically less than 10%. However, as explained later, the larger ^{30}Si addition in incubation 2 does not seem to have increased the measured biogenic silica production rates.

5.3.3 Reproducibility

			$^{30}Si \pm SD$, atom %	RSD, %	$^{28}Si \pm SD$, atom %	RSD, %	n
HR-SF-ICPMS (RMCA)	incubation 1	DSi initial	**10.33 ± 0.05**	0.44	**85.30 ± 0.05**	0.06	10
		DSi final	**10.21 ± 0.03**	0.33	**85.45 ± 0.05**	0.06	10
		$bSiO_2$ final	**5.72 ± 0.06**	1.01	**89.71 ± 0.04**	0.05	10
	incubation 2	DSi initial	**22.02 ± 0.19**	0.85	**74.18 ± 0.12**	0.16	4
			22.03 ± 0.13	0.60	**74.17 ± 0.12**	0.16	3
		DSi final	**19.45 ± 0.09**	0.48	**76.64 ± 0.13**	0.13	4
			19.35 ± 0.06	0.81	**76.73 ± 0.13**	0.13	3
		$bSiO_2$ final	**3.61 ± 0.03**	0.89	**91.74 ± 0.07**	0.07	8
	RMCA natural standard		**3.09 ± 0.01**	0.42	**92.23 ± 0.03**	0.03	30
	artificial solution		**4.00 ± 0.02**	0.58	**91.36 ± 0.03**	0.03	8
HR-SF-ICPMS (IUEM)	artificial solution		**4.03 ± 0.02**	0.50			12
TIMS (IUEM)	IUEM natural standard		**3.07 ± 0.02**	0.65			30

Table 5.5. Average $^{30-28}Si$ isotopic abundances with absolute and relative standard deviations. HR-SF-ICPMS data from incubations 1 and 2 were measured during several analytical sessions spread over several months (n, number of measurement). The two different rows for DSi initial and DSi final of incubation 2 represent complete chemical duplicates (i.e., including chromatography step). The natural standards (seawater for RMCA [Royal Museum for Central Africa, Tervuren, Belgium] and $NaSiO_3$ from Corvaisier et al. 2005 for IUEM [Institut Universitaire Européen de la Mer, Brest, France]) are the average of 30 successive measurements within the same analytical session. Note that natural ^{30}Si and ^{28}Si abundances are 3.09 and 92.23 atom %, respectively (Rossman and Taylor, 1998); abundances or artificial standards are 4.00 and 91.35 atom %, respectively (see text). RSD, relative standard deviation.

The Table 5.5 shows the results and the reproducibility in $^{30-28}Si$ abundance (Atom %) of the incubations and of artificial and natural solutions. The chromatographic step for the incubation 2 was fully duplicated (Table 5.5) and there was no significant difference between the duplicates. The reproducibility of, respectively, the $^{30-28}Si$ isotopic abundance was better than 1% and 0.2% for n ≥ 3 and similar to the one obtained by *Corvaisier et al.* (2005) (Table 5.5). Several Monte Carlo simulations have been run (n = 1000,

				^{30}Si		^{28}Si	
		model		$\rho_p \pm SD$ µmol L^{-1} day^{-1}	$\rho_d \pm SD$ µmol L^{-1} day^{-1}	$\rho_p \pm SD$ µmol L^{-1} day^{-1}	$\rho_d \pm SD$ µmol L^{-1} day^{-1}
incubation 1	^{30}Si	2		5.43 ± 0.57	0.11 ± 0.03	5.59 ± 0.56	0.18 ± 0.09
	^{30}Si	1	initial	3.43 ± 0.39	0.58 ± 0.02	3.47 ± 0.35	0.66 ± 0.02
	^{30}Si	1	final	5.18 ± 0.59	0.47 ± 0.02	5.24 ± 0.53	0.54 ± 0.01
	^{30}Si	1	mean	4.31 ± 0.27	0.52 ± 0.03	4.35 ± 0.22	0.60 ± 0.03
incubation 2	^{30}Si	2		0.032 ± 0.004	0.246 ± 0.019	0.058 ± 0.004	0.241 ± 0.019
	^{30}Si	1	initial	0.036 ± 0.004	0.273 ± 0.011	0.036 ± 0.004	0.274 ± 0.007
	^{30}Si	1	final	0.024 ± 0.003	0.287 ± 0.012	0.024 ± 0.003	0.288 ± 0.007
	^{30}Si	1	mean	0.030 ± 0.006	0.280 ± 0.017	0.030 ± 0.006	0.281 ± 0.013
	^{32}Si			0.027 ± 0.003			

Table 5.6. Production (ρ_p) and dissolution (ρ_d) rates with standard deviations for incubations 1 and 2 with the $^{30-28}Si$ method; production and dissolution rates for both one-compartmental model (model 1) (initial, final, and mean concentration values [Nelson and Goering, 1977a, b]) and two compartmental model (model 2) (Beucher et al., 2004a; de Brauwere et al., 2005; Elskens et al., 2007); production rates for incubation 2 is also given by the ^{32}Si method (Tréguer et al., 1991; Leynaert, 1993).

using a normal distribution) to have an alternative evaluation of the precision of the ^{30}Si isotopic abundance measurements (after the different instrumental corrections). The relative precision obtained was typically 0.5-1.5%, well in the range of the reproducibility (Table 5.5). Since with n≥ 3, the reproducibility was improved to better than 1% we recommend to triplicate the isotopic measurements.

For the incubations 1 and 2 respectively, the reproducibilities of production and dissolution rates given by the models are given in Table 5.6 and were similar to the ones obtained by *Corvaisier et al.* (2005). These standard deviations are satisfactory given the usual temporal and/or spatial range of the production and dissolution rates measured in coastal and/or open ocean ecosystems (*Nelson and Goering*, 1977a, 1977b; Nelson et al., 1981; *Nelson and Gordon*, 1982; *Brzezinski and Nelson*, 1989; *Nelson et al*., 1995; *Brzezinski et al*., 1995, 2001, 2003b; *DeMaster et al.*, 1996; *Beucher et al*., 2004a, 2004b). The two different models described above give similar precision, as previously described in Elskens et al. (2007), independently if we use ^{30}Si or ^{28}Si (Table 5.6). In the case of the two compartmental model, the incubation 1 has a much larger relative uncertainty (30-50%) on Si dissolution rate compared to the one compartmental model (8%) despite the fact that absolute errors are comparable (0.03 vs. 0.02 µmol l^{-1} d^{-1} respectively). This low dissolution rate might be explained by the characteristics of incubation 1: an exponentially growing monospecific culture at low temperature (3°C) free of bacteria and grazers.

5.3.4 Sensitivity

To test empirically if this new method can actually measure a ^{30}Si isotopic difference of 1%, ^{30}Si tracer in increasing amounts was added to the same preconcentrated seawater. A set of 6 solutions ranging from 8.05 to 8.30 Atom % ^{30}Si was prepared (with a ~0.5 % relative ^{30}Si isotopic abundance difference between two consecutive solutions) and analyzed in triplicate (Table 5.7). This table shows that the samples with relative difference of 1% have measured Atom % ^{30}Si abundances significantly different. This empirical demonstration agrees with the reproducibility better than 1% in Table 5.5. The results for the Atom % ^{28}Si values (which are the preferred abundances used for calculation Si dissolution rates with the one compartmental model) present the same trends (Table 5.7) with smaller relative Atom % ^{28}Si abundance variations. Overall, Table 5.7 shows that we are able to differentiate absolute abundance changes at the level of ~ 0.1 Atom % $^{28,30}Si$.

5.3.5 Accuracy

The results for the RMCA standards (natural seawater) showed that the accuracy of the isotopic abundances is good since our average measured on 30 analyses is exactly the one expected from the

^{30}Si ± SD, atom %	^{28}Si ± SD, atom %
8.04 ± 0.03	87.52 ± 0.04
8.07 ± 0.05	87.50 ± 0.05
8.11 ± 0.03	87.44 ± 0.01
8.16 ± 0.03	87.40 ± 0.03
8.21 ± 0.03	87.36 ± 0.02
8.29 ± 0.06	87.27 ± 0.07

Table 5.7. Triplicates (analyzed during the same session) of the same batch of preconcentrated seawater spiked with increasing ^{30}Si amounts. The relative difference between two consecutive solutions prepared is 0.5%, and the abundances measured follow this trend as expected. The measurements are significantly different for a difference of 1% (e.g., between solutions 1 and 3, 2 and 4, etc).

crustal abundance (Table 5.5). It has been further confirmed on artificial solutions prepared by mixing a natural isotopic solution (prepared from dissolution of Na_2SiF_6) with the spike solution (Table 5.5). The solution was measured on two different HR-SF-ICP-MS instruments (RMCA, Tervuren, Belgium and IUEM, Plouzané, France) following the same analytical procedure and gave 4.00 ± 0.02 Atom % and 4.03 ± 0.02 Atom % respectively, which agreed with calculated ^{30}Si abundance of this solution (4.00 %). A third assessment for accurate measurement has been made from the comparison with a parallel incubation using ^{32}Si performed during the SAZ-SENSE cruise by K. Leblanc (COM, Marseille) following the method developed by *Tréguer et al.* (1991) and *Leynaert* (1993). The production rate obtained with the ^{32}Si method on the parallel incubation 2 was 0.027 ± 0.003 µmol l^{-1} Si day^{-1} (Table 5.6) which was in agreement with our estimate (0.032 ± 0.004 µmol l^{-1} Si day^{-1} for the two compartmental model and 0.030 ± 0.006 µmol l^{-1} Si day^{-1} for the one compartmental model). Moreover, this good agreement between ^{32}Si and ^{30}Si methods for incubation 2 provides further evidence that the over-spiking of 20% with ^{30}Si did not affect the production rates.

This is in the lower range of Si-production rate measured in the world ocean. Although this comparison cannot be regarded as an absolute evidence of accuracy, it is so far the first published cross-comparison of the well-established ^{32}Si and ^{30}Si methods and their convergence provides good confidence for the whole ^{30}Si methodology. The analyses are currently underway for the 36 ^{30}Si spiked incubations performed in parallel with ^{32}Si incubations during SAZ-SENSE. The preliminary results are particularly encouraging since for 36 incubations we obtain a slope of 1.0 with a r^2 of 0.85 (not shown). This whole dataset will then permit a better comparison between the two approaches (chapter 8).

Table 5.6 allows to compare the two different models in terms of accuracy. First, the use of ^{30}Si or ^{28}Si to calculate the rates gives not significantly different values. For the incubation 1, the two compartmental model gives higher production rate and lower dissolution rates. It is in agreement with Elskens et al. (2007) who discuss about (1) the potential underestimation of the production rate by the one compartmental model as it does not take into account the increase of DSi due to the dissolution of biogenic silica and, (2) the overestimation of the dissolution rate as it does not take into account the decrease of DSi due to the production of biogenic silica. For the incubation 2, the two models give not

	Volume, L		
	2	**1**	**0.5**
HR-SF-ICP-MS			
DSi, µmol L^{-1}, without chromatographic purification	2.80	2.80	2.80
DSi, µmol L^{-1}, with chromatographic purification	0.04	0.07	0.18
$bSiO_2$, µmol L^{-1}	0.05	0.09	0.18
TIMS			
DSi, µmol L^{-1}	0.50	1.00	2.00
$bSiO_2$, µmol L^{-1}	0.50	1.00	2.00

Table 5.8. Comparison of detection limits for HR-SF-ICP-MS and TIMS as function of volume sampled. These theoretical estimations take into account an average HR-SF-ICP-MS sensitivity of 1.10^6/100 ppb (Table 5.1), the salinity of the MAGIC solution of 80 ± 8‰ per L seawater coprecipitated (average of 132 measurements), the salinity of alkaline digestion (~10‰), the salinity of solution by chromatography, which is less than 0.1‰ (8 measurements), the concentration factor of the alkaline digestion and the MAGIC solution (±400 and 50 respectively), and the Si-requirement per ion-exchange column (2.0 – 3.6 µg Si).

significantly different production rates. In contrast, the one compartmental model seems to overestimate the dissolution rate as discussed above.

5.3.6 Si-requirement

The Si-requirement, as defined above, was controlled both by the maximum salinity (2‰) of the solution that could be introduced in the HR-SF-ICP-MS and the initial content of Si in seawater. For 1 liter of sample, the detection limit of HR-SF-ICP-MS method is more than one order of magnitude better than when using the TIMS (Table 5.8). To obtain the same sensitivity with a TIMS, incubation volumes of 16 l would be necessary which is unrealistic to handle. The detection limit in Table 5.8 cover the whole range of Si content encountered in the ocean since the DSi contents are commonly below 0.5 µmol l^{-1} in the oligotrophic areas such SubTropical gyres and SubAntarctic Zone in late summer. In the case of biogenic silica, we are frequently below 0.5 µmol l^{-1} in diatoms non-growth period in the productive areas and almost every time in the oligotrophic areas.

5.4 Discussion

This new HR-SF-ICP-MS method improves significantly the two former methods using TIMS (*Corvaisier et al. (*2005) or IRMS (*Goering et al.,* 1973*; Nelson and Goering,* 1977a, 1977b) because it is 2, 3 or 4 times quicker (for dissolved silicon with chromatographic purification step, dissolved silicon without chromatographic purification step, and biogenic silica, respectively) and improves the sensitivity by more than one order of magnitude. Indeed a complete analysis takes ~20 minutes (blank-standard-sample-standard-blank) and can be processed with an auto-sampler. The chemical preparation for DSi can be completely processed on board (MAGIC-preconcentration) when the Si-content of the seawater is larger than 2.8 µmol l^{-1}. If not, a complete set of samples (depending on the number of columns available, usually 20-30) can be purified in one working day using the cation-exchange chromatography developed by *Georg et al.* (2006a). For $bSiO_2$, a simple alkaline digestion is applied (*Ragueneau et al.*, 2005). In the case of the pre-existing methods for DSi and $bSiO_2$, the chemical preparation of a limited set of samples takes several days (*Goering et al.*, 1973; *Nelson and Goering*, 1977a, 1977b; *Brzezinski and Nelson*, 1989, 1995; *Brzezinski et al*., 2001, 2003b; *Corvaisier et al.,* 2005). Since these instruments are now widespread it will help to expand the biogenic silica production-dissolution dataset which is currently poorly documented. *In fine* this method will help to improve quantifications of the silicon budget in the surface ocean.

5.5 Comments and recommendations

The analytical method presented here could be easily applicable to measure Si fluxes in environments extremely different from the sole system of marine diatoms. The most direct application would be for studies on freshwater environments (limnology and rivers) where diatoms can also play a major role (*Alleman et al.*, 2005). No chromatographic or MAGIC preconcentration steps are to be expected on such samples since salinity is low and DSi contents usually high. This method could also expand the studies over Si adsorption – desorption processes in batch experiments on sediments (e.g., *Van Cappelen et al.*, 2002) and soils (*Delstanche et al.*, 2009). It should permit more particularly to measure low rates on short time scales. Finally we foresee potential applications to trace the origin and fate of Si in the course of complex processes such as reverse weathering in sediments (*Michalopoulos and Aller,* 2004), the formation of

chemical complexes like hydroxyaluminisilicates (e.g., *Doucet et al.*, 2001) and/or Si uptake, transport and precipitation within higher organisms such as plants, (e.g., *Opfergelt et al., 2006, Carneiro et al., 2008*).

Part III. Natural Silicon isotopic composition

Chapter 6. Isotopic constraints on the Si-biogeochemical cycle of the Antarctic Zone in the Kerguelen area (KEOPS)[2]

Abstract

The estimation of the silicon mass balance in the ocean from direct measurements (Si uptake-dissolution rates) is plagued by their strong temporal and spatial variability. Additional tracers with different sensitivities to physical and biological processes would be of great complementary use. Silicon isotopic composition is a promising proxy to improve our constraint on the Si-biogeochemical cycle since it integrates longer timescale than with direct measurements. Si isotopic signatures of seawater [$Si(OH)_4$] and biogenic silica ($bSiO_2$) were investigated in late summer 2005 during the KEOPS experiment focused on two contrasted biogeochemical areas in the Antarctic Zone: a natural iron fertilized area above the Kerguelen plateau (<500m water depth) and the High Nutrient Low Chlorophyll area (HNLC) East of the plateau (>1000m water depth). Using the Si-isotopic constraint, we identify for the HNLC area the ultimate Si source as being the Upper Circumpolar Deep Water which supplies to the mixed layer, via the Antarctic Surface water (AASW), 4.0 ± 0.7 mol Si m^{-2} each year, representing the net annual $bSiO_2$ production. This is higher than the seasonal depletion estimated from simple mass balance in the mixed layer (2.5 ± 0.2 mol Si m^{-2} yr^{-1}) indicating that some Si-supply (1.5 ± 0.7 mol Si m^{-2} yr^{-1}) occurs during the stratification period. The silicon isotopic composition is mainly controlled by the Si-uptake in surface and mixing below with no significantly influence of $bSiO_2$ dissolution. In contrast, for the fertilized plateau bloom area, a low mixed layer $\Delta^{30}Si$ probably reflects a significant impact of $bSiO_2$ dissolution on the Si isotopic signature. $\delta^{30}Si$ signatures suggest that the HNLC AASW is the most likely source of $Si(OH)_4$ for the plateau. We estimate a net integrated $bSiO_2$ production of 10.5 ± 1.4 mol Si m^{-2} yr^{-1} in the AASW which includes a significant contribution of $bSiO_2$ production below the euphotic layer. Along with silicate pump and iron-light co-limitation, such deep silicification where no photosynthesis occurs, might contribute to the enhanced

[2] Adapted from Fripiat F., Cavagna A.-J., Savoye N., Dehairs F., André L., Cardinal D. (submitted). Isotopic constraints on the Si-biogeochemical cycle of the Antarctic Zone in the Kerguelen area (KEOPS). Marine Chemistry.

depletion of $Si(OH)_4$ compared to NO_3, a characteristic feature in the Antarctic Zone. For the plateau area, our results indicate that Si isotopic fractionation follows an open system for Si supply while they cannot be reconciled with a closed system; for the HNLC area the closed system could not be ruled out though an open system is more likely. Finally, combining the KEOPS Si isotopic data with those of previous studies we refine the average Si isotopic fractionation factor to -1.2 ± 0.2‰ for the Antarctic Circumpolar Current.

6.1 Introduction

The Southern Ocean (SO) plays a major role in the global circulation, redistributing nutrients to the surface layer at the global scale (*Sarmiento et al.*, 2004, 2007) via the upper limb of the meridional circulation (*Trull et al*., 2001). The biogeochemical processes occurring in surface water of the SO have a significant impact on the availability of nutrients in surface water of three-quarters of the global ocean (*Sarmiento et al*., 2004). In the SO, diatoms are key players in the carbon biological pump exporting both biogenic silica ($bSiO_2$) and organic carbon to the deep ocean (*Buesseler et al.*, 1998, 2001). The SO is the largest High-Nutrient Low Chlorophyll (HNLC) area and macronutrients (nitrates and phosphate) concentrations remain high throughout the year across much of the Antarctic Circumpolar Current (ACC). Dissolved silicon mainly present in the form of silicic acid, $Si(OH)_4$ (sometimes referred to as silicate), behaves differently from other macro-nutrients. Unlike nitrate concentration, which remains relatively constant, the region of the ACC between the Antarctic Polar Front (APF) and the Seasonal Ice Zone is marked by an extremely strong latitudinal gradient in $Si(OH)_4$ increasing southward (*Brzezinski et al.*, 2001; *Quéguiner and Brzezinski*, 2002). Surface waters north to the APF are Si-limited during the whole productive season while those south to the front become Si-limited only at the end of the growth season (*Nelson et al.*, 2001). The Si-N decoupling and the HNLC characteristic feature have been attributed to iron, light and Si co-limitations (*Brzezinski et al*., 2005; *De Baar et al.*, 2005; *Boyd et al.*, 2007) along with the processes involved in the so called “silicate pump” (*Dugdale et al.*, 1995).

The KErguelen Ocean and Plateau compared Study (KEOPS) was conducted to investigate a naturally iron-fertilized area located to the south-east of the Kerguelen Islands in the Indian sector of the SO where a well-developed bloom is observed annually (*Mongin et al.*, 2008). Results from KEOPS have provided evidence that deep iron-rich waters supply iron to the surface layer over the Kerguelen Plateau through enhanced vertical mixing triggered by internal wave activities (*Blain et al.*, 2007; *Park et al.*, 2008b).

Due to the strong Si-C coupling in the SO, a better understanding of the Si-biogeochemical cycle is necessary to assess the SO biological carbon pump and the fertility of the waters which are exported out the ACC to the low latitude thermocline. The interpretation of integrated $bSiO_2$ production-dissolution rates and $bSiO_2$ export is plagued by their strong temporal and spatial variability and by artefacts associated with the measurements (e.g., bottle effects, snapshots and or sediment traps biases). The isotopic composition of silicon ($\delta^{30}Si$) is a promising proxy to overcome both spatial and temporal variabilities since it integrates over longer timescales compared to direct measurements and is able to trace back the Si sources. $Si(OH)_4$ uptake by diatoms leaves a clear imprint on the isotopic compositions of both $Si(OH)_4$ and $bSiO_2$. Field studies (*Varela et al.*, 2004; *Alleman et al.*, 2005; *Cardinal et al*., 2005, 2007; *Reynolds et al.*, 2006; *Fripiat et al*., 2007; *Beucher et al*., 2008; *Cavagna et al.,* in revision) and controlled laboratory studies (*De La Rocha et al.*, 1997; *Milligan et al*., 2004) have revealed isotopic fractionation associated with Si-uptake by diatoms due to preferential incorporation of ^{28}Si into $bSiO_2$. The $^{30}\varepsilon$

fractionation factor (-1.1 ± 0.4‰) reported by De La Rocha et al. (1997) seems to be independent of temperature, species (*De La Rocha et al.*, 1997) and cell size (*Cardinal et al.*, 2007). Consequently, $\delta^{30}Si$ signatures of $Si(OH)_4$ or $bSiO_2$ allow to estimate the relative Si-utilisation of the reservoir.

In this study we compare Si isotopic compositions during KEOPS from different water masses above (fertilised area) and outside (HNLC area) the southern Kerguelen Plateau. We then use these signatures to trace the routes of $Si(OH)_4$ supply to the euphotic layer and make an attempt to close the Si-biogeochemical budget in this area.

6.2 Material and methods

6.2.1 The Kerguelen Ocean and Plateau compared Study (KEOPS)

KEOPS cruise was conducted around Kerguelen Islands from 19 January to 13 February 2005, aboard R.V. Marion Dufresne. Using a multiproxy approach to investigate the biological pump under natural iron fertilization by the plateau (*Blain et al.*, 2007), 18 stations from three distinct transects (A, B, C) were sampled, among which 7 stations were sampled for Si-isotopic analyses (Figure 6.1). Each transect covered a wide range of depths from stations above the plateau (bathymetry <500m) to off-plateau stations characteristic of the HNLC area (bathymetry >1000m). Two reference stations, A3 and C11, were respectively defined as representative of the plateau and the HNLC off-plateau area and were visited several times. From satellite-derived Chl-a concentration of the season 2004-2005, the bloom started in early November, reached its maximum in December and collapsed in February. Thus KEOPS took place during the demise of the bloom (*Mongin et al.*, 2008).

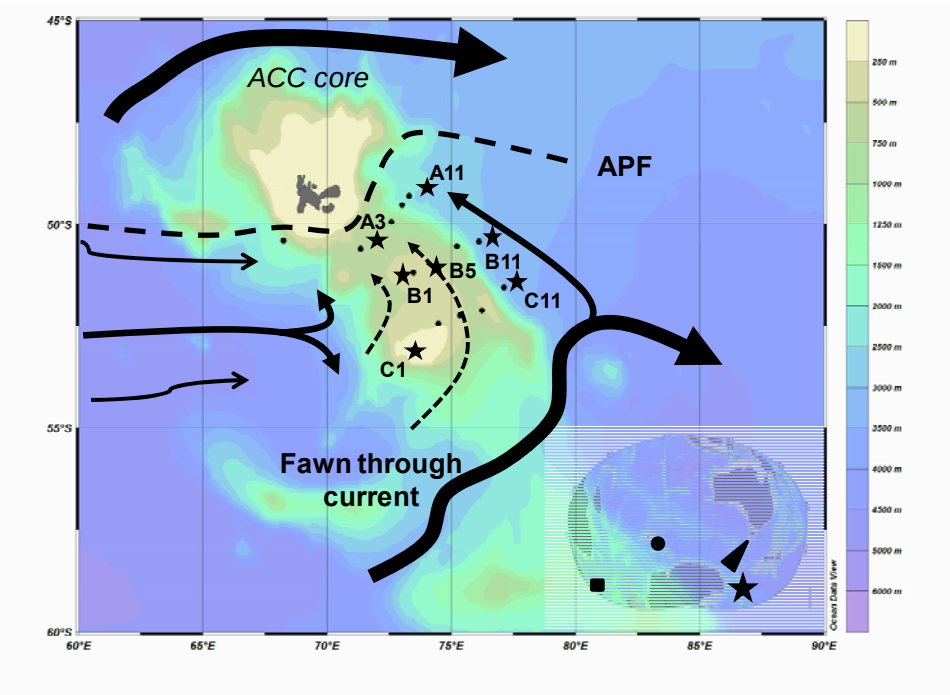

Figure 6.1. Map of the study area with bathymetry and main hydrodynamic features (following Park et al., 2008a; Zhang et al., 2008). The KEOPS stations are represented by the black dots, stars refer to the stations with Si-isotopic signatures available in this study. The hemispheric projection indicates the different Si-isotopic studies in the Southern Ocean: star: Varela et al. (2004); triangle: Cardinal et al. (2005, 2007); square: Cavagna et al. (in revision), and dot: KEOPS (this study). ACC: Antarctic Circumpolar Current; APF: Antarctic Polar Front.

6.2.2 Sampling and analyses

Biogenic silica samples were generally collected for $\delta^{30}Si$ measurement at four depths between surface and ~ 200 m. $Si(OH)_4$ samples were collected for $\delta^{30}Si$ measurement with a higher resolution from the surface to 1000 m, and an additional sample was taken at 2000m.

Seawater was collected using CTD Rosette Niskin bottles. Sampling for silicon isotopic composition of $bSiO_2$ and $Si(OH)_4$ was performed at 7 stations (plateau: A3, B1, B5, C1; off plateau: A11, B11, C11; Figure 6.1). Reference stations A3 and C11 were sampled twice with a sampling time interval of 18 and 10 days respectively. Water samples were immediately filtered on Perspex filtration units under pressure through *0.4 µm polycarbonate membranes to collect $Si(OH)_4$ and stored at room temperature in the dark, in acid*-cleaned polypropylene bottles. The membranes were stored in polycarbonate Petri dishes for $bSiO_2$, and dried overnight at 50°C. Samples were processed at the home-based laboratory (RMCA, Tervuren). Air supplying the filtration units was also filtered with the same type of membranes to avoid particles contamination during filtration.

We applied a wet-alkaline digestion on $bSiO_2$ samples (adapted from *Ragueneau et al.*, 2005), dissolving $bSiO_2$ with a 0.2 µmol l^{-1} NaOH solution (pH 13.3) at 100°C for 40 min. Since this digestion can also dissolve a part of lithogenic silica, we also analyze aluminum in the digested solution, to check possible lithogenic contamination. For all $bSiO_2$ samples, Al remained below the ICP-AES detection limit (0.05 ppm). Taking a Si:Al ratio of 3.74 (*Taylor and McLennan*, 1985) and a $\delta^{30}Si$ ranging from -2 to 0 ‰ for the clays signatures (*Basile-Doelsch,* 2006) the maximum potential contribution of lithogenic Si appears to be negligible (*Cardinal et al.*, 2007).

$Si(OH)_4$ and $bSiO_2$ concentrations were measured on the same samples used for Si isotopic analysis, with a colorimetric method according to *Grasshoff et al.* (1983). Since $Si(OH)_4$ concentrations at stations A3, B1, A11 were too low (<10 µmol Si l^{-1}) to directly apply the Si purification procedure required for Si-isotopic measurements (*De La Rocha et al*., 1996), a $Si(OH)_4$ preconcentration step was performed. It was achieved using a protocol adapted by *Reynolds et al.* (2006) from the MAGIC method (*Karl and Tien,* 1992): a two-step quantitative scavenging of $Si(OH)_4$ by the brucite [$Mg(OH)_2$] precipitate was obtained by adding 20 ml of 1 µmol l^{-1} NaOH per liter of seawater. The precipitate was recovered by filtration (0.8 µm, polycarbonate membrane) and 10 ml of NaOH 1 µmol l^{-1} was again added to the filtrate, and again the precipitate was recovered by filtration (to ensure a 100% recovery). They were then redissolved in 15 ml of HCl 3 µmol l^{-1}.

Silicon was precipitated following the triethylamine molybdate co-precipitation method (*De La Rocha et al.*, 1996). After combustion of the silicomolybdate precipitate in covered Pt crucibles, the pure cristobalite phase was transferred to pre-cleaned polypropylene vials. Dissolution of cristobalite was done in a dilute HF/HCl mixture as described in *Cardinal et al.* (2003).

The isotopic measurements were carried out on a Nu Plasma MC-ICP-MS (ULB-RMCA, Brussels) using Mg external doping in dry plasma mode. Most of the Si-isotopic measurements (78 % of $Si(OH)_4$ samples; 8 % of $bSiO_2$ samples; 55 % of total samples) were performed following the methodology described by *Cardinal et al.* (2003). This method uses a low-resolution mode and cannot resolve the interference on ^{30}Si (mainly due to $^{14}N^{16}O$), and silicon isotopic signatures are measured as $\delta^{29}Si$ only. Following an upgrade of

the Nu Plasma instrument, high resolution and pseudo high resolution could be achieved allowing the measurement of both $\delta^{29}Si$ and $\delta^{30}Si$ as described in *Abraham et al.* (2008). Results will be discussed using the $\delta^{30}Si$ notation only. When only $\delta^{29}Si$ was measured, results have been converted into $\delta^{30}Si$ using the theoretical conversion factor of 1.96 calculated from the kinetic fractionation law (*Young et al.*, 2002) as expected for Si-uptake (section 1.5.1).

The precision and reproducibility (±2sd) of the measurements are ± 0.10 % ($\delta^{29}Si$) and ± 0.15 % ($\delta^{30}Si$). The accuracy of the measurements is checked on a daily basis on secondary reference materials (Diatomite and Big Batch) whose Si isotopic compositions are well known from an inter-comparison exercise (e.g., *Reynolds et al.*, 2007).

6.3 Results

6.3.1 Hydrology and biogeochemical characteristics of the KEOPS area

During KEOPS, the different water masses characteristic of the summer Antarctic Zone (AZ) are present (*Park et al.*, 1998a, 1998b, 2008a). A relatively warm, fresh, well Mixed Layer (ML) caps the subsurface temperature minimum layer, hereinafter referred to as winter water (WW). The WW is the remnant of the former winter ML, thereinafter referred to as Antarctic Surface Water (AASW), capped by seasonal warming and freshening, as shown by time-series observations at station KERFIX southwest of Kerguelen Island (*Park et al*., 1998a). Over the plateau, the geostrophic circulation is relatively sluggish and directed to the northwest parallel to the local bathymetry (Figure 6.1, *Park et al.*, 2008a). All stations were located south of the APF and separated from the direct influence of Kerguelen Island by a strong current (Fig. 6.1), yielding an unproductive area according to satellite images (*Blain et al*., 2007). However, regarding the mesoscale eddy activity of the APF, the northernmost stations (e.g. A11) could have been sporadically influenced by waters from north of the APF (*Mongin et al.*, 2008).

	Stations	$Si(OH)_4$	NO_3[a]	Mixed Layer Depth[b]	Primary production[c]	$bSiO_2$ standing stock[d]	Export production (EP)[e]
		µmol Si l^{-1}	µmol N l^{-1}	m	g C m^{-2} d^{-1}	mmol Si m^{-2}	mg C m^{-2} d^{-1}
bloom area	A1-5 B1-B5	2.1	23.0	70-100	~1	1100 ± 600	222
HNLC area	B9-B11 C transect	27.2	29.4	70-100	~0.3	350 ± 100	85

[a]Autoanlyser onboard

[b]from Park et al., 2008a

[c]integrated on the euphotic layer (from Uitz et al., 2009)

[d]integrated from 0 - 200m (from Mosseri et al., 2008)

[e]export at 125m (from Savoye et al., 2004)

Table 6.1. Biogeochemical properties during KEOPS.

Based on the productivity criteria in *Uitz et al.* (2009), stations A1 to A3 and B1 to B5 are located within the bloom area (hereafter referred to as fertilized bloom area), while off-shelf stations C11 and B11 and the stations at the entrance of the plateau (C1-C7) are located within the HNLC area (Table 6.1). The remaining stations are in between these two contrasted groups (e.g. A11). The fertilised bloom area is characterized by high primary and export production (*Uitz et al., 2009* ; *Savoye et al.*, 2008) as well as high $bSiO_2$ concentrations (*Mosseri et al.*, 2008) (Table 6.1). A massive bloom was observed on the Kerguelen

Plateau in the course of the 2005 austral summer (*Mongin et al.*, 2008). This bloom was almost exclusively composed of relatively large diatoms (*Armand et al.*, 2008). The HNLC area contrasts by its low biogenic silica content, and its low primary and export productions (Table 6.1) (*Mosseri et al.*, 2008; *Savoye et al.*, 2008; *Uitz et al*., 2009).

In the fertilized bloom area low $Si(OH)_4$ coinciding with high NO_3 concentrations indicated a strong decoupling between both nutrients (*Mosseri et al*., 2008), while the HNLC area had high concentrations of both $Si(OH)_4$ and NO_3 (Table 6.1).

6.3.2 Dissolved silicon

Profiles of $Si(OH)_4$ concentration and isotopic composition display a heavier isotopic composition in surface relative to deep waters coinciding with Si-depletion (Table 6.2; Figure 6.2). Similar conditions have been reported earlier for the Atlantic, Southern and Pacific Oceans (*De La Rocha et al*. 2000b; *Cardinal et al.,* 2005; *Reynolds et al.,* 2006; *Beucher et al.* 2008). Such vertical gradients are driven by diatom production combined with vertical mixing (*Cardinal et al*., 2005; *Reynolds et al.,* 2006). For the different water masses identified by *Park et al.* (2008a), average $\delta^{30}Si_{Si(OH)4}$ signatures, were (Table 6.3): ML [0 to ~ 100 m], 2.4 ± 0.3 ‰ (n = 23); WW [~100 to ~400 m], 1.7 ± 0.2 ‰ (n = 32); Upper Circumpolar Deep Water (UCDW) [~400 to ~1400 m], 1.3 ± 0.2 ‰ (n = 16); and Lower Circumpolar Deep Water (LCDW) [~1400 to ~2600; sampling was done only at 2000 m], 1.1 ± 0.2 ‰ (n = 3). These values are in good agreement with previous values reported for the AZ (Table 6.3; see Figure 6.1 for the location of these studies), indicating a wide spatial biogeochemical uniformity of this zone regarding the silicon cycle. Notwithstanding this uniformity, seasonality can be clearly discerned in surface waters. The summer ML $\delta^{30}Si_{Si(OH)4}$ values in the present study (2.4 ± 0.3 ‰ = average of the fertilized bloom and HNLC areas) as well as those obtained during the Atlantic EIFEX expedition (2.6 ± 0.1 ‰; out patch values; summer 2004; *Cavagna et al.,* in revision) are heavier than the spring values reported for the Australian sector: 1.9 ± 0.1 ‰ (*Cardinal et al.*, 2005). This is consistent with the ML becoming more depleted in $Si(OH)_4$ with progress of the growth season yielding to an enrichment of the $Si(OH)_4$ pool in ^{30}Si due to the preferential ^{28}Si-uptake by diatoms and export of these ones. Such a seasonal concentration and isotopic effect was also observed by *Varela et al.* (2004) during a bloom propagating from the APF southward through the Pacific sector of the AZ.

The A3-1, A3-2, B1 stations in the fertilized bloom area had low $Si(OH)_4$ concentrations (on average 2.1 µmol Si l^{-1}) in the ML and heavier $\delta^{30}Si_{Si(OH)4}$ (2.5 to 2.7 ‰) compared to off-shelf stations (Figure 6.2a,b). Station B5, located at the edge of a $Si(OH)_4$ gradient between A3 and C11, is an exception with higher $Si(OH)_4$ concentration reaching 13.9 µmol Si l^{-1} but has similar $\delta^{30}Si_{Si(OH)4}$ values than the other stations in the fertilized bloom area (Figure 6.2b). *Mosseri et al.* (2008) measured the highest biogenic silica production rates at B5. In contrast, biogenic silica production rates at A3 were low and similar to those at station C11 (*Mosseri et al.*, 2008). This situation probably reflects the shift of the bloom from A3 to B5

Depth m	$Si(OH)_4$ µmol Si L^{-1}	$\delta^{30}Si_{Si(OH)4}$ ‰ ± 2sd	n
Station A11 - CTD 11 - 20/01/2005			
49.09°S		74.00°E	
8-76	3.6	2.78 ± 0.12	2
126	22.3	2.08	recalc
151	32.2	2.01 ± 0.15	1
201	41.5	1.62	recalc
202	50.8	1.73 ± 0.13	1
353	61.4	1.31	recalc
403	65.7	1.52	recalc
504	74.8	1.03	recalc
655	79.1	1.41 ± 0.16	1
807	82.9	1.37	recalc
2020	108.0	1.34 ± 0.13	2
Station B11 - CTD 50 - 28/01/2005			
50.30°S		76.60°E	
11	25.9	2.30 ± 0.08	2(*)
52	25.1	2.18 ± 0.13	2(*)
76	25.4	2.14 ± 0.21	2(*)
101	31.6	2.26	recalc
151	42.7	1.68	recalc
201	51.0	1.54	recalc
252	62.5	1.37	recalc
302	67.5	1.46	recalc
403	78.1	1.37	recalc
504	77.7	1.23 ± 0.20	2(*)
654	83.1	1.41	recalc
805	90.4	1.10	recalc
2025	115.0	0.97	2(*)
Station C11 - CTD 42 - 26/01/2005			
51.37°S		77.57°E	
9	25.9	2.28	recalc
49	25.4	2.30	recalc
76	27.3	2.39	recalc
99	30.6	2.12	recalc
151	41.7	1.69	recalc
201	54.4	1.41	recalc
252	59.5	1.41	2 recalc
304	68.6	1.51	2 recalc
353	74.6	1.37	recalc
404	80.3	1.35	recalc
504	82.1	1.26	recalc
555	81.8	1.21	recalc
656	89.8	1.26	recalc
807	90.6	1.42	recalc
2022	111.0	0.91	recalc

Depth m	$Si(OH)_4$ µmol Si L^{-1}	$\delta^{30}Si_{Si(OH)4}$ ‰ ± 2sd	n
Station C11 repeat - CTD 83 - 05/02/2005			
51.37°S		77.57°E	
11	25.7	2.14	recalc
51	26.8	2.30	recalc
74	27.4	1.93	recalc
100	29.1	1.97	recalc
151	43.5	1.56	recalc
202	55.2	1.56	recalc
303	75.2	1.52	recalc
Station A3 - CTD 32 - 23/01/2005			
50.38°S		72.05°E	
0-80	1.6	n.a.	n.a.
151	17.4	2.09	recalc
201	30.2	1.80	recalc
302	48.4	1.79	recalc
352	56.0	1.50	recalc
403	61.6	1.34	recalc
Station A3 repeat - CTD 119 - 12/02/2005			
50.38°S		72.05°E	
12-52	1.3	2.51	2 recalc
151	18.7	2.10	recalc
202	31.3	2.22 ± 0.14	1
353	50.6	1.64	recalc
Station B1 - CTD 68 - 02/02/2005			
51.30°S		73.00°E	
51	2.4	2.67 ± 0.09	1
100	10.6	1.94 ± 0.13	1
127	22.3	2.00 ± 0.07	2(*)
153	27.8	1.94 ± 0.14	2(*)
201	41.0	1.77 ± 0.15	2(*)
300	50.1	1.87 ± 0.08	2
Station B5 - CTD 60 - 30/01/2005			
51.06°S		74.36°E	
11	12.2	2.42	recalc
52	12.1	2.68 ± 0.14	1
77	17.3	2.55	recalc
100	21.1	2.12	recalc
151	33.7	1.68	recalc
201	39.1	1.87	recalc
252	45.8	1.70	recalc
352	59.7	1.30	recalc
404	70.9	1.33	recalc
456	71.0	1.30	recalc
Station C1 - CTD 100 - 08/02/2005			
53.11°S		73.52°E	
10	27.2	1.83	recalc
50	25.7	1.95	recalc
103	25.7	2.08 ± 0.09	2(*)
132	28.1	2.02 ± 0.02	1

Table 6.2. $Si(OH)_4$ concentrations and isotopic compositions. The ML for A11 and A3 repeat represent 2 merged depths. 'n': number of replicates: 'recalc' for single analysis in Low Resolution, '1' for a single analysis in Medium Resolution, '2' for duplicate both in MR, '2(*)' for duplicates with one analysis in LR and one in MR, '2recalc' for duplicates both in LR. The dashed lines indicate the position of the mixed layer depth.

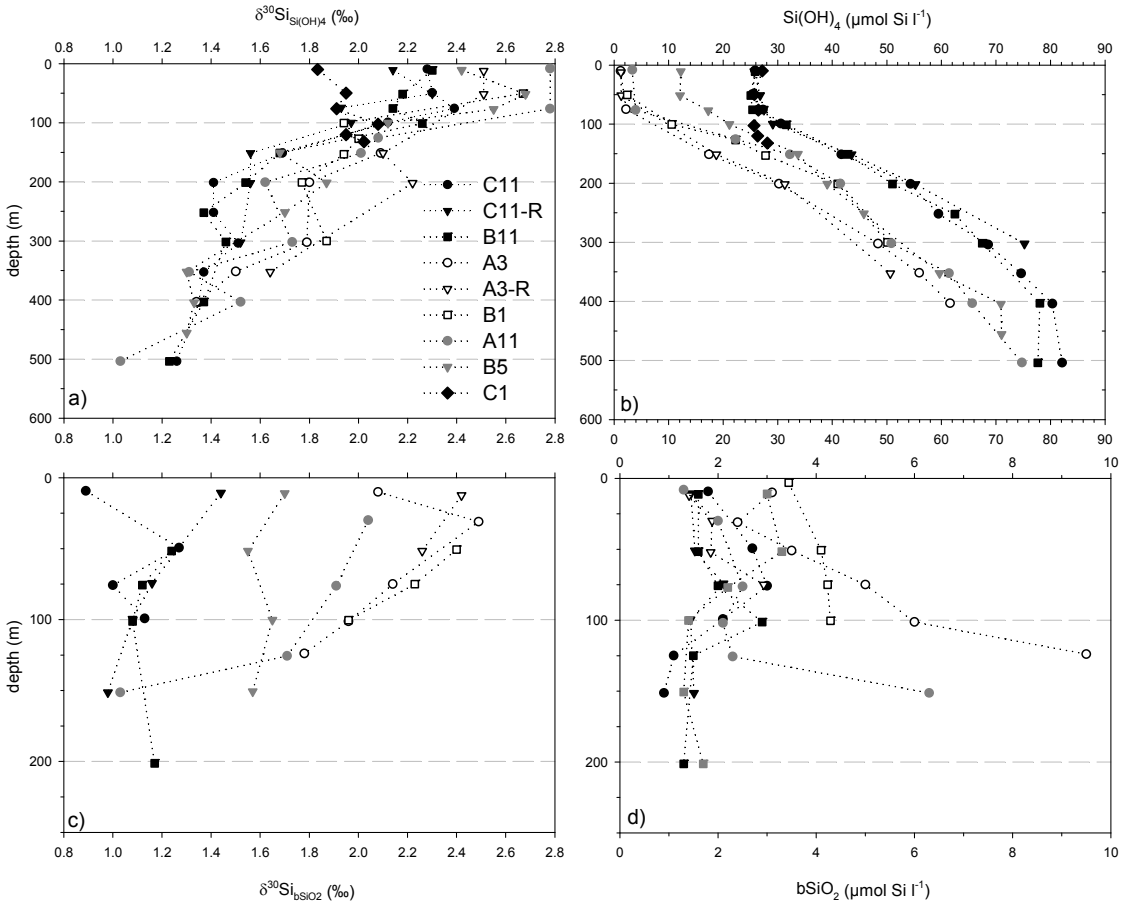

Figure 6.2. Upper 550m profiles for the stations characteristic of the fertilized (plateau) bloom area (white symbols), HNLC area (black symbols), and the two intermediates stations, A11 (grey dots), and B5 (grey triangles). (a) $\delta^{30}Si_{Si(OH)4}$, (b) $Si(OH)_4$ concentration, (c) $\delta^{30}Si_{bSiO2}$, and (d) $bSiO_2$ concentrations. The symbol with standard deviation (±1sd) in the panel (c) represents the average uncertainty of the isotopic measurements. The first two points for $\delta^{30}Si_{Si(OH)4}$ of A11 and A3 are values for merged samples.

observed by satellite images in *Mongin et al*., (2008) and predicted by a phytoplankton class-specific primary production model (*Uitz et al.*, 2009) towards more Si-replete areas.

The low productive HNLC stations C11-1, C11-2, B11 (*Uitz et al*., 2009) are characterized by high ML $Si(OH)_4$ concentrations (~27.2 µmol Si l^{-1}) and light $\delta^{30}Si_{Si(OH)4}$ (2.1 to 2.3 ‰) (Figure 6.2a,b). In contrast, we observed the heaviest ML $\delta^{30}Si_{Si(OH)4}$ (2.8 ± 0.1 ‰) at A11 (Figure 6.2a) coinciding with near complete Si-depletion (4.6 ± 2.6 µmol Si l^{-1}) (Figure 6.2b). The occurrence of such a heavy isotopic signature fits with an advection of Si-depleted water from north of the APF associated with heavier $\delta^{30}Si_{Si(OH)4}$ as observed in previous studies (*Varela et al.*, 2004; *Cardinal et al.*, 2005) and in agreement with a mesoscale eddy activity associated with the APF (*Mongin et al.,* 2008). The low productive station C1 (*Uitz et al*., 2009) at the southern end of the Plateau exhibited lighter $\delta^{30}Si_{Si(OH)4}$ (1.9 ‰) than HNLC area but with similar $Si(OH)_4$ concentration (26.6 µmol Si l^{-1}; Figure 6.2a,b). This station was located close to Heard Islands and the ML was directly in contact with the underlying basalt. Knowing that ocean island basalts bear $\delta^{30}Si_{Si(OH)4}$ of -0.4 ± 0.1 ‰ (*Georg et al*., 2007b), this light isotopic composition probably reflected a significant contribution of dissolving basalt to the $Si(OH)_4$ pool of the ML (also observed with neodynium isotopes, C. Jeandel, pers. comm. 2009). It is so far not possible to determine the contribution of this pool

		KEOPS[a]		EIFEX[b]	CLIVAR SR3[c]	AESOPS[d]	SOFeX[e]
		plateau	out plateau	out patch			
ML	$\delta^{30}Si_{Si(OH)4}$ (‰	2.6 ± 0.2	2.2 ± 0.2	2.6 ± 0.1	1.8 ± 0.2	2.5 ± 0.9	2.1 ± 0.7
	$Si(OH)_4$ (µmol	2.1 ± 0.6	27.2 ± 0.2	10.3 ± 2.4	28.5 ± 0.5	50 - <10	60 - <10
WW	$\delta^{30}Si_{Si(OH)4}$ (‰	1.9 ± 0.1	1.5 ± 0.0	1.6 ± 0.2	1.3 ± 0.2		
	$Si(OH)_4$ (µmol	34.2 ± 1.9	52.5 ± 3.3	37.3 ± 2.8	60.9 ± 9.3		
UCDW	$\delta^{30}Si_{Si(OH)4}$ (‰	1.3 ± 0.2		1.3 ± 0.2	1.3 ± 0.1		
	$Si(OH)_4$ (µmol	78.4 ± 8.5		75.5 ± 3.2	89.8 ± 8.8		
LCDW	$\delta^{30}Si_{Si(OH)4}$ (‰	1.1 ± 0.2			1.1		
	$Si(OH)_4$ (µmol	111.3 ± 3.5			117.2		
$\delta^{30}Si_{bSiO2}$ (‰)							
ML		2.3 ± 0.1	1.2 ± 0.2	1.5 ± 0.4	0.8 ± 0.2	1.2 ± 2.1	1.0 ± 1.6
under ML		1.9 ± 0.1	1.0 ± 0.1		0.7 ± 0.2		

[a]This study, January - February 2005

[b]Cavagna et al., in revision, January - March 2004

[c]Cardinal et al., 2005, 1 profile (61°S), October - December 2001

[d]Varela et al., 2004, AESOPS October 1997 - March 1998, SOFEX January - February 2002

Table 6.3. Average $\delta^{30}Si_{Si(OH)4}$, and $\delta^{30}Si_{bSiO2}$ for different water masses of the Antarctic Zone (± 1sd). ML : Mixed Layer ; WW : Winter Water ; UCDW : Upper Circumpolar Deep Water ; LCDW : Lower Circumpolar Deep Water. See Fig. 6.1 for locations of these studies.

on a single station with few samples since several processes are potentially involved fractionating Si-isotopes from multiple sources: diatom Si-uptake (*De La Rocha et al.*, 1997) and Si-dissolution from basalt and/or $bSiO_2$ (*Demarest et al.*, 2009). For these reasons, this station will not be discussed any further.

The bloom and HNLC areas exhibited significantly different $\delta^{30}Si_{Si(OH)4}$ signatures reflecting different degrees of Si-utilization by diatoms which were dominant throughout KEOPS (*Armand et al.*, 2008). There is a trend in the composition of WW between the fertilized bloom and the HNLC waters (Table 6.3 and Fig. 2a, b). In the fertilized area WW (100 – 400 m water depth) has a lower $Si(OH)_4$ concentration (34.2µmol l^{-1}) and a heavier $\delta^{30}Si_{Si(OH)4}$ composition (1.9‰) than WW in the HNLC area (52.5µmol l^{-1} and 1.5‰).

6.3.3 Biogenic silica

As observed for $\delta^{30}Si_{Si(OH)4}$ the fertilized bloom and HNLC areas differed in mean mixed layer $\delta^{30}Si_{bSiO2}$ (2.3 ± 0.1‰, vs. 1.1 ± 0.1‰, respectively) (Figure 6.2c and Table 6.4). These area averages and errors bars have been calculated based on the mean values for each station. Stations A11 and B5 had intermediate ML Si-isotopic compositions (2.0 ± 0.1‰ and 1.6 ± 0.1‰, respectively) as for $Si(OH)_4$. $\delta^{30}Si_{bSiO2}$ were systematically lighter than $\delta^{30}Si_{Si(OH)4}$, in agreement with the preferential uptake of light Si-isotopes by diatoms (*De La Rocha et al.*, 1997; *Milligan et al.*, 2004; *Varela et al.*, 2004; *Alleman et al.*, 2005; *Cardinal et al.*, 2007, *Cavagna et al.,* in revision) (Tables 6.2,4). The average ML $\Delta^{30}Si$ [= $\delta^{30}Si_{Si(OH)4} - \delta^{30}Si_{bSiO2}$] in the fertilized area (0.3 ± 0.1‰) was lower than in the HNLC area (1.0 ± 0.2‰) with intermediate values at B5 and A11 (0.9 and 0.8‰ respectively) closer from the HNLC value. For the fertilized and the HNLC areas we observe a gradient toward lighter $bSiO_2$ isotopic composition with increasing depth. This is particularly salient for the HNLC area. *Cardinal et al.* (2007) also report a decrease of $\delta^{30}Si_{bSiO2}$ from ML to underlying waters for the PFZ of the Australian sector, while no such feature was observed in the AZ. Below the ML, $\delta^{30}Si_{bSiO2}$ were lighter than the corresponding $\delta^{30}Si_{Si(OH)4}$ by 0.3‰ (B11 and C11), 0.2‰ (B5), 0.0‰ (B1), and 0.4‰ (A11) (Figure 6.2a,c). Such differences were too low to be explained only by in situ growth of diatoms and are in agreement with the fact that at the time of sampling diatoms below the ML

Depth m	$bSiO_2$ µmol Si L^{-1}	$\delta^{30}Si_{bSiO2}$ ‰ ± 2sd	n
Station A11 - CTD 11 - 20/01/2005			
49.09°S		74.00°E	
8	1.3	n.a.	
30	2.0	2.04 ± 0.15	1
76	2.5	1.91 ± 0.13	1
102	2.1	n.a.	
126	2.3	1.71 ± 0.14	1
151	6.3	1.03 ± 0.16	1
Station B11 - CTD 50 - 28/01/2005			
50.30°S		76.60°E	
9	1.5	n.a.	
52	1.6	1.24 ± 0.14	1
76	2.0	1.12 ± 0.16	1
101	2.9	1.08 ± 0.02	2
125	1.3	n.a.	
201	1.3	1.17 ± 0.11	1
Station C11 - CTD 42 - 26/01/2005			
51.37°S		77.57°E	
9	1.8	0.89	recalc
49	2.7	1.24 ± 0.21	2
76	3.0	1.00 ± 0.11	1
99	2.4	1.13 ± 0.13	1
125	1.1	n.a.	
151	0.9	n.a.	
Station C11 repeat - CTD 83 -05/02/2005			
51.37°S		77.57°E	
11	1.5	1.44 ± 0.12	1
51	1.5	n.a.	
74	2.1	1.16	recalc
100	1.4	1.08 ± 0.10	2
151	0.7	0.98 ± 0.15	1

Depth m	$bSiO_2$ µmol Si L^{-1}	$\delta^{30}Si_{bSiO2}$ ‰ ± 2sd	n
Station A3 - CTD 32 - 23/01/2005			
50.38°S		72.05°E	
10	3.1	2.08 ± 0.02	2(*)
31	2.4	2.49 ± 0.22	2(*)
51	3.5	n.a.	
75	5.0	2.14 ± 0.10	1
101	6.0	1.96 ± 0.12	1
124	9.5	1.78 ± 0.12	1
Station A3 repeat - CTD 119 - 12/02/2005			
50.38°S		72.05°E	
12	1.4	2.42 ± 0.16	1
30	1.9	n.a.	
52	1.9	2.26 ± 0.15	1
75	2.9	n.a.	
Station B1 - CTD 68 - 02/02/2005			
51.30°S		73.00°E	
3	3.4	n.a.	
51	4.1	2.4 ± 0.13	2
75	4.2	2.23 ± 0.11	1
100	4.3	1.96 ± 0.14	1
Station B5 - CTD 60 - 30/01/2005			
51.06°S		74.36°E	
11	3.0	1.70 ± 0.15	1
52	3.3	1.55 ± 0.12	1
77	2.2	n.a.	
100	1.4	1.65 ± 0.12	1
151	1.3	1.57 ± 0.12	1
201	1.7	n.a.	

Table 6.4. $bSiO_2$ concentration and isotopic compositions. 'n' : number of replicates : 'recalc' for one analysis in Low Resolution, '1' for one analysis in Medium Resolution, '2' for duplicates both in MR, '2(*)' for duplicates with one analysis in LR and one in MR, '2recalc' for duplicates both in LR. The dashed lines indicate the position of the mixed layer depth.

represented mainly accumulated diatoms that settled out from the surface waters (*Mosseri et al.*, 2008; *Uitz et al*., 2009).

Our $\delta^{30}Si_{bSiO2}$ values are on the heavy side of the reported range for the AZ (Table 6.3). This reflects the fact that the season during KEOPS was already well advanced, with maximal $Si(OH)_4$ depletion and associated enrichment in heavy Si-isotopes in particulate and dissolved Si-phases (*Brzezinski et al*., 2001; *Quéguiner and Brzezinski*, 2002; *Varela et al.,* 2004).

6.4 Discussion

6.4.1 General considerations

The fractionation of Si isotopes during biological production by diatoms could be described using one of two simple models. The Rayleigh model (or closed system model; *De la Rocha et al.*, 1997; *Sigman et al.*,

1999) assumes a closed system (i.e. nutrient consumption is not replenished by external sources) and describes the evolution of the isotopic signatures of $Si(OH)_4$ (Eq. 6.1), instantaneous $bSiO_2$ (Eq. 6.2) and accumulated $bSiO_2$ (Eq.6.3) when a reservoir of $Si(OH)_4$ is consumed and biogenic silica exported:

$$\delta^{30}Si_{Si(OH)4} = \delta^{30}Si_{Si(OH)4\ initial} + {}^{30}\varepsilon \,.\, \ln(f) \quad (6.1)$$

$$\delta^{30}Si_{bSiO2\ inst} = \delta^{30}Si_{Si(OH)4} + {}^{30}\varepsilon \quad (6.2)$$

$$\delta^{30}Si_{bSiO2\ acc} = \delta^{30}Si_{Si(OH)4\ initial} - {}^{30}\varepsilon \,.\, \frac{f.\ln(f)}{1-f} \quad (6.3)$$

In Eqs. (6.1) and (6.3), f is defined by:

$$f = \frac{[Si(OH)_4]_{observed}}{[Si(OH)_4]_{initial}} \quad (6.4)$$

The alternative to the Rayleigh model is the steady state model (or the open system model) in which $Si(OH)_4$ is supplied continuously and partially consumed. In this steady-state model the $Si(OH)_4$ supply equals the sum of the biogenic silica produced-exported and the residual $Si(OH)_4$ exported. *Sigman et al*. (1999) describe this model in detail for nitrate. The evolution of the isotopic signatures in such system is as follows:

$$\delta^{30}Si_{Si(OH)4} = \delta^{30}Si_{Si(OH)4\ initial} - {}^{30}\varepsilon \,.\, (1-f) \quad (6.5)$$

$$\delta^{30}Si_{bSiO2} = \delta^{30}Si_{Si(OH)4\ initial} + {}^{30}\varepsilon \,.\, f \quad (6.6)$$

$$\Delta^{30}Si = \delta^{30}Si_{Si(OH)4} - \delta^{30}Si_{bSiO2} \quad (6.7)$$

$\Delta^{30}Si$ equals ${}^{30}\varepsilon$ when an open system is followed or for the Rayleigh model when $\delta^{30}Si_{bSiO2}$ represents the instantaneous $bSiO_2$ (Eq. 6.2).

The evolution of $\delta^{30}Si_{Si(OH)4}$ vs. $[Si(OH)_4]$ described by the Rayleigh and the steady state models, follows a curved and straight lines, respectively. It is also possible that natural systems proceed in a mixed way, with a part following open system mode and another closed system mode. This would be the case for instance if uptake of the nutrient exceeds supply with a final result being intermediate between those for the theoretical open and closed systems (*Fry*, 2006). Mixing between two water masses with their Si isotopic and concentration characteristics can be calculated with the resulting mixing product falling on a mixing curve defined by the two original end-members (*Albarède*, 1996).

6.4.2 Estimation of the fractionation factor

Only the data for the HNLC off-plateau region will be used here in order to limit possible biases on local ${}^{30}\varepsilon$ estimates induced by larger mixing and difficulties in selecting the appropriate Si-source above the plateau (see section 6.4.4.). Moreover the $bSiO_2$:$Si(OH)_4$ ratio of the HNLC area was much lower than in the fertilised bloom area (Tables 6.2, 4), thus reducing the possible impact of $bSiO_2$ dissolution on the $Si(OH)_4$ isotopic balance in the ML. Using WW $Si(OH)_4$ pool as the Si-source (cf. section 6.4.3.1.), the Rayleigh and the steady state models (Eqs 6.1 and 6.5) we calculate for the HNLC area a ${}^{30}\varepsilon$ of -1.0 ± 0.3‰ and -1.3 ± 0.2‰, respectively.

To date, only four in situ studies have estimated the fractionation factor in the ACC and our estimates are not significantly different: -1.5 ± 0.3‰ (*Varela et al*. 2004), -0.9 ± 0.3 ‰ (*Cardinal et al.,* 2005), -1.3 ± 0.4‰ (*Cardinal et al.,* 2007), and -1.3 ± 0.1‰ (*Cavagna et al.* in revision). This relatively large variability in the fractionation factor probably results from the difficulty in accurately determining Si-source(s) and from mixing of waters having silicic acid pools that have experienced different degrees of biological consumption (*Cardinal et al.*, 2005; *Reynolds et al.*, 2006; *Beucher et al.*, 2008). The estimates reported in *Cardinal et al.* (2007) and *Cavagna et al.* (in revision) are based on $\Delta^{30}Si$. Since $\delta^{30}Si_{bSiO2}$ results from processes which may not be synchronous with those setting $\delta^{30}Si_{Si(OH)4}$ (*Cardinal et al.*, 2007; *Demarest et al.*, 2009), we decided not to include these estimates in the average $^{30}\varepsilon$ for the ACC region, even though differences between different $^{30}\varepsilon$ values are not significant. In addition for the same reasons, we only consider $^{30}\varepsilon$ estimated from $\delta^{30}Si_{Si(OH)4}$ (excluding $\delta^{30}Si_{bSiO2}$) of *Varela et al*. (2004) data. The average $^{30}\varepsilon$ value obtained for the ACC is -1.2 ± 0.2‰ (from this study, *Cardinal et al*. 2005 and $\delta^{30}Si_{Si(OH)4}$ of *Varela et al*., 2004), which is close to the value obtained from *in vitro* incubations under tropical conditions (-1.1 ± 0.4 ‰, *De la Rocha et al.*, 1997).

6.4.3 Si-isotopic constraints in the HNLC area

6.4.3.1 Silicon isotopes dynamics

Figure 6.3a shows the isotopic fractionation trends due to Si-uptake given by the models, taking the WW as the Si-source and using the global ACC $^{30}\varepsilon$ average of -1.2 ± 0.2‰ (see section 6.4.2). The ML $\delta^{30}Si_{Si(OH)4}$ falls on these trends (Figure 6.3a), in agreement with the seasonal evolution of the ML. Since WW is the remnant of the former winter ML [also referred to as Antarctic Surface Water (AASW)] it should represent the initial conditions prevailing before the summer stratification (*Park et al.*, 1998a, 1998b) and the start of the bloom. *Pondaven* et al. (2000a) show this is the case for the AZ in the Indian sector, with early summer – late winter surface ocean $Si(OH)_4$ contents being less than 7% different from the WW $Si(OH)_4$ concentrations. Such a small difference is undetectable in $\delta^{30}Si_{Si(OH)4}$. Therefore for the HNLC area it seems reasonable to consider the prevailing WW Si-pool characteristics conditions as the initial ones. Averages WW $Si(OH)_4$ concentrations and isotopic compositions are 52.5 ± 3.3 µmol l^{-1}; 1.5 ± 0.0 ‰ (Table 6.3).

Figure 6.3a shows that Si-utilisation in the KEOPS HNLC area was not large enough to resolve between steady state and Raleigh operational modes. Since biogenic silica can represent an accumulated or an instantaneous product pool, $\Delta^{30}Si$ (Eq. 6.7) could help determining whether the system operates in Rayleigh or steady state mode. $\Delta^{30}Si$ is 1.0 ± 0.2 ‰, a value not significantly different from the $^{30}\varepsilon$ value for the ACC reported elsewhere (= -1.2 ±0.2 ‰; see section 6.4.2). This similarity between $\Delta^{30}Si$ and $^{30}\varepsilon$ can be achieved either in the steady state configuration or in the Rayleigh configuration when produced biogenic silica does not accumulate in the system (Eq. 6.2). Taking the average ACC $^{30}\varepsilon$ value of (see section 6.4.2) and the Si characteristics of the HNLC WW, the theoretical $\delta^{30}Si$ value of accumulated $bSiO_2$ (Eq. 6.3) should be 0.7 ± 0.2‰, significantly different from the measured $\delta^{30}Si_{bSiO2}$ in the HNLC area (1.1 ± 0.1‰) and thus indicates the biogenic silica in the system rather represents an instantaneous pool. Since the isotopic composition for instantaneous $bSiO_2$ [Rayleigh; Eq. 6.2] and steady state $bSiO_2$ [Eq. 6.6] are similar, the use of $\Delta^{30}Si$ to constrain the dynamics of this system is precluded. However, a closed system for ML Si-pool would hardly persist because of propagation of high internal tide activity above the plateau to the surrounding HNLC areas (*Park et al.,* 2008b) causing turbulence diffusion and vertical mixing events.

Therefore a steady state mode, or at least a combination of Rayleigh and steady state depending of the ratio of Si-supply vs. Si-uptake is more likely.

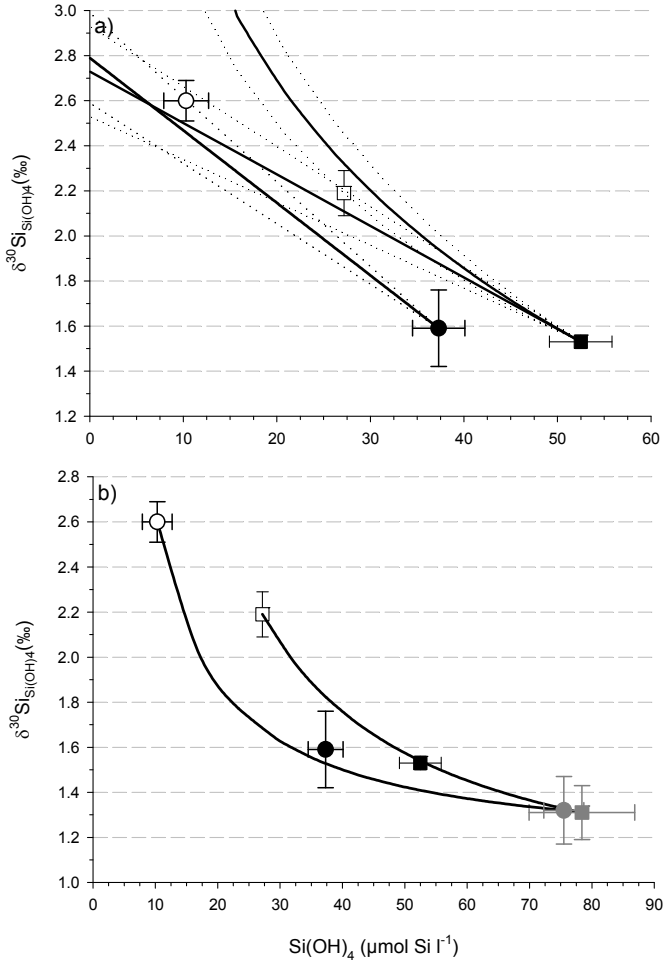

Figure 6.3. $\delta^{30}Si_{Si(OH)4}$ vs. $[Si(OH)_4]$ for the different Si-pools in the HNLC area (±1sd) during KEOPS and EIFEX out patch (Cavagna et al., in revision): (a) fractionation trends following the steady state (straight line) or Rayleigh (curved line) models calculated with HNLC WW as Si-source and an average ACC fractionation factor of -1.2 ± 0.2‰, (b) mixing curves between HNLC ML and UCDW. The square and circle represents KEOPS and EIFEX, respectively; the white, black, and gray symbols represent ML, WW, and UCDW, respectively.

6.4.3.2 Silicon mass balance

Since the KEOPS cruise covered the senescent phase of the bloom (*Blain et al.*, 2007; *Mosseri et al.*, 2008; *Mongin et al.*, 2008), in the following we consider the summer ML conditions to reflect the conditions before overturning ends the stratification. ML and UCDW can thus be considered end-members which, as a result of convective mixing at the onset of winter, will generate a homogenous layer in the upper 400 m (AASW, *Park et al.*, 2008a). In Figure 6.3b we plot the mixing curve between HNLC ML and

UCDW waters. HNLC WW during KEOPS falls perfectly on the mixing curve. The relative mass contribution of the UCDW (= f_{UCDW}) to the AASW can then be estimated with $\delta^{30}Si_{Si(OH)4}$ using Eq. 6.8 (*Fry*, 2006).

$$f_{UCDW} = \frac{\delta^{30}Si_{WW} - \delta^{30}Si_{HNLC-ML}}{\delta^{30}Si_{UCDW} - \delta^{30}Si_{HNLC-ML}} \cdot 100 \quad (6.8)$$

We estimate that UCDW contributes to 78 ± 12 % of the $Si(OH)_4$ standing stock of the HNLC AASW as a result of this mixing. As discussed in the section above, it is most likely that during the stratification period the $Si(OH)_4$ pool in remnant WW is still being supplied from the UCDW below. When integrating the observed WW $Si(OH)_4$ concentration over the whole water layer between surface and WW (i.e. the winter AASW depth range, 0 to 400m; *Park et al.*, 2008a) times the f_{UCDW} (Eq. 6.8), we calculate that UCDW accounts for 16.0 ± 2.8 mol Si m^{-2} to the AASW, of which 25%, i.e. 4.0 ± 0.7 mol Si m^{-2} yr^{-1} replenishes the ML in the upper 100m. Since WW reflects the initial condition for the ML and the fraction f of $Si(OH)_4$ remaining at the time of sampling calculated with Eq. (6.4) is 0.52 ± 0.03, the relative utilisation of the initial $Si(OH)_4$ standing stock in the ML since the start of the productive season is therefore 48 % yielding to a net $Si(OH)_4$ uptake integrated over the mixed layer (0-100 m) of 2.5 ± 0.2 mol Si m^{-2} yr^{-1}. This value is 1.5 ± 0.7 mol Si m^{-2} yr^{-1} lower than the annual UCDW Si-supply to the ML calculated above. Calculated seasonal nutrient depletion in surface water (based on Eq. 6.4) is a lower estimate of annual net $bSiO_2$ production since resupply during the stratified period is ignored (*Wang et al*., 2001). If the system operates in steady state mode (supply equalling export) at seasonal scale, this implies that the effective annual net $bSiO_2$ production is equal to the annual UCDW Si-supply (4.0 ± 0.7 mol Si m^{-2} yr^{-1}). The difference between annual Si-supply from UCDW and seasonal depletion could then represent the Si-supply from WW during the stratified period. This supply is probably sustained by highly dynamical area above Kerguelen plateau propagating to the surrounding area. This annual net $bSiO_2$ production was in the higher range of the previous net $bSiO_2$ production estimates for the AZ (1.3, 1.1, 3.3, 2.4, 0.1, 2.7 mol Si m^{-2} yr^{-1}; *Pondaven et al.*, 1998, 1999, 2000a; *Nelson et al.*, 2002; *Quéguiner et al.*, 2002, *Pollard et al.*, 2006, respectively). *Jin et al*. (2006) diagnosed, using an inverse modelling approach of the nutrients distribution, opal export out the euphotic layer in the Indian sector of the Southern Ocean in a range of 1-5 mol Si m^{-2} yr^{-1} comprising our estimate of net $bSiO_2$ production.

6.4.3.3 Comparison between two HNLC areas (Indian and Atlantic Sectors of SO)

Cavagna et al. (in revision) investigated Si-isotopic composition of biogenic silica and silicic acid during EIFEX, an artificial iron fertilization experiment in a mesoscale cyclonic eddy detached from the APF in the Polar Front Zone with water masses characteristic from the northern part of the AZ (~ 50°S - 2°E). While *Cavagna et al*. (in revision) focused on the temporal variations of the bloom in the artificial Fe fertilized patch of the eddy, we used the EIFEX data out-patch which should represent the cross frontal Si-supply at the APF in late summer 2004 in the Altantic sector. Indeed, EIFEX out-patch waters (Table 6.3) behave in a similar way than KEOPS (Figure 6.3b): seasonal Si-depletion with WW as initial Si-pool = 72 ± 7 %, (Eq. 6.4) or 84 ± 21 % (Eq. 6.5) and mixing line f_{ucdw} = 79 ± 16 % (Eq. 6.8). The relative Si contribution of the UCDW to the AASW is close to ours (78 ± 12 %). To estimate (1) the annual UCDW Si-supply to the AASW and (2) the seasonal Si-depletion in the ML for EIFEX we apply the same assumptions as for the KEOPS HNLC area. The annual UCDW Si-supply is estimated at 2.9 ± 0.6 mol Si m^{-2} yr^{-1} significantly lower than in KEOPS (4.0 ± 0.7 mol Si m^{-2} yr^{-1}). The seasonal Si-depletion was estimated at 2.7 ± 0.4 mol Si m^{-2} yr^{-1}; this is not

significantly different from the annual UCDW Si-supply. In this case, seasonal Si-depletion seems to agree well with net $bSiO_2$ production, i.e. with no significant influence of the Si-supply during the stratification period. This might appear to be in contradiction with *Cavagna et al*. (in revision) who estimated a Si-supply in the fertilized patch from the WW at 6.5 ± 1.1 mmol Si m^{-2} d^{-1}. The sensitivity of our estimations is however not sufficient to determine such small fluxes. Moreover different suspected dynamics between fertilized and unfertilized patch, respectively at the centre and margin of the eddy, preclude further comparison between these two mass balances.

6.4.4 Si-isotopic constraints in the Fe-fertilised area

6.4.4.1 Processes involved in the ML Si-isotopic balance

In contrast to HNLC area, estimates of the fractionation factor on the plateau using the Rayleigh model (Eq. 6.1) are unrealistically low ($^{30}\varepsilon$ smaller than -0.5 ‰) compared to published $^{30}\varepsilon$ estimates, whatever source and conditions considered for the initial Si-pool (UCDW, WW on or off plateau). The plateau ML $\delta^{30}Si_{Si(OH)4}$ falls slightly below the steady state trend but clearly off the Rayleigh trend (Figure 6.4a) which were calculated considering an average ACC $^{30}\varepsilon$ fractionation factor of -1.2 ± 0.2 ‰ (see section 6.4.2) and assuming the plateau WW is the Si-source. This indicates that the Si-isotopic fractionation in the ML does not behave as a closed system on the plateau, probably because of high vertical nutrient input due to high internal wave activity (*Park et al.*, 2008b). Noteworthy the ML fits the steady state fractionation trend when taking HNLC WW as the Si-source instead of plateau WW (Figure 6.4b), suggesting significant ventilation of plateau waters by AASW from HNLC areas located southward. This agrees with the residence time of the water above the plateau of 4 to 9 months (*Venchiarutti et al.,* 2008; *Park et al.,* 2008a) while the length of the growth season in the area is about 3 months (*Mongin et al*., 2008), implying significant water renewal of plateau waters which are advected from the south (*Park et al.*, 2008a). Therefore the whole water mass above the plateau may be significantly ventilated with AASW from the HNLC area over the season's time scale. This condition could explain why HNLC WW represents a more relevant source and initial Si-pool conditions for the plateau ML.

Although the near complete $Si(OH)_4$ utilization in plateau surface waters should have resulted in $\delta^{30}Si_{bSiO2}$ close to the initial $\delta^{30}Si_{Si(OH)4}$ value, the average $\delta^{30}Si_{bSiO2}$ in the ML is 2.3 ± 0.1 ‰ (Table 6.4), significantly heavier than the initial $\delta^{30}Si_{Si(OH)4}$ value (1.9 or 1.5 ‰ for initial condition taken as fertilized or HNLC WW, respectively). For short time scales $\delta^{30}Si_{bSiO2}$ may be controlled by processes which are not synchronous with those controlling $\delta^{30}Si_{Si(OH)4}$, thereby violating the equilibrium assumption needed for approximating $^{30}\varepsilon$ by $\Delta^{30}Si$ (*Wischmeyer et al.*, 2003; *Cardinal et al.*, 2007; *Demarest et al.*, 2009). This may be especially the case for dynamic conditions such as prevailing above the plateau (*Park et al.*, 2008b) where vertical mixing events can bring some light Si-isotopes into the ML (*Wischmeyer et al.*, 2003) but this process cannot explain a $bSiO_2$ isotopic composition heavier than the source. This could be explained in a Rayleigh model with $bSiO_2$ exported and ML $bSiO_2$ representing instantaneous product (Eq. 6.2) but for several reasons discussed above, a closed model cannot explain our $\delta^{30}Si_{Si(OH)4}$ signatures on the plateau. A more likely explanation is dissolution of biogenic silica with preferential release of light Si-isotopes (*Demarest et al.*, 2009). This would partly counteract the isotopic fractionation associated with biogenic silica production and decrease $\Delta^{30}Si$ with $bSiO_2$ and $Si(OH)_4$ isotopic composition becoming heavier and lighter, respectively. It could be especially the case above the plateau because (i) significant heterotrophic activity was taking place (*Lefèvre et al.*, 2008) in a senescent bloom phase (*Blain et al.*, 2007;

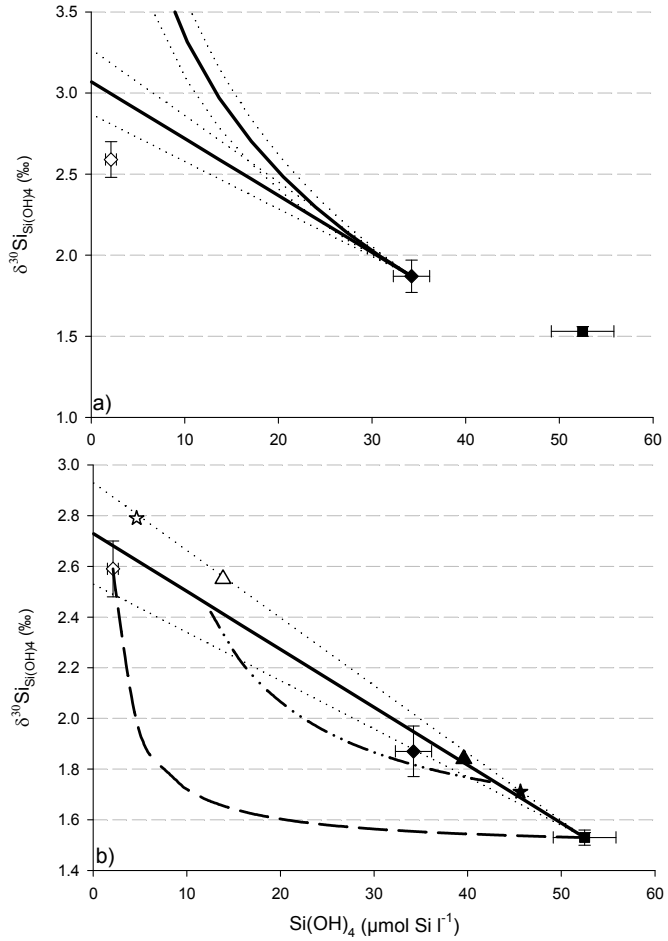

Figure 6.4. $\delta^{30}Si_{Si(OH)4}$ vs. $[Si(OH)_4]$ for the different Si-pools in the HNLC area and in the fertilized (plateau) bloom area (±1sd): (a) Plateau fractionation trends following the steady state (straight line) or Rayleigh (curve) models with fertilized WW as Si-source and the average ACC fractionation factor (-1.2 ± 0.2‰), (b) fractionation trend following the steady state model with HNLC WW as Si-source and the average ACC fractionation factor (-1.2 ± 0.2‰). Mixing lines with HNLC WW and fertilized ML (dashed line). Example of mixing line between hypothetical fertilized ML and a WW having undergone Si uptake (dashed-dotted line). The empty and filled symbols represent respectively ML and WW. The square, diamonds, triangles, and stars represent HNLC, plateau, B5 and A11, respectively.

Mosseri et al., 2007); (ii) dead diatom cells contributed on average to as much as 15 ± 4 % of total diatom cells at A3 (*Armand et al.*, 2008), and (iii) the biogenic silica pool was larger than the $Si(OH)_4$ pool (Tables 6.1, 4; Figure 6.2). At B5 on the contrary the $\Delta^{30}Si$ of 0.9‰ is not significantly different from the ACC $^{30}\varepsilon$ value (-1.2 ± 0.2‰), suggesting that the conditions at B5 are close to steady state. Though a shift of the bloom towards B5 was observed at the end of KEOPS (*Mongin et al.*, 2008), the $bSiO_2$:$Si(OH)_4$ ratio at B5 is 0.2 (compared to 1.5 ± 0.6 for A3-1, A3-2, B1), indicating that at B5 any isotopic effect due to dissolution of biogenic silica was not (yet) significant compared to a relatively larger $Si(OH)_4$ pool. A mixing effect on $\Delta^{30}Si$ should also be less relevant since the concentration difference between surface and subsurface was less significant than at A3.

6.4.4.2 Processes involved in the WW Si-isotopic balance

There is a significant gradient in WW $Si(OH)_4$-pool characteristics between HNLC (52.5 µmol Si l^{-1}, $\delta^{30}Si_{Si(OH)4}$ = 1.5 ± 0.0 ‰) and the fertilized bloom areas (34.2 µmol Si l^{-1}, $\delta^{30}Si_{Si(OH)4}$ = 1.9 ± 0.1 ‰) (Figure 6.2a,b). This gradient in WW $Si(OH)_4$ concentration was also observed from stations on the plateau towards off-plateau stations, the margin stations being intermediate (not shown). This gradient follows the eastward flow out plateau (*Park et al.*, 2008a). It seems to be controlled by isopycnal mixing at the margin of the plateau which represents an interface between altered WW (i.e. with $Si(OH)_4$ concentration and isotopic composition modified) above the plateau and original HNLC WW. Two processes could explain the summer alteration of the WW in the fertilized area.

(1) This gradient could be driven by active (i.e. silicifying) diatoms below the ML inducing a seasonal Si-depletion and $\delta^{30}Si_{Si(OH)4}$ increase in the WW above the plateau. Indeed, a deep $bSiO_2$ maximum was observed during KEOPS, associated with chlorophyll-a maximum (*Mosseri et al.,* 2008; *Uitz et al.,* 2009). This is a recurrent feature in the SO (e.g. *Parslow et al*., 2001; *Holm-Hansen and Hewes*, 2004) and several mechanisms could be responsible for the formation of this feature (*Cullen et al*., 1982; *Quéguiner et al*., 1997; *Parslow et al*., 2001; *Holm-Hansen and Hewes*, 2004). For the KEOPS bloom area *Uitz et al.* (2009) argue that the deep $bSiO_2$ maximum can be explained by the presence of a deep, temperature driven, pycnocline (well below the ML and the euphotic layer) and the sedimentation of living, though inactive algal cells of which the sinking rate was likely under environmental control. *Brzezinski et al*. (1989) report that diatoms can produce substantial amounts of $bSiO_2$ at depths where little or no photosynthesis is taking place. It is in agreement with numerous studies (cf. review by *Martin-Jézéquel et al*., 2000) showing that energy implicated in silicifying process was mainly of respiratory origin and so decoupled from photosynthesis. It is thus possible that the deep $bSiO_2$ maximum observed in the WW below the ML consists also of silicifying diatoms which settled out of the surface waters and accumulated at density gradient as suggested from Figure 6.4b where plateau WW is on the steady state fractionation trend with HNLC WW as Si-source. The ML and WW of stations B5 and A11 also fall on the same fractionation trend (Figure 6.4b). Si-utilization in the ML and WW at B5 is less than in the fertilized area. Since there is a temporal shift of the bloom location in the fertilized area from A3-B1 towards B5 (*Mongin et al.*, 2008; *Mosseri et al.*, 2008) this supports the fact that at B5 the bloom was at a less developed stage than at A3-B1. At A11 we observe a large deep $bSiO_2$ maximum (6.3 µmol l^{-1} at 150m), indicating that WW might also have undergone seasonal Si-uptake (Figure 6.4b).

(2) A mixing between ML and WW should also decrease WW $Si(OH)_4$ concentration and increase WW $\delta^{30}Si_{Si(OH)4}$. We have already indicated that WW HNLC is likely to supply bloom area WW during the growth period. To test the hypothesis of a non Si-uptake at bloom area WW, we plotted on Fig. 4b the mixing line between bloom area ML and HNLC WW. The bloom area WW falls completely out of such mixing line, whereas it is on the steady state fractionation line. Mixing lines with HNLC WW and ML for B5 and A11 also cannot explain their WW Si characteristics. This suggests that Si-uptake in subsurface largely dominates the fertilized bloom area, A11 and B5 WW $Si(OH)_4$ contents and isotopic composition. An example of mixing between ML and WW having undergone Si uptake is also provided on Fig. 4b. Such process cannot be rejected but it is not quantifiable by this approach and would require anyway Si uptake in subsurface.

6.4.4.3 Silicon mass balance

Using HNLC WW characteristics to represent initial conditions (52.5 ± 3.3 µmol l^{-1}; 1.5 ± 0.0 ‰) we estimate the net integrated $bSiO_2$ production in the ML (0-100m) at 5.0 ± 0.3 mol Si m^{-2} yr^{-1}. Such a value is close to total depletion of the surface $Si(OH)_4$-pool, in agreement with a higher uptake of the $Si(OH)_4$ above the fertilized area than in the HNLC area (*Mosseri et al.*, 2008). Using the $Si(OH)_4$ concentration differences in WW between HNLC and fertilized areas we calculate for the sub-euphotic part (WW layer of 100-400m) a net $bSiO_2$ production of 5.5 ± 1.1 mol Si m^2 yr^{-1}. As discussed in the section 6.4.3.2, the use of the Si-depletion to estimate the net $bSiO_2$ production in ML probably leads to an underestimation because of continuous input of silicic acid from deeper layers, particularly important above the plateau (*Park et al.*, 2008b). However, this underestimation should be balanced by an overestimation of the net $bSiO_2$ production in subsurface since both estimates are biased by the same mixing process of ML with WW. From section 6.4.4.2 and Figure 6.4b, it seems that the WW Si-isotopic signature was mainly driven by Si-uptake or at least a combination of mixing and uptake processes. In the HNLC area we estimated the summer Si-supply from HNLC WW was estimated at 1.5 ± 0.7 mol Si m^{-2} yr^{-1}. Since the fertilized area is a more dynamic than the HNLC area (*Park et al*., 2008a), we suggest that the HNLC WW Si-supply could represent a lower estimate for the fertilised area. We can then refine the distribution of annual net $bSiO_2$ production in surface (lower estimation) and subsurface (upper estimation) at respectively, 6.5 ± 0.8 and 4.0 ± 1.4 mol Si m^{-2} yr^{-1}.

Therefore, the total net $bSiO_2$ production in the fertilized area can be calculated summing up our ML and WW estimates, i.e. 10.5 ± 1.4 mol Si m^{-2} yr^{-1}. Compared to previous net $bSiO_2$ production estimation in the Antarctic Zone (1.3, 1.1, 3.3, 2.4, 0.1, 2.7 mol Si m^{-2} yr^{-1}; in *Pondaven et al*., 1998, 1999, 2000a; *Nelson et al.*, 2002; *Quéguiner et al.*, 2002, respectively), the Kerguelen plateau sustained an extremely high integrated net $bSiO_2$ production (see also *Mosseri et al.,* 2008) in the higher range of the opal export estimation for the Southern Ocean (*Jin et al*., 2006). Natural iron fertilization as discussed in *Mosseri et al.* (2008) clearly boosts diatoms productivity as observed in artificial iron fertilization (*de Baar et al*., 2005).

Active diatoms can be brought by vertical mixing event below the ML and/or accumulating at the density gradient (*Uitz et al*., 2009). This process might have significant biogeochemical consequences for Si fluxes and participates to the decoupling between Si and C-N in the Antarctic Zone with preferential depletion of $Si(OH)_4$ with regard to NO_3, along with processes of silicate pump (*Dugdale et al*., 1995) and iron-light co-limitation (*Takeda*, 1998; *Hutchins and Bruland*, 1998; *Claquin et al*., 2002; *Franck et al*., 2003; *Timmermans et al*., 2004; *Leynaert et al*., 2004; *Moore et al*., 2007).

6.5 Conclusions

Two contrasted areas in terms of silicon cycle were studied during KEOPS (KErguelen Ocean and the Plateau compared Study) in the Antarctic Zone: the HNLC area outside the plateau and the natural iron fertilised area above the plateau. Our Si-isotopic data allow a better constraining of the silicon mass budget, by identifying the initial conditions before diatom uptake and the different potential Si-pools involved. Seasonal Si uptake and export could then be calculated by mass and isotopic balances.

In the HNLC area, remnant Winter Water represents the initial Si-pool of the summer Mixed Layer. This Winter Water is supplied in Si by an Upper Circumpolar Deep Water contribution to the Antarctic Surface

Water (AASW) at 4.0 ± 0.7 mol Si m^{-2} yr^{-1} which should represent the annual net $bSiO_2$ production. However, the annual Si-depletion from mass balance is only 2.5 ± 0.2 mol Si m^2 yr^{-1}, i.e. 1.5 ± 0.7 mol Si m^{-2} yr^{-1} lower than the UCDW supply. As the seasonal Si-depletion does not take into account Si-supply during the stratification season, this difference could represent a mixing supply from below the mixed layer, favouring a view of the system behaving more like an open mode with significant continuous Si-supply from WW.

In the natural iron fertilised waters above the Kerguelen plateau, the Si isotopic signatures could not be described by Rayleigh (closed system) equations which provides firm evidence of continuous Si supply to the ML during the growth season. This is in accordance with physics showing that the Kerguelen plateau is a highly dynamic system. HNLC WW represents the most likely Si source (initial conditions). We estimate a net $bSiO_2$ production for the AASW in the bloom area at 10.5 ± 1.3mol Si m^{-2} yr^{-1} with a significant contribution (< 38%) of diatoms silicifying in the deep $bSiO_2$ maximum. Moreover, $\delta^{30}Si_{bSiO2}$ suggests that a significant part of the senescent $bSiO_2$ pool in the Mixed Layer was probably already dissolved. These results strongly support the view of the Southern Ocean as a highly dynamic system with important implications on the biogeochemical Si cycle and call on the preferential use of open model rather than closed system rationale for quantitative paleoceanography reconstructions from $\delta^{30}Si$.

Finally, using the off-plateau KEOPS $\delta^{30}Si_{Si(OH)4}$ where the silicon mass balance is better constrained along with previous studies in the Antarctic Circumpolar Current we refine the ACC fractionation factor estimate ($^{30}\varepsilon$) at -1.2 ± 0.2 ‰.

Chapter 7. Origin and fate of silicic acid pools across the summer Antarctic Circumpolar Current inferred from Si isotopes

Abstract

We report in this study the first isotopic compositions of silicic acid ($\delta^{30}Si$) across the whole summer Antarctic Circumpolar Current and adjacent subsystems, SubTropical Zone and Weddell Gyre, on complete water column profiles (BONUS-Goodhope transect; Feb-March 2008). The results are discussed in terms of sources and fates of the different ACC Si-pools since Si isotopes integrate at the seasonal scale biogenic Si production and dissolution along with mixing processes.

We show that large $\delta^{30}Si$ variations in the Southern Ocean are limited to the upper 1000m reflecting (1) the isopycnal shoaling of the water masses southward (Circumpolar Deep Water), (2) Si-uptake during the northward surface water advection in the Ekman layer, and (3) subsequently spreading and deepening northward to form intermediate water masses (Antarctic Intermediate Water and SubAntarctic Mode Water). During the circumpolar eastward pathway, biogenic silica dissolution is likely to be responsible for the progressive lightening of the $\delta^{30}Si$ of Circumpolar Deep Water. This isotopic imprint is then transmitted to the surface and intermediate water masses which Si-supplied by CDW. Si-isotopes track these processes and are in agreement with the current understanding of Southern Ocean physics.

Relatively simple mass and isotopic balances assuming steady-state at the an annual time scale for the Antarctic Surface Waters have been performed and have allowed to estimate the following Si-fluxes: annual Upper Circumpolar Deep Water Si-supply to AASW corresponding to the annual $bSiO_2$ production and summer Si-supply from the imbalance between seasonal mixed layer Si-depletion and annual $bSiO_2$ production estimates. Annual and summer Si-supplies increase progressively from respectively 2.9 to 6.0 and 0.2 to 3.6 mmol Si l^{-1} from Antarctic Polar Front to Weddell Gyre reflecting probably the isopycnal shoaling of the CDW with increasing silicic acid content southward..

Estimation of fractionation factor across the ACC from BONUS-Goodhope section is similar (-1.2 ± 0.2‰) with previous ACC estimates. This supports the use of $\delta^{30}Si$ in sediment as a tracer of past silicic acid

utilization. Nevertheless, due to the variety of the Si-sources and potential past change in oceanic circulation, we argue that a better understanding of modern and past $\delta^{30}Si$ distribution is a prerequisite for a quantitative application of this proxy.

7.1 Introduction

Southern Ocean biogeochemical processes affect global biogeochemical cycles via the upper limb of the meridional Southern Ocean (SO) circulation redistributing nutrients at global scale (*Toggweiler et al*., 1991; *Sarmiento et al*., 2004). This circumpolar ocean represents the largest High Nutrient Low Chlorophyll (HNLC) area in the world ocean. In the HNLC area of the SO, diatoms' productivity drives a significant part of primary production and export (*Pondaven et al.,* 2000a; *Nelson et al*., 2002; *Buesseler,* 1998; Buesseler et al., 2001; *Honjo et al*., 2008). Large decoupling between NO_3 and $Si(OH)_4$ is occurring as a result of a complex interplay with (i) low iron and light limitation favoring heavily silicified diatoms (*Takeda,* 1998; *Hutchins and Bruland*, 1998; *Martin-Jézéquel et al*., 2000; *Claquin et al*., 2002; *Franck et al.,* 2003; chapter 8), (ii) processes involved in the silicate pump – the deeper export of Si compared to N which is more efficiently remineralized (*Dugdale et al*., 1995; *Brzezinski et al*., 2003a), (iii) microbial food web structure (*Smetacek et al.,* 2004; *Pondaven et al*., 2007) and (iv) SO circulation with nutrient rich waters upwelling near Antarctica continent and Ekman transport northward of these surface waters (*Trull et al*., 2001; *Sarmiento et al*., 2004). As a result SO diatoms drive the largest world $Si(OH)_4$ gradient across the water column through uptake in surface, vertical mixing and subsequently intermediate water masses formation (*Pondaven et al*., 2000a; *Brzezinski et al*., 2001; *Sarmiento et al*., 2004, 2007). Deciphering the importance of these different processes is a necessary step to better constrain the role of the SO in the global C and Si cycles at different time scales (past, present, future).

The isotopic composition of silicon ($\delta^{30}Si$) is a promising proxy to overcome both spatial and temporal variabilities of marine Si cycle since it integrates longer timescales compared to direct measurements such as Si uptake estimated from 24h-incubations and is able to trace back the Si sources. $Si(OH)_4$ uptake by diatoms leaves a clear imprint on the isotopic compositions of both $Si(OH)_4$ and biogenic silica ($bSiO_2$). Field studies (*Varela et al.*, 2004; *Alleman et al.*, 2005; *Cardinal et al*., 2005, 2007; *Reynolds et al.*, 2006; *Fripiat et al*., 2007; *Beucher et al*., 2008; *Cavagna et al.,* in revision; *Fripiat et al*., Submitted) and controlled laboratory studies (*De La Rocha et al.*, 1997; *Milligan et al*., 2004) have revealed isotopic fractionation associated with Si-uptake by diatoms due to preferential incorporation of light ^{28}Si into $bSiO_2$. The fractionation factor ($^{30}\varepsilon$ = -1.1 ± 0.4‰) reported by *De La Rocha et a*l. (1997) seems to be independent of temperature, species (*De La Rocha et al.*, 1997) and cell size (*Cardinal et al.*, 2007) and relatively constant across contrasted hydrological environments including fresh waters (*Alleman et al*., 2005). The discovery of a Si-isotopic fractionation during biogenic silica dissolution, preferentially releasing light Si-isotopes ($^{30}\varepsilon$ = -0.55‰), should dampen the overall fractionation factor (*Demarest et al*., 2009). $\delta^{30}Si$ is a powerful tool to constrain mass and isotopic balance, both in modern (*Fripiat et al*., submitted; *Cavagna et al*., in revision) and past ocean (*Beucher et al*., 2007). Currently spatial and seasonal coverage of $\delta^{30}Si$ measurements in the global ocean are limited and additional measurements, controlled experiments, and modelling effort need to be done to better constrain origin and fate of isotopic composition and *in facto* better assessed modern and past distributions.

In this study, we present the first complete summer Antarctic Circumpolar Current transect of $\delta^{30}Si_{Si(OH)4}$ (surface to bottom) including adjacent systems (SubTropical Zone and Weddell Gyre). The results are discussed in terms of source, pathway and fate of silicon across different Southern Ocean water masses.

7.2 Materials and methods

7.2.1 Sampling and hydrology

BONUS-Goodhope (BGH) cruise covered a transect from Cape Town (South Africa) up to 58°S in the Southern Ocean close to 0° meridian from 8 February to 8 March 2008, aboard R/V Marion Dufresne (Fig. 1). The general aim of BGH, a GEOTRACES-IPY endorsed project, is to understand the interactions between the contemporary physics and biogeochemistry in the Atlantic sector of the Southern Ocean and its exchanges with the Indo-Atlantic connection in the wake of the Agulhas system. 11 stations were sampled for Si-isotopes distributed across the different subsystems crossed (Figure 7.1) on complete water column profiles (~ 13 depths/station).

BGH cruise track crosses the several frontal systems (Figure 7.1) of Antarctic Circumpolar Current (ACC) (*Orsi et al.*, 1995) and oceanographic regimes that extend beyond its northern and southern boundaries (i.e. respectively Subtropical Zone and Weddell gyre), that are from North to South: the southern branch of the South SubTropical Front (S-STF; 42.5°S), the SubAntarctic Front (SAF; 44.0°S), the Antarctic Polar Front (APF; 50.22°S), the Southern Antarctic Circumpolar Current Front (SACCF; 51.5°S), and the Southern

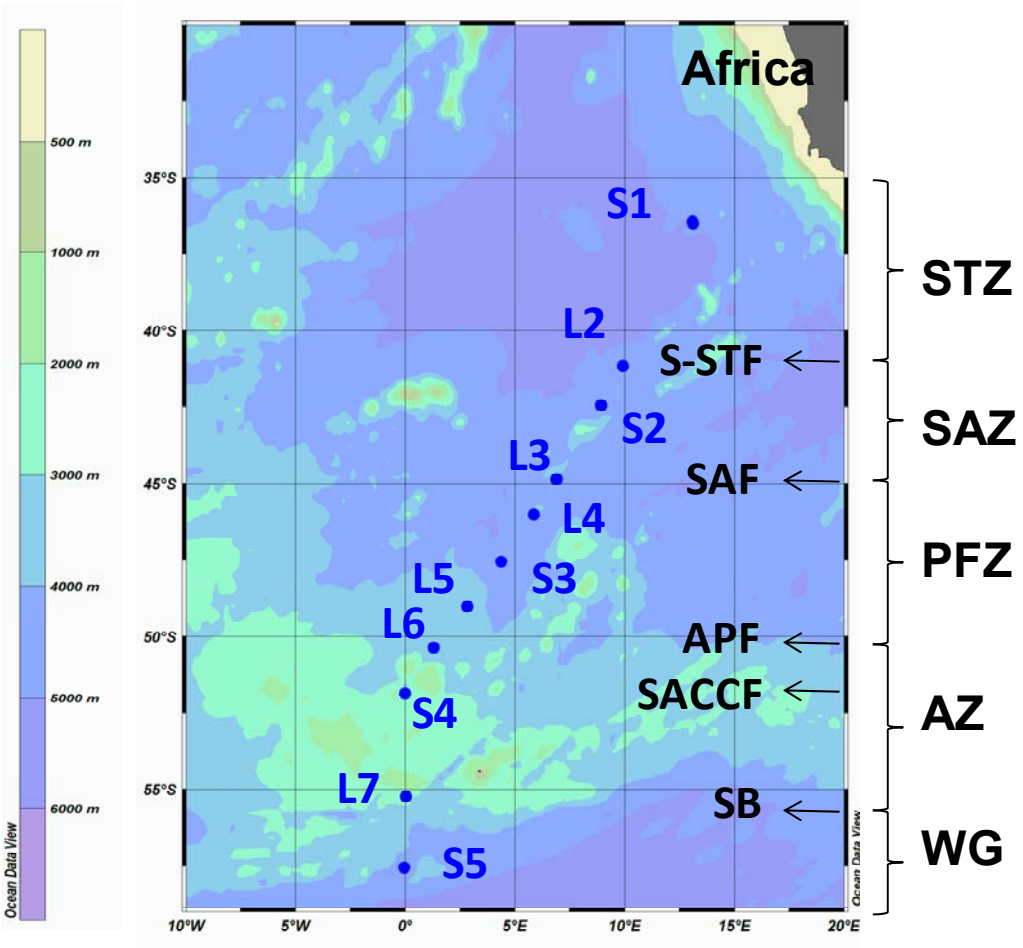

Figure 7.1. Map of the study area with bathymetry and main hydrodynamic features. See text for definition of acronyms.

Boundary (SB; 55.5°S). The narrow jets and fronts separate several oceanic provinces that distinguish each other by their horizontal and vertical hydrological and biogeochemical properties. Namely, the SubTropical Zone (STZ) is North to S-STF, the SubAntarctic Zone (SAZ) between S-STF and SAF, the Polar Frontal Zone (PFZ) between APF and SAF, the Antarctic Zone between APF and SB, and Weddell gyre systems (WG) South of SB. The 11 stations sampled for $\delta^{30}Si$ are characteristics of the following fronts or zones (Fig.1): S1 (CTD casts# 23 and 19): STZ; L2 (cast# 37): S-STF; S2 (casts# 44 and 41) SAZ; L3 (casts# 53 and 54) SAF; L4 (cast# 57) PFZ; S3 (casts#66 and 63) PFZ; L5 (casts# 72 and 70) PFZ; L6 (cast# 77) APF; S4 (casts# 87 and 84) AZ-SACCF; L7 (casts# 99) AZ; S5 (casts# 110 and 106) WG. S refer to "Super stations" where samplings for all other biogeochemical BGH parameters have been performed, while L refer to "Large stations" with less extensive sampling.

Si-isotopes stations covered the water masses variability encountered in summer ACC, WG and STZ. In the Weddell Gyre systems (S5) and in Antarctic Zone (L7, S4), a subsurface temperature minimum identifying Winter Water (WW; *Park et al*., 1998b) was found below the summer mixed layer (ML). The WW is the remnant of the former winter Mixed Layer, thereinafter referred to as Antarctic Surface Water (AASW), capped by seasonal warming and freshening (*Park et al*., 1998b). Below the AASW, different water masses distribution seems to prevail in WG and AZ. In the WG, the temperature maximum layer below AASW is representative of the Lower Circumpolar Deep Water (LCDW, Figure 7.2). In the AZ, the salinity maximum associated with a O_2 minimum represents Upper Circumpolar Deep Water (UCDW). Below UCDW, the Lower Circumpolar Deep Waters (LCDW) are observed. In the PFZ (L4, S3, L5), no WW were observed during BGH below the summer mixed layer. Nevertheless, Antarctic Intermediate Water (AAIW) characterized with a salinity minimum was present. This intermediate water masses is formed from fresh AASW and the low salinity signature is expanding and deepening northward of SAF below SAZ and STZ thermocline. In SAZ (S2), a SubAntarctic thermocline is observed as a transition zone between ML and AAIW, respectively above and below. Both in PFZ and SAZ, from below AAIW to bottom depth, UCDW, LCDW and AABW are observed. In STZ (S1), a SubTropical Thermocline is also observed with AAIW below. Below the AAIW in STZ, diluted form of North Atlantic Deep Water (NADW) with AABW are observed. There is a shoaling of MLD equatorwards from ~ 80m in the South to ~60m in the North of the BGH section.

Seawater was collected using CTD Rosette equipped with 12-L Niskin bottles. Water samples were immediately filtered on Perspex filtration units under pressure through 0.4 µm polycarbonate membranes to collect $Si(OH)_4$ and stored at room temperature in the dark, in acid-cleaned polypropylene bottles. Air supplying the filtration units was also filtered with the same type of membranes to avoid particles contamination during filtration.

7.2.2 Analyses

$Si(OH)_4$ concentrations were measured onboard with an auto-analyser (*LeMoigne et al*., in prep.). Since $Si(OH)_4$ concentration of surface and some subsurface waters at stations north to the Antarctic Polar Front (APF) were too low (<10 µmol Si l^{-1}) to directly apply the Si purification procedure required for Si-isotopic measurement (*De La Rocha et al*., 1996), a $Si(OH)_4$ preconcentration step was performed. It was achieved using a protocol adapted by *Brzezinski et al*. (2003b) and *Reynolds et al*. (2006) from the MAGIC method (*Karl and Tien*, 1992): one or two step (depending of the Si-recovery of the first step) scavenging of $Si(OH)_4$ by brucite, $Mg(OH)_2$, precipitate was obtained by increasing pH either with NaOH 1 µmol l^{-1} (20 ml / L

seawater *Reynolds et al.*, 2006) or NH_4OH 13.5 µmol l^{-1} (6 mL/L seawater *Brzezinski et al*., 2003b). The precipitates were recovered by centrifugation and redissolved with HCl. Both methods were compared for recovery and gave not significantly different results.

Silicon was then co-precipitated with triethylamine molybdate (*De La Rocha et al*., 1996) with a minimum Si requirement of ~1.5µmol Si. After combustion of the silicomolybdate precipitate in covered Pt crucibles at 1000°C, the pure cristobalite phase was transferred to pre-cleaned polypropylene vials. Dissolution of cristobalite was done in a dilute HF/HCl mixture as described in *Cardinal et al*. (2003).

Isotopic measurements were carried out on a Nu Plasma MC-ICP-MS (ULB, Brussels) using Mg external doping in dry plasma mode following *Abraham et al.* (2008) which is adapted from *Cardinal et al*. (2003). Both $\delta^{30}Si$ and $\delta^{29}Si$ measurements are possible since interferences on ^{30}Si described in *Cardinal et al*. (2003) could be overcome thanks to an instrumental upgrade (*Abraham et al*., 2008). The average precision and reproducibility of the measurements are ± 0.15 ‰ (± 2 sd) for $\delta^{30}Si$. The accuracy of the measurements is checked on a daily basis on secondary reference materials (e.g. Diatomite) whose Si isotopic compositions are well known from an inter-comparison exercise (e.g. *Reynolds et al*., 2007).

7.3 Results

In the mixed layer $\delta^{30}Si_{Si(OH)4}$ and $[Si(OH)_4]$ display an opposite pattern with latitude (Table 7.1 and Figure 7.2). There is ^{30}Si enrichment associated to the decreasing $Si(OH)_4$ gradient close to APF propagating in AZ and PFZ as already observed, both for $\delta^{30}Si_{Si(OH)4}$ (*Varela et al*., 2004; *Cardinal et al*., 2005) and $Si(OH)_4$ concentration (*Brzezinski et al*., 2001; *Quéguiner and Brzezinski*, 2002). It is mainly driven by preferential

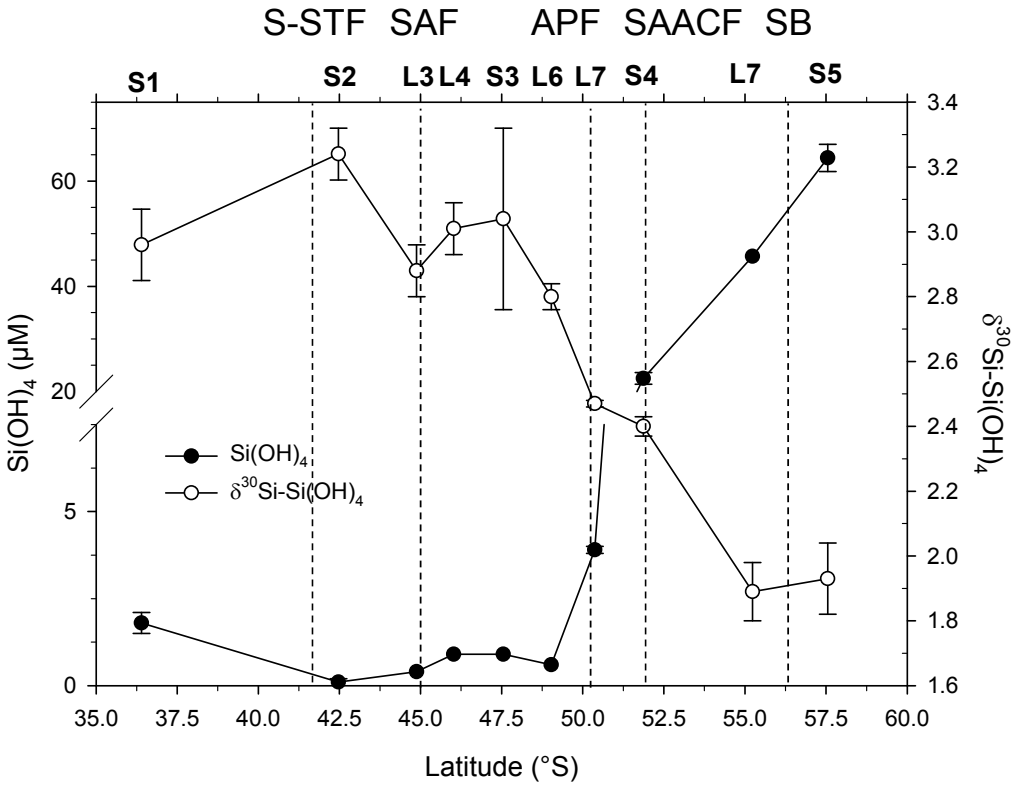

Figure 7.2. The $\delta^{30}Si_{Si(OH)4}$ (open circles) and $[Si(OH)_4]$ (filled circles) with error bars (1sd) of surface waters across the large-scale latitudinal gradient in $Si(OH)_4$.

depth m	$Si(OH)_4$ µmol Si l^{-}	$\delta^{30}Si_{Si(OH)4}$ ‰ ± 1sd	n	depth m	$Si(OH)_4$ µmol Si l^{-}	$\delta^{30}Si_{Si(OH)4}$ ‰ ± 1sd	n	depth m	$Si(OH)_4$ µmol Si l^{-1}	$\delta^{30}Si_{Si(OH)4}$ ‰ ± 1sd	n
Super 5 - CTD 110-106 - 03/16/2008				Large 5 - CTD 72-70 - 03/07/2008				Large 3 - CTD 54-53 - 03/02/2008			
57.55°S		0.04°W		49.03°S		2.83°E		44.88°S		6.89°E	
29	66.2	1.85 ± 0.07	1	9	0.6	2.77 ± 0.06	1	28	0.4	2.88 ± 0.20	2
88	62.6	2.00 ± 0.07	1	70	0.7	2.84 ± 0.08	2	101	4.5	2.32 ± 0.12	2
151	85.9	1.52 ± 0.07	1	100	1.9	1.99 ± 0.03	2	149	5.5	2.07 ± 0.05	1
251	103.0	1.41 ± 0.04	1	151	7.2	2.07 ± 0.06	1	298	10.1	2.06 ± 0.05	1
499	124.0	1.47 ± 0.04	1	200	13.8	1.92 ± 0.07	1	400	15.5	1.83 ± 0.10	2
700	129.5	1.44 ± 0.20	2	300	27.0	1.36 ± 0.07	1	1251	66.4	1.54 ± 0.07	1
1003	126.1	1.27 ± 0.04	1	600	45.8	1.63 ± 0.06	1	1997	70.5	1.51 ± 0.06	1
1499	130.4	1.13 ± 0.05	1	1000	72.6	1.58 ± 0.06	1	3001	95.9	1.36 ± 0.06	1
1999	132.1	1.12 ± 0.06	2	2001	77.7	1.41 ± 0.04	1	3601	111.8	1.22 ± 0.07	1
2500	133.8	1.20 ± 0.05	1	3001	113.3	1.37 ± 0.06	1	4371	120.1	1.24 ± 0.09	1
3000	131.3	1.11 ± 0.08	2	4080	130.7	1.60 ± 0.23	2	Super 2 - CTD 44-41 - 02/27/2008			
3979	131.3	1.08 ± 0.05	1	Super 3 - CTD 66-60 - 03/06/2008				42.47°S		8.93°E	
Large 7 - CTD 99 - 03/14/2008				47.55°S		4.38°E		10	0.1	3.24 ± 0.05	1
55.23°S		0.04°E		5	0.9	3.24 ± 0.01	2	80	1.0	2.07 ± 0.06	2
4	45.7	1.95 ± 0.07	1	41	0.9	2.85 ± 0.07	1	100	0.7	1.89 ± 0.08	2
80	45.7	1.83 ± 0.05	1	79	1.3	2.36 ± 0.07	1	150	1.5	2.09 ± 0.05	1
149	74.0	1.51 ± 0.06	1	100	3.9	2.57 ± 0.19	2	300	6.3	2.01 ± 0.14	2
300	82.5	1.61 ± 0.08	1	149	9.0	2.30 ± 0.07	1	601	19.0	1.83 ± 0.04	1
600	102.2	1.25 ± 0.08	4	200	10.6	2.42 ± 0.05	1	1001	47.1	1.50 ± 0.01	2
1002	110.2	1.34 ± 0.05	1	401	23.6	1.93 ± 0.35	2	1400	62.8	1.29 ± 0.11	2
2096	125.3	1.38 ± 0.05	1	600	40.1	1.67 ± 0.04	1	2000	68.5	1.28 ± 0.05	1
2768	131.2	1.43 ± 0.03	2	1002	65.6	1.43 ± 0.04	1	2501	64.7	1.42 ± 0.09	2
Super 4 - CTD 87-84 -03/11/2008				1403	47.8	1.42 ± 0.08	1	3500	85.5	1.30 ± 0.07	1
51.88°S		0.01°E		2000	82.4	1.34 ± 0.04	1	4057	107.5	1.36 ± 0.06	1
11	23.3	2.42 ± 0.07	1	2301	86.5	1.26 ± 0.01	2	Large 2 - CTD 37 - 02/25/2008			
79	21.7	2.37 ± 0.07	1	2900	102.3	1.39 ± 0.34	2	41.78°S		9.92°E	
149	30.0	2.03 ± 0.08	1	3500	115.6	1.16 ± 0.04	1	101	1.2	1.96 ± 0.05	1
300	74.7	1.41 ± 0.09	2	4101	117.3	1.37 ± 0.07	1	200	3.1	1.89 ± 0.06	1
553	84.1	1.37 ± 0.16	2	4532	123.1	1.28 ± 0.06	1	504	14.4	1.77 ± 0.06	1
704	92.0	1.53 ± 0.04	1	Large 4 - CTD 57 - 03/03/2008				600	18.8	1.73 ± 0.07	1
1201	103.5	1.35 ± 0.05	1	46.03°S		5.87°E		1000	47.9	1.55 ± 0.07	2
1601	115.2	1.47 ± 0.05	1	32	0.9	3.01 ± 0.06	1	2001	62.3	1.48 ± 0.05	1
2001	123.6	1.30 ± 0.05	1	90	4.2	2.72 ± 0.06	1	2900	73.6	1.57 ± 0.06	1
2551	139.5	1.13 ± 0.05	1	151	7.2	2.41 ± 0.06	1	4200	110.5	1.44 ± 0.08	1
Large 6 - CTD 77 - 03/08/2008				300	16.9	1.90 ± 0.05	1	4570	112.2	1.13 ± 0.01	2
50.37°S		1.30°E		501	30.3	1.70 ± 0.08	1	Super 1 - CTD 23-19 - 02/21/2008			
3	3.0	2.47 ± 0.08	1	749	51.1	1.68 ± 0.07	2	36.43°S		13.1°E	
48	3.9	2.48 ± 0.08	1	1000	66.3	1.45 ± 0.06	1	4	1.6	3.04 ± 0.24	2
98	4.8	2.47 ± 0.07	1	1502	71.1	1.51 ± 0.07	1	25	2.0	2.89 ± 0.07	2
129	21.2	2.03 ± 0.05	1	1999	73.8	1.36 ± 0.09	2	75	4.1	2.07 ± 0.01	2
200	44.8	2.04 ± 0.08	1	2497	86.6	1.36 ± 0.06	1	220	5.0	1.99 ± 0.07	1
401	69.4	1.42 ± 0.13	2	3001	100.9	1.43 ± 0.06	1	420	6.7	1.79 ± 0.07	1
602	81.7	1.39 ± 0.06	1	3500	111.2	1.40 ± 0.08	1	701	19.5	1.36 ± 0.06	1
801	84.8	1.46 ± 0.06	1	4148	124.7	1.47 ± 0.06	1	1000	48.9	1.64 ± 0.04	1
999	83.0	1.37 ± 0.15	2					1499	64.5	1.48 ± 0.06	1
1501	90.7	1.44 ± 0.06	1					2001	56.4	1.37 ± 0.04	1
2002	100.8	1.28 ± 0.06	1					2559	58.4	1.40 ± 0.01	2
2500	116.7	1.36 ± 0.06	1					2900	61.4	1.18 ± 0.05	1
2998	125.1	1.38 ± 0.06	1					3499	112.3	1.51 ± 0.06	1
3596	128.4	1.62 ± 0.06	1					4199	139.3	1.30 ± 0.14	2
								4600	144.3	1.06 ± 0.06	1
								5000	145.3	1.05 ± 0.05	1

Table 7.1. Seawater $\delta^{30}Si$ (‰ vs. NBS28) and $[Si(OH)_4]$ data. 'n': number of replicates. The dashed lines indicate the position of the mixed layer depth.

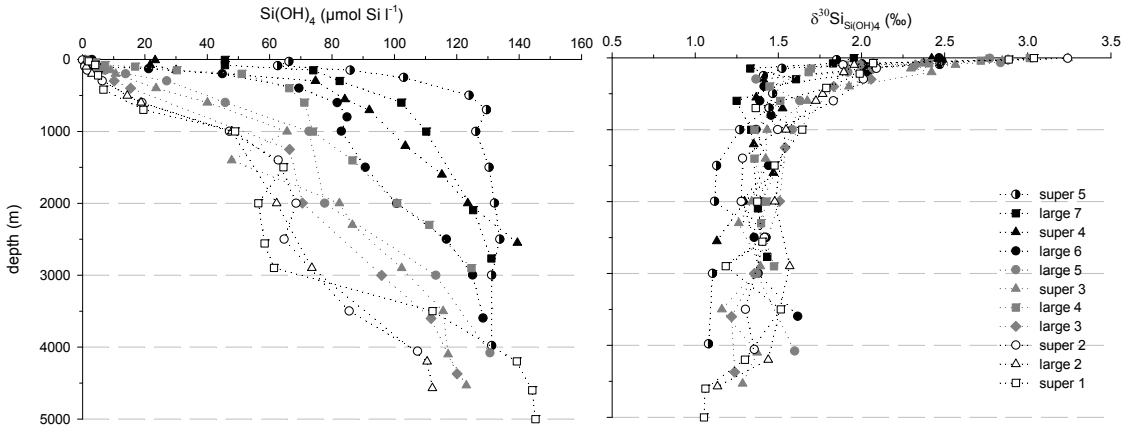

Figure 7.3. $\delta^{30}Si_{Si(OH)4}$ (right panels) and $[Si(OH)_4]$ (left panels) vertical distribution during BONUS-Goodhope.

^{28}Si uptake by diatoms (*De La Rocha et al*., 1997; *Brzezinski et al*., 2001) followed by their export out of the ML (*Nelson et al*., 2002).

The water column profiles of $Si(OH)_4$ concentration and $\delta^{30}Si_{Si(OH)4}$ show ^{30}Si enrichment and $Si(OH)_4$ depletion towards the surface (Figures 7.3 and 7.4) as classically observed in the ocean (*De La Rocha et al*., 2000b; *Cardinal et al*., 2005; *Reynolds et al*., 2006; *Beucher et al*., 2008 ; *Fripiat et al*., submitted ; *Cavagna et al*., submitted). Most of $\delta^{30}Si_{Si(OH)4}$ variation is in the upper 1000 m (Figures 7.3 and 7.4) as in *Cardinal et al*. (2005) with a similar, though much smaller, north-south gradient for mesopelagic water (100-1000m) than in surface water. This latitudinal variation in mesopelagic layer reflects the shoaling of isopycnal water masses surfaces polewards towards Antarctic divergence (*Pollard et al*., 2006) in agreement with meridional circulation of the Southern Ocean (*Trull et al*., 2001). From the South to North, the water masses (Figure 7.4) reflecting mesopelagic layer were: LCDW (WG), UCDW (AZ), AAIW (PFZ), SubAntarctic thermocline and AAIW (SAZ), and subTropical thermocline and AAIW (STZ). Our averaged deep-water (below 1000m) signature (1.4 ± 0.1 ‰) is constant despite large variation in $Si(OH)_4$ content with a north-south gradient as for surface and mesopelagic waters (Figure 7.3). This large $Si(OH)_4$ gradient in deep water come from an isopycnal mixing between NADW and CDW with contrasted $Si(OH)_4$ concentration but similar $\delta^{30}Si_{Si(OH)4}$ (*De La Rocha et al*., 2000b).

7.4 Discussion

The strong link between $Si(OH)_4$ utilization and Si isotopes in the Southern Ocean observed (*Varela et al*., 2004; *Cavagna et al*., in revision) is confirmed by our new data (Figures 7.2, 7.3, 7.4). A comparison between spring (*Cardinal et al*., 2005) and summer (this study) in the ACC, from two distinct transects (Australian and Atlantic sectors, respectively), reveals in surface heavier $\delta^{30}Si_{Si(OH)4}$ in summer in agreement with larger seasonal $Si(OH)_4$ depletion (Figure 7.4) while $\delta^{30}Si_{Si(OH)4}$ are relatively more homogeneous in subsurface and deep waters. The fractionation of Si isotopes during Si uptake by diatoms could be described using one of two simple models assuming constant fractionation factor ($^{30}\varepsilon$) and source. We recently refined the ACC $^{30}\varepsilon$ estimate by compiling several studies at -1.2 ± 0.2 ‰; (*Fripiat et al*., submitted). The Rayleigh model (or closed system model; *De La Rocha et al.*, 1997; *Sigman et al.*, 1999) assumes a closed system (i.e. nutrient consumption is not replenished by external sources) and describes

the evolution of the isotopic signatures of $Si(OH)_4$ (Eq. 7.1), instantaneous $bSiO_2$ (Eq. 7.2) and accumulated $bSiO_2$ (Eq.7.3) when a reservoir of $Si(OH)_4$ is consumed and biogenic silica exported:

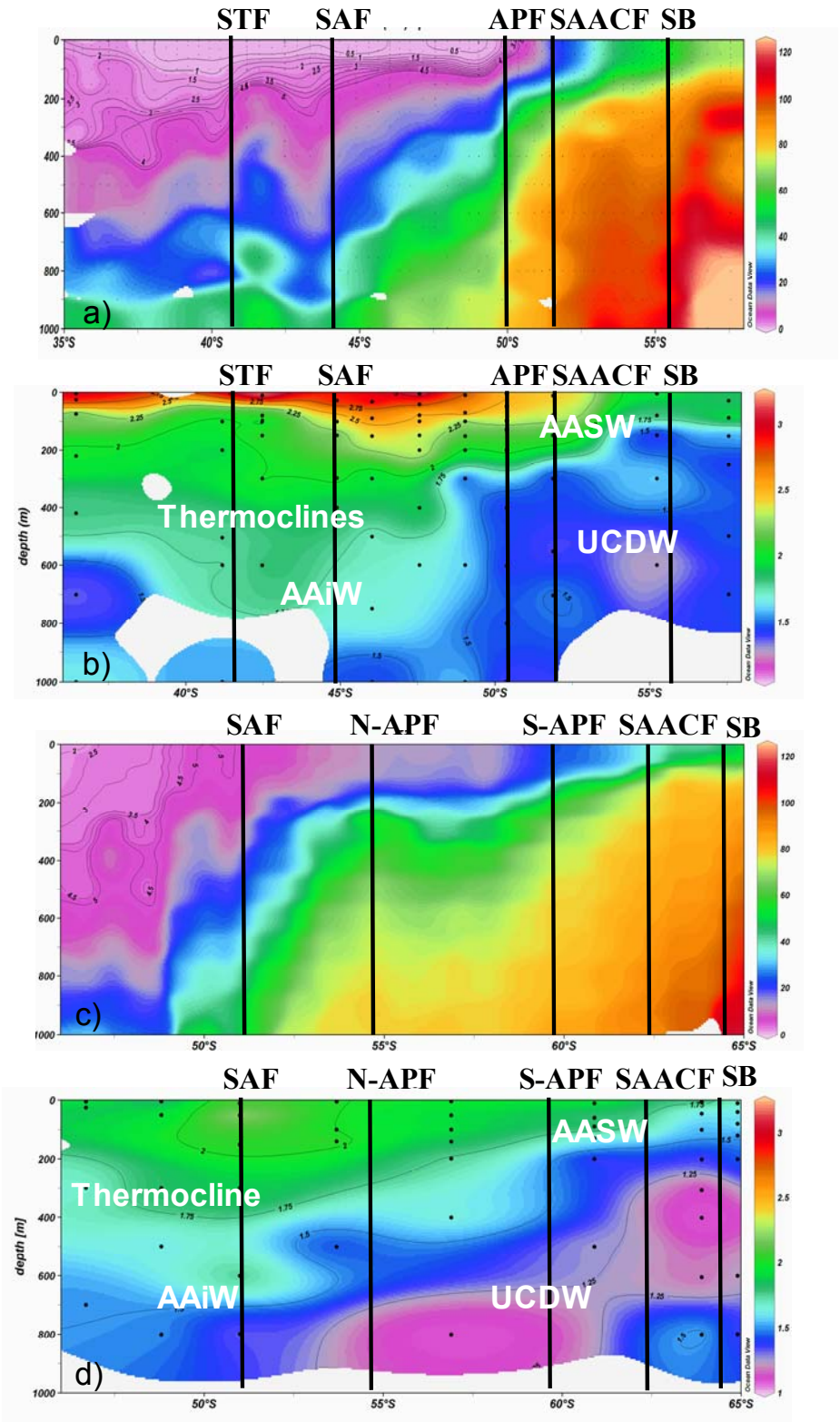

Figure 7.4. Interpolation of $\delta^{30}Si_{Si(OH)4}$ (panels b and d) and $[Si(OH)_4]$ (panels a and c) distribution in upper 1000m during BONUS-goodhope (panels a and b) and Clivar-SR3 (panels c and d, from Cardinal et al., 2005). Interpolation is from R. Schlitzer (Ocean Data View, 2003, available at http://www.awi-bremerhaven.de/GEO/ODV).

$$\delta^{30}Si_{Si(OH)4} = \delta^{30}Si_{Si(OH)4initial} + {}^{30}\varepsilon \cdot \ln(f) \quad (7.1)$$

$$\delta^{30}Si_{bSiO2inst} = \delta^{30}Si_{Si(OH)4} + {}^{30}\varepsilon \quad (7.2)$$

$$\delta^{30}Si_{bSiO2acc} = \delta^{30}Si_{Si(OH)4initial} + {}^{30}\varepsilon \frac{f \cdot \ln(f)}{1-f} \quad (7.3)$$

In Eqs. (7.1) and (7.3), f, is defined by:

$$f = \frac{[Si(OH)_4]_{measured}}{[Si(OH)_4]_{initial}} \quad (7.4)$$

The alternative to the Rayleigh model is the steady state model (or the open system model) in which $Si(OH)_4$ is supplied continuously and partially consumed. In this steady-state model the $Si(OH)_4$ supply equals the sum of the biogenic silica produced-exported and the residual $Si(OH)_4$, both leaving the system. *Sigman et al*. (1999) describe this model in detail for nitrate. The evolution of the isotopic signatures in such system is as follows:

$$\delta^{30}Si_{Si(OH)4} = \delta^{30}Si_{Si(OH)4initial} + {}^{30}\varepsilon \cdot (1-f) \quad (7.5)$$

$$\delta^{30}Si_{bSiO2} = \delta^{30}Si_{Si(OH)4initial} + {}^{30}\varepsilon \cdot f \quad (7.6)$$

On a $\delta^{30}Si_{Si(OH)4}$ vs. $[Si(OH)_4]$ graph, the Rayleigh and the steady state models yield to a curved and straight lines, respectively. These two models represent ideal situations. Depending on the Si-uptake:Si-supply ratio, natural systems could proceed in a mixed way with real fractionation trends lying between true Rayleigh and steady state fractionation trends (*Altabet and François*, 2001; *Varela et al*., 2004). *Demarest et al.* (2009) observe an isotopic fractionation during $bSiO_2$ dissolution. This fractionation counteracts the one occurring during $bSiO_2$ production at about half of its magnitude (-0.55‰). By increasing the euphotic D:P ratio, the overall fractionation factor associated with Si-uptake would dampened as follows assuming a system in steady state at cellular scale:

$${}^{30}\varepsilon = {}^{30}\varepsilon_{uptake} + {}^{30}\varepsilon_{dissolution} \cdot \frac{D}{P} \quad (7.7)$$

In contrast to biological uptake, mixing does not fractionate Si-isotopes, and a mixing curve can be calculated defined by the two original end-members on a $\delta^{30}Si_{Si(OH)4}$ vs. $[Si(OH)_4]$ plot (*Albarède*, 1996; *Fripiat et al.,* submitted). In the following we will use these contrasted behaviour of Si-isotopic signatures to identify sources and attempt to quantify mixing and Si uptake on the BGH transect.

7.4.1 Surface and subsurface processes

7.4.1.1 Antarctic Zone and Weddell Gyre area (S4, L7, S5)

7.4.1.1.1 Surface Water Si-pool dynamic

Fripiat et al. (submitted) and *Cavagna et al*. (in revision) confirmed that Si-sources for the AZ mixed layers was Winter Waters (WW) centred at the temperature minimum, 125-150 m (Cardinal et al., 2005).

This is in agreement with the seasonal evolution of the ML since WW is the remnant of the Antarctic Surface Waters forming by deep winter convective mixing (*Park et al*., 1998a, 1998b; *Chaigneau et al*., 2004). *Pondaven et al*. (2000a) and *Altabet and François* (2001) observed no significant differences in the Si-properties of summer WW and winter AASW. Figure 7.5a shows that ML in AZ (L7 and S4) and in WG (S5) fall on the fractionations trends caused by Si-uptake (Eqs 7.1 and 7.5), with WW as Si-source and using global ACC $^{30}\varepsilon$ average of -1.2 ± 0.2 ‰ (*Fripiat et al*., submitted).

Except in the WG where the Si-utilization was not sufficient enough to distinguish if the $Si(OH)_4$ pool behaves as an open or closed system, the mass and isotopic balances seem more in agreement with a system continuously supplying silicic acid via diapycnal mixing or turbulence diffusion from WW during seasonal Si-depletion (Eq. 7.5; Figure 7.5a). Nevertheless given the relatively small difference between the projections of the two models (Figure 7.5a) and the existence of other uncertainties (e.g $bSiO_2$ dissolution

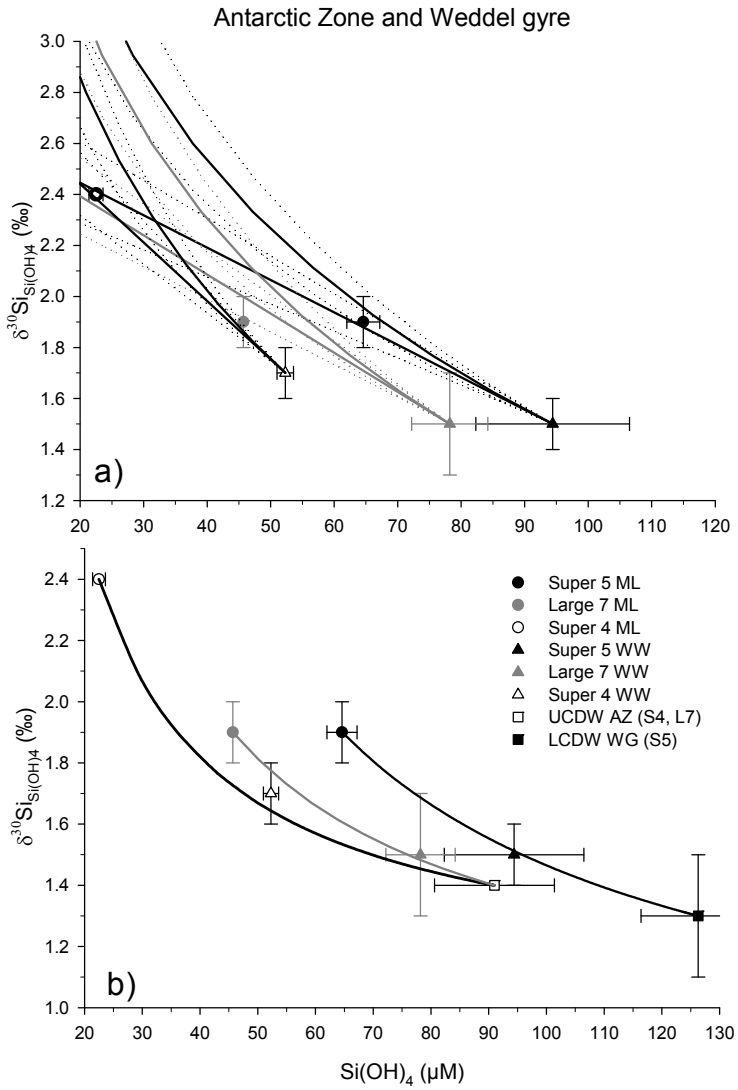

Figure 7.5. $\delta^{30}Si_{Si(OH)4}$ vs. $[Si(OH)_4]$ for the different Si-pools in Antarctic Zone and Weddell gyre): (panel a) fractionation trends following the steady state (straight line) or Rayleigh (curved line) models calculated with HNLC WW as Si-source and an average ACC fractionation factor of -1.2 ± 0.2‰, (panel b) mixing curves between HNLC ML and UCDW-LCDW. Each water mass representing by a symbol (see legend) is the average (with 1sd) of all the corresponding depth (determined with T-S-O_2 diagrams) with a concentration and an isotopic values.

isotopic discrimination), we cannot definitely reject Rayleigh model. However, the steady state model seems to fit better all observations and Rayleigh model was already shown to be unlikely to describe correctly $\delta^{30}Si$ variations in the Southern Ocean (*Cardinal et al*., 2005; *Fripiat et al*., submitted, *Cavagna et al.* in revision). Therefore a steady state mode, or at least a combination of Rayleigh and steady state depending of the ratio of Si-supply vs. Si-uptake is more likely (*Altabet and François*, 2001; *Varela et al*., 2004).

7.4.1.1.2 Mass balance

As observed in *Fripiat et al*. (submitted) in AZ, the temperature minimum layer (WW) for each station in the AZ falls on a mixing line between UCDW and ML (Figure 7.5b). In the WG, UCDW is absent, and LCDW is upwelled in surface. This explains why for these stations WW falls on a mixing line between ML and LCDW (Figure 7.5b). These observations further confirm that subsurface $\delta^{30}Si_{Si(OH)4}$ in AZ and WG are mainly due to Si-uptake in surface and vertical mixing (*Cardinal et al*., 2005; *Fripiat et al*., submitted). As in *Fripiat et al*. (submitted) and in Cavagna et al., (in revision), BGH cruise covered the end of the diatoms growth (Feb.-March) with $bSiO_2$ productions rates in the lower range of the global oceanic measurements (annex 1). Therefore, late summer ML probably represents conditions at the end of the growth season just before overturning ends stratification. ML and UCDW can thus be considered end-members which, as a result of convective mixing at the onset of winter, will generate a homogenous AASW. Mass contribution of the UCDW (=f_{UCDW}) to the AASW can then be estimated with $\delta^{30}Si(OH)_4$ using Eq. 7.8 (Fry, 2006).

$$f_{UCDW} = \frac{\delta^{30}Si_{WW} - \delta^{30}Si_{ML}}{\delta^{30}Si_{UCDW} - \delta^{30}Si_{ML}} \cdot 100 \quad (7.8)$$

Relative mass contribution of LCDW (f_{LCDW}) can be estimated for the station in WG also with Eq. 7.8 replacing $\delta^{30}Si_{UCDW}$ by $\delta^{30}Si_{LCDW}$. Estimated UCDW and LCDW Si-contribution to AASW respectively in AZ and WG is shown in Table 7.2. These estimations are very similar than in AZ off Kerguelen (f_{UCDW} = 78 ± 12 %, KEOPS campaign) and from a previous study in the same sector as BGH (f_{UCDW} = 79 ± 16 %, EIFEX campaign) (*Fripiat et al*., submitted). This suggests a relative homogeneity in UCDW contribution to AASW. When integrating WW $Si(OH)_4$ concentration over the whole water layer between surface and WW (i.e. winter AASW depth range, 0 to 300m) times the f_{UCDW} for AZ and f_{LDCW} for WG (Eq. 7.8), we calculate that UCDW contributes to 14.1 ± 5.9 and 11.0 ± 1.7 mmol Si m^{-2} to AASW for L7 and S4, respectively, and LCDW contributes to 22.7 ± 7.0 mmol Si m^{-2} to AASW at S5. Since the average summer MLD represents 27% of the AASW (80 vs. 300m), we can estimate the winter overturning replenishing what has been consumed from the previous summer ML (AASW annual Si-supply; Table 7.2). Using the same approach implemented first in *Fripiat et al*. (submitted), if we assume steady state at annual time scale (i.e., supply equaling export) this supply should represent the annual integrated ML net $bSiO_2$ production (i.e. AASW $bSiO_2$ export). The imbalance between annual integrated net $bSiO_2$ production and seasonal integrated depletion should be an estimation of the summer vertical Si-supply into mixed layer (Table 7.2). Indeed, the estimated seasonal nutrient depletion in surface water (taking into account WW $[Si(OH)_4]$ as initial conditions and ML $[Si(OH)_4]$ as final conditions) is a conservative estimate since resupply during the stratified period is ignored (*Wang et al*., 2001). This analysis showed than the $bSiO_2$ production estimated from the seasonal Si-drawdown alone could significantly underestimate from ~20 to ~60% (Table 7.2).

A pattern of latitudinal Si-supply and $bSiO_2$ production can then be proposed for the AZ. Table 7.2 shows that this Si-supply, both initially from UCDW during deep winter convective mixing regime and during summer from either continuous turbulence diffusion or regular vertical mixing events, seems stronger southward. It is in agreement with the shoaling of isopycnal with higher Si-content southward (*Pollard et al*., 2006) boosting diatoms productivity. *Nelson et al.* (2002) in the Pacific sector observe also a southward increase in both gross and net $bSiO_2$ production and suggest the role of higher standing stock of $Si(OH)_4$ in the winter ML southward for this pattern. Our study highlights the role of this winter silicic content but also the significant contribution of the summer Si-supply. Moreover, during BGH, this pattern is also reflected in the instantaneous $bSiO_2$ production rate (using ^{30}Si spiked incubations; appendix) and

		WG		AZ		APF
		Super 5	Large 7	Super 4	Keops[1]	Eifex[1-2]
relative seasonal Si-utilization	**%**	32 ± 9	42 ± 5	43 ± 2	48 ± 3	72 ± 7
f_{ucdw}	**%**	80 ± 22	60 ± 25	70 ± 10	0.78 ± 12	79 ± 16
Seasonal Si depletion	**mmol Si m^{-2}**	2.4 ± 0.9	2.6 ± 0.5	2.4 ± 0.1	2.5 ± 0.2	2.7 ± 0.2
AASW annual Si-supply	**mmol Si m^{-2}**	6.0 ± 1.9	3.8 ± 1.6	2.9 ± 0.4	4.0 ± 0.7	2.9 ± 0.6
ML seasonal Si-supply	**mmol Si m^{-2}**	3.6 ± 1.7	1.2 ± 1.6	0.5 ± 0.5	1.5 ± 0.7	0.2 ± 0.6

[1]Fripiat et al., submitted

[2]Cavagna et al., in revision

Table 7.2. Mass balances for Antarctic Zone and Weddell Gyre during BONUS-Goodhope. Estimations from EIFEX and KEOPS are shown to compare (Fripiat et al., submitted).

$bSiO_2$ concentration (*LeMoigne et al.,* in prep). *Jin et al*. (2006) by combining a restoring approach of global oceanic nitrate, silicic acid, and alkalinity with a size-dependent ecological/biogeochemical model, observe a high opal export in the Antarctic Zone from 1 to 10 mol Si m^{-2} d^{-1} covering the range of our estimates and also with higher values southward.

7.4.1.2 Polar Frontal Zone

Two $Si(OH)_4$ sources are plausible for ML PFZ (Figure 7.6), (1) AAIW which formed in this area the summer subsurface layer (~100 to ~700m) and (2) unaltered AASW (represented by the WW closer of APF advected northward in the Ekman layer: S4). These two potential Si-sources cannot be discerned since by applying steady state fractionation trends both could explain Si mass and isotopic signatures in the PFZ despite a large difference in terms of $Si(OH)_4$ content (Eq. 7.5; Figure 7.6). Since a surface water particle needs several years to cross the PFZ (Speich, pers. com. 2009), several wintertime deep convective mixings should set the initial $Si(OH)_4$ pool close to the subsurface properties, here AAIW. Unaltered AASW source cannot be totally expressed especially in the northern part of PFZ.

In contrast to AZ, PFZ $\delta^{30}Si_{Si(OH)4}$ indicate clearly that the mixed layer was behaving in a steady state mode whatever source is used since a Rayleigh model (Eq. 7.1) using, either AASW (WW from S4) or AAIW as Si-sources, cannot explain ML PFZ isotopic signatures (Figure 7.6). Better fit on steady state is also in agreement with *Cardinal et al.* (2005) in spring ACC suggesting a ML mainly operating in an open mode along seasonal Si-depletion.

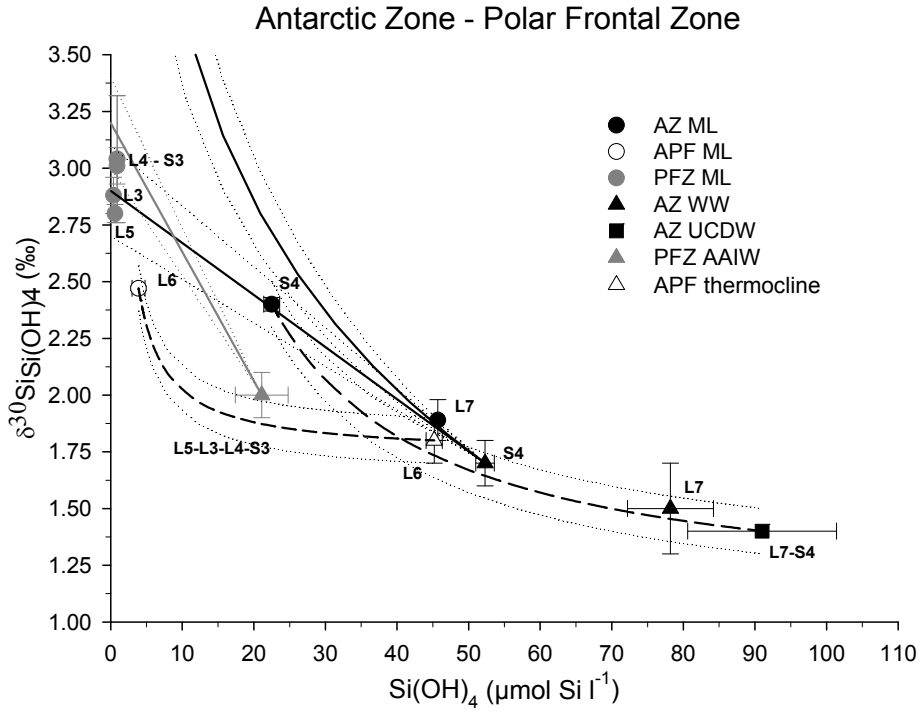

Figure 7.6. $\delta^{30}Si_{Si(OH)4}$ vs. $[Si(OH)_4]$ for the different Si-pools in Antarctic Zone (filled black symbols), Antarctic Polar Front (empty black symbols) and Polar Frontal Zone (filled gray symbols): with fractionation trends following the steady state (straight line) or Rayleigh (curved line) models calculated with WW (Super 4) as Si-source and an average ACC fractionation factor of -1.2 ± 0.2‰, and mixing curves between HNLC ML and UCDW, and between APF ML and APF WW. Each water mass representing by a symbol (see legend) is the average (with 1sd) of all the corresponding depth (determined with T-S-O_2 diagrams) with a concentration and an isotopic values.

Depending on the Si-source chosen (AAIW or AASW from S4), different integrated seasonal depletions are estimated. PFZ depletion estimate assuming each corresponding AAIW as a Si-source and taking an average summer ML depth at 80m is 1.8 ± 0.3 mol Si m^{-2} yr^{-1}. It is clearly lower than the estimations with AASW as source yielding to 4.1 ± 0.6 mol Si m^{-2} yr^{-1}. These seasonal depletions as explained in section 7.4.1.1.2 are lower estimates of integrated net $bSiO_2$ production since they are not taking into account potential Si-supply from subsurface during summertime (*Wang et al*., 2003; *Fripiat et al*., submitted). Due to the impossibility to discern the two potential Si-sources probably co-occurring, it is difficult to establish a simple mass balance as perform in Antarctic Zone with a unique Si-source and a relatively simple annual dynamics approach. Nevertheless, these estimations could be regarded as upper and lower estimates of the annual net $bSiO_2$ production. *Quéguiner and Brzezinski* (2002) observed in spring specifically high diatoms productivity in the Atlantic PFZ instead of AZ more in agreement with AASW mass balance. Nevertheless, the diatoms productivity peak occurs in the Southern Part of PFZ close to APF where unaltered AASW could be easily expressed. More complex model with multisource to constrain the isotopic and mass balance should improve our understanding on this significant Southern Ocean subsystems for Si-biogeochemical cycle.

7.4.1.3 Antarctic Polar Front

The fronts of ACC delimit zones relatively impermeably with similar physical, chemical and biological properties (*Tréguer and Jacques*, 1992; *Rintoul and Trull*, 2001; *Chaigneau et al*., 2004; *Sokolov and*

Rintoul, 2007b). The ACC dynamic is essentially dominated by ACC fronts split in several jets or branches associated with higher eastward baroclinic transport (*Sokolov and Rintoul*, 2002; 2007a; 2009). Other mesoscale processes as meanders and eddies are added to this jet dynamics and are directly involved in the cross frontal mixing mainly at the proximity of sharp topographic features (*Sokolov and Rintoul*, 2007b; S.Speich, pers. com. 2009).

Except APF (L6), all the ML $\delta^{30}Si$ data of AZ (S4, L7) and PFZ (L4, S3, L5) fall on the steady state trends (Eq. 7.5; Figure 7.6) either with AASW (represented by the WW closer to APF and thus from a potential AASW source for APF and PFZ, i.e. S4 in the Northern AZ) or also with AAIW (only for PFZ ML) as Si-sources and using average ACC fractionation factor of -1.2 ± 0.2 ‰ (*Fripiat et al*., submitted).

APF ML (L6) falls below since the $\delta^{30}Si_{Si(OH)4}$ is similar than S4 in AZ but with a lower $Si(OH)_4$ content (Figure 7.2). Intensive vertical mixing with subsurface easily occurs at these fronts driving the surface mixed layer towards lighter isotopic values as suggested by *Sigman et al*. (1999) for $\delta^{15}N_{NO3}$ near the SAF. This processes could also explain potentially the slight lower Si-isotopic composition observed in the SAF (L3; Figure 7.2).

This process at the APF could have driven AAIW formation since this water mass falls on a mixing line between APF ML and APF subsurface layer as end-members. AASW seems to be the main source of AAIW but are significant altered via intensive vertical mixing with highly Si-depleted summer ML during cross frontal exchange. During wintertime when AASW formed a homogeneous surface layer in AZ, vertical mixing during cross frontal exchange should alter less initial AASW (Figure 7.6). Nevertheless, the subsequent mixing between AASW and highly PFZ Si-depleted surface waters could also contribute to the formation of AAIW (Figure 7.6). Whereas that the involvement of AASW to form AAIW is well established, the exact mechanisms at stake are still unclear (*Molinelli*, 1981; *England et al*., 1993; *Sloyan and Rintoul*, 2001; *Morrow et al*., 2004). *Ribbe and Tomczak* (1997) concluded that both circumpolar cross-frontal mixing and PFZ local deep mixing play a role in agreement with our data. This link is also easily seen on Figure 7.4, both for Australian and Atlantic section, since the AASW $\delta^{30}Si_{Si(OH)4}$ (green color) is spreading and deepening northward following the salinity minimum characteristic of AAIW (not shown).

Sigman et al. (1999) suggested that the main source for NO_3 mixed layer in the PFZ was unaltered AASW advected northwards by Ekman transport. Decoupling between $Si(OH)_4$ and NO_3 in the ACC could explain this difference in term of sources: as $[NO_3]$ is still high at the APF (~ 22 µmol N l^{-1}) in comparison to $[Si(OH)_4]$ (~ 4 µmol Si l^{-1}) and with WW (~ 35 and ~ 45 µmol l^{-1}, for Si and N respectively), AAIW NO_3-biogeochemical properties should be closer to AASW in agreement with unaltered AASW as the main source for summer mixed layer NO_3 pool (*Sigman et al*., 1999). In contrast, highly $Si(OH)_4$ depleted surface water at APF decreases $Si(OH)_4$ content of the resulting mixing product without significant change in $\delta^{30}Si_{Si(OH)4}$.

7.4.1.4 SubAntarctic and SubTropical Zones

Both in SAZ and in STZ, the thermocline (respectively ~80 to ~300m and ~80 to 600m) appears to be the main Si-source since mixed layer fit the steady state fractionation trends (Figure 7.7a). In the STZ, the mixed layer falls not far of the Rayleigh trends, indicating a system probably operating in a mixed way between open vs. closed mode. These suggestions are in agreement with *Cardinal et al*. (2005) in spring

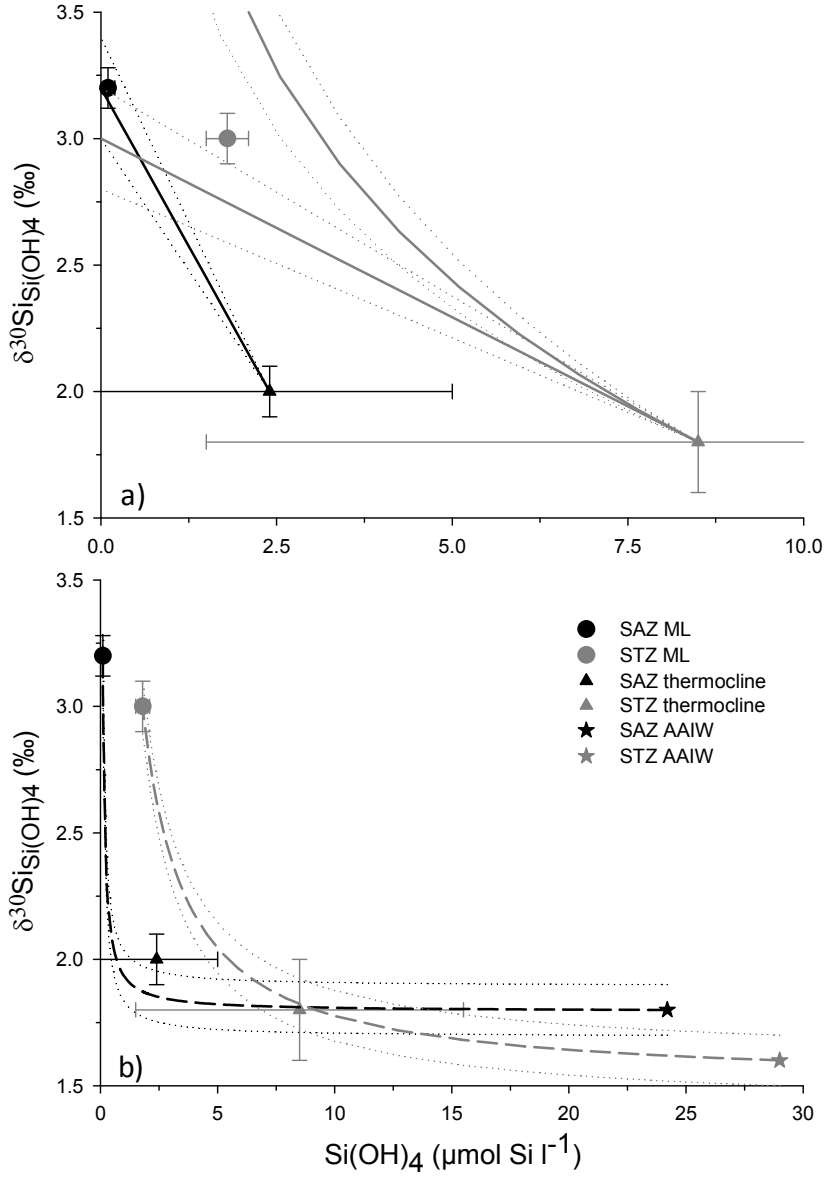

Figure 7.7. $\delta^{30}Si_{Si(OH)4}$ vs. [$Si(OH)_4$] for the different Si-pools in SubAntarctic Zone (black symbols) and SubTropical Zone (gray symbols): (a, upper panel) fractionation trends following the steady state (straight line) or Rayleigh (curved line) models calculated with thermocline as Si-sources and an average ACC fractionation factor of -1.2 ± 0.2‰, (b, lower panel) mixing curves between SAZ-STZ ML and SAZ-STZ AAIW. Each water mass representing by a symbol (see legend) is the average (with 1sd) of all the corresponding depth (determined with T-S-O_2 diagrams) with a concentration and an isotopic values.

ACC for SAZ (STZ was not sampled in this study). In SAZ and STZ, diatoms productivity is low and seems significantly sustained by $bSiO_2$ dissolution (*Nelson and Gordon*, 1982; *Beucher et al*., 2004b; Chapter 8). I*n situ* estimations of $^{30}\varepsilon$ associated with $bSiO_2$ production in areas with significant $bSiO_2$ dissolution are likely to be biased by the dampening isotopic effect of dissolution, with the measured value representing the combined net effect of these two processes rather than that the biological production alone (Eq. 7.7; *Demarest et al*., 2009).

Nevertheless, $\delta^{15}N_{NO3}$ studies suggested that close to the SAZ isotopic and mass balance, a significant proportion of the summertime SAZ nitrate is supplied from south to SAF (*Sigman et al*., 1999; *DiFiore et al*., 2006) as shown with salinity distribution (*Rintoul and Trull*, 2001). Such contrast between $\delta^{30}Si_{Si(OH)4}$

and $\delta^{15}N_{NO3}$ could again be explained by the strong decoupling between $Si(OH)_4$ and NO_3 in the Southern Ocean (*Sarmiento et al*., 2004). The waters south to PFZ are strongly depleted in $Si(OH)_4$ but not in NO_3. Such depleted environment are unable to supply significantly SAZ in $Si(OH)_4$ by cross frontal exchanges.

Thermocline in SAZ and STZ seems clearly to be a mixing interface between AAIW below and mixed layer above (Figure 7.7b). This process is in agreement with *Sarmiento et al*. (2004) hypothesis in which AAIW and SAMW replenish in nutrient low latitude thermocline. The SAZ thermocline could also provide $Si(OH)_4$ by Subtropical Thermocline (lateral mixing) as suggested by *Sigman et al.* (2000) with $\delta^{15}N_{NO3}$ (Figure 7.7b).

In SAZ, deep winter convective mixing should mostly set the initial summer mixed layer close to the thermocline Si-properties (*Rintoul and Bullister*, 1999; *Lourey and Trull*, 2001). Due to the low silicic acid content of the SAZ thermocline (2.4 µmol Si l^{-1}), diatoms productivity could be strongly Si-limited (*Nelson et al*., 2001; *Hutchins et al*., 2001; *Sedwick et al*., 2002) confirming a minor role of this subsystem in the ACC Si-budget (*Quéguiner*, 2001; *Leblanc et al*., 2002, in prep; Chapter 8). In the Australian sector, SAZ thermocline has higher $Si(OH)_4$ concentration *circa* 4-5 µmol Si l^{-1} with summer ML close to Si-depletion (as S2; *Lourey and Trull*, 2001) suggesting a circumpolar variation of the potential diatoms productivity in SAZ. Notwithstanding, one station is clearly not representative of all SAZ area since large variability is classically observed in this area in term of C and Si productivity (*Griffiths et al*., 1999; *Boyd et al*., 1999b; *Quéguiner*, 2001; *Cavagna et al*., submitted; *Leblanc et al*., in prep; Chapter 8). This is mainly resulting from the several potential co-limitation (light, iron, silicic acid) occurring in a complex temporal and spatial pattern especially in summer (*Boyd et al*., 1999b; *Boyd*, 2002).

7.4.2 Intermediate and deep water masses

Figure 7.8a shows that corresponding water masses in Australian sector (*Cardinal et al*., 2005) have systematically lighter $\delta^{30}Si_{Si(OH)4}$ than their Atlantic counterparts probably reflecting a progressive ^{28}Si enrichment of the deep water masses (CDW) from $bSiO_2$ dissolution along the circumpolar water path (*De La Rocha et al*., 2000b; *Reynolds*, 2009). As these deep water masses feed in Si the surface and intermediate water masses via the upper limb of the meridional circulation (Trull et al., 2001a), the isotopic influence of $bSiO_2$ dissolution in CDW is transmitted. The circumpolar view of AAIW and SAMW formation is inaccurate (Speer et al., 2001). Indeed, these water masses has different origin (Atlantic, Indian, Pacific) across a same latitudinal section mainly advected either eastward with the ACC or westwards, as in its cases in BGH STZ or partly in Clivar-SR3 SAZ (*Rintoul and Bullister*, 1999; S. Speich, pers. com. 2009).

During the AAIW northward component transport across the BGH section, basically from PFZ to SAZ and then STZ with a progressive deepening, this water mass is altered by diapycnal mixing with underlying Si-rich UCDW which supplies light Si-isotopes (Figure 7.8c). In the Australian sector (Clivar-SR3 section), AAIW is not formed locally by deep convection (*Rintoul and Bullister*, 1999). *Rintoul and Bullister* (1999) suggest that AAIW south of Australia is supplied by a number of water types with distinct sources, and the source waters are poorly ventilated or sufficiently distant that significant “aging” occurs by the time the water mass is advected in this sector. AAIW is found at this sector in SAZ below the corresponding SAZ-thermocline. In Figure 7.8c, AAIW from the Australian sector seems significantly altered by mixing with

adjacent water masses (SAZ thermocline and UCDW) in agreement with *Rintoul and Bullister* (1999) hypothesis.

The difference observed between the SAZ thermoclines of the two sections could be explained by different AAIW Si-properties (Figure 7.8b). Indeed as discussed in section 4.1.3, SAZ thermocline seems to be a mixing interface between SAZ ML and underlying AAIW. As AAIW in the Australian sector has lower $\delta^{30}Si$ value with higher silicic acid concentration, the resulting mixing product is influenced by these distinct properties.

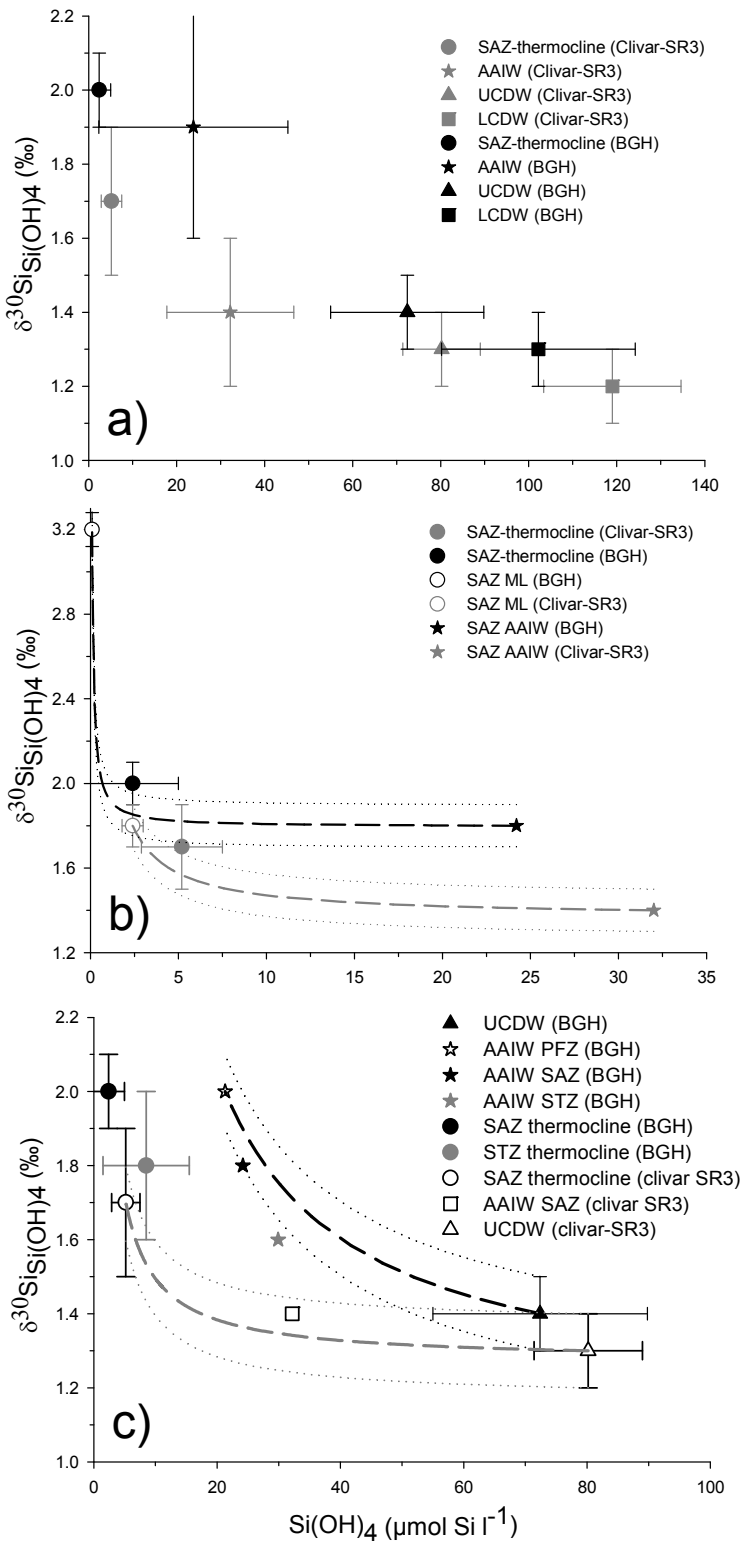

Figure 7.8. $\delta^{30}Si_{Si(OH)4}$ vs. $[Si(OH)_4]$ for the different Si-pools from BGH section and Clivar-SR3 section (from Cardinal et al., 2005): (a) comparison between BGH (black symbols) and Clivar-SR3 (gray symbols) deep and intermediate water masses, (b) mixing curves between SAZ ML and SAZ AAIW for BGH (black symbols) and Clivar-SR3 (gray symbols) sections, (c) mixing curves between PFZ AAIW and UCDW from BGH section and between SAZ thermocline and UCDW from Clivar-SR3 section. Each water mass representing by a symbol (see legend) is the average (with 1sd) of all the corresponding depth (determined with T-S-O_2 diagrams) with a concentration and an isotopic values.

7.4.3 Palaeoceanography implications

To track variation of $Si(OH)_4$ utilization at glacial-interglacial timescales using $\delta^{30}Si_{bSiO2}$ in sediment (*De La Rocha et al*., 1998; *Brzezinski et al*., 2002; *Beucher et al*., 2007; *Pichevin et al*., 2009), we need to understand the processes involved in origin and fate of $bSiO_2$ in the water column and at sediment-water interface which is not the aim of this study. $\delta^{30}Si$ of Si-sources and the amplitude of isotope discrimination associated with $Si(OH)_4$ utpake-$bSiO_2$ incorporation are also two key parameters relating $Si(OH)_4$ utilization to the isotopic composition of $Si(OH)_4$ in oceanic surface waters and the sinking flux to the seafloor.

The average isotopic fractionation factor ($^{30}\varepsilon$) estimate for BGH is -1.2 ± 0.2 ‰, not significantly different from *in vitro* estimates under tropical conditions (-1.1 ± 0.4 ‰; *De La Rocha et al*., 1997) and from recent ACC compilations (-1.2 ± 0.2 ‰; *Fripiat et al*., submitted). This supports that $^{30}\varepsilon$ does not vary significantly with latitudes, diatoms species, temperature, biogeochemical and hydrological properties, and $Si(OH)_4$ concentration as previously observed in contrasted areas (*De La Rocha et al*., 1997; *Cardinal et al*., 2005, 2007, *De La Rocha et al*., 2000; *Reynolds et al*., 2006; *Beucher et al*., 2008).

Our study, along with most of Southern Ocean studies (*Cardinal et al*., 2005; *Cavagna et al*., submitted, *Fripiat et al*., submitted), show that subsurface waters are the main Si-sources for mixed layer, both initially by deep winter convective mixing and in by supplying $Si(OH)_4$ to the mixed layer during growth period. Moreover, the origin and fates of the subsurface water masses has significant effect on the Si-isotopic fractionation extent in the surface water. From the palaeoceanographic perspective, this represents a complexity since glacial Southern Ocean circulation and hydrology is expected to be different from today (*Toggweiler et al*., 2006). As suggested in *Beucher et al*. (2007), different oceanic circulations altering probably Si-biogeochemical properties of water masses and subsequently $\delta^{30}Si_{Si(OH)4}$ of Si-sources need to be better assess to estimate isotopic and mass balance involved in the glacial Southern Ocean. It requires a better understanding of Si-isotopic distribution through process-oriented modeling effort. In a first time, Global Coupled Model (e.g. PISCES; Aumont et al., 2003) should be test first reproducing present Si-isotopic distribution. Secondly, apply different past circulation scenario (Toggweiler et al., 2006) should be useful to assess potential variation of Si-source properties.

7.5 Conclusions

This study confirms that Si-isotopes in the Southern Ocean seem to be mainly driven by uptake in surface and mixing in subsurface with no significantly direct influence of $bSiO_2$ dissolution except in the expression of the fractionation factor in the mixed layer (Demarest et al., 2009). This process is however currently difficult to assess. Nevertheless $bSiO_2$ dissolution isotopic effect is recorded in Circumpolar Deep Water with longer residence time as suggested by the enrichment in ^{28}Si in CDW during the circumpolar eastward baroclinic transport. As the CDW are the ultimate Si-sources for surface and intermediate ACC water masses, this imprint is propagated via the upper limb of the meridional circulation.

Mixed layer seems to better fit open system assumptions (steady state) with subsurface waters as Si-sources, both initially by deep winter convective mixing and during stratification period by diapycnal mixing events. It is in agreement with previous spring ACC $\delta^{30}Si$ suggesting that Si-depletion is occurring in an open system mode (*Cardinal et al*., 2005) and that net $bSiO_2$ production estimated from Si-drawdown only could be strongly underestimated.

In Antarctic Zone, our data suggest a single Si-source (Winter Water) with annual resetting during wintertime. In a similar way than in *Fripiat et al*. (submitted), simple mass and isotopic balances could be performed to estimate UCDW annual and summertime Si-supply. We observe that both winter and summer Si-supplies increase southward in AZ probably reflecting the progressive shoaling of isopycnal (Circumpolar Deep Water) with higher Si-content southward.

Si-isotopes allow tracking the origin and fates of the different ACC-Si-pools in agreement with SO physics, from upwelling (southern ACC), uptake in the Ekman layer, and subsequent downwelling (northern ACC). Box modeling effort should be useful to quantify the different associated Si-fluxes.

The reproducibility of Si-isotopic fractionation across the ACC and adjacent subsystems close to the previous *in situ* and *in vitro* estimates comforts the utilization of this proxy as a tracer of Si palaeo-utilization. Nevertheless, we argue that, as suggested by *Beucher et al*. (2007), a better understanding of past oceanic circulation potentially influencing the Si-sources and mixed layer dynamics need to be assessed for the quantitative palaeoceanographic utilization of this proxy.

Part IV. Biogenic silica production and dissolution rates

Chapter 8. Mid-summer silicon dynamic and diatoms productivity in Polar Frontal and SubAntarctic Zones, south of Tasmania[3]

Abstract

We studied the mid-summer carbon biological pump in the Southern Ocean with a special emphasis on the silicon cycle and diatoms contribution to primary production. Three sites, two in the SubAntarctic Zone (SAZ) southeast and southwest of Tasmania, and one in the Inter Polar Frontal Zone (IPFZ), were selected on the basis of their contrasted physico-chemical, biogeochemical and food web structure characteristics. Biogenic silica production and dissolution rates were measured in the euphotic layer at three different days for each station to investigate short-term and daily variability. The results are compared with carbon uptake rates and community structure.

An efficient silicon remineralization loop by accumulation of dissolving biogenic silica at the end of productive period (IPFZ), or following productive stratification events (Western SAZ), could sustain almost all Si-utpake in surface waters. In the eastern SAZ, which was not limited by iron, silicon limitation exerted a strong control on community structure favoring non-silicified phytoplankton and small lightly silicified diatoms also supporting an efficient silicon loop. The SAZ seemed to be a more efficient environment for biogenic silica dissolution due to higher temperature, bacterial activity and grazing pressure.

Strong Si-Fe co-limitation seemed to prevail in the IPFZ and to a lesser extent in the western SAZ. These conditions favored relatively heavily silicified and chain forming diatoms with low specific Si-uptake rates. Under iron-replete conditions as encountered in the eastern SAZ, biogenic silica specific production rates were higher, in agreement with an iron control on Si-uptake dynamics.

[3] Adapted from Fripiat F., Leblanc K., Cavagna A.-J., Elskens M., Armand L., André L., Cardinal D. (in prep). Mid-summer silicon dynamic and diatoms productivity in Polar Frontal and SubAntarctic Zones, south of Tasmania.

At all three stations diatoms contribution to primary production was low. A shift from diatoms dominated community towards flagellates dominated community was observed in the IPFZ. This evolution was reflected in Si:C particulate and uptake ratios and was in agreement with seasonal pattern of $Si(OH)_4$ limitation in summer in this area. In the western SAZ, this evolution was less marked and seemed to follow a stratification event. Our results in the SAZ suggest that stratification events and/or $Si(OH)_4$ pulse events could boost diatoms productivity and subsequently diatoms contribution to primary production as typically observed in oligotrophic systems or Si-addition bottle fertilization experiment.

A relation between Si:C uptake ratios and light level was found, in agreement with the fact that C uptake is light dependent through photosynthesis while Si uptake mainly occurs using energy coming from respiration. Such decoupling between C and Si with silicate pump processes and iron limitation should partly participate to the strong decoupling between NO_3 and $Si(OH)_4$ observed in the Southern Ocean.

8.1 Introduction

The Southern Ocean (SO) plays a key role in the global climate system by controlling a significant part of the CO_2 atmospheric concentration through a complex interplay between physical and biological processes (*Takahashi et al*., 2002; *Watson and Orr,* 2003). The SubAntarctic Zone (SAZ) and Polar Frontal Zone (PFZ) merit particular attention not only because of the extensive uptake of CO_2 from the atmosphere, particularly in the SAZ (*Metzl et al.*, 2001), but also because these regions are where the SubAntarctic Mode Water (SAMW) and Antarctic Intermediate Water (AAIW) are formed via the 'upper limb' of the meridional overturning circulation (*Trull et al*., 2001a). SAMW and AAIW ventilate the main oceanic thermocline and supply nutrients to the sub-tropical and tropical ocean on decadal to century timescales (*Toggweiler et al.*, 1991). Up to 75% of global oceanic production may rely on this nutrient supply (*Sarmiento et al.*, 2004). Its efficiency at lower latitudes depends closely on the efficiency on nutrient uptake and on the export of biogenic matter to deep ocean in the PFZ and SAZ (*Sigman and Boyle*, 2000). Limitation by macronutrients (N, Si, P) or micronutrients (trace metals) diminishes phytoplankton growth and ultimately the export of organic carbon to the deep sea. Carbon export is also governed by the relative use of new and recycled nutrients by the phytoplankton, which sets an upper limit on the fraction of primary production that can be exported to depth (*Dugdale and Goering*, 1967). None of these factors is the sole factor determining the magnitude and efficiency of the biological carbon pump. Rather, they and others interact through their combined effect on phytoplankton physiology and food web structure (*Brzezinski et al*., 2003a). Diatoms are major players of the biological pump in the Southern Ocean (*Buesseler et al*., 2001; *Trull et al*., 2001b; *Honjo et al*., 2008) and have an absolute requirement for silicon to build their cell wall (frustule). From a mooring study south of Tasmania, *Trull et al*. (2001b) reported that calcium carbonate dominate export fluxes in the SAZ while fluxes are dominated by biogenic silica in the PFZ. Nevertheless, biogenic silica contributes significantly to particles export in the SAZ during late summer (*Trull et al*., 2001b). Up to now, diatoms productivity in the SAZ was only investigated in four studies (*Nelson and Gordon*, 1982; *Quéguiner*, 2001; *Leblanc et al.*, 2002; *Beucher et al*., 2004b) but only two of them investigated $bSiO_2$ dissolution with only two profiles available, one in spring and one in summer (respectively *Nelson and Gordon*, 1982; *Beucher et al*., 2004b). In the PFZ, diatoms productivity was investigated by more extensive studies (*Nelson and Gordon*, 1982; *Brzezinski et al*., 2001; *Quéguiner and Brzezinski*, 2002; *Leblanc et al*., 2002). Two of them only investigated $bSiO_2$ dissolution through 19 profiles, 17 in spring and 2 in summer (*Nelson and Gordon*, 1982; *Brzezinski et al*.,

2001). A striking feature from these studies is the large variability observed in diatoms Si-uptake and dissolution, ranging in the PFZ from respectively 0.2 to 60.7 and 0.2 to 5.8 mmol Si m^{-2} d^{-1} and in the SAZ from respectively 0.01 to 3.05 and 0.4 to 5.2 mmol Si m^{-2} d^{-1}. Clearly, a better assessment of this variability is required to quantify the role of diatoms on C productivity and the strength of the silicate pump in both regions.

The SAZ-Sense cruise ('Sensitivity of the SubAntarctic zone to environmental change') was conducted in waters East, West and South of Tasmania and represents an excellent approach to examine biogeochemical cycling in the Southern Ocean in contrasted environments. The SAZ region West of Tasmania (135 to 145°E) is usually characterized by low phytoplankton biomass while the SAZ East of Tasmania (150-160°E) exhibits relatively high phytoplankton biomass (*Griffiths et al.*, in prep). This contrast for the same Southern Ocean zone is possibly linked with spatial and temporal changes in light, Fe and $Si(OH)_4$ availability in SAZ surface waters (*Boyd et al.*, 1999b; *Boyd*, 2002).

The objectives of this study were (1) to understand processes which drive Si-biogeochemical budget (Dissolution:production ratios) in surface waters using the ^{30}Si stable isotope method initially developed by *Nelson and Goering* (1977a, 1977b) but with a new analytical method which improves sensitivity (Fripiat et al., 2009) and to compare it with the ^{32}Si radioactive isotope labeling (*Tréguer et al.*, 1991; *Brzezinski et al*., 1997). These measurements were coupled to others measurements (e.g., siliceous biomass, PDMPO labeling (*Leblanc and Hutchins,* 2005), diatom community composition, and bacterial activity; see *Armand et al*., in prep; *Leblanc et al.*, in prep; *Dumont et al*., submitted) in order to fully characterize the Si-biogeochemical cycle during SAZ-Sense; (2) to compare the Si cycle with gross primary production (*Cavagna et al*., submitted), to provide an estimation of the contribution of diatoms to primary production and to understand the dynamic of nutrients' uptake and their degree of coupling.

8.2 Materials and methods

8.2.1 Oceanographic settings and sampling strategy

The SAZ-Sense cruise track (21 January – 19 February 2007, R/V Aurora Australis) followed a diamond-shaped grid in the Australian sector of the Southern Ocean south of Tasmania (Figure 8.1) from the SubTropical to the (Inter) Polar Front through the SubAntarctic Zones, thereinafter referred to as STZ, (I)PFZ and SAZ, respectively. The area is characterized from north to south by several circumpolar fronts: the SubTropical Front (STF), the SubAntarctic Front (SAF), and the northern branch of the Antarctic Polar Front (APF) (*Trull et al*., 2001a; *Griffiths et al*., in prep; Figure 8.1). Three Process stations were selected on the basis of their contrasted hydrodynamics, physico-chemical and ecosystem's characteristics. The aim of Process stations was to have a station occupation of 6 to 8 days to conduct incubation experiments and replicate samplings over several days. Process station 1 (P1, 140.6°E, 46.3°S; 22-29 January 2007) was located in the northwestern SAZ waters, Process station 2 (P2, 145.9°E, 54.0°S; 01-06 February 2007) in the Inter Polar Frontal Zone as indicated by the presence of a temperature minimum layer between 100 and 250 m (remnant winter waters), Process Station 3 (P3, 153.2°E, 45.5°S; 10-15 February 2007) was located in an highly dynamic region at the northernmost edge of the SAZ (Figure 8.1). P3 was indeed strongly influenced by the lateral mixing of warm, salty subtropical waters driven by eddies of the Eastern Antarctic Current extension with cooler fresh SAZ waters (*Ridgway*, 2007).

^{30}Si incubations were performed at process stations on three different days to cover short-term temporal variability. Samplings (always at dawn) were performed simultaneously (same CTD casts) with ^{32}Si incubations, PDMPO labeling (*Leblanc et al.*, in prep), taxonomic composition (*Armand et al.*, in prep), ^{13}C/^{15}N incubations (*Cavagna et al.*, submitted), and bacterial production/activity (*Dumont et al.*, submitted). Details of the individual data sets and associated methodology (except Si) considered here have been published in the before mentioned articles and will not be repeated here. Uptake rates were determined at four depths corresponding to 100, 50, 25, and 1% of PAR (Photosynthetically Active Radiation) light depths sampled with Niskin bottles mounted on a CTD rosette. Samples were incubated in deck incubators equipped with blue Lee filters screens to simulate the light intensity at depth of collection for 24 (t24) and 48 (t48) hours. Circulating surface seawater was used to maintain ambient surface temperatures within the incubators.

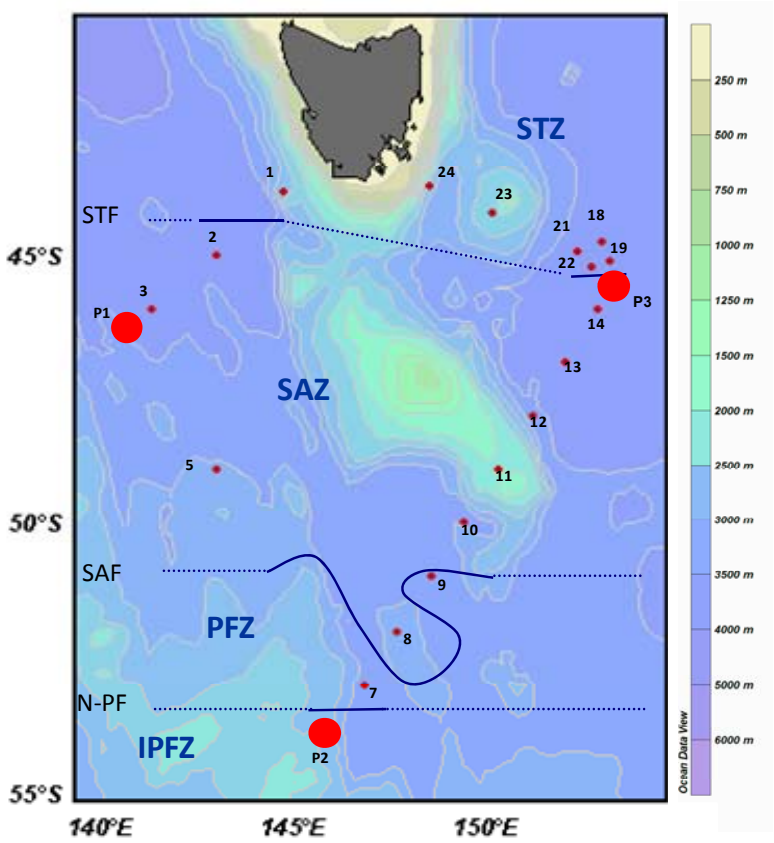

Figure 8.1. Map of the study area with bathymetry and main hydrographic features. The SAZ-Sense process stations are represented by large red dots.

8.2.2 Nutrients and particulate matter measurements

$Si(OH)_4$ concentrations were analyzed onboard on a segmented flow auto-analyzer (Lachat Quickchem series 8000 FIA). The $bSiO_2$ filtered onto polycarbonate membranes (Nucleopore 0.4 µm porosity, 47 mm Ø), was dried at 60°C and stored at room temperature. It was digested at the laboratory in one step with 0.2M NaOH during 40 min at 100°C followed by neutralization with HCl 1M (adapted from *Ragueneau et al.,* 2005). Biogenic silica ($bSiO_2$) concentrations were determined with a spectrophotometer (Genesys 10S UV, VWR) following *Grasshoff et al.* (1983). Samples for Particulate Organic Carbon (POC) concentrations

were filtered on pre-combusted glass fiber filter (Wathmann, GF/F, 0.7 µm porosity, 25 mm Ø), stored in the dark at room temperature, and analyzed at the laboratory on an elemental analyzer – Isotopic ratio mass spectrometer using the method described in *Savoye et al.* (2004).

8.2.3 $bSiO_2$ production and dissolution rates

Seawater was spiked with ^{30}Si (*Nelson and Goering*, 1977a, 1977b) and incubated under controlled light conditions. The changes in isotopic composition of the particulate phase (increase in ^{30}Si) are used to estimate $bSiO_2$ production rates. To assess $bSiO_2$ dissolution rates, the increase in ^{28}Si in the dissolved phase due to the dissolution of initial biogenic silica is measured. Seawater was sampled following *Corvaisier et al.* (2005): For each light level, 8L of seawater were collected in a PC bottle. 2L were collected immediately as the unspiked standard. The remaining 6L were then spiked with ^{30}Si and homogenized. A second aliquot (2L) was again subsampled for the initial conditions, and the remaining volume was incubated in 4L PC bottles for 2 days (with subsampling (2L) at t24 and t48). For $Si(OH)_4$, we applied a preconcentration protocol adapted from the MAGIC method (*Karl and Tien*, 1992; *Rimmelin-Maury et al*., 2007) in order to increase the Si:salinity ratio (Fripiat et al., 2009). As $Si(OH)_4$ concentrations in seawater during SAZ-Sense were too low (<2.8 µmol Si l^{-1}; expect 1% PAR at P2) and too saline to be introduced into the mass spectrometer without purification, even after Si-preconcentration, a cation-exchange chromatography developed by *Georg et al.* (2006a) was applied to remove the saline matrix to all samples including at the 1% PAR at P2 (*Fripiat et al.*, 2009). Purified $Si(OH)_4$ samples and digested $bSiO_2$ solutions were diluted at ~ 100 ppb Si in bidistilled 0.65% HNO_3 and analyzed by a standard High Resolution Sector Field Inductively Coupled Plasma Mass Spectrometer (HR-SF-ICP-MS, ELEMENT2, Thermo, Bremen, Germany) to determine silicon isotopic abundances. This new method is described in details in *Fripiat et al.* (2009). Each sample was fully duplicated and the reproducibility of ^{30}Si isotopic abundance (Atom %) was better than 1% (Relative Standard Deviation).

In order to calculate the production and dissolution rates of biogenic silica (respectively ρ_{Si} and ρ_D) from those measurements, it is necessary to postulate a model. Until now two different models existed, the linear one compartmental model described for production (*Nelson and Goering*, 1977a) and dissolution (*Neslon and Goering*, 1977b), and the nonlinear two compartmental model previously described in *Beucher et al.* (2004b), and *Elskens et al.* (2007). The mass balance is not taken into account in the one compartmental model (*Nelson and Goering*, 1977a,b). In the two compartmental model parameters are constrained by the requirement to fit mass and isotopic balances of dissolved and particulate phases (*Elskens et al*., 2007). This model takes into account both isotopic dilution and concentration changes occurring over the course of incubation which can induce biases in estimations when ignored. A detailed comparison on the two models is provided in *Elskens et al.*, (2007).

Si-uptake estimates from ^{30}Si and ^{32}Si methods were compared for the complete set of incubations (n = 36). For the ^{32}Si method, 275-ml seawater samples were spiked with $^{32}Si(OH)_4$ produced by Los Alamos laboratory (*Tréguer et al.*, 1991; *Brzezinski et al.*, 1997) and incubated in the same deck incubators as for ^{30}Si for 24h. After 24h, the samples were filtered (0.4 µm, PC membrane Nuclepore) and the filters stored in PE scintillation vials at ambient temperature until analysis. The radioactivity of the particulate biogenic silica was measured on a Packard 1600-TR scintillation counter. The relative precision on Si-uptake rates is 10%, similar to the ^{30}Si method (*Fripiat et al*., 2009). However, the ^{32}Si method does not allow quantification of $bSiO_2$ dissolution rates.

Integration of stock and fluxes was done using the trapezoidal integration method to the 1% light depth.

8.3 Results

8.3.1 Assessment of the accuracy of the $bSiO_2$ production-dissolution rates estimates

Several assumptions are taken into account to process the data which include a number of basic statements about the behaviour of the isotopic tracer (*Elskens et al.*, 2007). Briefly the assumptions are (i) the tracer $^{30}Si(OH)_4$ undergoes the same transformations than the unlabelled substrate $^{28}Si(OH)_4$, i.e. isotopic effects are negligible, (ii) there is no isotopic exchange between the labeled substrate and other Si pool than diatom, e.g. between $Si(OH)_4$ and lithogenic silica (iii) initially, the tracer is not in equilibrium with the studied system, and its change over time is quantifiable, (iv) dissolving $bSiO_2$ has the natural abundance ratio, i.e. it consists of non-labeled silicon, and (v) the tracer addition (less than 10% of in situ stock) does not perturb the steady state existing in the system. Assumptions (i) and (ii) are not significantly violated (*De La Rocha et al*., 1997; *Demarest et al*., 2009). Several indexes described in *Elskens et al*. (2007) allow estimating a potential violation of the statements (iii) and (iv) and no violation of these assumptions were observed on our data (not shown). Nevertheless, 12 of the 36 incubations had a tracer addition comprised between 10% and 20%, and one exceeded 30%. For these incubations the assumption (v) might have been violated. However, as shown later, the good comparison with ^{32}Si-uptake rates for which all Si additions were below 10% suggests that results have not been biased by over-addition of ^{30}Si.

In order to assess the discrepancy between the observations (y_i) and the model counterparts (x_i) for the four parameters used ($[Si(OH)_4]$, $[bSiO_2]$, atom % $^{30}Si_{Si(OH)4}$, and atom % $^{30}Si_{bSiO2}$), the residual ($y_i - x_i$) needs to be transformed to a common scale by the standardized residual (SR_i) approach (*Elskens et al.,* 2007) :

$$SR_i = \frac{y_i - x_i}{\sqrt{2} \cdot \sigma_i} \quad (8.1)$$

where ρ_i represents the relative standard deviation expected for each parameter. Hence, SR_i represents the deviation of the modeled parameter from the measurement normalized by the expected uncertainty of the parameter. Taking into account all the sampling treatments and analyses, we consider an expected relative standard deviation of 2, 7 and 1% for $[Si(OH)_4]$, $[bSiO_2]$, and ^{30}Si-isotopic abundances, respectively. These standard deviations have been constrained during BONUS-Goodhope (R.V. Marion Dufresne in 2008) cruise on 42 incubations which were triplicated (annex 1).

If the model correctly describes the main features of uptake and dissolution processes, it is expected that SR_i-scores for each parameter will be symmetrically distributed around a mean of zero and < 3 (i.e. less than 3 times the expected standard deviation) (*Elskens et al.* 2007).

Figure 8.2a and b presents the SR_i's for the one and two compartmental models. The one compartmental model (Figure 8.2a) has SR_i-scores that do not behave as standard normal variables. Medians generally differ from 0, and there are too many unacceptable scores above 3. The SR_i-scores are even worse at t48. This is an evidence of a model failure which especially appears for small Si-fluxes (P1 cast #34, and P3) as well as for larger Si-fluxes (P1 casts #9 and #17, and P2) for which the SR_i-scores distribution is not satisfactory either (not shown). In contrast, the SR_i-scores of the two compartment model better fit the ideally zero-centered distribution whatever the intensity of the Si-fluxes (Figure 8.2b): there is no evidence of systematic error (as already observed in *Elskens et al.*, 2007). At t48, the model does not fit perfectly the zero-centered distribution but it is still within expected error.

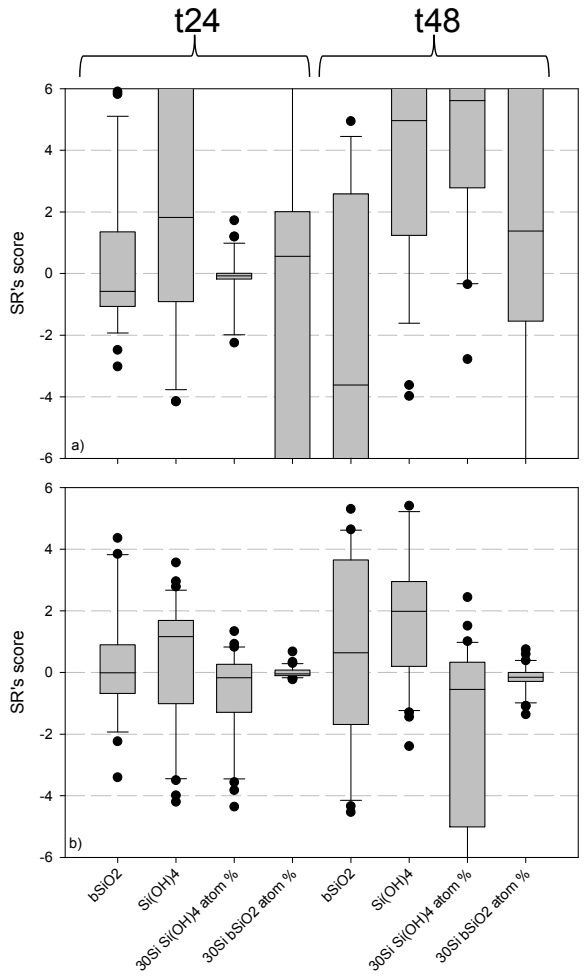

Figure 8.2. SR's scores for one compartmental model (panel a) and two compartmental model (panel b). The boxes, whiskers and symbols cover the twenty-fifth to seventy-fifth, the tenth to ninetieth and the fifth to ninety-fifth percentiles respectively.

Si-uptake rates estimated at t24 and t48 are not significantly different (Figure 8.3a; slope = 1.01 ± 0.03, R^2=0.94, p value <0.01) suggesting little influence of short-term light variability on silicification processes in agreement with previous studies (review in *Martin-Jézéquel et al*., 2000). As the SR_i's scores seem to indicate that the mass and isotopic balances are better respected in t24 incubations, in the following ^{30}Si-uptake estimates from t24 will be used. Si-uptake estimates from ^{30}Si and ^{32}Si methods were also compared on the complete set of incubations (n = 36). There was a good correlation between the two (R^2 = 0.85; p value < 0.01, Figure 8.3b) with a slope not significantly different from 1.0 (0.96 ± 0.06). At P3 however, ^{32}Si uptake rates were 2-3 times higher than ^{30}Si uptake rates but were still very low (<10 nmol Si d^{-1}, Table 8.1). $bSiO_2$ concentration for ^{30}Si-measurements was systematically higher than for ^{32}Si-measurements (respectively 0.025 ± 0.004 and 0.016 ± 0.001 µmol Si l^{-1}) suggesting a potential Si-contamination. Such contamination with the natural isotopic background should decrease the final ^{30}Si-isotopic abundance of $bSiO_2$ subsequently underestimating Si-uptake. Due to the very low natural background ^{32}Si-concentration, a contamination is less easily expressed on ^{32}Si-incubation. The fact that P3 was just after P2 where much higher Si-content was measured, could explain this. Indeed, for the cast #34

(P1; before P2) with similar $bSiO_2$ concentration and Si-fluxes, no systematic difference is observed between the two methodologies. Moreover, larger volumes were manipulated for ^{30}Si-measurements incidentally increasing the probability of Si-contamination at such level of $bSiO_2$ concentration.

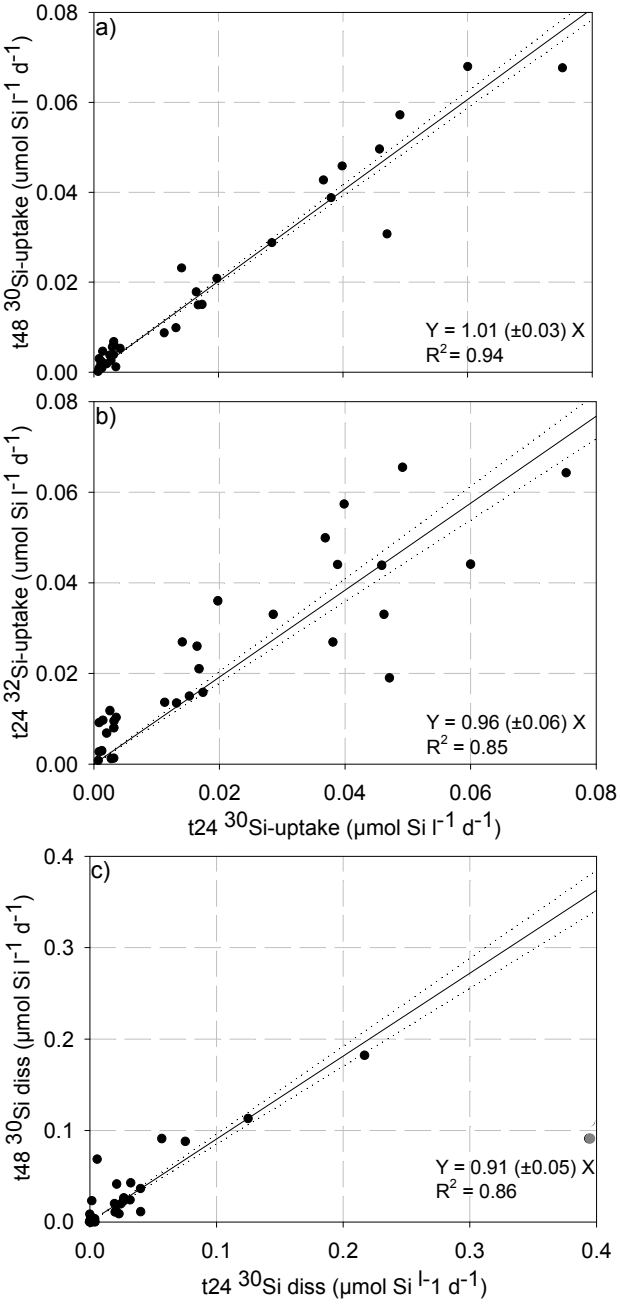

Figure 8.3. Panel a shown the correlation between $Si(OH)_4$ uptake estimates at t24 in relation with t48, both with ^{30}Si method. Panel b shown the correlation between $Si(OH)_4$ uptake estimates at t24 with ^{30}Si method in relation with the estimates with ^{32}Si method. Panel C shown the correlation between $bSiO_2$ dissolution estimates at t24 in relation with t48. In panel c, 1% PAR of P2 (cast 58) is not taken into account in the regression (gray dot).

$bSiO_2$ dissolution rates from t24 and t48 were generally also almost the same (R^2 = 0.86; slope of 0.91 ± 0.05, p value < 0.01; Figure 8.3c, excluding one outlier). The outlier is the deep $bSiO_2$ maximum of cast #58 (PAR 1%) where $bSiO_2$ dissolution at t24 largely exceeded that at t48. For the deep $bSiO_2$ maximum at P2, t48-^{30}Si uptake is more in agreement with ^{32}Si uptake rates and t48 exhibits in this case better SR's score than t24 (not shown). Therefore both for uptake and dissolution, t48 estimates will be used in the discusion for deep P2 samples. For all the other, we will use rates calculated from t24 incubations. This slight model failure at t24 could result from Si-efflux outward the cells (*Martin-Jézéquel et al*., 2000): the

intracellular silicon pool (turnover less than 1 day; Ragueneau et al., 2000) is not initially in isotopic equilibrium with extracellular spiked silicic acid pool and could bias the measured $bSiO_2$ dissolution by releasing ^{28}Si-isotopic in the incubation water. Indeed, at the deep $bSiO_2$ maximum, higher silicic acid concentration and accumulation of settling cells from Si-depleted mixed layer could favor Si-efflux (*Sulivan*, 1976; *Thamatrakoln and Hildebrand*, 2008). This process could explain the relative bad SR's score at t24 found in deep $bSiO_2$ maximum.

The detection limit for ^{30}Si-isotopic dilution is shown in Figure 8.4. It was estimated by solving the mass and isotopic balance using as constraint that the difference between initial and final ^{30}Si-isotopic abundances should be at least 1% (~ 1 relative standard deviation). Variable $Si(OH)_4$ concentrations (from 0.25 to 6 µmol Si l^{-1}) and initial silicic acid ^{30}Si-isotopic abundances (12 ± 6 atom % ^{30}Si which represents a spike addition of *circa* 10 ± 5%) have been tested, while $bSiO_2$ production and content have no significant influence on the value of the detection limit for $bSiO_2$ dissolution. All the dataset, except for P3 and cast #34 of P1, are above the detection limit estimate.

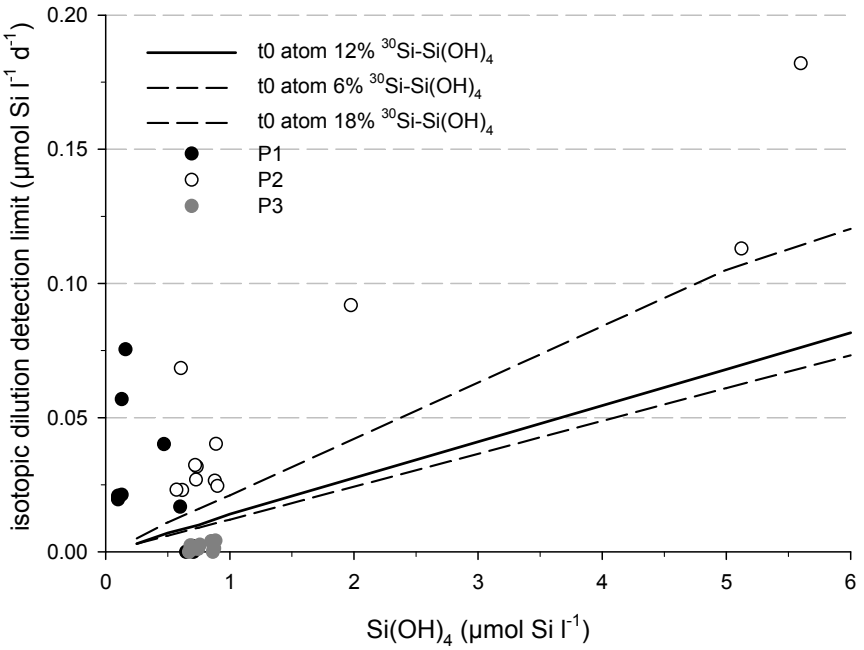

Figure 8.4. Detection limit for ^{30}Si-isotopic dilution for measuring $bSiO_2$ dissolution as a function of $Si(OH)_4$ concentration and spike addition. Black dots represent the SAZ-sense dataset.

8.3.2 Distribution of $Si(OH)_4$, $bSiO_2$, Si-uptake and $bSiO_2$ dissolution rates

The complete data used for discussion are provided in Table 8.1 and displayed on figure 8.5. Euphotic layer (Z_e) and mixed layer depth are given in Table 8.2. As in *Quéguiner* (2001) in the same area, an increasing north-south gradient was observed for $Si(OH)_4$ in the SAZ (range = 0.1 - < 2 µmol Si l^{-1}), in agreement with lateral advection from nutrient-rich PFZ surface water via Ekman transport (*Trull et al.*, 2001b). The SAMW formed by deep winter convective mixing (*Trull et al*., 2001b) is characterized by $Si(OH)_4$ concentrations close to 4-5 µmol Si l^{-1} reflecting past biological activity in the mixed layer since SAMW could be considered as the mixed layer initial condition (*Lourey and Trull*, 2001; *Cardinal et al*.,

2005). From *Leblanc et al*., (in prep) and *Westwood et al*., (in prep), the three Process stations covered the whole range of C and Si productivity encountered during SAZ-Sense.

Process date	cast #	depth m	$Si(OH)_4$ µmol Si l^{-1}	$bSiO_2$ µmol Si l^{-1}	Si-utpake (^{30}Si) µmol Si l^{-1} d^{-1}	Si-utpake (^{32}Si) µmol Si l^{-1} d^{-1}	$bSiO_2$ dissolution µmol Si l^{-1} d^{-1}
Process 1	9	5	0.16	0.176	0.039	0.044	0.075
22-01-07		10	0.13	0.184	0.046	0.033	0.057
		17	0.13	0.174	0.047	0.019	0.021
		50	0.47	0.295	0.020	0.036	0.040
Process 1	17	5	0.10	0.109	0.029	0.033	0.020
24-01-07		10	0.10	0.105	0.017	0.021	0.021
		15	0.10	0.085	0.016	0.026	0.020
		50	0.60	0.118	0.015	0.015	0.017
Process 1	34	5	0.65	0.016	0.003	0.001	0.000
29-01-07		10	0.70	0.020	0.003	0.001	0.002
		15	0.71	0.017	0.001	0.001	0.001
		50	0.71	0.016	0.001	0.003	0.000
Process 2	42	5	0.88	0.702	0.049	0.065	0.027
02-02-07		12	0.89	0.777	0.040	0.057	0.040
		24	0.90	0.852	0.060	0.044	0.025
		80	5.60	2.768	0.067	0.064	0.182
Process 2	47	10	0.73	0.909	0.046	0.044	0.027
03-02-07		20	0.73	0.817	0.037	0.050	0.032
		30	0.72	0.782	0.038	0.027	0.032
		80	5.12	3.098	0.062	0.046	0.113
Process 2	58	10	0.62	0.450	0.017	0.016	0.023
06-02-07		20	0.57	0.418	0.011	0.014	0.023
		30	0.61	0.412	0.013	0.013	0.068
		80	1.98	1.310	0.023	0.027	0.092
Process 3	81	5	0.70	0.029	0.001	0.010	0.001
12-02-07		10	0.70	0.028	0.001	0.009	0.001
		15	0.67	0.029	0.004	0.010	0.000
		30	0.68	0.028	0.002	0.007	0.002
Process 3	85	5	0.76	0.025	0.003	0.012	0.003
13-02-07		10	0.75	0.022	0.003	0.010	0.001
		15	0.74	0.022	0.003	0.008	0.001
		30	0.86	0.018	0.001	0.003	0.000
Process 3	96	5	0.85	0.025	0.003		0.004
15-02-07		10	0.89	0.025	0.004		0.004
		15	0.88	0.022	0.001		0.001
		30	0.87	0.022	0.001		0.001

Table 8.1. $[Si(OH)_4]$, $[bSiO_2]$, Si-uptake (both with ^{30}Si and ^{32}Si), $bSiO_2$ dissolution for each casts of each process.

A significant daily variation was observed in $Si(OH)_4$ concentration at P1 (Figure 8.5a). Casts #9 and #17 exhibited the highest $Si(OH)_4$ depletion (<0.2 µmol Si l^{-1} in the surface layer) and cast #34 the highest concentration (~ 0.7 µmol Si l^{-1} in the mixed layer). Temperature-salinity profiles indicated that casts #9 and #17 were sampled within the same water mass while the ship had drifted to the South-West for cast #34, which presented a deeper mixed layer depth explaining $Si(OH)_4$ variations (*Griffiths et al*., in prep). At P2 in the IPFZ, higher $Si(OH)_4$ concentrations were observed with a more pronounced $Si(OH)_4$ vertical gradient as usually observed in this zone (*Quéguiner*, 2001; *Leblanc et al*., 2002). Casts #42 and #47 had similar $Si(OH)_4$ concentrations, which were higher than those measured on cast #58 for the whole euphotic layer (Figure 8.5b). At P3 in the Eastern SAZ, $Si(OH)_4$ concentration were higher (~0.8 µmol Si l^{-1}) and less variable than in the Western SAZ (Figure 8.5c).

Large $bSiO_2$ variations were also observed at P1. $bSiO_2$ concentrations in the euphotic layer decreased over the course of the station occupation (Figure 8.5a). A slight $bSiO_2$ increase was observed at 1% PAR (50 m) on cast #9 and was also observed at the other transect stations studied during SAZ-SENSE (*Leblanc et al*., in prep). A similar feature (deep Si maximum) was observed in this area in mid-summer by *Beucher et al*. (2004b). At P2, $bSiO_2$ concentrations for casts #42 and #47 were similar in the ML (0.7-0.9 µmol Si l^{-1}) while a significant deep $bSiO_2$ maximum (2.8-3.1 µmol Si l^{-1}) was observed below the ML at 1% PAR (~80 m) (Figure 8.5b). Cast #58 presented the same features but with lower $bSiO_2$ concentrations, as for $Si(OH)_4$. P3 exhibited extremely low and constant $bSiO_2$ concentrations (0.024 ± 0.004 µmol Si l^{-1}; Figure 8.5c).

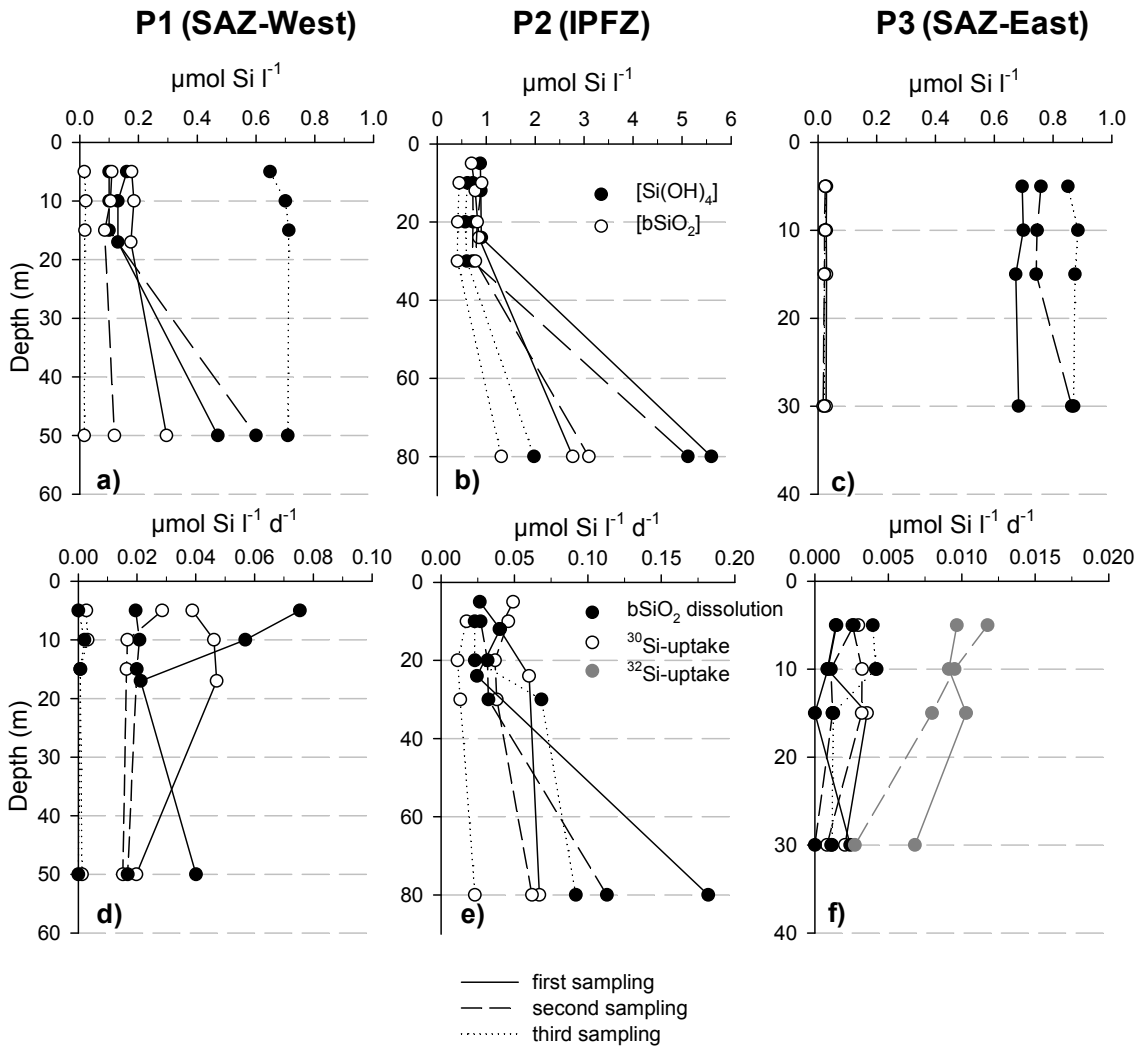

Figure 8.5. Upper panels: vertical distribution of $bSiO_2$ and $Si(OH)_4$ concentrations (a, b, c, for P1, P2, P3, respectively). Lower panels: $Si(OH)_4$ uptake and $bSiO_2$ dissolution (d, e, f for P1, P2, P3, respectively). The full, dashed, and dotted lines are respectively casts #9, #17, #34 for P1, casts #42, #47, #58 for P2, and casts #81, #85, #96 for P3. In panel f, $Si(OH)_4$ uptake measured with ^{32}Si are shown with gray dots.

As for $bSiO_2$ concentration at P1, $Si(OH)_4$ uptake (ρ_{Si}) decreased during the station occupation (Figure 8.5d). It also decreased slightly with depth. At P2 in contrast to $bSiO_2$ concentration, ρ_{Si} was slightly higher than P1 (Figure 8.5d,e). ρ_{Si} for casts #42 and #47 were similar and higher than cast #58, similarly to Si concentrations (Figure 8.5b,e). At P3, extremely low ρ_{Si} values were measured (0.002 ± 0.001 µmol Si l^{-1}). ^{32}Si method gave significantly higher ρ_{Si} estimate (0.008 ± 0.003 µmol Si l^{-1}; only casts 81 and 85 are available), but only at this station. As discussed in section 8.3.1, a potential Si-contamination with natural isotopic background has probably underestimated ^{30}Si-uptake. Highly contrasted specific Si uptake rates, V_{Si} (in d^{-1}), calculated by $\rho_{Si}/[bSiO_2]$ with ^{30}Si and ^{32}Si methodologies, between the different process stations was observed (Figure 8.6). V_{Si} was very low in the IPFZ (respectively 0.04 ± 0.02 and 0.06 ± 0.03 d^{-}

Site	date	Cast #	Mixed layer depth (m)[1]	Eupthotic layer depth (m)	POC[2] mmol C m^{-2}	$bSiO_2$ mmol Si m^{-2}	^{13}C-GPP[2] mmol C m^{-2} d^{-1}	^{30}Si-uptake mmol Si m^{-2} d^{-1}	$bSiO_2$:POC	Si:C uptake
Process 1	22-01-07	9	20	50	577	10.8	147.8	1.84	0.019	0.012
	24-01-07	17	43	50	462	5.1	70.8	0.89	0.011	0.013
	29-01-07	34	73	50	170	0.84	13.6	0.07	0.005	0.005
Process 2	02-02-07	45	57	80	599	119.8	36.8	4.70	0.200	0.128
	03-02-07	47	47	80	589	122.7	34.2	3.75	0.208	0.110
	06-02-07	58	62	80	410	56.0	36.2	1.35	0.137	0.037
Process 3	12-02-07	81	13 80	30	535	0.9	52.9	0.07	0.002	0.001
	13-02-07	85	15 80	30	543	0.7	51.2	0.07	0.001	0.001
	15-02-07	96	14 75	30	648	0.7	65.9	0.06	0.001	0.001

[1] see Mongin et al. (in prep) for details about the 2 density gradients (2 mixed layer depths) observed at P3

[2] Cavagna et al. (submitted)

Table 8.2. Integrated POC, $bSiO_2$, Gross Primary Production, and Si-uptake for each casts of each process. Integrated $bSiO_2$:POC, and Si:C uptake ratios are shown.

^{1}), intermediate in the Western SAZ (respectively 0.17 ± 0.08 and 0.14 ± 0.09 d^{-1}), and intermediate or high in the Eastern SAZ depending of the methodology (respectively 0.11 ± 0.06 and 0.54 ± 0.20 d^{-1}). For the reasons discussed before, ^{32}Si-estimates are taken at P3.

$bSiO_2$ dissolution rates decreased, as for ρ_{Si}, during the station occupation at P1 (Figure 8.5d) down to values below the detection limit for cast #34 (~ 0.008 µmol Si l^{-1}; Figure 8.4). For casts #9 and #17, $bSiO_2$ dissolution decreased with depth. P2 exhibited constant $bSiO_2$ dissolution rates in the mixed layer during the station occupation (Figure 8.5e). At the deep $bSiO_2$ maximum, the $bSiO_2$ dissolution was significantly higher than in the mixed layer. The two compartmental model yielded extremely low $bSiO_2$ dissolution rates at P3 (0.002 ± 0.001 µmol Si l^{-1} d^{-1}; Figure 8.5f) below the detection limit of ^{28}Si-isotopic dilution (~ 0.008 µmol Si l^{-1}; Figure 8.4).

8.4 Discussion

As a general feature during SAZ-Sense, the SubAntarctic Zone was characterized by higher Particulate Organic Carbon (POC) content and Gross Primary Production (GPP, C-utpake) than the IPFZ (*Cavagna et al*., submitted; *Westwood et al*., in prep) in accordance with previous studies conducted in austral summer (*Griffiths et al*., 1999; *Boyd et al*., 1999b; *Elskens et al*., 2002; *Leblanc et al*., 2002; *Reuer et al*., 2007). The biogenic silica and Si-fluxes exhibited an inverse pattern with higher stock and Si-fluxes in the IPFZ compared to the SAZ (this study; *Leblanc et al*., in prep) as previously observed in this area (*Quéguiner*, 2001) and in agreement with a larger contribution of diatoms to primary production towards polar waters (*Wright et al*., 1996; *Popp et al*., 1999; *Kopczynska et al*., 2001, 2007; *Safi et al*., 2007). In the following, we will discuss in more details these results and attempt to make quantitative estimates of the Si biogeochemical cycle.

8.4.1 Control of $bSiO_2$ production and dissolution rates

8.4.1.1 $bSiO_2$ production rates

Such gradient in specific Si-uptake rate (Figure 8.6) was already observed for the IPFZ and the non iron-fertilized SAZ (*Quéguiner*, 2001; *Leblanc et al*., 2002). Calculated V_{Si} represents a lower estimation of specific uptake rate since detrital biogenic silica or inactive diatoms are taken into account in the calculation. Moreover, V_{Si} represents a mean of the bulk diatoms community and can erase interspecific variability in $Si(OH)_4$ affinity (*Leblanc and Hutchins*., 2005; Leblanc et al., in prep).

In the IPFZ (P2), low V_{Si} suggests that siliceous phytoplankton populations were strongly limited either by light and/or iron (*Boyd et al*., 2001) influencing Si-uptake processes (*De la Rocha et al*., 2000a; *Claquin et al*., 2002*; Franck et a*l., 2003; *Leynaert et al*., 2004). Moreover, low $Si(OH)_4$ concentration in the mixed layer (<1 µmol Si l^{-1}) fall in the range of concentrations known to limit diatoms growth (*Nelson and Tréguer*, 1992; *Nelson et al*., 2001; *Sedwick et al*., 2002). These different potential co-limitations (*Boyd*, 2002) in addition to the fact that SAZ-Sense occurred at the end of productive period likely explain these low Si specific uptake rates, which are classically observed in the Southern Ocean (*Nelson et al*., 2001).

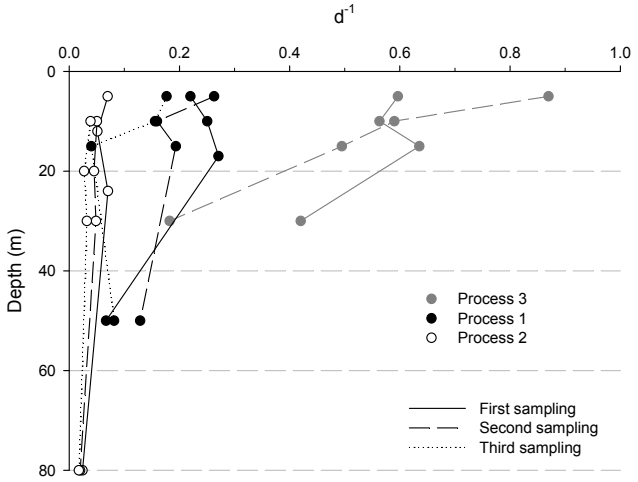

Figure 8.6. Vertical distribution of specific Si-uptake rates for each casts of each process stations. The black, white, and gray dots represent respectively process stations 1, 2, 3. The full, dotted, and dashed lines are respectively casts #9, #17, #34 for P1, casts #42, #47, #58 for P2, and casts #81, #85 for P3. For P3, only the ^{32}Si results are presented (section 8.3).

In the Western SubAntarctic Zone (P1) several co-limitations potentially also occurred. The relatively higher specific Si-uptake rates compared to the IPFZ suggests that the extent of these potential co-limitations should be lower and/or the SAZ diatoms species have higher Si-affinity (*Claquin et al*., 2002; *Leynaert et al*., 2004; *Timmermans et al*., 2001, 2004). The productive period was still ongoing since higher primary production rates (both gross and new) and chla content were measured (*Cavagna et al*., submitted; *Wright et a*l., in prep.) suggesting a higher proportion of active diatoms which may also explain the higher specific Si-uptake rates (Figure 8.6).

In the Eastern SAZ (P3) where iron concentrations were sufficient for growth (0.48 ± 0.10 nmol Fe l^{-1}; *Lannuzel et al*., submitted), the alleviation of Fe limitation seemed to stimulate Si uptake as previously observed in other studies even if conflicting results on the impact of Fe on Si uptake kinetic parameters still persist (*De La Rocha et al*., 2000a; *Hutchins et al.*, 2001; *Franck et al*., 2003; *Leynaert et al*., 2004; *Brzezinski et al*., 2005, 2008; *Mosseri et al*., 2008).

8.4.1.2 $bSiO_2$ dissolution rates

$bSiO_2$ dissolution in the marine environment has been shown to be influenced by temperature, diatom species, trace metal content of the frustule, grazing, bacterial activity, and the percentage of dead diatoms (review in *Nelson et al*., 1995*; Bidle and Azam*, 1999, 2001; *Van Cappellen et al*., 2002; *Bidle et al*., 2003; *Beucher et al*., 2004b). During SAZ-Sense, there was a coarse positive relationship (R^2 = 0.72; p value < 0.01) between $bSiO_2$ concentration and $bSiO_2$ dissolution rates: dissolution rates were higher when biogenic silica (i.e. probably also more dead/inactive diatoms) concentrations were higher. Nevertheless, there were some differences between process stations. In the Western SAZ (P1), the linear regression slope between $bSiO_2$ dissolution rates and $bSiO_2$ concentrations was 0.21 (R^2 = 0.70, p value < 0.01) larger than in the IPFZ (P2, slope = 0.05, R^2 = 0.79, p value < 0.01). The SAZ environment seemed more proned to $bSiO_2$ dissolution than the IPFZ. The temperature differences between these two areas could partly explain this (Figure 8.7a). In this figure, specific dissolution rates for casts # 34 (P2), #81, #85, and #96 (P3) are not shown due to the uncertainties on these fluxes (section 8.3.1). There is evidence from the

literature that higher temperature enhances specific $bSiO_2$ dissolution rates (*Kamatani*, 1982; Hurd and Birdwhistell, 1983). Another process which could explain this difference is bacterial activity. It efficiently denudes the organic matrix isolating $bSiO_2$ from the surrounding Si undersaturated environment, allowing subsequent chemical dissolution of the naked frustules (*Bidle and Azam*, 1999, 2001; *Bidle et al.*, 2003). As shown in *Dumont et al*. (in prep), bacterial production and activity during SAZ-Sense were higher in the

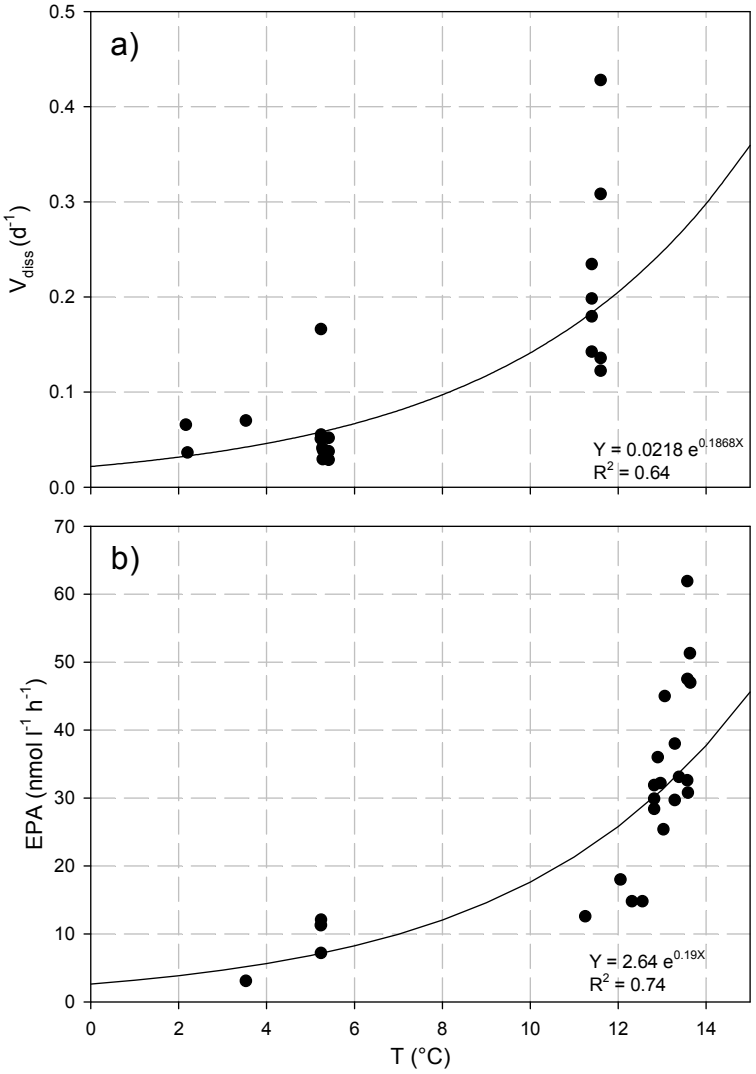

Figure 8.7. Specific $bSiO_2$ dissolution rates (panel a) and ectoenzymatic activity (panel b, from Dumont et al., submitted) both vs. temperature. For panel A, only the values significantly different from zero are shown (± 1RSD).

SAZ than in the IPFZ, also probably due to temperature difference and higher substrate availability. *Bidle et al.* (2002) demonstrated a temperature regulation on ectoprotease activities, the main hydrolytic ectoenzyme of the organic protective coating. This relationship was also found in our study (R^2 = 0.74; Figure 8.7b; *Dumont et al.,* submitted). This complex interplay between bacterial activity and temperature, which is likely to be influenced by the type of organic substrate and phytoplankton species composition, could explain the relatively weaker correlation (R^2 = 0.63) between specific $bSiO_2$ dissolution rate and temperature (Figure 8.7a). Indeed, C and Si regeneration rates show significant variability (~ fourfold) among different bacterial assemblages and isolates (*Bidle and Azam*, 1999, 2001), implying that species

composition, colonization dynamics, metabolic state and ectoprotease activity are important variables. Moreover, *Pearce et al*. (in prep) report higher grazing rates in the SAZ than in the IPFZ, a process which can also enhance $bSiO_2$ dissolution depending on the type of grazers (Nelson et al., 1995). To conclude, SAZ waters with higher temperature and microbial food wed is a more efficient dissolution environment in agreement with the fact that temperature controls the carbon export efficiency (Laws et al., 2000).

8.4.2 Diatoms productivity and comparison with previous studies

Figure 8.8 shows integrated (over Z_e) Si-fluxes for each day at each process station compared to averages from previous studies in the PFZ-IPFZ and SAZ in summer (*Caubert*, 1998; *Quéguiner*, 2001; *Brzezinski et al*., 2001; *Leblanc et al*., 2002; *Beucher et al*., 2004b).

8.4.2.1 Western SAZ (P1)

The western SAZ (P1) was dominated by nano- and dinoflagellates (*Wright et al*., in prep) with a low contribution of diatoms to the total biomass in agreement with low integrated $bSiO_2$:POC ratios (0.005-0.019) (Table 8.2). Si:C uptake ratios were similarly low (0.005-0.013), and one order of magnitude lower than Si:C ratios sustained by nutrient replete diatoms (0.09-0.13; *Brzezinski*, 1985). *Leblanc et al.* (2002) reported similar ratios for the SAZ in the Indian sector (averaged $bSiO_2$:POC ratios of 0.018 and Si:C uptake ratios of 0.011). These observations suggest low diatoms - though significant- contribution to primary production in the SAZ area during summer.

Large variability was observed in integrated Si-uptake rates during P1 occupation (Figure 8.8a). The diminution of Si:C ratios between the beginning and the end of the survey, both for particulate content and uptake rates (Table 8.2), indicates a decrease of diatoms contribution to both biomass and primary production along the station occupation. Si-uptake rates decreased significantly in association with a decrease of $bSiO_2$ concentrations (Figure 8.5a). This trend was also observed for gross primary production, new production via the f ratio (*Cavagna et al*., submitted) and chla content (*Wright et al*., in prep). A deepening of the mixed layer depth from 20, to 43, and 73 m (respectively for casts #9, #17, and #34) with a constant euphotic layer depth (1% PAR) at ~ 50m could explain a decrease of the productivity for both Si and C, during the station occupation due to a light/mixing regime becoming less favourable for productivity (*Nelson and Smith*, 1991; *Cavagna et al*., submitted). Here diatoms, both biomass and productivity, seemed to co-vary with primary production, new primary production, and carbon export efficiency (*Cavagna et al*., submitted; *Jacquet et al*., submitted). Nutrients [NO_3, $Si(OH)_4$, NH_4] exhibited an inverse pattern with increasing concentrations towards the end of station occupation whereas there was no trend in dissolved iron concentration (*Lannuzel et al.,* submitted). Thus, the variation in productivity and export efficiency during P1 occupation does not seem to be driven by variations in nutrient limitation. The diatom community was constituted by relatively large or chain forming diatoms at P1 (*Leblanc et al.,* in prep). A large part of the diatom community was not actively silicifying suggesting an accumulation of inactive diatoms after a past period of higher productivity and potentially Si export, maybe in the beginning of the stratification event not sampled during SAZ-sense.

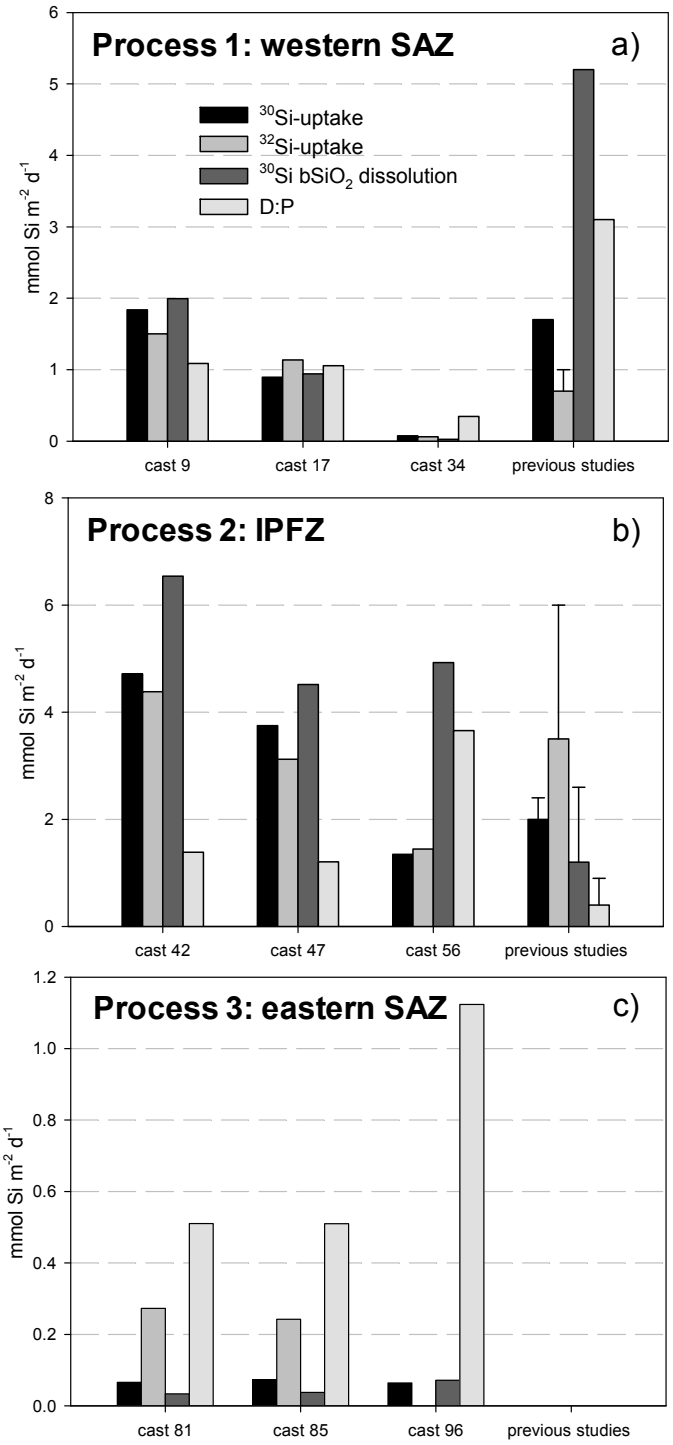

Figure 8.8. Integrated (100-1 % PAR) $Si(OH)_4$ uptake (both with ^{30}Si and ^{32}Si) and $bSiO_2$ dissolution rates, and dissolution:uptake ratios (D:P). Panels a, b, c represent respectively P1, P2, and P3. Previous studies show the summer values of previous studies for each area (Caubert, 1998; *Brzezinski et al*., 2001; *Quéguiner*, 2001; *Leblanc et al*., 2002; *Beucher et al*., 2004b). When no error bars is available, the value represent only one vertical integrated profiles.

Casts #9 and #17 were in the range of the previous studies in summer in the SAZ for Si-uptake (Figure 8.8a) (*Quéguiner*, 2001; *Leblanc et al*., 2002; *Beucher et al., 2004b)*. The lowest Si-uptake value reported

so far in summer was measured on the last day (cast #34) with 0.003 µmol Si l^{-1} d^{-1}. Only one profile in spring is available for the SAZ and integrated Si-uptake rate was estimated at 1.4 mmol Si l^{-1} d^{-1} (*Nelson and Gordon*, 1982), in the range of summer estimates. During summer, due to the variability of the limiting factors (*Boyd,* 2002) and to the fact that C export and productivity seem to be higher in transient disequilibrium conditions (*Cavagna e al*., submitted), it is difficult to assess SAZ variability in productivity with this sampling resolution and quite high productivity events could be easily missed.

8.4.2.2 Eastern SAZ (P3)

Extremely low integrated Si:C ratios, both in particulate content and uptake rates were observed (Table 8.2), suggesting low contribution of diatoms to C productivity, in agreement with CHEMTAX analysis (*Wright et al*., in prep). This area exhibited the lowest Si-uptake rates of the cruise (Figure 8.8c). Low silicic acid concentrations in austral summer in this area could have impaired the response of diatoms to higher Fe inputs from subtropical waters (Bowie et al., accepted) as previously observed (*Franck et al*. 2000; *Hutchins et al,*. 2001, *Sedwick et al*. 2002, and *Brzezinski et al*. 2005). *Leblanc et al*. (in prep) observed at P3 a large contribution of small lightly silicified diatoms species to cell abundance and to Si uptake. *Hutchins et al*. (2001) suggested that addition of Fe to Si-depleted SAZ waters can result in rapid growth of lightly silicified diatoms species which are adapted to low Si-conditions thus outcompeting the larger diatoms with higher Si requirements (*Timmermans et al*., 2004). Moreover, P3 is an area where primary production is limited by the lack of macro-nutrients (N, P, Si; Lannuzel et al., submitted). It is likely that small lightly silicified diatoms were able to take advantage of increased Fe availability and depleted a large part of the ambient silicic acid pool (<1 µmol Si l^{-1}). Nevertheless, these small diatoms species are more prone to be grazed than large diatoms preventing $bSiO_2$ accumulation. A very efficient microbial loop was observed in this area (*Pearce et al*., submitted) and together with grazing, these processes may well explain the low $bSiO_2$ concentrations (24 ± 4 nmol Si l^{-1}; Figure 8.5c) and the high specific uptake rates (0.54 ± 0.20 d^{-1}; Figure 8.6). *Petrou et al*. (submitted) showed that the in eastern SAZ after Si-addition only to the medium, diatoms contributions to phytoplankton increased from 4 to 50% with a larger contribution of large diatoms (*Pseudo-Nizschia* and *Nizschia species*) with different increases in cell size if iron was added. This study clearly shows a silicon control on community structure and probably export as previously shown by *Hutchins et al*. (2001), *Sedwick et al*. (2002), *Brzezinski et al.* (2005), and Leblanc *et al*. (2005b).

To our knowledge, no studies reporting Si-uptake rates exist in natural iron fertilized SAZ precluding any comparisons with this study.

8.4.2.3 Inter Polar Frontal Zone (P2)

IPFZ (P2) was dominated by nano and dinoflagellates (mainly haptophytes; *Wright et al*., in prep) in terms of chla. Integrated $bSiO_2$:POC ratios were 0.20, 0.21, and 0.14 respectively for casts #42, #47, and #58 (table 8.2). These ratios were higher than the values given for nutrient-replete diatoms (0.13 to 0.09; *Brzezinski*, 1985) which would indicate a diatoms contribution to C biomass higher than 100%, in opposition to CHEMTAX results (*Wright et al*., in prep). This high $bSiO_2$:POC ratios could indicate the presence of healthy heavily silicified diatoms or the presence of a large amount of senescent diatom cells. As pigment determination indicated an important contribution of nano- and dinoflagellates, it is likely that the these elevated ratio rather reflect the presence of a large pool of senescent diatom cells that have not yet sunk out of surface waters.

Integrated Si:C uptake ratios (table 8.2) were lower than particulate contents ratios whereas processes associated with iron-light limitation should increase these ratios to the same extent (*Hutchins and Bruland*, 1998; *Takeda*, 1998; *Claquin et al*., 2002; *Franck et al.,* 2003) which might yield to the erroneous interpretation that diatoms sustain entirely C-uptake (*Brzezinski*, 1985; *Brzezinski et al*., 2003a). Fe is required for photosynthetic carbon acquisition, Fe-starved diatoms exhibit dramatically reduced carbon fixation (*Geider and La Roche*, 1994; *Franck et al*., 2003; *Bucciarelli et al*., 2009) while continuing to take up Si at slightly lowered rates inducing higher silicification. Two processes could explain this difference between uptake and particulate ratios: (1) the preferential remineralization of organic matter instead of $bSiO_2$ through the microbial loop (Brzezinski et al., 2003a) and (2) the presence of senescent diatom cells with healthy flagellate cells. Particulate matter accumulated in the mixed layer and in subsurface waters integrate longer timescale than daily uptake rates which could explain these variations in Si:C ratios.

The community shift toward a community dominated by flagellates was likely observed during the station occupation, as evidenced by the continuous decrease of both particulate and uptake ratios (Table 8.2). Moreover, relatively high surface F_v/F_m ratios (0.58) imply that phytoplankton was not significantly stressed by nutrient availability (*Ralph et al*., in prep). The high F_v/F_m ratios could result from a shift in phytoplankton community with early dominance of diatoms towards nanoflagellates in late summer which exhibited higher (micro)-nutrients affinities (*Sunda and Huntsman*, 1997) in a similar way than with pico-phytoplankton (*Timmermans et al*., 2005).

Si uptake rates at P2 cover the range of values encountered in summer in the PFZ-IPFZ in previous studies (*Caubert*, 1998; *Quéguiner*, 2001; *Brzezinski et al*., 2001; *Leblanc et al*., 2002). In spring, integrated Si-utpake could be very high with value up to 60.7 mmol Si m^{-2} d^{-1} (*Brzezinski et al*., 2001; *Quéguiner and Brzezinski*, 2002). This seasonal pattern is again in agreement with an early dominance of diatom over the growing season followed by a flagellate community towards the end of the productive period. This is in agreement with seasonal Si depletion transects (*Lourey and Trull*, 2001) and Si-kinetic measurements suggesting high Si-limitation in late summer (*Nelson et al*., 2001). Our study thus covered the end of the diatom growth period in the IPFZ.

8.4.3 Euphotic layer silicon budget (D:P)

Figure 8.8 shows that $bSiO_2$ dissolution could sustain Si-uptake in the euphotic layer almost everywhere in SAZ-Sense area.

High D:P ratios (~3), significantly higher than the D:P ratio of *circa* 1 measured at P1 (Figure 8.8a), were observed in late summer in the Western SAZ area *(Beucher et al*., 2004b). Larger $bSiO_2$ stock (~3 times) with higher proportion of inactive diatoms than for this study should explain this higher D:P ratio. The similar specific dissolution rates indicate a comparable dissolution environment in both studies.

In IPFZ (P2), higher $bSiO_2$ dissolution was measured during SAZ-Sense in comparison to the only available study in summer PFZ (*Brzezinski et al*., 2001). No deep $bSiO_2$ maximum was observed in this previous study and $bSiO_2$ content were lower than during SAZ-Sense, which could explain the difference as suggested in section 8.4.1.

Except at P3 and cast #34 at P1 where uptake and dissolution rates were below the detection limit (Figure 8.4; section 8.3.1), all the casts showed D:P ratios ≥ 1. Such D:P values were observed in the Atlantic, northwest to Africa (*Nelson and Goering*, 1977b) and also in late summer in the Southern Ocean (this study and *Beucher et al.*, 2004b). *Brzezinski et al*. (2003b) suggest a shift from $bSiO_2$ dissolution supporting a small fraction of gross silica production during diatoms blooms to silica dissolution

supporting the majority of gross $bSiO_2$ production during non-bloom periods when $bSiO_2$ production is low. As suggested in *Brzezinski et al*. (2003b), D:P should would increase following blooms either due to the increase in the relative proportion of detrital biogenic silica in the water column from cell death and/or grazing (*Brzezinski et al.,* 1989) or to a decrease of gross Si-uptake rates without significant changes in $bSiO_2$ dissolution rates (*Brzezinski et al*., 2001). Our study and that of *Beucher et al*. (2004b) are more in agreement with the former process since a relationship between $bSiO_2$ (this study) and dead diatoms percentage (Beucher et al., 2004b) was observed. Moreover, *Leblanc et al*. (in prep) observed at P1 and P2 that a large part of the diatom community was not actively silicifying. In mid-summer, an accumulation of dissolving $bSiO_2$ following past diatoms productive event, either seasonally (IPFZ) or following short productive period after favourable hydrological conditions (irradiance-mixing level) as in the western SAZ, can sustain an efficient silicon loop.

8.4.4 Particulate matter and gross uptake distribution across the euphotic layer

In this section, $bSiO_2$:POC and ρSi:GPP variations in euphotic layer are discussed. An efficient silicate pump would increase the $bSiO_2$:POC ratio since labile organic and nitrogen compounds are remineralized more quickly through metabolic processes than $bSiO_2$ (*Dudgale et al*., 1995; *Brzezinski et al*., 2003a). Such processes could explain the Si enrichment of the particulate phase from the initial uptake ratio (*Brzezinski et al*., 2003a) observed everywhere except at P1 casts #17 (only 1% PAR), #34 and P3 casts #81, #85, #96 (Figure 8.9). This process was accentuated in samples below MLD (1% PAR) such as P1 cast #9 and P2 casts #42, #47, #58. At these depths, a subsurface $bSiO_2$ maximum was observed (Figure 8.5a, b). Subsurface $bSiO_2$ maxima during SAZ-Sense seemed mainly due to an accumulation of $bSiO_2$ settling out of the mixed layer and partly composed of living cells. Settling cells already lost a significant part of their C content through remineralization processes. At P3 on the complete euphotic layer, $bSiO_2$:POC was lower than ρSi:GPP suggesting a very efficient silicon loop. This is in agreement with low new primary production and carbon export efficiency (*Cavagna et al*., submitted; *Jacquet et al*., submitted), high grazing and bacterial pressure (*Pearce et al*., submitted; *Dumont et al*., submitted), and questionable balance in Si-budget (section 8.3.1).

ρSi:GPP increased with depth for all casts (Figure 8.9a) similarly to $bSiO_2$:POC ratios. A relative enhancement of silicification could be linked to the intensity of limitation (light, N, P, trace metals) acting on growth rate (*Claquin et al*., 2002; *Leynaert et al*., 2004). During SAZ-Sense, N and P did not seem to be limiting factors for growth south of SubTropical Front (*Sedwick et al*., 2002; *Lannuzel et al*., submitted) while iron was constant in the euphotic layer (*Lannuzel et al.*, submitted). Variation in light intensity with depth could increase silicon cell-quotas. Numerous studies (*Martin-Jézéquel et al*., 2000; *Claquin et al*., 2002) have shown that the energy used for silicification was mainly of respiratory origin and thus decoupled from photosynthesis. The silicon metabolism is strongly connected to the cellular cycle (*Claquin et al*., 2002) while C and N metabolisms are interconnected and light-dependent since they are related to photosynthesis (*Vergera et al.*, 1998; *Falkowski and Raven*, 1997). For P1 casts #9 and #17 and P2, the uptake ratio increase with depth could also be linked to an increase in $Si(OH)_4$ concentrations with depth. Indeed under strong silicon limitation, diatoms grow thinner frustules (*Nelson and Brzezinski*, 1997; *Martin-Jézéquel et al.*, 2000) which could explain the lower silicification rates at the surface where $Si(OH)_4$ is strongly depleted. Nevertheless, variation in ρSi:GPP seemed mainly linked to variation in C-uptake with depth (*Cavagna et al*., submitted) precluding this hypothesis.

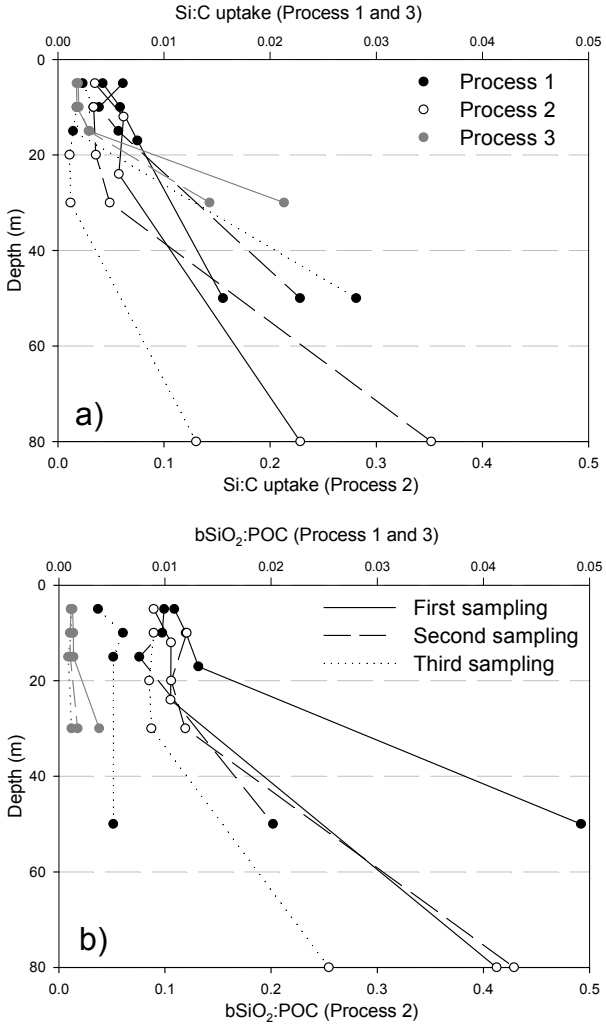

Figure 8.9. Vertical distributions of Si:C uptake ratios (panel a), and $bSiO_2$:POC ratios (panel b). For each panel and each stations, the full, dashed, and dotted lines are respectively casts #9, #17, and #34 for P1, #42, #47, and #58 for P2, and #81, #85, and #96 for P3. C uptakes are coming from *Cavagna et al.* (submitted).

8.5 Conclusions

During SAZ-sense, a complete set of ^{30}Si-incubations was coupled with ^{32}Si-incubations and both methods gave statistically similar results. The effect of incubation time was also tested. $bSiO_2$ production rates after 24 and 48h were not statistically different. $bSiO_2$ dissolution rates were also not significantly different between the two different incubations times except for the deep $bSiO_2$ maximum where dissolution at 24h seemed to be overestimated. A potential influence of Si-efflux on measured ^{28}Si-isotopic dilution could explain this with the intracellular Si-pool initially not ^{30}Si-spiked and characterized by a rapid turnover rate.

Our study on the silicon cycle in mid-summer in contrasted hydrological and biogeochemical environments shows that:

- The western SAZ presents a low diatom contribution to primary production whereas a co-variation of diatoms contribution with new primary production and export production is observed along station occupation (*Cavagna et al*., submitted; *Jacquet et al*., submitted). Stratification event should favor both new production and diatoms production. Accumulation of inactive diatoms along with higher temperature, grazing pressure and bacterial activity resulted in efficient $bSiO_2$ dissolution environnement, sufficient to sustain $Si(OH)_4$ uptake entirely. These results are in agreement with the only other available study in SubAntarctic waters in summer (1 profile; *Beucher et al*., 2004b).

-In the Eastern SAZ, which was enriched with iron due to subtropical southward advection (*Bowie et al*., accepted), silicon limitation exerted a control on the community structure preventing significant growth of diatoms. Nevertheless, small lightly silicified diatoms with higher Si-affinity were rapidly growing but no significant accumulation in the mixed layer was observed, probably due to a high grazing pressure and bacterial activity.

Higher $Si(OH)_4$ concentrations as usually observed in the beginning of the growth period in SAZ or induced by some pulse event should favor diatoms growth and export as suggested by *Hutchins et al*. (2001), *Sedwick et al*. (2002), *Boyd* (2002) and *Brzezinski et al*. (2005). This is also in accordance with the SAZ-Sense study of *Petrou et al.* (submitted) who shows that Si-additions in bottle experiments strongly favor diatoms growth. As suggested in *Brzezinski et al.* (2005), long-term Fe fertilization in the Si-limited SAZ during summer is likely to produce very different phytoplankton species assemblages with the dominance of non siliceous phytoplankton (such as dinoflagellates during SAZ-Sense) than in the southward Si-enriched waters.

-Inter Polar Frontal Zone at the end of the productive period probably encountered a shift in the microbial community from diatoms towards flagellates communities with lower resource requirement than diatoms. The summer deep $bSiO_2$ maximum, not associated with higher production rates and POC maximum, seems to result mainly from an accumulation of settling and dissolving diatoms on a second density gradient. As in the western SAZ, larger accumulation of inactive diatoms sustain really efficient silicon loop. However, due to lower temperatures, grazing pressure and bacterial activity, $bSiO_2$ dissolution environment was less efficient in the IPFZ than in the western SAZ.

There is a depth-dependent decoupling all across the study area between Si uptake and C-N uptake. It is well in accordance with physiological studies showing that Si uptake is mainly fueled with energy of respiratory origin (*Martin-Jézéquel et al*., 2000; *Claquin et al*., 2002) while photosynthesis is the main energy source for C and N assimilation (*Falkowski and Raven*, 1997). Such decoupling should partly explain, along with silicate pump processes and Fe-Si colimitation, the decoupling between $Si(OH)_4$ and NO_3 observed in the Southern Ocean (*Sarmiento et al*., 2004).

Part V. General Discussion and conclusions

Chapter 9. General Discussion

Our data confirm that consumption of silicic acid by diatoms results in a clear increase in the $\delta^{30}Si$ of the ocean silicic acid pool due to the preferential uptake of light Si-isotopes by diatoms. In the following discussion, efforts will be made to discuss the use of this proxy either in palaeoceanography to track past Si-utilization or in modern ocean as a constraint reacting with different sensitivity to physical and biological processes. *Anderson and Winckler* (2005) noted that every proxy is influenced by multiple factors, and the sensitivity of each proxy to these factors will likely change in space and time. It is necessary to develop firstly a quantitative understanding of each process involved in the contemporaneous Si-isotopic balance to safely use this proxy in palaeoceanography.

9.1 Processes involved in the modern Si-isotopic balance

Several processes are involved in the mass and isotopic balances of silicon: Si-uptake, $bSiO_2$ dissolution, and mixing. In the following, the mass and isotopic balances will be discussed from isotopic fractionation at cellular scale up to the level of a Si-pool in mixed layer. This implies to closely link dissolution:production ratio (D:P) to natural Si-isotopic fractionation which was one of the aims of this thesis.

9.1.1 Cellular Si-isotopic fractionation

De La Rocha et al. (1997) observe for the first time that diatoms growing *in vitro* use preferentially light Si-isotopes to construct their opaline cell walls with a fractionation factor of -1.1 ± 0.4% (n = 23). In this study, no influence of temperature (n = 3; 12-22°C) and species (n = 3) is observed whereas a large standard deviation is reported. Such fractionation was further confirmed by an increasing number of *in situ* observations (*De La Rocha et al*., 2000b; *Varela et al*., 2004; *Cardinal et al*., 2005, 2007; *Alleman et al*., 2005; *Reynolds et al*., 2006; *Beucher et al*., 2008; *Cavagna et al*., in revision; chapters 6 and 7). These in situ estimations have been realized in a large range of hydrological and biogeochemical conditions, and diverse diatoms communities. They cover all latitudes, from polar (*Varela et al*., 2004; *Cardinal et al*., 2005, 2007; *Reynolds et al*., 2006; *Cavagna et al*., in revision; this thesis) to tropical and equatorial oceans (*Reynolds et al*., 2006; *Beucher et al*., 2008), two profiles on coastal upwelling systems (*De La Rocha et al*.,

2000) as well as tropical freshwaters (*Alleman et al*., 2005). The average *in situ* fractionation factor estimated in the ocean by compiling either using the subsurface $Si(OH)_4$ pool as Si-source or using the difference in $\delta^{30}Si$ between $Si(OH)_4$ and $bSiO_2$ are respectively -1.2 ± 0.5‰ (n = 40) and -1.4 ± 0.5‰ (n = 38), and are not statistically different from *in vitro* estimations but also with a relatively large variability. Although $\delta^{30}Si$ and silicic acid concentration are highly correlated in the global ocean, the estimation of the *in situ* fractionation factor can potentially be significantly influenced by mixing of waters with silicic acid pools that have experienced different degrees of biological consumption (*Beucher et al*., 2008). This effect could partly explain the large variability encountered in $^{30}\varepsilon$ field estimations, especially in Si-depleted water (see section 9.1.2), but not *in vitro*.

The overall fractionation factor associated with transformation of $Si(OH)_4$ into $bSiO_2$ would be a balance between different isotopic discriminations associated to different cellular Si-fluxes (Figure 9.1; section 1.2; *Milligan et al*., 2004; *Demarest et al*., 2009). This overall balance could explain partly the relatively large variability on *in situ* and *in vitro* $^{30}\varepsilon$ estimations.

For decades models of saturable kinetics of Si-uptake (Michaelis-Menten type) have guided our understanding on how diatom cell translates nutrient availability into growth (*Sullivan*, 1976, 1977; *Del Amo and Brzezinski*, 1999). However, several studies suggest that Si-uptake, under certain conditions, is nonsaturable and in some case biphasic (e.g. *Thamatrakoln and Hildebrand*, 2008). Uptake at low $Si(OH)_4$ concentration was saturable and mediated by silicon transporters (SITs; specific membrane-associated proteins transporting $Si(OH)_4$ across the lipid bilayer membranes), while uptake at high $Si(OH)_4$ concentration was non-saturable and occurred mainly by diffusion. *Thamatrakoln and Hildebrand* (2008) revise the Si-uptake model by incorporating equilibrium effects. During exponential growth, intracellular soluble silicon binding components are in equilibrium with needs for silica incorporation into the cell wall; hence a portion of the components is available to bind newly taken up $Si(OH)_4$, but most are in the process of transport or release of $Si(OH)_4$ into the Silica Deposition Vesicle (SDV). During short-term Si-starvation the organic binding components release their $Si(OH)_4$ to the SDV without being replenished and the majority are then uncomplexed. Upon subsequent $Si(OH)_4$ replenishment intracellular capacity is high, facilitating surge uptake; at low $Si(OH)_4$ concentration, it is controlled by the SITs and hence saturable; at high $Si(OH)_4$ diffusional uptake occurs and uptake is non-saturable. Over time, equilibrium is re-established through utilization of intracellular silicon for cell wall deposition and by efflux. When cells are Si-starved for a prolonged time, the level of intracellular binding components is minimized and after $Si(OH)_4$ replenishment surge uptake was prevented and saturable kinetic result. *Hildebrand et al*. (2007) show that in prolonged incubation after $Si(OH)_4$ replenishment intracellular pool levels gradually increased, suggesting that abundance of binding components increase as well, leading to a new equilibrium.

Figure 9.1 shows a schematic view of the potential silicon pathways in a diatom cell. Two views are presented exhibiting different level of model complexity. Figure 9.1a exhibits only one intracellular Si-pool whereas in Figure 9.1b two intracellular Si-pools co-exist, the cytoplasm intracellular pool and SDV pool. The overall balance of these different cellular Si-fluxes should set the overall fractionation factor (ε_{tot}) as follows:

$$\varepsilon_{tot} = \varepsilon_{inf1} + f_{eff1} \cdot (\varepsilon_{poly} - \varepsilon_{eff1}) \quad (9.1)$$

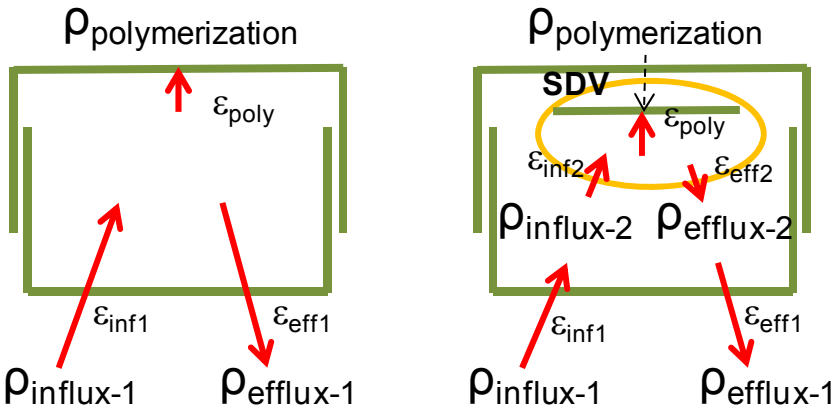

Figure 9.1. Silicon fluxes in a diatom's cell. Influx1: transport rate across the plasmalemma from outside to inside the cell; silica polymerization: the rate of frustule formation inside the silicon vesicle deposit (SDV); efflux1: the transport rate across the plasmalemma from inside to outside the cell; influx2: the transport rate across the SDV membrane from the cytoplasm to SDV; efflux2: the transport rate across the SDV membrane from the SDV to the cytoplasm. Green is biogenic silica. The difference between the left and right schematic views is the pathway of silicon inside the diatom cell.

$$\varepsilon_{tot} = \varepsilon_{inf1} + f_{eff1} \cdot (f_{eff2} \cdot (\varepsilon_{poly} - \varepsilon_{eff2}) + \varepsilon_{inf2} - \varepsilon_{eff1}) \quad (9.2)$$

Where ε_{inf1} is the isotopic discrimination of the transport across the plasmalemma from outside to the cytoplasm, ε_{inf2} the isotopic discrimination of the transport from the cytoplasm to the SDV, ε_{eff1} the isotopic discrimination associated with the transport from the cytoplasm to outside the cell, ε_{eff2} the isotopic discrimination of the transport from the SDV to the cytoplasm, and ε_{poly} the isotopic discrimination of silica polymerization. f_{eff1} is the ρ_{eff1}:ρ_{inf1} ratio and f_{eff2} is the ρ_{eff2}:ρ_{inf2} ratio. Derivation of these equations is detailed in appendix 2.

ρ_{influx} represents both transport across the cell membrane by carrier (SITs, active transport) and by diffusion (passive transport) depending on the external $Si(OH)_4$ concentration (*Thamatrakoln and Hildebrand*, 2008). The overall fractionation factor associated with influx should be also a balance between the kind of Si-transports across the cell membrane as follows:

$$\varepsilon_{inf} = f_a \cdot \varepsilon_a + f_p \varepsilon_p \quad (9.3)$$

where f_a and f_p are respectively the proportions of the active and passive transports ($f_a + f_p = 1$) with associated isotopic discrimination, ε_a and ε_p (see appendix 2 for detailed calculation).

Except the isotopic discrimination associated with the influx1, the others are more or less linearly expressed depending on the flux ratios (Eqs 9.1 and 9.2). Clearly the figure 9.1b better fit with reality since two distinct intracellular Si-pools have been clearly identified (*Martin-Jézéquel et al.*, 2000; *Hildebrand,* 2008). An easy way to simplify Eq (9.2) is to assume that silica polymerization consumes all the available Si inside the SDV, subsequently setting the f_{eff2} to 0. This is likely because energetically, this operating mode seems more favorable (Hildebrand, pers. comm. 2009). Thus except for the isotopic discrimination associated with influx1, the remaining isotopic discrimination should be depending of f_{eff1} when f_{eff2} is set at 0.

Efflux is a consequence of transient imbalances between uptake and polymerization during surge uptake caused by a level of transport that exceeds the capacity of intracellular silicon-binding component (*Martin-Jézéquel et al*., 2000; *Thamatrakoln and Hildebrand*, 2008). Average concentration of $Si(OH)_4$ in most of the ocean's euphotic zone is 10 µmol Si l^{-1} (*Tréguer et al*., 1995). $Si(OH)_4$ uptake by field assemblages would mostly be directly controlled by silicic acid transporters (SITs), which would minimize the associated costs of excess surge uptake and efflux (*Thamatrakoln and Hildebrand*, 2008). On the other side, our data are all from the Southern Ocean where high $Si(OH)_4$ concentrations are often present. These concentrations are expected to be in a range favoring diffusion mediated uptake incidentally increasing the probability of efflux to occur (*Thamatrakoln and Hildebrand*, 2008). Notwithstanding, *Milligan et al*. (2004) observe no influence of the influx:efflux ratio on the overall $^{30}\varepsilon$ (n = 2) using *in vitro* incubation (n=6) in *Thalassiosira weissflogii* suggesting that isotopic discrimination only takes place during influx. Clearly additional work is required to confirm this hypothesis. A potential explanation resides in the fact that once the $Si(OH)_4$ is complexed with the intracellular silicon binding component, the transport and affinity is only depending on the organic molecule without significant influence of the intrinsic binded silicon isotopic variation. An alternative option is that the ε_{inf2} equals ε_{eff1} cancelling each other (Eq. 9.2).

Demarest et al. (2009) report an isotopic fractionation during $bSiO_2$ dissolution. Indeed, dissolving biogenic silica preferentially releases light Si-isotopes ($^{30}\varepsilon$ = -0.55‰). This fractionation counteracts the one occurring during $bSiO_2$ production at about half of its absolute magnitude (i.e. compared to $^{30}\varepsilon$ for uptake of -1.1‰). By increasing the euphotic D:P ratio, the overall fractionation factor associated with Si-uptake would be dampened as follows assuming a system in steady state (appendix 2):

$$\varepsilon_{tot} = \varepsilon_{upt} + \frac{D}{P} \cdot \varepsilon_{diss} \quad (9.4)$$

where ε_{upt} is the isotopic fractionation factor associated with $bSiO_2$ production (ε_{tot} in Eqs (9.1 and 9.2)), and ε_{diss} is the isotopic discrimination associated with $bSiO_2$ dissolution. Although $bSiO_2$ production (Si-uptake) and dissolution occur simultaneously in marine surface waters, for a given $bSiO_2$ particle these processes are uncoupled temporally, since it is not until after diatom death and degradation of its protective organic coating that the $bSiO_2$ cell wall starts to dissolve (*Lewin*, 1961; *Kamatani*, 1982; *Bidle and Azam*, 1999). This decoupling is not recorded in the Eq. (9.4) assuming a steady state with no $bSiO_2$ accumulation. Additional studies that combine measurement of $\delta^{30}Si$ with those of $bSiO_2$ production and dissolution rates hold promise to reveal how silicon isotope distribution are affected by the fractionation of silicon isotopes during $bSiO_2$ dissolution (*Demarest et al*., 2009).

There is a shift in the mode of functioning of the surface silica cycle, from silica dissolution supporting a small fraction of gross silica production during diatoms bloom to silica dissolution supporting the majority of gross silica production during non-bloom periods when silica production is low (section 1.3.1; *Brzezinski et al.*, 2003b; *Beucher et al*., 2004b; chapter 8). We can suspect that Si-production and subsequently D:P is respectively positively and inversely correlated (not linearly) with $Si(OH)_4$ (*Nelson et al*., 1995; *Ragueneau et al*., 2000; *Brzezinski et al*., 2003b). We plot all the *in situ* fractionation factors, both $^{30}\varepsilon$ and $\Delta^{30}Si$, in function of $Si(OH)_4$ concentration (Figure 9.2). Low *in situ* fractionation factor are observed at decreasing silicic acid concentration in agreement with a significant influence of physicochemical $bSiO_2$ dissolution (*Cardinal et al*. , 2007; *Demarest et al*., 2009). Nevertheless, in these low $Si(OH)_4$ areas, vertical mixing

with subsurface ^{28}Si-enriched waters could easily interfere with dissolution processes to reduce the fractionation factor estimates in a way still difficult to assess. A statistically significant linear correlation exist between [$Si(OH)_4$] and Δ^{30}Si (r^2 = 0.54, p < 0.01). The Δ^{30}Si estimates are limited to the Southern Ocean (*Varela et al.*, 2004; *Cardinal et al.*, 2007; *Fripiat et al.*, submitted; *Cavagna et al.*, in revision). During KEOPS above the Kerguelen plateau (chapter 6), biogenic silica was significantly higher than silicic acid. Extremely low Δ^{30}Si are observed in this area. Dissolution of dead accumulated biogenic silica with preferential release of light Si-isotopes (*Demarest et al.*, 2009) should decrease Δ^{30}Si since $bSiO_2$ and $Si(OH)_4$ isotopic composition become heavier and lighter, respectively. This effect would be more significant when dead diatoms contribute more to the total biogenic silica pool. Unfortunately no extensive Si-biogeochemical studies have been realized during the beginning of the productive period (November-December) in the all-year Si-depleted (< 5µmol Si l^{-1}) SAZ when the main silicic acid depletion is occurring. In summer when the silicic acid pool is strongly depleted (< 1-2 µmol Si l^{-1}), the Si-cycle is mainly operating in a regenerative mode with a really efficient silicon loop (*Beucher et al.*, 2004b; chapter 8). This process could explain the relatively low spring *in situ* $^{30}\varepsilon$ estimates in SAZ with the open system (*Cardinal et al.*, 2005).

To conclude, a relatively large range in $^{30}\varepsilon$ is observed in the global ocean from -0.5 to -2.2‰. Clearly,

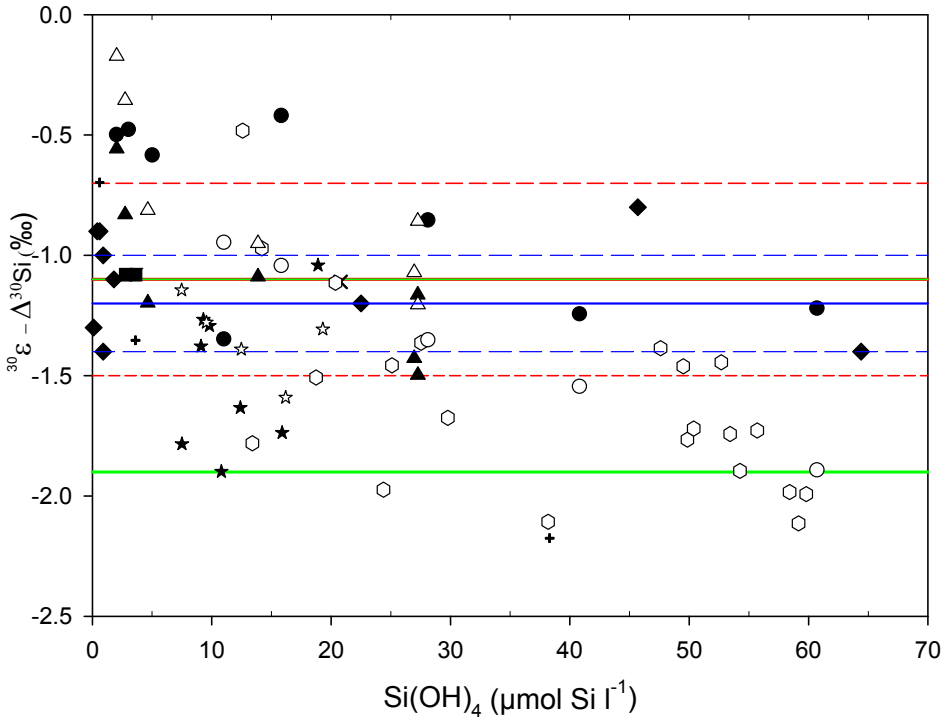

Figure 9.2. Global data set of *in situ* fractionation factor. White and black symbols represent respectively $^{30}\varepsilon$ and Δ^{30}Si estimates: cross, De La Rocha et al. (2000); hexagons, Varela et al., 2004; circles, Cardinal et al. (2005; 2007); plus, Reynolds et al. (2006); squares, Beucher et al. (2008); diamonds, BONUS-Goodhope; triangles, KEOPS; stars, Cavagna et al., (in revision). *In vitro* average fractionation factor [full red line; De La Rocha et al., 1997] with 1 standard deviation (dashed lines). The ACC average fractionation factor determined in chapter 4 (full blue line) with 1 standard deviation (dashed lines). The range of fractionation factor given by Varela et al. (2004) estimated with Rayleigh (lower) and steady state (higher) model is shown using green lines.

the location, nature and intensity of isotopic fractionation associated with each cellular Si-fluxes need to be better constrained (via e.g. chemostat and synchronous cultures) along with potential interspecific variability still poorly assessed (up to now only four species) and variable growth conditions (light, nutrient limitation, Si-availability …). In this context, we have acquired a set of new data which need to be further validated with complementary analyses (Appendix 3).

9.1.2 Si-isotopic fractionation at regional scale

The Southern Ocean dynamic is characterized by several jets associated to higher eastward baroclinic transport materializing the inner ACC fronts (*Sokolov and Rintoul*, 2007b). The ACC fronts represent almost impermeable barriers delimiting zones with relatively constant hydrological and biogeochemical properties, and lower baroclinic transport (*Tréguer and Jacques*, 1992; *Sokolov and Rintoul*, 2007a). Cross frontal exchanges occur but mainly locally, close to sharp topographic features. Incidentally, water particles spend several years in each zone and subsequently take part in several winter convective mixings (S. Speich, pers. comm. 2009). We can consider that a water parcel is surrounded by water with relatively similar properties and subject to the same seasonal evolution. With this perspective, we can implement a vertical view to apply mass and isotopic balances. These assumptions work for the open ocean but not for particular locations as e.g. the Kerguelen Plateau (Chapter 6) where intense biological productivity is taking place surrounded by waters with relatively low productivity. In such cases, advection from the surrounding areas seems necessary to close mass and isotopic balances.

Up to now there are only two models describing Si-isotopic fractionation during Si-consumption. They represent ideal situations operating either in closed (Rayleigh) or in open mode (steady state) (*Fry*, 2006):

- If a pool of silicic acid is consumed by algal assimilation with a constant isotopic fractionation and without resupply during the consumption process, then the isotopic evolution of the remaining silicic acid is given by the "substrate pool" equation in Rayleigh fractionation (Figure 1.22). Specifically, starting with an initial $[Si(OH)_4]$ and $\delta^{30}Si$, the silicic acid pool will increase exponentially in a graph $\delta^{30}Si$ versus $[Si(OH)_4]$ (Chapters 6 and 7). Rayleigh model can be appropriate for instance, when there are non-overlapping events of nutrient supply. In the Southern Ocean especially deep mixing occurs supplying mixed layer in silicic acid during summertime; thus the Rayleigh model alone is not adequate for the different zones as a whole as shown from previous Southern Ocean Si-isotopic studies (*Varela et al*., 2004; *Cardinal et al*., 2005) and this thesis (chapters 6 and 7). These studies suggest that turbulence diffusion and vertical mixing events would impose the ML Si-pool to operate in an open system mode or at least a balance between Rayleigh and the steady state model (see below) depending of the ratio of Si-supply vs. Si-uptake (*Varela et al*., 2004).

- The alternative to the Rayleigh model is the open system also referred to as steady state or open flow through system (Figure 1.22). This system describes the isotopic evolution with an Eulerian view since the water flow splits the silicic acid input in residual silicic acid pool and $bSiO_2$ product, both leaving the system (*Fry*, 2006). The steady state represents just a final snapshot of the system and does not represent a temporal evolution. Conceptually, this poses a problem since Si-isotopes track the history of a system taken as a whole (silicic acid and biogenic silica) from the beginning of silicic acid consumption.

In the following, we will focus on the seasonal mixed layer evolution of silicon isotopic composition, both in dissolved and particulate Si-pools. $bSiO_2$ dissolution and its associated isotopic discrimination dampens the $bSiO_2$ production mediated Si-isotopic fractionation by preferentialy releasing light Si-isotope through a bi-directional isotopic exchange (section 9.1.1; *Demarest et al*., 2009). Si-rich subsurface Si-pools are also acting in the same way, supplying summer mixed layer in light silicic acid. Mixing is expected to be relatively constant on a seasonal scale through turbulence diffusion and relatively regular vertical mixing events. This process should have a higher impact on Si-isotopes close to Si-depletion. On the contrary, $bSiO_2$ dissolution exhibits a seasonal pattern (sections 1.3.1 and 9.1.1; *Brzezinski et al*., 2003b). We will first work with zero order equations to subsequently discuss on the utility to use second order equations. To clarify the following discussion, open system refers to seasonal evolution and steady state system to a final stage.

We apply these simple mass and isotopic balances first on the Antarctic Zone, since this area is already quite well independently constrained. More specifically we use the KEOPS case study (chapter 6; Table 9.1) since (1) we know the duration of the productive period (*circa* 83 days; *Mongin et al*., 2008) and (2) both the biogenic silica and dissolved pools have been measured. Moreover, this analysis would be useful to compare seasonal isotopic dynamic in two systems with contrasted Si-depletion level. In this area, the winter mixed layer (also referred to as Antarctic Surface Water) is split by summer stratification in two layers, the summer mixed layer and the winter water keeping the biogeochemical properties from the previous deep winter convective mixing (*Pondaven et al*., 2000a; *Altabet and François*, 2001). With the assumptions discussed in chapters 6 and 7, the annual UCDW Si-supply could be estimated using the following relation and a simple annual dynamic:

$$f_{UCDW} = \frac{\delta^{30}Si_{WW} - \delta^{30}Si_{ML}}{\delta^{30}Si_{UCDW} - \delta^{30}Si_{ML}} \quad (9.5)$$

where f_{UCDW} represent the contribution of UCDW to AASW. This gives the annual flux but does not inform on the seasonal evolution. Assuming a system which consists of AASW as a whole, WW and summer mixed layer in steady state (supply = export) on an annual timescale, this annual Si-supply should represent the annual net $bSiO_2$ production (or annual Si-uptake) integrated over the mixed layer. The

Keops		HNLC area		Plateau area	
		initial	final	initial	final
$[Si(OH)_4]$	µmol Si l^{-1}	52.5	27.2	52.5	2.1
$[bSiO_2]$	µmol Si l^{-1}		2.0		3.2
$\delta^{30}Si_{Si(OH)4}$	‰	1.5	2.2	1.5	2.6
$\delta^{30}Si_{bSiO2}$	‰		1.1		2.3
mass balance (chapter 4)		mol si m^{-2} yr^{-1}		mol si m^{-2} yr^{-1}	
net $bSiO_2$ production		4.0 ± 0.7		6.5 - 10.5	
Summertime Si-supply		1.5 ± 0.7		> 1.5	

Table 9.1. initial and final, both for biogenic silica and silicic acid, concentration and $\delta^{30}Si$ for the two KEOPS areas. Mass balance determined using Eqs (9.5 and 9.6).

summer Si-supply can be then estimated using:

$$m_{input} = m_{final} - m_{initial} + m_{uptake} \quad (9.6)$$

where m is the Si mass integrated over the mixed layer. With Eqs 9.5 and 9.6, we have an independent estimate of the mass and isotopic balance that can be used to constrain the seasonal mass and isotopic evolutions.

Assuming a Lagrangian view and a mixed layer receiving Si-input from subsurface, the isotopic and mass balances associated with seasonal Si-depletion could be described using zero-order equations as follows:

$$\frac{d(m)}{dt} = m_{input} - m_{uptake} \quad (9.7)$$

$$m \cdot \frac{d(\delta^{30}Si)}{dt} = m_{input} \cdot \delta^{30}Si_{input} - {}^{30}\varepsilon \cdot m_{uptake} \quad (9.8)$$

$${}^{30}\varepsilon = {}^{30}\varepsilon_{uptake} + {}^{30}\varepsilon_{dissolution} \cdot \frac{D}{P} \quad (9.9)$$

Figure 9.3a shows the daily mass and isotopic evolutions of the residual silicic acid pool and accumulated $bSiO_2$ in KEOPS HNLC area assuming continuous Si-supply, or sporadic Si-supply via regular vertical mixing events (1.5 ± 0.7 mol Si m^{-2} yr^{-1}; Table 9.1) with a constant D:P ratio set at 0.4 (Kerfix; *Pondaven et al*., 1998, 2000b). The number of mixing events is arbitrary and corresponds to one mixing event every ~5 days. Decreasing the number of mixing event increases the scattering around the continuous mixing curve as average. The closed system is shown for comparison. Even if in this case the seasonal Si-isotopic balance is respected (Si-utilization not sufficient enough), this system does not respect the summertime Si-supply independently estimated (Eqs 9.5 and 9.6). For the HNLC area, the simulated

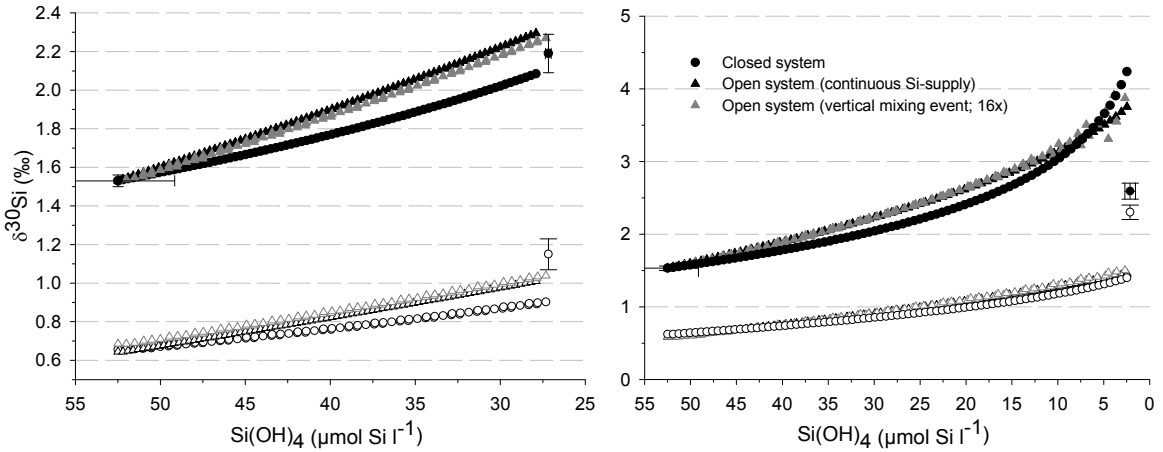

Figure 9.3. Seasonal isotopic and mass evolution in the KEOPS HNLC area (panel a) and Plateau area (panel b) using zero order Eqs. (9.7, 9.8, and 9.9). Observations are represented by white and black dots for biogenic silica and dissolved silicon, respectively with error bars (1sd). The initial silicic acid pool is the HNLC WW and the final silicic acid and biogenic silica pools are the ML average values (Table 8.1). $^{30}\varepsilon_{uptake}$ is set at -1.1‰ (De La Rocha et al., 1997) and $^{30}\varepsilon_{dissolution}$ at -0.55‰ (Demarest et al., 2005). The empty symbols represent biogenic silica (same than silicic acid).

open system is close to the isotopic fractionation described using simple steady state equations (Figure 1.22) and for such level of Si-utilization there are no large differences between the different described models.

Similar isotopic and mass seasonal evolutions have been run but this time on the KEOPS plateau area (near complete depletion) with a D:P ratio also sets at 0.4. The results are shown in the figure 9.3b. Since the Si-supply (2.4 mol Si m^{-2} yr^{-1}) is lower than the Si-uptake (7.4 mol Si m^{-2} yr^{-1}), the mass and isotopic evolution lie between an open and closed system with final $\delta^{30}Si_{Si(OH)4}$ heavier than an expected steady state values ($\delta^{30}Si_{source} - {}^{30}\varepsilon$; in this case 2.7‰) and observed value (Figure 9.3b). With sporadic vertical mixing events, the evolution is significantly scattered at low silicic acid concentrations due to the larger effect of Si-supply. This effect would be probably smoothed by mixing with surrounding water masses which have experienced not synchronously different degree of mixing. Modeled biogenic silica isotopic evolution does not fit with observations neither and are significantly lighter (Figure 9.3b). From this analysis, it seems clear that the simple zero-order equations are not able to describe correctly an open system up to near Si-depletion like the Kerguelen Plateau.

This decoupling between model outputs and observations is probably due to seasonal variations of $bSiO_2$ production (Pondaven et al., 2000a; *Brzezinski et al*, 2001; *Quéguiner and Brzezinski*, 2002) and D:P ratio (*Brzezinski et al*., 2003b) allowing to the different isotopic effects to be more or less expressed. We try in the following to take into account these temporal variations. The growth period uptake is described using a Michaelis-Menten relation type (*Pondaven et al*., 1998, 2000b; *Ragueneau et al.*, 2000; *Sarthou et al*., 2005) and D:P increases linearly (from 0.0 to 0.8; in the expected range: *Nelson et al*., 1982; *Brzezinski et al*., 2001, 2003b; *Beucher et al*., 2004b):

$$\frac{d(m_{Si(OH)4})}{dt} = m_{input} - V_{Si}(t)\cdot m_{bSiO2} + \frac{D}{P}(t)\cdot V_{Si}(t)\cdot m_{bSiO2} \quad (9.10)$$

$$\frac{d(m_{bSiO2})}{dt} = V_{Si}(t)\cdot m_{bSiO2} - \frac{D}{P}(t)\cdot V_{Si}(t)\cdot m_{bSiO2} - k_{export}\cdot m_{bSiO2} \quad (9.11)$$

$$m_{Si(OH)4}\cdot\frac{d(\delta^{30}Si_{Si(OH)4})}{dt} = m_{input}\cdot\delta^{30}Si_{input} - {}^{30}\varepsilon(t)\cdot\left[V_{Si}(t)\cdot m_{bSiO2} - \frac{D}{P}(t)\cdot V_{Si}(t)\cdot m_{bSiO2}\right]$$

$$m_{bSiO2}\cdot\frac{d(\delta^{30}Si_{bSiO2})}{dt} = \left[V_{Si}(t)\cdot m_{bSiO2} - \frac{D}{P}(t)\cdot V_{Si}(t)\cdot m_{bSiO2}\right]\cdot\left(\delta^{30}Si_{Si(OH)4} + {}^{30}\varepsilon(t)\right) \quad (9.13)$$

$$V_{Si}(t) = \frac{V_{max}\cdot[Si(OH)_4]}{k_{Si} + [Si(OH)_4]} \quad (9.14)$$

$$\frac{D}{P}(t) \rightarrow \frac{d\left(\frac{D}{P}\right)}{dt} = 0.01 \quad (9.15)$$

$${}^{30}\varepsilon(t) = {}^{30}\varepsilon_{uptake} + {}^{30}\varepsilon_{dissolution}\cdot\frac{D}{P}(t) \quad (9.16)$$

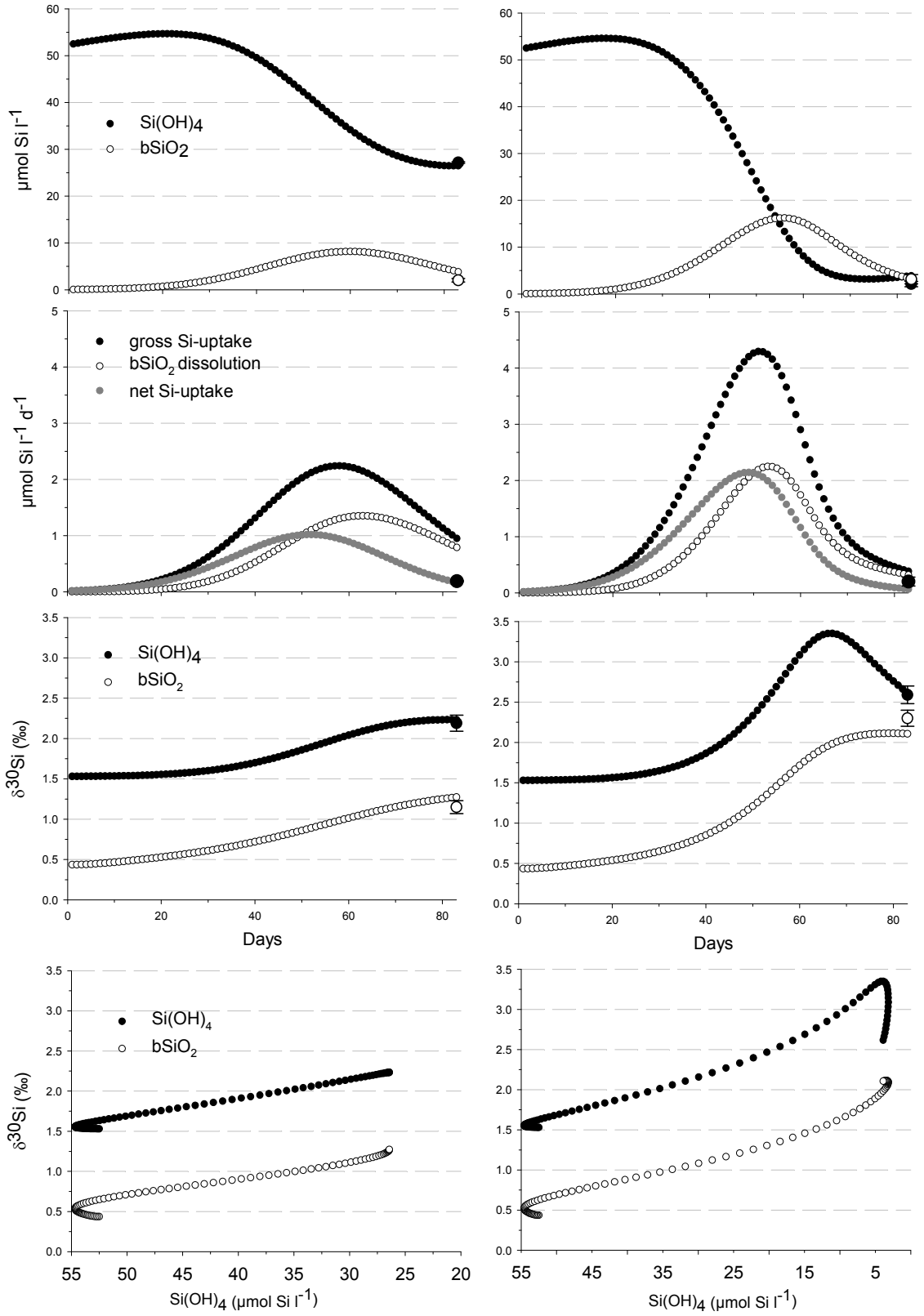

Figure 9.4. Seasonal evolution per days for the KEOPS HNLC area (left side) and Plateau area (right side), both biogenic and silicic acid, of the concentrations (upper panels; Eqs 9.10 and 9.11), Si-fluxes (upper middle panels; Eqs 9.14 and 9.15), and Si-isotopic composition (lower middle panels; Eqs 9.12, 9.13 and 9.16). Lower Panels present $\delta^{30}Si$, both for silicic acid and biogenic silica, in function of the silicic acid concentration. Observations are shown, both for biogenic silica and dissolved silicon, respectively white and black dots, with 1 standard deviation error bars. The measured $bSiO_2$ production rates are also shown (Mosseri et al., 2008).

where k_{export} is the fraction of biogenic silica which is exported (fixed to 0.1). This parameter has a large effect (not shown) and clearly would need to be better simulated. Figure 9.4 shows the run simulation for the KEOPS plateau and HNCL areas, both with a V_{max} at 0.4 and a K_{Si} respectively at 10 and 17 µmol Si l^{-1} (AZ range; 0.7 to 61 µmol Si l-1: *Jacques*, 1983; *Caubert*, 1998; *Pondaven et al*., 1998, 2000b; *Neslon et al*., 2001). These kinetic parameters have been chosen because the run fits with the data and they are close of expected values from previous Si-modeling efforts at KERFIX time series (K_{Si} = 8 µmol Si l^{-1}; *Pondaven et al*., 1998, 2000b). The sensitivity of the model to these kinetic parameters and D:P ratios is discussed later. The seasonal net $bSiO_2$ production is respectively for plateau and HNLC areas 7.0 and 4.0 mol Si m^{-2} and the summertime Si-supply 2.5 and 1.5 mol Si m^{-2}. This is in the range of expected values (Table 9.1). Figure 9.4a presents the seasonal evolution of silicic acid and biogenic silica concentration. For both areas, a peak in $bSiO_2$ production (Figure 9.4b) is observed and is associated with a biogenic silica concentration peak (respectively up to 7.2 and 19.3 µmol Si l^{-1}). Such high values were already observed in AZ by *Brzezinski et al*. (2001; 16 µmol Si l^{-1}), and in the beginning of KEOPS cruise (*Mosseri et al*., 2008; 22.6 µmol Si l^{-1}). *Mosseri et al*. (2008) note that the declining $bSiO_2$ biomass above the Kerguelen Plateau is unusually high, even for the Southern Ocean. Figure 9.4b shows also the evolution of the Si-fluxes. Overall, the seasonal evolution is in agreement with the bloom evolution (*Mongin et al*., 2008) and the seasonal expected D:P trends from *Brzezinski et al*. (2003b). Production rates are a little bit higher than measured values (*Mosseri et al*., 2008) but in the same order of magnitude. The isotopic evolution, both for silicic acid and biogenic silica, seems to be respected (Figure 9.4c). Once near complete depletion is reached, mixing and dissolution isotopic effects are becoming more significant inducing a decreasing in $Si(OH)_4$ isotopic composition and an increasing in $bSiO_2$ isotopic composition. Even though we acknowledge that additional work will be necessary to better simulate such evolution, for example using equations of different orders, adding constrains as biogenic silica accumulation leading to D:P ratio higher than 1 (*Beucher et al*., 2004b; chapter 8) and seasonality for kinetic uptake parameters (*Nelson et al*., 2001), our new approach seems to adequately describes Si biogeochemical seasonal evolution in two contrasting areas of the AZ.

Field observations close to Si-depletion (e.g. BONUS-Goodhope section; PFZ, SAZ, STZ, chapter 7) are close to the steady state expected value ($\delta^{30}Si_{source} + {}^{30}\varepsilon$) confirming that the system is there in a steady state mode. At the end of the productive period, several co-limitations (e.g. iron, light, Si) are potentially occurring which can induce a spatial heterogeneity in term of productivity (*Boyd*, 2002). SAZ-Sense area is quite representative of such view since large variability in C and Si-productivities were observed in late summer SAZ (*Cavagna et al*., submitted; chapter 8). The simple 1D vertical view might be inadequate for these typical late summer situations. Small variations in the model parameters bring significant variation in the late summer Si-isotopic evolution and are susceptible to be highly sensitive to environmental factors (Figure 9.5). Figure 9.5a shows the sensitivity of the model on kinetic uptake parameters (K_{Si}, V_{max}). In the Southern Ocean, there is no clear tendency for K_{Si} to change with latitude or with $[Si(OH)_4]$, but there was an apparent seasonal progression in which both the highest K_{Si} values and the variability in K_{Si} increased with time (*Nelson et al*., 2001). The seasonality and intensity of the productivity peak are strongly sensitive to these parameters (e.g. *Pondaven et al*., 1998). D:P ratio evolution has also a significant impact on the seasonality and intensity of the productivity peak (Figure 9.5b). The essential of the variability is observed under strong Si-depletion ($f < 0.20$; Figure 9.5 < 5 µmol Si l^{-1}). In the field, Si-isotopic composition might smooth such spatial heterogeneity through mixing with the surrounding waters

from a given area exhibiting large spatial heterogeneity in term of bloom collapse timing, D:P evolution, and growth controlling factors. This process should bring the resulting Si-isotopic composition around the expected steady state values as observed *in situ* ($\delta^{30}Si + {}^{30}\varepsilon$; on Figure 9.5 ~ 3.1‰).

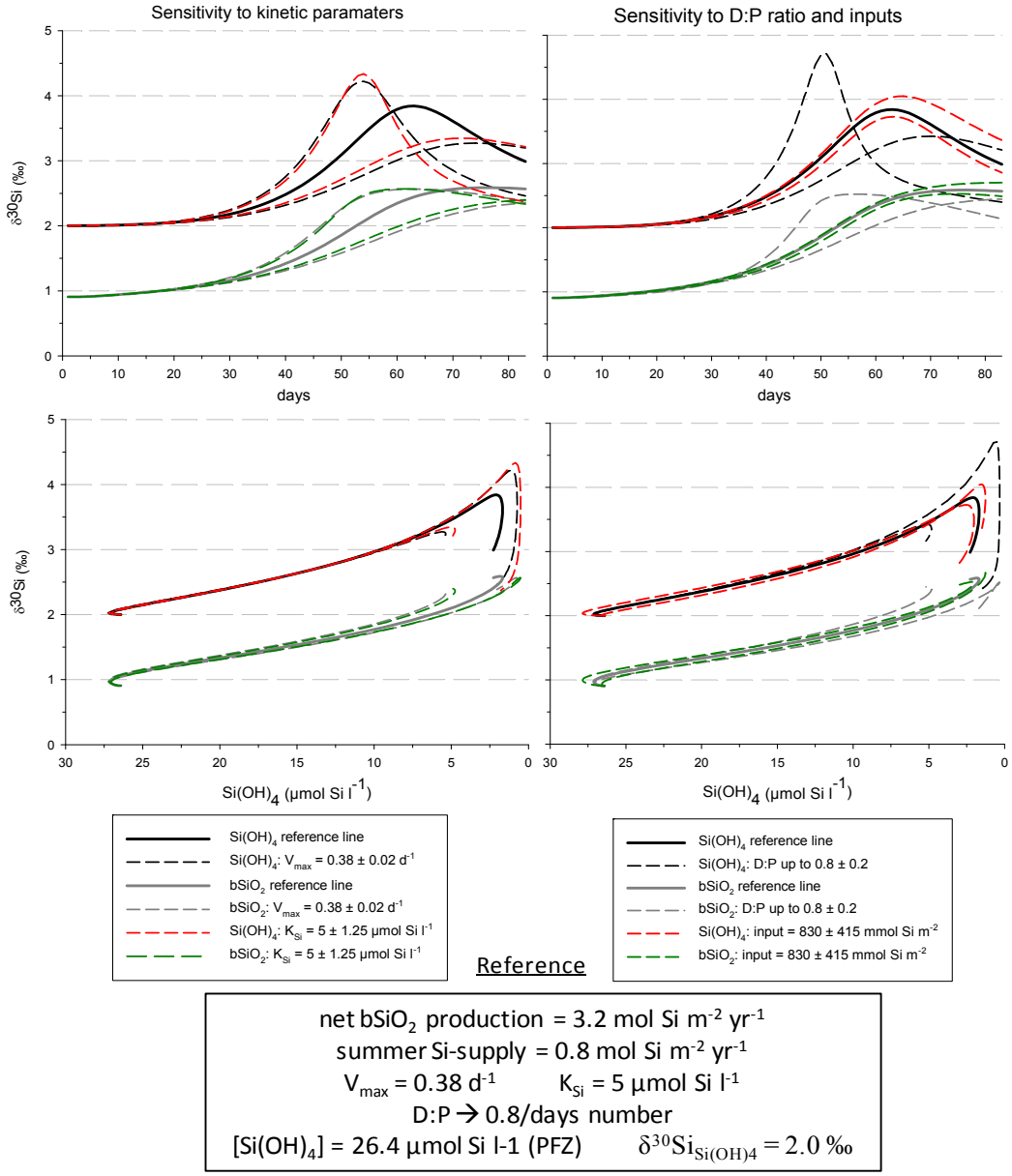

Reference

net $bSiO_2$ production = 3.2 mol Si m^{-2} yr^{-1}
summer Si-supply = 0.8 mol Si m^{-2} yr^{-1}
V_{max} = 0.38 d^{-1} K_{Si} = 5 µmol Si l^{-1}
D:P → 0.8/days number
$[Si(OH)_4]$ = 26.4 µmol Si l-1 (PFZ) $\delta^{30}Si_{Si(OH)4} = 2.0$ ‰

Figure 9.5. Seasonal evolution of Si-isotopic compositions of biogenic silica and silicic acid using Eqs (9.10 to 9.16). Reference simulation is described in the lower text box. Sensibility of the model outputs to kinetic parameters (left panel), D:P ratio, and Si-inputs (right panels) have been tested. Vertical full lines represents the period where the Si-utilization is at 80% (f=0.20, here for 5 µmol Si l^{-1}) with one standard deviation represented by vertical dashed lines.

9.1.3 Subsurface Si-isotopic signatures: origin and fates of silicic acid pools in the Southern Ocean

As discussed in chapters 6 and 7, the main Si-sources for surface mixed layer, independently of zones, are subsurface Si-pools, both initially by deep winter convective mixing and during summertime via turbulence diffusion or regular vertical mixing events. This view is in agreement with the study of *Cardinal*

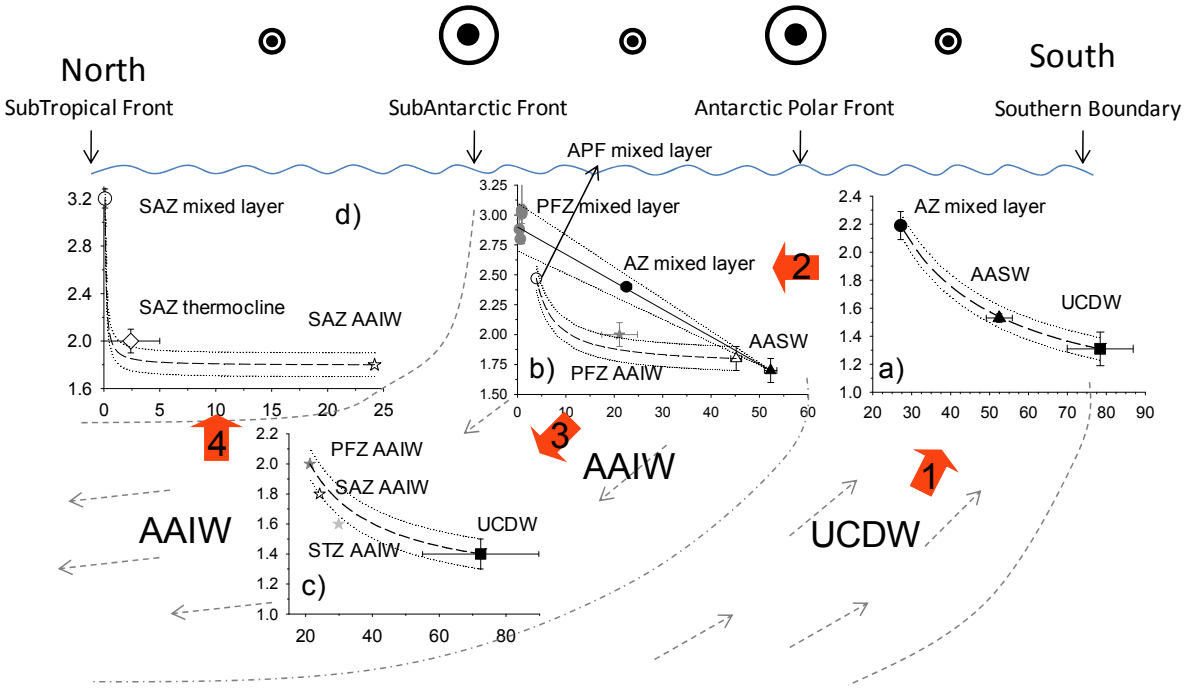

Figure 9.6. Schematic view of the processes involved in the alteration of the initial UCDW Si-pool during meridional Southern Ocean circulation (Figure 1.12). For each plot, the X axis is the silicic acid concentration and the Y axis is the $\delta^{30}Si_{Si(OH)4}$. (1) UCDW supply AASW in silicic acid mainly during winter time mixing. (2) During cross frontal exchange and locally (PFZ) by deep winter vertical mixing with PFZ mixed layers, AAIW are created. The straight line represents the steady state fractionation trends with AASW as Si-source. (3) During the northward transport, AAIW is furnished in silicic acid by diapycnal mixing with UCDW. (4) AAIW feeds in silicic acid the SAZ and STZ thermoclines.

et al. (2005) in the Australian sector where the mass and isotopic balances are respected only if we assume the subsurface Si-pools as the main Si-source ("multibox approach"). In the Southern Ocean, a clear north-south gradient of Si content in the mesopelagic layer is observed reflecting the shoaling of the Si-rich isopycnal south of the APF and the intermediate and mode waters subducted northwards via the upper limb of the Southern Ocean meridional circulation (Figure 7.4; *Trull et al*., 2001; *Pollard et al*., 2006). The magnitude of $\delta^{30}Si$ increase for a given $[Si(OH)_4]$ decrease in subsurface is small relative to what one observes for a given amount of silicic acid consumption, assuming a reasonable value for the fractionation factor. This suggests that the isotopic imprint of silicic acid consumption in the surface waters is transmitted deeper mainly by mixing processes. As suggested in *Fry* (2006), fractionation and mixing are just two sides of a coin, with fractionation acting to separate the isotopes and whereas water mixing recombines them. Both processes thus oppose and compensate each other.

On BONUS-Goodhope data, we have used these different sensitivities to track the origin and fates of the different ACC $Si(OH)_4$ pools (chapter 7). Figure 9.6 proposes a schematic meridional ACC overview of the different processes involved in silicic acid pathway. The Upper Circumpolar Deep Water, representing the ultimate ACC Si-source, upwells south to the Antarctic Polar Front. Mainly during deep winter convective mixing, UCDW supplies Antarctic Surface Water in silicic acid (Figure 9.6a). Summer stratification of the AASW advected northward in the Ekman layer separates the seasonal Si-depleted waters from the unaltered winter AASW (Winter Water; *Park et al*., 1998a, 1998b; *Pondaven et al*., 2000a; *Altabet and François*, 2001). During cross frontal exchange at the APF, intense vertical mixing between summer mixed

layer and unaltered WW seems to forms the AAIW. Locally deep winter vertical mixing with PFZ mixed layer could also participate to the AAIW formation (Figure 9.6b) in agreement with *Ribbe and Tomczak* (1997). AAIW is spreading and deepening northward. During its northward transport, AAIW is supplied significantly by UCDW (Figure 9.6c) and feed in silicic acid SAZ and STZ thermoclines (Figure 9.6d) as suggested in *Sarmiento et al*. (2004). As shown in Figure 9.6, natural silicon isotopic compositions are well in agreement with such view and seem to record the processes involved. This confirms $\delta^{30}Si$ is a powerful tool, for understanding modern marine Si-cycle. Modeling efforts are however required to have a better quantitative view of these processes.

9.1.4 Inter oceanic basin comparison

Figure 9.7a presents the locations of available data set of $\delta^{30}Si_{Si(OH)4}$ measurements in the world ocean: De La Rocha et al., (2000b), punctual silicic acid profiles in the world ocean; *Varela et al*., (2004), surface silicic acid transect in the spring-summer AZ (AESOPS, SOFEX); *Cardinal et al*., 2005, silicic acid profiles covering the spring ACC (Clivar SR-3); *Reynolds et al*., 2006, silicic acid profiles covering the spring SubArctic and Tropical gyres in the Western-North Pacific; *Beucher et al.,* 2008, silicic acid profiles in the eastern Equatorial Pacific (Biocomplexity); *Cavagna et al*., in revision, late summer silicic acid profiles close

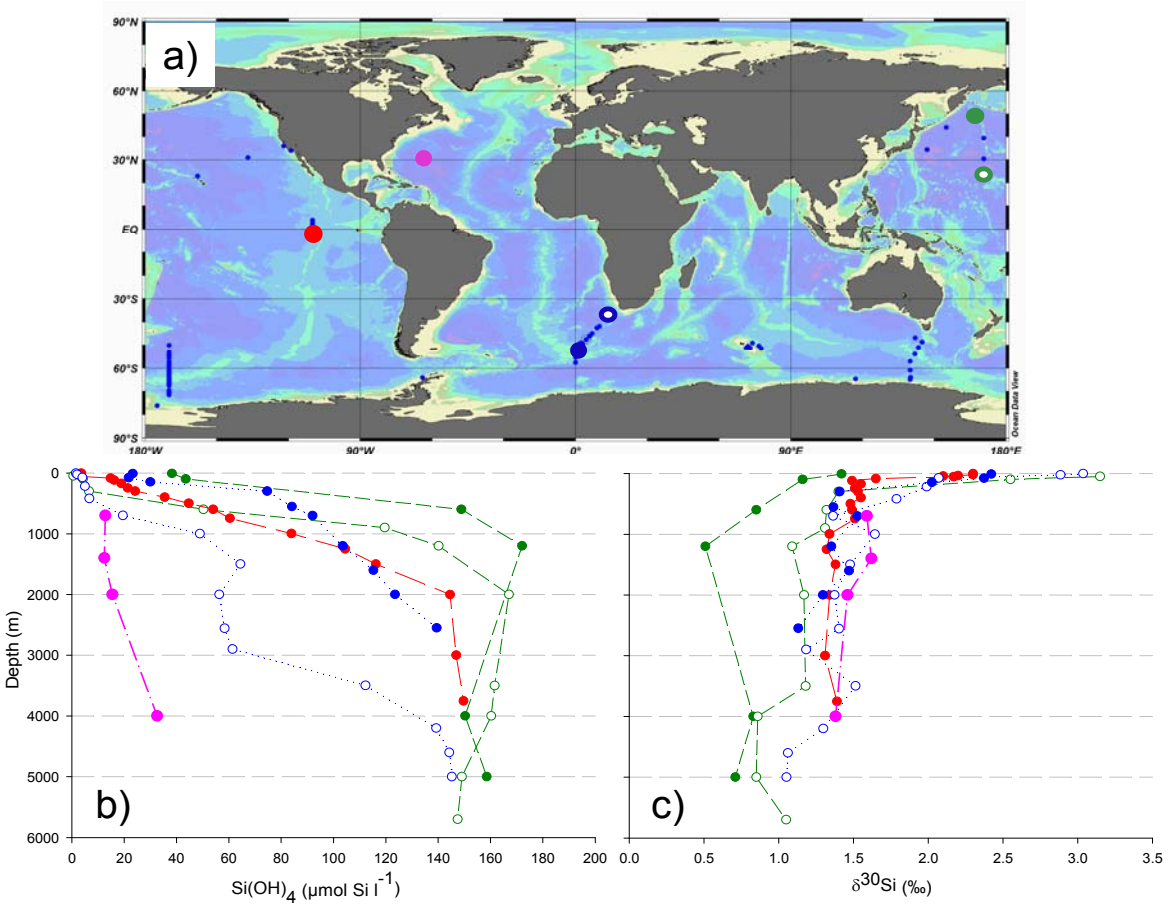

Figure 9.7. (a) Map of the Silicic acid isotopic studies in the World Ocean (Pink: De La Rocha et al., 2000b; Green: Reynolds et al., 2006 ; Red: Beucher et al., 2008; Blue: Varela et al., 2004; Cardinal et al., 2005; Fripiat et al., 2007 ; Cavagna et al., in revision ; chapters 4 and 5). (b) Silicic acid concentration profiles for some selected stations. (c) Silicic acid isotopic profiles for the corresponding stations. The color codes correspond to the ones on the map. See text for further information.

of the APF near the meridian 0 (Eifex); chapter 6, late summer silicic acid profiles around the Kerguelen plateau (KEOPS); chapter 7, late summer silicic acid profiles covering the complete ACC and adjacent systems close of the meridian 0 (BONUS-Goodhope).

Figures 9.7b and 9.7c show selected representative profiles of these different studies. The two selected silicic acid profiles in the Southern Ocean form like an envelope covering the variability encountered in the ACC (*De La Rocha et al*., 2000b*; Varela et al*., 2004; *Cardinal et al*., 2005, 2007; *Cavagna et al*., in revision; chapters 6 and 7), idem for the North Pacific studies from *Reynolds et al*. (2006). The Atlantic and North Pacific silicic acid profiles in the figure 9.7 represent the two end-members of the global meridional oceanic circulation (*Sarmiento et al*., 2007).

In the deep waters (> 2000m; Figure 9.8a), silicic acid distribution exhibits low concentration values in the North Atlantic Deep Water and increasing concentration along the pathway of the conveyor belt circulation upto the deep North Pacific. As explained hereafter, progressive dissolution of accumulating $bSiO_2$ is likely the main driver of this distribution and it is mostly confined in the Southern Ocean where the essential stripping of silicic acid in surface waters occurs (*Sarmiento et al*., 2004, 2007). Circumpolar Deep Water represents the crossroads of the deep oceanic circulation that blends together NADW, the corresponding deep water masses from the Indian (Indian Ocean Deep Water) and Pacific Ocean (North Pacific Deep Water) (*Sarmiento and Gruber*, 2006). The distribution of the $\delta^{30}Si$ of silicic acid decreases from ~ 1.4 ‰ in NADW to ~ 0.6‰ in NPDW (Figure 9.8a), and such features was first suggested by *De La Rocha et al.* (2000b) and further confirmed through modeling efforts (*Reynolds*, 2009). Progressive accumulation of silicic acid from $bSiO_2$ dissolution could sustain such features as for $\delta^{30}C_{DIC}$ with the remineralization of organic matter (*Kroopnick*, 1985). The lack of $\delta^{30}Si$ gradient along the path of deep circulation from North Atlantic to Circumpolar Deep Water stems fundamentally from the fact that silicic acid is completely consumed in most of the Atlantic surface ocean (*Conkright et al*., 2002). Therefore, the integrated $\delta^{30}Si$ of sinking biogenic silica converges to the one of the source (Figure 1.22), i.e. silicic acid

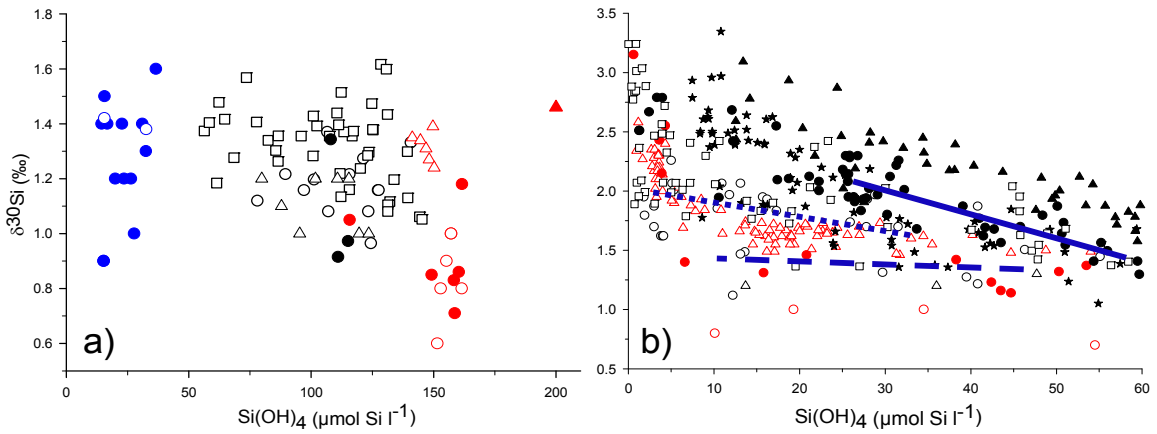

Figure 9.8. Complete world dataset of silicic acid isotopic composition for (a) below 2000m and (b) above 1500m. Atlantic: from De La Rocha et al. (2000; filled blue circles) and preliminary results from the GEOTRACES intercalibration (BATS; empty blue circles). Black symbols: Southern Ocean; empty triangles: De La Rocha et al. (2000b), filled triangles: Varela et al. (2004), empty circles: Cardinal et al. (2005), filled stars: Cavagna et al. (in revision), filled circles: KEOPS, (chapter 4), and empty squares: BONUS-Goodhope (chapter 5). Pacific: red symbols; empty circles: De La Rocha et al. (2000), filled circles: Reynolds et al. (2006), and empty triangles: Beucher et al. (2008). The blue lines represent the variations for three subsurface waters groups: AASW (filled line), AAIW-SAMW (dotted line), and NPIW (dashed line).

supply, so that the $\delta^{30}Si$ of the $bSiO_2$ rain out of the surface ocean is similar to that of subsurface silicic acid (ultimately Antarctic Intermediate Water; *Sarmiento et al*., 2004). The following Si-isotopic lightening from CDW to North Pacific could be attributed to the dissolution of settling diatoms in an area where silicic acid is partly used, both in the Southern Ocean and North Pacific (*Pondaven et al*., 1999, 2000a, 2000b; *Brzezinski et al*., 2001). *Reynolds* (2009) suggests that the $\delta^{30}Si$ gradient in deep waters results from both a heavy $\delta^{30}Si$ of silicic acid overturning in the North Atlantic and the dissolution of light $\delta^{30}Si$ of opal in the deep waters around the Southern Ocean that feed into the North Pacific. The subpartioning of the ocean's overturning in two compartments (Northern and Southern) that occupy distinct domains in the interior could enhance this difference (*Toggweiler et al*., 2006): the mid depth northern domain is North Atlantic Deep Water (NADW) and the southern domain is the bottom water formed around Antarctic and NPDW. Northern and southern water in the modern ocean mix together in the interior to form the water mass known as Circumplar Deep Water, which comes up to the surface along the southern flank of the ACC. The northern component of upwelled CDW is driven northward in the surface Ekman layer and then makes a long traverse through the thermoclines of the Indian, Pacific, and Atlantic before reaching its zone of sinking in the North Atlantic (*Gnanadesikan*, 1999). The southern component on the other hand, sinks almost immediately back into the deep ocean and is ventilated slowly than the northern counterpart (*Gordon*, 1971; *Toggweiler et al*., 2006). Most open ocean Si-producvities areas, e.g. the Southern ACC and North Pacific, seems to be furnished in silicic acid mainly through this southern domain and are areas where surface Si-pools are partly depleted. Incidentaly, this process is acting as a positive feedback in the observed $\delta^{30}Si$ between the different oceanic deep basins since dissolution should decrease the silicic acid isotopic composition only in the southern overturning component indicentaly lowering $\delta^{30}Si$ of furnished silicic acid to surface waters.

On Figure 9.7 and 9.8a, we see that this isotopic gradient is mainly restricted in the deep Pacific basins with a slight contribution across the ACC eastward circumpolar pathway (chapter 7). Indeed the data from the deep western North Pacific (*Reynolds et al*., 2006) and the deep Central North Pacific (*De La Rocha et al.*, 2000b) appear significantly lighter than the Equatorial Pacific and the Cascadia basin (*Beucher et al*., 2008) which are isotopically similar than the Southern Ocean (Figure 9.8a). The variability of the $\delta^{30}Si$ values in the deep waters of the North Pacific basin is extremely large (0.5‰) compared to Atlantic and SO basins. Isotopic variations of this magnitude within a single ocean basin are not predicted by models (*Wischmeyer et al*., 2003; *Reynolds*, 2009). Confirmation of large differences in Si isotopes values on these spatial scale will require a re-evaluation of the mechanisms controlling the distribution of silicon isotopes in the sea (*Beucher et al*., 2008).

The upwelling of deep water becomes confined primarily to the Southern Ocean but also in the North Pacific with significant vertical mixing and/or upwelling (*Sarmiento et al*., 2004; *Gnanadesikan et al*., 2004, 2007). In the AZ surface waters, this process brings extremely high nutrients concentration. As discussed in the section 9.1.3, winter mixing drives the Si-properties of the AASW representing a mixing interface between UCDW and partly Si-depleted summer mixed layer (Figure 9.6; Figure 9.9). This imposes a relatively heavy Si-isotopic composition in AASW relative to UCDW (Figure 9.8). Subsequently since AASW is the main Si-source for AZ surface waters, this latter can support the observed relatively heavier $\delta^{30}Si$ values through Si-consumption process (Figure 9.8b). The Ekman transport carries then these waters in the Northern ACC area where AAIW and SAMW are formed locally by deep convective mixing and by cross frontal exchanges (*Ribbe and Tomczak*, 1997) with AASW and highly Si-depleted surface waters as

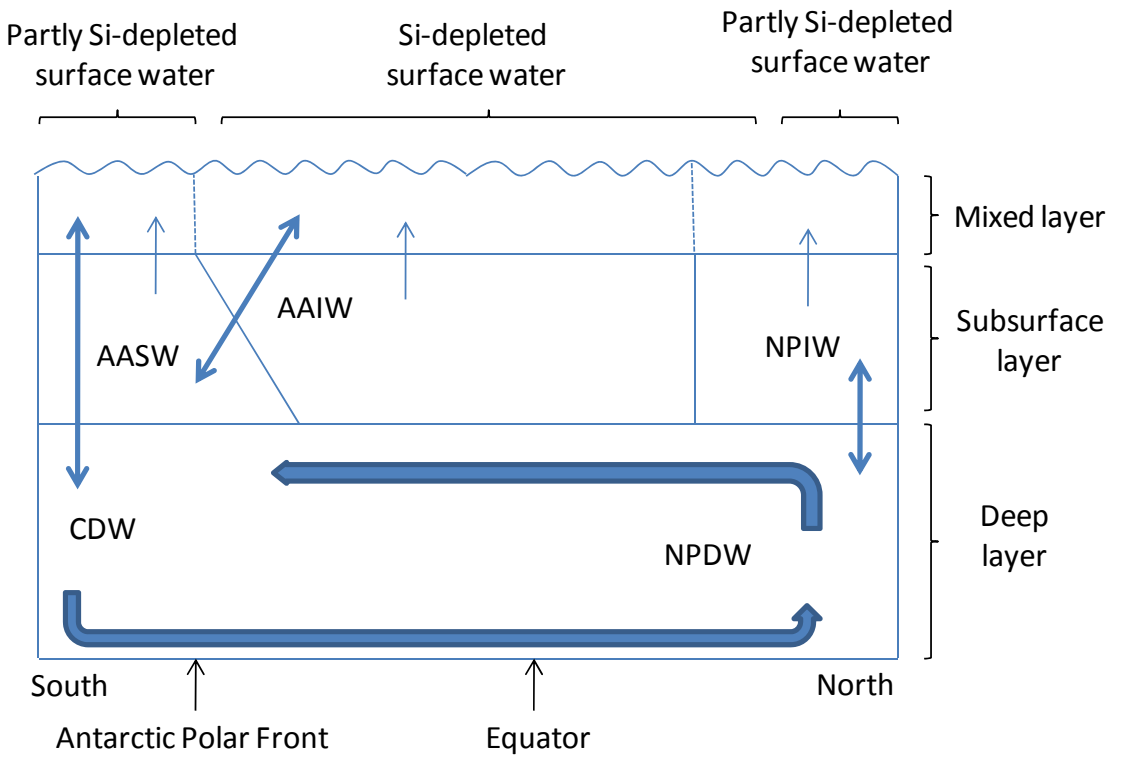

Figure 9.9. Schematic view of the responsible processes of the observed Si-isotopic distribution in subsurface waters across a Pacific section. AASW is a mixing interface between partly Si-depleted surface waters and CDW; AAIW is formed by mixing between AASW and highly Si-depleted surface waters; NPIW is furnished in silicic acid by NPDW by vertical mixing processes (Sarmiento and Gruber, 2006).

ulitmate end-members (Figure 9.9). This process dilutes significantly the initially Si-rich AASW without significant changing the AASW δ^{30}Si values (Figures 9.6 and 9.8b). Incidentally, Si-utilization in the northern ACC would give relatively the same δ^{30}Si range in surface waters than southern ACC but with lower corresponding silicic acid concentration (Figure 9.8b). AAIW and SAMW are spreadind northward feeding in silicic acid the main thermocline not only through-out the Southern hemisphere tropical gyres but also into the North Atlantic (*Sarmiento et al*., 2004). *Beucher et al*. (2008) noted that the main Si-source for the equatorial thermocline at 110°W is the AAIW which could explain the isotopic distribution similar than in the Northern ACC (Figure 9.8b). The North Pacific Ocean is an important exeption to the dominance of the AAIW-SAMW influence: in this area, the thermocline seems to be feeded in silicic acid by the North Pacific Intermediate Water (NPIW) presenting lighter δ^{30}Si values (Figure 9.8b). Strong vertical mixing supplying silicic acid from Si-rich NPDW is an important contributor to the processes that determine the biogeochemical properties of NPIW (*Sarmiento and Gruber*, 2006) including lighter measured δ^{30}Si values (Figures 9.8 and 9.9). Subsequently, for the same Si-utilization than in the AAIW counterpart, the δ^{30}Si of the resulting surface water should be lighter (Figure 9.8b).

9.2 Past Si-isotopic balance: proxy of past Si-utilization?

There are few means to reconstruct the history of diatom productivity and marine silicon cycle, and thus to explore the potential contribution of diatoms to past oceanic biogeochemistry. Indices based on the accumulation of sedimentary opal are often biased by winnowing and focusing of sediments and by opal dissolution (*Nelson et al*., 1995; *De La Rocha et al*., 1998; *Ragueneau et al*., 2000; *De La Rocha*, 2006). The

discovery that diatoms discriminate against the heavy silicon isotopes during the production of their siliceous cell walls (*De La Rocha et al*., 1997) has led to the use of silicon isotope data to gain insight into silicon utilization patterns (through its relation with f, the relative Si-utilization) by diatoms in past oceans (*De La Rocha et al*., 1998; *Brzezinski et al*., 2002; *Beucher et al*., 2007; *Reynolds et al*., 2008; *Pichevin et al*., 2009). To interpret such $\delta^{30}Si$ sedimentary records, we need to understand the processes involved in origin and fates of $bSiO_2$ in the water column and at the sediment interfaces. This is not the primary aim of this thesis but it clearly needs to be constrained especially since *Demarest et al*. (2009) reported a Si-isotopic fractionation during $bSiO_2$ dissolution. The $\delta^{30}Si$ of the silicic acid supply and the amplitude of isotope discrimination associated with silicic acid utilization are also two key parameters relating silicic acid utilization to the isotopic composition of silicic acid in oceanic surface waters and of the sinking flux to the seafloor. Both parameters require quantification in the modern ocean, assessments of their variability, and the development of a mechanistic understanding of the parameters that control them (section 9.1).

As shown previously in *Cardinal et al*. (2005) and in chapters 6 and 7, the possible sources of silicic acid have distinct silicic acid $\delta^{30}Si$-to-$[Si(OH)_4]$ relationships with a latitudinal gradient (also seen on figure 9.6). From the perspective of palaeoceanography studies, this represents an unwanted complexity since the past oceanic circulation was susceptible to be different from today, a feature still highly debated (see review in *Toggweiler et al*., 2006). For instance, *Beucher et al*. (2007) make quantitative paleoreconstructions from $\delta^{30}Si$ records assuming that the modern $\delta^{30}Si$ subsurface waters in SAZ are representative of the waters which should be upwelled if a northward shift of the upwelling area occurs during the Last Glacial Maximum. Such assumptions seem unrealistic however since this water mass should have been significantly altered by this processes and subsequently being not representative of the subsurface waters during the LGM. Modeling efforts (GCM) need to be done first to try to simulate modern Southern Ocean $\delta^{30}Si$ distribution and then to test the influence of different past oceanic circulation scenarios on this distribution.

Similarly, the amplitude of the fractionation factor and involved processes need to be better constrained (section 9.1.1). In chapter 6 of this manuscript and further confirmed in chapter 7, we did a compilation of the *in situ* fractionation factors estimates realized in the ACC. The average seasonally integrated ACC *in situ* fractionation factor was estimated at -1.2 ± 0.2‰, not so far from analytical precision (1sd *circa* 0.1‰). For this compilation, we remove the *in situ* estimates from $\Delta^{30}Si$ for the reasons discussed in section 9.1.1. We run several Montecarlo simulations (Normal distribution, n = 1000), with HNLC WW (KEOPS) as Si-source, the average ACC fractionation factor and different degrees of Si-utilization in the ML (different summer final ML $\delta^{30}Si$), in order to propagate the error on f estimates. These simulations show that for the steady state the precision on f deteriorates with the degree of Si-utilization from ±0.1 to ±0.2 when measuring $\delta^{30}Si_{Si(OH)4}$ (Figure 9.10a) while it is the reverse with $bSiO_2$ (Figure 9.10c). These trends result from the fact that the best known value is the Si-source and since the $Si(OH)_4$ departs from this signature while the $bSiO_2$ is getting closer to it, the precision improves near this value. In the case of Rayleigh for both $Si(OH)_4$ (Figure 9.10b) and instantaneous $bSiO_2$ (not shown), the precision on f estimation is better than ±0.1 and improves towards low f (high utilisation) since for a same variation of f, the $\delta^{30}Si$ change is more significant. It is difficult to run such kind of simulation on the accumulated $bSiO_2$ due to the non-linearity of the equation. Optimisations of the equation on each of 30 random generated parameters were realized. Such a number seems realistic since above 10 random generated parameters

and optimisations, no significant changes in the precision estimation are observed. The results are shown in Figure 9.10d. The same relation than for $Si(OH)_4$ is observed between $\delta^{30}Si$ and f estimation since the change of the isotopic signal is larger at low f value, but at high f value the change in $\delta^{30}Si$ is very small inducing worse precision (±0.25). In running these simulations but with a precision on the fractionation factor equals to the analytical precision which is so far the best that could be theoretically achieved on epsilon (±0.1‰), the precision on f estimation is only slightly improved (Figure 9.10). The same exercise is realized but this time with the precision from *in vitro* fractionation factor (± 0.4‰; *De La Rocha et al*., 1997). The precision is getting worse implying that it is difficult to have a quantitative estimation with this precision (Figure 9.10). However, except for ± 0.4‰, the precision is qualitatively relatively acceptable taking into account the potential Si-utilization variation in glacial (f~0.60)-interglacial (f close of 0) timescales (*De la Rocha et al.*, 1998; *Brzezinski et al.*, 2002; *Beucher et al.*, 2007). Therefore, it is crucial to pursue efforts to reduce the uncertainty on epsilon. Dissolution at depth and in the sediments would complicate the inferred relationship between opal isotopic signature acquired in surface waters and past Si-utilization by subsequently shifting the preserved material toward more positive values in a way still

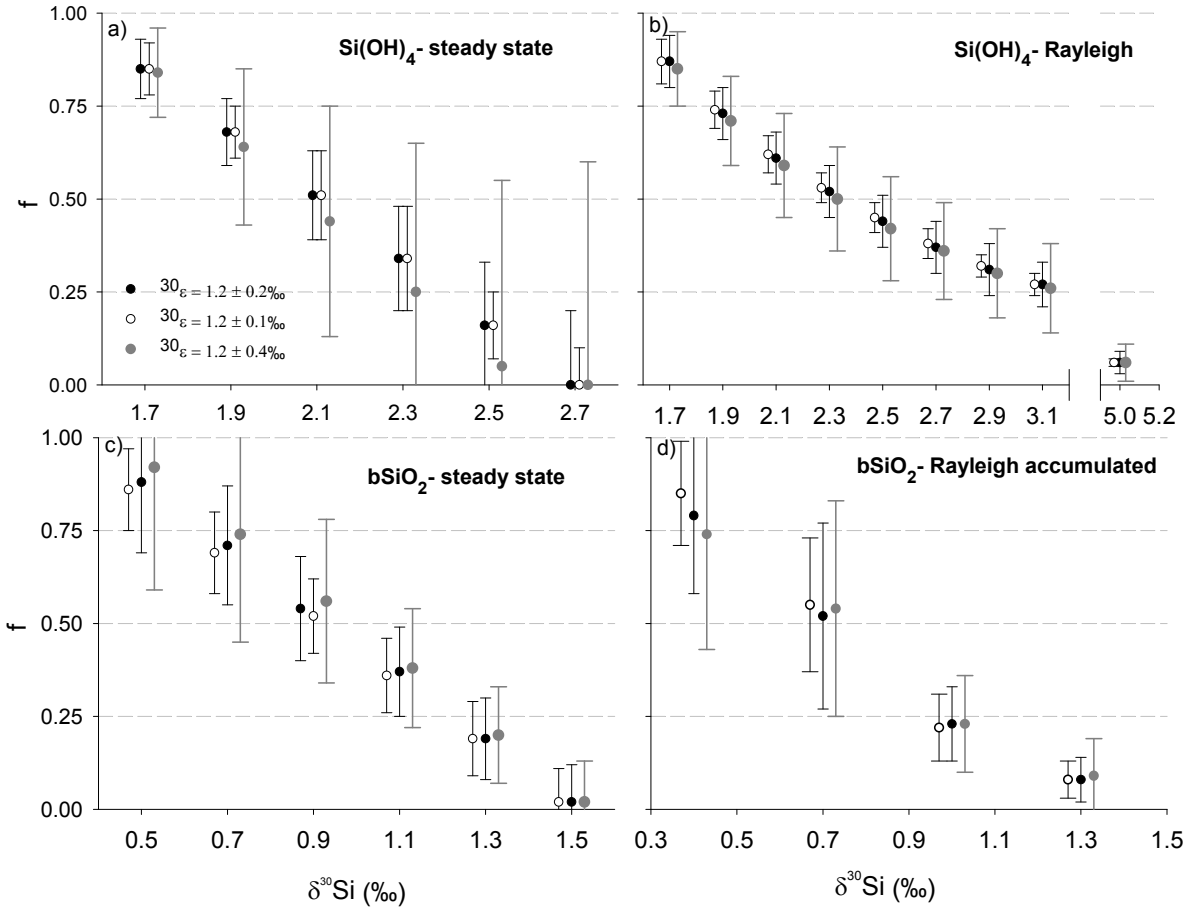

Figure 9.10. $\delta^{30}Si(OH)_4$ vs. f (f= $[Si(OH_4]_t/[Si(OH)_4]_{initial}$) showing the precision on the f estimation under KEOPS HNLC conditions (WW as Si-source) using average ACC fractionation factor of -1.2 ± 0.2‰ (black dots), or with the analytical precision ±0.1‰ (white dots), and the *in vitro* incubation precisions ±0.4‰ (gray dots: De La Rocha et al., 1997). The panels (a) show the steady state model for $Si(OH)_4$, (b) the Rayleigh model for $Si(OH)_4$, (c) the steady state model for $bSiO_2$, (d) the Rayleigh model for accumulated $bSiO_2$.

difficult to assess (*Demarest et al*., 2009). Ignoring this post-formational effect will cause an overestimation of the relative level of past surface $Si(OH)_4$ utilization that the measurement implies.

Varying the oceanic Si-inputs seems to have negligible effect on the average $\delta^{30}Si$ oceanic value at glacial-interglacial timescales (*De La Rocha and Bickle*, 2005; *Georg et al*., 2009a). Nevertheless as discussed in section 9.1.4, the $\delta^{30}Si$ of the northern and southern domain of the ocean's overturning circulation could be altered in a way keeping the average $\delta^{30}Si$ oceanic value constant. *Toggweiler et al*. (2006) suggest that the lowering of the pCO_2 during glacial periods could be due to a weakening of the southern component. Decreasing this ventilation rates should decrease the $\delta^{30}Si$ of silicic acid since larger accumulation of dissolving biogenic silica should be expected. Incidentally this process could partly participate to the lighter $\delta^{30}Si$ observed in biogenic silica from glacial AZ sediments and should partly reconcile the past $\delta^{15}N$ and $\delta^{30}Si$ Antarctic records (*Brzezinski et al*., 2002). This effect clearly needs to be constrained.

Chapter 10. Conclusions and perspectives

This thesis demonstrates the usefulness of coupling the measurement of an element (Si) with two complementary silicon isotopic approaches to investigate the Southern Ocean Si-biogeochemical cycle. They give an internal view of the silicon cycling from cellular to global scale (Figure 10.1). Indeed, the different sensitivity of the mass and isotopic balances in marine systems allows to track the sources and to discriminate between the different processes involved (10.1), e.g. $bSiO_2$ production and dissolution, and water mixing.

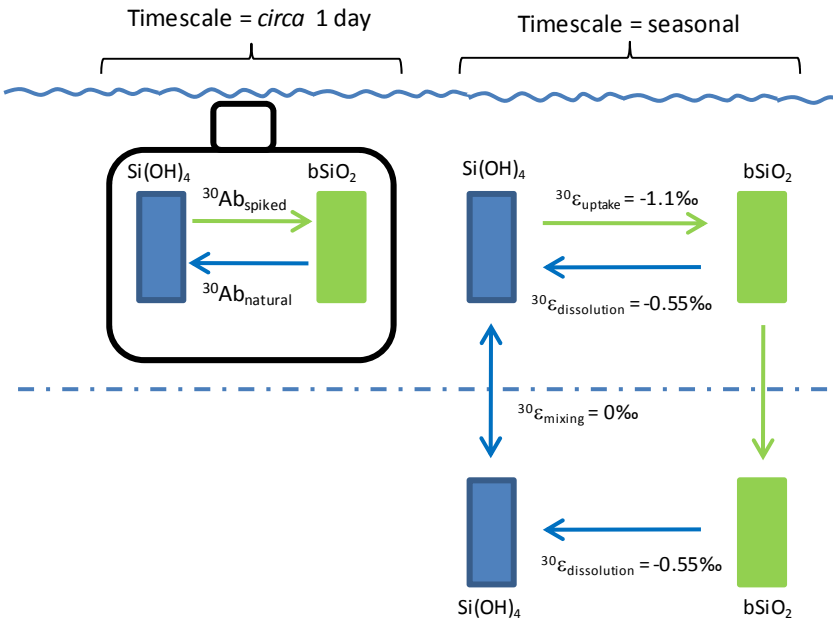

Figure 10.1. Schematic view of the two different isotopic approaches used in this thesis. The left side shows the ^{30}Si-tracer incubation experiment and the right side the processes which affect both the natural mass and isotopic balance.

10.1 Detection limit of the ^{30}Si-isotopic dilution method

We have developed a new method for the simultaneous determination of the rates of production and dissolution of biogenic silica. We use the same sampling method and integrating model described in *Corvaisier et al*. (2005) and *Elskens et al*. (2007) but we analyzed the isotopic composition by HR-SF-ICPMS instead of IRMS or TIMS (*Nelson et al*., 1977a, 1977b; *Corvaisier et al*., 2005). Our procedure has the same precision, requires a different sample processing protocol than the previous ones, but it is easier, 2-4 times faster, HF free and uses HRSF-ICPMS instruments which are available in many laboratories.

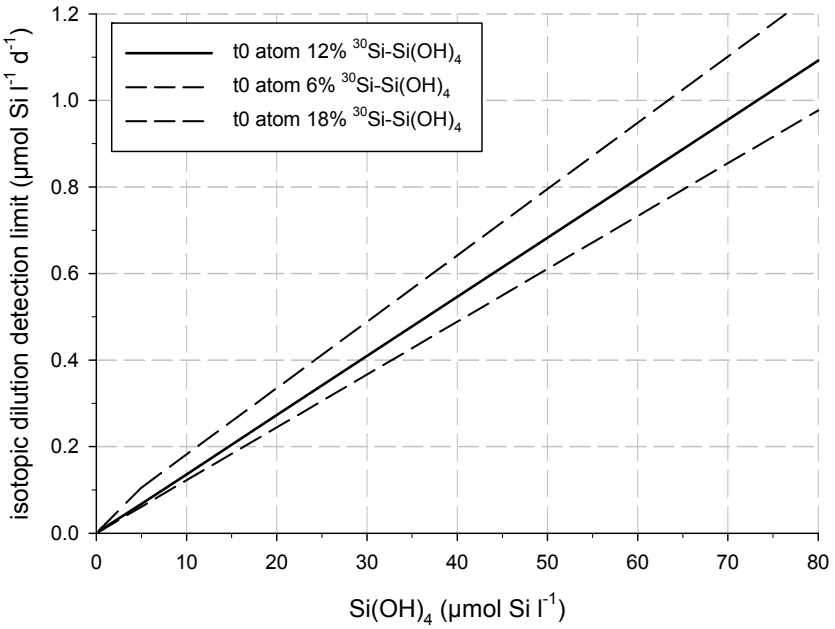

Figure 10.2. Detection limits of the ^{30}Si-isotopic dilution experiment corresponding to a spike addition of 10 ± 5% with the range of encountered Southern Ocean silicic acid concentrations in surface water.

With the help of the two compartmental models from *Elskens et al*. (2007), we precisely determine the detection limit of ^{30}Si-isotopic dilution required to estimate $bSiO_2$ dissolution rate (Figure 10.2). The mass and isotopic balance have been solved to get one relative standard deviation (1% = analytical precision) as difference between initial and final silicic acid isotopic abundances. The two main variables influencing this detection limit are silicic acid content and Si-isotopic abundances with a minor role of $bSiO_2$ content and production rates. Figure 10.2 covers the silicic acid concentration encountered in the surface waters of Antarctic Circumpolar Current. The initial Si-isotopic abundances correspond to a ^{30}Si-addition of *circa* 10 ± 5% of initial silicic acid content which is in the expected range. In regard of the estimated detection limit and taking into account the upper limit of biogenic silica dissolution rates measured in the ACC (0.25 µmol Si l^{-1} d^{-1}; *Brzezinski et al*., 2001), it is still difficult with the available method to determine $bSiO_2$ dissolution rate in the silicic acid rich surface waters of the Southern ACC. An alternative that we developed during BONUS-Goodhope cruise (collaboration with P. Pondaven and R. Corvaisier, IUEM) is to apply parallel incubations with two different ^{30}Si-spike additions (e.g. 10 and 100% of the initial silicic acid content) in order to decrease the detection limit (theoretically up to 10 times) in a similar way than *Brzezinski et al*. (2001) adding 30 µmol Si l^{-1} of ^{30}Si-spike to each incubation. So far, only the 10% results

are available (all below the detection limit, Annex 1) but samples from the 100% spike addition will be processed early 2010 by the IUEM team.

10.2 Si-budget in Northern Antarctic Circumpolar Current

The sensitivity of the available method (with 10% of ^{30}Si-addition) was appropriate enough to determine the generally low $bSiO_2$ dissolution rate during SAZ-Sense cruise south of Tasmania in mid-summer 2007 (Chapter 6). A complete set of incubations (n = 36) has been realized with parallel ^{32}Si-incubations (same CTD casts) to assess $bSiO_2$ production rates. The two methodologies give similar production rates (slope 0.96 ± 0.06; R^2 = 0.85, p value < 0.01). Actually efficient silicon loop with integrated (euphotic layer) dissolution:production rates ≥ 1 were observed. This loop is driven either by either (1) an accumulation of dissolving biogenic silica following productive period, both seasonal or sporadic (respectively Inter Polar Frontal Zone or western SubAntarctic Zone) or (2) a highly regenerated microbial food web comprising small silicified diatoms which are more prone to be grazed (eastern SubAntarctic Zone). These observations are in agreement with the seasonal evolution in the D:P ratio where $bSiO_2$ dissolution sustains a little part of the Si-uptake during bloom and a large part during non-bloom periods (*Brzezinski et al*., 2003b). As expected, the SubAntarctic Zone seems to be a more efficient dissolution environment than the IPFZ due to higher temperature, grazing pressure, and bacterial activity (*Hurd and Birdwhistell*, 1983; *Neslon et al*., 1995; *Bidle and Azam*, 1999, 2001; *Brzezinski et al*., 2003b; *Beucher et al*., 2004b). Complete characterization of the Si-cycle as during SAZ-Sense needs to be done systematically for process Si-studies: $bSiO_2$ production and dissolution rates (^{30}Si, ^{32}Si), kinetic parameters, taxonomy, silicifying species (PDMPO; *Leblanc and Hutchins*, 2005), δ^{30}Si, death diatoms percentage, size fraction, bacterial activity, and grazing dilution. By this way, the main different processes acting on the Si-cycle would be assessed, subsequently improving both Si-tracer integrating-models and potential mass and isotopic balance modeling efforts.

10.3 Si-isotopic distribution

This thesis expands widely the Si-isotopic data in the open ocean: 33% (209 on 638) for the δ^{30}Si of silicic acid and 15% (30 on 194) for biogenic silica. All the measurements for biogenic silica, except three in the North Pacific (*Rhizosolenia* mats; *De La Rocha et al*., 2000b), have been performed in the Southern Ocean south of the SubAntarctic Front (*Varela et al*., 2000; *Cardinal et al*., 2007; *Fripiat et al*., 2007; *Cavagna et al*., in revision; Chapter 4). A huge range of isotopic variations is observed for biogenic silica (-0.5 to 2.5‰) for a single oceanic basin. The variation of silicic acid composition in the surface waters of the Southern Ocean is more restricted (from 1.5 to 3.4‰). Such fractioned signature for biogenic silica is found at the end of summer just after productive period (*Varela et al*., 2004; chapter 4). We observe that at the end of the productive period as suggested with ^{30}Si-incubation, large accumulation of detrital biogenic silica in the surface waters increase the D:P ratio. This effect dampens the $bSiO_2$ production mediated isotopic fractionation with residual biogenic silica carrying heavier δ^{30}Si imposing a small isotopic different between silicic acid and biogenic silica (up to -0.4‰; chapter 4). Seasonal isotopic evolution is simulated and seems in agreement with our observations. These simulations strongly suggest working with non-zero order equations to fully assess the seasonal expression of the different processes involved: mixing, uptake, dissolution. In contrast, extremely low biogenic silica isotopic compositions are observed in the southern waters in the Seasonal Ice Zone with isotopic difference between the particulate and dissolved pool up to

-2.2‰ (*Varela et al*., 2004; *Cardinal et al*., 2007). This difference could not be just related to isotopic discrimination effect associated with the biogenic silica dissolution (-0.55‰; *Demarest et al*., 2009). Two hypotheses could explain such isotopic fractionation: an intraspecific variation (appendix 3) or an environmental control on the isotopic fractionation extent (Si-metabolism, Sea Ice, …). Clearly, biogenic silica needs to be systematically sampled to get an integrated view of the studied isotopic system. For such purposes, $bSiO_2$ isotopic composition on complete water column profiles (*in situ* pump) across BONUS-Goodhope section would be analyzed soon.

The Si-isotopic distribution in the deep waters with a progressive lightening of Si-isotopic composition across the global meridional circulation pathway (from the North Atlantic to the North Pacific) seems to reflect mainly the accumulation of dissolving biogenic silica in the Southern Ocean and northern Pacific where surface silicic acid pools are partly consumed. Subsequently, settling biogenic silica can carry lighter Si-isotopic composition than their Si-source and can participate to this trend (*De La Rocha et al*., 2000b; *Reynolds*, 2009). This thesis highlights a two step process (Figure 8.8): (1) slightly during the circumpolar pathway of the ACC (chapter 5) and (2) sharply in the North Pacific with large variation for a single oceanic basin. Such large variation is not predicted by the available model (*Reynolds*, 2009) and need to be clarified. A potential positive feedback to this deep water gradient is the partitioning of the overturning circulation in two components. The southern and deepest one with lower ventilation rates (*Toggweiler et al.*, 2006) can largely accumulate the isotopic imprint of biogenic silica dissolution since Si is remineralized deeper. Moreover this overturning component feeds in silicic acid the two most Si-productive areas in the World Ocean where surface Si-pools are partly depleted: the Southern ACC and North Pacific (*Pondaven et al*., 2000b).

For subsurface waters, we observe a counterintuitive Si-isotopic distribution (Figure 8.8b). Indeed, upwelling in the global ocean is mainly confined in the Southern Ocean (*Sarmiento et al*., 2007) supplying surface waters in light Si-isotopes. Nevertheless the subsurface waters in the Antarctic Zone (Antarctic Surface Water) are on the heavier Si-isotopic range found in subsurface. Antarctic Intermediate Waters furnishing silicic acid to the main low latitude thermocline (*Toggweiler et al*., 1991; *Sarmiento et al*., 2004) has similar Si-isotopic composition but much lower Si-concentration. The lightest Si-isotopic composition for the subsurface waters is found in the North Pacific Intermediate Water. Models do not fit well these observations and suggest an increase of the Si-isotopic composition both in the subsurface and surfaces ocean from the main upwelling area in the Southern Ocean (*Wischmeyer et al*., 2003; *Reynolds*, 2009). This measured distribution could be explained by the fact that the subsurface waters in the southern ACC, the AASW, are a mixing interface (Chapters 6 and 7) between partly Si-depleted surface waters and deep waters. The fact that the surface water end-members are partly Si-depleted has significant implications. AAIW seems mainly formed via mixing between AASW and highly Si-depleted surface waters. This process would dilute strongly the AASW silicic acid concentrations without significant changing its isotopic composition, as observed. The NPIW are fed in silicic acid through vertical mixing (*Sarmiento and Gruber*, 2006) with North Pacific Deep Water carrying the lightest oceanic Si-isotopic composition (*De La Rocha et al*., 2000; *Reynolds et al*., 2006). Since surface waters are mainly supplied in silicic acid by these water masses, this isotopic distribution controls the extent of isotopic fractionation found in the surface ocean: e.g. for the same level of Si-utilization, surface waters from the Southern Ocean can carry a heavier Si-isotopic composition than the North Pacific surface waters.

Global Coupled Modeling (e.g. PISCES; *Aumont et al.*, 2003) efforts should be useful to see to what extents the known processes can simulate the modern $\delta^{30}Si$ distribution and help in quantifying the processes involved. Too it is crucial to model different past oceanic circulation scenario to better constrain potential circulation feedbacks on the isotopic composition of past surface water Si-sources and subsequently settling biogenic silica (*Beucher et a*l., 2007). For such purposes, it is crucial to expand the available dataset.

10.4 Mass and isotopic balance in the Antarctic Zone

Most of our $\delta^{30}Si$ measurements have taken place in the Antarctic Zone south of the Antarctic Polar Front. Interestingly, all cruises were realized in late summer and should represent final conditions just before the onset of the winter convective regime (KEOPS, EIFEX, BONUS-Goodhope). Relatively simple mass and isotopic balances assuming a annual dynamics for the Antarctic Surface Waters (*Park et al.*, 1998a, 1998b; *Pondaven et al.*, 2000a; *Altabet and François*, 2001) have been performed to estimate various Si-fluxes: annual Upper Circumpolar Deep Water Si-supply to AASW corresponding to the annual $bSiO_2$ production using a system operating in steady state (supply = export), and summer Si-supply from the imbalance between seasonal mixed layer Si-depletion and annual $bSiO_2$ production estimates (Figure 10.3). It is the first time that Si-isotopes are used in a quantitative way in the modern ocean: we estimate regional net silica production (2.9 to 6.0 mol Si m^{-2} yr^{-1}) and quantify source waters fueling $bSiO_2$ productivity during summertime (0.2 to 3.6 mol Si m^{-2} yr^{-1}).

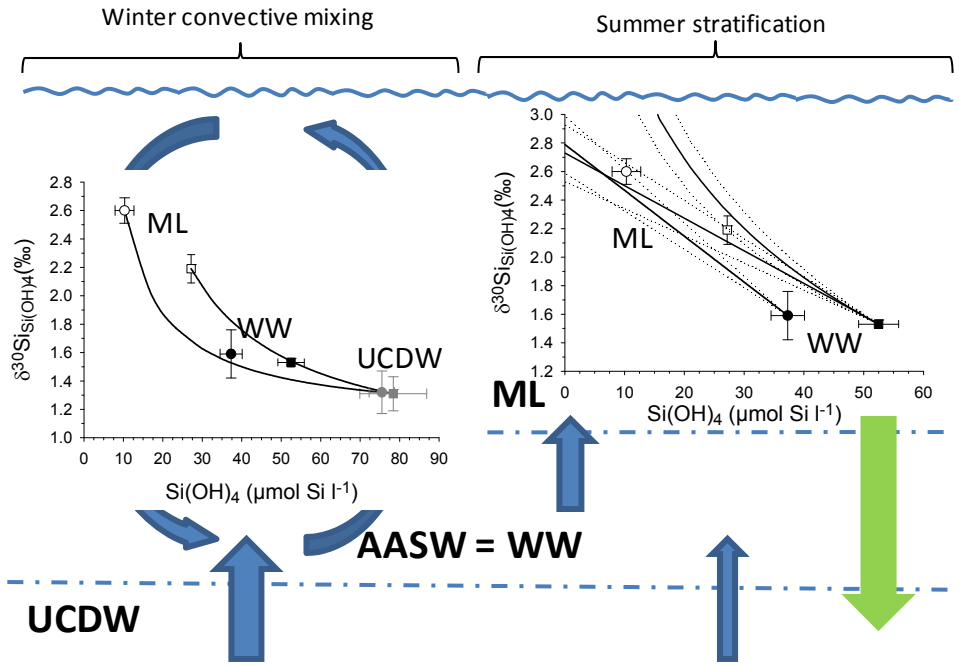

Figure 10.3. Schematic view of the estimated Si-fluxes from the annual mass and isotopic balance in the Antarctic Surface Waters (AASW). The left side shows the wintertime period characterized by deep winter convective mixings; the right side illustrates the summer stratification period when the winter mixed layer is split in a summer mixed layer (ML) and a residual Winter Water. The graphs present the water masses observed during KEOPS (squares) and Eifex (circles) with the mixing lines in the left panel and fractionation trends in the right panel.

Finally, we are developing an inverse box model (collaboration with A. de Brauwere and M. Elskens, VUB) solving the natural mass and isotopic balance in order to optimize the different Si-flux in a similar way than the models used in tracer incubation experiments (Figure 10.4). This model is tested in the Antarctic Zone but in the future, it will be adapted in function of the studied area and Si-sources.

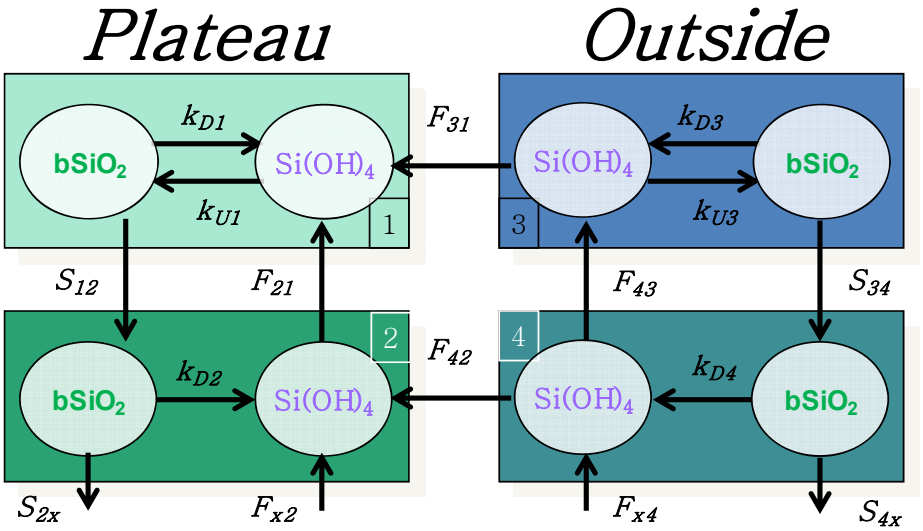

Figure 10.4. Inverse box models to solve mass and isotopic balance for KEOPS. Left boxes represents the Kerguelen Plateau area and the right boxes, the HNLC area eastward. Upper boxes are the surface boxes and lower boxes, the subsurface. K are constants of 1st order (uptake and dissolution), and F are constants of zero order (mixing).

Part VI. Appendix

Appendix 1. $bSiO_2$ production and dissolution data's

Location	# profiles	Production rates (mmol Si m^{-2} d^{-1})			Season	References
total	531	low	mean	high		
Coastal upwelling areas	**85**		**80.6**		**Spring**	
Baja California	25	2.3	89.0	307.0	Spring	Nelson and Goering, 1977
NW Africa	17	2.4	22.0	99.0	Spring	Nelson and Goering, 1977
Peru	25	2.6	27.0	97.0	Spring	Nelson et al., 1981
Monterey Bay	10	70.0	222.0	1140.0	Spring	Brzezinski and Phillips, 1996
Monterey Bay	8	4.8	42.8	108.0	spring	Brzezinski et al., 2003
Other Coastal areas	**133**		**11.5**			
Amazon river plumes	15	3.2	24	131.0	Spring/Summer	De Master et al., 1996
NW Black Sea Shelf	9	0.2	6.3	16.5	Spring/Summer	Ragueneau, unpublished results
(including Danube river plume)	5	4.4	10.6	16.5	Spring/Summer	Ragueneau, unpublished results
Bering Sea Shelf	31	1.8	17.7	51.0	Spring/Summer	Banahan and Goering, 1986
Lion Gulf	7	0.1	0.5	1.4	year	Leblanc et al., 2003
Santa Barbara basin	38	2.4	17.5	57.3	year	Shipe and Brzezinski, 2001
Amazon plumes	28	0.5	3.8	12.5	Summer/Fall	Shipe et al., 2006
Oceanic areas	**158**		**3.7**			
Gulf stream warm core	14	2	6.4	11.7	Spring	Brzezinski and Nelson, 1989
Equatorial Pacific (HNLC)	5		3.9		Fall	Blain et al., 1997
Equatorial Pacific (oligotrophic)	5	0.8	1.0	2.1	Fall	Blain et al., 1997
Equatorial Pacific	9	0.1	0.7	2.6	Fall	Leynaert et al., 2001
North Pacific	20	0.5	1.2	2.9	Summer	Brzezinski et al., 1998
North Atlantic	13	0.1	1.7	11.2	Spring/Fall	Leblanc et al., 2005
North Atlantic	3	0.5	0.9	1.3	Summer	Ragueneau et al., 1997
North Atlantic	9	6.0	38.0	166.0	Spring	Brown et al., 2003
Almeria-Oran Front	8	0.4	0.8	1.6	Winter	Leblanc et al., 2004
SubTropical Zone (Indian)	2	0.5	0.7	0.9	Summer	Leblanc et al., 2002
SubTropical Zone (Austrialian)	4	0.2	0.5	1.6	Summer	Quéguiner, 2001
SubTropical Zone (Atlantic)	1		0.0		Summer	Fripiat, 2009
Sargasso Sea	8	0.2	0.5	1.6	Spring	Brzezinski and Nelson, 1995
Sargasso Sea (BATS)	12	0.1	0.4	0.9	Year	Nelson and Brzezinski, 1997
Sargasso Sea	26		1.5		Winter/Spring 2004	Krause et al., 2009
Sargasso Sea	19		1.1		Winter/Spring 2005	Krause et al., 2009

Direct measurements of biogenic silica production in the world ocean (except Southern Ocean), by means of ^{30}Si and ^{32}Si isotopes. Updated from Ragueneau et al. (2000).

Location	# profiles	Production rates (mmol Si m^{-2} d^{-1})			Season	References
total	106.5	low	mean	high		
Southern Ocean	**24**		**9.4**			
CCSZ	**12**		**43.1**			
Ross Sea	8	7.1	37.6	92.6	Summer	Nelson and Smith, 1986
Ross Sea	3	25.5	34.0	49.6	Summer	Nelson et al., 1991
Australian sector	1		57.6		Summer	Beucher et al., 2004b
SIZ	**53**		**8.0**			
Weddel Sea	9	2.0	2.6	3.2	Winter	Leynaert et al., 1993
Weddel/Scotia Sea	18	2.3	10.9	22.9	Summer/Winter	Tréguer et al., 1991
Weddel Sea	1		4.0		Summer	BONUS-Goodhope
Pacific sector	1		6.8		Spring	Nelson and Gordon, 1982
Pacific sector	11	4.8	19.5	45.5	Spring/Summer	Brzezinski et al., 2001
Indian sector	4	5.7	7.0	8.9	Summer	Caubert, 1998
Australian sector	1		7.9		Summer	Beucher et al., 2004b
Atlantic sector	8	1.8	5.4	11.0	Spring	Quéguiner and Brzezinski, 2002
POOZ	**28**		**7.0**			
Pacific Sector	1		3.6		Spring	Nelson and Gordon, 1982
Pacific Sector	8	2.4	18.7	36.6	Spring/Summer	Brzezinski et al., 2001
Indian Sector	6	2.3	3.1	3.9	Summer	Caubert, 1998
Australian Sector	3	9.2	10.2	11.4	Summer	Beucher et al., 2004b
Atlantic Sector	7	2.4	4.1	6.9	Spring	Quéguiner and Brzezinski, 2002
Atlantic Sector	3	0.7	2.0	4.0	Summer	BONUS-Goodhope
PFZ	**47**		**6.4**			
Pacific Sector	1		3.6		Spring	Nelson and Gordon, 1982
Pacific Sector	17	0.2	7.9	24.8	Spring/Summer	Brzezinski et al., 2001
Australian Sector	9	0.5	2.6	5.2	Summer	Quéguiner, 2001
Australian Sector	3	1.3	3.3	4.7	Summer	chapter 8
Indian Sector	2	1.7	2.0	2.2	Summer	Caubert, 1998
Indian Sector	1		0.3		Summer	Leblanc et al., 2002
Atlantic Sector	10	12.6	30.8	60.7	Spring	Quéguiner and Brzezinski, 2002
Atlantic Sector	4	0.1	0.6	1.3	Summer	BONUS-Goodhope
SAZ	**15**		**0.9**			
Pacific Sector	1		1.4		Spring	Nelson and Gordon, 1982
Australian Sector	4	0.4	0.8	1.2	Summer	Quéguiner, 2001
Australian Sector	6	0.1	0.5	1.8	Summer	chapter 8
Australian Sector	1		1.7		Summer	Beucher et al., 2004b
Indian Sector	2	0.4	0.5	0.5	Summer	Leblanc et al., 2002
Atlantic Sector	1		0.7		Summer	BONUS-Goodhope

Direct measurements of biogenic silica production in the Southern Ocean, by means of ^{30}Si and ^{32}Si isotopes. Updated from Ragueneau et al. (2000).

Location	# profiles	Dissolution rates (mmol Si m^{-2} d^{-1})			Season	References
total	74	low	mean	high		
North-West Africa	7	15.7	27.4	40.5	Spring	Nelson and Goering, 1977b
Monteray bay	7	0.6	2.9	6.5	Spring	Brzezinski et al., 2003
Amazone plume	3	5.6	12.8	22	Summer	DeMaster et al., 1996
golf stream warm core	5	<1.9	<1.9	<1.9	Spring	Brzezinski and Nelson, 1989
golf stream warm core	3	4.4	4.9	5.4	Summer	Brzezinski and Nelson, 1989
SubTropical Zone (Atlantic)	1		0.9		Summer	Fripiat, 2009
Southern Ocean	39					
CCZS	**4**		**42.4**			
Ross Sea	3	16.2	21.6	27.5	Spring	Nelson et al., 1991
Australian sector	1		63.1		Summer	Beucher et al., 2004b
SIZ	**6**		**9.3**			
Pacific sector	1		2.3		Spring	Nelson and Gordon, 1982
Pacific sector	4	1.8	6.9	14.5	Spring/Summer	Brzezinski et al., 2001
Australian sector	1		18.8		Summer	Beucher et al., 2004b
POOZ	**9**		**5.4**			
Pacific sector	1		1.0		Spring	Nelson and Gordon, 1982
Pacific sector	5	4.7	7.3	10.9	Spring/Summer	Brzezinski et al., 2001
Australian sector	3		7.9		Summer	Beucher et al., 2004b
PFZ	**12**		**2.1**			
Pacific sector	3	0.5	0.7	1.0	Spring	Nelson and Gordon, 1982
Pacific sector	6	0.2	2.5	5.8	Spring/Summer	Brzezinski et al., 2001
Australian sector	3	1.5	3.0	4.4	Summer	chapter 8
SAZ	**8**		**2.1**			
Pacific sector	1		0.4		Spring	Nelson and Gordon, 1982
Australian sector	1		5.2		Summer	Beucher et al., 2004b
Australian sector	6	0.0	0.6	2.0	Summer	chapter 8

Direct measurements of biogenic silica dissolution in the world ocean, by means of the ^{30}Si isotopes. Updated from Beucher (2003)

Appendix 2. Cellular scale Si-isotopic fractionation : derivation

1) Three compartmental steady state model for Si-uptake

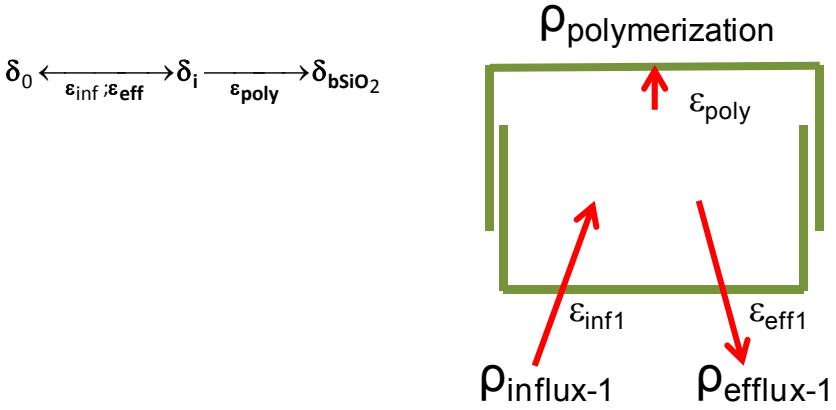

Let's define δ_0, δ_i, and δ_{bSiO2} as the isotopic signatures of the external source of $Si(OH)_4$, the internal silicon pool, and the biogenic silica. ε_{inf} is the fractionation associated with influx, ε_{eff} is the fractionation associated with efflux, and ε_{poly} is the fractionation associated with silica polymerization. This model is similar to the model developed for C-isotopic fractionation by phytoplankton by Popp et al. (1989), François et al. (1993), and Cassar (2003).

$$\delta_i = \delta_0 - \varepsilon_{inf} + f_{eff} \cdot \varepsilon_{diff} + (1 - f) \cdot \varepsilon_{poly} \quad (1)$$

where f_{eff} is the fraction of the internal silicon pool that leaks out of the cell.

$$\delta_{bSiO_2} = \delta_i - \varepsilon_{poly} \quad (2)$$

Hence,

$$\delta_{bSiO_2} = \delta_0 - \varepsilon_{inf} + f_{eff} \cdot \varepsilon_{eff} + (1 - f_{eff}) \cdot \varepsilon_{poly} - \varepsilon_{poly} \quad (3)$$

$$\delta_{bSiO_2} = \delta_0 - \varepsilon_{inf} + f_{eff} \cdot \varepsilon_{eff} - f_{eff} \cdot \varepsilon_{poly} \quad (4)$$

$$\delta_{bSiO_2} = \delta_0 - \varepsilon_{inf} + f_{eff} \cdot (\varepsilon_{eff} - \varepsilon_{poly}) \quad (5)$$

Therefore, ε_{tot}, the overall fractionation is

$$\varepsilon_{tot} = \delta_0 - \delta_{bSiO_2} = \varepsilon_{inf} + f_{eff} \cdot (\varepsilon_{poly} - \varepsilon_{eff}) \quad (6)$$

This equation is similar than one given by Milligan et al. (2004).

As noted in section 8.1 and similarly than for carbon (Cassar, 2003), the Si-transport through the cell membrane could be active (silicon transporters) or passive (diffusion) depending of the external $Si(OH)_4$ concentration (Thamatrakoln and Hildebrand, 2008). The silicon isotopic composition of the transported $Si(OH)_4$ across the membrane (δ_{inf}) should be;

$$\delta_{inf} = \mathbf{f_a} \cdot (\delta_0 - \boldsymbol{\varepsilon_a}) + \mathbf{f_p} \cdot (\delta_0 - \boldsymbol{\varepsilon_p}) \quad (7)$$

where f_a and f_b are respectively, the fraction of silicic acid which is transported actively or passively with $f_a + f_b$ equaling 1. The associated fractionation is respectively ε_a and ε_p.

$$\varepsilon_{inf} = \delta_0 - \delta_{inf} \quad (8)$$
$$\varepsilon_{inf} = \delta_0 - \mathbf{f_a} \cdot (\delta_0 - \boldsymbol{\varepsilon_a}) - \mathbf{f_p} \cdot (\delta_0 - \boldsymbol{\varepsilon_p}) \quad (9)$$
$$\varepsilon_{inf} = \delta_0 - \mathbf{f_a} \cdot \delta_0 + \mathbf{f_a} \cdot \boldsymbol{\varepsilon_a} - \mathbf{f_p} \cdot \delta_0 + \mathbf{f_p} \boldsymbol{\varepsilon_p} \quad (10)$$
$$\varepsilon_{inf} = \delta_0 (1 - \mathbf{f_a} - \mathbf{f_p}) + \mathbf{f_a} \cdot \boldsymbol{\varepsilon_a} + \mathbf{f_p} \boldsymbol{\varepsilon_p} \quad (11)$$
$$\varepsilon_{inf} = \mathbf{f_a} \cdot \boldsymbol{\varepsilon_a} + \mathbf{f_p} \boldsymbol{\varepsilon_p} \quad (12)$$

2) Four compartmental steady state model for Si-uptake (mathematical development from Cassar, 2003).

$$\delta_0 \xleftrightarrow[\varepsilon_{inf1};\varepsilon_{eff1}]{} \delta_i \xleftrightarrow[\varepsilon_{inf2};\varepsilon_{eff2}]{} \delta_{SDV} \xrightarrow[\varepsilon_{poly}]{} \delta_{bSiO_2}$$

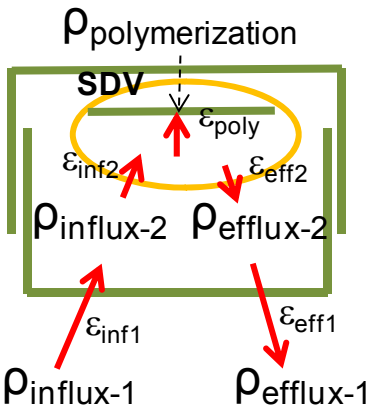

Let's define δ_0, δ_i, δ_{SDV} and δ_{bSiO2} as the isotopic signatures of the external source of $Si(OH)_4$, of the internal silicon pool, of the silicon pool in the Silicon Vesicle Deposit (SDV), and the biogenic silica. ε_{inf} is the fractionation associated with influx, ε_{eff} is the fractionation associated with efflux, the subscript 1 and 2 represent respectively the flux between the intracellular external medium, and between intracellular and SDV medium, and ε_{poly} is the fractionation associated with silica polymerization. This model is similar to the model developed for C-isotopic fractionation by phytoplankton by Cassar (2003). The proportion of silicon that enters the δ_{SDV} pool that actually leaks out before to be polymerized is f_{eff2}. The associated fluxes are ρ_{inf1}, ρ_{eff1}, ρ_{inf2}, ρ_{eff2}, and ρ_{poly}.
Mass and isotopic balances of the δ_{SDV} pool;

$$\rho_{inf2} \cdot (\delta_i - \varepsilon_{inf2}) = \rho_{poly} \cdot (\delta_{SDV} - \varepsilon_{poly}) + \rho_{eff2} \cdot (\delta_{SDV} - \varepsilon_{eff2}) \quad (13)$$

Isolating δ_i from Eq. 13;

$$\delta_i = \frac{\rho_{poly}}{\rho_{inf2}} \cdot (\delta_{SDV} - \varepsilon_{poly}) + \frac{\rho_{eff2}}{\rho_{inf2}} \cdot (\delta_{SDV} - \varepsilon_{eff2}) + \varepsilon_{inf2} \quad (14)$$
$$\delta_i = (1 - \mathbf{f_{eff2}}) \cdot (\delta_{SDV} - \varepsilon_{poly}) + \mathbf{f_{eff2}} \cdot (\delta_{SDV} - \varepsilon_{eff2}) + \varepsilon_{inf2} \quad (15)$$
$$\delta_i = \delta_{SDV} - \varepsilon_{poly} + \varepsilon_{inf2} + \mathbf{f_{eff2}} \cdot (\varepsilon_{poly} - \varepsilon_{eff2}) \quad (16)$$

Mass and isotopic balances of the δ_i pool;

$$\rho_{inf1} \cdot (\delta_0 - \varepsilon_{inf1}) + \rho_{eff2} \cdot (\delta_{SDV} - \varepsilon_{eff2}) = \rho_{inf2} \cdot (\delta_i - \varepsilon_{inf2}) + \rho_{eff1} \cdot (\delta_i - \varepsilon_{eff1}) \quad (17)$$

Mass and isotopic balances for the whole diatom cell;

$$\rho_{inf1} \cdot (\delta_0 - \varepsilon_{inf1}) = \rho_{\mathbf{eff1}} \cdot (\delta_{\mathbf{i}} - \varepsilon_{\mathbf{eff1}}) + \rho_{\mathbf{poly}} \cdot (\delta_{\mathbf{SDV}} - \varepsilon_{\mathbf{poly}}) \quad (18)$$

Since,

$$\rho_{\mathbf{eff1}} = \rho_{inf1} - \rho_{\mathbf{poly}} \quad (19)$$

We can replace ρ_{eff1} in Eq (18) by the right-hand-side of Eq (19) and rearrange

$$\rho_{inf1} \cdot (\delta_0 - \varepsilon_{inf1} + \varepsilon_{\mathbf{eff1}} - \delta_{\mathbf{i}}) = \rho_{\mathbf{poly}} \cdot (\varepsilon_{\mathbf{eff1}} - \delta_{\mathbf{i}} + \delta_{\mathbf{SDV}} - \varepsilon_{\mathbf{poly}}) \quad (20)$$

Assuming that the proportion of silicon that enters δ_i that leaks out the cell is represent by $f_{eff1}=(\rho_{inf}-\rho_{poly})/\rho_{inf}$. Hence the Eq. (20) can be simplified to

$$\delta_0 - \varepsilon_{inf1} + \varepsilon_{\mathbf{eff1}} - \delta_{\mathbf{i}} = (1 - \mathbf{f_{eff1}}) \cdot (\varepsilon_{\mathbf{eff1}} - \delta_{\mathbf{i}} + \delta_{\mathbf{SDV}} - \varepsilon_{\mathbf{poly}}) \quad (21)$$

Replacing δi in Eq. (21) by the right-hand side of Eq. (16)

$$\begin{aligned} &\delta_0 - \varepsilon_{inf1} + \varepsilon_{\mathbf{eff1}} - \delta_{\mathbf{SDV}} - \varepsilon_{inf2} + \varepsilon_{\mathbf{poly}} - \mathbf{f_{eff2}} \cdot (\varepsilon_{\mathbf{poly}} - \varepsilon_{\mathbf{eff2}}) \\ &= (1 - \mathbf{f_{eff1}}) \cdot (\varepsilon_{\mathbf{eff1}} - \varepsilon_{inf2} - \mathbf{f_{eff2}} \cdot (\varepsilon_{\mathbf{poly}} - \varepsilon_{\mathbf{eff2}})) \end{aligned} \quad (22)$$

And since

$$\delta_{\mathbf{bSiO2}} = \delta_{\mathbf{SDV}} - \varepsilon_{\mathbf{poly}} \text{ and } \varepsilon_{\mathbf{tot}} = \delta_0 - \delta_{\mathbf{bSiO2}} \quad (23 \text{ and } 24)$$

Eq. (22) can be simplified to

$$\varepsilon_{\mathbf{tot}} - \varepsilon_{inf1} + \varepsilon_{\mathbf{eff1}} - \varepsilon_{inf2} - \mathbf{f_{eff2}} \cdot (\varepsilon_{\mathbf{poly}} - \varepsilon_{\mathbf{eff2}}) = (1 - \mathbf{f_{eff1}}) \cdot (\varepsilon_{\mathbf{eff1}} - \varepsilon_{inf2} - \mathbf{f_{eff2}} \cdot (\varepsilon_{\mathbf{poly}} - \varepsilon_{\mathbf{eff2}})) \quad (25)$$

Rearranging and simplifying Eq. (25)

$$\varepsilon_{\mathbf{tot}} = \varepsilon_{inf1} + \mathbf{f_{eff1}} \cdot (\mathbf{f_{eff2}} \cdot (\varepsilon_{\mathbf{poly}} - \varepsilon_{\mathbf{eff2}}) + \varepsilon_{inf2} - \varepsilon_{\mathbf{eff1}}) \quad (26)$$

3) Three compartmental steady state model to assess $bSiO_2$ dissolution isotopic effect

$$\delta_0 \xleftrightarrow[\varepsilon_{upt};\varepsilon_{diss}]{} \delta_{bSiO2}$$

The mass and isotopic balance of the δ_{bSiO2} pool

$$(\rho_{\mathbf{upt}} - \rho_{\mathbf{diss}}) \cdot \delta_{\mathbf{bSiO2}} = \rho_{\mathbf{upt}} \cdot (\delta_0 - \varepsilon_{\mathbf{upt}}) - \rho_{\mathbf{diss}} \cdot (\delta_{\mathbf{bSiO2}} + \varepsilon_{\mathbf{diss}}) \quad (27)$$

Rearranging Eq. (27)

$$\rho_{\mathbf{upt}} \cdot \delta_{\mathbf{bSiO2}} - \rho_{\mathbf{diss}} \cdot \delta_{\mathbf{bSiO2}} = \rho_{\mathbf{upt}} \cdot \delta_0 - \rho_{\mathbf{upt}} \cdot \varepsilon_{\mathbf{upt}} - \rho_{\mathbf{diss}} \cdot \delta_{\mathbf{bSiO2}} - \rho_{\mathbf{diss}} \cdot \varepsilon_{\mathbf{diss}} \quad (28)$$

$$\rho_{\mathbf{upt}} \cdot \delta_{\mathbf{bSiO2}} = \rho_{\mathbf{upt}} \cdot \delta_0 - \rho_{\mathbf{upt}} \cdot \varepsilon_{\mathbf{upt}} - \rho_{\mathbf{diss}} \cdot \varepsilon_{\mathbf{diss}} \quad (29)$$

$$\delta_{bSiO2} = \delta_0 - \varepsilon_{upt} - \frac{\rho_{diss}}{\rho_{upt}} \cdot \varepsilon_{diss} \quad (30)$$

Since

$$\varepsilon_{tot} = \delta_0 - \delta_{bSiO2}$$

Eq. (30) can be simplified

$$\varepsilon_{tot} = \varepsilon_{upt} + \frac{\rho_{diss}}{\rho_{upt}} \cdot \varepsilon_{diss} \quad (31)$$

This equation is similar to the one given by Demarest et al. (2009).

Appendix 3. *In vitro* incubations under Antarctic conditions to assess $bSiO_2$ production mediated $^{30}\varepsilon$.

Temperature	Concentration	Species	$\delta^{30}Si_{Si(OH)4\ final}$ (‰)	$\delta^{30}Si_{bSiO2\ final}$ (‰)	$^{30}e_{Si(OH)4\text{-}bSiO2}$ (‰)
1°C	40 µmol Si l^{-1}	*Ch.brevis*	-0.2	-1.3	-1.0
		Ch.brevis	0.0	-1.0	-1.0
		Th.antarctica	-0.3	-1.9	-2.2
	70 µmol Si l^{-1}	*Ch.brevis*	0.5	-1.5	-1.9
		Ch.brevis	0.1	-1.4	-1.4
3°C	40 µmol Si l^{-1}	*Ch.brevis*	0.3	-1.0	-1.3
		Ch.brevis	0.3	-0.8	-1.1
		Ch.dichaeta	0.5	-1.0	-1.5
		Th.antarctica	0.2	-1.6	-1.8
	70 µmol Si l^{-1}	*Th.antarctica*	0.1	-1.9	-2.0
		Th.antarctica	0.2	-1.9	-2.0
7°C	70 µmol Si l^{-1}	*Ch.brevis*	0.8	0.3	-0.5
		Ch.brevis	1.0	0.4	-0.7
				total	**-1.6 ± 0.4**
				1°C	**-1.5 ± 0.5**
				3°C	**-1.6 ± 0.4**
				Ch.brevis	**-1.3 ± 0.3**
				Ch. Dichaeta	**-1.5**
				Th.antarctica	**-2.0 ± 0.2**
				40 µmol Si l^{-1}	**-1.4 ± 0.5**
				70 µmol Si l^{-1}	**-1.8 ± 0.3**

***In vitro* incubations (in batch) at three different temperatures, two different silicic acid concentrations, and with three Antarctic species.**

Part VII. Bibliography

Abraham, K., S., Opfergelt, F., Fripiat, A.-J., Cavagna, J.T.M., de Jong, S.F., Foley, L., André, D., Cardinal, 2008. δ^{30}Si and δ^{29}Si determinations on USGS BHVO-1 and BHVO-2 reference materials with a new configuration on an Nu Plasma Multi-Collector ICP-MS. Geost. and Geoanal. Res. 32 (2), 193-202.

Albarede, F., 1996. Introduction to geochemical modeling. Cambridge University Press, Cambridge, pp. 564.

Alleman, L. , D., Cardinal, C., Cocquyt, P.D., Plisnier, J.-P., Descy, I., Kimirei, D., Sinyinza, L., André, 2005. Silicon isotopic fractionation in Lake Tanganyika and its main tributaries. J. Gt. Lakes Res. 31, 509-519.

Altabet, M.A., R., François, 2001. Nitrogen isotope biogeochemistry of the Antarctic Polar Frontal Zone at 170°W. Deep-Sea Res. II 48: 4247-4273.

Alvain, S., C., Moulin, Y., Dandonneau, H., Loisel, 2008. Seasonal distribution and succession of dominant phytoplankton groups in the global ocean : a satellite view. Global Biogeochem. Cycles 22, GB3001, doi:10.1029/2007GB003154.

Anderson, R.F., Z., Chase, M.Q., Fleisher, J., Sachs, 2002. The Southern Ocean's biological pump during the Last Glacial Maximum. Deep-Sea Res. II 49: 1909-1938.

Anderson, R.F., G., Winckler, 2005. Problems with paleoproductivity proxies. Paleoceanography 20, PA3012, doi:10.1029/2004PA001107.

André, L., D., Cardinal, L.Y., Alleman, S. Moorbath, 2006. Silicon isotopes in 3.8 Ga West Greenland rocks as clues to the Eoarchaean supracrustal Si cycle. Earth and Planetary Science Letters, 245(1-2):162-173.

Armand, L.K., V., Cornet-Barthaux, J., Mosseri B., Quéguiner, 2008. Late summer diatom biomass and community structure on and around the naturally iron-fertilised Kerguelen Plateau in the Southern Ocean. Deep-Sea Res. II 55, 653-678.

Armand et al., in prep 2009. Observations on the diatom distribution and biomass in the Southwest Pacific Ocean.

Arrigo, K.R., G.L., van Dijken, S., Bushinsky, 2008. Primary production in the Southern Ocean, 1997-2006. J. Geophys. Res. 113, C08004, doi:10.1029/2007JC004551.

Azam, F., B., Volcani, 1984. Role of silicon in diatom metabolism. VI. Active transport of Germanic acid in the heterotrophic diatom Nitzschia alba. Arch. Microbiol. 101: 1-8.

Barling, J., G.L., Arnold, A.D., Anbar, 2001. Natural mass dependent variations in the isotopic composition of molybdenum. Earth Planet. Sci. Lett. 193: 447-457.

Basile-Doelsch, I., 2006. Si stable isotopes in the earth's surface: a review. J. Geochem. Explor. 88: 252-256.

Becker, J.S., H.-J. Dietze (2000). Precise and accurate isotope ration measurements by ICP-MS. Fresenius J. Anal. Chem. 368: 23-30.

Becker, J.-S., 2002. State of the art and progress in precise and accurate isotope ratio measurements by ICP-MS and LA-ICP-MS. J. Anal. At. Spectrom. 17, 1172, doi:10.1039/b203028.

Becker, J.S., 2005. Recent developments in isotope analysis by advanced mass spectrometric techniques. J. Anal. At. Spectrom. 20, 1173-1184.

Behrenfeld, M.J., P.G., Falkowski, 1997. Photosynthetic rates derived from satellite-based chlorophyll concentration. Limnol. Oceanogr. 42: 1-20.

Belkin, I.M., A.L., Gordon, 1996. Southern Ocean fronts from the Greenwich meridian to Tasmania. J. Geophys. Res., 101: 3675-3696, doi:10.1029/95JC02750.

Belshaw, N.S., P.A., Freedman, R.K., O'Nions, M., Frank, Y., Guo, 1998. A new variable dispersion double-focusing plasma mass spectrometer with performance illustrated for Pb isotopes. Int. J. Mass Spectrom. 181: 51-58.

Benitez-Nelson, C.R., R.R., Bidigare, T.D., Dickey, M.R., Landry, C.L., Leonard, S.L., Brown et al., 2007. Mesoscale eddies drive increased silica export in the Subtropical Pacific Ocean. Science 316: 1017-1021.

Beucher, C., P., Tréguer, R., Corvaisier, A.M., Hapette, M., Elskens, 2004a. Production and dissolution of biosilica, and changing microphytoplankton dominance in the Bay of Brest (France). Mar. Ecol. Prog. Ser. 267:57-69.

Beucher, C., P., Tréguer, A.-M., Hapette, R., Corvaisier. 2004b. Intense summer Si-recycling in the surface Southern Ocean. Geophys. Res. Lett. 31: doi:10.1029/2003GL018998.

Beucher, C.P., M.A., Brzezinski, X., Crosta, 2007. Silicic acid dynamics in the glacial sub-Antarctic: Implications for the silicic acid leakage hypothesis. Global Biogeochem. Cycles 21, GB3015, doi:10.1029/2006GB002746.

Beucher, C.P., M.A., Brzezinski, J.L., Jones, 2008. Sources and biological fractionation of silicon isotopes in the Eastern Equatorial Pacific. Geochim. Cosmochim. Acta 72, 3063-3073.

Bidle, K.D., F., Azam, 1999. Accelerated dissolution of diatom silica by marine bacterial assemblages. Nature 397: 508-512.

Bidle, K.D., F., Azam, 2001. Bacterial control of silicon regeneration from diatom detritus: significance of bacterial ectohydrolases and species identity. Limnol. Oceanogr. 46: 1606-1623.

Bidle, K.D., M., Manganelli, F., Azam, 2002. Regulation of oceanic silicon and carbon preservation by temperature control on bacteria. Science 298, 1980-1984.

Bidle, K.D., M.A., Brzezinski, R.A., Long, J.L., Jones, F., Azam, 2003. Diminished efficiency in the oceanic silica pump caused by bacteria-mediated silica dissolution. Limnol. Oceanogr. 48(5): 1855-1868.

Blain, S., B., Quéguiner, L., Armand, S., Belviso, B, Bombled, L., Bopp, A., Bowie, C., Brunet, C., Brussaard, F., Carlotti, U., Christaki, A., Corbière, I., Durand, F., Ebersback, J.-L., Fuda, N., Garcia, L., Gerringa, B., Griffiths, C., Guigue, C., Guillerm, S., Jacquet, C., Jeandel, P., Laan, D., Lefèvre, C., Lo Monaco, A., Malits, J., Mosseri, I., Obernosterer, Y.-P., Park, M., Picheral, P., Pondaven, T., Remenyi, V., Sandroni, G., Sarthou, N., Savoye, L., Scouarnec, M., Souhaut, D., Thuiller, K., Timmermans, T., Trull, J., Uitz, P., van Beek, M., Veldhuis, D., Vincent, E., Viollier, L., Vong, T., Wagener, T., 2007. Effect of natural iron fertilization on carbon sequestration in the Southern Ocean. Nature 446: doi:10.1038/nature05700, 1070-1075.

Blank, G.S., C.W., Sullivan, 1979. Diatom mineralization of silicic acid III. $Si(OH)_4$ binding and light dependent transport in Nitzschia angularis. Arch. Microbiol. 123: 157-164.

Bopp, L., P., Monfray, O., Aumont, J.L., Dufresne, H., Le Treut, G., Madec, L., Terray, J.C., Orr, 2001. Potential impact of climate change on marine export production. Global Biogeochem. Cycles 15: 81-99.

Boyd, P.W., P., Newton, 1995. Evidence of the potential influence of planktonic community structure on the interannual variability of particulate carbon flux. Deep-Sea Res. I 42: 619-639.

Boyd, P.W., P., Newton, 1999a. Does planktonic community structure determine downward particulate organic carbon flux in different oceanic provinces. Deep-Sea Res. I 46: 63-91.

Boyd, P.W., J., LaRoche, M., Gall, R., Frew, R.M.L., McKay. 1999b. Role of iron, light, and silicate in controlling algal biomass in subantarctic waters SE of New Zealand. J. Geophys. Res. 104: 13395-13408.

Boyd, P.W., A.C., Crossley, G.R., DiTullio, F.B., Griffiths, D.A., Hutchins, B., Quéguiner, P.N., Sedwick, T.W., Trull. 2001. Control of phytoplankton growth by iron supply and irradiance in the subantarctic Southern Ocean: experimental results from SAZ Project. J. Geophys. Res. 106(C12): 31573-31583.

Boyd, P.W., 2002. Environmental factors controlling phytoplankton processes in the Southern Ocean. J. Phycol. 38: 844-861.

Boyd, P.W., T.W., Trull, 2007. Review: Understanding the export of biogenic particle in oceanic waters: Is there consensus? Progr. Oceanogr. 72: 276-312.

Boyd, P.W., 2007. Biogeochemistry: Iron findings. Nature 446, 989-991.

Bowie, A.R., D., Lannuzel, T., Remenyi, T., Wagener, P.J., Lam, P.W, Boyd, C., Guieu, A.T., Townsend, T.W., Trull, 2009. Biogeochemical iron budgets of the Southern Ocean south of Australia demonstrate that summertime supply decouples iron and nutrient cycles in the subantarctic zone. Global Biogeochem. Cycles, in press.

Broecker, W.S., 1982. Glacial to interglacial changes in ocean chemistry. Prog. Oceanogr. 11: 151-197.

Broecker, W.S., 1991. The great ocean conveyor. Oceanography 4: 79-90.

Broecker, W.S., G.M., Henderson, 1998. The sequence of events surrounding termination II and their implication for the cause of glacial-interglacial CO_2 change. Paleoceanography 13: 352-364.

Brzezinski, M.A., 1985, The Si:C:N ratios of marine diatoms: interspecific variability and the effect of some environmental variables. J. Phycol. 21: 345-357.

Brzezinski, M.A., D.M., Nelson, 1989. Seasonal changes in the silicon cycle within a Gulf Stream warm-core ring. Deep-Sea Res. 36, 1009-1030.

Brzezinski, M.A., D.M., Nelson. 1995. The annual cycle in the Sargasso sea near Bermuda. Deep-Sea Res. I 36: 1215-1237.

Brzezinski, M.A., D.R., Phillips, 1997. Evaluation of Si-32 as a tracer for measuring silica production rates in marine waters. Limnol. Oceanogr. 42: 856-865.

Brzezinski, M.A., D.M., Nelson, V.M., Franck, D.E., Sigmon, 2001. Silicon dynamics within an intense open-ocean diatom bloom in the Pacific sector of the Southern Ocean. Deep-Sea Res. II 48, 3997-4018.

Brzezinski, M.A., C.J., Pride, V.M., Franck, D.M., Sigman, J.L., Sarmiento, K., Matsumoto, N., Gruber, G., Rau, K.H., Coale, 2002. A switch from $Si(OH)_4$ to NO_3 depletion in the glacial Southern Ocean. Geophys. Res. Let. 29: 12, 10.1029/2001GL014349.

Brzezinski, M.A., M.-L., Dickson, D.M., Nelson, R., Sambrotto, 2003a. Ratios of Si, C and N uptake by microplankton in the Southern Ocean. Deep Sea Res. II, 50, 619-633.

Brzezinski M.A., J.L., Jones, K.D., F., Azam, 2003b. The balance between silica production and silica dissolution in the sea: Insights from Monteray Bay, California, applied to the global data set. Limnol. Oceanogr. 48(5):1846-1854.

Brzezinski, M.A., Jones, L.J., Demarest, M.S., 2005. Control of silica production by iron and silicic acid during the Southern Ocean iron experiment (SOFeX). Limnol. Oceanogr. 50(3), 810-824.

Brzezinski, M.A., J.L., Jones, C.P., Beucher, M.S., Demarest, H.L., Berg H.L., 2006. Automated determination of silicon isotope natural abundance by the acid decomposition of cesium hexafluosilicate. Anal. Chem., doi:10.1021/ac0606406.

Brzezinski, M.A., C., Dumousseaud, J., Krause, C.I., Measures, D.M., Nelson. 2008. Iron and silicic acid concentrations together regulate Si uptake in the equatorial Pacific Ocean. Limnol. Oceangr. 53(3): 875-889.

Brzezinski, M.A., et al. preliminary results of the first GEOTRACE cruise. Talk in GEOTRACE intercalibration meeting , San Francisco, december 2008.

Bucciarelli, E., P., Pondaven, G., Sarthou. 2009. Effects of an iron-light co-limitation on the elemental composition (Si, C, N) of the marine diatoms Thalassiosira oceanica and Ditylum brightwelli. Biogeosciences Discuss. 6: 7175-7205.

Buesseler, K.O., 1998. The decoupling of production and particulate export in the surface ocean. Global Biogeochem. Cycles 12(2), 297-310.

Buesseler, K.O., L., Ball, J., Andrews, J.K., Cochran, D.J., Hirschberg, M.P., Bacon, A., Fleer, M.A., Brzezinski, 2001. Upper ocean export of particulate organic carbon and biogenic silica in the Southern Ocean along 170°W. Deep-Sea Res. II 48, 4275-4297.

Buesseler, K.O., J.E., Andrews, S.M., Pike, M.A., Charette, L.E., Goldson, M.A., Brzezinski, 2005. Particle export during the Southern Ocean Iron Experiment (SOFeX). Limnol. Oceanogr. 50(1): 311-327.

Claquin, P., V., Martin-Jézéquel, J.C., Krompkamp, M.J., Veldhuis, G.W., Kray, 2002. Uncoupling of silicon compared to carbon and nitrogen metabolisms and the role of the cell cycle in continuous cultures of *Thalassiosira pseudonana* (Bacillariophyceae) under light, nitrogen, and phosphorus control. J. Phycol. 38, 922-930.

Cardinal, D., L.Y., Alleman, J., de Jong, K., Ziegler, L., André, 2003. Isotopic composition of silicon measured by multicollector plasma source mass spectrometry in dry plasma mode. J. Anal. Atom. Spectrom. 18, 213-218.

Cardinal, D., L.Y., Alleman, F., Dehairs, N., Savoye, T.W., Trull, L., André, 2005. Relevance of silicon isotopes to Si-nutrient utilization and Si-source assessment in Antarctic waters. Global Biogeochem. Cycles 19, GB2007, doi:10.1029/2004GB002364.

Cardinal, D., N., Savoye, T.W., Trull, F., Dehairs, E.E., Kopczynska, F., Fripiat, J.-L.., Tison, L., André, 2007. Silicon isotopes in spring Southern Ocean diatoms: large zonal changes despite homogeneity among size fractions. Mar. Chem. 106, 46-62.

Cardinal, D., 2008. Etude des cycles biogéochimiques du carbone et du silicium par une approches multi-traceurs. Habilitation à Diriger les Recherches : 152pp.

Carneiro, J.M.T., L.R.M.R., Alexssandra, J.A., Bendassolli, 2008. Isotopic determination of silicon by mass spectrometry in plants and soils labelled with ^{30}Si. Anal. Lett. 41(9): 1640-1647.

Carrignan, J., D., Cardinal, A., Eisenhauer, A., Galy, M., Rehkämper, F., Wombacker, N., Vigier, 2004. A reflection on Mg, Cd, Ca, Li and Si isotopic measurements and related reference materials. Geost. Geoanal. Res. 28(1): 139-148.

Cassar, N., 2003. Carbon-concentrating mechanisms and β-carboxylation: their potential contribution to marine photosynthetic carbon isotope fractionation. Ph.D. dissertation.

Cassar, N., M.L., Bender, B.A., Barnett, S., Fan, W.J., Moxim, H., Levy II, B., Tilbrook, 2007. The Southern Ocean biological response to aeolian iron deposition. Science 317: 1067-1070.

Cavagna, A.-J., M., Elskens, F.B., Griffiths, F., Fripiat, S.H.M., Jacquet, F., Dehairs. 2009. Contrasting regimes of productivity and potential for carbon export in the SAZ and PFZ south of Tasmania. Submitted in Deep-Sea Res. II.

Cavagna, A.-J., F., Fripiat, F., Dehairs, D., Wolf-Gladrow, N., Savoye, L., André, D., Cardinal, 2009. Silicon isotopic signal during EIFEX: diatom uptake vs. mixing, biological fractionation and iron fertilization impact. In revision for Limmol. Oceanogr.

Chaigneau, A., R.A., Morrow, S.R., Rintoul, 2004. Seasonal and interannual evolution of the mixed layer in the Antarctic Zone south of Tasmania. Deep-Sea Res. II 51: 2047-2072.

Charles, C.D., P.N., Froelich, M.A., Zibello, R.A., Mortlock, J.J., Morley, 1991. Biogenic opal in Southen Ocean sediments over the last 450000 years: implications for surface water chemistry and circulation. Paleoceanography 6: 697-728.

Chishlomn, S.W., 1992. Phytoplankton size. In: Falkowski, P.G., Woodhead, A.D. (Eds.), Primary productivity and biogeochemical cycles in the sea. Plenum, New York, pp. 213-238.

Comiso, J.C., C.R., McClain, C.W., Sulivan, J.P., Ryan, C.L., Leonard, 1993. Coastal Zone Color Scanner pigment concentrations in the Southern Ocean and relationships to geophysical surface features. J. Geophys. Res. 98: 2419-2451.

Conkright, M.E., R.A., Locarnini, H.E., Garcia, T.D., O'Brien, T.P., Boyer, C., Stephens, J.I., Antonov (2002), World Ocean Atlas 2001; Ojective Analyses, Data Statistics, and Figures, CD-ROM Documentation, Natl. Oceanogr. Data Cent., Silver Spring, Md.

Conley, D.J., 2002. Terrestrial ecosystems and the global biogeochemical silica cycle. Global Biogeochem. Cycles 16(4), 1121, doi:10.1029/2002GB001894.

Conte, M.H., T.D., Dickey, J.C. Weber, R.J., Jonhson, A.H., Knap, 2003. Transient physical forcing fo pulsed export fo bioreactive material to the deep Sargasso Sea, Deep-Sea Res. I 50: 1157-1187.

Corvaisier, R., P., Tréguer, C., Beucher, M., Elskens, 2005. Determination of the rate of production and dissolution of biosilica in marine waters by thermal ionisation mass spectrometry. Anal. Chim. Acta 534:149-155.

Cullen, J.J., 1982. The deep chlorophyll maximum: comparing vertical profiles of chlorophyll a. Can. J. Fish. Aquat. Sci. 39(5), 791-803.

Criss, R.E., 1999. Principles of stable isotope distribution. Oxford Univ. Press, New York.

Deacon, G.E.R., 1937. The hydrology of the Southern Ocean. Discov. Rep. 15: 1-124.

De Baar, H.J.W., P.W., Boyd, K.H., Coale, M.R., Landry, A., Tsuda, P., Assmy, D.C.E., Bakker, Y., Bozec, R.T., Barber, M.A., Brzezinski, K.O., Buesseler, M., Boyé, P.L., Croot, F., Gervais, M.Y., Gorbunov, P.J., Harrison, W.T., Hiscock, P., Laan, C., Lancelot, C.S., Law, M., Levasseur, A., Marchetti, F.J., Millero, J., Nishioka, H., Nojiri, S., Takeda, K.R., Timmermans, M.J.W., Veldhuis, A.M., Waite, C.S., Wong, 2005. Synthesis of iron fertilization experiments: from the iron age in age of enlightenment. J. Geophys. Res. 110 : C09S16, doi:10.1029/2004JC002601.

de Brauwere, A., F., De Ridder, R., Pintelon, M., Elskens, J., Schoukens, W., Baeyens, 2005. Model selection through a statistical analysis of the minimum of a Weighted Least Squares cost function. Chemom. Intell. Lab. 76: 163-173.

de Freitas, A.S.W., A.W., McCulloch, A.G., McInnes, 1991. Revovery of silica from aqueous silicate solution via trialkyl or tetraalkylammnonium silicomolybdate. Canadian J. Chem. 69: 611-614.

Del Amo, Y., M.A., Brzezinski, 1999. The chemical form of dissolved Si taken up by marine diatoms. J. Phycol. 35: 1162-1170.

De La Rocha, C.L., Brzezinski, M.A., DeNiro, M.J., 1996. Purification recovery and laser-driven fluorination of silicon from dissolved and particulate silica for the measurement of natural stable isotope abundances. Anal. Chem. 68, 3746-3750.

De La Rocha, C.L., Brzezinski, M.A., DeNiro, M.J., 1997. Fractionation of silicon isotopes by marine diatoms during biogenic silica formation. Geochim. Cosmochim. Acta 61(23), 5051-5056.

De La Rocha, C.L., M.A., Brzezinski, M.J., DeNiro, 1998. Silicon-isotope composition of diatoms as an indicator of past oceanic change. Nature 395: 680-683.

De La Rocha, C.L., M.A., Brzezinski, D.A., Hutchins, Y., Zhang, 2000. Effects of iron and zinc efficiency on elemental composition and silica production of diatoms. Mar. Ecol. Prog. Ser. 195: 71-79.

De La Rocha, C.L., Brzezinski, M.A., DeNiro, M.J., 2000. A first look at the distribution of the stable isotopes of silicon in natural waters. Geochim. Cosmochim. Acta 64(14), 2467-2477.

De la Rocha, C.L., 2002. Measurement of silicon stable isotope natural abundances via multicollector inductively coupled plasma mass spectrometry (MC-ICP-MS). Geochem. Geophys. Geosyst. 3(8): 10.1029/2002GC000310.

De La Rocha, C.L., 2003. Silicon isotope fractionation by marine sponges and the reconstruction of the silicon isotope composition of ancient deep water. Geology 31(5): 423-426.

Delmas, R.J., J.M., Ascencio, M., Legrand, 1980. Polar ice evidence that atmospheric CO_2 20000 yr BP was 50% of present. Nature 284: 155-157.

Delstanche, S., S., Opfergelt, D., Cardinal, F., Elsass, L., André, B., Delvaux, 2009. Silicon isotopic fractionation during adsorption of aqueous monosilicic acid onto iron oxide. Geochim.Cosmochim. Acta., doi:10.1016/j.gca.2008.11.014.

Demarest, M.S., M.A. Brzezinski, C.P., Beucher, 2009. Fractionation of silicon isotopes during biogenic silica dissolution. Geochim. Cosmochim. Acta, doi: 10.1016/j.gca.2009.06.019.

DeMaster, D.J., B.A., McKee, W.S., Moore, D.M. Nelson, 1991. Geochemical processes occuring in the waters at the Amazon river/ocean boundary. Oceanography 4: 15-20.

DeMaster, D.J., W.O., Jr Smith, D.M., Nelson, J.Y., Aller. 1996. Biogeochemical processes in Amazon shelf waters: chemical distributions and uptake rates of silicon, carbon and nitrogen. Cont. Shelf Res. 16: 617-643.

DeMaster, D.J., 2002. The accumulation and cycling of biogenic silica in the Southern Ocean: Revisiting the marine biogeochemical budget. Deep Sea Res. II 49: 3155-3167.

DiFiore P.J., D.M., Sigman, T.W., Trull, M.J., Lourey, K., Karsh, G., Cane, H., Ruby, 2006. Nitrogen isotope constraints on subantarctic biogeochemistry. Journal of Geophysical Research 111, C08016, doi:10.1029/2005JC003216.

Ding, T., S., Jiang, D., Wan, Y., Li, J., Li, H., Song, Z., Liu, X., Yao, 1996. Silicon Isotope Geochemistry. Geological Publishing House, Bejing, China.

Ding, T., D., Wan, C., Wang, F., Zhang, 2004. Silicon isotope compositions of dissolved silicon and suspended matter in the Yangtze river, China. Geochim. Cosmochim. Acta, 68(2): 205-216.

Ding, T. P., G.R., Ma, M.X., Shui, D.F., Wan, R.H., Li, 2005b. Silicon isotope study on rice plants from the Zhejiang province, China. Chem. Geol., 218:41-50.

Ding, T.P., S., Tian, J., Gao, 2007. Silicon isotope compositions of the underground water, limestone and soil from karst caves in Guilin city, Guangxi, China. Geochim. Cosmochim. Acta 71 (15S), A225.

Ding, T. P., J.X., Zhou, D.F., Wan, Z.Y., Chen, C.Y., Wang, F., Zhang, 2008. Silicon isotope fractionation in bamboo and its significance to the biogeochemical cycle of silicon. Geochim. Cosmochim. Acta,72(5): 1381-1395.

Ding, T.P., J.X., Zhou, D.F., Wan, Z.Y. Chen, C.Y. Wang, F. Zhang, 2009. Silicon isotope fractionation in bamboo and its significance to the biogeochemical cycle of silicon. Geochim. Cosmochim. Acta, 72, 1381-1395.

Doucet, F.J., C., Schneider, S.J., Bones, A., Kretchmer, I., Moss, P., Tekely, C., Exley. 2001. The formation of hydroxyaluminosilicate of geochemical and biological significance. Geochim. Cosmochim. Acta 65(15): 2461-2467.

Douglas, D.J., S.D., Tanner, 1998. Fundamental considerations in ICPMS. In: Inductively coupled plasma mass spectrometry, A. Montaser (Ed.). Wiley-VCH: 615-679.

Douthitt, C.B., 1982. The geochemistry of the stable isotopes of silicon. Geochim. Cosmochim. Acta 46: 1449-1458.

Dugdale, R.C., J.J., Goering, 1967. Uptake of new and regenerated form of nitrogen in primary productivity. Limnol. Oceanogr. 12: 196-206.

Dugdale, R.C., F.P., Wilkerson, H.J., Minas, 1995. The role of a silicate pump in driving new production. Deep-Sea Res. I 42(5): 697-719.

Dumont, I., F., Masson, S.H.M., Jacquet, V., Shoemann, S., Becqevort, 2009. Bacterial remineralization in epilagic and mezopelagic waters in SubAntarctic and Polar frontal zones south of Tasmania. Submitted in Deep-Sea Res. II.

Durbin, E.G., 1977. Studies on the autoecology of the marine diatom *Thalassiosira nordenskioeldii*. II. The influence of cell size on growth rate and carbon, nitrogen, chlorophyll a and silica content. J. Phycol. 31: 1004-1012.

Dunne, J., R.A., Armstrong, A., Gnanadesikan, J.L., Sarmiento, R.D., Slater, 2005. Empirical and mechanistic models for particle export ratio. Global Biogeochem. Cycles 19: GB4026, doi:10.1029/2004GB002390.

El-Sayed, S.-Z., J.T., Turner, 1975. Productivity of the Antarctic and tropical/subtropical regions: a comparative study. In: Dunbar, M. (Ed.), Polar Oceans, Arctic Institute of North America, Montreal, pp. 463-503.

Elskens, M., W., Baeyens, T., Cattaldo, F., Dehairs., 2002. N uptake conditions during summer in the Subantarctic and Polar Frontal Zones of the Australian sector of the Southern Ocean. J. Geophys. Res., 107, 3182-3193.

Elskens, M., A., de Brauwere, C., Beucher, R., Corvaisier, N., Savoye, P., Tréguer, W., Baeyens, 2007. Statistical process control in assessing production and dissolution rates of biogenic silica in marine environments. Mar. Chem. 106:272-286.

England, M.H., J.S., Godfrey, A.C., Hirst, M., Tomczak, 1993. The mechanism for Antarctic Intermediate Water renewal in a world Ocean Model. J. Phys. Oceanogr. 23: 1553:1560.

Eppley, R.W., W., Holmes, et al., 1967. Periodicity in cell division and physiological behavious of *Ditylum brightwellii*, a marine planktonic diatom. Arch. Microbiol. 56: 305-323.

Falkowski, P.G., J.A., Raven, 1997. Aquatic photosynthesis, Blackwell Science, Malden, M.A

Falkowski, P.G., R.T., Barber, V., Smetacek, 1998. Biogeochemical controls and feedbacks on ocean primary production. Science 281: 200-206.

Falkowski, P.G., R.J., Scholes, E.A., Boyle, J., Canadell, D., Canfield, J., Elser, N., Gruber, K., Hibbard, P., Hogberg, S., Linder, F.T., Mackenzie, B.I., Moore, T., Perdersen, Y., Rosenthal, S., Seitzinger, V., Smetacek, W., Steffen, 2000. The global carbon cycle: a test of our knowledge of Earth as system. Science 290: 291-296.

Falkowski, P.G., E.A., Laws, R.T., Barber, J.W. Murray, 2003. Phytoplankton and their role in primary, new, and export production. In: Fasham, M.J.R. (Ed.), Ocean biogeochemistry: The role of ocean carbon cycle in global change. Springer, Berlin, pp. 99-118.

Feely, R.A., C.L., Sabine, K., Lee, W., Berelson, J., Kleypas, V.J., Fabry, F.J., Millero, 2004. Impact of anthropogenic CO_2 on the $CaCO_3$ system in the Ocean. Science 305: 362-366.

Franck, V.M., M.A., Brzezinski, K.H., Coale, D.M., Nelson, 2000. Iron and silicic acid concentration regulate Si uptake north and south of the Polar Frontal Zone in the Pacific Sector of the Southern Ocean. Deep-Sea Res. II 47: 3315-3338.

Franck, V.M., K.W., Bruland, D.A., Hutchins, M.A., Brzezinski. 2003. Iron and zinc effects on silicic acid and nitrate uptake kinetics in three high-nutrient, low-chlorophyll (HNLC) regions. Mar. Ecol. Prog. Ser. 252: 15-33.

François, R., M.A., Altabet, R., Goericke, D.C., McCorkle, C., Brunet, A. Poisson, 1993. Changes in the $\delta^{13}C$ of surface water particulate organic matter across the subtropical convergence in the SW Indian Ocean. Global Biogeochem. Cycles 7(3): 627-644.

Francois, R., M.A., Altabet, E.F., Yu, D.M., Sigman, M.P., Bacon, M., Frank, G., Bohrmann, G., Bareille, L.D., Labeyrie, 1997. Contribution of Southern Ocean surface water stratification to low atmospheric CO_2 concentration during the last glacial period. Nature 389: 929-935.

Fripiat, F., D., Cardinal, J.-L., Tison, A., Worby, L., André, 2007. Diatom-induced silicon isotopic fractionation in Antarctic sea ice. J. Geophys. Res. 112, G02001, doi:10.1029/2006JG000244.

Fry, B., 2006. Stable Isotope Ecology. Springer, New York, pp 308.

Galy, A., N.S., Belshaw, L., Halicz, R.K., O'nions, 2001. High-precision measurement of magnesium isotopes by multiple-collector inductively coupled plasma mass spectrometry. Int. J. Mass Spectrom., 208: 89-98.

Geider, R.J., J., La Roche, 1994. The role of iron in phytoplankton photosynthesis, and the potential for iron-limitation of primary productivity in the sea. Photosynth. Res. 39: 275-301.

Georg, R.B., B.C., Reynolds, M., Frank, A.N., Halliday, 2006a. New sample preparation techniques for the determination of Si isotopic compositions using MC-ICPMS. Chem. Geol. 235: 95-104.

Georg, R.B., B.C., Reynolds, M., Frank, A.N., Halliday, 2006b. Mechanisms controlling the silicon isotopic compositions of river waters. Earth Planet. Sci. Let., 249(3-4): 290-306.

Georg, R.B., B.C., Reynolds, A.J., West, K.W., Burton, A.N., Halliday, 2007a. Silicon isotope variations accompanying basalt weathering in Iceland. Earth Planet. Sci. Let. 261: 476-490.

Georg, R.B., A.N., Halliday, E.A, Schauble, B.C, Reynolds, 2007b. Silicon in the Earth's core. Nature, 447, 1102-1106.

Georg, R.B., A.J., West, A.R., Basu, A.N., Halliday, 2009a. Silicon fluxes and isotope composition of direct groundwater discharge into the Bay of Bengal and the effect on the global ocean silicon isotope budget. Earth Planet. Sci. Let. 283: 67-74.

Georg, R.B., C., Zhu, B.C., Reynolds, A.N., Halliday, 2009b. Stable silicon isotopes of groundwater, feldspars, and clay coating in the Navajo Sandstone aquifer, Black Mesa, Arizona, USA. Geochim. Cosmochim. Acta 73: 2229-2241.

Gnanadesikan, A., 1999. A global model of silicon cycling sensitivity to eddy parametreization and dissolution. Global Biogeochem. Cycles 13: 199-220.

Gnanadesikan, A., J.P., Dunne, R.M., Key, K., Matsumoto, J.L., Sarmiento, R.D., Slater, P.S., Swathi, 2004. Oceanic ventilation and biogeochemical cycling: understanding the physical mechanisms that produce realistic distributions of tracers and productivity. Global Biogeochem. Cycles 13: 199-220.

Goering, J.J., D.M., Nelson, J.A., Carter, 1973. Silicic acid uptake by natural populations of marine phytoplankton. Deep-Sea Res. 20:777-789.

Grasshoff, K., M., Erhardt, K., Kremling, 1983. Methods of seawater analysis. 2nd ed. Verlag Chemie.

Griffiths, B.F., T.S., Bates, P.Q, Quinn, L.A., Clementson, J.S., Parslow, 1999. Oceanographic context of the First Aerosol Characterization Experiment (ACE 1): a physical, chemical and biological overview. J. Geophys. Res., 104 (C17), 21,649-21,671.

Griffiths, F.B., A.R., Bowie, F., Dehairs, T.W., Trull, 2009. The SAZ-Sense experiment: a biogeochemical comparison of Sub-Antarctic and Polar Frontal waters southwest and southeast of Tasmania. Deep Sea Research Part II, submitted.

Hallberg, R.W., A., Gnanadesikan, 2007. The role of eddies in determining the structure and response of the wind-driven Southern Hemisphere overturning: results from the modeling eddies in the Southern Ocean project. J. Phys. Oceanogr. 36: 2232-2252.

Halliday, A.N., D.-C., Lee, J.N., Christensen, M., Rehkämper, W., Yi, X., Luo, C.M., Hall, C., Ballentine, T., Pettke, C., Stirling, 1998. Applications of mulitple collector-ICPMS to cosmochemistry, geochemistry, and paleoceanography. Geochim. Cosmochim. Acta 62(6): 919-940.

Hildebrand, M., B.E., Volcani, W., Gassmann, J.I., Schroeder, 1997. A gene family of silicon transporters. Nature 385: 688-689.

Hildebrand, M., K., Dahlin, B.E., Volcani, 1998. Characterization of a silicon transporter gene family in *Cylindrotheca fusiformis*: sequences, expression analysis, and identification of homologs in other diatoms. Mol. Gen. Genet. 260: 480-486.

Hildebrand, M., L.G., Frigeri, A.K., Davis, 2007. Synchronized growth of *Thalassiosira pseudonana* (Bascillariophyceae) provides novel insights into cell wall synthesis processes in relation to the cell cycle. J. Phycol. 43: 730-740.

Hildebrand, M., 2008. Diatoms, biomineralization processes, and genomics. Chem. Rev. 108: 4855-4874.

Hoefs, J., 2009. Stable isotopic geochemistry, springer verlag, New York, pp. 241.

Holm-Hansen, O., C.D., Hewes, 2004. Deep chlorophyll-a maxima (DCMs) in Antarctic waters: I. Relationships between DCMs and the physical, chemical, and optical conditions in the upper water column. Polar. Biol. 27, 699-710.

Honjo, S., S.J., Manganini, R.A., Krishfield, R., François, 2008. Particulate carbon fluxes to the ocean interior and factors controlling the biological pump : A synthesis of global sediment trap programs since 1983. Progr. Oceanogr. 76: 217-285.

Hurd, D.C, 1972. Factors affecting solution rate of biogenic opal in seawater. Earth Planet. Sci. Lett. 15: 411-417.

Hurd, D.C., S., Birdwhistell, 1983. On producing a general model for biogenic silica dissolution. Am. J. Sci. 283: 1-28.

Hutchins, D.A., K.W., Bruland. 1998. Iron-limited diatom growth and Si:N uptake ratios in a coastal upwelling regime. Nature 393: 561-564.

Hutchins, D.A., P.N., Sedwick, G.R., DiTullio, P.W., Boyd, B., Quéguiner, F.B., Griffiths, C., Crossley, 2001. Control of phytoplankton growth by iron and silicic acid availability in the subantarctic Southern Ocean: experimental results from SAZ Project. J. Geophys. Res. 106 (C12): 31559-31572.

Indermühle, A., E., Monnin, B., Stauffer, T.F., Stocker, M., Wahlen, 2000. Atmospheric CO_2 concentration from 60 to 20 kyr BP from the Taylor Dome ice core, Antarctica. Geophys. Res. Let. 27: 735-738.

Jacques, G., 1983. Some ecophysiological aspects of the Antarctic phytoplankton. Polar Biol. 2: 27-33.

Jacquet, S.H.M, P., Lam, T.W., Trull, F., Dehairs, 2009. ^{234}Th-determined shallow export flux from the Subantarctic and Polar Frontal Zones of the Southern Ocean. Deep-Sea Res. II, submitted.

Jacobson, D.M., D.M., Anderson, 1986. Thecate heterotrophic dinoflagellates: feeding behavior and mechanism. J. Phycol. 22: 249-258.

Jin, X., N., Gruber, J.P., Dunne, J.L., Sarmiento, J.L., R.A., Amstrong, 2006. Diagnosing the contribution of phytoplankton functional groups to the production and export of particulate organic carbon, $CaCO_3$, and opal from global nutrient and alkalinity distributions. Global Biogeochem. Cycles 20, GB2015, doi:10.1029/2005GB002532.

Johnson, C.M., B.L., Beard, F., Albarède, 2004. Overview and general concepts. Reviews in Mineralogy and Geochemistry 55: 1-24.

Joubert et al., in prep 2009. A comparison of the O_2/Ar and new production fluxes.

Kamatani, A., J.P., Riley, 1979. Rate of dissolution of diatom silica walls in seawater. Mar. Chem. 68: 219-229.

Kamatani, A., 1982. Dissolution rates of silica from diatoms decomposing at various temperatures. Mar. Biol. 68: 29-35.

Kamatani, A., N., Ejiri, P., Tréguer, 1988. The dissolution kinetics of diatom ooze from the Antarctic area. Deep-Sea Res. 35: 1195-1203.

Karl, D.M., G., Tien, 1992. MAGIC : a sensitive and precise method for measuring dissolved phosphorus in aquatic environments. Limnol. Oceanogr. 37: 105-106.

Kara, A.B., P.A., Rochford, H.E., hurlburt, 2003. Mixed layer depth variability over the gloval ocean. J. Geophys. Res. 108, doi: 10.1029/2000C0007.

Keeling, R.F., M., Visbeck, 2001. Paleoceanography-Antarctic stratification and glacial CO_2. Nature 412: 605-606.

Key, R.M., A., Kozyr, C.L., Sabine, K., Lee, R., Wanninkhof, J., Bullister, R.A., Feely, F., Millero, C.W. Mordy, T.H. Peng, 2004. A global ocean carbon climatology: Results from Global Data Analysis Project (GLODAP), Global Biogeochem. Cycles 18, GB4031, doi:4010.1029/2004GB002247.

Klemens, P., K.G., Heumann, 2001. Development of an ICP-HRIDMS method for accurate determination of traces of silicon in biological and clinical samples. Fresenius J. Anal. Chem., 371, 758-763.

Knox, F., M.B., McElroy, 1984. Changes in atmospheric CO_2: influence of the marine biota at high latitude. J. Geophys. Res. 89: 4629-4637.

Kopczynska, E.E., M., Fiala, C., Jeandel. 1998. Annual and interannual variability in phytoplankton at a permanent station off Kerguelen Islands, Southern Ocean. Polar Biol. 20: 342-351.

Kopczynska, E.E., F., Dehairs, M., Elskens, S., Wright. 2001. Phytoplankton and microzooplankton variability between the Subtropical and Polar Fronts south of Australia: thriving under regenerative and new production in late summer. J. Geophys. Res. 106 (C12): 31597-31609.

Kopczynska, E.E., N., Savoye, F., Dehairs, D., Cardinal, M., Elskens. 2007. Spring phytoplankton assemblages in the Southern Ocean between Australia and Antarctica. Polar Biol. 31: 77-88.

Krause, J.W., D.M., Nelson, M.W., Lomas, 2009. Biogeochemical responses to late-winter storms in the Sargasso Sea: II. Increased rates of biogenic silica production and export. Deep-Sea Res. I, doi:10.1016/j.dsr.2009.01.002.

Kroopnick, P.M., 1985. The distribution of ^{13}C of TCO_2 in the world oceans. Deep-Sea Res. A 32: 57-84.

Lannuzel, D., T., Remenyi, P.J., Lam, A., Townsend, E., Ibisanmi, E., Butler, T., Wagener, V., Schoemann, A.R., Bowie, 2009. Distribution of dissolved and particulate iron in the sub-Antarctic and Polar Frontal Southern Ocean (Australian sector). Deep-Sea Res. II, submitted.

Laws, E.A., P.G., Falkowski, W.O., Smith, H., Ducklow, H., MacCarthy J.J., 2000. Temperature effects on export production in the open ocean. Global Biogeochem. Cycles 14: 1231-1246.

Lawson, D.S., D.C., Hurd, H.S., Pankratz, 1978. Silica dissolution rates of decomposing assemblages at various temperatures. Am. J. Sci. 278: 1373-1393.

Leblanc, K., B., Quéguiner, M., Fiala, S., Blain, J., Morvan, R., Corvaisier, 2002. Particulate biogenic silica and carbon production rates and particulate matter distribution in the Indian sector of the Subantarctic Ocean. Deep-Sea Res. II 49: 3189-3206.

Leblanc, K., B., Quéguiner, N., Garcia, P., Rimmelin, P., Raimbault, 2003. Silicon cycle in the NW Mediterranean Sea : seasonal study of a coastal oligotrophic site. Oceanol. Acta 26: 339-355.

Leblanc K., A. Leynaert, I., Fernandez, P., Rimmelin, T., Moutin, P., Raimbault, J., Ras, B., Quéguiner, 2005a. A seasonal study of diatom dynamics in the North Atlantic during the POMME experiment (2001):

Evidence for Si limitation of the spring bloom. J. Geophys. Res. 110, C07S14, doi:10.1029/2004JC002621.

Leblanc, K., C.E., Hare, P.W., Boyd, K.W., Bruland, B., Sohst, S., Pickmere, M.C., Lohan, K., Buck, M., Ellwood D.A., Hutchins, 2005b. Fe and Zn effects on the Si cycle and diatom community structure in two contrasting high and low-silicate HNLC areas. Deep-Sea Res. I 52: 1842-1864.

Leblanc, K., D.A., Hutchins, 2005c. New applications of a biogenic silica deposition fluorophore in the study of oceanic diatoms. Limnol. Oceanogr.: Methods 3: 462-476.

Leblanc et al, in prep 2009. Species-specific silicification rates using a new fluorescent probe (PDMPO) in the Southern Ocean.

Lefèvre, D., C., Guigue, I., Obernosterer, 2008. The metabolic balance at two contrasting sites in the Southern Ocean: The iron-fertilized Kerguelen area and HNLC waters. Deep-Sea Res. II 55, 766-776.

Legendre, L., J., Le Fèvre, 1989. Hydrodynamical singularities as controls of recycled versus export production in oceans. In: Berger, W.H., Smetacek, V., Wefer, G. (Eds.), Productivity of the ocean: present and past. Wiley, S. Bernard, Dahlem Konferenzen, pp. 49-63.

LeMoigne et al., in prep 2009. Nutrients, particulate matters, chlorophyll and phaeopigments across the BONUS-Goodhope section.

Levitus, S., et al., 1998. World Ocean Database Vol 1, Introduction, NOAA, NESDIS, Washington D.C.

Lewin, J.C., 1961. The dissolution of biogenic silica from diatom walls, Geochim. Cosmochim. Acta 21: 182-195.

Leynaert, A., P., Tréguer, D.M., Nelson, Y., Del Amo. 1993. The silica cycle in the Antarctic Ocean: is the Weddell Sea atypical? Mar. Ecol. Prog. Ser. 96: 1-15.

Leynaert, A., E., Bucciarelli, P., Claquin, R.C., Dugdale, V., Martin-Jézéquel, P., Pondaven, O., Ragueneau, 2004. Effect of iron deficiency on diatom cell size and silicic acid uptake kinetics. Limnol. Oceanogr. 49(4), 1134-1143.

Lobel, K.D., J.K., West, L.L., Hench, 1996. Computational model for protein-mediated Biomineralization of the diatom frustule. Mar. Biol. 126: 353-360.

Lourey, M.J., T.W., Trull, 2001. Seasonal nutrient depletion and carbon export in the Subantarctic and Polar Frontal Zones of the Southern Ocean south of Australia. J. Geophys. Res., 106(C12), 31,463-31,487.

Luce, R.W., Bartlett, R.W., Parks, G.A., 1972. Dissolution kinetics of magnesium silicates. Geochim. Cosmochim. Acta 36: 35-50.

Maréchal, C.N., P., Télouk, F., Albarede, 1999. Precise analysis of copper and zinc isotopic compositions by plasma-source mass spectrometry. Chem. Geol. 156: 251-273.

Margalef, R., 1978. Life-forms of phytoplankton as survival alternatives in an unstable environment. Oceanol. Acta 1: 493-509.

Marriotti, A., J.C., Germon, P., Hubert, P., Kaiser, R., Letolle, A., Tardieux, P., Tardieux, 1981. Experimental determination of nitrogen kinetic isotope fractions: some principles ; illustration for the denitrification an nitrification processes. Plant and Soil 62: 413-430.

Martin, J.H., 1990. Glacial-Interglacial CO_2 change: the iron hypothesis. Paleoceanography 5: 1-13.

Martin-Jézéquel, V., M., Hildebrand, M.A., Brzezinski, 2000. Review: Silicon metabolism in diatoms: implications for growth. J. Phycol. 36: 821-840.

Matsumoto, K., J., Lynch-Stieglitz, R.F., Anderson, 2001. Similar glacial and Holocene Southern Ocean hydrography. Paleoceanography 16(5): 445-454.

Matsumoto, K., J.L., Sarmiento, 2008. A corollary to the silicic acid leakage hypothesis. Paleoceanography 23, PA2203, doi:10.1029/2007/PA001515.

McGillicuddy, D.J., L.A., Anderson, N.R., Bates, T., Bibby, K.O., Buesseler, C.A., Carlson, C.S., Davis, C., Ewart, P.G., Falkowski, S.A., Goldthwait, D.A., Hansell, W.J., Jenkins, R., Johnson, V.K., Kosnyrev, J.R., Ledwell, Q.P., Li, D.A., Siegel, D.K., Steinberg. 2007. Eddy/Wind interactions stimulate extraordinary mid-ocean plantkon blooms. Science 316: 1021-1026.

McNeil, J.D., H.W., Jannasch, T., Dickey, D.J., McGillicuddy, M.A., Brzezinski, C.M., Sakamato, 1999. New chemical, bio-optical and physical observations of upper ocean response to the passage of a mesoscale eddy off Bermuda. J. Geophys. Res. 104: 15537-15548.

Mehard, C.W., C.W., Sullivan, F., Azam, B.E., Volcani, 1974. Role of silicon in diatom metabolism. IV. Subcellular localization of silicon and germanium in Nitzschia alba and Cylindrotheca fusiformis. Physiol. Plant. 30: 265-272.

Mengesha, S., F., Dehairs, M., Fiala, M., Elskens, L., Goeyens. 1998. Seasonal variation of phytoplankton community structure and nitrogen uptake regime in the Indian Sector of the Southern Ocean. Polar Biol. 20: 259-272.

Metzl, N., B., Tilbrook, A., Poisson, 1999. The annual fCO_2 cycle and the air-sea CO_2 flux in the sub-Antarctic Ocean. Tellus. Series B. Chemical and Physical Meteorology 51(4): 849-861.

Michalopoulos, P., R.C., Aller, 2004. Early diagenesis of biogenic silica in the Amazon delta: alteration, authigenic clay formation, and storage. Geochim. Cosmochim. Acta, 68, 1061-1085

Milligan, A.J., D.E., Varela, M.A., Brzezinski, F.M.M., Morel, 2004. Dymanics of silicon metabolism and silicon isotopic discrimination in a marine diatom as a function of pCO_2. Limnol. Oceanogr. 49(2), 322-329.

Mitchell, B.G., O., Holm-Hansen, 1991. Observations and modeling of the Antarctic phytoplankton crop in relation to mixing depth. Deep-Sea Res. II 38: 981-1007.

Miller, C.B., D.M., Nelson, C., Weiss, A.H., Soeldner, 1990. Morphogenesis of opal teeth in calanoid copepods. Mar. Biol. 106: 91-101.

Minas, H.J., M., Minas, 1992. Net community production in “High Nutrient Low Chlorophyll” waters of the tropical and Antarctic Ocean: grazing vs. iron hypothesis. Oceanol. Acta 15: 145-162.

Molinelli, E.T., 1981. The Antarctic influence on Antarctic Intermediate Water. J. Mar. Res. 39: 267-293.

Mongin, M., E., Molina, T.W., Trull, 2008. Seasonality and scale of the Kerguelen plateau phytoplankton bloom: a remote sensing and modeling analysis of the influence of natural iron fertilization in the Southern Ocean. Deep-Sea Res. II 55, 880-892.

Monnin, E., A., Indermühle, A., Dallenback, J., Fluckiger, B., Stauffer, T.F., Stocker, D., Raynaud, J.M., Barnola, 2001. Atmospheric CO_2 concentrations over the last glacial termination. Science 291: 112-114.

Moore, J.K., M.R., Abbott, J.G., Richman, 1999. Location and dynamic of the Antarctic Polar Front from satellite sea surface temperature data. J. Geophys. Res. 104: 3059-3073.

Moore, J.K., M.R., Abbott, 2000. Phytoplankton chlorophyll distributions and primary production in the Southern Ocean. J. Geophys. Res. 105: 28709-28722.

Moore, C.M., A.E., Hickman, A.J., Poulton, S., Seeyave, M.I., Lucas, 2007. Iron-light interactions during the CROZet natural iron bloom and EXport experiment (CROZEX): II-Taxonomic responses and elemental stoichiometry. Deep-Sea Res. II 54, 2066-2084.

Morrow, R.A., R., Coleman, J.A., Church, D.B., Chelton, 1994. Surface eddy momentum flux and velocity variances in the Southern Ocean from geosat altimetry. J. Phys. Oceanogr. 24: 2050-2071.

Mosseri, J., B., Quéguiner, L., Armand, V., Cornet-Barthaux, 2008. Impact of iron on silicon utilization by diatoms in the Southern Ocean: a case study of Si/N cycle decoupling in a naturally iron enriched area. Deep-Sea Res. II 55, 801-819.

Neftel, A., H., Oeschger, J., Schwander, B., Stauffer, R., Zumbrunn, 1982. Ice core sample measurements give atmospheric CO_2 content during the past 40000 yr. Nature 295: 220-223.

Nelson D.M., J.J., Goering, S.S., Kilham, R.R.L., Guillard, 1976. Kinetics of silicic acid uptake and rates of silica dissolution in the marine diatom *Thalassiosira pseudonana*. J. Phycol 12: 246-252.

Nelson, D.M., and J.J. Goering. 1977a. A stable isotope tracer method to measure silicic acid uptake by marine phytoplankton. Anal. Biochem. 78:139-147.

Nelson, D.M., and J.J. Goering. 1977b. Near-surface silica dissolution in the upwelling region off northwest Africa. Deep-Sea Res. 24:65-73.

Nelson, D.M., J.J., Goering, W., Boisseau, 1981. Consumption and regeneration of silicic acid in three coastal upwelling systems. In: Richard FA (ed) Coastal upwelling. American Geophysical Union, Washington, DC: 242-256.

Nelson, D.M., L.I., Gordon. 1982. Production and pelagic dissolution of biogenic silica in the Southern Ocean. Geochim. Cosmochim. Acta 46:491-500.

Nelson, D.M., W.O., Smith Jr., 1991. Sverdrup revisited: critical depths, maximum chlorophyll levels, and the control of Southern Ocean productivity by the irradiance-mixing regime. Limnol. Oceanogr. 36(8): 1650-1661.

Nelson, D.M., P., Tréguer, M.A., Brzezinski, A., Leynaert, B., Quéguiner, 1995. Production and dissolution of biogenic silica in the ocean: revised global estimates, comparison with regional data and relationship to biogenic sedimentation. Glob. Biogeochem. Cycles 9(3): 359-372.

Nelson, D.M., M.A., Brzezinski, 1997. Diatom growth and productivity in an oligotrophic mid-ocean gyre: A 3-yr record from the Sargasso Sea near Bermuda. Limnol. Oceanogr. 42: 473-486.

Nelson, D.M., Brzezinski, M.A., Sigmon, D.E., Franck, V.M., 2001. A seasonal progression of Si limitation in the Pacific sector of the Southern Ocean. Deep-Sea Res. II 48, 3973-3995.

Nelson, D.M., R.F., Anderson, R.T., Barber, M.AT., Brzezinski, K.O., Buesseler, Z.., Chase, R.W., Collier, M.L., Dickson, R., François, M.R., Hiscock, S., Honjo, J., Marra, W.R., Martin, R.J., Sambrotto, F.L., Sayles, D.E., Sigmon, 2002. Vertical budgets for organic carbon and biogenic silica in the Pacific sector of the Southern Ocean, 1996-1998. Deep-Sea Res. II 49, 1645-1674.

Nowlin, W.D., M., Clifford, 1982. The kinematic and thermohaline zonation of the Antarctic Circumpolar Current at Drake Passage. J. Mar. Res. 40: 481-507.

Opfergelt, S., D., Cardinal, C., Henriet, X., Draye, L., André, B., Delvaux, 2006. Silicon isotopic fractionation by banana (Musa spp.) grown in a continuous nutrient flow device. Plant and Soil, 285, 333-345.

Opfergelt, S., B., Delvaux, L., André, D., Cardinal, 2008. Plant silicon isotopic signature might reflect soil weathering degree. Biogeochemistry, 91, 163-175.

Opfergelt, S., 2008. Silicon cycle in the soil-plant system: biogeochemical tracing using Si isotopes. Ph.D. thesis: 327pp.

Opfergelt, S., G., de Bournonville, D., Cardinal, L., André, S., Delstanche, B., Delvaux, 2009. Impact of soil weathering degree on silicon isotopic fractionation during adsorption onto iron oxides in basaltic ash soils, Cameroon. Geochim. Cosmochim. Acta 73: 7226-7240.

Orsi A.H., T., Whitworth, W.D., Nowlin, 1995. On the meridional extent and fronts of the Antarctic Circumpolar Current. Deep-Sea Res. I 42(5): 641-673.

Park, Y.-H., E., Charriaud, D., Ruiz Pino, C., Jeandel, 1998a. Seasonal and interannual variability of the mixed layer properties and steric height at station KERFIX, southwest of Kerguelen. J. Mar. Sys. 17, 571-586.

Park, Y.-H., E., Charriaud, M., Fieux, 1998b. Thermohaline structure of the Antarctic Surface Water/Winter Water in the Indian sector of the Southern Ocean. J. Mar. Sys. 17, 5-23.

Park, Y.-H., F., Roquet, I., Durand, J.L., Fuda, 2008a. Large-scale circulation over and around the Northern Kerguelen Plateau. Deep-Sea Res. II 55, 566-581.

Park, Y.-H., J.L., Fuda, I., Durand, A.C., Naveira Garabato, 2008b. Internal tides and vertical mixing overt the Kerguelen Plateau. Deep-Sea Res. II 55, 582-593.

Parslow, J.S., P.W., Boyd, S.R., Rintoul, F.B., Griffiths, 2001. A persistent subsurface chlorophyll maximum in the Interpolar Frontal Zone south of Australia: seasonal progression and implications for phytoplankton-light-nutrient interactions. J. Geophys. Res. 106 (C12): 31543-31557.

Pearce, I., A.T., Davidson, P.G., Thomson, S., Wright, R., van der Eden, 2009. Marine microbial ecology in the Sub-Antarctic Zone: rates of bacterial and phytoplankton growth and grazing by heterotrophic protists. Deep Sea Research Part II. Submitted.

Petit, J.R., J., Jouzel, D., Raynaud, N.I., Barkov, J.M., Barnola, I., Basile, M., Bender, J., Chappellaz, M., Davis, G., Delaygeu, M., Delmotte, V.M., Kotlyakov., M., Legrand, V.Y., Lipenkov, C., Lorius, L., Pepin, C., Ritz, E., Saltzman, M. Stievenard, 1999. Climate and atmosheric history of the past 420000 years from the Vostok ice core, Antarctica. Nature 399: 429-436.

Petrou, K., C.S., Hassler, M.A., Doblin, K., Shelly, V., Shoemann, R., van den Enden, S., Wright, P.J., Ralph. 2009. Iron-limitation and high light stress on phytoplankton populations from the Australian Sub-Antarctic Zone (SAZ). Submitted in Deep-Sea Res. II.

Pichevin, L.E., B.C., Reynolds, R.S., Ganeshram, I., Cacho, L., Pena, K., Keefe, R.M., Ellam, 2009. Enhanced carbon pump inferred from relaxation of nutrient limitation in the glacial ocean. Nature 459, doi:10.1038/nature081101.

Pickett-Heaps, J., A.-M.M., Schmid, I.A., Edgar, 1990. The cell biology of diatom valve formation. Progr. Phycol. Res. 7: 1-168.

Pollard, R.T., P., Tréguer, J., Read, 2006. Quantifying nutrient supply to the Southern Ocean. J. Geophys. Res. 111: C05011, doi.10.1029/2005JC003076.

Pollard, R.T., I., Salter, R.J., Sanders, M.I., Lucas, M., Moore, R.A., Mills, P.J., Statham, J.T., Allen, A.R., Baker, D.C.E., Bakker, M.A., Charette, S., Fielding, G.R., Fones, M., French, A.E., Hickman, R.J., Holland, J.A., Hughes, T.D., Jickells, R.S., Lampitt, P.J., Morris, F.H., Nédélec, M., Nieldottir, H., Planquette, E.E., Popova, A.J., Poulton, J.F., Read, S., Seeyave, T., Smith, M., Stinchcombe, S., Taylor, S., Thomalla, H.J., Venables, R., Williamson, M.V., Zubkov, 2009. Southern Ocean deep-water carbon export enhanced by natural iron fertilization. Nature 457, doi:10.1038/nature07716, 577-581.

Pondaven, P., C., Fravalo, D., Ruiz-Pino, P., Tréguer, B., Quéquiner, C., Jeandel, 1998. Modelling the silica pump in the Permanently Open Ocean Zone of the Southern Ocean. J. Mar. Sys. 17, 578-619.

Pondaven, P., D., Ruiz-Pino, J.N., Druon, C., Fravalo, P., Tréguer, 1999. Factors controlling silicon and nitrogen biogeochemical cycles in high nutrient, low chlorophyll systems (the Southern Ocean and the North Pacific): Comparison with a mesotrophic system (the North Atlantic). Deep-Sea Res. I 46, 1923-1968.

Pondaven, P., Ragueneau, O., Tréguer, P., Hauvespre, A., Dezileau, L., Reyss, J.L., 2000a. Resolving the « opal paradoxe in the Southern Ocean. Nature 405,168-172.

Pondaven, P., D., Ruiz-Pino, C., Fravalo, P., Tréguer, C., Jeandel, 2000b. Interannual variability of Si and N cycles at the time-series station KERFIX between 1990 and 1995 – a 1-D modelling study. Deep-Sea Res. I 47: 223-257.

Pondaven, P., M., Gallinari, S., Chollet, E., Bucciarelli, G., Sarthou, S., Schultes, F., Jean, 2007. Grazing-induced changes in cell wall silicification in a marine diatoms. Protist 158: 21-28.

Popp, B.N., R., Takigiku, J.M., Hayes, J.W., Louda, E.W., Baker, 1989. The post-paleozoic chronology and mechanism of ^{13}C depletion in primary marine organic matter. Am. J. Sci. 289: 436-454.

Popp, B.N., T.W., Trull, F., Kenig, S.G., Wakeham, T.M., Rust, B., Tilbrook, B., Griffiths, S.W., Wright, H.J., Marchant, R.R., Bidigare, E.A., Laws. 1999. Controls on the carbon isotopic composition of Southern Ocean phytoplankton. Global Biogeochem. Cycles 13(4): 827-843.

Quéguiner, B., P., Tréguer, I., Peeken, R., Scharek, 1997. Biogeochemical dynamics and the silicon cycle in the Atlantic sector of the Southern Ocean during austral spring 1992. Deep-Sea Res. II 44, 69-89.

Quéguiner, B. 2001. Biogenic silica production in the Australian sector of the Subantarctic Zone of the Southern Ocean in late summer 1998. J. Geophys. Res. 106(C12): 31627-31636.

Quéguiner, B., M.A., Brzezinski, 2002. Biogenic silica production rates and particulate matter distribution in the Atlantic sector of the Southern Ocean During austral spring 1992. Deep-Sea Res. II 49, 1765-1786.

Ragueneau, O., P., Tréguer, A., Leynaert, R.F., Anderson, M.A., Brzezinski, D.J., DeMaster, R.C., Dugdale, J., Dymond, G., Fischer, R., François, C., Heinze, E., Maier-Reimer, V., Martin-Jézéquel, D.M., Nelson, B., Quéguiner, 2000. A review of the Si cycle in the modern ocean: recent progress and missing gaps in the application of biogenic opal as a paleoproductivity proxy. Global Planet. Change 26: 317-365.

Ragueneau, O., N., Dittert, P., Pondaven, P., Tréguer, L., Corrin, 2002. Si/C decoupling in the world ocean : is the Southern Ocean different? Deep-Sea Res. II 49: 3127-3154.

Ragueneau, O., N., Savoye, Y., Del Amo, J., Cotten, B., Tardiveau, A., Leynaert, 2005. A new method for the measurement of biogenic silica in suspended matter of coastal waters : using Si :Al ratios to correct for the mineral interference. Cont. Shelf Res. 25, 697-710.

Ralph et al, in prep 2009. Photophysiological interaction of iron and high light on Southern Ocean phytoplankton.

Rau, G.H., P.N., Froelich, A 450 kyr record of bulk sediment δ^{13}Corg and δ^{15}N at 54°S: Significant glacial-interglacial changes in Southern Ocean C and N supply/demand? Transaction, American Geophysical Union, 74: 998.

Raven, J.A., 1983. The transport and function of silicon in plants. Biol. Rev. 58: 179-207.

Rehkämper, M., A.N., Halliday, 1998. Accuracy and long-term reproducibility of lead isotopic measurements by multiple-collector ICP-MS: verification and application of optimized analytical protocols. J. Anal. At. Spectrom. 15: 1451-1460.

Rehkämper, M., M., Schöpnbachler, C.H., Stirling, 2001. Multiple collector ICP-MS: Introduction to instrumentation, measurement techniques and analytical capabilities. Geostand. Newslett. 25: 23-40.

Rehkämper, M., F., Wombacher, J.K., Aggarwal, 2004. Stable isotope analysis by Multiple Collector ICP-MS. IN: de Groot P.A. (Ed.), Handbook of stable isotope analytical techniques: volume 1, Elsevier, Amsterdam, pp 692-725.

Reuer, M.K., B.A., Barnett, M.L., Bender, P.G., Falkowski, M.B., Hendricks, 2007. New estimates of Southern Ocean biological production rates from O_2/Ar ratios and the triple isotope composition of O_2. Deep-Sea Res. I 54: 951-974.

Reynolds, B.C., M., Frank, A.N., Halliday, 2006. Silicon isotope fractionation during nutrient utilization in the North Pacific. Earth Planet. Sci. Lett. 244, 431-443.

Reynolds, B.C., J., Aggarwal, L., André, D., Baxter, C., Beucher, M.A., Brzezinski, E., Engström, R.B., Georg, M., Land, M.J., Leng, S., Opfergelt, I., Rodushkin, H.J., Sloane, H.J.M., van den Boorn, P.Z., Vroon, D., Cardinal, D., 2007. An inter-laboratory comparison of Si isotope reference materials. J. Anal. Atom. Spectrom. 22, 561-568.

Reynolds, B.C., M., Frank, A.N., Halliday, 2008. Evidence for a major change in silicon cycling in the subarctic North Pacific at 2.73 MA. Paleoceanography 23, PA4219, doi:10.1029/2007PA001563.

Reynolds, B.C., 2009. Modeling the modern marine δ^{30}Si distribution. Global Biogeochem. Cycles 23, GB2015, doi:10.1029/2008GB003266.

Ridgway, K.R., 2007. Seasonal circulation around Tasmania: an interface between eastern and western boundary dynamics. J. Geophys. Res. 112, C10016, doi:10.1029/2006JC003898.

Rimmelin-Maury, P., T., Moutin, B., Quéguiner, 2007. A new method for nanomolar determination of silicic acid in seawater. Anal. Chim. Acta 587, 281-286.

Rintoul, S.R., J.L., Bullister, 1999. A late winter hydrographic section from Tasmania to Antarctica. Deep-Sea Research I 46: 1417-1454.

Rintoul, S.R., T.W., Trull, 2001. Seasonal evolution of the mixed layer in the Subantarctic Zone south of Australia. J. Geophys. Res. 106(C12): 31447-31462.

Robert, F., M., Chaussidon, 2006. A palaeotemperature curve for the Precambrian oceans based on silicon isotopes in cherts. Nature 443, doi:10.1038/nature05239.

Rogerson, A., A.S.W., DeFreitas, A.G., McInnes, 1987. Cytoplasmic silicon in the centric diatom *Thalassiosira pseudonana* by electron spectroscopic imaging. Can. J. Microbiol. 33: 128-131.

Rosman, K.J.R., and P.D. Taylor. 1998. Isotopic compositions of the elements 1997. Pure and Appl. Chem. 70(1):217-236.

Round, F.E., 1972. The formation of girdle, intercalary bands and septa in diatoms. Nova Hedwiga 23: 449-463.

Rayleigh, L., 1902. On the distillation of binary mixtures. Phil. Mag. S.6 4: 521-537.

Sabine, C.L., R.A., Feely, N., Gruber, R.M., Key, K., Lee, J.L., Bullister, R., Wanninkhof, C.S., Wong, D., Wallace, B. Tilbrook, F.J., Millero, T.H., Peng, A., Kozyr, T., Ono, A.F., Rios, 2004. The oceanic sink for anthropogenic CO_2. Science 305: 367-371.

Safi, K.A., F.B., Griffiths, J.A., Hall, 2007. Microzooplankton composition, biomass and grazing rates along the WOCE SR3 line between Tasmania and Antarctica. Deep-Sea Res. I, 54, 1025-1041, doi:10.1016/j.dsr.2007.05.003.

Sambrotto, R.N., B.J., Mace, 2000. Coupling of biological and physical regimes across the Antarctic Polar Front as reflected by nitrogen production and recycling. Deep-Sea Res. II 47: 3339-3368.

Sarmiento, J.L., J.R., Toggweiler, 1984. A new model for the role of the oceans in determining atmospheric CO_2. Nature 308: 621-624.

Sarmiento, J.L., T.M.C., Hughes, R.J., Stouffer, S., Manabe, 1998. Simulated response of the ocean carbon cycle to anthropogenic climate warming. Nature 393: 245-249.

Sarmiento, J.L., N., Gruber, M.A., Brzezinski, J.P., Dunne, 2004. High-latitude controls of thermocline nutrients and low latitude biological productivity. Nature 427: 56-60.

Sarmiento, J.L., N., Gruber, 2006. Ocean biogeochemical dynamics. Princeton University Press, Princeton NJ.

Sarmiento, J.L., J., Simeon, A., Gnanadesikan, N., Gruber, R.M., Key, R., Schlitzer, 2007. Deep ocean biogeochemistry of silicic acid and nitrate. Global Biogeochem. Cycles 21: GB1S90, doi.10.1029/2006GB002720.

Sarthou, G., K.R., Timmermans, S., Blain, P., Tréguer. Growth physiology and fate of diatoms in the ocean: a review. J. Sea Res. 53: 25-42.

Savoye, N., F., Dehairs, M., Elskens, D., Cardinal, E.E., Kopczyńska, T.W., Trull, S., Wright, W., Baeyens, B.F., Griffiths, 2004. Regional variation of spring N-uptake and new production in the Southern Ocean. Geophys. Res. Let., 31, L03301.

Savoye, N., K.O., Buesseler, D. Cardinal, F., Dehairs, 2004b. ^{234}Th deficit and excess in the Southern Ocean during spring 2001: Particle export and remineralization. Geophys. Res. Let. 31, L12301, doi:10.1029/2004GL019744.

Savoye, N., T.W., Trull, S.H.M., Jacquet, J., Navez, F., Dehairs, 2008. ^{234}Th-based export fluxes during a natural iron fertilization experiment in the Southern Ocean (KEOPS). Deep-Sea Res. II 55, 841-855.

Schlitzer, R., 2002. Caron export fluxes in the Southern Ocean: Results from inverse modeling and comparison with satellite-based estimates. Deep-Sea Res. II 49: 1623-1644.

Sedwick, P.N., S., Blain, B., Quéguiner, F.B., Griffiths, M., Fiala, E., Bucciarelli, M., Denis, 2002. Resource limitation of phytoplankton growth in the Crozet Basin, SubAntarctic Southern Ocean. Deep-Sea Res. II 49: 3327-3349.

Sherbakova, T.A., Y., Masyokova, T., Safonova, D., Petrova, A., Vereshagin, T., Minaeva, R., Adelshin, T., Triboy, I., Stonik, N., Aizdaitcher, et al., 2005. Conserved motif CMLD in silicic acid transport proteins of diatoms. Mol. Biol. (Mosk) 39: 269-280.

Siegenthaler, U., T., Wenk, 1984. Rapid atmospheric CO_2 variation and ocean circulation. Nature 308: 624-626.

Sigman, D.M., M.A., Altabet, D.C., McCorkle, R., François, G., Fischer, 1999. The $\delta^{15}N$ of nitrate in the Southern Ocean: Consumption of nitrate in surface waters. Global Biogeochem. Cycles 13, 1149-1166.

Sigman, D.M., M.A., Altabet, D.C., McCorkle, R., Francois, G. Fischer, 2000. The $\delta^{15}N$ of nitrate in the Southern Ocean: Nitrogen cycling and circulation in the ocean interior. J. Geophys. Res. 105(C8): 19599-19614.

Sigman, D.M., E.A., Boyle 2000. Glacial / interglacial variations in atmospheric carbon dioxide. Nature, 407, 859-869.

Sigman, D. M., K.L., Karsh, K.L., Casciotti, 2009. Nitrogen isotopes in the ocean, in Encyclopedia of Ocean Sciences (update from 2001), edited by J.H. Steele, K.K. Turekian, and S.A. Thorpe, Academic Press, London.

Sjöberg, S., A., Norden, I., Nils, 1981. Equilibrium and structural studies of silicon (IV) and aluminium (III) in aqueous solution. Mar. Chem. 10: 521-532.

Sloyan, B.M., S.R., Rintoul, 2001. Circulation, renewal, and modification of Antarctic mode and intermediate water. J. Phys. Oceanogr. 31: 1005-1030.

Smetacek, V., 1999. Diatoms and the ocean carbon cycle. Protist 150: 25-32.

Smetacek, V., 2001. The giant diatom dump. Nature 406:574-575.

Smetackek, V., P., Assmy, J., Henjes, 2004. The role of grazing in structuring Southern Ocean pelagic ecosystems and biogeochemical cycles. Antarct. Sci. 16: 541-558.

Sokolov, S., S.R., Rintoul, 2002. Structure of Southern Ocean fronts at 140°E. J. Mar. Syst. 37: 151-184.

Sokolov, S., S.R., Rintoul, 2007a. On the relationship between fronts of the Antarctic Circumpolar Current and surface chlorophyll concentration in the Southern Ocean. J. Geophys. Res. 112, C07030, doi:10.1029/2006JC004072.

Sokolov, S., S.R., Rintoul, 2007b. Multiple jets of the Antarctic Circumpolar Current south of Australia. J. Phys. Oceanogr. 37: 1394-1412.

Sokolov, S., S.R., Rintoul, 2009. Circumpolar structure and distribution of the Antarctic Circumpolar fronts: 1. Mean circumpolar path. J. Geophys. Res. 114, C11018, doi:10.1029/2008JC005108.

Speer, K.G., S.R., Rintoul, B.M., Sloyan, 2000. The diabatic Deacon cell. J. Phys. Oceanogr. 30: 3212-3222.

Sunda, W.G., S.A., Huntsman, 1995. Iron uptake an growth limitation in oceanic and coastal phytoplankton. Mar. Chem. 50: 189-206.

Stumm, W., J.J., Morgan, 1981. Aquatic Chemistry. 2nd edn. Wiley, New York, 780pp.

Sullivan, B.K., C.B., Miller, W.T. Peterson, A.H., Soeldner, 1975. A scanning electron microscope study of the mandibular morphology of boreal copepods. Mar. Biol. 30: 175-182.

Sullivan, C.W., 1976. Diatom mineralization of silicic acid. I. $Si(OH)_4$ transport characteristic in Naviculla pelliculosa. J. Phycol. 12: 390-396.

Swart, S., S., Speich, I.J., Ansorge, G.J., Goni, S., Gladyshev, J.R.E., Lutjeharms, 2008. Transport and variability of the Antarctic Circumpolar Current south of Africa. J. Geophys. Res. 113, C09014, doi:10.1029/2007JC004223.

Takahashi, T., S.C., Sutherland, C., Sweeney, A., Poisson, N., Metzl, B., Tilbrook, N., Bates, R., Wanninkhof, R.A., Feely, C., Sabine, J., Olafsson, Y., Nojiri, 2002. Global sea-air CO_2 flux based on climatological surface ocean pCO_2 and seasonal biological and temperature effects. Deep-Sea Res. II, 49, 1601-1622.

Takeda, S. 1998. Influence of iron availability on nutrient consumption ratio of diatoms in oceanic waters. Nature 393: 774-777.

Taylor, N.J., 1985. Silica incorporation in the diatom *Coscinodiscus granii* as affected by light intensity. Br. Phycol. J. 20: 365-374.

Taylor, S.R., S.M., McLennan, S.M., 1985. The continental crust: its composition and evolution. Blackwell Scientific Publications, Oxford, pp 312.

Thamatrakoln, K., A.J., Alverson, M., Hildebrand, 2006. Comparative sequence analysis of diatom silicon transporters: towards a mechanistic model of silicon transport. J. Phycol. 42: 822-834.

Thamatrakoln, K., M., Hildebrand, 2007. Analysis of *Thalassiosira pseudonana* silicon transporters indicates distinct regulatory levels and transport activity through the cell cycle. Eukaryotic Cell 6(2): 271-279.

Thamatrakoln, K., M., Hildebrand, 2008. Silicon uptake in diatoms revisited: a model for saturable and nonsaturable uptake kinetics and the role of silicon transporters. Plant. Physiol. 146: 1397-1407.

Thomas, R., A beginners guide to' ICP-MS. http://spectroscopyonline.findanalytichem.com/

Timmermans K.R., L.J.A., Gerringa, H.J.W., de Baar, B., van der Wagt, M.J.W., Veldhuis, J.T., de Jong, P.L. Croot, 2001. Growth rates of large and small Southern Ocean diatoms in relation to availability of iron in natural seawater. Limnol. Oceanogr. 46(2): 260-266.

Timmermans, K.R., B., van der Wagt, H.J.W., de Baar, 2004. Growth rates, half-saturation constants, and silicate, nitrate, and phosphate depletion in relation to iron availability of four large, open-ocean diatoms from the Southern Ocean. Limnol. Oceanogr. 49(6), 2141-2151.

Timmermans, K.R., B., van der Wagt, M.J.W., Veldhuis, A., Maatman, H.J.W., de Baar. 2005. Physiological responses of three species of marine pico-phytoplankton to ammonium, phosphate, iron and light limitation. J. Sea Res. 53: 109-120.

Toggweiler, J.R., K., Dixon, W.S., Broecker, 1991. The Peru upwelling and the ventilation of the South Pacific thermocline. J. Geophys. Res., 96(C11), 20467-20497.

Toggweiler, J.R., 1999. Variation of atmosheric CO_2 by ventilation of the ocean's deepest water. Paleoceanography 14: 571-588.

Toggweiler, J.R., J.L., Russell, S.R., Carson, 2006. Midlatitudes westerlies, atmospheric CO_2, and climate change during the ice ages. Paleoceanography 21, PA2005, doi:10.1029/2005PA001154.

Tomczak, M., J.S., Godfrey, 1994. Regional Oceanography: An Introduction. Pergamon, New York.

Tréguer, P., A., Kamatani, S., Gueneley, B., Quéguiner, 1989. Kinetics of dissolution of Antarctic diatom frustules and the biogeochemical cycle of silicon in the Southern Ocean. Polar Biol. 9: 397-403.

Tréguer, P., L. Lindner, A.J. van Bennekom, A. Leynaert, M. Panouse M., and G. Jacques. 1991. Production of biogenic silica in the Weddell-Scotia Seas measured with ^{32}Si. Limnol. Oceanogr. 36, 1217-1227.

Tréguer, P., G., Jacques, 1992. Dynamics of nutrients and phytoplankton, and fluxes of carbon, nitrogen and silicon in the Antarctic Ocean, Polar Biol. 12: 149-162.

Tréguer, P., D.M., Nelson, A.J., van Bennekom, D.J., DeMaster, A., Leynaert, B., Quéguiner, 1995. The silica balance in the world ocean: a re-estimate. Science 268:375-379.

Tréguer, P., P., Pondaven, 2000. Silica control of carbon dioxide. Nature 406:358-359.

Trenberth, K.E., J.G., Olsen, W.G., Large, 1989. A global ocean wind stress climatology based on ECMWF analysis. NCAR Technical Note NCAR/TN-338#STR, 93 pp.

Trull, T.W., S.G., Bray, S.J., Manganini, S., Honjo, R., François. 2001. Moored sediment trap measurements of carbon export in the subantarctic and polar frontal zones of the Southern Ocean, south of Australia. J. Geophys. Res. 106 (C12): 31489-31509.

Trull, T.W., S.R., Rintoul, M., Hadfield, E.R., Abraham, 2001. Circulation and seasonal evolution of polar waters south of Australia: Implications for iron fertilization of the Southern Ocean. Deep-Sea Res. II 48, 2439-2466.

Uitz, J., H., Claustre, F.B., Griffiths, J., Ras, N., Garcia, V., Sandroni, 2009. A phytoplankton class-specific primary production model applied to the Kerguelen Islands region (Southern Ocean). Deep-Sea Res. I 56, 541-560.

Van Bennekom, A.J., J.H.F., Jansen, S.J., Van der Gaast, J.M., Van Ieperen, J., Pieters, 1989. Aluminum-rich opal: an intermediate in the preservation of biogenic silica in the Zaire (Congo) deep-sea fan. Deep-Sea Res. 36: 173-190.

Van Bennekom, A.J., A.G.J., Buma, R.F., Nolting, 1991. Dissoved aluminium in the Weddel-Scotia confluence and the effect of Al on the dissolution kinetics of biogenic silica. Mar. Chem. 35: 423-434.

Van Beusekom, J.E.E., A.J., Van Bennekom, P., Tréguer, J., Morvan, 1997. Aluminium and silicic acid in water and sediments of the Enderby and Crozet basins. Deep-Sea Res. II 44: 987-1004.

Van Cappellen, P., S., Dixit, J., van Beusekom, 2002. Biogenic silica dissolution in the oceans: Reconciling experimental and field-based dissolution rates. Global Biogeochem. Cycles, 16(4), 1075, doi: 10.1029/2001GB001431

Varela, D.E., C.J., Pride, M.A., Brzezinski, 2004. Biological fractionation of silicon isotopes in Southern Ocean surface waters. Global Biogeochem. Cycles 18 : GB1047, doi.10.1029/2003GB002140.

Veldhuis, M. J. W., W., Admiraal, 1987. Influence of phosphate depletion on the growth and colony formation of *Phaeocystis pouchetii*. Mar. Biol. 95: 47–54.

Vergara, J.J., J.A., Berges, P., Falkowski, 1998. Diel periodicity of nitrate reductase activity and protein levels in the marine diatom *Thalssiosira Weissflogii* (Bacillariophyceae). J. Phycol. 34: 952-961.

Venchiarutti, C., C., Jeandel, M., Roy-Barman, 2008. Particle dynamics study in the wake of Kerguelen Island using thorium isotopes. Deep-Sea Res. I 55, 1343-1363.

Volcani, B.E., 1981. Cell wall formation in diatoms: morphogenesis and biochemistry. In Simpson, T.L. & Volcani, B.E. (Eds.), Silicon and siliceous structures in biological systems. Springer-Verlag, New York, pp. 157-200.

Volk, T., M.I., Hoffert, 1985. Ocean carbon pumps: analysis of relative strengths and efficiencies in ocean-driven atmospheric CO_2 changes. In: Sundquist, E., Broecker, W.S., (Eds.), The carbon cycle and atmospheric CO_2: Natural variations Archean to present. AGU, Washington, DC, pp. 99-110.

Vrieling, E.G., W.W.C., Gieskes, T.P.M., Beelen, 1999. Silicon deposition in diatoms: control by the pH inside the silicon deposition vesicle. J. Phycol. 35: 548-559.

Walder, A.J., I., Platzner, P.A., Feedman, 1993. Isotope measurement of lead, neodymium and neodymium-samarium mixtures, hafnium and hafnium-lutetium mixtures with a double focusing multiple collector inductively coupled plasma mass spectrometer. J. Anal. At. Spectrom. 8: 19-23.

Wang, X., R.J., Matear, T.W., Trull, 2001. Modeling seasonal phosphate export and resupply in the Subantarctic and Polar Frontal Zones in the Australian sector of the Southern Ocean. J. Geophys. Res. 106: C12, 31525-31541.

Westwood, K.J., F.B., Griffiths, J., Webb, 2009. Primary productivity in the Subantarctic and Polar Frontal zones south of Tasmania, Australia; SAZ-Sense survey 2007. Deep Sea Research Part II, submitted.

Wischmeyer, A.G., C.L., De La Rocha, E., Maier-Reimer, D.A., Wolf-Gladrow, 2003. Control mechanisms for the oceanic distribution of silicon isotopes. Global Biogeochem. Cycles 17(3): 1083, doi:10.1029/2002GB002022.

Wright, S.W., D.P., Thomas, H.J., Marchant, H.W., Higgins, D.M., Mackey, D.J., Mackey, 1996. Analysis of phytoplankton of the Australian sector of the Southern Ocean: comparisons of microscopy and size frequency data with interpretations of pigments HPLC data using the "Chemtax" matrix factorization program. Mar. Ecol. Progr. Ser. 144: 285-298.

Wright, S., R., van den Enden, I., Pearce, M., Doblin, 2009. Phytoplankton pigments in the Sub-Antarctic and Polar Frontal Zones waters south-west and south-east of Tasmania. Deep-Sea Res. Part II, submitted.

Ziegler, K., O.A., Chadwick, M.A., Brzezinski, E.F., Kelly, 2005. Natural variations of δ^{30}Si ratios during progressive basalt weathering, Hawaiian Islands. Geochim. Cosmochim. Acta 69 (19): 4597-4610.

Watson, A.J., J.C., Orr, 2003. Carbon dioxide fluxes in the global ocean. In: Fasham, M.J.R. (Ed.), Ocean biogeochemistry: The role of ocean carbon cycle in global change. Springer, Berlin, pp. 123-141.

Whitworth, T., A.H., Orsi, S.J., Kim, W.D., Nowlin, 1998. Water masses and mixing near the Antarctic slope front. In: Jacobs, S.S., Weiss, R.F. (Eds.), ocean, ice and atmosphere interactions at the Antarctic continental margin, Antarctic Research Series, vol 75. American Geophysical Union, Washington, DC, USA, pp 1-27.

Wollast, R., and F.T. Mackenzie. 1983. The global cycle of silica. In: S.R. Aston (eds.), Silicon geochemistry and biogeochemistry. Academic Press.

Young, E.D., A., Galy, H., Nagahara, 2002. Kinetic and equilibrium mass-dependent isotope fractionation laws in nature and their geochemical and cosmochemical significance. Geochim. Cosmochim. Acta 66(6), 1095-1104.

Zhang, Y., F., Lacan, C., Jeandel, 2008. Dissolved rare earth elements tracing lithogenic inputs over the Kerguelen Plateau (Southern Ocean). Deep-Sea Res. II 55, 638-652.

Part VIII. Annex

Late summer diatoms productivity across the Antarctic Circumpolar Current and adjacent subsystems in Indo-Atlantic sector

Abstract

Si-cycle in surface waters was investigated in late summer 2008 during a transect (BONUS-goodhope) across the Antarctic Circumpolar Current and adjacent subsystems (Weddell Gyre and SubTropical Zone) In the Indo-Pacific sector. Biogenic silica concentration and production were in the lower range of previous observations in the Southern Ocean reflecting the end of diatoms productive period. This is also reflected in the low specific rate of Si-uptake (<0.1 d^{-1}) in agreement with several co-occurring co-limitations (Si, light, Fe, …). In the southern part of the section, diatoms productivity and biomass were higher along with a more significant contribution to total primary production than in the northern part. This north-south expression, already well documented, results from a increasing of silicic acid limitation towards the north since $Si(OH)_4$ concentration are relatively high south of APF (> 5µmol Si l^{-1}) and low north of it (<2 µmol Si l^{-1}). Areas associated with significant contribution of diatoms, south of SAF, exhibit higher carbon export efficiency as expected.

The ^{28}Si-isotopic dilution carrying by $bSiO_2$ dissolution was not sufficient enough to carefully quantify this Si-flux. In this article, the limit of detection of ^{30}Si-incubation methodology is discussed in term of mass and isotopic balance. All the BONUS-goodhope stations are falling below and the upper estimate of $bSiO_2$ dissolution, equaling detection limit, proper for each station is given. Nevertheless by comparing Si:N ratio in particulate and uptake, silicate pump processes preferentially depleting the mixed layer in silicic acid instead of NO_3 through biological pump processes are actively occurring even if more efficient silicon loop is expected due to mainly an increase of detrital biogenic silica following productive period.

1.1. Introduction

The marine Si-biogeochemical cycle is dominated by biogenic silica production and dissolution in the euphotic zone (Tréguer et al., 1995). The balance between integrated silica production and dissolution in the euphotic zone, which we will referred to in the following as the integrated dissolution to production rate ratio (∫D:∫P), is a key determinant to assess the strength of the silicate pump (Brzezinski et al., 2003). Despite the scarcity of data (up to now only 74 vertical profiles; Nelson et al., 1995; Brzezinski et al., 2001, 2003; Beucher et al., 2004a, 2004b; Fripiat et al., in prep, this study), the range of measured ∫D:∫P ratios spans an order of magnitude, with values as low as 0.1 and others exceeding 1.0. This implies that there is a high degree of variability in the extent of silica recycling in the ocean. The magnitude and variability of ∫D:∫P is one of the greatest uncertainties in the global marine budget (Nelson et al., 1995; Brzezinski et al., 2003). The scarcity of data mainly results from analytical difficulties to measure $bSiO_2$ dissolution by isotopic dilution, but progress has been made recently for a more sensitive and faster methodology (Fripiat et al., 2009).

Southern Ocean plays a key role in the global Si-biogeochemical cycle since diatoms are major player of the biological pump in this area (Buesseler et al., 2001; Jin et al., 2006; Honjo et al., 2008) driving a dramatic silicic acid (also referred as $Si(OH)_4$) gradient (Pondaven et al., 2000; Brzezinski et al., 2001; Quéguiner and Brzezinski, 2002). This feature observed on the whole circumpolar Southern Ocean coincides with the largest burial area of biogenic silica (also referred as $bSiO_2$) in the global ocean (DeMaster, 1981; Tréguer et al., 1995; DeMaster, 2002). This North-South $Si(OH)_4$ gradient which is not observed with such extent, for other major nutrients, has significant implications, both in modern and

past ocean, on global biogeochemistry since the upper limb of the Southern Ocean meridional circulation redistributes nutrient into the main global ocean thermocline driven 75% of the low-latitude productivity (Trull et al., 2001; Sarmiento et al., 2004).

In this study, we investigate the late summer diatoms productivity across the ACC in the Indian-Atlantic sector. We discuss the potential factors controlling it along with the limit of the isotopic dilution technique to measure dissolution:production ratios in contrasted biogeochemical zones of the Southern Ocean.

1.2. Materials and methods

BONUS-Goodhope cruise covered a transect from Cape Town (South Africa) to 58°S in the Southern ocean along the 0° meridian from 8 February to 8 March 2008, aboard R/V Marion Dufresne. The aim of BONUS-Goodhope, an International Polar Year and GEOTRACES cruise, was to understand the interactions between physics, geochemistry, and biogeochemistry in the water column. 79 stations were sampled among which 9 stations were sampled to measure Si production and dissolution rates. These stations were distributed across the following different subsystems (Figure 1): SubTropical Front Zone (n=1), SubAntarctic Zone (n=1), Polar Frontal Zone (n=3), Antarctic Polar Front (n=1), Southern Antarctic Circumpolar Current Front (n=1), Antarctic Zone (n=1), and Weddell Gyre (n=1).

^{30}Si incubations were performed at three depths (each time triplicated) corresponding to 100, 25, and

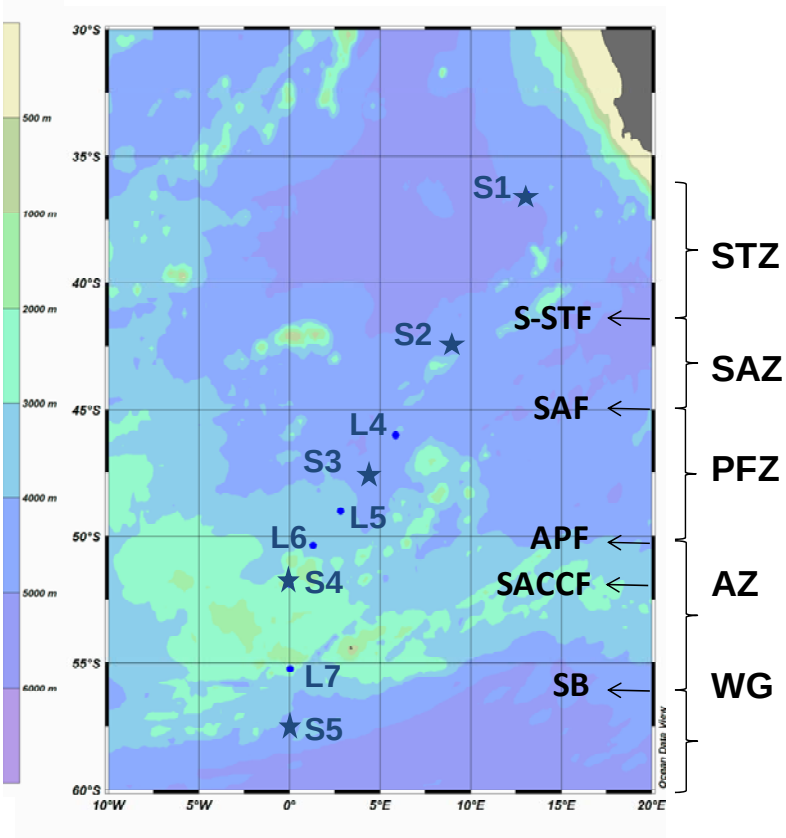

Figure 1. Map of the study area with bathymetry and main hydrodynamic features. Stations represented by a star are "Super station" where ^{30}Si-incubation were realised a two incubation times (t24 and t48). The dots stations are "Large Station" where only t24 were realized.

1% light level depths (determined by PAR=Photosynthetically Active Radiation) sampled with Niskin bottles mounted on a CTD rosette. Samples were incubated in deck incubators for 24h (t24) and 48h (t48; only stations represented by a star in Figure 1) equipped with neutral density light screens to simulate the light intensity at original depth of collection. Surface seawater was used to maintain ambient temperatures within the incubators. Seawater sampling was performed following Corvaisier et al. (2005). For the 24h incubations, 9 liters per depth were sampled and divided in three 1-liter aliquots for initial conditions, and three 2-liter aliquots for final conditions. For the stations with two incubations times (24 and 48h), a total of 15 liters per depth were sampled and divided in three 1-liter aliquot for initial conditions, three 2-liter aliquots for t24, and three 2-liter aliquots for t48.

Silicic acid concentration was analyzed with a segmented flow auto-analyzer (Technicon; IUEM, Plouzané, France). The biogenic silica ($bSiO_2$) filtered onto polycarbonate membranes (Nucleopore 0.4 µm porosity, 47mm Ø), was dried at 60°C and stored in the dark at room temperature. It was digested at home laboratory (RMCA, Tervuren, Belgium) in one step with 0.2M NaOH during 40 min at 100°C followed by neutralization with HCL 1M (Ragueneau et al., 2005). Biogenic silica concentrations were determined with a spectrophotometer (Genesys 10S UV, VWR) following Grasshoff et al. (1983). For both biogenic silica and silicic acid concentrations, these measurements are well in agreement with onboard data (for silicic acid) and alkaline digestion (for biogenic silica) performed at higher spatial resolution on different CTD cast: 0.9 ± 9.8% for $bSiO_2$ (Lemoigne et al., in prep).

The basic concept of Si incubation is isotopic dilution which consists to spike seawater with ^{30}Si and leave the incubation under controlled conditions for a specified time (here 24h and 48h) (Nelson and Goering, 1977a, 1977b). The ^{30}Si addition should represent less than 10% of the ambient $Si(OH)_4$ concentration in order to avoid significant perturbation in the samples. The increase in ^{30}Si of particulate phase is used to estimate $bSiO_2$ production rate while the increase in ^{28}Si from death dissolving biogenic silica in dissolved phase is used to assess $bSiO_2$ dissolution rate.

We apply a preconcentration step following a protocol adapted for Si from the MAGIC method (Karl and Tien, 1992; Rimmelin-Maury et al., 2007). As $Si(OH)_4$ concentration in seawater north of Antarctic Polar Front (S1, S2, L4, S3, L5) during BONUS-Goodhope was too low (<2.8 µmol Si l^{-1}) and too saline to be directly introduced into the mass spectrometer without purification (Fripiat et al., 2009), a cation-exchange chromatography developed by Georg et al. (2006) was required to remove saline matrix after the MAGIC preconcentration step. Stations on Antarctic Polar Front and south (L6, S4, L7, S5) had $Si(OH)_4$ concentration higher than the threshold limit, these diluted MAGIC solutions were directly introduced into the mass spectrometer.

Purified and non-purified $Si(OH)_4$ samples as well as digested $bSiO_2$ solutions were diluted at ~ 100 ppb Si in bidistilled 0.65% HNO_3 and analyzed using a standard High Resolution Sector Field Inductively Coupled Plasma Mass Spectrometer (HR-SF-ICP-MS, ELEMENT2, Thermo, Bremen, Germany) to determine silicon isotopic abundances (Fripiat et al., 2009). The average reproducibility of ^{30}Si isotopic abundance (Atom %) for each triplicates (from sampling to measurements) was lower than 1% (Relative Standard Deviations) as determined in Fripiat et al. (2009).

In order to calculate the silicon fluxes (production and dissolution rates of biogenic silica) from those measurements, two different models exist: the linear one compartmental model described in Nelson and

Goering (1977a, 1977b), and the two nonlinear two compartmental model previously described in Beucher et al. (2004) and Elskens et al. (2007). In the two compartmental model parameters are constrained by the requirement to fit mass and isotopic balances of dissolved and particulate phases (Elskens et al., 2007). We will preferentially use this two compartmental model since it takes into account both isotope dilution and concentration changes occurring in the course of incubation which can induce biased estimations when using only the one compartmental model. A detailed comparison on the two models is provided in Elskens et al. (2007). Integration of stock and fluxes were assessed using the trapezoidal integration method to the 1% light depth.

1.3. Results and discussion

2.1.1 Assessment of the accuracy of the $bSiO_2$ production-dissolution rates

$bSiO_2$ production rates estimated at t24 and t48 using the two compartmental model are strongly correlated around a 1:1 slope (slope = 1.09x ± 0.04, R^2 = 0.93, p value < 0.01, not shown) as for $bSiO_2$ production from one and two compartmental models (slope = 1.04 ± 0.04, R^2 = 0.99, p value < 0.01, not shown). In the following discussion, only $bSiO_2$ production rate at t24 estimated with two compartmental model will be used.

Although $bSiO_2$ production and dissolution occur simultaneously in marine surface waters, for a given $bSiO_2$ particle these processes are uncoupled temporally, since it is not until after diatom death and degradation of its protective organic coating that the $bSiO_2$ cell wall becomes subject to dissolution (Lewin, 1961; Kamatani, 1982; Biddle and Azam, 1999; Ragueneau et al., 2000). During BONUS-Goodhope in most of the cases (87%), ^{28}Si-isotopic dilution carrying by death diatom cells was not sufficient enough analytically, incidentally precluding the estimation of $bSiO_2$ dissolution. Indeed final silicic acid atom % ^{30}Si was in most of the case not statistically different from initial silicic acid atom % ^{30}Si: < 1 relative standard deviation determined at 1% in Corvaisier et al. (2005) and Fripiat et al. (2009). In the following, effort would be made to determine the limit of the detection for the ^{30}Si-isotopic dilution.

To safely quantify this limit of detection, the overall precision (including sampling, processing, and analyze) need to be accurately assessed. BONUS-Goodhope data has allowed to assess the precisions through a complete set of triplicate incubations (n=81) from spiking to model outputs (following Fripiat et al., 2009). The relative standard deviations for each measured parameter was estimated at 7, 2, 1% for respectively [$bSiO_2$], [$Si(OH)_4$], and atom % ^{30}Si, both for $bSiO_2$ and $Si(OH)_4$. The limit of detection for ^{30}Si-isotopic dilution was estimated by solving the mass and isotopic balance by constraining the difference between initial and final ^{30}Si-isotopic abundance at 1% (~ 1RSD; Corvaisier et al., 2005; Fripiat et al., 2009) with variable [$Si(OH)_4$] and initial atom % ^{30}Si-$Si(OH)_4$ value. The detection limit for isotopic dilution is relatively well constrained (Figure 2). $bSiO_2$ production and content have not significant influence on isotopic dilution detection limit.

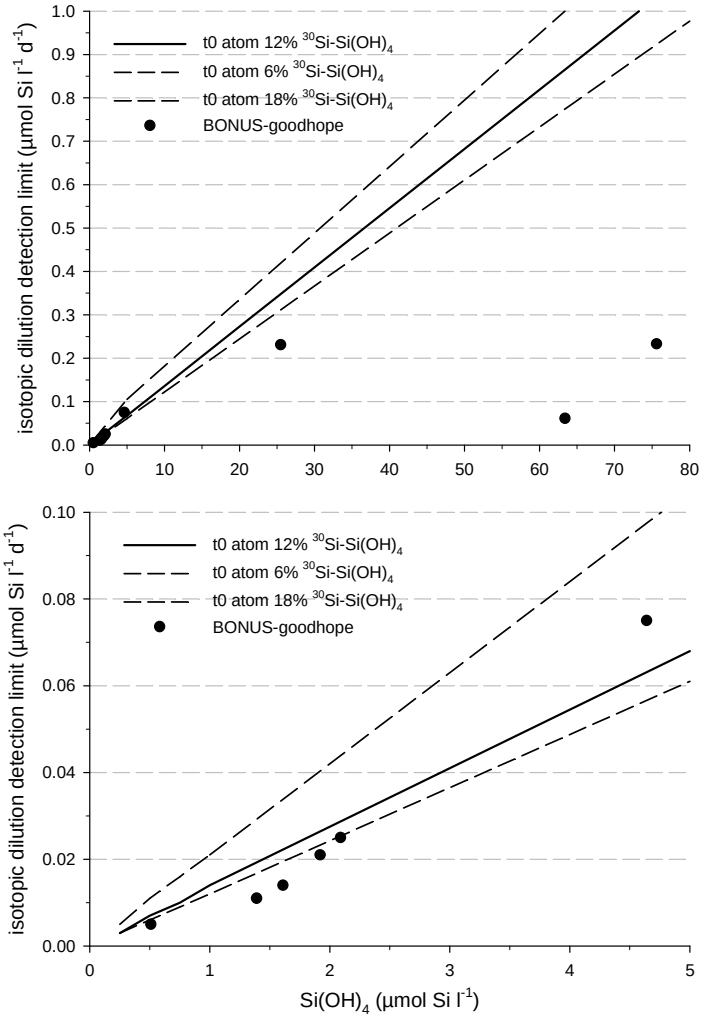

Figure 2. Detection limit for ^{30}Si-isotopic dilution carrying by $bSiO_2$ dissolution in function of $Si(OH)_4$ concentration. Panel b is a closed view for lower $Si(OH)_4$ concentration than panel a.

All BONUS-Goodhope depth average $bSiO_2$ dissolution rates calculated fall below the estimated detection limit (Figure 2). Therefore, in the following, dissolution rates will always been discussed using a range from zero to the detection limit. The latter being different for each station since it is dependent of the station Si-characteristics (Table 1).

2.1.2 $bSiO_2$ production across the BONUS-Goodhope section

Table 1 shows values of $bSiO_2$, $Si(OH)_4$, Si-uptake and $bSiO_2$ dissolution. No significant trends with depth are observed for the whole ACC euphotic zone in term of Si-biogeochemical properties (Figure 3). A vertical trends towards lower biogenic silica production rates with depth is observed at several station (Table 1; Figure 3) and was already observed previously in the ACC (Brzezinski et al., 2001; Quéguiner, 2001; Leblanc et al., 2002; Quéguiner and Brzezinski, 2002; Beucher et al., 2004b).

	PAR	depth	$bSiO_2$	$Si(OH)_4$	ρ_{Si}[1]	ρ_{diss}[2] (t24)	ρ_{diss} (t48)	ρ_{diss} max (DL^3)
	%	m	µmol Si l^{-1}	µmol Si l^{-1}	µmol Si l^{-1} d^{-1}	µmol Si l^{-1} d^{-1}	µmol Si l^{-1} d^{-1}	µmol Si l^{-1} d^{-1}
Super 1: CTD #20								
02/21/2008	100%	3	0.088 ± 0.017	2.18 ± 0.01	0.001 ± 0.000	0.038 ± 0.024	0.022 ± 0.009	0.031
13.1°E	25%	15	0.024 ± 0.001	1.64 ± 0.04	0.001 ± 0.000	0.008 ± 0.001	0.005 ± 0.000	
30.5°S	1%	54	0.049 ± 0.004	1.95 ± 0.09	0.000 ± 0.000	0.019 ± 0.007	0.008 ± 0.005	
Super 2: CTD #45								
02/28/2008	100%	3	0.086 ± 0.001	0.45 ± 0.01	0.009 ± 0.001	0.000 ± 0.000	0.002 ± 0.003	0.007
8.5°E	25%	10	0.096 ± 0.004	0.45 ± 0.03	0.008 ± 0.002	0.005 ± 0.006	0.001 ± 0.002	
42.3°S	1%	50	0.295 ± 0.028	0.64 ± 0.03	0.021 ± 0.002	0.021 ± 0.005	0.003 ± 0.003	
Large 4: CTD #58								
3/03/2008	100%	11	0.084 ± 0.005	1.42 ± 0.05	0.003 ± 0.000	0.013 ± 0.002		0.019
5.5°E	25%	19	0.075 ± 0.006	1.38 ± 0.02	0.003 ± 0.000	0.005± 0.002		
46.0°S	1%	48	0.073 ± 0.006	1.40 ± 0.04	0.002 ± 0.000	0.014 ± 0.014		
Super 3: CTD #62								
3/04/2008	100%	4	0.534 ± 0.110	1.53 ± 0.01	0.033 ± 0.006	0.013 ± 0.005	0.012 ± 0.002	0.021
4.2°E	25%	9	0.565 ± 0.008	1.65 ± 0.03	0.032 ± 0.001	0.009 ± 0.010	0.006 ± 0.002	
47.3°S	1%	60	0.487 ± 0.059	1.66 ± 0.04	0.024 ± 0.004	0.020 ± 0.015	0.012 ± 0.007	
Large 5: CTD #71								
3/07/2008	100%	4	0.140 ± 0.006	2.02 ± 0.02	0.007 ± 0.002	0.009 ± 0.005		0.029
2.5°E	25%	9	0.146 ± 0.010	2.04 ± 0.03	0.006 ± 0.001	0.017 ± 0.011		
49.0°S	1%	60	0.167 ± 0.026	2.20 ± 0.09	0.005 ± 0.001	0.048 ± 0.018		
Large 6: CTD #78								
3/09/2008	100%	7	0.433 ± 0.018	3.65 ± 0.24	0.013 ± 0.001	0.131 ± 0.015		0.064
1.2°E	25%	10	0.385 ± 0.020	4.24 ± 0.09	0.015 ± 0.003	0.017 ± 0.018		
50.2°S	1%	78	0.425 ± 0.033	6.04 ± 0.09	0.008 ± 0.000	0.076 ± 0.016		
Super 4: CTD #83								
3/10/2008	100%	2	0.541 ± 0.038	24.87 ± 0.09	0.021 ± 0.000	0.156 ± 0.049	0.030 ± 0.028	0.350
0.0°E	25%	11	0.625 ± 0.044	25.06 ± 0.10	0.021 ± 0.001	0.231 ± 0.040	0.054 ± 0.040	
51.5°S	1%	125	0.683 ± 0.038	26.55 ± 0.13	0.009 ± 0.002	0.305 ± 0.095	0.100 ± 0.011	
Large 7: CTD #100								
3/14/2008	100%	5	1.034 ± 0.024	61.47 ± 0.17	0.072 ± 0.005	0.073 ± 0.026		0.857
0.0°E	25%	14	0.985± 0.048	61.21 ± 0.31	0.071 ± 0.003	0.016 ± 0.027		
55.3°S	1%	110	1.108 ± 0.027	67.49 ± 0.11	0.035 ± 0.005	0.093 ± 0.012		
Super 5: CTD #108								
3/16/2008	100%	4	1.461 ± 0.030	75.49 ± 0.36	0.084 ± 0.016	0.337 ± 0.176	0.089 ± 0.019	1.05
0.0°E	25%	9	1.522 ± 0.034	76.14 ± 0.09	0.102 ± 0.002	0.195 ± 0.038	0.113 ± 0.028	
57.3°S	1%	90	1.646 ± 0.067	75.35 ± 0.19	0.041 ± 0.000	0.168 ± 0.103	0.113 ± 0.097	

[1] biogenic silica production rate

[2] biogenic silica dissolution rate

[3] Detection limit (section 3.1)

Table 1. $bSiO_2$ and $Si(OH)_4$ concentration, $bSiO_2$ production and dissolution rates (t24, t48, and upper station average estimates). Each value excepted for upper estimates of $bSiO_2$ dissolution rates represents the average and standard deviation (1sd) of triplicates.

A sharp north-south gradient (Figure 4a), both in $Si(OH)_4$ and $bSiO_2$ content, is a recurrent features in the spring-summer ACC (Pondaven et al., 2000; Brzezinski et al., 2001; Quéguiner and Brzezinski, 2002). Higher diatoms biomass in the southern ACC results much as probably from Si-limitations north of the APF with $Si(OH)_4$ values lower than 2 µmol Si l^{-1} (Franck et al., 2000; Nelson et al., 2001; Sedwick et al., 2002; Brzezinski et al., 2005). Nevertheless, even if there is also a gradient for $bSiO_2$ production towards higher values southward (Figure 4b), it is in the lower range of biogenic silica production encountered in the Southern Ocean similar than for oligotrophic areas (Ragueneau et al., 2000). Integrated $bSiO_2$ production (euphotic layer) rates during BONUS-goodhope along with previous estimates in the Southern Ocean are shown for corresponding area (appendix 1). BONUS-goodhope in late summer 2008 seems to represent the background of biogenic silica production after the growth period occurring previously in the season

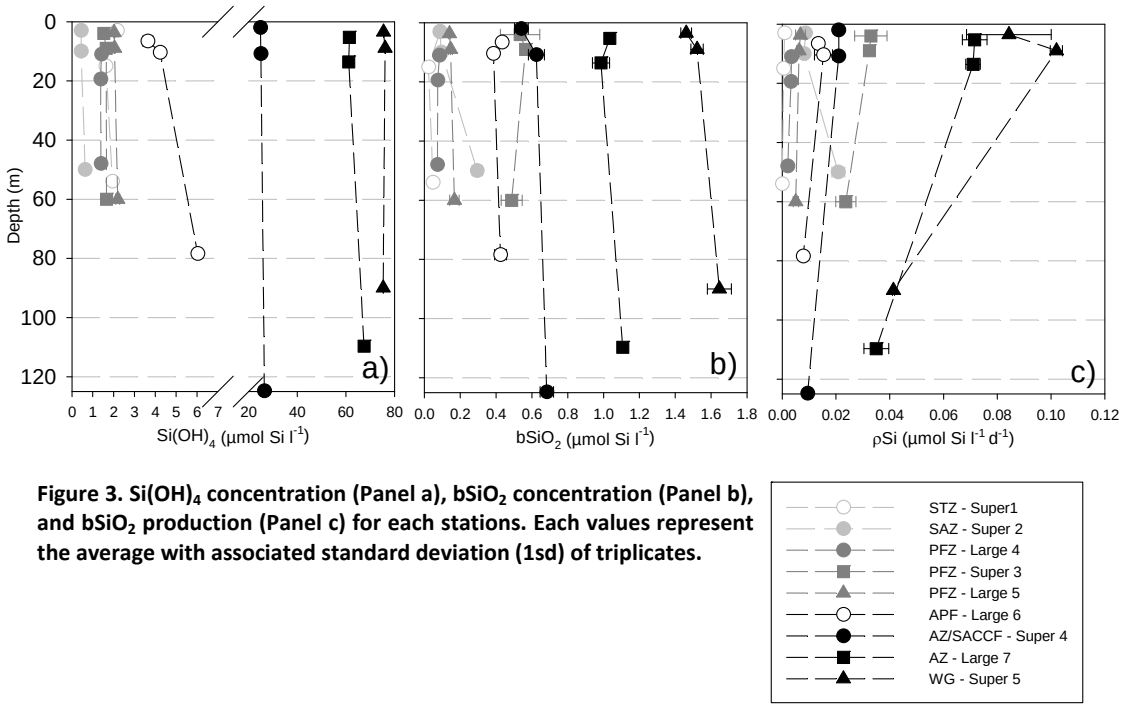

Figure 3. $Si(OH)_4$ concentration (Panel a), $bSiO_2$ concentration (Panel b), and $bSiO_2$ production (Panel c) for each stations. Each values represent the average with associated standard deviation (1sd) of triplicates.

with especially higher expected values in PFZ, AZ, and SIZ (Pondaven et al., 2000; Brzezinski et al., 2001; Quéguiner and Brzezinski, 2002).

This north-south expression of diatoms productivity seems mainly results, as from diatom biomass, from the north-south gradient in $Si(OH)_4$ with biogenic silica production in the northern side of ACC limited by Si-availability (Nelson et al., 2001). Joubert et al. (in prep) observed higher primary production for the same casts and depths in the northern part of the ACC and relatively low values of primary production in the southern part of the transect. This pattern is recurrently observed in the ACC (Griffiths et al., 1999; Boyd et al., 1999; Elskens et al., 2002; Leblanc et al., 2002; Reuer et al., 2007; Cavagna et al., submitted) and reproduced by PP models (Behrenfeld and Falkowski, 1997). The inverse pattern for biogenic silica production indicates that diatoms, as expected (Leblanc et al., 2002; Brzezinski et al., 2003a; chapter 8), contribute more significantly to primary production in the southern part and that primary production in the northern part is dominated by non-siliceous phytoplankton. This distribution is also reflected in Si:N ratios, both for particulate and uptake (N pools and fluxes from Joubert et al., in prep), with higher ratios in the southern than northern parts of the transect (Figure 5). At the Antarctic divergence (south of APF), high values, as expected (Brzezinski et al., 2003a), are observed for Si:N particulate (0.8 to 2.6) and uptake (0.2-0.9) ratios. Since microbial community contains a lot of non-siliceous organisms and that diatoms growing under repleted condition had Si:N ratio of ~1 (Brzezinski, 1985), preferential N remineralization instead of Si during metabolic processes is actively occurring, via the "silicate pump" (Dugdale et al., 1995), giving particulate ratio higher than uptake ratio (Brzezinski et al., 2003a), and above 1. Uptake ratios lower than 1 but anyways still significant indicate that diatoms significantly contributes to primary production in late summer in this area whereas primary production seems mainly driven by non-siliceous phytoplankton much prone to take part in regenerative microbial food web (Smetacek et al., 2004; Safi et al., 2007). Even if one station in the southern Antarctic Zone (Large 7) present Si:N uptake ratio close of 1.

This ratio is also strongly impacted by co-occurring limitations acting on growth rates subsequently increasing silicification processes in most of the cases (Claquin et al., 2002; Brzezinski et al., 2003a; Leynaert et al., 2004; Bucciarelli et al., 2009) and given the false impression than phytoplankton community is driven by repleted diatoms (Brzezinski et al., 2003a).

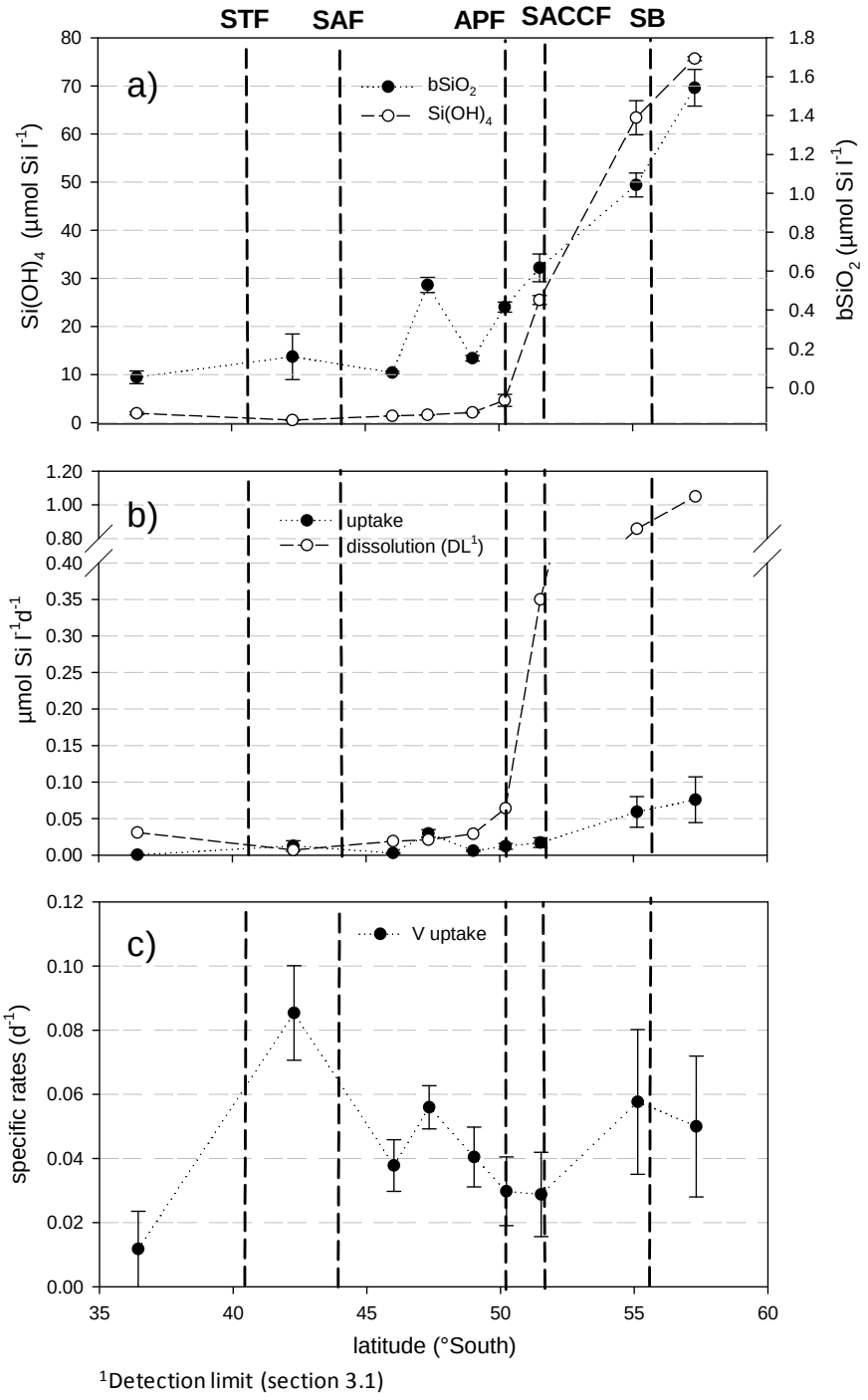

Figure 4. Distribution of station average (with one standard deviation, 1sd) of $Si(OH)_4$ and $bSiO_2$ concentration (Panel a), $bSiO_2$ production and upper estimate of dissolution (Panel b), and specific Si-uptake rates (Panel c) versus latitude.

North of APF in the PFZ, both for particulate and uptake, Si:N ratio are always lower than 1 (Figure 5) but still also anyways significant (respectively 0.1 to 0.8 and 0.0 to 0.3). Late summer PFZ diatoms contribution is lower than south of APF but same processes are also increasing the Si:N ratios from uptake to particulate through metabolic processes (Brzezinski et al., 2003a). PFZ exhibits some variability in term of $bSiO_2$ production and Si:N ratios. Diatoms productivity and contribution to total productivity is more significant at Super 3. At this station, euphotic layer seems more in concordance with mixed layer depth than for the two other stations in PFZ (Larges 4 and 5) with deeper mixed layer than euphotic layer. It is in agreement with the fact that a more favorable irradiance-mixing regime induces higher productivity (Nelson and Smith, 1991; Sambrotto and Mace, 2000; Boyd et al., 2001; de Baar et al., 2005; Cavagna et al., submitted). Arrigo et al. (1999) in the Ross Sea and Fripiat et al. (in prep) in SAZ observed that stratification events could be more favorable to diatoms growth. Krause et al. (2009) in agreement with these observations, suggest that diatoms productivity in the oligotrophic area could be boosted after stratification events following vertical mixing events along with carbon export (McNeil et al., 1999; Conte et al, 2003; McGillicuddy et al., 2007). In PFZ where intense biogenic silica production is occurring in spring especially in this area (Quéguiner and Brzezinski, 2002), the summer mixed layer is strongly depleted, both in iron and $Si(OH)_4$, which may favor the growth of non siliceous, ammonium-driven, iron-efficient phytoplankton species (Brzezinski et al., 2005; Timmermans et al., 2005; Safi et al., 2007). Hydrological dynamic could strongly impact the community structure and subsequently export in late summer in this

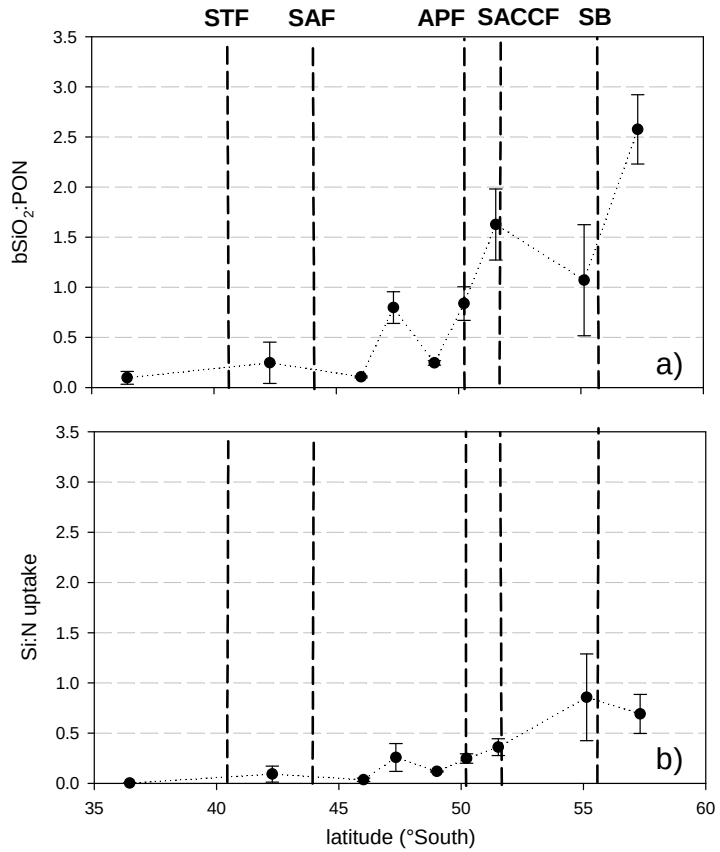

Figure 5. Distribution of station average (with one standard deviation, 1sd) of particulate (Panel a), and uptake (Panel b) Si:N ratios versus latitude. N-stock and fluxes are provided in Joubert et al. (in prep).

area in supplying nutrients and forming favorable light mixing regimes.

In STZ and SAZ, especially low values, both for particulate and uptake Si:N ratios, are observed (respectively 0.1 and 0.2 for STZ and SAZ, and 0.0 and 0.1). As observed in Lourey and Trull (2003), in Leblanc et al. (2002) and in Fripiat et al. (in prep), diatoms contribution to primary production and C-export is low and similar than in the oligothropic area mainly due to $Si(OH)_4$ limitation. Large variability is classically observed in this area in term of C and Si productivity due to several co-limitations occurring in a complex temporal and spatial interplay (Boyd, 2002). One station is clearly not representative of all the corresponding area, STZ or SAZ, especially in this Southern Ocean sector where intense mesoscale dynamics is observed via exchange processes allowing Indo-Atlantic oceanic connection. As suggested in Fripiat et al. (chapter 8) from observation in oligotrophic area (Krause et al., 2009) and discussed for PFZ sector, some mixing and stratification event inducing non-equilibrium conditions could allows significant contribution of diatoms to primary production and export difficult to assess with this sampling resolution.

Dehairs et al. (in prep) and Verdeny et al. (in prep) observed higher C-export south of SAF suggesting higher export efficiency than in SAZ and STZ where a higher primary production is observed triggering mainly by regenerative process inducing lower C export efficiency (Joubert et al., in prep). Buesseler (1998) observed that diatoms are located in areas of relatively high carbon export efficiency and that there is strong decoupling between production and particulate export in the ocean. These observation are in agreement with the BONUS-goodhope transect since area where diatoms significantly contribute to primary production are areas corresponding with higher export efficiency but with lower primary production. Nevertheless, C-export is it in the lower range of C export for Southern Ocean (Buesseler et al., 2001) since BONUS-goodhope covering the end of productive period.

Low specific Si-uptake rates (V_{Si}) prevail for complete BONUS-goodhope transect (Brzezinski et al., 2001; Quéguiner, 2001; Fripiat et al., in prep). South of SAF, the V_{Si} is relatively constant (~ 0.05 d^{-1}). North of SAF, SAZ and STZ exhibit respectively the lowest and highest V_{Si} value (0.09 and 0.01 d^{-1}). Such values result from potential strong Si-Fe (trace metals)-Light co-limitations evolving in a different temporal and spatial pattern especially in late summer (Boyd, 2002; Bucciarelli et al., in prep). Such low values are already observed in the Southern Ocean where several factors, especially light and iron (de Baar et al. , 2005) control productivity forming the highest world HNLC area (Martin et al., 1990; Minas and Minas, 1992) subsequently impacting the diatom Si-metabolisms (Martin-Jézéquel et al., 2000).

1.4. Conclusions

This study was investigated in late summer 2008 (8 February to 8 March) across the end of the productive period for the ACC. Whereas to be in the lower range of oceanic observations, diatoms productivity is higher south of APF where $Si(OH)_4$ is high (> 5µmol Si l^{-1}) in comparison with the other part of the transect (<2 µmol Si l^{-1}). Diatoms contributed significantly to total primary production south of APF and in less degree in PFZ. Areas where diatoms contribute significantly to primary production are associated with higher export efficiency in agreement with previous studies which highlighted the key role of diatoms to carbon export in the Southern Ocean (Buesseler et al., 2001; Jin et al., 2006; Honjo et al., 2008). Strong co-limitation processes impose specific uptake rate (< 0.1) to be in the lower range of oceanic observations. BONUS-goodhope transect sampled the end of productive period (Quéguiner and Brzezinski, 2002; Lemoigne et al., in prep; Fripiat et al., in prep). Silicate pump process are still actively

occurring suggesting that whereas more suspected efficient silicon loop triggering mainly by detrital $bSiO_2$ accumulation, the biological pump would still preferentially depleted $Si(OH)_4$ than NO_3 in late summer with significant implication for global biogeochemical properties.

Diatom-induced silicon isotopic fractionation in Antarctic sea ice

JOURNAL OF GEOPHYSICAL RESEARCH, VOL. 112, G02001, doi:10.1029/2006JG000244, 2007

Diatom-induced silicon isotopic fractionation in Antarctic sea ice

François Fripiat,[1,2] Damien Cardinal,[1] Jean-Louis Tison,[3] Anthony Worby,[4] and Luc André[1]

Received 12 June 2006; revised 19 October 2006; accepted 5 December 2006; published 5 April 2007.

[1] In this study, we measure the silicon-isotopic composition δ^{29}Si,‰, relative to NBS28 quartz standard) of dissolved silicon and biogenic silica collected by sequential melting from spring Antarctic pack ice collected near 117°E-64.5°S. This work aims to investigate the use of Si isotopes to quantify the activity of sea-ice diatoms in the different brine structures and the influence of sea-ice diatoms on the spring ice edge blooms. From three cores with contrasted physico-chemical characteristics, we report significant isotopic fractionations linked to diatom activity with distinct silicon biogeochemical dynamics between different brine structures. The diatoms in snow ice and in brine pockets of frazil or congelation ice have the heavier silicon-isotopic composition (+0.53 to +0.86‰), indicating that they grow in a closed system and use a significant fraction of the small dissolved silicon pool available. In the brine channels and skeletal layer, diatoms display a relatively lower silicon-isotopic composition (+0.41 to +0.70‰), although it is still relatively positive compared to expected equilibrium fractionation. This suggests that the diatoms have grown in a semi-closed system where the dissolved silicon pool (i.e., brine) is partially replenished. The silicon-isotopic composition (+0.63‰) of the sea-ice diatoms is much heavier than the one of biogenic silica in the seasonal ice zone mixed layer (+0.09‰). Our results suggest that sea-ice diatoms either contribute to an insignificant part of the whole diatom biomass in the upper water layer, or that they are directly exported below the mixed layer.

Citation: Fripiat, F., D. Cardinal, J.-L. Tison, A. Worby, and L. André (2007), Diatom-induced silicon isotopic fractionation in Antarctic sea ice, *J. Geophys. Res.*, *112*, G02001, doi:10.1029/2006JG000244.

1. Introduction

[2] Sea-ice diatom-dominated primary production plays a leading role in the ecology of the polar oceans because it is the sole source of fixed carbon for the upper trophic levels of sea-ice covered waters [*Arrigo*, 2003; *Arrigo and Thomas*, 2004]. In fact, sea-ice diatoms represent 65–95% of the sea-ice biomass [*Mathot et al.*, 1991] because they are physiologically able to maintain higher growth rates under sea-ice conditions than the other phytoplankton groups [*Gleitz et al.*, 1998; *Lizotte*, 2003]. Moreover, once released into the surface seawater during melting, they have been shown to have a seeding effect that may trigger spring phytoplankton blooms [*Smith and Nelson*, 1985, 1986; *Garrison et al.*, 1987; *Garrison and Buck*, 1989; *Michel et al.*, 1993; *Lancelot et al.*, 2000; *Goffart et al.*, 2000]. Other studies, however, favor rapid export out of the mixed layer soon after melting, either by grazing or aggregation [*Mathot et al.*, 1991; *Riebesell et al.*, 1991; *Lancelot et al.*, 1993; *Sharek et al.*, 1994; *Michel et al.*, 1996, 1997].

[3] Sea-ice diatom productivity is likely to be a significant factor in Southern Ocean biogeochemical cycling of C, N, Si, P, S and Fe, and this is presently the focus of investigation in the context of climate change. The algae activity can be qualitatively estimated from the composition of brine nutrients (nitrate, phosphate, silicic acid, nitrite and ammonium) and their deviation, either by consumption or remineralization/dissolution, relative to the dilution curve of seawater [*Clarke and Ackley*, 1984; *Meese*, 1989; *Dieckmann et al.*, 1991; *Gleitz et al.*, 1995; *Thomas and Papadimitriou*, 2003]. However these estimates only represent a final snapshot of the nutrient content of the brine at the time of sampling, and are not representative of the bulk diatom history. This implies difficulties in evaluating the initial nutrient concentrations of the different sea-ice structures, including brine channels, brine pockets, intracrystalline brine layers, and brine feeder tubes. Bias can occur either when sporadic nutrient replenishments or brine drainage processes take place that are not in synch with the diatom activity, or when past diatom generations preserved in the brine structure dissolve. Si isotopes have been proposed as a means to measure the relative dissolved silicon

[1]Department of Geology and Mineralogy, Section of Mineralogy and Petrography, Royal Museum for Central Africa, Tervuren, Belgium.
[2]Also at Laboratoire de Glaciologie Polaire, Département des Sciences de la Terre et de l'Environnement, Université Libre de Bruxelles, Brussels, Belgium.
[3]Laboratoire de Glaciologie Polaire, Département des Sciences de la Terre et de l'Environnement, Université Libre de Bruxelles, Brussels, Belgium.
[4]Department of the Environment and Water, Australian Antarctic Division and Antarctic Climate and Ecosystems Cooperative Research Centre, Hobart, Tasmania, Australia.

0148-0227/07/2006JG000244$09.00

use by diatoms because these organisms preferentially incorporate light isotopes, with apparently no dependence on temperature or species [*De La Rocha et al.*, 1997], pH [*Milligan et al.*, 2004] or salinity [*Alleman et al.*, 2005]. Their potential has been confirmed through marine and fresh water studies [*De La Rocha et al.*, 2000; *Varela et al.*, 2004; *Cardinal et al.*, 2005, 2007; *Alleman et al.*, 2005] which have demonstrated their usefulness in quantifying diatom dynamic growth and their effect on the dissolved silicon pool. From this perspective, this study is the first to provide sea-ice silicon isotope data, both in the biogenic fraction and in the brine, and to explore their use for quantifying the diatom activity in the pack ice. As the physical ice characteristics, such as temperature, salinity, brine and crystal structure, have important effects on biological processes [e.g., *Clarke and Ackley*, 1984; *Cota et al.*, 1987; *Cota and Horne*, 1989; *Eicken*, 1992], the Si-isotopic composition of different ice types such as snow ice, frazil and congelation ice are compared. Furthermore by confronting the Si-isotopic signature of the sea-ice diatoms to that of the upper water column diatoms (collected in the seasonal ice zone [*Varela et al.*, 2004; *Cardinal et al.*, 2007]), we investigate the influence of sea-ice diatoms on the Si-isotopic composition of the spring ice edge bloom.

2. Materials

[4] In spring, Antarctic pack-ice primary productivity occurs in various layers within the ice [e.g., *Horner*, 1985; *Arrigo*, 2003; *Arrigo and Thomas*, 2004]. In the bottom section, where the temperature is above $-5°C$, a threshold above which the brine network becomes interconnected in ice with >5‰ bulk ice salinity [*Golden et al.*, 1998; *Golden*, 2001], allowing exchanges with the underlying seawater. This section includes the so-called ''skeletal layer'' which has increased porosity consisting of intracrystalline brine layers and a complex connecting brine network running through it. In the upper section, which is below $-5°C$, the primary productivity is sparse because the environmental conditions (low temperature, confined space, high salinity) are unfavorable. An exception to this is the surface snow ice layer where primary productivity can occur, linked with the sporadic input of nutrients from seawater flooding of snow and subsequent refreezing. Our study will investigate ice core samples from each of these environments that are potentially favorable to diatom growth.

[5] Ice cores were collected during the ARISE (AU0301) campaign aboard RV *Aurora Australis* in 2003, which took place in the beginning of spring (September–October). The physical properties of the ice at this time of year change rapidly and this affects the sea-ice biogeochemistry. A total of 13 ice stations were undertaken during the voyage, of which three have been selected for detailed analysis in this paper. These are sites III, IV, and V from the pack ice region located at $\sim$64.5°S, 117°E, located just offshore from Australia's Casey station. Vertical profiles of ice texture, in situ temperature, ice salinity, relative brine volume (V_b/V = ratio between brine volume and ice volume) and chl-a are available from *Lannuzel et al.* [2007] and *Tison et al.* [2004], and summarized in Table 1. These parameters were measured on different cores, collected within 20 cm of each other, at each station. Stations IV and V show the typical binomial layering of first year pack ice, which consists of frazil ice (ice with equigranular crystals formed under turbulent conditions) at the top and congelation ice below (ice with vertically elongated crystals formed by downward growth under quiescent conditions). The ice at Station III was thicker (155 cm) and of peculiar origin since it shows no columnar ice (80% of frazil ice, 20% of snow ice). Stations III and V display a snow ice layer (equigranular ice formed when seawater infiltrates the snow cover by flooding) of 30 cm and 20 cm respectively. The ice of Station IV is $<-5°C$ (except for the bottom 20 cm), and therefore in a ''cold regime'' with a brine network mostly not connected [*Golden et al.*, 1998; *Golden*, 2001; *Lannuzel et al.*, 2007]. This is supported by thin section analysis [*Tison et al.*, 2004] which shows no sign of a warming-cooling event [*Tucker et al.*, 1987; *Tison et al.*, 2002]. In contrast, stations III and V are mostly under a milder temperature regime [*Tison et al.*, 2004; *Lannuzel et al.*, 2007] as the $-5°C$ isotherm is near the surface of the ice floe and most of the brine network are interconnected. This strong contrast in the temperature regime of cores from the same region is most likely caused by the large difference in the insulating snow cover thickness between sites (Table 1). These three cores were therefore chosen for their very distinct physico-chemical characteristics.

[6] In situ dissolved Si was sampled using the ''sackhole'' method. This involves drilling a hole at two different depths in the ice cover, based on the temperature profile. One hole is drilled above the $-5°C$ isotherm, and one below it. This enables the brine to seep out of the surrounding ice and be collected in the bottom of the hole. This method allows the sampling of large brine volumes but has the disadvantage that the ice volume feeding the collected sample is unknown. The samples were filtered onto 0.4-μm polycarbonate membranes, but unfortunately these filters were not available for the measurements of isotopic composition of bulk biogenic silica.

[7] For laboratory biogenic and dissolved silicon extractions, blocks $\sim$10 cm thick (200–400 mL) were cut from ice cores with a steel saw in a cold room at $-25°C$. The exact depth intervals are reported in Table 1. Each block was sequentially melted, either naturally at +3°C or in a microwave oven using warming cycles of 10 s. This enabled us to separate the different phases (brine vs. pure ice) by their melting point, in order to collect the most saline fractions first, followed by the less saline aliquots. The melted samples were collected every $\sim$10–50 mL and immediately filtered through a 0.4 μm polycarbonate membrane to separate biogenic silica (BSi) from dissolved silicon (DSi). Unlike the sackhole sampling method, the sequential melting does not provide a sufficient sample of DSi to perform isotopic analyses. However, it does allow us to separate the different brine structures (see below) which is not possible using the bulk brines collected from sackholes.

3. Analytical Methods

[8] We apply a wet-alkaline digestion on filter samples (adapted from *Ragueneau et al.* [2005]), which involves dissolving biogenic silica with a 0.2 M NaOH solution (pH 13.3) at 100°C for 40 min. As this digestion can also dissolve a part of lithogenic silica, we also analyze

Table 1. Si-Isotopes Data With Physico-Chemical and Biological Characteristics for Studied Ice Cores and Blocks[a]

Station	Coring Date	Total Length, cm	Depth of −5°C Isotherm, cm[b]	Block	Depth, cm[b]	Ice Texture	T°C	V_b/V[c]	Chla, $\mu g\ L^{-1}$	Bsi Fraction[d]	Sal,[d] ‰	Dsi,[d] $\mu mol\ L^{-1}$	Bsi,[d] $\mu mol\ L^{-1}$	$\delta^{29}Si_{BSi}$,[d] ‰ ± $2\sigma_M$	Depth, cm[b]	$\delta^{29}Si_{DSi}$,[e] ‰ ± $2\sigma_M$
III	30-Sep-03	ice: 155	12	A	0–10	snow ice	−5.5	0.06	4.0	bulk	14.0	10.8	7.3	0.68 ± 0.09		
		snow cover: 25		C	145–155	frazil	−2.0	0.05	1.2	t_1	9.7	7.3	31.1	0.61 ± 0.08	0–60	1.17 ± 0.08
										t_2	4.0	5.1	22.3	0.49 ± 0.07		
IV	1-Oct-03	ice: 48	30	B	22–28	congelation	−6.0	0.04	0.1	t_1, t_2	5.8	5.4	11.9	0.41 ± 0.07	0–25	n.a
		snow cover: 2		C	40–48	congelation	−3.0	0.10	18.0	bulk	9.0	9.1	163.4	0.58 ± 0.08		
										t_1	18.3	21.5	443.0	0.52 ± 0.08	0–40	0.88 ± 0.08
										t_2	14.4	10.1	113.0	0.63 ± 0.08		
										t_3	4.2	3.7	77.6	0.72 ± 0.09		
										t_4	0.5	4.3	82.1	0.53 ± 0.08		
V	7-Oct-03	ice: 80	11	A	07–17	snow ice	−5.0	0.07	5.0	bulk	3.2	3.2	7.0	0.73 ± 0.07		
		snow cover: 20		C	70–80	congelation	−2.0	0.24	26.0	bulk	6.0	n.a	105.3	0.68 ± 0.08		
										t_1	14.8	n.a	68.9	0.70 ± 0.08	0–45	n.a
										t_2	4.7	n.a	180.3	0.60 ± 0.07		
										t_3	2.1	n.a	120.7	0.67 ± 0.07		
										t_4	0.2	n.a	64.0	0.86 ± 0.07		

[a]A, surface; B, internal; C, bottom. Here n.a. means ''not available.'' The notations (t_1, t_2, t_3, t_4) are the same as in Figure 1. Ice temperature, relative brines volume (Vb/V), and chl-a are from *Tison et al.* [2004] and *Lannuzel et al.* [2007].

[b]Depth from the surface.

[c]Relative brines volume.

[d]Si_{BSi}, Si_{DSi}, and Sal sampled with the sequential melting (bulk $\delta^{29}Si_{BSi}$ has been calculated by weighted average of the different BSi fractions collected by sequential melting, and DSi and Sal is the weighted average of the DSi fraction merged to do BSi fraction).

[e]Si_{DSi} sampled with the sackholes method.

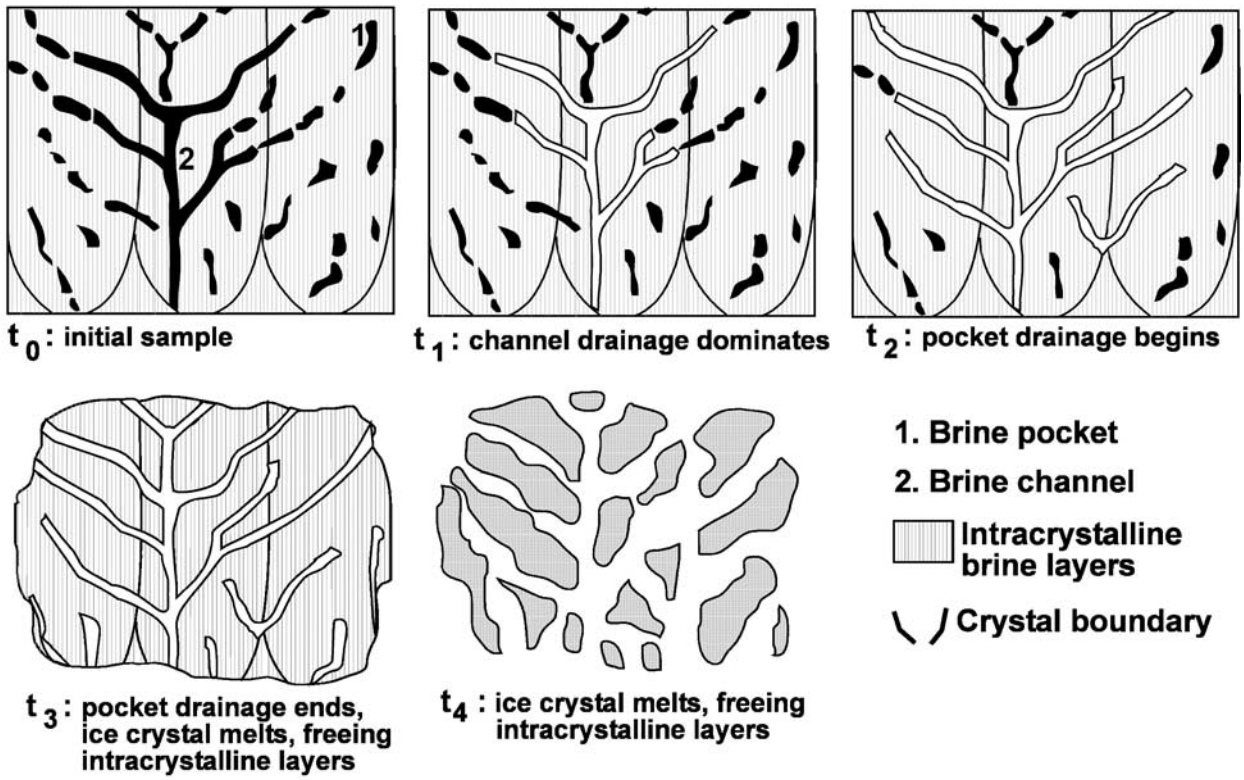

Figure 1. Sketch showing the potential stages of the drainage process within a sea-ice sample as it is progressively warmed up (sequential melting). Sal_{t1}(‰) = 19 ± 10, Sal_{t2}(‰) = 8 ± 6, Sal_{t3}(‰) = 3 ± 1.5, Sal_{t4}(‰) = 0.5 ± 0.5.

aluminium in the digested solution, which provides a proxy of the potential lithogenic source. Al remains below the ICP-AES detection limit (0.05 ppm) supporting a negligible lithogenic Si-derivation. For each aliquot from the sequential melting, salinity was estimated by measuring the concentrations of major cations (Ca^{2+}, Mg^{2+}, K^{+} and Na^{+}) along with the concentration of the biogenic and dissolved silicon by ICP-AES. This method only provides an estimate of the bulk salinity of the aliquots and has been used here for the purpose of having a relative term of comparison between samples of limited volume.

[9] Silicon was purified through its quantitative reaction with triethylamine-molybdate [*De La Rocha et al.*, 1996]. Si-isotopic compositions were then measured on a Nu Plasma MC-ICP-MS, using Mg external doping in dry plasma mode, following *Cardinal et al.* [2003]. The results are presented relative to NBS28 quartz standard as δ^{29}Si (‰), = $[(^{29}Si/^{28}Si)_{sample}/(^{29}Si/^{28}Si)_{NBS28} - 1] \times 1000$, because ^{30}Si cannot be measured on the Nu Plasma because of an irresolvable $^{14}N^{16}O$ interference. Assuming a kinetic mass-dependent fractionation [*Young et al.*, 2002], δ^{29}Si can be converted to δ^{30}Si by applying a multiplying factor of 1.96. The triethylamine-molybdate step requires a minimal quantity of 2.5 μmol of silicon, so we sometimes had to merge samples in order to measure the isotopic composition. Owing to this sample size limitation, we could not analyze replicates. Nevertheless full replications (including the triethylamine-molybdate step) are usually within ±0.08‰ (±2σ) [*Cardinal et al.*, 2003, 2005; *Carignan et al.*, 2004].

4. Results

[10] The salinity of the first fractions collected during the sequential melting experiments was 19 ± 10‰ which is much lower than the expected range of brine salinity (37.6‰ < S < 209.9‰) within the potential −2°C to −20°C temperature interval [*Cox and Weeks*, 1983]. This indicates that the sequential melting procedure does not collect pure brine samples because: (1) both the relatively small volume of the sample block and the geometry of the apparatus result in simultaneous melting of the pure water ice areas in contact with the container's walls and (2) the sampling of brine pockets and intracrystalline brine layers requires partial melting of some surrounding pure ice crystals (Figure 1). However the sequential melting produced a continuous sequence of liquid with decreasing salinity (19 ± 10‰ to 0.5 ± 0.5‰). This suggests that the volumetrically large connected brine structures (intracrystalline layers in the skeletal layer, channels and their feeder branches) were likely to be drained before the smaller and more isolated brine pockets which are trapped within the ice structure as shown schematically in Figure 1.

[11] (Figure 2) presents the two trends usually observed for the dissolved silicon (DSi) with regards to the dilution curve of seawater (at the ice-water interface; DSi = 61 μmol L^{-1}

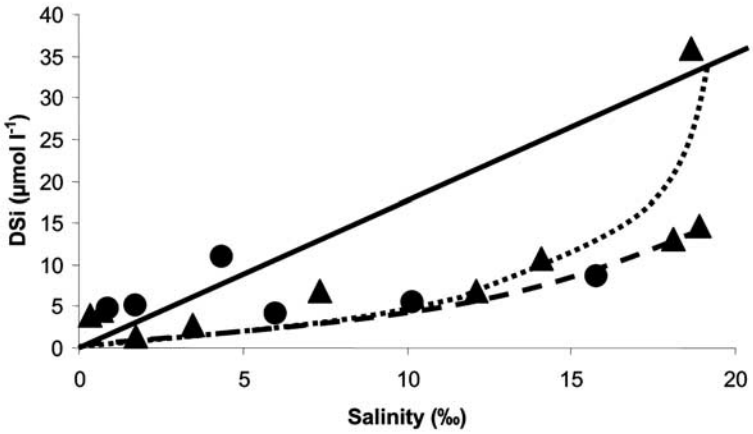

Figure 2. DSi versus brine salinity trends for sequential melting in snow ice (dashed line) and congelation or frazil ice (dotted line) compared to the theoretical seawater dilution curve (solid line). The triangles represent the results for the block IV C (bottom) and the circles the block III A (snow ice).

and S = 34.5‰). All blocks with the exception of the snow ice (III A and V A), show the same trend: the first fraction collected during the sequential melting lies on the seawater dilution curve but all other successive fractions are below. In the case of snow ice all fractions, including the first one, are below the seawater dilution curve. The fact that some aliquots lie slightly above the sea water conservative dilution curve probably results from uncertainties in the bulk salinity estimates (see section 3).

[12] Table 1 summarizes the main physico-chemical and biological characteristics of the studied ice samples. It also provides the Si-isotopic signatures along with their standard deviation (2σ) of both the bulk brine from in situ sackholes and the biogenic fractions collected during the sequential melting experiments (steps t_1, t_2, t_3, t_4 of Figure 1). In snow ice, biogenic silica has similar positive signatures at two different stations ($\delta^{29}Si_{BSi}$ at +0.67‰ and +0.73‰ for cores III and V respectively). The ''internal'' ice sample at temperature below −5°C (block IV B) shows the lowest measured $\delta^{29}Si_{BSi}$ (+0.41‰) of the data set presented here. The ''bottom'' samples (blocks C), which are the only samples where it has been possible to measure the Si-isotopic signature on the different fractions collected during the sequential melting, have $\delta^{29}Si_{BSi}$ in the range of +0.49 to +0.86‰ (Table 1). The biogenic silica of fractions t_1 and t_2 display a less positive Si-isotopic composition (+0.49 to +0.70‰) than fractions t_3 and t_4 (+0.53 to +0.86‰), with the exception of fraction t_4 of the block IV C which exhibits the same $\delta^{29}Si_{BSi}$ as the first fraction (+0.53 and +0.52‰ respectively). All the other Si-isotopic compositions of fractions t_3 and t_4 lay between +0.67 and +0.86‰.

[13] The isotopic composition of the dissolved silicon source, i.e., the seawater at the ice-water interface, is the same for two stations (average = +0.91 ± 0.02‰) and is almost exactly the same as the one measured for seawater in the seasonal ice zone during spring 2001 at 140°E (+0.93 ± 0.04‰) by *Cardinal et al.* [2005]. The $\delta^{29}Si_{DSi}$ measured in sackhole brine of core IV (>−5°C) is not significantly different (+0.89‰) from the one measured in seawater at the interface. On the contrary, sackhole brine from core III (>−5°C), shows the heaviest $\delta^{29}Si_{DSi}$ (+1.17‰) of the data set.

5. Discussion

5.1. Bulk Sackhole Brines Si Signature

[14] Interpretation of the dissolved Si-isotopic signature of bulk sackhole brine is complex because of the unconstrained origin of the sample from the surrounding sea-ice cover. For the same reason, caution must be exercised when comparing these values to the results of the biogenic silica analyses from the sequential ice melting experiments described above.

[15] The Si-isotopic signature of the bulk brines for the lower part of station IV (above −5°C) is not significantly different from the seawater underneath (Table 1). This supports negligible Si consumption relative to the DSi pool, even though the BSi content was high and the bulk $\delta^{29}Si_{BSi}$ relatively positive (+0.58‰), suggesting significant diatom activity. This can be explained by important exchanges with the underlying seawater, which has a constant Si-isotopic signature. The $\Delta^{29}Si$ ($=\delta^{29}Si_{BSi} - \delta^{29}Si_{DSi}$) is smaller (−0.21‰) than the equilibrium fractionation factor, $^{29}\varepsilon$, (−0.57 ± 0.21‰ [*De La Rocha et al.*, 1997]), indicating a mixing process, either by convection or diffusion [*Eide and Martin*, 1975; *Wakatsuchi and Ono*, 1983; *Worster and Wettlaufer*, 1997; *Wettlaufer et al.*, 1997] which would entrain isotopically light silicic acid from underlying seawater into the brine network. This would act to diminish the difference between the Si-isotopic signature of the diatoms previously formed and the DSi pool [*Cardinal et al.*, 2007].

[16] Sackhole brine collected in the lower part of the ice cover at Station III (above −5°C) at +1.17‰ indicates an enrichment of the brine in the heavy isotopes, providing evidence for a significant consumption of the DSi pool by diatoms. This is in apparent contradiction with the thermal regime of the ice (>−5°C) that should favor important silicon exchanges with the underlying seawater reservoir. However, the ice here is exclusively of granular texture, which probably hampers brine exchanges compared to

congelation ice. Indeed, *Tison and Verbeke* [2001] have shown that brine channel density is lower in granular sea ice than in columnar sea ice, at equivalent growth rates. In addition, the ice cover is 2 to 3 times thicker at Station III. Thus the sackhole brine sample integrates a depth range that includes some ice located far away from the ice-water interface. The greater thickness should also decrease the exchange rates with the water reservoir, as described by *Thomas and Papadimitriou* [2003].

5.2. Si Dynamics in Sea-Ice Brine

5.2.1. In Search of an Isotopic Model

[17] Our Si-isotopic measurements on sequential melting fractions demonstrate different biogeochemical Si dynamics for different ice types and thermal regimes. Two simple models have been proposed to account for isotopic fractionation induced by the formation of a product (in our case silica) from a dissolved pool (dissolved Si): the Rayleigh model [*Mariotti et al.*, 1981] and the steady state model [*Sigman et al.*, 1999], for a closed or open system respectively. In sea ice, the Rayleigh model should be more appropriate to account for the Si-isotopic fractionation by diatoms in closed systems such as brine pockets, intracrystalline brine layers or snow ice. Furthermore, our measurements of the integrated Si-isotopic signature were made from several generations of diatoms, rather than from diatoms grown at a given time, and would therefore be best described by the accumulated biogenic silica rather than the instantaneous biogenic silica. The steady state model can be thought of as an open system with the addition of continuous, infinitesimal mixing events that supply dissolved silicon with the same isotopic signature as the source [*Sigman et al.*, 1999]. It requires a strict equilibrium with the inflows of Si in the dissolved pool equaling the uptake into the biogenic pool, thereby keeping the DSi concentration constant. Although the steady state model is conceivable in the open ocean where the surrounding waters can be considered as "isotropic" in terms of nutrient availability at the diatom scale, the situation is likely to be much more complex in the permeable sea-ice brine network. There, nutrient availability will be strongly dependent on the brine network geometry (predominantly vertically structured). Isotopic fractionation could indeed be close to the predictions of an open steady state model for the diatoms located at the ice-ocean interface. However, for those living further inside the permeable brine network, nutrient input will depend on the distance to the ice-ocean interface and on the depletion history of the DSi pool related to the uptake from the diatoms closer to the interface. This could be seen, in a simplified way, as a boundary layer fractionation model, in which the transport of the isotopic species toward the diatom membrane is driven by diffusion only, but with a varying boundary layer thickness, depending on the location of the diatom within the permeable brine network. The larger the boundary layer thickness, the closer the model will be to a Rayleigh case. During the sequential melting procedure, the first aliquot collects the majority of the diatoms attached within the whole interconnected brine network. It therefore integrates different steady state conditions (both spatially and temporally) in its biogenic δ^{29}Si signal. In the absence of a more sophisticated isotopic model, the steady state model might be used, at least semiquantitatively, as a high estimation of the relative use of the DSi pool. However this will only provide an average relative use of the DSi pool for all diatom populations and generations from the same complex permeable structure.

[18] These models will give us "f" (= $DSi_{measured}/DSi_{initial}$), the remaining silicon fraction, which is a measure of exhaustion of the DSi pool and so the diatom activity. Two parameters must be known for characterizing "f."

[19] Firstly, the isotopic signature of the source of dissolved silicon ($\delta^{29}Si_{DSi0}$), i.e., the underlying seawater, has been determined at +0.91 ± 0.2‰. Since the primary production under the ice sheet is not significant [*Arrigo*, 2003], the Si-isotopic composition remains unchanged from the beginning of the formation of the ice sheet until its break up. This assumption might not be valid for brine pockets in frazil ice which form in autumn from seawater with potentially significant diatom activity [*Arrigo and Thomas*, 2004] that may induce local isotopic changes. Since we have not measured the Si-isotopic composition in this ice type, it is not an issue for this study. It should also be noted that there is limited spatial variability at the regional level, since the Si-isotopic composition of the underlying seawater at two different stations (III and V) is similar. This is supported by *Cardinal et al.* [2005] who also measured the same Si-isotopic signature for seawater in the seasonal ice zone during spring 2001 at 140°E.

[20] Secondly, the diatom-water Si-isotopic equilibrium fractionation factor ($^{29}\varepsilon$), which has been established experimentally at −0.57 ± 0.21‰ by *De La Rocha et al.* [1997] and confirmed, within the reported error, by *Milligan et al.* [2004] (−0.79 ± 0.1‰). In the Southern Ocean, *Varela et al.* [2004] have determined a fractionation factor in summer varying between −0.52‰ and −0.88‰, calculated by the Rayleigh model and open steady state models respectively. In spring, under a more intense mixing regime, and using a multibox approach, *Cardinal et al.* [2005] estimated a fractionation factor (−0.53 ± 0.16‰) similar to the one of *De La Rocha et al.* [1997] measured south of the polar front.

[21] In the following sections, we will apply the Rayleigh and the open steady state models to our data set, using the experimental fractionation factor of *De La Rocha et al.* [1997] to assess the state of exhaustion of the DSi pool with the "f" value (= diatoms activity) of the remaining silicon fraction. In view of the assumptions inherent in the models discussed above, and because some recent indications suggest a possible dependency of the fractionation factor on various experimental parameters [*Cardinal et al.*, 2007], these "f" values have to be considered as "first-order" approximations. Further work is clearly needed to improve the sampling resolution, the fractionation factor estimates, and the concept of the fractionation model, before a precise quantitative use of silicon isotopes in sea ice can be achieved.

5.2.2. Frazil and Congelation Ice Signatures

[22] All the first fractions sampled during sequential melting from frazil and congelation ice are on the dilution curve (trend shown in Figure 2), which indicates either a lack of consumption by diatoms or remineralization of biogenic silica, or that the consumption-remineralization processes are somehow balanced by large exchanges with seawater. Note that with the exception of aliquot t_1 from

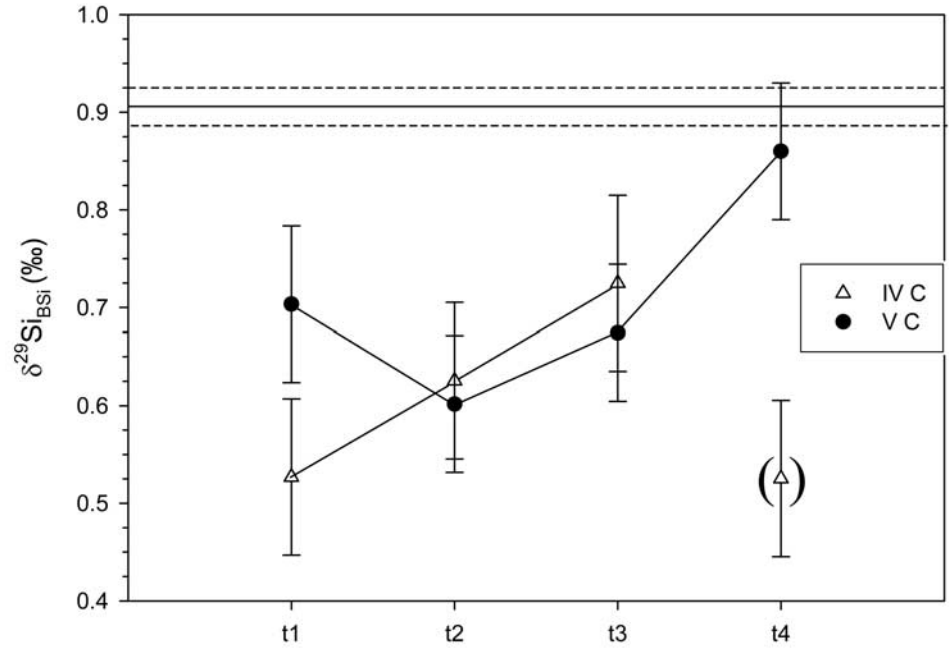

Figure 3. Silicon isotopic signatures of biogenic silica ($\delta^{29}Si_{BSi}$) in the bottom blocks (block C of the Stations IV and V, Table 1). The notation (t_1, t_2, t_3, t_4) is the same that in the Figure 1. The horizontal line at +0.91 ± 0.02‰ is the value of the dissolved silicon source (seawater at the ice-water interface) with two error bars (two dashed lines). The brackets for the samples IV C t_4 indicate that it is out of the trend (see text).

sample V C (which probably did not collect all the diatoms fixed on the brine channels' walls), these fractions exhibit the highest concentration of biogenic silica (Table 1). This is evidence that some DSi must have been consumed by diatoms. These fractions represent open brine structures where significant exchanges with seawater are likely to have occurred [*Weeks and Ackley*, 1986]. The next samples collected, which are all below the dilution curve in the DSi/Salinity diagram, indicate a net consumption of dissolved silicon by diatoms, and therefore a rather closed system. The last fractions sampled sometimes plot slightly above the sea water dilution curve which, as suggested earlier, may reflect an underestimate of the bulk salinity. This suggests a progressive closure of the system.

[23] This is confirmed by the biogenic silica isotopic signatures of the bottom congelation ice (blocks IV C, V C) which exhibit a general trend toward more positive values throughout the sequential melting process (Table 1 and (Figure 3); the block III C is not shown in Figure 3 because we have only the Si-isotopic compositions of the fractions t_1 and t_2 for this sample). Hence the initial fractions collected are representative of the brine channels, or layers trapped within the skeletal layer, both of which are characterized by large primary production and potential exchanges of nutrients with seawater [*Weeks and Ackley*, 1986]. However, the isotopic signatures of the biogenic silica in these brine aliquots are relatively positive (+0.49 to +0.70‰; station III included), supporting a significant use of the DSi pool. Applying the open steady state model gives DSi pool use estimates between 25 and 60%. Therefore these brine structures are likely to represent a semi-closed system, where the diatoms consume DSi before the pool has been replenished by exchanges with the underlying seawater. Consequently our $\delta^{29}Si_{BSi}$ data suggest that convection or diffusion in the brine system [*Eide and Martin*, 1975; *Wakatsuchi and Ono*, 1983; *Worster and Wettlaufer*, 1997; *Wettlaufer et al.*, 1997] cannot be fast enough to replenish the DSi pool at all times.

[24] The last fractions collected represent the closed brine pockets and intracrystalline layers, with limited primary production or potential for nutrient exchange [*Weeks and Ackley*, 1986]. In these cases, the observed Si-isotopic composition of biogenic silica supports a more significant relative use of the DSi pool than in the open structures. However, the lower biogenic silica isotopic signature of the last fraction from block IV C (t_4) stands out as an exception to the trend described above (Figure 3). A plausible explanation can be the proximity of the −5°C isotherm, suggesting that the environmental conditions of the corresponding brine pockets and intracrystalline brine layers were favorable for primary production for only a short time before sampling. Consequently the diatoms have used a less significant part of the dissolved silicon pool than in the other more readily accessible brine inclusions of samples IV C t_2-t_3. The DSi pool use estimates range here between 50 and 100% when applying the Rayleigh model. Removing the outlier IV C t_4 brings this range between 80 and 100%.

[25] The first fractions of the internal blocks, at in situ temperatures below −5°C (IV-B, Table 1), display the lowest measured biogenic silica isotopic signature of the data presented in this paper (0.41‰, Table 1). This suggests that the diatoms were incorporated in the sea ice at the very beginning of the DSi use, probably when they were at the ice-water interface at the beginning of the winter. Afterward their growth probably stopped owing to the unfavorable environmental conditions [e.g., *Gleitz et al.*, 1995], and they have

therefore had little effect on the available DSi pool (the open steady state gives a Si utilization estimate of less than 10%). The relatively low chl-a peak (0.140 μg/L) and the high percentage of dead diatom frustules (S. Becquevort, personal communication, 2006) are in agreement with this hypothesis.

5.2.3. Snow Ice Signatures

[26] Because snow ice is an environment where the diatoms are only supplied with nutrients by sporadic seawater infiltration [*Arrigo and Thomas*, 2004], diatoms can easily be cut off from their nutrient supply. According to our $\delta^{29}Si_{BSi}$ data (III-A and V-A in Table 1), diatoms have consumed a large part of their available dissolved silicon pool: 80 to 90% from the Rayleigh model.

5.3. Potential Contribution of Sea-Ice Diatoms to Spring Ice Edge Blooms

[27] The isotopic signature of biogenic silica in sea ice (mean = +0.63 ± 0.12‰, Table 1) is much more positive than those reported for biogenic silica in the seasonal ice zone mixed layer during spring (AESOPS survey and process 1, +0.12 ± 0.12‰ [*Varela et al.*, 2004]; CLIVAR-SR3, +0.06 ± 0.18‰ [*Cardinal et al.*, 2007]). The sea-ice diatoms therefore represent either an insignificant part of the diatom biomass in the mixed layer after the sea-ice break up, or are directly exported out of the mixed layer. Such a large difference is very significant analytically and, in the following, we discuss the possibility to use it as a tracer of diatoms grown within sea ice. The contribution of such diatoms to the deep ocean BSi flux is unknown. *Gersonde and Zielinski* [2000] have measured large sea-ice diatom fluxes in sediment traps soon after ice melt, but it is impossible to determine the proportion of diatoms grown in sea ice vs. those grown in surface waters after seeding, because both processes result in diatom assemblages typical of sea ice. We suggest that the isotopic composition of BSi in sediment traps could be used to estimate the sea-ice contribution to this flux. In contrast, for paleoceanography studies, given the relatively low BSi budget in sea ice compared to the mixed layer integrated over the growth season, it is unlikely that such isotopic differences could be measurable in sediments as a means to track sea-ice extent. Indeed, *Gersonde and Zielinski* [2000] observed in surface sediments that the sea-ice diatoms represent a maximum of 15% in the marginal ice zone. Even if all these diatoms grew within sea ice (which is obviously an overestimate), giving a mean sea-ice Si-isotopic signature of +0.63 ± 0.12‰, they would induce a shift in the Si-isotopic composition in surface sediments close to 0.08‰, which is the standard deviation (2σ) of the measurements. A similar approach has been proposed for carbon isotopes [*Arrigo and Thomas*, 2004] but the C isotopic difference is much larger (up to 22‰) than for silicon. Clearly further work is required to confirm that the Si isotopic difference between diatoms in sea-ice and in the mixed layer is a recurrent feature.

6. Conclusions and Perspectives

[28] This study provides the very first data on the dissolved and biogenic Si-isotopic signature in sea ice. Our isotopic data indicate that diatom activity and the Si-biogeochemical dynamic in sea ice vary significantly between different brine structures. The brine channels, their feeder branches, and the intracrystalline brine layers in the skeletal layer represent semiclosed systems where diatoms consume a significant part of the DSi pool (i.e., brine) which is only partially replenished by convection or diffusion with the underlying seawater. The brine pockets and the intracrystalline brine layers trapped in the ice structure behave as closed systems, where a more significant part of the small DSi pool is consumed. In snow ice, the diatoms can be cut off from the nutrient supply initially provided by seawater infiltration and will therefore use a large part of their available dissolved silicon pool.

[29] We propose that the contrasted Si-isotopic signature between sea-ice diatoms and surface seawater diatoms might be used to determine the proportion of the biogenic silica flux to the deep sea, contributed by diatoms which have grown in sea ice vs. diatoms which have grown in seawater after sea-ice melting.

[30] Future work should focus on the seasonal evolution of the Si-isotopic signature in distinct sea-ice environments (pack ice versus landfast ice; Antarctic versus Arctic) and develop a dedicated Si-isotopic fractionation model for sea-ice diatoms. This, in turn, should allow us to study the spatial and temporal variations of diatom activity in sea ice and the influence of sea ice on the Si-isotopic budget of the polar oceans and the biogenic fluxes to the deep sea.

[31] **Acknowledgments.** Our warm thanks go to the officers and crew of the ARISE *Aurora Australis* cruise (AU0301) and also to I. Allison (Chief Scientist). We are also grateful to J. de Jong and N. Matielli (ULB) for the management of the MC-ICP-MS lab in Brussels and to L. Monin, N. Dahkani (MRAC), and S. El Amri (ULB) for their help in sample processing and ICP-AES analyses. The comments from two anonymous reviewers were greatly appreciated and have substantially improved the manuscript. This work was conducted under the SIBCLim Program (ARC contract 02/07-287) funded by the Communauté Française de Belgique, and the BELCANTO II and III network (contracts EV/37/7C and SD/CA/03A of SPSDII and III, Support Plan for Sustainable Development) funded by BELSPO, the Belgian Science Policy. L. A. thanks the FNRS for its financial support in the frame of the FRFC project 2.4512.00. This work was supported by the Australian Government's Cooperative Research Centres Programme through the Antarctic Climate and Ecosystems Cooperative Research Centre (ACE CRC).

References

Alleman, L. Y., D. Cardinal, C. Cocquyt, P. D. Plisnier, J. P. Descy, I. Kimirei, D. Sinyianza, and L. André (2005), Silicon isotopic fractionation in Lake Tanganyika and its tributaries, *J. Great Lakes Res.*, *31*, 509–519.

Arrigo, K. R. (2003), Primary production in sea ice, in *Sea Ice: An Introduction to Its Physics, Chemistry, Biology and Geology*, edited by D. N. Thomas and G. S. Dieckmann, pp. 143–179, Blackwell, Malden, Mass.

Arrigo, K. R., and D. N. Thomas (2004), Large scale importance of sea ice biology in the Southern Ocean, *Antarct. Sci.*, *16*(4), 471–486, doi:10.1017/S0954102004002263.

Cardinal, D., L. Y. Alleman, J. De Jong, K. Ziegler, and L. André (2003), Isotopic composition of silicon measured by multicollector plasma source mass spectrometry in dry plasma mode, *J. Anal. At. Spectrom.*, *18*, 213–218.

Cardinal, D., L. Y. Alleman, F. Dehairs, N. Savoye, T. W. Trull, and L. André (2005), Relevance of silicon isotopes to Si-nutrient utilisation and Si source assessment in Antarctic waters, *Global Biogeochem. Cycles*, *19*, GB2007, doi:10.1029/2004GB002364.

Cardinal, D., N. Savoye, T. W. Trull, F. Dehairs, E. E. Kopczynska, F. Fripiat, J. L. Tison, and L. André (2007), Silicon isotopes in spring Southern Ocean diatoms: Large zonal changes despite homogeneity among size fractions, *Mar. Chem.*, doi:10.1016/j.marchem.2006.04.006, in press.

Carignan, J., D. Cardinal, A. Eisenhauer, A. Galy, M. Rehkämper, F. Wombacher, and N. Vigier (2004), A reflection on Mg, Cd, Ca, Li and Si–isotopic measurements and related references materials, *Geostand. Geoanal. Res.*, *28*, 139–148.

Clarke, D. B., and S. F. Ackley (1984), Sea ice structure and biological activity in the Antarctic marginal ice zone, *J. Geophys. Res.*, *89*(2), 2087–2095.
Cota, G. F., and E. P. W. Horne (1989), Physical control of arctic ice algal production, *Mar. Ecol. Prog. Ser.*, *52*, 111–121.
Cota, G. F., S. J. Prinsenberg, E. B. Bennet, J. W. Loder, M. R. Lewis, J. L. Aming, N. H. F. Watson, and L. R. Harris (1987), Nutrient flux during extended blooms of arctic ice algae, *J. Geophys. Res.*, *92*(4), 1951–1962.
Cox, G. F. N., and W. F. Weeks (1983), Equations for determining the gaz and brine volumes in sea-ice samples, *J. Glaciol.*, *29*(102), 306–316.
De La Rocha, C. L., M. A. Brzezinski, and M. J. DeNiro (1996), Purication, recovery and laser-driven fluorination of silicon from dissolved and particulate silica for the measurement of natural stable isotope abundances, *Anal. Chem.*, *68*, 3746–3750.
De La Rocha, C. L., M. A. Brzezinski, and M. J. DeNiro (1997), Fractionation of silicon isotopes by marine diatoms during biognic silica formation, *Geochim. Cosmochim. Acta*, *61*, 5051–5056.
De La Rocha, C. L., M. A. Brzezinski, and M. J. DeNiro (2000), A first look at the distribution of the stable isotopes of silicon in natural waters, *Geochim. Cosmochim. Acta*, *64*, 2467–2477.
Dieckmann, G. S., M. A. Lange, S. F. Ackley, and J. C. Jennings (1991), The nutrient status in sea ice of the Weddel Sea during winter: Effects of sea ice texture and algae, *Polar Biol.*, *11*, 449–456.
Eicken, H. (1992), Salinity profiles of Antarctic sea ice: Field data and model results, *J. Geophys. Res.*, *97*(10), 15,545–15,557.
Eide, L. I., and S. Martin (1975), The formation of brine drainage features in young sea ice, *J. Glaciol.*, *14*(70), 137–154.
Garrison, D. L., and K. R. Buck (1989), The biota of Antarctic pack ice in the Weddel Sea and Antarctic Peninsula regions, *Polar Biol.*, *10*, 211–219.
Garrison, D. L., K. R. Buck, and G. Fryxell (1987), Algal assemblages in Antarctic pack ice and ice-edge plankton, *J. Phycol.*, *23*, 564–572.
Gersonde, R., and U. Zielinski (2000), The reconstruction of late quaternary Antarctic sea-ice distribution-the use of diatoms as a proxy for sea-ice, *Palaeogeogr. Paleoclimatol. Palaeoecol.*, *162*, 263–286.
Gleitz, M., M. Rutgers van der Loeff, D. N. Thomas, G. S. Dieckmann, and F. J. Millero (1995), Comparison of summer and winter inorganic carbon, oxygen and nutrient concentrations in Antarctic sea ice brine, *Mar. Chem.*, *51*, 81–91.
Gleitz, M., A. Bartsch, G. S. Dieckmann, and H. Eicken (1998), Composition and succession of sea ice diatom assemblages in the eastern and southern Weddel Sea, Antarctica, in *Antarctic Sea: Ice Biological Processes, Interactions and Variability*, *Antarct Res Ser.*, vol. 73, edited by M. Lizotte and K. R. Arrigo, pp. 107–120, AGU, Washington, D. C.
Goffart, A., G. Catalano, and J. H. Hecq (2000), Factors controlling the distribution of diatoms and Phaeocystis in the Ross Sea, *J. Mar. Syst.*, *27*, 161–175.
Golden, K. M. (2001), Brine percolation and the transport properties of sea ice, *Ann. Glaciol.*, *33*, 28–36.
Golden, K. M., S. F. Ackley, and V. I. Lytle (1998), The percolation phase transition in sea ice, *Science*, *282*(5397), 2238–2241.
Horner, R. (1985), *Sea Ice Biota*, 215 pp., CRC Press, Boca Raton, Fla.
Lancelot, C., S. Mathot, C. Veth, and H. deBaar (1993), Factor controlling phytoplancton ice-edge blooms in the marginal ice-zone of the northwestern Weddel Sea during sea ice retrait 1988, *Polar Biol.*, *13*, 337–387.
Lancelot, C., E. Hannon, S. Becquevort, C. Veth, and H. De Baar (2000), Modeling phytoplankton blooms and carbon export production in the Southern Ocean: Dominant controls by light and iron in the Atlantic sector in Austral spring 1992, *Deep Sea Res., Part I*, *47*, 1621–1662.
Lannuzel, D., V. Schoemann, J. de Jong, J.-L. Tison, and L. Chou (2007), Distribution and biogeochemical behaviour of iron in the East Antarctic sea ice, *Mar. Chem.*, doi:10.1026/j.marchem.2006.06.010, in press.
Lizotte, M. P. (2003), The microbiology of sea ice, in *Sea Ice: An Introduction to Its Physics, Chemistry, Biology and Geology*, edited by D. N. Thomas and G. S. Dieckmann, pp. 184–209, Blackwell, Malden, Mass.
Mariotti, A., J. C. Germon, P. Hubert, P. Kaiser, R. Letolle, A. Tardieux, and P. Tardieux (1981), Experimental determination of nitrogen kinetic isotope fractionation: Some principles; illustration for the denitrification and nitrification processes, *Plant Soil*, *62*, 413–430.
Mathot, S., S. Becquevort, and C. Lancelot (1991), Microbial communities from the sea ice and adjacent water column at the time of ice melting in the northwestern part of the Weddel Sea, in *Proceeding of the Pro Mare Symposium on Polar Marine Ecology*, edited by E. Sakshaug, C. C. E. Hopkins, and N. A. Oritsland, *Polar Res.*, *10*, 267–275.
Meese, D. A. (1989), The chemical and structural properties of sea ice in the sourthern Beaufort Sea, *Rep. 89-25*, pp. 1–97, Cold Reg. Res. and Eng., Hanover, N. H.
Michel, C., L. Legendre, J.-C. Therriault, S. Demers, and T. Vandevelde (1993), Springtime coupling between ice algal and phytoplankton assemblages in southeastern Hudson bay, Canadian Arctic, *Polar Biol.*, *13*, 441–449.
Michel, C., L. Legendre, R. G. Ingram, M. Gosselin, and M. Levasseur (1996), Carbon budget of sea-ice algae in spring: Evidence of a significant transfer to zooplankton grazers, *J. Geophys. Res.*, *101*(C8), 18,345–18,360.
Michel, C., L. Legendre, and S. Taguchi (1997), Coexistence of microalgal sedimentation and water column recycling in a seasonnaly ice-covered ecosystem (Saroma-ko Lagoon, Sea Okhotsk, Japan), *J. Mar. Syst.*, *11*, 133–148.
Milligan, A. J., D. E. Varela, M. A. Brzezinski, and F. M. M. Morel (2004), Dynamics of silicon metabolism and silicon isotopic discrimination in a marine diatom as a function of pCO_2, *Limnol. Oceanogr.*, *49*, 322–329.
Ragueneau, O., N. Savoye, Y. Del Amo, J. Cotton, B. Tardiveau, and A. Leynaert (2005), A new method for the measurement of biogenic silica in suspended matter of coastal waters: Using Si:Al ratios to correct for the mineral interference, *Cont. Shelf Res.*, *25*, 697–710.
Riebesell, U., I. Schloss, and V. Smetacek (1991), Aggregation of algae released from melting sea ice: Implications for seeding and sedimentation, *Polar Biol.*, *11*, 239–248.
Sharek, R., V. Smetacek, E. Fahrback, L. I. Gordon, G. Rohardt, and S. Moore (1994), The transition from winter to early spring in the eastern Weddell Sea, Antarctica: Plankton biomass and composition in relation to hydrography and nutrients, *Deep Sea Res., Part II*, *41*, 1231–1250.
Sigman, D. M., M. A. Altabet, D. C. McCorkle, R. François, and G. Fischer (1999), The $\delta^{15}N$ of nitrate in the Southern Ocean: Consumption of nitrate in surface waters, *Global Biogeochem. Cycles*, *13*(4), 1149–1166.
Smith, W. O., Jr., and D. Nelson (1985), Phytoplankton bloom produced by a receding ice edge in the Ross Sea: Spatial coherence with the density field, *Science*, *227*, 163–166.
Smith, W. O., Jr., and D. M. Nelson (1986), Importance of ice edge phytoplankton production in the Southern Ocean, *BioScience*, *36*(4), 251–257.
Thomas, D. N., and S. Papadimitriou (2003), Biogeochemistry of sea ice, in *Sea Ice: An Introduction to its Physics, Chemistry, Biology and Geology*, edited by D. N. Thomas and G. S. Dieckmann, pp. 267–294, Blackwell, Malden, Mass.
Tison, J.-L., and V. Verbeke (2001), Chlorinity/salinity distribution patterns in experimental granular sea ice, *Ann. Glaciol.*, *33*, 13–20.
Tison, J.-L., C. Haas, M. M. Gowing, S. Sleewaegen, and A. Bernard (2002), Tank study of physico-chemical controls on gas content and composition during growth of young sea ice, *J. Glaciol.*, *48*(161), 177–191.
Tison, J.-L., R. Lorrain, V. Verbeke, C. Lancelot, V. Shoemann, S. Becquevort, L. Chou, and J. De Jong (2004), Sea Ice Biogeochemistry in a CLIMate change perspective (SIBCLIM): Works progress report, October 2002–December 2003, report, 57 pp., Univ. Libre de Bruxelles, Brussells, Belgium.
Tucker, W. B., III, A. J. Gow, and W. F. Weeks (1987), Physical properties of summer sea ice in the Fram Strait, *J. Geophys. Res.*, *92*(7), 6787–6803.
Varela, D. E., C. J. Pride, and M. A. Brzezinski (2004), Biological fractionation of silicon isotopes in Southern Ocean surface waters, *Global Biogeochem. Cycles*, *18*, GB1047, doi:10.1029/2003GB002140.
Wakatsuchi, M., and N. Ono (1983), Measurements of salinity and volume of brine excluded from growing sea ice, *J. Geophys. Res.*, *88*(5), 2943–2951.
Weeks, W. F., and S. F. Ackley (1986), The growth, structure, and properties of sea ice, in *The Geophysics of Sea Ice*, *NATO ASI Ser.*, vol. 146, edited by N. Understeiner, pp. 9–164, Springer, New York.
Wettlaufer, J. S., M. G. Worster, and H. E. Huppert (1997), The phase evolution of young sea ice, *Geophys. Res. Lett.*, *24*(10), 1251–1254.
Worster, M. G., and J. S. Wettlaufer (1997), Natural convection, solute trapping, and channel formation during solidification of salwater, *J. Phys. Chem.*, *101*, 6132–6136.
Young, E. D., A. Galy, and H. Nagahara (2002), Kinetic and equilibrium mass-dependent isotope fractionation laws in nature and their geochemical and cosmochemical significance, *Geochim. Cosmochim. Acta*, *66*, 1095–1104.

L. André, D. Cardinal, and F. Fripiat, Department of Geology and Mineralogy, Section of Mineralogy and Petrography, Royal Museum for Central Africa, Leuvensesteenweg 13, B-3080 Tervuren, Belgium. (lucandre@africamuseum.be; damien.cardinal@africamuseum.be; ffripiat@africamuseum.be)

J.-L. Tison, Unité de Glaciologie, Département des Sciences de la Terre et de l'Environnement, Université Libre de Bruxelles, CP 160/03, 50 Av. F. D. Roosevelt, B-1050 Brussels, Belgium. (jtison@ulb.ac.be)

A. Worby, Department of the Environment and Water, Australian Antarctic Division, 203 Channel Highway, Kingston, Tasmania 7050, Australia. (a.worby@utas.edu.au)

Silicon isotopes in spring Southern Ocean diatoms: Large zonal changes despite homogeneity among size fractions

Available online at www.sciencedirect.com
ScienceDirect
Marine Chemistry 106 (2007) 46–62
MARINE CHEMISTRY
www.elsevier.com/locate/marchem

Silicon isotopes in spring Southern Ocean diatoms: Large zonal changes despite homogeneity among size fractions ☆

Damien Cardinal [a,*], Nicolas Savoye [b,1], Thomas W. Trull [c], Frank Dehairs [b], Elzbieta E. Kopczynska [d], François Fripiat [a,e], Jean-Louis Tison [e], Luc André [a]

[a] *Department of Geology and Mineralogy, Section of Mineralogy and Petrography, Royal Museum for Central Africa, Tervuren, Belgium*
[b] *Department of Analytical and Environmental Chemistry, Vrije Universiteit Brussel, Brussels, Belgium*
[c] *Antarctic Climate and Ecosystem Cooperative Research Centre, CSIRO Marine Research, University of Tasmania, Hobart, Australia*
[d] *Department of Antarctic Biology, Polish Academy of Science, Warsaw, Poland*
[e] *Laboratoire de Glaciologie Polaire, Département des Sciences de la Terre et de l'Environnement, Université Libre de Bruxelles, Bruxelles, Belgium*

Received 5 October 2005; received in revised form 17 March 2006; accepted 26 April 2006
Available online 30 June 2006

Abstract

We determine Southern Ocean diatom silicon isotopic signatures and compare them with the previously published data for dissolved silicic acid from the same locations. Five stations distributed along the WOCE SR-3 transect (Australian Sector of the Southern Ocean) in different biogeochemical provinces are presented: Polar Front and Inter-Polar Front Zones (PFZ–IPFZ), Southern Antarctic Zone (AZ-S), Seasonal Ice Zone (SIZ). Total (>0.4 μm), medium-sized (20–70 μm), and large diatoms (>70 μm) were sampled at 2–4 depths in the upper 150 m. Silicon isotopic compositions of biogenic silica (diatoms) and seawater were then measured by MC-ICP-MS, in dry plasma mode using external Mg doping. Results are expressed as δ^{29}Si relative to the NBS28 standard. The isotopic composition of diatoms ($\delta^{29}Si_{BSi}$) is generally homogeneous in the mixed layer and does not exhibit a systematic isotopic fractionation linked to a size effect. $\delta^{29}Si_{BSi}$ are always lighter than the ambient dissolved silicic acid signatures ($\delta^{29}Si_{DSi}$), reflecting the preferential uptake of light isotopes by diatoms. A trend of lighter isotopic signatures southward is observed both in diatoms and seawater samples but the $\delta^{29}Si_{BSi}$ latitudinal gradient is much steeper. A diatom signature as low as −0.26‰ in the southernmost SIZ station strongly contrasts with the +0.65‰ signature measured on PFZ diatoms. The difference between the ambient dissolved silicic acid and diatom isotopic signatures, Δ^{29}Si, strongly increases southward: from 0.4 in the PFZ up to 1.08‰ in the SIZ. This points toward occurrence of mixing events in the PFZ–IPFZ with diatoms not being under equilibrium with their surrounding water and/or, possible variation of the diatom–seawater equilibrium fractionation factor, $^{29}\varepsilon$. Apart from mixing, we found that the other parameters likely responsible of such variation are temperature, dissolved Si contents and, Si specific uptake and dissolution rates although at this stage none of these could be clearly recognized as the leading cause. Thorough examination of these parameters through in vitro experiments reflecting the extreme Southern Ocean conditions is needed to determine whether the observed latitudinal variation of Δ^{29}Si reflects real variable fractionation or results from non-equilibrium or different time-scales recorded between dissolved and biogenic Si isotopic signatures. Our results also call for the development of more realistic models for describing short-term isotopic composition changes due to e.g. Si consumption, export

☆ This work is gratefully dedicated to the memory of Roland Wollast as a special recognition of the excellence of his pioneer work on the silicon cycle. His brilliance, intuitive insights, kindness and zest for life are sadly missed.

* Corresponding author.
E-mail address: damien.cardinal@africamuseum.be (D. Cardinal).
[1] Now at: Observatoire Aquitain des Sciences de l'Univers, UMR 5805 EPOC, Arcachon, France.

doi:10.1016/j.marchem.2006.04.006

and resupply via mixing. Finally, by comparing $\delta^{29}Si_{BSi}$ within and below the mixed layer, we could identify a two-step history of the PFZ–IPFZ bloom in contrast to the recently started diatom bloom in the SIZ.

Keywords: Diatoms; Silicon isotopes; Silicon cycle; Isotope fractionation; Nutrient cycles; Southern Ocean

1. Introduction

The Southern Ocean is a major carbon sink owing to its large physical and biological C uptake capacity (Takahashi et al., 2002; Sabine et al., 2004). Diatoms have a key role in this biological carbon pump because they often dominate the phytoplankton biomass from the Polar Front Zone southward (Kopczynska et al., 2001, submitted for publication) and are prone to be easily exported from the mixed layer because of their opal frustules. Indeed due to the near absence of coccolithophorids south of the Polar Front, they are the leading Antarctic phytoplankton group accountable for this so-called ballast effect (François et al., 2002; Klaas and Archer, 2002). Therefore the silicon cycle in the Southern Ocean and its close link to that of carbon is being increasingly scrutinised (e.g. Ragueneau et al., 2002).

The strong South–North dissolved silicon (also referred to as silicates or silicic acid, H_4SiO_4) gradient from replete conditions in the Seasonal Ice Zone to depleted conditions in the Subantarctic Zone is a prominent feature of the Southern Ocean. It can be explained by the progressive diatom-controlled Si drawdown and export to the intermediate ocean in the course of northward transport of surface waters by Ekman drift (e.g., Trull et al., 2001; Brzezinski et al., 2002; Sarmiento et al., 2004) along with diapycnic mixing (Pollard et al., 2002). While the high-nutrient low chlorophyll (HNLC) modern Southern Ocean, appears to be non-limited in macro-nutrients such as phosphate and nitrate, this is not the case for the micro-nutrient iron (Martin et al., 1990; Boyd et al., 2000). Some uncertainty remains about the relative importance of other limiting factors such as grazing pressure (Becquevort, 1997; Smetacek et al., 2004), light (Lancelot et al., 2000), and Si availability (Nelson et al., 2001; Trull et al., 2001), in comparison to Fe-limitation. Nonetheless, it is clear that Fe stress not only limits phytoplankton growth, but also affects the diatom Si:NO_3 uptake ratio, leading to increased Si-uptake relative to NO_3-uptake (Takeda, 1998; Hutchins and Bruland, 1998). For that reason considerable attention has been paid to the understanding of processes influencing Si:N ratios in solution and diatoms, both in the natural environment and in laboratory experiments (e.g., Claquin et al., 2002; Brzezinski et al., 2003; Wang et al., 2003; Sarmiento et al., 2004).

Variations of the diatom Si:N ratio through time have been proposed as a possible contributor to changes in global ocean production and ocean–atmosphere partitioning of carbon dioxide. In this "silica leakage hypothesis" iron control of the Si:N ratio supports higher silicate:nitrate ratio of subducting Antarctic Intermediate Waters (AAIW) and Subantarctic Mode Waters (SAMW) during glacial stages (Brzezinski et al., 2002; Matsumoto et al., 2002; Sarmiento et al., 2004). Such changed nutrient ratios would then change the carbonate rain ratio at lower latitude by favouring diatom over coccolithophorid predominance. The N and Si isotopic signatures of diatoms in the Southern Ocean sediments, which are proxies of relative N and Si utilisation, have provided major support to this view (e.g. François et al., 1997; De La Rocha et al., 1998; Sigman et al., 1999a; Brzezinski et al., 2002; Crosta et al., 2005), despite the fact that processes acting on the isotopic signatures of Si and N are far from being constrained, especially as concerns the fractionation factor.

Several studies on seawater and, suspended and sinking particles have addressed controls on N isotope variations in a very thorough way recently, gradually building a more constrained but also a more complex picture of N isotopic fractionation in the ocean, in particular in the Southern Ocean (Sigman et al., 1999b; Altabet and François, 2001; Lourey et al., 2003; Karsh et al., 2003; Needoba and Harrison, 2004; Needoba et al., 2004). The marine isotopic system for Si should be simpler compared to N, because silicon is taken up only as silicic acid (mainly the H_4SiO_4 form; Del Amo and Brzezinski, 1999; Wischmeyer et al., 2003) and mostly by one phytoplankton group (diatoms), while N occurs as different chemical species and is utilised by all phytoplankton groups. Yet, the marine studies on Si isotopes are particularly scarce and the results are sometimes conflicting. This is especially the case for the fractionation factor between diatoms and seawater as well as the assessment of parameters and accurate models to describe the Si isotopic system at the local to ocean basin scale (De La Rocha et al., 1997, 2000; Varela et al., 2004; Milligan et al., 2004; Cardinal et al., 2005a).

This study presents the first dataset of natural Si isotopic composition for size-fractionated diatoms, from the Polar Front to the Seasonal Ice Zones during spring in the Southern Ocean south of Australia (WOCE SR-3 transect). The isotopic compositions of biogenic silica are compared with those for dissolved silicate, obtained for the same cruise and published previously (Cardinal et al., 2005a). We also compare our results with other Southern Ocean data reported by Varela et al. (2004). The results are discussed with reference to the significant findings concerning Southern Ocean physics, diatom silicification and Si isotopes (De La Rocha et al., 1997; Martin-Jézéquel et al., 2000; Claquin et al., 2002; Claquin and Martin-Jézéquel, 2005; Milligan et al., 2004).

2. Sampling and methods

2.1. Sampling

A total of five stations (seven samplings) were sampled along the WOCE SR-3 transect at 139–140°E for Si isotope studies. During the southbound transect we sampled one station each in the Polar Front Zone (PFZ at 53.7°S), the Inter-Polar Front Zone (IPFZ at 56.9°S), the Southern Antarctic Zone (AZ-S at 60.9°S) and two stations in the Seasonal Ice Zone (SIZ at 63.9 and 64.9°S, called SIZ-1 and SIZ-2, respectively). At the time of SIZ-1 sampling (24 Nov. 2001) sea ice coverage was ~40%, whereas for SIZ-2, located 1° latitude further south but

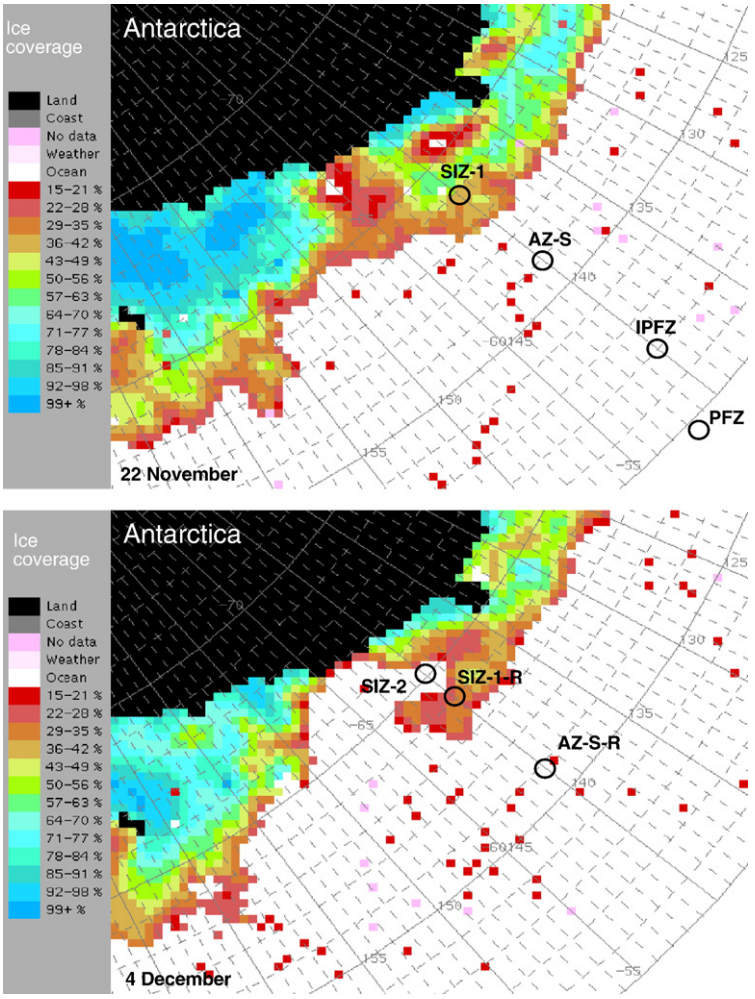

Fig. 1. Sea ice coverage on two sampling dates. 22 November 2001 (upper panel) was 2 days after AZ-S sampling and 2 days before SIZ-1 sampling. On 4th December 2001 (lower panel) SIZ-2 was sampled (one day before SIZ-1-R on the way back). Locations of stations are also indicated on the panel closest to their sampling dates. Actual date for each station is given in Table 2. See text for the definitions of acronyms. Sea ice concentrations from the NASA Earth Observing System SSM/I passive microwave remote sensing 25 × 25 km gridded product from the Distributed Active Archive Center (DAAC) at the U.S. National Snow and Ice Center, University of Colorado, Boulder, USA (data and documentation available on-line at http://nsidc.org/data/seaice/pm.html).

sampled 9 days later, large melting had taken place leaving the area ice-free (Fig. 1). Two repeat stations were sampled on the northbound transect: AZ-S on 8 Dec., and SIZ-1 on 6 Dec., i.e. 17 and 11 days after the first visits, respectively. These latter stations are referred to further as AZ-S-R and SIZ-1-R. Surface ocean physics of the study area are described in detail in Chaigneau et al. (2004).

Particulate silica samples (largely dominated by diatoms) were obtained from both Niskin bottles mounted in a CTD rosette and a submersible electrical pump which returns water to the ship via a hose (Trull and Armand, 2001) hereafter referred to as the "bow pump".

Seawater from the Niskin bottles was filtered through 0.4 μm polycarbonate membranes in Perspex filtration units under pressure. The air supplying the filtration unit was also filtered with the same type of membranes. The detailed sampling procedure is given in Cardinal et al. (2005b).

In general for the bow pumps, there were two sampling depths within the mixed layer, varying from 5–20 m for the upper part of the mixed layer and between 40 m (64.9°S) and 75 m (53.7 and 60.9°S) for the deeper part of the mixed layer. A third depth was sampled just below the mixed layer (100–120 m) for collecting diatoms and particles recently exported from the mixed layer. Two fractions of phytoplankton (20–70 μm and >70 μm) were sampled by filtering 30 to 1100 l of water in series through 142 mm diameter nylon mesh sieves. These particles were then resuspended and filtered onto 0.4 μm pore size polycarbonate membranes filters. All the filters were then dried at 50 °C before storage for analysis in the laboratory.

2.2. Methods

Biogenic silica (BSi) was extracted by a single leaching step in order to minimise potential lithogenic contamination (40 min at 100 °C with 0.2 M NaOH; Ragueneau et al., 2005). Such alkaline leaching has been shown to extract quantitatively 10–15 μmol BSi for every 4 ml NaOH 0.2 M. To optimise the single leaching step for Si isotopes analyses we first measured precisely BSi contents in a 2 to 3-step alkaline leaching performed on other filters (i.e., different CTD for the >0.4 μm Niskin samples) or different filter aliquots (for the bow pumps). The 1-step leaching for Si-isotopic analyses was then adapted from the previous BSi measurements, i.e. NaOH was added in small excess. Due to natural BSi variation between samples this leaching might not have been 100% quantitative. Our concern for natural Si-isotopic composition was actually to avoid as much as possible lithogenic Si contamination (see below) rather than a strict 100% BSi recovery. This approach is also supported by the current consensus that chemical dissolution does not fractionate Si isotopes as reported by De La Rocha et al. (1998). Therefore it is unlikely that incomplete BSi dissolution could have led to Si isotopic bias. Al was analysed in this leachate and found to be below ICP-AES detection limit (0.05 ppm) confirming only a negligible contribution, if any, of lithogenic Si. The Si isotopic composition of clays varies within the −1 to 0‰ range (Douthitt, 1982; Ding et al., 1996; De La Rocha et al., 2000; Basile-Doelsch, 2006) which is relatively close to the one we expect for Antarctic diatoms (−0.2 to +1.5; Varela et al., 2004). Maximising the lithogenic Si isotopic contamination for the heaviest diatom δ^{29}Si composition (+1.5‰) by taking Al content at the ICP-AES detection limit, an upper crust Si:Al mass ratio at 3.74 (Taylor and McLennan, 1985) with a δ^{29}Si signature at −1‰ (lightest end member for clays) induces a shift of less than 0.1‰. This maximal potential bias is less than the ±0.07‰ obtained from full replication at the $\pm 2\sigma_D$ level (see below). Therefore lithogenic Si contamination should not significantly alter our measured BSi isotopic signature after this 1-step NaOH leaching, even if the Si:Al ratio is significantly lower than 3.74. Si was subsequently purified through its quantitative reaction with triethylamine–molybdate (De La Rocha et al., 1996). After final dissolution in dilute HF/HCl, silicon isotopic compositions were then measured on a Nu Plasma MC-ICP-MS in dry plasma mode following Cardinal et al. (2003). The results are presented as δ^{29}Si relative to NBS28 quartz standard because ^{30}Si cannot be measured on the Nu Plasma due to an irresolvable $^{14}N^{16}O$ interference. This method has been intercalibrated (Cardinal et al., 2003; Carignan et al., 2004) and sample replicates (including the triethylamine–molybdate step) are within ±0.07‰ ($\pm 2\sigma_D$, Cardinal et al., 2005a). Assuming a mass dependent Si isotope fractionation under thermodynamic equilibrium (Young et al., 2002), δ^{29}Si can be converted to δ^{30}Si by applying a multiplying factor of 1.93.

3. Results

All BSi isotopic signatures ($\delta^{29}Si_{BSi}$) are presented in Table 1. Due to time and sample limitations it was not possible to replicate every single isotopic composition. Among the 39 BSi samples, eight were fully replicated starting from the NaOH step, and four were duplicated from the same HF/HCl final digestion solution. The average difference between the replicated $\delta^{29}Si_{BSi}$ is 0.07‰ (0.05‰ when removing an outlier, Table 1), well in accordance with previous results as obtained for the dissolved silicon phase (Cardinal et al., 2005a) and for in-house standards (Cardinal et al., 2003).

Table 1
Complete $\delta^{29}Si_{BSi}$ analyses from CLIVAR-SR3

Depth (m)	Size fraction (μm)	$\delta^{29}Si_{BSi}$ (‰ ± 1 st. error)
53.7°S — PFZ — CTD51		
10	>70	0.55±0.04
″	″	0.59±0.05
17.5	>0.4	0.57±0.04
50	>0.4	0.55±0.03
75	>70	0.66±0.04
″ ″	″ ″	0.57±0.04
120	20–70	0.49±0.04
120	>70	0.49±0.04
56.9°S — IPFZ — CTD63		
5	>0.4	0.48±0.03
10	20–70	0.45±0.04
10	>70	0.60±0.03
″	″	0.62±0.04
50	>0.4	0.45±0.04
75	>70	0.59±0.04
″	″	0.51±0.03
120	20–70	0.41±0.03
120	>70	0.37±0.04
60.8°S — AZ-S — CTD73		
5	>0.4	0.47±0.04
10	20–70	0.20±0.03
10	>70	0.21±0.04
50	>0.4	0.38±0.05
″ ″	″ ″	0.33±0.04
75	>70	0.24±0.04
120	20–70	0.34±0.04
60.8°S — AZ-S-R — CTD130		
5	>0.4	0.55±0.04
10	20–70	0.38±0.04
10	>70	0.36±0.04
50	>0.4	0.33±0.06
100	>0.4	0.47±0.05
″	″	0.41±0.03
120	20–70	0.36±0.03
″ ″	″ ″	0.38±0.05
120	>70	0.25±0.04
″ ″	″ ″	0.57±0.04
63.9°S — SIZ-1 — CTD85		
5	>0.4	0.27±0.04
10	20–70	0.21±0.04
10	>70	0.17±0.04
″ ″	″ ″	0.28±0.04
55	20–70	0.28±0.04
55	>70	0.23±0.03
120	20–70	0.18±0.03
″ ″	″ ″	0.15±0.05
120	>70	0.16±0.04
″	″	0.14±0.04
63.9°S — SIZ-1-R — CTD127		
5	>0.4	−0.05±0.04
50	>0.4	0.11±0.04

Table 1 (*continued*)

Depth (m)	Size fraction (μm)	$\delta^{29}Si_{BSi}$ (‰ ± 1 st. error)
64.9°S — SIZ-2		
10	20–70	−0.06±0.04
10	>70	−0.23±0.04
40	20–70	−0.09±0.04
40	>70	−0.26±0.04
120	20–70	−0.05±0.04
″ ″	″ ″	−0.07±0.04
120	>70	−0.18±0.04

st. error refers to the analytical error of the isotopic ratios measured on the standard and samples runs and propagated to $\delta^{29}Si$ (Cardinal et al., 2003). See section Sampling for the definition of acronyms. CTD numbers refer for Niskin samplings only (i.e.>0.4 μm size fraction).
″ ″ indicate full replicates.
″ indicate analytical replicate.

Profiles of dissolved Si isotopic compositions ($\delta^{29}Si_{DSi}$) have been acquired from close CTD casts and discussed in a previous paper (Cardinal et al., 2005a). In Table 2 average mixed layer isotopic data are presented along with main characteristics relevant to silicon. Fig. 2 displays the latitudinal trend of the BSi and DSi isotopic compositions. Note that large size fraction may contain some radiolarians even if the diatom valves to radiolarian cells ratio is 10^4–10^5 in Antarctic waters (Abelmann and Gersonde, 1991). $\delta^{29}Si_{BSi}$ are systematically lighter than the ones of silicic acid in agreement with the preferential uptake of light isotopes by diatoms (De La Rocha et al., 1997; Milligan et al., 2004; Varela et al., 2004; Alleman et al., 2005). We observe a southward trend of $\delta^{29}Si_{BSi}$ becoming lighter, whatever the size fraction. A much smoother southward trend is also observed for $\delta^{29}Si_{DSi}$.

Over the whole north to south SR-3 transect, there is no systematic size or depth related variation of the $\delta^{29}Si_{BSi}$ signature. Mixed layer $\delta^{29}Si_{BSi}$ values appear homogeneous for all size fractions at PFZ and SIZ-1, and to a lesser extent at AZ-S-R. However, significant differences are recorded for the other stations: large diatoms are isotopically heavier in the IPFZ, whereas they are lighter for AZ-S (mixed layer) and SIZ-2 (both depths). SIZ-2 is the only station exhibiting size related differences in the isotopic composition of mixed layer and exported diatoms (i.e. within the deeper layer). Comparing isotopic signatures for mixed layer diatoms with those for sub-mixed layer samples ('exported' diatoms) reveals significantly lighter isotopic compositions below the mixed layer at the two northern stations (PFZ–IPFZ). Signatures of these 'exported' diatoms are heavier in the AZ-S, while they are homogeneous for the two SIZ stations and in AZ-S-R.

Table 2
Summary of Si contents and isotopic measurements averaged per depth layer: mixed layer and just below

		PFZ	IPFZ	AZ-S	AZ-S- R	SIZ-1	SIZ-1 R	SIZ-2
Latitude	(°S)	53.7	56.9	60.8	60.8	63.9	63.9	64.9
Sampling date (2001)		13 Nov.	16 Nov.	20 Nov.	7 Dec.	24 Nov.	5 Dec.	4 Dec.
Mixed layer depth [a]	(m)	76	92	97	97	41	38	104
Mixed layer temperature	(°C)	2.94	1.58	−0.08	0.08	−1.68	−1.5	−1.42
$[DSi]_{initial}$ [a]	(μmol l^{-1})	19.8	31.5	55.1	55.1	77.4	77.4	72.1
$[DSi]_{ML}$ [a]	(μmol l^{-1})	11.0	15.8	28.1	27.3	40.8	43.4	60.7
$[BSi]_{ML}$ >0.4 μm	(μmol l^{-1})	0.39±0.15	0.86±0.61	1.66±0.21	3.92±1.30	0.83±0.01	1.41±0.59	0.40±0.09
$[BSi]_{ML}$ 20–70 μm	(μmol l^{-1})	nd	0.08±0.01	1.26±0.36	1.44	0.61	0.00	0.07±0.02
$[BSi]_{ML}$ >70 μm	(μmol l^{-1})	0.28±0.05	0.25±0.05	0.85±0.13	1.45	0.56	na	0.04±0.01
$\delta^{29}Si_{DSi\text{-}ML}$ [a]	(‰)	1.02	0.99±0.01	0.97±0.04	1.09±0.08	0.97	0.97	0.84±0.03
$\delta^{29}Si_{BSi\text{-}ML}$ >0.4 μm	(‰)	0.56±0.01	0.46±0.03	0.40±0.07	0.44±0.15	0.27	−0.05	
$\delta^{29}Si_{BSi\text{-}ML}$ 20–70 μm	(‰)	na	0.45	0.20	0.38	0.21	na	−0.08±0.02
$\delta^{29}Si_{BSi\text{-}ML}$ >70 μm	(‰)	0.59±0.05	0.58±0.05	0.22±0.02	0.36	0.22±0.07	na	−0.24±0.03
$\delta^{29}Si_{BSi\text{-}deep}$ >0.4 μm	(‰)	na	na	na	0.44±0.04	na	0.11	na
$\delta^{29}Si_{BSi\text{-}deep}$ 20–70 μm	(‰)	0.49	0.41	0.34	0.37±0.02	0.20±0.07	na	−0.06±0.02
$\delta^{29}Si_{BSi\text{-}deep}$ >70 μm	(‰)	0.49	0.37	na	0.41±0.23	0.18±0.05	na	−0.18

DSi: dissolved Si. BSi: Biogenic Si. R: repeat stations. ML: Mixed Layer. Deep: from bow pumps sampling below ML.
1 standard deviation calculated on all analyses available per depth layer (i.e. ML or deep) is given (see Table 1 for the complete dataset).
No standard deviation indicates single measurement at this depth layer.
na: no data available; nd: not detectable.
See section Sampling for the definition of acronyms.
[a] Data from Cardinal et al. (2005a). Initial: refers to the conditions before start of Si consumption as discussed in Cardinal et al. (2005a).

Fig. 3 displays the latitudinal trend of BSi concentration ([BSi]) and diatom cell concentration (the latter data from Savoye et al., 2004a; Kopczynska et al., submitted for publication). There is a good correlation (r^2=0.87, not shown) between diatom cell numbers and [BSi] (>20 μm). The maximum [BSi] was observed in the AZ-S, and the

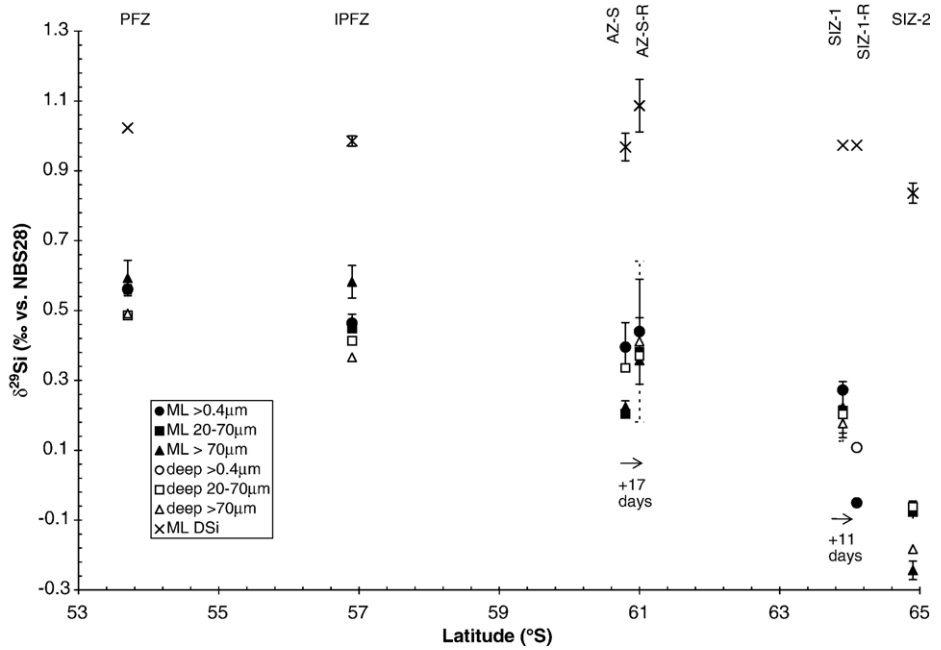

Fig. 2. Zonal variation of the isotopic composition of silicic acid (also referred to as silicate) (crosses: mixed layer data from Cardinal et al., 2005a) and biogenic silica: circles: >0.4 μm fraction; squares: 20–70 μm; triangles: >70 μm; filled symbols: mixed layer average; empty symbols: below mixed layer depth. Arrows link two repeat samplings at the same location (delay is given). Latitudes displayed for repeat stations have been slightly shifted in the figure to avoid overlap with first sampling (AZ-S-R has been put at 61.2°S instead of 60.8°S and SIZ-1-R at 65.1°S instead of 64.9°S). Error bars are the standard deviation calculated when several analyses have been acquired (see Tables 1 and 2). See section sampling for the definition of acronyms.

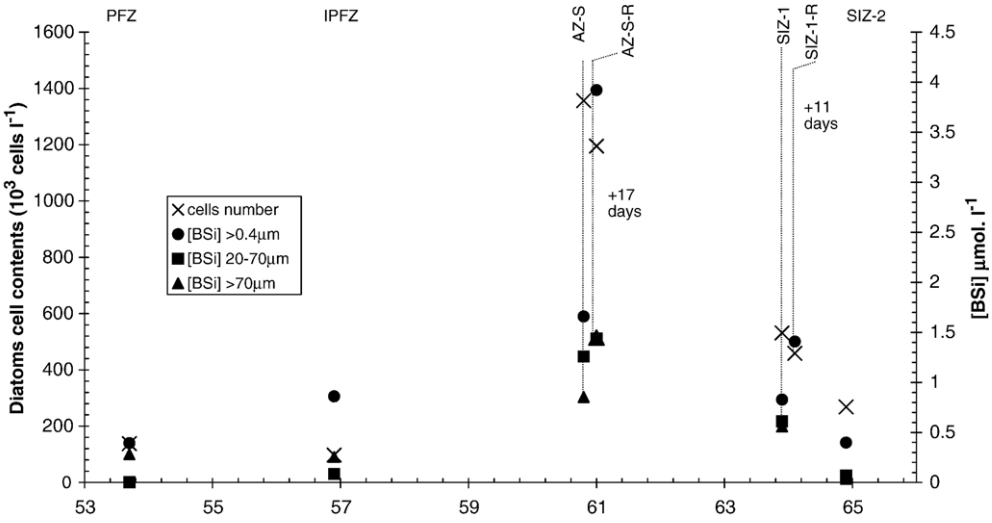

Fig. 3. Mixed layer average BSi contents (filled symbols) and upper 70-m diatom cell contents (crosses) vs. latitude °S. Vertical lines indicate two repeat samplings at the same location (delay is given). Latitudes displayed for repeat stations have been slightly shifted in the figure to avoid overlap with first sampling (AZ-S-R has been put at 61.2°S instead of 60.8°S and SIZ-1-R at 65.1°S instead of 64.9°S). See section sampling for the definition of acronyms.

lowest at the northern (PFZ–IPFZ) and southern (SIZ-2) edges of the transect. Diatom cell numbers follow the same pattern. The medium (20–70 μm) and large (>70 μm) size fractions have similar [BSi] contents in the SIZ (and AZ-S-R), whereas in the PFZ–IPFZ [BSi] of the >70 μm size fraction exceeds that of the 20–70 μm size fraction.

Overall, micro-sized diatoms (>20 μm) are dominant and account for 80±45% of the BSi concentration of the >0.4 μm size fraction (assuming this fraction reflects total [BSi] even if under sampling with Niskin can occur). A similar size distribution has been reported by Quéguiner and Brzezinski (2002) in the spring Southern Ocean. A significant increase of BSi was observed at the repeat stations; at AZ-S-R diatom biomass increased more than twofold in between successive visits, but this increase was mainly carried by the smaller sized diatoms. Indeed, [BSi] in the >0.4 μm size fraction increased by 2.2 μmol l^{-1}, while [BSi] in the >20 μm fraction increased only by 0.8 μmol l^{-1}. Diatom cell counts, on the contrary, decreased by 12–14% between repeat visits of the AZ-S and SIZ-1 sites (Fig. 3) indicating that diatoms were more silicified at the repeat visits. In both cases, the increase of [BSi] over time was not counterbalanced by a decrease in [DSi] (Table 2).

4. Discussion

4.1. Apparent fractionation factor

In vitro experiments of De La Rocha et al. (1997) have established the basic understanding of Si isotopes as a proxy of relative Si utilisation by showing that the equilibrium fractionation factor, expressed as $^{29}\varepsilon$ or $^{30}\varepsilon$ (with $^{30}\varepsilon = 1.93 \times {}^{29}\varepsilon$), between diatoms and dissolved silicon ($^{29}\varepsilon = -0.56 \pm 0.2$‰) appeared to be independent of temperature (12–22 °C range), species (three tropical species) and cell growth rate. It is worth noting that such incubations have however never been performed on conditions close to the ones found in the Southern Ocean. Milligan et al. (2004) have recently made important progress on physiological aspects and provide strong support for the idea that isotopic fractionation takes place only during membrane transport and not during the polymerisation–precipitation process. Therefore, the step involved in Si-isotopic fractionation differs from the main process involved for N isotopic fractionation which is the intra-cellular reduction of NO_3^- by nitrate reductase (Needoba and Harrison, 2004; Granger et al., 2004). Actually the difference in the mechanisms involved for the Si vs. N isotopic fractionation processes is not surprising as the Si cycle in a diatom's cell is decoupled from C and N cycles (e.g. Claquin et al., 2002; Claquin and Martin-Jézéquel, 2005).

Going a step beyond laboratory experiments, data on silicon isotopic signatures in the modern ocean are limited to the studies by De La Rocha et al. (2000), Varela et al. (2004), and Cardinal et al. (2005a), with the most two recent providing detailed datasets exclusively for the Southern Ocean. Our $\delta^{29}Si_{BSi}$ data are actually very similar to the ones of Varela et al. (2004) acquired for several repeat samplings (mostly in summer) along a North–South transect in the S.O. eastward to the SR-3 line (SOFeX and AESOPS programs at 170°W). Based

on their summer BSi and DSi data Varela et al. (2004) deduced a fractionation factor ($^{29}\varepsilon$) ranging between −0.55 and −0.98‰ and showing no latitudinal gradient. In their approach Varela et al. considered the section between the Polar Front and the Southern Antarctic Circumpolar Current Front as one single system (i.e. with same Si contents and isotopic signature of the source). Furthermore, they applied the open steady-state (Sigman et al., 1999b) or closed system Rayleigh type (Mariotti et al., 1981) models to their data in which biological activity appears to have had a larger impact than physical mixing (spring or samples taken after strong mixing events were excluded from this calculation). The description of these models is given in Fig. 4. In contrast, Cardinal et al. (2005a), studying $\delta^{29}Si_{DSi}$ in spring, applied an open system, multi-box approach and deduced a fractionation factor very close (−0.54±0.2‰) to the value reported by De La Rocha et al. (1997). The equations of these open steady-state and closed systems assume a constant equilibrium fractionation factor between diatoms and dissolved silicon and describe the evolution of $\delta^{29}Si_{DSi}$ and $\delta^{29}Si_{BSi}$ as function of ε, relative Si utilisation (f= [DSi]/[DSi]$_{initial}$, ratio of actual silicic acid content over initial content) and $\delta^{29}Si_{DSi}$ isotopic signature of the substrate before any consumption had started (Fig. 4). While providing new ε estimates, Varela et al. (2004) and Cardinal et al. (2005a) reported that none of these models is likely to adequately describe the Southern Ocean system at the seasonal and regional scales. In particular we have shown that during the CLIVAR-SR3 spring cruise the system could hardly be considered to operate as a single closed one, but rather that each site rather functioned as an independent open system (Cardinal et al., 2005a). Therefore, applying the same closed system approach Varela et al. (2004) used for summer data to this spring $\delta^{29}Si_{BSi}$ CLIVAR-SR3 dataset is likely to lead to a flawed interpretation. Indeed, comparing $\delta^{29}Si_{BSi}$ with relative Si utilisation for a closed system makes sense only if (i) it is assumed that source silicon at all sites has the same isotopic composition and (ii) initial Si contents are well constrained. Furthermore, combining results from multiple sites can introduce sampling biases — for example in our case the observations at 64.9°S, where relative Si utilisation appears to be much lower than at the other sites would bias the overall interpretation by controlling one extremity of the regression line drawn (see Fig. 5 in Cardinal et al., 2005a).

$^{29}\varepsilon$ could be independently assessed from the chosen theoretical model using the "apparent" fractionation factor, $\Delta^{29}Si$, which is the difference between the isotopic composition of the product, biogenic silica ($\delta^{29}Si_{BSi}$) and the ambient dissolved silicon ($\delta^{29}Si_{DSi}$). For both steady-state open system (Fig. 4b) and closed system assuming that $\delta^{29}Si_{BSi}$ represents the instantaneous (i.e., non-accumulated) product signature (Fig. 4a), $\Delta^{29}Si$, should be an estimate of the fractionation factor, $^{29}\varepsilon$. This condition only holds if the isotopic compositions of both phases represent instantaneous equilibrium conditions (Fig. 4). For instance if a closed system applies, $\Delta^{29}Si$ should increase along with DSi consumption as $\delta^{29}Si_{BSi}$ reflects the accumulated rather than the instantaneous product. As such, $\Delta^{29}Si$ is no longer representative of $^{29}\varepsilon$ (Fig. 4a). Assuming $\Delta^{29}Si \sim {}^{29}\varepsilon$, Varela et al. (2004) obtained an average of −0.83‰, giving additional support for a significantly larger ε value than deduced from laboratory experiments (De La Rocha et al., 1997), whereas recent $\Delta^{29}Si$ values reported by Alleman et al. (2005) for tropical freshwater lake diatoms are in the range of De La Rocha et al. (1997).

In the present study, the latitudinal trend for $\delta^{29}Si_{BSi}$ is much steeper than for $\delta^{29}Si_{DSi}$ inducing latitudinal varying $\Delta^{29}Si$ values. A similar trend could also be seen in Fig. 5 for the data from Varela et al. (2004). This suggests a possible latitudinal change in the water-diatom silicon fractionation factor and/or a bias induced by sporadic physical mixing events on our spring data. In Varela et al. (2004) the slope of $\delta^{29}Si_{BSi}$ vs. f, was significantly more negative (slope=$^{30}\varepsilon$=−2.1±0.2) than the one for $\delta^{29}Si_{DSi}$ vs. f (slope=$^{30}\varepsilon$=−1.7±0.1). In our previous study on $\delta^{29}Si_{DSi}$, we also observed a latitudinal trend in the fractionation factor, with values being more negative (larger fractionation) in the southern waters compared to those in the north (Cardinal et al., 2005a). Although those differences for $^{29}\varepsilon$ were not statistically significant, the fact that they were present in Varela et al. (2004) and are observed in the present BSi dataset calls for a closer look at this aspect. For the PFZ–IPFZ zone, $\Delta^{29}Si$ falls well in the range of our previous $^{29}\varepsilon$ estimates (De La Rocha et al., 1997; Cardinal et al., 2005a) but becomes progressively more negative southward (i.e. larger isotopic difference between BSi and DSi phases). SIZ-2 and SIZ-1-R are particularly off the expected range. In the following sections we discuss this latitude-related variation of $\Delta^{29}Si$ with respect to the likely factors that might have some control over it: 1) Sea ice diatoms, 2) Iron, 3) Temperature, 4) Si uptake and dissolution rates, 5) Sporadic physical mixing events in the frontal zones. Before entering into these discussions, we note that variations in the extent of product accumulation do not offer a simpler explanation of the latitudinal variations in $\Delta^{29}Si$ — because biogenic silica accumulations do not increase southward from the PFZ to the SIZ (Fig. 3). This issue is addressed in more detail in Section 4.1.5.

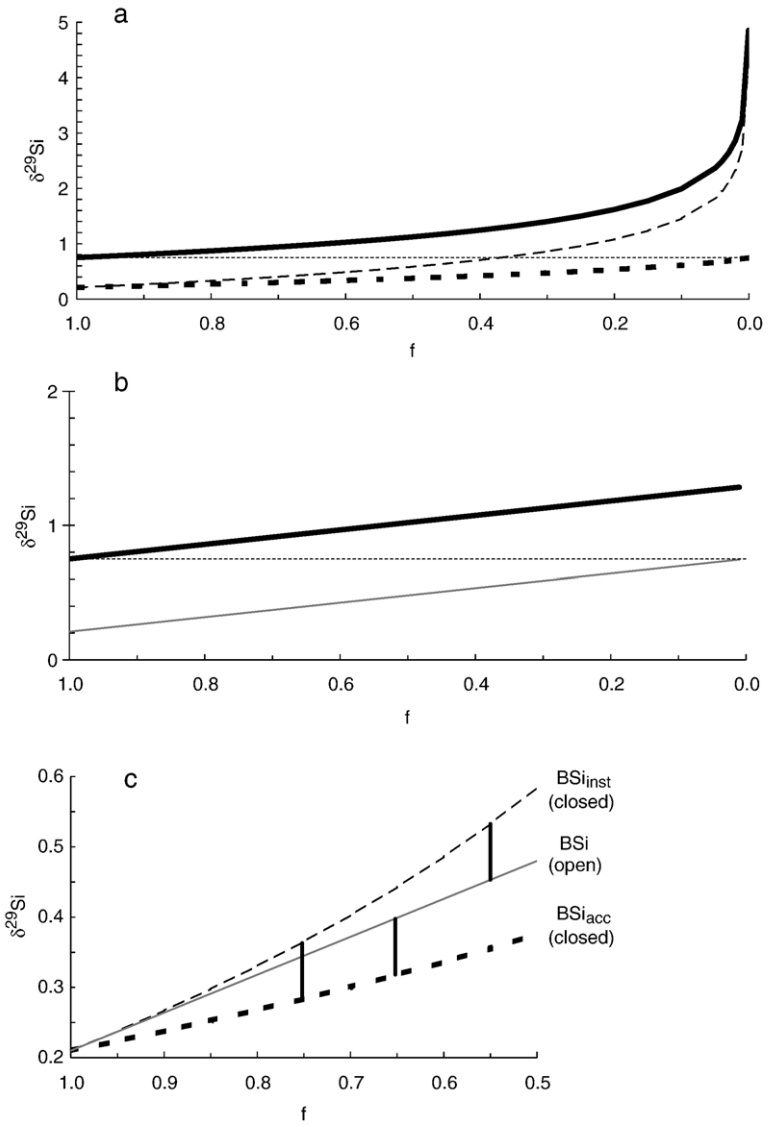

Fig. 4. Steady-state models describing the theoretical evolution of Si isotope signatures as a function of f (f=[DSi]/[DSi]$_{initial}$). Conditions set were expected in the SIZ as based on results from a previous study, i.e. $^{29}\varepsilon=-0.54‰$ and $\delta^{29}Si_{DSi\text{-}initial}=0.75‰$ (Cardinal et al., 2005a). Plain thick line: $\delta^{29}Si_{DSi}$; horizontal light dotted line indicates $\delta^{29}Si_{DSi\text{-}initial}$ (a): Closed Rayleigh system (Mariotti et al., 1981): $\delta^{29}Si_{DSi}=\delta^{29}Si_{DSi\text{-}initial}+^{29}\varepsilon\times\ln f$; $\delta^{29}Si_{BSi\text{-}inst}=\delta^{29}Si_{DSi}+^{29}\varepsilon$; $\delta^{29}Si_{BSi\text{-}acc}=\delta^{29}Si_{DSi\text{-}initial}-^{29}\varepsilon\times f(\ln f/(1-f))$. $\delta^{29}Si_{BSi\text{-}inst}$ (light dashed curve) is the isotopic composition of diatom produced for a specific f_t (referred to as the instantaneous product), and $\delta^{29}Si_{BSi\text{-}acc}$ (thick dashed curve) is the resulting isotopic composition of the total diatoms population grown from f=1 up to f_t without export (referred to as the accumulated product). (b) Open system (Sigman et al., 1999b). $\delta^{29}Si_{DSi}=\delta^{29}Si_{DSi\text{-}initial}-^{29}\varepsilon\times(1-f)$; $\delta^{29}Si_{BSi}=\delta^{29}Si_{DSi\text{-}initial}+^{29}\varepsilon\times f$. Note that in the open steady-state system diatoms all have the same isotopic signature (light plain line); i.e. the isotopic difference between $\delta^{29}Si_{BSi\text{-}inst}$ and $\delta^{29}Si_{BSi\text{-}acc}$ does not apply. (c) Comparison of $\delta^{29}Si_{BSi}$ signatures for the two systems. Vertical lines indicate where the difference between $\delta^{29}Si_{BSi}$ curves starts to become analytically significant (i.e., 0.08‰). Note that there is no significant difference for the three lines between f=1 and f=0.75 (i.e. 0–25% DSi utilisation). Significant differences between open and closed systems are for $f<0.65$ (i.e., >35% DSi utilisation) and $f<0.55$ (i.e. >45% DSi utilisation) considering accumulated or instantaneous $\delta^{29}Si_{BSi}$ respectively. Based on estimated winter mixed layer depth and DSi profiles, we calculate for the SIZ DSi that silicic acid utilisation during CLIVAR-SR3 ranged between 15 and 45% (Cardinal et al., 2005a), indicating non-significant model dependence for our SIZ $\delta^{29}Si_{BSi}$.

4.1.1. Sea ice diatoms

SIZ stations were still under sea ice influence at the time of sampling, with reduced ice coverage (SIZ-2-R) or recent ice-free conditions (SIZ-1) (Fig. 1). Antarctic sea ice contains a significant amount of diatoms and their release during melting has been identified as an

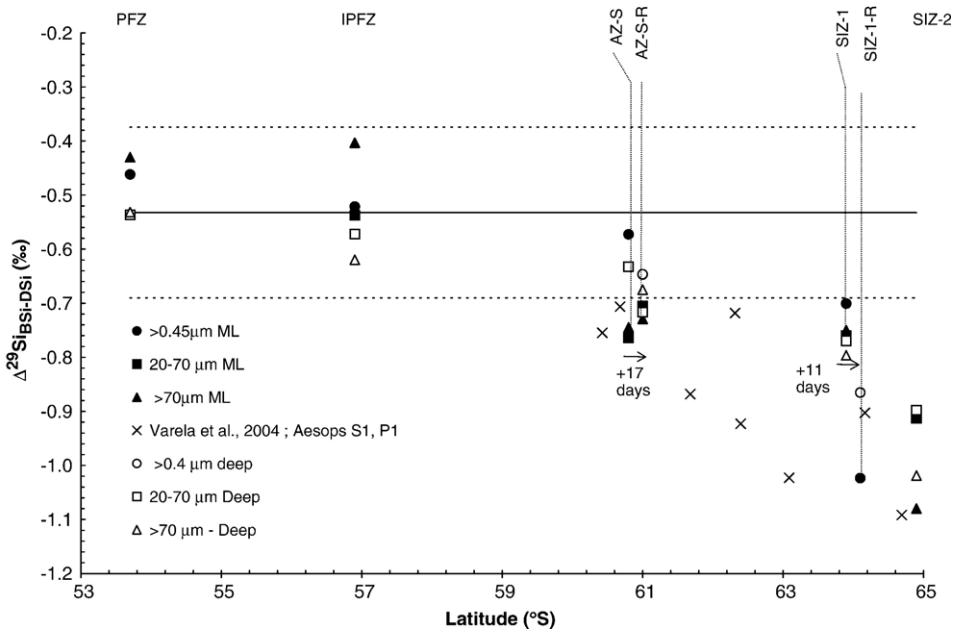

Fig. 5. Latitudinal variation of $\Delta^{29}Si$ ($\Delta^{29}Si = \delta^{29}Si_{BSi} - \delta^{29}Si_{DSi}$). Latitudes displayed for repeat stations have been slightly shifted in the figure to avoid overlap with first sampling (AZ-S-R has been put at 61.2°S instead of 60.8°S and SIZ-1-R at 65.1°S instead of 64.9°S). Filled symbols: average values for mixed layer (ML). Open symbols (deep): difference between $\delta^{29}Si_{BSi}$ below the ML and $\delta^{29}Si_{DSi}$ within the ML. Circles: >0.4 µm fraction; squares: 20–70 µm; triangles: >70 µm; crosses: spring data from Varela et al. (2004), i.e. AESOPS Survey 1 and Process 1. The straight horizontal line reflects the average fractionation factor estimate, $^{29}\varepsilon$, based on $\delta^{29}Si_{DSi}$ data only for the zone PFZ to SIZ, (Cardinal et al., 2005a). This value is similar to the one of De La Rocha et al. (1997). Dashed lines indicate ±1 standard deviation from this average estimate. See section sampling for the definition of acronyms.

important factor to initiate blooms in the SIZ (Lancelot et al., 1993; Goffart et al., 2000; Moore and Abbott, 2000; Riaux-Gobin et al., 2005). Diatom assemblages at SIZ-2 and SIZ-1-R (Kopczynska et al., submitted for publication) reveal the presence of characteristic sea ice related species such as *F. cynlindrus* and *F. curta* (e.g. Armand et al., 2005) and these were not present in such abundance at SIZ-1 or at northern stations. A preliminary investigation does not support specific light isotopic signatures for sea ice diatoms. Indeed $\delta^{29}Si_{BSi}$ of diatoms sampled directly within sea ice cores during the ARISE spring 2003 cruise are much heavier (+0.63±0.12‰, $n=13$; Fripiat, 2005 and Fripiat et al., submitted for publication) than the ones we obtained for BSi in the SIZ mixed layer during CLIVAR-SR3 (0.06± 0.18‰ Fig. 2 and Table 1) whereas silicate in brines has either a similar isotopic composition as in the surface mixed layer or is slightly heavier (Fripiat et al., submitted for publication). It is therefore unlikely that light $\delta^{29}Si_{BSi}$ values encountered at SIZ-2 and SIZ-1-R reflect the signature of sea ice diatoms. Indeed, diatoms in ice have a heavier Si isotopic composition, and there is no reason why they should become that light once released and in the course of blooming, given the $\delta^{29}Si_{DSi}$ signature of their Si source in the mixed layer (~0.92‰). The fact that Varela et al. (2004) reported similar negative BSi isotopic compositions at such southern latitudes for situations without evidence of recent sea ice influence corroborates this view.

4.1.2. Iron

Iron is a key factor for diatom's cell silicification and nitrate assimilation and its limitation increases the diatom Si:N ratios 2–8 fold (e.g. Hutchins and Bruland, 1998; Franck et al., 2000). Dissolved Fe concentrations during CLIVAR-SR3 were low and quite homogeneous (~0.1 nM) in the PFZ–IPFZ, AZ-S and SIZ and no Fe enrichment linked to sea ice melting was observed (Sedwick et al., submitted for publication). Timmermans et al. (2001) report that the extent of Fe limitation differs between small (nano) and large (micro) diatom species. Because Fe concentrations were homogenous and bulk $\delta^{29}Si_{BSi}$ signal was supported mostly by micro-sized diatoms (>20 µm; Table 2), we suspect that Fe stress was limiting diatom growth to a similar degree all along the transect studied here as reported by Sedwick et al. (submitted for publication). This argues against Fe availability as a leading factor of Si-isotopic fractionation during CLIVAR-SR3.

4.1.3. Temperature

A role of temperature on the fractionation factor can be invoked since it is well known that both equilibrium and kinetic isotopic fractionations are temperature dependent. No temperature effect has been detected in incubation experiments (De La Rocha et al., 1997) but this could have been because of the higher temperature (12–22 °C) and/or masked by the relative high standard deviation of $^{29}\varepsilon$ estimates (±0.2‰). Plotting Δ^{29}Si vs. mixed layer temperature (Fig. 6a) reveals a significant correlation on CLIVAR-SR3 data with larger fractionation for lower temperatures although sea ice Δ^{29}Si from Fripiat et al. (submitted for publication) are completely off-trend. In the Southern Ocean many parameters vary latitudinally which renders it difficult to decipher which factor is leading. In this regard, we note that a correlation also exists between [DSi] and Δ^{29}Si (Fig. 6b). The correlation is even better and is not in complete opposition with the sea ice results, in contrast to the temperature relationship (this is briefly discussed in the next section). Moreover, low temperatures mostly affect the biomineralisation process (Sullivan, 1980) and, according to Milligan et al. (2004), this step is not thought to induce a measurable Si-isotopic fractionation. For these reasons, although temperature cannot be ruled out yet, it does not explain our variations satisfactorily. The possibility of a temperature effect remains to be addressed carefully by experimental growth experiments to verify if the non-dependency of ε on temperature (De La Rocha et al., 1997) can be extended to the very low temperatures (−1.0 to 3 °C). A better understanding of diatom growth and associated silicon isotope fractionation in sea ice must also be tackled.

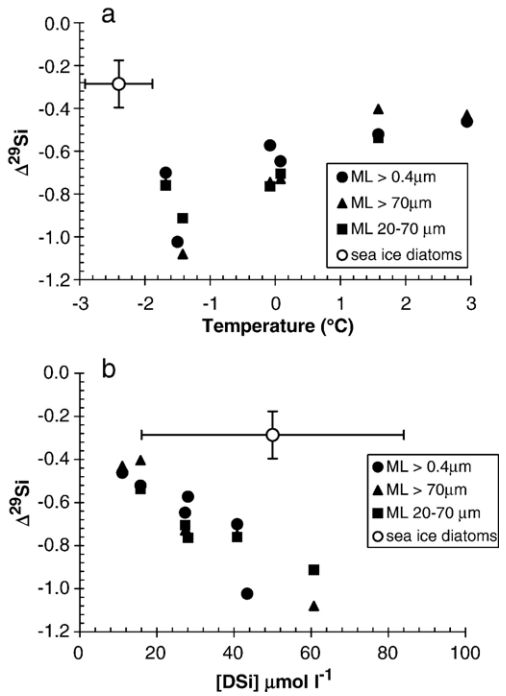

Fig. 6. Mixed layer Δ^{29}Si vs. temperature (a) and [DSi] (b). Filled circles: >0.4 µm; filled squares: 20–70 µm; filled squares: >70 µm; empty circles: sea ice diatoms. Temperatures and isotopic composition of sea ice diatoms (n=10) are from Fripiat et al. (in prep.) in cores sampled during the ARISE 2003 cruise (R/V *Aurora Australis*, October–November 2003, at ~64.5°S, 117°E). Only data for temperatures>−5 °C are presented because above this temperature the brine channels are open (Golden, 2001) and therefore $\delta^{29}Si_{BSi}$ is not likely to be biased by $\delta^{29}Si_{BSiacc}$ (Fig. 4a). As no [DSi] contents were measured directly in the brine pockets during this cruise we have taken the range obtained by Gleitz et al. (1995).

4.1.4. Si uptake and dissolution rates

Si is incorporated actively within a diatom cell by different types of silicon transporters, SIT (Hildebrand et al., 1997). Silicification in diatoms takes place during the G2 and M phases of cell division when no photosynthetic energy is involved and the necessary energy is supplied via respiration (cf. the review by Martin-Jézéquel et al., 2000). Consequently, silicification (Si content per cell) is enhanced at reduced light levels or when the ratio of dark over light period is high, i.e. when cell growth rate is lower (Claquin et al., 2002). This implies a decoupling between cell growth rate (cell division rate) and specific Si uptake rate (Vb in time^{-1}), which actually reflects the Si turn-over in the diatoms. Reaction kinetics usually have a strong impact on isotopic fractionation processes (Young et al., 2002). However, the current level of analytical precision for Si isotope ratio measurement precludes deciphering whether the biogenic isotopic fractionation is a kinetic or an equilibrium process (De La Rocha et al., 1997). In vitro measurements support the view that variable cell growth rate does not generate a variable fractionation factor (De La Rocha et al., 1997), but as Si specific uptake rate is decoupled from cell division rate (Martin-Jézéquel et al., 2000) this conclusion cannot be extended to Vb. Actually little is known about the influence of Si uptake and dissolution rates on the fractionation factor but we observed that there is a significant positive relationship between the Δ^{29}Si data from Varela et al. (2004) and the balance of Si uptake and Si release (Vb−Vd), Brzezinski et al. (2001) report for the same AESOPS stations. Si release from a diatom cell can occur according to two processes (Milligan et al., 2004): dissolution (depolymerisation of opal to silicic acid) and efflux (outward Si transport across the membrane). This efflux can take place via Si transporters or simple diffusion. Milligan et al. (2004) show that “Si dissolution

rates" assessed from ^{29}Si isotope enrichment experiments actually result from both Si efflux and dissolution. Since SIT are the loci of the Si isotopic fractionation during uptake (Milligan et al., 2004), it is likely that their involvement during efflux also fractionates Si isotopes. It would be worth looking at the relation between δ^{29}Si and the specific Si uptake and dissolution rates but such data are not available for CLIVAR-SR3. Further experimental evidence for the observed relationship between ε and (Vb−Vd) is needed since we cannot exclude that the balance between specific uptake and release rate (Vb−Vd) impacts on fractionation. Other likely explanations for the significant relationship between (Vb−Vd) and Δ^{30}Si during AESOPS are: (i) physical mixing that could have driven the Vb−Vd vs.Δ^{30}Si relationship by biasing the assumption $\Delta^{30}\mathrm{Si} \sim {}^{30}\varepsilon$ (a process inducing such artefact is discussed in more detail in Section 4.1.5); (ii) indirect control of diatom silicification by the light:dark cycle (Claquin et al., 2002); (iii) the specific Si uptake rate is partly depending on the external DSi contents (e.g., Brzezinski et al., 2005) and therefore, in general, exhibits a latitudinal trend in the Southern Ocean (Nelson and Gordon, 1982; Brzezinski et al., 2001; Beucher et al., 2004). The stronger relationship between Δ^{29}Si and [DSi] compared to Δ^{29}Si and temperature seems to corroborate this (Fig. 6b). In this regard, hydroponic experiments on higher plants also support a larger Δ^{29}Si when DSi content of the continuous nutrient supply is higher (Opfergelt et al., in press).

4.1.5. Mixing and export as possible biases between Δ^{29}Si and $^{29}\varepsilon$

4.1.5.1. Mixing. Mixing events are frequent in the spring Southern Ocean especially in frontal zones such as PFZ and IPFZ. Indeed during CLIVAR-SR3, PFZ and IPFZ upper water layers were less stratified than SIZ upper waters as seen for instance in density profiles (Cardinal et al., 2005b). Mixing would entrain isotopically light silicic acid into the euphotic zone from depth, diminishing the difference between the isotopic signature of the diatoms previously formed and dissolved Si recently supplied. It also would reduce the latitudinal gradient of $\delta^{29}\mathrm{Si}_{\mathrm{DSi}}$ in the mixed layer, since mixed layer δ^{29}Si isotopic signatures would then result from the combined effects of vertical mixing (inducing changes of the source isotopic signature) and biological uptake (Cardinal et al., 2005a). Such processes are qualitatively (but not straightforwardly) similar to the ones setting latitudinal changes of silicic acid contents (Pollard et al., 2002). A steady-state open system model (Fig. 4b) takes into account mixing provided that nutrient is continuously supplied (with invariable source isotopic composition) and partially consumed, with residual nutrient being exported at a steady-state rate, such that gross nutrient supply is balanced by biomass produced and the residual nutrient exported. When these conditions are fulfilled, mixing of surface and deeper waters tends to recombine waters which have experienced fractionation along the same isotopic path. This situation would not strongly influence ε estimates (Sigman et al., 1999b). However $\delta^{29}\mathrm{Si}_{\mathrm{BSi}}$ is the result of time-scale processes which may not be synchronous with those setting $\delta^{29}\mathrm{Si}_{\mathrm{DSi}}$, thus precluding the steady-state assumption needed for $\Delta^{29}\mathrm{Si} \sim {}^{29}\varepsilon$ as discussed below.

In particular if recent and intense mixing events occurred at the PFZ–IPFZ locations just before sampling, they could have shifted $\delta^{29}\mathrm{Si}_{\mathrm{DSi}}$ towards lighter values before the δ^{29}Si of the diatoms population actually sampled had been affected by the recent isotopic change of the silicic acid source. We cannot rule out such a possibility, but some evidences go against this explanation. First it would imply that the true PFZ–IPFZ fractionation factor lies within the range of values found for Δ^{29}Si in the SIZ (i.e. around −0.9 to −1.1‰). Though Varela et al. (2004) provide some indication that the $^{29}\varepsilon$ might be larger than the 0.56‰ as expected from in vitro incubations on tropical marine diatoms (De La Rocha et al., 1997), this was not confirmed by our previous work (Cardinal et al., 2005a) and has not yet been quantified by others. Clearly this underlines the urgent need for reducing uncertainties on ε by means of in vitro incubations reproducing Southern Ocean conditions (temperature, species, DSi). Such studies are underway. Second, models predict that increasing vertical mixing enhances downwelling of Chl-a beneath the mixed layer (Larsson, 2004). Therefore, it is expected that high vertical mixing would diminish the (isotopic) heterogeneity between mixed layer and deep diatoms. However, the reverse is observed, i.e. BSi isotopic composition is more homogenous with depth in the SIZ than in PFZ–IPFZ (see discussion in Section 4.2).

4.1.5.2. Export. In case a significant amount of BSi is subject to export the open steady-state or closed system conditions are violated. Grazing pressure was high all along the SR3 section (Safi et al., submitted for publication; Kopczynska et al., submitted for publication) and other studies indicate that export was occurring (Savoye et al., 2004b; Cardinal et al., 2005b). SIZ stations were somewhat different in that grazing pressure was highest for the nano-phytoplankton (<20 μm) and lowest for the micro-phytoplankton cells, which dominated (Safi et al., submitted for publication). Indeed an export of most recently formed

diatoms (supposed to be isotopically heavier than the older ones, Fig. 4) could bias $\Delta^{29}Si$ toward larger values.

In a closed system with accumulation of BSi, $\Delta^{29}Si$ will also increase during the DSi drawdown as illustrated in Fig. 4a. By taking a constant equilibrium fractionation factor $^{29}\varepsilon$ of −0.54‰ and an initial $\delta^{29}Si_{DSi}$ ranging from 0.77‰ and 0.92‰ (Cardinal et al., 2005a), it is impossible to reconcile a $\Delta^{29}Si$ value of −1.0‰ with the $\delta^{29}Si_{DSi}$ and $\delta^{29}Si_{BSi}$ measured in the SIZ-2 and SIZ-1-R. In the SIZ during CLIVAR-SR3 we assessed Si utilisation to be less than 40% (Cardinal et al., 2005a) and it is worth underlining that whatever model is chosen, there is no significant (i.e. measurable) difference among $\delta^{29}Si_{BSi}$ values for a Si utilisation less than 35–45% (see Fig. 4c).

Therefore the most likely bias on the $\Delta^{29}Si \sim {}^{29}\varepsilon$ assumption would rest on processes moving away $\delta^{29}Si_{DSi}$ and $\delta^{29}Si_{BSi}$ from models described in Fig. 4 such as different time-scales for the dissolved and particulate phases, i.e. mixing and/or export. Our data are snapshots and are very sensitive to short-term environmental changes, yielding to large variability. It is possible that at the annual or multi-annual time-scales, this short-term seasonal variation is smoothed out. Looking at seasonal or inter-annual variability from sediment trap isotopic signatures may provide key information on this aspect, as initiated by Varela et al. (2004).

4.2. BSi dynamics within zones

Even if the fractionation factor would be more variable than previously expected, it is likely that this variability during CLIVAR-SR3 was – directly or indirectly – related to latitude, as supported by the discussion above. Therefore we discuss the Si isotopic signatures in relation to spring diatoms and Si cycles within zones.

4.2.1. PFZ–IPFZ vs. SIZ

In the PFZ–IPFZ, deep $\delta^{29}Si_{BSi}$ are lighter than the surface signatures, giving support to the occurrence of two different populations of diatoms: below the mixed layer, we have diatoms that were rapidly exported at the beginning of the bloom (with lighter isotopic signature at the onset of Si consumption, as expected), whereas in the mixed layer the diatom population (getting progressively isotopically heavier) has not yet experienced export. Such decoupling would have been possible if stratification had occurred recently. The exported diatoms originally grew in an unstratified, open system before being exported and sealed off from the surface after stratification occurred. On the other hand, diatoms sampled from the mixed layer grew in a partly closed system and/or accumulated in the mixed layer for a while due to stronger stratification. Since, on the contrary there is no depth-related Si-isotopic difference at stations SIZ-1, SIZ-2 and AZ-S, located further south, the deeper diatoms there must have been exported recently and should therefore have the same history as the ones still in the mixed layer. Likewise, for the PFZ in spring (Atlantic sector) Quéguiner and Brzezinski (2002) also report important peaks of BSi down to 200 m contrasting with more southern zones. Their BSi production rates provided additional support for significant BSi export while the bloom was still expanding. This overall picture is also consistent with the temporal dynamics of the diatom bloom in the Southern Ocean, which starts in the PFZ and then propagates southward when environmental conditions evolve favourably (Nelson et al., 2001; Brzezinski et al., 2001).

4.2.2. Repeat stations

4.2.2.1. AZ-S. At 60.8°S many parameters converge to indicate that a bloom was going on during the first visit (AZ-S) but that its intensity had decreased during the second visit (AZ-S-R). New production at AZ-S was the second highest of the whole transect but had decreased by one third at AZ-S-R (Savoye et al., 2004a). Diatom cell numbers were the highest at the first visit but had decreased by 20% (Fig. 3) while diatoms biomass increased by 45% (Cardinal et al., 2005b) along with a 2.3-fold increase of BSi contents (Table 2). This bloom clearly induced some particle export (Savoye et al., 2004b) and mesopelagic carbon remineralisation (Cardinal et al., 2005b) in accordance with the highest grazing pressure found at AZ-S for the <20 μm size fraction (Safi et al., submitted for publication). Whereas between successive visits Si isotopic signatures for both, dissolved and biogenic phases increased, with the most significant enrichment being measured for the larger (>20 μm) micro-sized diatoms (Fig. 2), only a very small DSi depletion had occurred in the mixed layer (0.8 μM Si; Table 2). Note that the signature of deep diatoms did not significantly change between the two samplings. Such variation in isotopic signature would result from silicate consumption, but cannot easily be reconciled with the open steady-state or closed systems since any significant isotopic shift should be accompanied by a significant Si depletion (Fig. 4). Varela et al. (2004) and Cardinal et al. (2005a) have shown that none of these models are likely to describe adequately the Southern Ocean at the seasonal time-scale. In particular, if the open model is preferred for the CLIVAR-SR3 spring conditions as discussed in Cardinal et al. (2005a), it cannot describe non-steady-state conditions which are likely to occur when sporadic mixing and/or export events

take place (Varela et al., 2004). The fact that the isotopic change for large diatoms is larger than the change for $\delta^{29}Si_{DSi}$ could be due to a recent mixing event having resupplied the mixed layer in DSi, and thereby dampening $\delta^{29}Si_{DSi}$ without having affected $\delta^{29}Si_{BSi}$.

4.2.2.2. SIZ-1 vs. SIZ-1-R. As observed for the AZ-S situation, [BSi] (from 0.9 to 1.4 μM), diatom biomass (10 to 13 μg C l^{-1}; Cardinal et al., 2005b), Chl-a and ^{234}Th deficit (Savoye et al., 2004a,b) all increased in between the two visits, while diatom cell numbers decreased (−12–14%; Fig. 3). The $\delta^{29}Si_{BSi}$ of the >0.4 μm fraction shifted from +0.32 to −0.08‰ in the mixed layer within 11 days. This shift was also present (though to a lesser extent) below the mixed layer (Fig. 2 and Table 2) while DSi slightly increased (from 40.8 to 43.8 μM). Decreasing $\delta^{29}Si_{BSi}$ and increasing silicate concentrations are a priori inconsistent with increasing diatom biomass and Chl-a characteristic of a bloom situation unless a sporadic mixing event occurred in between both visits at the SIZ-1 site, a kind of process described and discussed in Section 4.1.5.

5. Conclusions and perspectives

By reporting on Si-isotopic composition of Southern Ocean diatoms during spring this study complements our previous work on dissolved silicate from the same CLIVAR-SR3 cruise (Cardinal et al., 2005a). The Si-isotopic signatures of diatoms appear generally to be unrelated to particle size. The latitudinal trend toward lighter particulate isotopic composition ($\delta^{29}Si_{BSi}$) in the South is much steeper than the one for dissolved silicon in surface waters ($\delta^{29}Si_{DSi}$). Such discrepancy between dissolved and particulate phases might indicate a variable equilibrium fractionation factor between diatoms and seawater and/or non-equilibrium conditions. Taking into account the large amount of information available from the CLIVAR-SR3 cruise, we found that the factors most likely to produce such change are temperature, DSi contents, and, the specific Si uptake and dissolution rates. These factors are different from the ones controlling N isotopic fractionation which strengthens the picture of a decoupling between the Si and N cycles in diatoms as underlined by recent studies (Martin-Jézéquel et al., 2000; Claquin et al., 2002). Yet, these results are far from proving that Si-isotopic fractionation by diatoms is variable. As discussed, many parameters vary with latitude in the Southern Ocean and finding a significant relationship among the two, as in Fig. 6, does not necessarily mean that one causes the other. Moreover a decoupling between $\delta^{29}Si_{BSi}$ and $\delta^{29}Si_{DSi}$ resulting from different and/or too small time windows is also possible. In particular, the latitudinal $\Delta^{29}Si$ trend could result from more intense and sporadic vertical mixing events in the PFZ–IPFZ which would result in undermining the assumption that apparent fractionation factor ($\Delta^{29}Si$) approximates equilibrium fractionation factor ($^{29}\varepsilon$) as based on the simple models currently available. Such biases from model rationales recorded by snapshot sampling could be dampened at the annual or multi-annual time-scales and hence do not yet invalidate the potential of Si isotopes as a useful paleo-proxy.

Comparison of $\delta^{29}Si_{BSi}$ in the mixed layer with $\delta^{29}Si_{BSi}$ just below the mixed layer supports the view of dynamic changes in the Southern Ocean during spring, involving spatial differentiation due to progressive (latitudinal) delay of the season's onset as controlled by light, temperature and stratification. Although sampled in early October, the PFZ–IPFZ had already exported diatoms which were isotopically lighter than the ones found in the mixed layer. Farther south no depth-related isotopic change was observed in agreement with an ongoing recently started bloom.

Overall even if these results highlight important gaps in the understanding of the oceanic Si isotope system, the differences with previous estimates are significant only in the seasonal ice zone given the standard deviation of the fractionation factor estimates and the uncertainties linked to the choice of the model. Therefore further steps must be especially undertaken in order to (i) improve modelling of the Si isotope cycle in the upper water column at the seasonal scale and quantify the isotopic effect of mixing events, (ii) constrain the effect of low temperature, DSi contents, Si specific uptake and dissolution rates and species by in vitro experiments, (iii) measure the isotopic signature of exported diatoms on time series (sediment traps) to verify if the same variability is obtained on a larger time window, (iv) examine the special environment of sea ice hosted diatoms, and (v) investigate efflux and dissolution rates by detailed physiological studies: it should be of particular importance to know whether efflux is mostly controlled by silicon transporters (SIT) and/or diffusion, and identify the implications for the Si isotopic system.

Acknowledgements

We thank the CLIVAR-SR3 party on board the R/V *Aurora Australis* (AU0103), especially the officers and crew and S. Rintoul (chief scientist) for their efficient help as well as K. Safi and P. Sedwick for having provided their data prior to publication. We are grateful to J. de Jong and N. Mattielli (ULB) for the management of the MC-ICP-MS lab in Brussels and to S. Pollet (U. Gent and VUB), L. Alleman, L. Monin and N. Dahkani (MRAC) for their help

in sample processing and ICP-AES analyses. This work was conducted under the BELCANTO II network funded by the Belgian Science Policy on Sustainable Development (SPSDII, contracts EV/37/7C and EV/03/7A). We thank the "Fonds National de la Recherche Scientifique" (contract FRFC n°2.4.512.00F) for funding the purchase of the MC-ICP-MS. Fieldwork was supported by the Australian Antarctic Science program via projects ASAC 1156 (T.W.T.) and ng1343 (F.D.). T.W.T. acknowledges support of the Australian Commonwealth Cooperative Research Centre Program. Work of E. Kopczynska was partly supported by grant 2 PO4 F 024 26 of the Polish Committee for Scientific Research. The sea ice dataset was collected in the framework of the SIBClim Program (ARC contract n° 02/07-287 of the Communauté Française de Belgique). The officers and crew of the ARISE *Aurora Australis* cruise (AU0301) and I. Allison (Chief Scientist) are especially acknowledged for their kind collaboration in that respect. The constructive comments of two anonymous reviewers have significantly helped in clarifying and balancing the discussion.

References

Abelmann, A., Gersonde, R., 1991. Biosiliceous particle flux in the Southern Ocean. Marine Chemistry 35, 503–536.

Alleman, L.Y., Cardinal, D., Cocquyt, C., Plisnier, P.-D., Descy, J.-P., Kimirei, I., Sinyianza, D., André, L., 2005. Silicon isotopic fractionation in Lake Tanganyika and its tributaries. Journal of Great Lakes Research 31, 509–519.

Altabet, M.A., François, R., 2001. Nitrogen isotope biogeochemistry of the Antarctic Polar Frontal Zone at 170°W. Deep-Sea Research. Part 2. Topical Studies in Oceanography 48, 4247–4273.

Armand, L.K., Crosta, X., Romero, O., Pichon, J.-J., 2005. The biogeography of major diatom taxa in Southern Ocean sediments: 1. Sea ice related species. Palaeogeography, Palaeoclimatology, Palaeoecology 223, 93–126.

Basile-Doelsch, I., 2006. Si stable isotopes in the Earth's surface: a review. Journal of Geochemical Exploration 88, 252–256.

Becquevort, S., 1997. Nanoprotozooplankton in the Atlantic sector of the Southern Ocean during early spring: biomass and feeding activities. Deep-Sea Research. Part 2. Topical Studies in Oceanography 44, 355–373.

Beucher, C., Tréguer, P., Hapette, A.-M., Corvaisier, R., Metzl, N., Pichon, J.-J., 2004. Intense summer Si-recycling in the surface Southern Ocean. Geophysical Research Letters 31, L09305. doi:10.1029/2003GL018998.

Boyd, P.W., Watson, A.J., Law, C.S., Abraham, E.R., Trull, T., Murdoch, R., Bakker, D.C.E., Bowie, A.R., Buesseler, K.O., Chang, H., Charette, M., Croot, P., Downing, K., Frew, R., Gall, M., Hadfield, M., Hall, J., Harvey, M., Jameson, G., LaRoche, J., Liddicoat, M., Ling, R., Maldonado, M.T., McKay, R.M., Nodder, S., Pickmere, S., Pridmore, R., Rintoul, S., Safi, K., Sutton, P., Strzepek, R., Tanneberger, K., Turner, S., Waite, A., Zeldis, J., 2000. A mesoscale phytoplankton bloom in the polar Southern Ocean stimulated by iron fertilization. Nature 407, 695–702.

Brzezinski, M.A., Nelson, D.M., Franck, V.M., Sigmon, D.E., 2001. Silicon dynamics within an intense open-ocean diatom bloom in the Pacific sector of the Southern Ocean. Deep-Sea Research. Part 2. Topical Studies in Oceanography 48, 3997–4018.

Brzezinski, M.A., Pride, C.J., Franck, V.M., Sigman, D.M., Sarmiento, J.L., Matsumoto, K., Gruber, N., Rau, G.H., Coale, K.H., 2002. A switch from $Si(OH)_4$ to NO_3^- depletion in the glacial Southern Ocean. Geophysical Research Letters 29, 12. doi:10.1029/2001GL014349.

Brzezinski, M.A., Dickson, M.-L., Nelson, D.M., Sambrotto, R., 2003. Ratios of Si, C and N uptake by microplankton in the Southern Ocean. Deep-Sea Research. Part 2. Topical Studies in Oceanography 50, 619–633.

Brzezinski, M.A., Jones, J.L., Demarest, M.S., 2005. Control of silica production by iron and silicic acid during the Southern Ocean Iron Experiment (SOFeX). Limnology and Oceanography 50, 810–824.

Cardinal, D., Alleman, L.Y., De Jong, J., Ziegler, K., André, L., 2003. Isotopic composition of silicon measured by multicollector plasma source mass spectrometry in dry plasma mode. Journal of Analytical Atomic Spectrometry 18, 213–218.

Cardinal, D., Alleman, L.Y., Dehairs, F., Savoye, N., Trull, T.W., André, L., 2005a. Relevance of silicon isotopes to Si-nutrient utilization and Si source assessment in Antarctic waters. Global Biogeochemical Cycles 19, GB2007. doi:10.1029/2004GB002364.

Cardinal, D., Savoye, N., Trull, T.W., André, L., Kopczynska, E.E., Dehairs, F., 2005b. Variations of carbon remineralisation in the Southern Ocean illustrated by the Baxs proxy. Deep-Sea Research. Part 1. Oceanographic Research Papers 52, 355–370.

Carignan, J., Cardinal, D., Eisenhauer, A., Galy, A., Rehkämper, M., Wombacher, F., Vigier, N., 2004. A reflection on Mg, Cd, Ca, Li and Si isotopic measurements and related reference materials. Geostandards and Geoanalytical Research 28, 139–148.

Chaigneau, A., Morrow, R.A., Rintoul, S.R., 2004. Seasonal and interannual evolution of the mixed layer in the Antarctic Zone south of Tasmania. Deep-Sea Research. Part 1. Oceanographic Research Papers 51, 2047–2072.

Claquin, P., Martin-Jézéquel, V., 2005. Regulation of the Si and C uptake and of the soluble free-silicon pool in a synchronised culture of *Cylindrotheca fusiformis* (Bacillariophyceae): effects on the Si/C ratio. Marine Biology 146, 877–886.

Claquin, P., Martin-Jézéquel, V., Kromkamp, J.C., Veldhuis, M.J.W., Kraay, G.W., 2002. Uncoupling of silicon compared with carbon and nitrogen metabolisms and the role of the cell cycle in continuous cultures of *Thalassiosira pseudonana* (Bacillariophyceae) under light, nitrogen and phosphorus control. Journal of Phycology 38, 922–930.

Crosta, X., Shemesh, A., Etourneau, J., Yam, R., Billy, I., Pichon, J.J., 2005. Nutrient cycling in the Indian sector of the Southern Ocean over the last 50,000 years. Global Biogeochemical Cycles 19, GB3007. doi:10.1029/2004GB002344.

Del Amo, Y., Brzezinski, M.A., 1999. The chemical form of dissolved Si taken up by marine diatoms. Journal of Phycology 35, 1162–1170.

De La Rocha, C.L., Brzezinski, M.A., DeNiro, M.J., 1996. Purification, recovery and laser-driven fluorination of silicon from dissolved and particulate silica for the measurement of natural stable isotope abundances. Analytical Chemistry 68, 3746–3750.

De La Rocha, C.L., Brzezinski, M.A., DeNiro, M.J., 1997. Fractionation of silicon isotopes by marine diatoms during biogenic silica formation. Geochimica et Cosmochimica Acta 61, 5051–5056.

De La Rocha, C.L., Brzezinski, M.A., DeNiro, M.J., Shemesh, A., 1998. Silicon-isotope composition of diatoms as an indicator of past oceanic change. Nature 395, 680–683.

De La Rocha, C.L., Brzezinski, M.A., DeNiro, M.J., 2000. A first look at the distribution of the stable isotopes of silicon in natural waters. Geochimica et Cosmochimica Acta 64, 2467–2477.

Ding, T., Wan, D., Li, J., Jiang, S., Song, H., Li, Y., Liu, Z., 1996. Silicon Isotope Geochemistry. Geological Publishing House, Beijing.

Douthitt, C.B., 1982. The geochemistry of the stable isotopes of silicon. Geochimica et Cosmochimica Acta 46, 1449–1458.

Franck, V.M., Brzezinski, M.A., Coale, K.H., Nelson, D.M., 2000. Iron and silicic acid concentrations regulate Si uptake north and south of the Polar Front Zone in the Pacific Sector of the Southern Ocean. Deep-Sea Research. Part 2. Topical Studies in Oceanography 47, 3315–3338.

François, R., Altabet, M.A., Yu, E.-F., Sigman, D., Bacon, M.P., Frank, M., Bohrmann, G., Bareille, G., Labeyrie, L.D., 1997. Contribution of Southern Ocean surface-water stratification to low atmospheric CO_2 concentrations during the last glacial period. Nature 389, 929–935.

François, R., Honjo, S., Krishfield, R., Manganini, S., 2002. Factors controlling the flux of organic carbon to the bathypelagic zone of the ocean. Global Biogeochemical Cycles 16, 1087. doi:10.1029/2001GB001722.

Fripiat, F., 2005. Etude structurale et isotopique du silicium dans la glace de banquise Antarctique, M. Sc. Thesis, Université Libre de Bruxelles, 117pp.

Fripiat, F., Cardinal, D., Tison, J.-L., Worby, A., André, L., submitted for publication. Diatom-induced Si-isotopic fractionation in Antarctic sea-ice. Journal of Geophysical Research-Biogeosciences.

Gleitz, M., Rutgers van der Loeff, M., Thomas, D.N., Dieckmann, G.S., Millero, F.J., 1995. Comparison of summer and winter inorganic carbon oxygen and nutrient concentrations in Antarctic sea ice brine. Marine Chemistry 51, 81–91.

Goffart, A., Catalano, G., Hecq, J.H., 2000. Factors controlling the distribution of diatoms and *Phaeocystis* in the Ross Sea. Journal of Marine Systems 27, 161–175.

Golden, K.M., 2001. Brine percolation and the transport properties of sea ice. Annals of Glaciology 33, 28–36.

Granger, J., Sigman, D.M., Needoba, J.A., Harrison, P.J., 2004. Coupled nitrogen and oxygen isotope fractionation of nitrate during assimilation by cultures of marine phytoplankton. Limnology and Oceanography 49, 1763–1773.

Hutchins, D.A., Bruland, K.W., 1998. Iron-limited diatom growth and Si:N uptake ratios in a coastal upwelling regime. Nature 393, 561–564.

Hildebrand, M., Volcani, B.E., Gassmann, W., Schroeder, J.I., 1997. A gene family of silicon transporters. Nature 385, 688–689.

Karsh, K.L., Trull, T.W., Lourey, M.J., Sigman, D.M., 2003. Relationship of nitrogen isotope fractionation to phytoplankton size and iron availability during the Southern Ocean Iron RElease Experiment (SOIREE). Limnology and Oceanography 48, 1058–1068.

Klaas, C., Archer, D.E., 2002. Association of sinking organic matter with various types of mineral ballast in the deep sea: implications for the rain ratio. Global Biogeochemical Cycles 16, 1116. doi:10.1029/2001GB001765.

Kopczynska, E.E., Dehairs, F., Elskens, M., Wright, S., 2001. Phytoplankton variability between the Subtropical and Polar Fronts south off Australia: thriving under regenerative and new production in late summer. Journal of Geophysical Research 106, 31597–31609.

Kopczynska, E., Savoye, N., Dehairs, F., Cardinal, D., Elskens, M., submitted for publication. Spring phytoplankton assemblages in the Southern Ocean between Australia and Antarctica; relationship to nitrogen regime. Deep-Sea Research I.

Lancelot, C., Mathot, S., Veth, C., de Baar, H.W.J., 1993. Factors controlling phytoplankton ice-edge blooms in the marginal ice-zone of the north western Weddell Sea during sea ice retreat 1988: field observations and mathematical modelling. Polar Biology 13, 377–387.

Lancelot, C., Hannon, E., Becquevort, S., Veth, C., De Baar, H.J. W., 2000. Modeling phytoplankton blooms and carbon export production in the Southern Ocean: dominant controls by light and iron in the Atlantic sector in Austral spring 1992. Deep-Sea Research. Part 1. Oceanographic Research Papers 47, 1621–1662.

Larsson, A.-M., 2004. The role of mixing in an Antarctic ocean ecosystem: observations and model computations of vertical distributions of related parameters. Deep-Sea Research. Part 2. Topical Studies in Oceanography 51, 2807–2825.

Lourey, M.J., Trull, T.W., Sigman, D.M., 2003. Sensitivity of $\delta^{15}N$ of nitrate, surface suspended and deep sinking particulate nitrogen to seasonal nitrate depletion in the Southern Ocean. Global Biogeochemical Cycles 17, 1081. doi:10.1029/2002GB001973.

Mariotti, A., Germon, J.C., Hubert, P., Kaiser, P., Letolle, R., Tardieux, A., Tardieux, P., 1981. Experimental determination of nitrogen kinetic isotope fractionation: some principles; illustration for the denitrification and nitrification processes. Plant and Soil 62, 413–430.

Martin, J.H., Fitzwater, S.E., Gordon, R.M., 1990. Iron deficiency limits phytoplankton growth in Antarctic waters. Global Biogeochemical Cycles 4, 5–12.

Martin-Jézéquel, V., Hildebrand, M., Brzezinski, M.A., 2000. Silicon metabolism in diatoms: implications for growth. Journal of Phycology 36, 821–840.

Matsumoto, K., Sarmiento, J.L., Brzezinski, M.A., 2002. Silicic acid leakage from the Southern Ocean: a possible explanation for glacial atmospheric pCO_2. Global Biogeochemical Cycles 16, 3. doi:10.1029/2001GB001442.

Milligan, A.J., Varela, D.E., Brzezinski, M.A., Morel, F.M.M., 2004. Dynamics of silicon metabolism and silicon isotopic discrimination in a marine diatom as a function of pCO_2. Limnology and Oceanography 49, 322–329.

Moore, J.K., Abbott, M.R., 2000. Phytoplankton chlorophyll distributions and primary production in the Southern Ocean. Journal of Geophysical Research 105, 28709–28722.

Needoba, J.A., Harrison, P.J., 2004. Influence of low light and a light: dark cycle on NO_3^- uptake, intracellular NO_3^- and nitrogen isotope fractionation by marine phytoplankton. Journal of Phycology 40, 505–516.

Needoba, J.A., Sigman, D.M., Harrison, P.J., 2004. The mechanism of isotope fractionation during algal nitrate assimilation as illuminated by the $^{15}N/^{14}N$ of intracellular nitrate. Journal of Phycology 40, 517–522.

Nelson, D.M., Gordon, L.I., 1982. Production and pelagic dissolution of biogenic silica in the Southern Ocean. Geochimica et Cosmochimica Acta 46, 491–501.

Nelson, D.M., Brzezinski, M.A., Sigmon, D.E., Franck, V.M., 2001. A seasonal progression of Si limitation in the Pacific sector of the Southern Ocean. Deep-Sea Research. Part 2. Topical Studies in Oceanography 48, 3973–3995.

Opfergelt S., Cardinal D., Henriet, C., Draye, X., André, L., Delvaux B., in press. Silicon isotope fractionation by banana (*Musa spp.*) grown in a continuous nutrient flow device. Plant and Soil. doi:10.1007/s11104-006-9019-1.

Pollard, R.T., Lucas, M.I., Read, J.F., 2002. Physical controls on biogeochemical zonation in the Southern Ocean. Deep-Sea

Research. Part 2. Topical Studies in Oceanography 49, 3289–3305.

Quéguiner, B., Brzezinski, M.A., 2002. Biogenic silica production rates and particulate matter distribution in the Atlantic sector of the Southern Ocean during austral spring 1992. Deep-Sea Research. Part 2. Topical Studies in Oceanography 49, 1765–1786.

Ragueneau, O., Dittert, N., Pondaven, P., Tréguer, P., Corrin, L., 2002. Si/C decoupling in the world ocean: is the Southern Ocean different? Deep-Sea Research. Part 1. Oceanographic Research Papers 49, 3127–3154.

Ragueneau, O., Savoye, N., Del Amo, Y., Cotten, J., Tardiveau, B., Leynaert, A., 2005. A new method for the measurement of biogenic silica in suspended matter of coastal waters: using Si:Al ratios to correct for the mineral interference. Continental Shelf Research 25, 697–710.

Riaux-Gobin, C., Tréguer, P., Dieckmann, G., Maria, E., Vétion, G., Poulin, M., 2005. Land-fast ice off Adélie Land (Antarctica): short-term variations in nutrients and chlorophyll just before ice break-up. Journal of Marine Systems 55, 235–248.

Sabine, C., et al., 2004. The oceanic sink for anthropogenic CO_2. Science 305, 367–371.

Safi, K.A., Griffiths, F.B., Hall, J.A., submitted for publication. Microzooplankton composition, biomass and grazing rates along WOCE SR3 line between Tasmania and Antarctica. Deep-Sea Research I.

Sarmiento, J.L., Gruber, N., Brzezinski, M.A., Dunne, J.P., 2004. High-latitude controls of thermocline nutrients and low latitude biological productivity. Nature 427, 56–60.

Savoye, N., Dehairs, F., Elskens, M., Cardinal, D., Kopczyñska, E.E., Trull, T.W., Wright, S., Baeyens, W., Griffiths, F.B., 2004a. Regional variation of spring N-uptake and New Production in the Southern Ocean. Geophysical Research Letters 31, L03301. doi:10.1029/2003GL018946.

Savoye, N., Buesseler, K.O., Cardinal, D., Dehairs, F., 2004b. ^{234}Th deficit and excess in the Southern Ocean during spring 2001: particle export and mineralization. Geophysical Research Letters 31, L12301. doi:10.1029/GL019744.

Sedwick, P., Bowie, A.R., Trull, T.W., submitted for publication. Dissolved iron in the upper ocean along the CLIVAR SR3 section (Australian sector of the Southern Ocean): Meridional and seasonal trends. Deep-Sea Research I.

Sigman, D.M., Altabet, M.A., François, R., McCorkle, D.C., Gaillard, J.-F., 1999a. The isotopic composition of diatom-bound nitrogen in Southern Ocean sediments. Plaeoceanography 14, 118–134.

Sigman, D.M., Altabet, M.A., McCorkle, D.C., François, R., Fischer, G., 1999b. The δ^{15}N of nitrate in the Southern Ocean: consumption of nitrate in surface waters. Global Biogeochemical Cycles 13, 1149–1166.

Smetacek, V., Assmy, P., Henjes, J., 2004. The role of grazing in structuring Southern Ocean pelagic ecosystems and biogeochemical cycles. Antarctic Science 16, 541–558.

Sullivan, C.W., 1980. Diatom mineralization of silicic acid. V. Energetic and macromolecular requirements for $Si(OH)_4$ mineralization events during the cell cycle of *Navicula pelliculosa*. Journal of Phycology 16, 321–328.

Takahashi, T., Sutherland, S.C., Sweeney, C., Poisson, A., Metzl, N., Tilbrook, B., Bates, N., Wanninkhof, R., Feely, R.A., Sabine, C., Olafsson, J., Nojiri, Y., 2002. Global sea–air CO_2 flux based on climatological surface ocean pCO_2, and seasonal biological and temperature effects. Deep-Sea Research. Part 2. Topical Studies in Oceanography 49, 1601–1622.

Takeda, S., 1998. Influence of iron availability on nutrient consumption ratio of diatoms in oceanic waters. Nature 393, 774–777.

Taylor, S.R., McLennan, S.M., 1985. The Continental Crust: Its Composition and Evolution. Blackwell Scientific Publications, Oxford.

Timmermans, K.R., Gerringa, L.J.A., de Baar, H.J.W., van der Wagt, B., Veldhuis, M.J.W., de Jong, J.T.M., Croot, P.L., 2001. Growth rates of large and small Southern Ocean diatoms in relation to availability of iron in natural seawater. Limnology and Oceanography 46, 260–266.

Trull, T.W., Armand, L., 2001. Insights into Southern Ocean carbon export from the δ^{13}C of particles and dissolved inorganic carbon during the SOIREE iron release experiment. Deep-Sea Research. Part 2. Topical Studies in Oceanography 48, 2655–2680.

Trull, T.W., Rintoul, S.R., Hadfield, M., Abraham, E.R., 2001. Circulation and seasonal evolution of polar waters south of Australia: implications for iron fertilization of the Southern Ocean. Deep-Sea Research. Part 2. Topical Studies in Oceanography 48, 2439–2466.

Varela, D., Pride, C.J., Brzezinski, M.A., 2004. Biological fractionation of silicon isotopes in Southern Ocean surface waters. Global Biogeochemical Cycles 18, GB01047. doi:10.1029/2003GB002140.

Wang, X., Matear, R.J., Trull, T.W., 2003. Nutrient utilization ratios in the Polar Frontal Zone in the Australian sector of the Southern Ocean: a model. Global Biogeochemical Cycles 17, 1009. doi:10.1029/2002GB001938.

Wischmeyer, A.G., Del Amo, Y., Brzezinski, M., Wolf-Gladrow, D.A., 2003. Theoretical constraints on the uptake of silicic acid species by marine diatoms. Marine Chemistry 82, 13–29.

Young, E.D., Galy, A., Nagahara, H., 2002. Kinetic and equilibrium mass-dependent isotope fractionation laws in nature and their geochemical and cosmochemical significance. Geochimica et Cosmochimica Acta 66, 1095–1104.

δ^{30}Si and δ^{29}Si Determinations on USGS BHVO-1 and BHVO-2 Reference Materials with a New Configuration on a Nu Plasma Multi-Collector ICP-MS

Vol. 32 — N° 2 06 08 p. 193–202

GEOSTANDARDS and GEOANALYTICAL RESEARCH

$\delta^{30}Si$ and $\delta^{29}Si$ Determinations on USGS BHVO-1 and BHVO-2 Reference Materials with a New Configuration on a Nu Plasma Multi-Collector ICP-MS

Kathrin **Abraham** (1, 2)*, Sophie **Opfergelt** (2, 3), François **Fripiat** (2, 5), Anne-Julie **Cavagna** (2, 4), Jeroen T.M. **de Jong** (5), Stephen F. **Foley** (1), Luc **André** (2) and Damien **Cardinal** (2)

(1) Institut für Geowissenschaften, Universität Mainz, Becherweg 21, D 55099 Mainz, Germany
(2) Section de Mineralogie-Pétrographie-Géochimie, Musée Royal de l'Afrique Centrale, Leuvensesteenweg 13, B 3080 Tervuren, Belgium
(3) Université catholique de Louvain, Unité Sciences du Sol, Place Croix du Sud 2/10, B 1348 Louvain-la-Neuve, Belgium
(4) Vrije Universiteit Brussel, Department of Analytical and Environmental Chemistry, Pleinlaan 2 B-1050 Brussels, Belgium
(5) Université Libre de Bruxelles, Département des Sciences de la Terre et de l'Environnement, Avenue F.D. Roosevelt 50, B-1050 Brussels, Belgium
* Corresponding author. e-mail: abraha@uni-mainz.de

We report silicon isotopic determinations for USGS rock reference materials BHVO-1 and BHVO-2 using a Nu Plasma multi-collector (MC)-ICP-MS, upgraded with a new adjustable entrance slit, to obtain medium resolution, as well as a stronger primary pump and newly designed sampler and skimmer cones ("B" cones). These settings, combined with the use of collector slits, allowed a resolution to be reached that was sufficient to overcome the $^{14}N^{16}O$ and $^{14}N_2$ interferences overlying the ^{30}Si and the ^{28}Si peaks, respectively, in an earlier set-up. This enabled accurate measurement of both $\delta^{30}Si$ and $\delta^{29}Si$. The δ value is expressed in per mil variation relative to the NBS 28 quartz reference material. Based on data acquired from numerous sessions spread over a period of six months, we propose a recommended average $\delta^{30}Si$ of -0.33 ± 0.05‰ and -0.29 ± 0.11‰ (2*se*) for BHVO-1 and BHVO-2, respectively. Our BHVO grand mean silicon isotope composition ($\delta^{30}Si$ = -0.31 ± 0.06‰) is significantly more negative than the only published value for BHVO-2, but is in very good agreement with the recently established average value of ocean island basalts (OIB), confirming the conclusion that the OIB reservoir has a distinct isotopic composition from the solar reservoir as sampled by chondrites.

Keywords: reference materials, BHVO-1, BHVO-2, ocean island basalt, silicon isotopes, MC-ICP-MS.

Dans cette étude nous présentons des analyses isotopiques du silicium sur les materiaux de référence de roches USGS BHVO-1 et BHVO-2 en utilisant un spectromètre de masse multi-collecteurs à source de plasma (MC-ICP-MS) Nu Plasma qui a été préalablement amélioré par une nouvelle fente d'entrée ajustable de meilleure qualité, ainsi que par une pompe primaire plus puissante et des cônes d'un nouveau modèle (cônes de type "B"). Ces paramètres combinés à l'utilisation de deux fentes situées sur les collecteurs permettent d'atteindre une résolution suffisante pour séparer les interférences $^{14}N^{16}O$ et $^{14}N_2$ qui se superposaient respectivement aux pics ^{30}Si et ^{28}Si dans la configuration initiale. Ces modifications permettent des mesures justes à la fois de $\delta^{30}Si$ et de $\delta^{29}Si$. Les valeurs δ sont exprimées en pour mille relativement au materiau de référence de quartz NBS 28. Sur la base de données acquises lors de nombreuses sessions analytiques étalées sur six mois, nous proposons de recommander les valeurs moyennes de $\delta^{30}Si$ à -0.33 ± 0.05‰ et -0.29 ± 0.11‰ (2se) pour respectivement BHVO-1 et BHVO-2. Notre valeur moyenne pour la composition isotopique de silicium de BHVO ($\delta^{30}Si$ = -0.31 ± 0.06‰) est significativement plus négative que la seule moyenne publiée pour BHVO-2 mais est en très bon accord avec les valeurs moyennes des basaltes des îles océaniques (OIB) confirmant la conclusion que le réservoir OIB a une composition isotopique différente du réservoir solaire tel qu'enregistré dans les chondrites.

GEOSTANDARDS and GEOANALYTICAL RESEARCH

Received 03 Sep 07 — Accepted 18 Dec 07

Mots-clés : materiaux de référence, BHVO-1, BHVO-2, basaltes des îles océaniques, isotopes du silicium, MC-ICP-MS.

During the last decade, there has been renewed interest in the measurement of silicon (Si) isotope variations in water and biological samples because of the importance of Si in global biogeochemical cycles through its incorporation in diatoms (e.g., De La Rocha *et al.* 1998, Varela *et al.* 2004, Cardinal *et al.* 2005, 2007, Alleman *et al.* 2005 and Fripiat *et al.* 2007) and its pathways in plants (Ding *et al.* 2005, Opfergelt *et al.* 2006). Interest has been recently extended to water-rock interaction and core formation processes focused on various mineral and rock samples: clays (Ziegler *et al.* 2005a, b), cherts (André *et al.* 2006, Robert and Chaussidon 2006), silcretes (Basile-Doelsch *et al.* 2005), metabasalts (André *et al.* 2006), metasediments (André *et al.* 2006), and basalts, lherzolites and meteorites (Georg *et al.* 2007a).

Naturally occurring mass fractionation processes between aquatic dissolved Si and biological/mineral Si-rich phases are generally limited (max. 1.5‰, Alleman *et al.* 2005 and Opfergelt *et al.* 2006, Méheut *et al.* 2007, Georg *et al.* 2006a, 2007b) producing rather small variations in the relative abundances of the three naturally occurring stable isotopes (^{28}Si, ^{29}Si and ^{30}Si). Improved gas source isotope ratio measurement (IRMS) techniques (Brzezinski *et al.* 2006) and the advance of MC-ICP-MS now provide the required precision to constrain aquatic and biological systems. This has been confirmed recently by an inter-laboratory Si isotope comparison of three pure silica reference materials (Carignan *et al.* 2004, Reynolds *et al.* 2007): (1) IRMM-018 (a SiO_2 reference material); (2) Big Batch (an artificial SiO_2 material) and (3) a diatomite sample (natural opal sample). These comparisons demonstrated that published $\delta^{30}Si$ data can be reliably compared between laboratories within 0.2‰ precision for pure silicon materials.

Chemically more complex specimens such as soils and rocks require appropriate analytical dissolution and elemental separation/purification procedures, which may differ between laboratories. As yet, there are no cross-calibration data available to assess the accuracy of the whole Si isotopic analytical procedure on these matrices. So far only two U.S. Geological Survey (USGS) reference materials AGV-2 (andesite, Oregon) and BHVO-2 (Hawaiian basalts) have been analysed for Si isotopes (van den Boorn *et al.* 2006). Their $\delta^{30}Si$ measurements (at -0.01 ± 0.24‰ and -0.09 ± 0.31‰, 2*s*, respectively) fall outside the 95% confidence intervals of representative rocks from the basaltic rock range of upper mantle lherzolites ($\delta^{30}Si$ = -0.37 ± 0.10‰, n = 4, 2*s*, Georg *et al.* 2007a), terrestrial mafic and ultramafic igneous rocks ($\delta^{30}Si$ = -0.4‰, Douthitt 1982), ocean island basalts (OIB) ($\delta^{30}Si$ = -0.37 ± 0.14‰, n = 5, 2*s*, Georg *et al.* 2007b) and bulk Iceland basalt value ($\delta^{30}Si$ = -0.35 ± 0.10‰, n = 2, 2*s*, Georg *et al.* 2007b). The compilation with Douthitt Si rock data needs no correction, since the Caltech Rose Quartz reference material is shown to be similar to NBS 28 (Georg *et al.* 2007a). These differences may reflect either analytical artefacts or natural variations that are known to affect other trace or isotopic ratios in andesitic or basaltic rocks. The first aim of this contribution is to answer this question by providing additional measurements on both BHVO-1 and BHVO-2 OIB reference materials using a different sample preparation and analytical methodology.

One of the largest drawbacks in MC-ICP-MS analysis is the occurrence of interferences of isobaric polyatomic ions, inhibiting correct determination of various elements with m/z ‹ 100, notably Fe and Si. The interferences are mostly molecular species derived from reactions in the plasma and cannot be avoided by chemical purification. In particular, the determination of $\delta^{30}Si$ on a conventional Nu Plasma instrument has proved elusive until now because of the insufficient resolution of the $^{14}N^{16}O$ interference overlying the ^{30}Si peak. $\delta^{30}Si$ was calculated from $\delta^{29}Si$ using theoretical multiplying factors based either on kinetic ($\delta^{30}Si = 1.96*\delta^{29}Si$) or equilibrium ($\delta^{30}Si = 1.93*\delta^{29}Si$) simplified mass-dependent fractionation law, based on an approximation valid for small ranges of isotopic fractionations (Johnson *et al.* 2004). In order to eliminate these interferences and to obtain high precision measurements, the Nu Plasma MC-ICP-MS was upgraded with a new high quality adjustable entrance slit, newly designed B-type cones (as opposed to the regular A-type cones) and a more powerful primary pump. The second objective of this paper is to demonstrate precise and accurate $\delta^{30}Si$ determinations on a conventional Nu Plasma instrument in high resolution mode.

Instrumental

New configuration of the Nu Plasma mass spectrometer

The measurements were performed on a Nu Plasma MC-ICP-MS (Nu Instruments, Wrexham UK, described in detail by Belshaw *et al.* 1998) at the Université Libre de Bruxelles (Belgium). For $\delta^{30}Si$ determinations our Nu Plasma instrument was upgraded with the combination of two sets of adjustable slits (entrance and collector slits), high transmission B cones and a new vacuum rotary pump (BOC Edwards E2M80), in order to accomplish a compromise between complete interference separation, flat-topped peak shape and sufficient signal intensity on all Si stable isotopes: ^{28}Si, ^{29}Si and ^{30}Si.

A newly designed entrance slit was installed in 2006 with three selectable narrower slit settings: 0.3 mm, 0.05 mm and 0.03 mm, corresponding to true low (~ 400 M/ΔM), medium (~ 1500 M/ΔM) and high resolution (~ 3000 M/ΔM). For Si isotope measurements, this slit was set at medium resolution. A higher resolution mode reduced the transmission and overall sensitivity. Contrary to the Nu Plasma HR, the Nu Plasma instrument used in this study was not equipped with so-called "Alpha" slits, used to reduce beam aberrations, which could cause a blurred peak image at the detector. As an alternative to improve the peak shape, the edge-resolving power was improved by setting the High Voltage 5 lens to 0 V. This led to steeper peak edges and improved peak top flatness. However, sensitivity was further reduced by a factor of approximately 2.

Two collector slits were installed in 2001 on the Nu Plasma instrument at ULB in Brussels in front of the L4 and H5 Faraday cups, where respectively ^{28}Si and ^{30}Si are measured. They were used to clip the interfering $^{14}N_2$ and $^{14}N^{16}O$ ion beams from the ^{28}Si and ^{30}Si beams to achieve full separation from the interference and to help peak-centring the instrument in dynamic mode (Figure 1).

The data acquisition was done in high resolution mode. The peak centring was performed according to the 10% valley rule on ^{28}Si or ^{30}Si. The source slit was set to give medium resolution, while the collector slit was optimised for each session to give spatially resolved beams on the collector. The interfered parts of the beams were clipped by the collector slits on the high mass end of the peaks. Given that $^{14}N_2$ and $^{14}N^{16}O$ are slightly heavier than ^{28}Si and ^{30}Si and do not enter the detector, this allowed only the analyte beam to enter the Faraday cup. In doing so the signal for each isotope was measured at the mid-point of the analyte peak. This configuration could be used when all interfering species are located at the high-mass side of the peak. As there was no collector slit on the axial Faraday cup where ^{29}Si was measured, this did not allow full separation of analyte and interference peaks (10% valley). This isotope was analysed in the so-called "pseudo-high resolution mode", i.e., the ^{29}Si peak was wider than ^{28}Si and ^{30}Si but measurement was performed on the lower mass side of the peak where no interference was present (Figure 1).

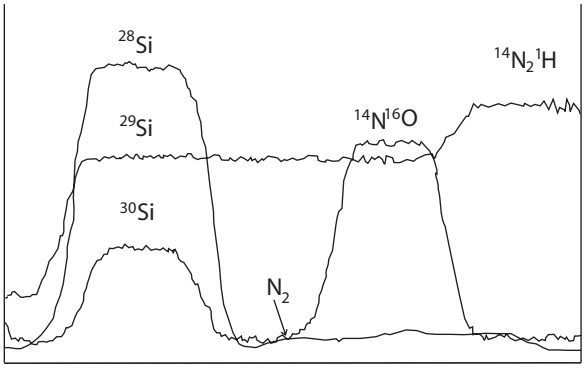

Figure 1. Magnet scan of an acid blank solution. Abscissa characterises the magnet scan mass range on the axial collector. Ordinate indicates signal intensity (different scales per curve, ^{28}Si-peak ~ 17 mV, ^{29}Si-peak ~ 1.4 mV and ^{30}Si-peak ~ 0.8 mV). Interferences were identified by calculation of ΔM (Reed *et al.* 1994). The ^{29}Si-peak was not separated from its $^{14}N_2{}^1H$ interference due to the absence of a collector slit in front of the axial collector. Given that the analysis is centred on the ^{28}Si or ^{30}Si peak, the measurements of ^{29}Si took place on the interference-free left side of the ^{29}Si-peak. Note that the $^{14}N_2{}^1H$ interference was much higher, as in Cardinal *et al.* (2003), who report insignificant levels (‹ 0.1 mV), probably related to the use of the Big80 pump in combination with B-cones, causing a higher transmission of plasma-entrained atmospheric nitrogen into the mass spectrometer.

The "Big 80" (BOC Edwards E2M80) vacuum rotary pump with a capacity of 80 $m^3\ hr^{-1}$ was installed for a better vacuum in the expansion chamber to improve

Table 1.
Operation conditions for Si isotope determination using the MC-ICP-MS Nu Plasma instrument

Parameter	Running conditions
RF power	1350 W
Acceleration voltage	4 kV
Plasma mode	Dry plasma
Introduction system	Cetac ARIDUS (I) desolvator
Coolant gas flow rate	13 l min^{-1}
Auxiliary gas flow rate	0.7 l min^{-1}
Nebuliser gas flow rate	0.9 l min^{-1}
Nebuliser type	100 µl min^{-1} PFA microconcentric nebuliser (ESI)
Aridus sweep gas flow rate	3.5 - 4.0 l min^{-1}
PFA Spray chamber temperature	105 °C
Membrane temperature	160 °C
Running concentrations	Si = 1.7-2.5 µg ml^{-1}, Mg = 0.9-1.25 µg ml^{-1}
Intensity yields	^{28}Si = 5-7 V
Backgrounds on HCl-HF (~ 1 mmol l^{-1}) running solutions	^{28}Si ~ 40 mV, ^{24}Mg ~ 5 mV
Washout time	7 minutes
Stabilisation time before analysis	7 minutes
Cup configuration	L4(^{28}Si), Ax(^{29}Si), H5(^{30}Si); L5(^{24}Mg), Ax(^{25}Mg), H6(^{26}Mg)

the transmission and balance the loss of sensitivity related to the medium resolution mode. The Big 80 evacuated the interface region between the sampler and skimmer cones. It improved the vacuum to approximately 1 mbar in comparison to the standard E2M28 rotary pump of 28 m^3 hr^{-1} (2 mbar). Furthermore, higher sensitivity was obtained by running in dry plasma mode using a Cetac Aridus desolvating sample introduction system in combination with B-type cones with a slightly different geometry than regular A-type cones: a B-type skimmer is characterised by a flatter tip and a B-type sample cone by a smaller interior angle compared to the former A-type design. Sample desolvation greatly reduced potential polyatomic isobaric interferences. The sensitivity on Si decreased with increasing resolution and decreasing entrance slit width.

Analytical conditions

The measurements were carried out using the calibrator-sample bracketing technique in dry plasma mode. The isotopic variations were expressed as δ-values in per mil deviation from a reference material (NBS 28 or an in-house reference sample: $pSiO_2$ or Quartz Merck). We applied mass bias correction using external Mg doping and measured Si and Mg in dynamic mode. Typical operation conditions for Si isotope analysis on this instrument are reported in Cardinal *et al.* 2003 except that a single analysis is now split in four blocks of fifteen runs instead of three blocks of twenty runs (5 second integration). Peak centring was required before each block, as the narrower plateau of ^{28}Si and ^{30}Si in high resolution resulted in an increased sensitivity to magnet drift during the measurement.

In contrast to the low resolution mode (Cardinal *et al.* 2003), the analyte concentrations were doubled (1.7-2.5 µg ml^{-1} Si, 0.9-1.25 µg ml^{-1} Mg, for an uptake rate of 100 µl min^{-1}) (Table 1) to compensate for the loss of sensitivity in medium resolution mode. Conversely, in order to minimise the use of HF, which induces a loss of Si in the desolvator (Cardinal *et al.* 2003, Georg *et al.* 2006b), the HF/HCl content was reduced by a factor of ~ 2 compared to the procedure of Cardinal *et al.* (2003). Acid molarities of the running solutions were usually in the range of 0.7-1.2 mmol l^{-1} for both HF and HCl. Silicon-rich sample solutions were diluted and spiked with Mg in order to reach approximately a 1:1 voltage intensity ratio (^{28}Si:^{24}Mg) at the mass spectrometer (Cardinal *et al.* 2003). The Mg/Si intensity ratios ranged between 1.01 and 1.34 and generally did not vary by more than ± 3% between a sample and calibrator. Indeed HF, HCl, Mg and Si contents of the running solutions were adjusted daily and kept constant throughout each analytical session. The δ-values are expressed relative to NBS 28 or with acid attack digested in-house reference samples Quartz Merck and $pSiO_2$. The average values of -0.03 ± 0.06‰ ($\delta^{29}Si$) and -0.04 ± 0.11‰ ($\delta^{30}Si$) for $pSiO_2$ (n = 10, 1*s*) and -0.01 ± 0.07‰ ($\delta^{29}Si$) and 0.00 ± 0.03‰ ($\delta^{30}Si$) for Quartz Merck (n = 2, 1*s*) confirm that the in-house reference samples measured versus NBS 28 were not significantly different from zero. The $pSiO_2$ was already used and calibrated as an internal in-house reference sample by Cardinal *et al.* (2003).

Experimental

Reference material preparation

Secondary Si isotope reference materials Diatomite and Big Batch were dissolved using single step HF-HCl dissolution at atmospheric pressure (Cardinal *et al.* 2003) in order to check the accuracy of the new MC-ICP-MS configuration on these previously inter-compared reference materials (Reynolds *et al.* 2007). For each aliquot we dissolved about 800 μg silicate powder with HCl (~ 1 mol l^{-1}) - HF (~ 2.3 mol l^{-1}). After dissolution the solution was diluted to reach a ~ 100 μg ml^{-1} Si solution with acid concentrations of ~ 0.05 mol l^{-1} and ~ 0.04 mol l^{-1} for HCl and HF, respectively.

USGS BHVO-1 and BHVO-2 Hawaiian rock reference materials were taken from the same location from the surface layer of a pahoehoe lava that overflowed from the Halemaumau crater in late 1919 (*cf.* Flanagan *et al.* 1976). They thus should be considered as two aliquots from the same lava flow. Because the low pressure HF/HCl acid attacks were inefficient in dissolving rock samples, aliquots of BHVO powders were digested using an alkaline flux attack procedure adapted from the techniques proposed by Georg *et al.* (2006b). The generated glass is easily dissolvable in low concentration acids (Georg *et al.* 2006b). A series of tests were performed to determine the appropriate flux for the alkaline fusion method. In addition to $LiBO_2$ we tested alternative fluxes like Cs_2CO_3 and Na_2CO_3 for the fusion step, but they resulted in poor yields of recovery of about 60 to 90% and were therefore thought to potentially fractionate the Si isotopes. Therefore the fusion step was carried out with $LiBO_2$ as the most appropriate flux due to its providing the highest yield (› 98%, see below). About 5 mg of silicate powder was mixed with 30 mg of $LiBO_2$ flux in a platinum crucible. After one hour of melting at 1000 °C, the fusion beads were quickly quenched in 50 ml double distilled 5% HNO_3 (0.8 mol l^{-1}) to inhibit crystallisation and avoid potential Si isotope fractionation that might result from such a process. Silicon was purified through its quantitative co-precipitation with triethylamine-molybdate (TEA) (De La Rocha *et al.* 1996). The pure cristobalite was dissolved with HCl (~ 1 mol l^{-1}) - HF (~ 2.3 mol l^{-1}) solution. The same alkaline procedure was also applied to the diatomite reference material and four quartz Merck aliquots (Table 2) in order to compare results from acid and alkaline attacks.

All sample preparation steps were carried out in a clean environment. Procedural blanks were prepared for all samples and found to contain non-measurable quantities of Si (with a sample : blank ratio › 350). Concentrations were measured by ICP-AES after fusion to calculate Si recovery (Table 3) and before Si-purification in order to check the absence of major elements and Mo contaminants. Our average calculated yield was 100.9 ± 2.9% (1*s*).

Results

Results for Diatomite and Big Batch secondary reference material are reported in Table 2 and Figure 2. For the silica reference material Diatomite the average delta value of +0.64 ± 0.05‰ and +1.25 ± 0.07‰ (1*s*) for $\delta^{29}Si$ and $\delta^{30}Si$, respectively with a $\delta^{30}Si/\delta^{29}Si$

Table 2.
Bulk average isotopic compositions for Diatomite and Big Batch: (1) prepared by acid attack and alkaline fusion (this study) and (2) from the inter-laboratory comparison (Reynolds *et al.* 2007) and average isotopic composition of Quartz Merck digested by alkaline attack (Quartz Merck is not an inter-laboratory compared reference material in Reynolds *et al.* (2007))

	$\delta^{29}Si$ (‰)	Std. dev (1*s*)	n	$\delta^{30}Si$ (‰)	Std. dev (1*s*)	n	Ratio δ^{30}/δ^{29}
Diatomite							
This study	0.64	0.05	24	1.25	0.07	24	1.95
Reynolds *et al.* (2007)	0.64	0.07	100	1.26	0.10	82	1.97
Big Batch							
This study	-5.38	0.05	5	-10.53	0.07	5	1.96
Reynolds *et al.* (2007)	-5.35	0.15	198	-10.48	0.27	159	1.96
Quartz Merck							
This study	0.00	0.07	4	-0.01	0.12	4	-

Standard deviation is expressed as 1*s* as for respective literature values. Attention should be paid to the standard deviation of inter-laboratory comparison where variability is also resulting from different laboratories using different methodologies and instrumentation.

Table 3.
Delta values, precision and recovery of individual BHVO-1 and BHVO-2 analyses

BHVO-1	Date of analysis	δ^{29}Si (‰)	Std. error (1*se*)	δ^{30}Si (‰)	Std. error (1*se*)	Recovery (%)
BHVO-1 1	6/07/06	-0.18	0.03	n.a.	n.a.	102.4%
BHVO-1 3	7/07/06	-0.25	0.03	n.a.	n.a.	99.3%
BHVO-1 1	23/10/06	-0.10	0.04	n.a.	n.a.	103.1%
BHVO-1 2	23/10/06	-0.16	0.04	n.a.	n.a.	98.8%
BHVO-1 b-I	15/01/07	-0.12	0.04	-0.28	0.06	101.0%
BHVO-1 2	24/02/07	-0.26	0.03	-0.41	0.05	106.2%
BHVO-1 3	24/02/07	-0.18	0.03	-0.29	0.06	99.9%
BHVO-1 1	24/02/07	-0.17	0.04	-0.22	0.05	102.8%
BHVO-1b-II	7/03/07	-0.20	0.05	-0.37	0.08	103.0%
BHVO-1a-I	9/03/07	-0.12	0.05	-0.31	0.09	98.0%
BHVO-1a-Li	10/03/07	-0.17	0.04	-0.41	0.06	105.0%
Average	**BHVO-1**	δ^{29}Si (‰)	**2*se***	δ^{30}Si (‰)	**2*se***	**Recovery (%)**
		-0.17	**0.03**	**-0.33**	**0.05**	**101.8 ± 2.6 (1*s*)**
BHVO-2	**Date of analysis**	δ^{29}Si (‰)	**Std. error (1*se*)**	δ^{30}Si (‰)	**Std. error (1*se*)**	**Recovery (%)**
BHVO-2 1	24/10/06	-0.24	0.03	n.a.	n.a.	99.0%
BHVO-2 3	24/10/06	-0.16	0.04	n.a.	n.a.	102.5%
BHVO-2 2	16/01/07	-0.11	0.03	-0.17	0.05	99.5%
BHVO-2 3	23/02/07	-0.10	0.04	-0.22	0.08	95.4%
BHVO-2 1	23/02/07	-0.15	0.04	-0.19	0.06	102.5%
BHVO-2 1	24/02/07	-0.23	0.04	-0.44	0.06	102.1%
BHVO-2 2	24/02/07	-0.26	0.03	-0.47	0.05	95.2%
BHVO-2b-II	9/03/07	-0.12	0.03	-0.22	0.07	101.0%
Average	**BHVO-2**	δ^{29}Si (‰)	**2*se***	δ^{30}Si (‰)	**2*se***	**Recovery (%)**
		-0.17	**0.04**	**-0.29**	**0.11**	**99.7 ± 2.9 (1*s*)**
Average	**BHVO-total**	δ^{29}Si (‰)	**2*se***	δ^{30}Si (‰)	**2*se***	**Recovery (%)**
		-0.17	**0.03**	**-0.31**	**0.06**	**100.9 ± 2.9 (1*s*)**

The recovery noted here was achieved by concentration measurements after the fusion. n.a. stands for not analysed. 1*se* is the standard error of the mean for each individual analysis. 2*se* represents two times the standard error of the mean of the average values. All data biasing more than 2*se* away from their mean of δ^{29}Si were rejected and are not shown in this table (n = 3 for BHVO-1 and n = 4 for BHVO-2).

of 1.95 are in good agreement with the recommended values from the recent inter-laboratory comparison (+0.64 ± 0.07‰ and +1.26 ± 0.10‰, 1*s*; Reynolds *et al.* 2007). No significant difference was observed between samples prepared by acid and alkaline attack, including for Quartz Merck showing that the alkaline flux procedure does not introduce any analytical bias relative to those obtained with our previous acid procedure (Cardinal *et al.* 2003). For the Big Batch reference material, we obtained values of -5.38 ± 0.05‰ (δ^{29}Si, 1*s*) and -10.53 ± 0.07‰ (δ^{30}Si, 1*s*) with a δ^{30}Si/δ^{29}Si of 1.96, which also fits closely with the recommended values (-5.35 ± 0.15‰ and -10.48 ± 0.27‰, 1*s*, Reynolds *et al.* 2007). These accurate results demonstrate clearly the high data quality of the δ^{30}Si measurements with our new alkaline fusion procedure and the upgraded configuration of the Nu Plasma MC-ICP-MS.

The BHVO-1 and BHVO-2 datasets are given in Table 3. The average values of BHVO-1 and BHVO-2 are identical at -0.17 ± 0.03‰ for δ^{29}Si and -0.33 ± 0.05‰ and -0.29 ± 0.11‰ (2*se*) for δ^{30}Si, respectively. The reproducibility of BHVO measurements is slightly inferior to that obtained for the mono-elemental materials (Diatomite and Big Batch), probably due to the alkaline fusion step, to the purification procedure or to a combination of both, which induces additional variability for samples with more complex matrix. Considering that BHVO-1 and BHVO-2 are derived from the same rock sampled at the same location, we use their grand mean as the representative isotopic composition of the BHVO lava flow (see Table 3). These grand mean values (δ^{29}Si = -0.17 ± 0.10‰ and δ^{30}Si = -0.31 ± 0.20‰, 2*s*) fall within the error brackets of the previous data on BHVO-2 (δ^{29}Si = -0.03 ± 0.17‰ (n = 14, 2*s* and δ^{30}Si = -0.09 ± 0.31‰

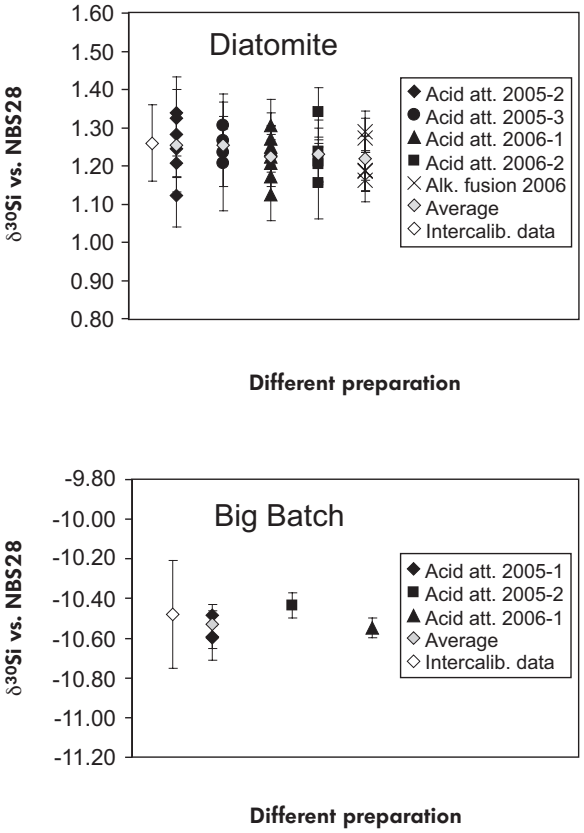

Figure 2. Individual analyses of Diatomite and Big Batch prepared in different years and by different methods (alkaline fusion and acid attack) are indicated by black symbols, with error bars showing 1*se*. Open diamonds on the left side of each figure represent the mean of inter-calibrated reference materials (Reynolds *et al.* 2007); their error bars stand for 1*s*. Grey coloured points indicate the average values for each digestion, with error bars representing 1*s*. Alkaline attack analysis corresponds to different chemical preparations.

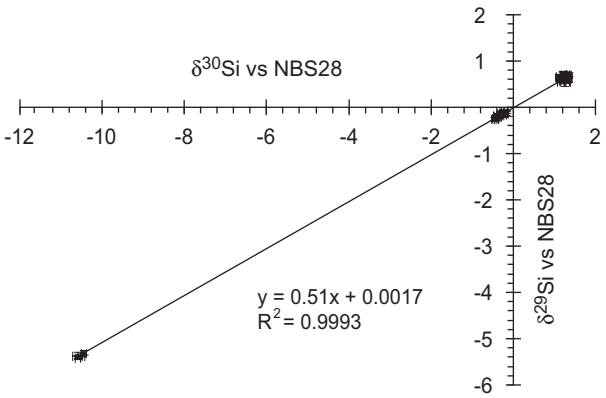

Figure 3. Three isotope plot of δ^{29}Si versus δ^{30}Si for all reference materials Diatomite, BHVO-1, BHVO-2 and Big Batch with linear regression line (error bars indicate 1*se*). All groups of reference materials fall along a mass dependent line. The best fit line with an intercept of zero has a gradient of 0.510, which is principally controlled by the kinetic fractionation of Big Batch (Reynolds *et al.* 2007).

(n = 14, 2*s*) by van den Boorn *et al.* (2006). Besides, our δ^{30}Si BHVO estimate is fully consistent with the average value of four Ocean Island Basalt (OIB) samples by Georg *et al.* (2007a, δ^{30}Si = -0.37 ± 0.14‰, 2*s*). In contrast, it slightly differs from Ziegler *et al.* (2005b) evaluation of a Hawaiian basalt (δ^{30}Si = -0.5‰), that relies on a single measurement and cannot thus be used as an actual reference value.

The three-isotope plot shown in Figure 3 on all reference materials Diatomite, BHVO-1, BHVO-2 and Big Batch is an additional way to demonstrate high data quality and the interference-free determination of δ^{30}Si and δ^{29}Si. The slope of 0.510, mostly driven by the Big Batch set of data, is not significantly different from that in Reynolds *et al.* (2007) observed on Big Batch, Diatomite and IRMM018 (0.511). This slope is again in close agreement with kinetic fractionation law (0.509), as expected for large isotopic fractionation process such as the one likely to have led to the Big Batch isotopic signature.

Discussion

Our BHVO grand mean (δ^{30}Si = -0.31 ± 0.06‰, 2*se*) is significantly heavier than the chondritic reservoir (δ^{30}Si = -0.55 ± 0.08‰, Molini-Velsko *et al.* 1986; δ^{30}Si = -0.58 ± 0.06‰, (1*s*), Georg *et al.* 2007a), but is consistent with the average compositions of upper mantle spinel lherzolites, recent OIB basalts (both at -0.37 ± 0.06‰ (1*s*), Georg *et al.* 2007a) and bulk Iceland basalts (δ^{30}Si = -0.35 ± 0.10‰, 2*s*, Georg *et al.* 2007b). Four processes may be invoked to account for the non-chondritic δ^{30}Si signature within OIBs. First, water-rock interactions may have modified Si isotopic compositions of altered rocks (e.g., Ziegler *et al.* 2005a, b), which can be discounted considering the lack of any surface weathering on BHVO reference materials (Flanagan *et al.* 1976). Second, Si-rich rocks from the continental crust and sedimentary components derived from them bear heavier signatures (δ^{30}Si = -0.07 ± 0.05‰, Douthitt 1982, Ding *et al.* 1996,

André *et al.* 2006), indicating that crustal contamination may shift the Si isotopic compositions of basaltic melts towards more positive $\delta^{30}Si$ values. This hypothesis can obviously be disregarded for Hawaii, which lies within an oceanic plate. Third, the BHVO $\delta^{30}Si$ signature might mirror a widespread mantle-derived geochemical feature related to the incorporation of Si as a light element in the core during the early history of the Earth as proposed by Georg *et al.* (2007a). Finally, the BHVO $\delta^{30}Si$ signature might reflect recycling of old oceanic crust through the mantle. Indeed, much of the trace element and isotopic variability observed in Hawaiian basalts has been attributed to mantle sources that contain various proportions of old (~ 3 Ga) recycled oceanic basaltic crust with or without sediments (e.g., Hofmann 1986). Because highly silicified early Archaean metabasalts bear heavy Si isotopic compositions ($\delta^{30}Si$ › 0‰, André *et al.* 2006, Abraham *et al.* 2007), their recycling through the mantle is a process by which mantle sources with super-chondritic signatures ($\delta^{30}Si$ › -0.55‰) might be generated. The feasibility of such a scenario may be evaluated through a simple (SiO_2-$\delta^{30}Si$) mass balance using a lherzolitic chondritic mantle with a silica content of *ca.* 45% m/m and the 3.47 Ga "Barberton Silicified Basalts" (BSB: 70 ‹ SiO_2 ‹ 75% m/m, +0.4‰ ‹ $\delta^{30}Si$ ‹ +0.6‰) as the recycled component. With these end-members, the offset of +0.24‰ between the Hawaiian basalts and the chondritic reservoir requires between 13% (for SiO_2 = 75% m/m, $\delta^{30}Si$ = +0.6‰ in BSB) and 28% (for SiO_2 = 70% m/m, $\delta^{30}Si$ = +0.4‰ in BSB). These percentages match well the recent estimates of recycled inputs in the source of Hawaiian basalts (~ 16% m/m, Sobolev *et al.* 2007). Therefore, Si isotopes might have some potential in tracing early oceanic crust recycling in the source of OIBs. To decipher whether crustal recycling or core formation (or both) is the ultimate cause of the non-chondritic OIB composition will need further detailed examination based on larger Si-isotopic datasets on various basaltic rock populations with improving accuracy and reproducibility. After accurate inter-laboratory calibration, BHVO-1 and BHVO-2 rock reference materials may serve as ideal reference materials to test new appropriate sample preparation procedures and provide insights to answer this question.

Conclusions

We have demonstrated that accurate and precise $\delta^{30}Si$ data can be acquired on a Nu Plasma MC-ICP-MS. A new simple alkaline flux digestion method followed by purification by TEA co-precipitation has been tested successfully on secondary reference materials (Big Batch and Diatomite). This $LiBO_2$ alkaline fusion method seems to be suitable also for chemically more complex samples such as soils and rocks, since it produces consistent and reproducible silicon isotopic signatures. We provide the second silicon isotope characterisation of international basaltic rock reference materials, BHVO-1 and BHVO-2. Our $\delta^{30}Si$ values agree with isotope signatures of average Ocean Island Basalts, (Georg *et al.* 2007a) and fall in the middle of previous Hawaiian basalt estimates by Ziegler *et al.* (2005b) and van den Boorn *et al.* (2006). As no certified rock reference material exist so far for silicon isotopic composition, our study is a first step to fill this gap. Further isotopic determinations of the BHVO reference material through inter-calibration should now be carried out.

Acknowledgements

The authors greatly thank N. Mattielli for managing the MC-ICP-MS facility in ULB. F. Planchon, L. Monin and N. Dahkani for laboratory assistance at the MRAC, and Jamie Williams and Ian Bowen from Nu Instruments Ltd. for advice. We thank B. Georg and one anonymous reviewer whose comments have greatly helped in improving this manuscript. S.O. is supported by the "Fonds National de la Recherche Scientifique" (FNRS) of Belgium as a Research Fellow. A.J.C. receives a grant from EUR-OCEANS (EC FP6 NoE 511106). D.C. and F.F. are supported by the Belgian Science Policy, BELSPO (SD/CA/03A and IAP P6/13). K.A. is funded by the Geocycles excellence cluster of the state of Rheinland-Pfalz. L.A. thanks the "Fonds National de la Recherche Scientifique" (contract FRFC n°2.4.512.00F) and the Federal Belgian Research Policy for funding the Nu Plasma MC-ICP-MS. L.A. is also grateful to the Federal Belgian Research Policy and European Union for supporting analytical Si-isotopic developments, in the frame of the "Second Supporting actions of the scientific support plan for a sustainable development policy SPSD 2" (contract n° EV/37/7C) and CONTINENT FP5 network (contract n°EVK-CT-2000-00057), respectively. This paper is Geocycles Publication No. 312.

References

Abraham K., Opfergelt S., Cardinal D., Hofmann A., Foley S. and André L. (2007) Si isotopes as a clue for understanding Eoarchean sillicifications. **Geochimica et Cosmochimica Acta, 71,** A3 (Suppl. 1).

references

Alleman L.Y., Cardinal D., Cocquyt C., Plisnier P.D., Descy J.-P., Kimirei I., Sinyianza D. and André L. (2005)
Silicon isotopic fractionation in Lake Tanganyika and its tributaries. Journal of Great Lakes Research, 31, 509-519.

André L., Cardinal D., Alleman L.Y. and Moorbath S. (2006)
Silicon isotopes in ~ 3.8 Ga West Greenland rocks as clues to the Eoarchean supracrustal Si cycle. Earth and Planetary Science Letters, 245, 162-173.

Basile-Doelsch I., Meunier J.D. and Parron C. (2005)
Another continental pool in the terrestrial silicon cycle. Nature, 433, 399-402.

Belshaw N.S., Freedman P.A., O'Nions R.K., Frank M. and Guo Y. (1998)
A new variable dispersion double-focusing plasma mass spectrometer with performance illustrated for Pb isotopes. International Journal of Mass Spectrometry, 181, 51-58.

Brzezinski M.A., Jones J.L., Beucher C.P., Demarest M.S. and Berg H.L. (2006)
Automated determination of silicon isotope natural abundance by the acid decomposition of cesium hexafluosilicate. Analytical Chemistry, 78, 6109-6114.

Cardinal D., Alleman L.Y., de Jong J., Ziegler K. and André L. (2003)
Isotopic composition of silicon measured by multicollector plasma source mass spectrometry in dry plasma mode. Journal of Analytical Atomic Spectrometry, 18, 213-218.

Cardinal D., Alleman L.Y., Dehairs F., Savoye N., Trull T.W. and André L. (2005)
Relevance of silicon isotopes to Si-nutrient utilization and Si-source assessment in Antarctic waters. Global Biochemical Cycles, 19, GB2007, doi:10,1029/2004GB002364.

Cardinal D., Savoye N., Trull T.W., Dehairs F., Kopczynska E.E., Fripiat F., Tison J.-L. and André L. (2007)
Silicon isotopes in spring Southern Ocean diatoms: Large zonal changes despite homogeneity among size fractions. Marine Chemistry, 106, 46-62.

Carignan J., Cardinal D., Eisenhauer A., Galy A., Rehkämper M., Wombacher F. and Vigier N. (2004)
A reflection on Mg, Cd, Ca, Li and Si isotopic measurements and related reference materials. Geostandards and Geoanalytical Research, 28, 139-148.

De La Rocha C.L., Brzezinski M.A. and DeNiro M.J. (1996)
Purification, recovery and laser-driven fluorination of silicon from dissolved and particulate silica for the measurement of natural stable isotope abundances. Analytical Chemistry, 68, 3746-3750.

De La Rocha C.L., Brzezinski M.A. and DeNiro M.J. and Shemesh A. (1998)
Silicon isotope composition of diatoms as an indicator of past oceanic change. Nature, 395, 680-683.

Ding T., Jiang S., Wan D., Li Y., Li J., Song H., Liu Z. and Yao X. (1996)
Silicon isotope geochemistry. Geological Publishing House (Beijing), 125pp.

Ding T.P., Ma G.R., Shui M.X., Wan D.F. and Li R.H. (2005)
Silicon isotope study on rice plants from the Zhejiang province, China. Chemical Geology, 218, 41-50.

Douthitt C.B. (1982)
The geochemistry of stable isotopes of silicon. Geochimica et Cosmochimica Acta, 46, 1449-1458.

Flanagan F.J., Wright T.L., Taylor S.R., Annell C.S., Christian R.C. and Dinnin J.I. (1976)
Basalt, BHVO-1, from Kilauea crater, Hawaii. U.S. Geological Survey Professional Paper, 840, 33-39.

Fripiat F., Cardinal D., Tison J.-L., Worby A. and André L. (2007)
Diatom-induced silicon isotopic fractionation in Antarctic sea ice. Journal of Geophysical Research, 112, G02001, doi:10.1029/2006JG000244.

Georg R.B., Reynolds B.C., Frank M. and Halliday A.N. (2006a)
Mechanisms controlling the silicon isotopic composition of river waters. Earth and Planetary Science Letters, 249, 290-306.

Georg R.B., Reynolds B.C., Frank M. and Halliday A.N. (2006b)
New sample preparation techniques for the determination of Si isotopic compositions using MC-ICP-MS. Chemical Geology, 235, 95-104.

Georg R.B., Halliday A.N., Schauble E.A. and Reynolds B.C. (2007a)
Silicon in the Earth's core. Nature, 447, 1102-1106.

Georg R.B., Reynolds B.C., West A.J., Burton K.W. and Halliday A.N. (2007b)
Silicon isotope variations accompanying basalt weathering in Iceland. Earth and Planetary Science Letters, 261, 476-490.

Hofmann A.W. (1986)
Nb in Hawaiian magmas: Constraints on source composition and evolution. Chemical Geology, 57, 17-30.

Johnson C.M., Beard B.L. and Albarède F. (2004)
Overview and general concepts. In: Johnson C.M., Beard B.L. and Albarède F. (eds), Geochemistry of non-traditional stable isotopes. Reviews in Mineralogy and Geochemistry, 55, 1-24.

references

Méheut M., Lazzeri M., Balan E. and Mauri F. (2007)
Equilibrium isotopic fractionation in the kaolinite, quartz, water system: Prediction from first-principles density-functional theory. Geochimica et Cosmochimica Acta, 71, 3170-3181.

Molini-Velsko C., Mayeda T.K. and Clayton R.N. (1986)
Isotopic composition of silicon in meteorites. Geochimica et Cosmochimica Acta, 50, 2719-2726.

Opfergelt S., Cardinal D., Henriet C., André L. and Delvaux B. (2006)
Silicon isotopic fractionation by banana (*Musa* spp.) grown in a continuous nutrient flow device. Plant and Soil, 285, 333-345.

Reed N.M., Cairns R.O., Hutton R.C. and Takaku Y. (1994)
Characterization of polyatomic ion interferences in inductively coupled plasma mass spectrometry using a high resolution mass spectrometer. Journal of Analytical Atomic Spectrometry, 9, 881-896.

Reynolds B.C., Aggarwal J., André L., Baxter D., Beucher C., Brzezinski M.A., Engström E., Georg B., Land M., Leng M.J., Opfergelt S., Rodushkin I., Sloane H.J., Van den Boorn S.H.J.M., Vroon P.Z. and Cardinal D. (2007)
An inter-laboratory comparison of Si isotope reference materials. Journal of Analytical Atomic Spectrometry, 22, 561-568.

Robert F. and Chaussidon M. (2006)
A paleotemperature curve for the Precambrian oceans based on silicon isotopes in cherts. Nature, 443, 969-972.

Sobolev A.V., Hofmann A.W., Kuzmin D.V., Yaxley G.M., Arndt N.T., Chung S.L., Danyushevsky L.V., Elliott T., Frey F.A., Garcia M.O., Gurenko A.A., Kamenetsky V.S., Kerr A.C., Krivolutskaya N.A., Matvienkov V.V., Nikogosian I.K., Rocholl A., Sigurdsson I.A., Sushchevskaya N.M. and Teklay M. (2007)
The amount of recycled crust in sources of mantle-derived melts. Science, 316, 412-417.

van den Boorn S.H.J.M., Vroon P.Z., van Belle C.C., van der Wagt B., Schwieters J. and van Bergen M.J. (2006)
Determination of silicon isotope ratios in silicate materials by high-resolution MC-ICP-MS using a sodium hydroxide sample digestion method. Journal of Analytical Atomic Spectrometry, 21, 734-742.

Varela D.E., Pride C.J. and Brzezinski M.A. (2004)
Biological fractionation of silicon isotopes in Southern Ocean surface waters. Global Biochemical Cycles, 18, GB1047, doi:10.1029/2003GB002140.

Ziegler K., Chadwick O.A., White A.F. and Brzezinski M.A. (2005a)
δ^{30}Si systematics in a granitic saprolite, Puerto Rico. Geology, 33, 817-820.

Ziegler K., Chadwick O.A., Brzezinski M.A. and Kelly E.F. (2005b)
Natural variations of δ^{30}Si ratios during progressive basalt weathering, Hawaiian Islands. Geochimica et Cosmochimica Acta, 69, 4597-4610.